

Aimé Lay-Ekuakille
Subhas Chandra Mukhopadhyay (Eds.)

Wearable and Autonomous Biomedical Devices and Systems for Smart Environment

Issues and Characterization

Lecture Notes in Electrical Engineering

Volume 75

Aimé Lay-Ekuakille and
Subhas Chandra Mukhopadhyay (Eds.)

Wearable and Autonomous Biomedical Devices and Systems for Smart Environment

Issues and Characterization



Springer

Aimé Lay-Ekuakille, Guest Editor
Dipartimento d’Ingegneria dell’innovazione
University of Salento
Lecce, Italy
E-mail: aime.lay.ekuakille@unisalento.it

Subhas Chandra Mukhopadhyay, Guest Editor
School of Engineering and Advanced Technology (SEAT),
Massey University (Turitea Campus)
Palmerston North, New Zealand
E-mail: S.C.Mukhopadhyay@massey.ac.nz

ISBN 978-3-642-15686-1

e-ISBN 978-3-642-15687-8

DOI 10.1007/978-3-642-15687-8

Library of Congress Control Number: 2010934865

© 2010 Springer-Verlag Berlin Heidelberg

This work is subject to copyright. All rights are reserved, whether the whole or part of the material is concerned, specifically the rights of translation, reprinting, reuse of illustrations, recitation, broadcasting, reproduction on microfilm or in any other way, and storage in data banks. Duplication of this publication or parts thereof is permitted only under the provisions of the German Copyright Law of September 9, 1965, in its current version, and permission for use must always be obtained from Springer. Violations are liable to prosecution under the German Copyright Law.

The use of general descriptive names, registered names, trademarks, etc. in this publication does not imply, even in the absence of a specific statement, that such names are exempt from the relevant protective laws and regulations and therefore free for general use.

Typeset & Coverdesign: Scientific Publishing Services Pvt. Ltd., Chennai, India.

Printed on acid-free paper

9 8 7 6 5 4 3 2 1

springer.com

Guest Editorial

The human body, with its articulations, is a complex physical bio-system that needs a constant check-up not only for remedial reasons (bio-psycho-physical degradation) but also for compensating limitations imposed by impairments and for improving performances in particular situations. Beyond the above reasons there are others related to the use of external non-invasive biomedical devices and instrumentation necessary for monitoring physiological parameters and for allowing diagnosis. Further issues connecting previous aspects regard technologies of managing intrinsic and extrinsic phenomena that surround the human body according to information processing. The quick growth of smart sensors, low-power embedded devices and new materials from physical and technological viewpoints, represents a stimulus to provide new applications for the human body well-being.

Hence, continuous advances in wearable and portable sensors for many applications and especially for biomedical issues have been sufficient reasons that are encouraged the necessity to collect variety of experience in this field; thanks to that, a new book has been prepared which title is “Wearable and autonomous biomedical devices and systems: New issues and characterization” and included in the book series of “Lecture Notes in Electrical Engineering”. This special issue dedicated to wearable and autonomous systems, including devices, offers to variety of users, namely, master degree students, researchers and practitioners, an opportunity of a dedicated and a deep approach in order to improve their knowledge in this specific field. The special issue draws the attention about interesting aspects, as for instance, advanced wearable sensors for enabling applications, solutions for arthritic patients in their limited and conditioned movements, wearable gate analysis, energy harvesting, physiological parameter monitoring, communication, pathology detection , etc..

The book, on one hand, illustrates theoretical aspects and applications, and it displays new criteria in characterizing devices and systems, at the other hand. Characterization is a key issue since it allows to know the performance of devices and systems described in the book by showing some statistics and result representation. The book contains 20 contributions from colleagues working in the topic and under different approaches and aspects; these co-ordinated approaches are the true richness of the book. The editors gracefully thank the contributors for their single papers included in this special issue. The editors hope this special

issue will be a good omen for all neophytes who approach the topic for the first time but also for readers with experience who can breathe fresh life into their research.

Aimé Lay-Ekuakille, Guest Editor

Dipartimento d'Ingegneria dell'innovazione

University of Salento

Lecce, Italy

aime.lay.ekuakille@unisalento.it

Subhas Chandra Mukhopadhyay, Guest Editor

School of Engineering and Advanced Technology (SEAT),

Massey University (Turitea Campus)

Palmerston North, New Zealand

S.C.Mukhopadhyay@massey.ac.nz



Dr. Subhas Chandra Mukhopadhyay graduated from the Department of Electrical Engineering, Jadavpur University, Calcutta, India in 1987 with a Gold medal and received the Master of Electrical Engineering degree from Indian Institute of Science, Bangalore, India in 1989. He obtained the PhD (Eng.) degree from Jadavpur University, India in 1994 and Doctor of Engineering degree from Kanazawa University, Japan in 2000.

During 1989–90 he worked almost 2 years in the research and development department of Crompton Greaves Ltd., India. In 1990 he joined as a Lecturer in the Electrical Engineering department, Jadavpur University, India and was promoted to Senior Lecturer of the same department in 1995.

Obtaining Monbusho fellowship he went to Japan in 1995. He worked with Kanazawa University, Japan as researcher and Assistant professor till September 2000.

In September 2000 he joined as Senior Lecturer in the Institute of Information Sciences and Technology, Massey University, New Zealand where he is working currently as an Associate professor. His fields of interest include Sensors and Sensing Technology, Electromagnetics, control, electrical machines and numerical field calculation etc.

He has authored over 200 papers in different international journals and conferences, edited nine conference proceedings. He has also edited six special issues of international journals as guest editor and seven books with Springer-Verlag.

He is a Fellow of IET (UK), a senior member of IEEE (USA), an associate editor of IEEE Sensors journal and IEEE Transactions on Instrumentation and Measurements. He is in the editorial board of e-Journal on Non-Destructive Testing, Sensors and Transducers, Transactions on Systems, Signals and Devices (TSSD), Journal on the Patents on Electrical Engineering, Journal of Sensors. He is in the technical programme committee of IEEE Sensors conference, IEEE IMTC conference and IEEE DELTA conference. He was the Technical Programme Chair of ICARA 2004 and ICARA 2006. He was the General chair of ICST 2005, ICST 2007. He has organized the IEEE Sensors conference 2008 at Lecce, Italy as General Co-chair and the IEEE Sensors conference 2009 at Christchurch, New Zealand as General Chair during October 25-28, 2009.



Aimé Lay-Ekuakille has a Master Degree in Electronic Engineering, a Master Degree in Clinical Engineering, a Ph.D in Electronic Engineering from Polytechnic of Bari. He has been technical manager of different private companies in the field of: Industrial plants, Environment Measurements, Nuclear and Biomedical Measurements; he was director of a Health & Environment municipal Department. He has been a technical advisor of Italian government for high risk plants. From 1993 up to 2001, he

was adjunct professor of Measurements and control systems in the University of Calabria, University of Basilicata and Polytechnic of Bari. He joined the Department of Innovation Engineering, University of Salento, in september 2000 in the Measurement & Instrumentation Group. Since 2003, he became the leader of the scientific group; hence, he is the co-ordinator of Measurement and Instrumentation Lab in Lecce. He has been appointed as UE Commission senior expert for FP-VI (2005–2010). He is the Editor-in-Chief of the International Journal of Measurement Technologies and Engineering Instrumentation - IJMTIE (IGI-Global, USA). He is still: chair of IEEE-sponsored SCI/SSD Conference, member of Transactions on SSD and Sensors & Transducers Journal editorial board. He is Associate Editor of the International Journal on Smart Sensing and Intelligent Systems. He is currently organizing the next ICST2010 in Lecce, Italy. He is a member of the following boards and TCs: Association of the Italian Group of Electrical and Electronic Measurements (GMEE), SPIE, IMEKO TC19 Environmental Measurements, IEEE, IEEE TC-25 Medical and Biological Measurements Subcommittee on Objective Blood Pressure Measurement, IEEE-EMBS TC on Wearable Biomedical Sensors & System and included in different IPCs of conferences. Aimé Lay-Ekuakille is a scientific co-ordinator of different international projects. He has authored and co-authored more than 110 papers published in international journals, books and conference proceedings. His main researches regard Environmental and Biomedical instrumentation & measurements and, measurements for renewable energy.

Contents

Design and Integration of Fall and Mobility Monitors in Health Monitoring Platforms	1
<i>Pepijn van de Ven, Alan Bourke, John Nelson, Hugh O'Brien</i>	
Smart Nano-systems for Tumour Cellular Diagnoses and Therapies.....	31
<i>Conversano Francesco, Greco Antonio, Casciaro Sergio</i>	
Miniature Differential Mobility Spectrometry (DMS) Advances towards Portable Autonomous Health Diagnostic Systems	55
<i>Weixiang Zhao, Abhinav Bhushan, Michael Schivo, Nicholas J. Kenyon, Cristina E. Davis</i>	
A Distributed Telemedical System for Monitoring of the Respiratory Mechanics by Enhanced Interrupter Technique	75
<i>Ireneusz Jabłoński, Janusz Mroczka</i>	
Nonlinear Dynamics, Materials and Integrated Devices for Energy Harvesting in Wearable Sensors.....	97
<i>Bruno Andò, Salvatore Baglio, Marco Ferrari, Vittorio Ferrari, Luca Gammaitoni, Carlo Trigona</i>	
Wearable Sensors for Foetal Movement Monitoring in Low Risk Pregnancies	115
<i>Luís M. Borges, Pedro Araújo, António S. Lebres, Andreia Rente, Rita Salvado, Fernando J. Velez, J. Martinez-de-Oliveira, Norberto Barroca, João M. Ferro</i>	

An Embedded System for EEG Acquisition and Processing for Brain Computer Interface Applications	137
<i>A. Palumbo, F. Amato, B. Calabrese, M. Cannataro, G. Cocorullo, A. Gambardella, P.H. Guzzi, M. Lanuzza, M. Sturniolo, P. Veltri, P. Vizza</i>	
Micro Systems for the Mechanical Characterization of Isolated Biological Cells: State-of-the-Art	155
<i>Denis Desmaële, Mehdi Boukallel, Stéphane Régnier</i>	
On-Body Chemical Sensors for Monitoring Sweat	177
<i>Shirley Coyle, Fernando Benito-Lopez, Robert Byrne, Dermot Diamond</i>	
A Wearable Measurement System for the Risk Assessment Due to Physical Agents: Whole Body Mechanical Vibration Injuries	195
<i>Rosario Morello, Claudio De Capua</i>	
A Measurement System Design Technique for Improving Performances and Reliability of Smart and Fault-Tolerant Biomedical Systems	207
<i>Rosario Morello, Claudio De Capua</i>	
A Self-controlled Master-Slave Robot and Its Application for Upper Limb Rehabilitation.....	219
<i>Tao Liu, Chenguang Li, Yoshio Inoue, Kyoko Shibata</i>	
Advanced Wearable Sensors and Systems Enabling Personal Applications	237
<i>Andreas Lymberis</i>	
Fall Detection of Patients Using 3-Axis Accelerometer System	259
<i>Petar Mostarac, Hrvoje Hegeduš, Marko Jurčević, Roman Malarčić, Aimé Lay-Ekuakille</i>	
Unobtrusive and Non-invasive Sensing Solutions for On-Line Physiological Parameters Monitoring	277
<i>Octavian Postolache, Pedro Silva Girão, Eduardo Pinheiro, Gabriela Postolache</i>	
The Method of Increasing the Accuracy of Mean Opinion Score Estimation in Subjective Quality Evaluation	315
<i>A. Ostaszewska, S. Żebrowska-Lucyś</i>	
Wearable Assistive Devices for the Blind	331
<i>Ramiro Velázquez</i>	

Intrabody Communication in Biotelemetry	351
<i>Željka Lučev, Igor Krois, Mario Cifrek</i>	
SPINE-HRV: A BSN-Based Toolkit for Heart Rate Variability Analysis in the Time-Domain	369
<i>Alessandro Andreoli, Raffaele Gravina, Roberta Giannantonio, Paola Pierleoni, Giancarlo Fortino</i>	
Measuring Finger Movement in Arthritic Patients Using Wearable Glove Technology.....	391
<i>J. Condell, K. Curran, T. Quigley, P. Gardiner, M. McNeill, J. Winder, E. Xie, Zhang Qi</i>	
Author Index	407

Design and Integration of Fall and Mobility Monitors in Health Monitoring Platforms

Pepijn van de Ven, Alan Bourke, John Nelson, and Hugh O'Brien

University of Limerick, Limerick, Ireland
pepijn.vandeven@ul.ie

1 Introduction

This chapter discusses the design and integration of fall and mobility sensor platforms for mobile and remote health signs monitoring. With a steadily increasing elderly population in Europe [1] and indeed throughout significant parts of the rest of the world, health services for elderly people are placing a growing strain on national health budgets [2] and the availability of nursing and care taker staff. Additionally, perhaps due to the advent of technology in general and changing social relations in society, there is an ever-increasing wish amongst our elderly citizens to live independently and be mobile for as long as possible. Recent advances in telecommunications, medical devices and technology in the home environment have enabled elderly people to live independently for longer than ever before. However, integrated systems targeting the monitoring of these elders' health in the home environment are at best scarce. The use of these systems would enable medical practitioners to perform an early diagnosis of potential issues, which in turn would result in a better chance of full recovery and lower hospitalization costs. A common problem encountered by elderly people is a reduction in their mobility. It is estimated that one in three elderly people 65 years or older in the UK experience a serious fall each year [3]. The results of a fall can be dramatic, leading to long hospitalization and, not seldom, death as a direct or indirect consequence of the fall [3, 4]. The resulting emotional and financial cost to individuals and society is significant. In a recently published paper [5], Gannon et al. estimated the annual cost of falls amongst elderly citizens in Ireland, which has a population of 4 million, to be EUR 404 Million. In the United States the cost of falls for people aged 65 and over were estimated at over \$19 billion for the year 2000 [6]. People experiencing reduced mobility, in particular the elderly, can greatly benefit from having a fall and mobility sensor for several reasons. In the event of a fall, it is of great importance that help is requested immediately to prevent a so-called long-lie event. All too often, elderly citizens spend hours or longer on their own after having fallen. Getting help immediately has shown to lower the risk of hospitalization by 26%, and

death as a result of the fall by 80% [7]. To prevent falls from happening in the first place, it is important that elderly people (or other groups of citizens at higher risk of falling) and their health providers have access to an early warning system that indicates an increased risk of falling. Mobility monitoring is a proven means of predicting fall risk and continuous assessment of an elderly person's mobility is therefore crucial. Current solutions focus on providing a stand-alone solution to fall and mobility monitoring; the sensors may share interfaces with other health signs sensors, but the measurements are not correlated with other health signs or used to optimize the measurement of those other health signs. For example, if an elderly person's blood pressure or heart rate is measured just after vigorous exercise (walking stairs could easily fall in this category), results may be interpreted as alarming if there is no information regarding the recent activity. The importance of including fall and mobility monitors in mobile health monitoring systems is evident. However, the close and careful integration of the functionality added by the fall and mobility monitor with all the other sensor functionality is extremely important to take full benefit of the extra information. This chapter discusses such an integration effort. After an overview of existing fall and mobility algorithms and sensors in section 2, fall and mobility sensor hardware, made in the University of Limerick, is presented in section 3. The software implementing the fall and mobility monitoring algorithms is discussed in section 4 after which a generic sensor interface for use on resource-constrained mobile platforms is discussed in section 5. After this description of fall and mobility monitoring hardware and software, section 6 discusses trials performed with the fall and mobility sensors as part of a large project funded by the European Commission.

2 Methods of Fall Detection

In 1987 the Kellogg international working group on the prevention of falls in the elderly defined a fall as 'unintentionally coming to ground, or some lower level not as a consequence of sustaining a violent blow, loss of consciousness, sudden onset of paralysis as in stroke or an epileptic seizure' [8]. This definition has been used in many research studies, and sometimes extended to include falls resulting from dizziness, syncope and consequences of an epileptic fit or cardiovascular collapse. The World Health Organization has defined a fall as 'an event, which results in a person coming to rest inadvertently on the ground or some other lower level.' Thus fall detection systems should be able to detect falling onto the ground in an unexpected and uncontrolled way, whatever the cause of this accidental collapse.

2.1 Fall Detection Algorithms

The end of a fall may be characterized by an impact (which causes the physical damage) and by near horizontal orientation of the faller. Fall-detection

systems must detect one if not both of these characteristics associated with a fall [4]. The most obvious method of fall detection involves the sensing of the shock received by the body upon impact. The preferred sensor for this purpose is the accelerometer. Attached to the body it is used to measure deceleration of the body when it is arrested by the ground following a fall. This method is used in many subject-worn fall-detection systems [9, 10, 11, 12, 13, 14]. Also included in some fall-detection systems is the detection of the orientation of the subject [11, 12, 14, 15, 16, 17]. The body orientation characteristic is used as a confirmation that the person has fallen and not just bumped into someone or something. The measurement of the body orientation is accomplished using tilt switches incorporated into the subject-worn fall-detection device, or through extraction of the orientation specific part of the accelerometer signal.

Academic research efforts

In 1991 Lord and Colvin [9] reported some early work on fall detection using a tri-axial accelerometer. Their work described a data-logging unit to measure accelerometer signals for later analysis. Williams in 1998 [11] described the concept of an autonomous device, carried on the belt, which featured a piezoelectric sensor to detect the impact when the person hit the ground, as well as a mercury tilt switch to detect when the person was horizontal. The detection thresholds for impact were determined by attaching the sensors to a mannequin, which fell onto a wooden floor. This work was later continued by Doughty [18], who patented a two-stage fall-detection system and algorithm and a commercial version of this system was developed and marketed by the company Tunstall (Whitley lodge, Yorkshire, England). Doughty's fall-detector wakes up from the sleep state when a strong impact is detected. Then a second sensor estimates the body orientation of the wearer and determines whether the subject is in a lying state for a set period of time. If both these decision rules are satisfied an alarm is raised. Wu [19] from the University of Vermont-USA showed, using video analysis of markers placed on the subject, that vertical and horizontal speeds are 3 times higher during a fall than for any other controlled normal activity. Wu also showed that both speeds are of the same amplitude at the time of the fall whereas they are strongly dissimilar during 30 normal activities. This work inspired Nait-Charif [20] to detect falls from computer vision techniques using particle filters to track movement of the subject's head. Successful fall detection results were obtained through the use of fixed thresholds on vertical and longitudinal velocities. Tamura [17] proposed an ambulatory monitor that records falling time over a long period. When the subject is falling a photo-interrupter outputs a trigger signal and the microprocessor records the falling time. In a preliminary study, the system was tested for normal adults and hemiplegic patients, and operated without any trouble. However, fundamentally the sensor is just a tilt switch and thus false-positives occurred when subjects lay down or rode a

bike. Noury [15, 16, 14], from the University of Grenoble-France, designed an autonomous sensor module, attached under the armpit, which comprised accelerometers, inclinometers and a vibration sensor. The sensor module detected when the velocity of the movement exceeded a specific threshold, the sequence from a vertical posture to the lying posture, as well as the absence of movements after the fall. The device was first tested on 5 persons who performed 15 fall scenarios 5 times and was shown to achieve a sensitivity and specificity close to 85%. Demongeot [21] developed a ‘tele-monitoring’ system to remotely detect the physical and physiological health aspects of elderly people living at home. The system also incorporated a fall detection feature. A fall was detected when a combination of, subject-worn sensors and local environment or embedded sensors triggered simultaneously. The sensors include infrared-volumetric sensors, magnetic door contacts and the accelerometer readings (attached to the subject). The combination of information from all of these sensors was used to indicate that a fall might have occurred. A heart-rate monitor was used to ensure that the subject wore the device. This fall-detection system is part of an over-all ‘health-smart-home’ and is an example of a secondary-fall detection system. A fall is detected when certain criteria are fulfilled and the system detects a deviation from normal habit in the persons activity. As a result, a fall may not be detected straightaway unlike primary fall-detection systems. Degen [22] developed a fall detector wrist watch which obtained a 65% sensitivity and 100% specificity. The device consists of a tri-axial accelerometer and uses three thresholds to distinguish falls from Activities of Daily Living (ADL). If all three exceed their thresholds, a fall is detected. Three subjects performed a number of falls. Results show a 100% detection of forward falls, 58% detection of backwards falls and 45% detection of sideways falls. One subject then wore the device for 48 hours in which time no false-positives occurred. Karantonis [23] developed a subject worn fall-detector and mobility monitor which incorporated a single tri-axial accelerometer. The algorithm for the fall-detection algorithm operates on the device itself and is not processed in a remote location. If at least two consecutive peaks in the signal vector magnitude exceed a threshold of 1.8g a possible fall flag is set. The subject is then monitored continuously for 60 seconds after the possible fall and after an initial 5-second settling period. If the subject is motionless during this time. Then the event is reclassified as a fall. This would require immediate attention. The algorithm was tested using five young healthy subjects. Each performed three different fall types and a number of sitting, lying and walking ADL at different speeds. A number of the lying activities were incorrectly detected as possible falls. The overall sensitivity of the fall detection algorithm was 95.6%. Prado [13] developed an intelligent 4-axis accelerometer unit (IAU) worn like a patch, fixed to the back at the height of the sacrum. Further evaluation by Diaz [10] in a laboratory study carried out over 8 volunteers, showed that the device was able to distinguish true fall events from normal activities like fast walking or going up/downstairs. The device produced a 100% sensitivity and

92.5% specificity. Kangas et al. [24] evaluated different low-complexity fall detection algorithms, using tri-axial accelerometers attached at the waist, wrist, and head. Fall data was recorded from three middle-aged subjects who performed nine intentional fall types in three directions (forward, backward, and lateral). High sensitivities (97% – 98%) and specificities (100%) were achieved in this study with quite low-complexity algorithms, however only a small subject group ($n=3$) performing very few scripted ADL was used and no long-term unsupervised testing was performed. The same researchers also continued the evaluation of the algorithms on data recorded by a group of 20 middle-aged (40-65 years old) volunteers performing falls (six different falls each performed twice) and four scripted ADL, also these same ADL were also recorded from 21 older people (aged 58-98 years) from a residential care unit. Chao et al. [25] recorded tri-axial accelerometer data from the chest and waist of seven young healthy male subjects as they performed falls as well as functional normal and dynamic activities including jumping. They examined the use of acceleration cross-product and magnitude as well as post fall posture and developed and tested algorithms of varying complexity. The various algorithms were analysed under the following categories; threshold selection, sensor placement and post-fall posture. Results showed that a fall detection algorithm based on the data from the chest shows better global accuracy. With post-fall posture detection leading to lower false alarm ratios.

2.2 Sensor Location

In several studies performed in the area of falls, fractures of the hip and proximal femur were identified as typical injuries sustained during a fall-event [26, 27, 28]. Indeed this is a large area of concern, with hip fractures being the most common and frequent of all serious injuries sustained by the elderly population following a fall [9]. But as statistics have shown, injuries from falls are not confined to this region. A large amount of wrist, radius and elbow fractures as well as shoulder and head injuries occur from falls also [29, 30]. According to Veltink et al. [31] to provide general kinematic data from a subject using subject-worn sensors, sensors should be easily mountable on the body and stay reliably in place at all times. Sensors should not be uncomfortable to the subject and not impede their activity of daily living, so they should not cross any joints and only require short cables. Thus to provide comprehensive detection of all collisions to all major body parts due to fall-events, the proposed sensors should measure the impact occurring to both the upper and lower extremities during a fall-event, as well as being non-intrusive and not cumbersome. Most of the fall detection devices and systems that will be discussed use one or more sensors placed on the upper part of the body, at the upper trunk and at the pelvic region. Doughty et al. [18] placed piezoelectric shock sensors on the trunk (chest), thigh, waist and wrist, but later confined the sensor locations to the waist and chest. One of the major issues with fall detection devices is the lack of compliance with

wearing these sensors. The idea of a wrist worn fall detector is highly suitable as the sensor would replace the already acceptable wrist watch. A fall-detector placed at the wrist was investigated as a possible location by Doughty et al. [18] and Degen et al. [22]. According to the authors the wrist would be a very appealing location as ‘A fall detector in the form of a wrist watch will not feel alien to the wearer’, and it could be worn comfortably during high risk fall situations like showering or going to bed. However, according to the same authors ‘The major disadvantage of this solution is the complexity of the fall detection algorithm in detecting impact from a fall. The arm can move and rotate, thus has six degrees of freedom in its movement.’ Doughty et al. [18] also conceded that the results obtained with a wrist-worn sensor for different fall types varied too widely for a fall detector to be placed there.

2.3 Sensor Attachment

Most accelerometer based fall detection and mobility monitoring systems located on the trunk have used either chest straps [31, 12, 32, 33, 34, 35] or patches [10, 13, 36]. These methods of attachment have significant draw backs:

- They normally result in systems which are uncomfortable to wear
- The system is not easily donned
- Sensors can be easily placed incorrectly
- More than one person may be required to attache the sensors

Fall detection systems incorporated in wearable garments eliminate many of these problems. A number of garments that incorporate fall detection sensors exist and are detailed here.

- MEMSWear smart shirt

The MEMSWear smart shirt was developed by Tay [37]. It incorporates a tri-axial accelerometer into the shoulder. By setting a threshold of 4.8g on the summation of the peak values from the acceleration signals, separation between gathered fall and ADL data is achieved, however these peaks do not occur at the same time and it is not clear what time window, if any, is used.

- VTAMN

Garment based mobility monitoring has been attempted by Noury [38] who developed a smart vest for ambulatory remote monitoring of physiological parameters and activity. A fall detection system is incorporated into the vest under the left-arm, it consists of a bi-axial accelerometer and a micro-controller embedded on a flexible electronic board. The fall detection algorithm is based on research also performed by Noury [15, 16, 14]. In clinical trials where the vest was worn by 3 healthy adults for 4 days the VTAMN was found easy to put on and the thermal comfort was acceptable, even with high ambient temperatures (36°). The vest delivers physiological information on the subject including heart rate, respiratory

rate and temperature as well as environmental parameters (ambient temperature) and can be used to perform fall detection.

- Lifeshirt by Vivometrics
The lifeshirt developed by Vivometrics (www.vivometrics.com) is a lightweight, machine washable shirt with embedded sensors. The respiratory sensors are woven into the shirt around the wearer's chest and abdomen. A single channel ECG measures heart rate, and a three axis accelerometer located at the sternum, records posture and activity. Optional peripheral devices measure EEG/EOG, periodic leg movement, temperature, end tidal CO₂, blood oxygen saturation, blood pressure and coughing.
- The smartshirt by sensatex
The sensatex smartshirt (www.sensatex.com) is a seamless light breathable, nylon fabric with fully integrated conductive fibres, creating connectivity to acquire and transfer physiological signals. The shirt is designed to monitor an individual's heart rate, respiration, body temperature and movement wirelessly and remotely. The SmartShirt collects physiological signals from the wearer's body which are converted to digital signals using a small personal controller and sent wirelessly to a base station through either Bluetooth or ZigBee wireless technology.

3 Fall Sensor Hardware

This section describes the hardware used by the authors in several projects. In these projects the objectives are to accurately identify falls, monitor mobility or perform both. The fall and mobility sensor is based on a Freescale tri-axial accelerometer controlled by a Texas Instruments low power microprocessor. The microprocessor is used for AD conversion of the accelerometer data, extraction of mobility and fall data, storage of the data on a microSD card and communication with a PC or mobile phone. A block schematic of the fall and mobility sensor system is shown in figure □. The Bluetooth module used in this design is the Roving Networks RN-24.

3.1 Microprocessor

The Texas Instruments MSP430F1611 was chosen for its low power consumption, sizeable memory (48kB flash with 256B user flash and 10kB RAM) and relatively high speed (8MHz). Using the IAR workbench or similar software, the MSP430 can be programmed using C/C++ or assembler. The MSP430F1611 is equipped with a 16 bit Reduced Instruction Set Computer (RISC) processor, 3 Direct Memory Access (DMA) channels, a 12 bit Analogue to Digital Converter (ADC) with 16 channels, a 12 bit Digital to Analogue (DA) converter, a hardware multiplier, 2 independent timers, 2 communication ports which can implement Universal Asynchronous Receiver Transmitter (UART), Serial Peripheral Interface (SPI) or Inter-Integrated Circuit

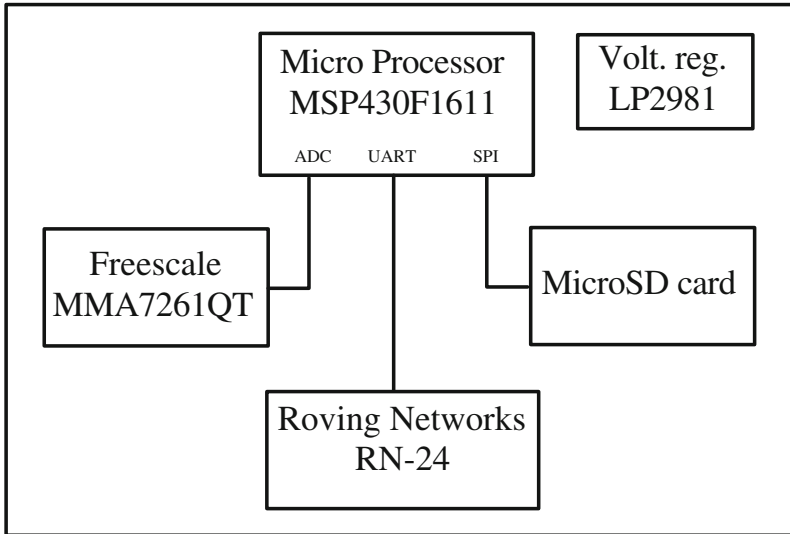


Fig. 1. Block diagram of fall and mobility sensor

(I2C) communication protocols and a watch dog. Due to this impressive selection of hardware interfaces and the availability of three DMA channels, it is possible to implement significant functionality without the need to have the core of the microprocessor running continuously.

3.2 Freescale Accelerometers

The Freescale MMA7261QT tri-axial accelerometer is a low cost accelerometer with selectable outputs between $\pm 2.5 - 10g^1$. The principle of operation is based on sensing changes in capacity due to flexing of moveable beams under the influence of accelerations. With a power consumption of $500\mu A$, the sensor is ideally suited for low-power applications. The measured accelerations are filtered using on-board single pole switched capacitor filters and can be directly fed to an AD converter.

3.3 Bluetooth Module

The Roving Networks RN-24 can be obtained as a class 1 or 2 module on a small Printed Circuit Board (PCB), which allows for through-hole, and thus easy, integration on prototype PCB's. The module offers sustainable data rates of up to 100 kb/s at transmit/receive powers of around 30-50 mA with which it is by far the biggest consumer on the board. Power consumption can be minimized by using appropriate sleep modes. The RN-24 was chosen

¹ g Is the gravitational constant in $\frac{m}{s^2}$.

for its ease of integration in prototype hardware, but it should be noted that any radio with a UART or similar interface could be used. The use of a Zigbee radio is for example appealing from an energy efficiency aspect, but introduces challenges due to the relatively limited number of available Zigbee interfaces for PCs and mobile phones.

3.4 Power Requirements

Due to the use of a low power microprocessor with the ability to turn off peripherals and thus lower power consumption further, a low energy sensor can be obtained. The potential for this power reduction is determined by the functional requirements of the sensor. To indicate a ceiling for the energy consumption, the power requirements of the sensor without explicit power reducing measures is here discussed. In this scenario, the processor core and accelerometers are powered continuously. This results in a quiescent current of $370\mu A$ at 3.3V. However, whilst communicating the sensor consumes 38.4 mA and this clearly inhibits long term autonomous use of this sensor. For the prototype of this platform a rather large Lithium Ion battery with capacity of 1000mAh was chosen. With this battery it is possible to transmit mobility data constantly for periods exceeding 26 hours. For monitoring applications, in which mobility data will normally only be stored locally and only urgent information is relayed using Bluetooth, the battery can be chosen far smaller. Although the cost of communication is likely to drop significantly with the imminent use of Bluetooth Low Energy, Bluetooth is a rather power hungry communication channel. Its widespread availability makes Bluetooth the ideal wireless technology for clinical use of the sensor. For stand-alone applications a low-power wireless technology, such as Zigbee (802.15.4) or a proprietary technology may be more appropriate.

3.5 Communication

Although the Bluetooth standard incorporates methods for guaranteed message delivery through resending of messages, the respective functionality is normally not exposed to the designer. Moreover, the exact implementation is dependant on the drivers used and as a result message receptions can be quite unpredictable at times (on less powerful platforms messages can get ‘lost’ in the stack or buffers can overflow). In addition to these issues, there exist different ways of making the identity of the sender and receiver known. The Bluetooth standards specify ‘services’ that can be used to identify devices and Media Access Control (MAC) addresses can also be used. Again, due to the various abstraction levels in the software, it may not always be straight forward to identify an arbitrary Bluetooth radio in the software on the Bluetooth master device.

For these reasons a high level protocol with sender and receiver identification can be extremely useful. A message protocol was defined for bi-directional communication with the fall and mobility sensor. The payload

of the message, with a maximum length of 226 bytes², is preceded by a delimiter (0xFC) and 8 byte header and followed by a second delimiter (0xFD). As the second byte of the header contains the message type, the protocol allows for early decisions on whether or not to read a message. The number of bytes to be read is stored in the first field of the header. In combination with the delimiters, the message length is used to decide on the integrity of the received message prior to further processing. The integrity of the message is further tested using a checksum.

4 Fall Sensor Software

4.1 Embedded Software

The fall and mobility sensing algorithm is largely interrupt driven. Figure 2a shows the main loop of the software, in which the software continuously checks for incoming and outgoing messages. The main loop of the program is periodically interrupted by various interrupts. Two interrupts occur at fixed intervals. The first of these interrupts is a timer interrupt which triggers a reading from the AD converter, as depicted in figure 2b. Upon finishing the conversion, the AD converter will send an interrupt indicating a new reading is ready for further processing, which will trigger the process depicted in figure 2c. First and foremost, in this interrupt handler the fall algorithm is implemented and used to analyze the latest data for high impacts and, if necessary, to start a further analysis into the origin of detected impacts. If event or alert messages result from this analysis, these are stored on a stack and a transmission will be initiated in the program's main loop. This is done by sending characters one by one to the UART (Universal Asynchronous Receiver/Transmitter). Once the UART is ready to accept the next character, it sends an interrupt request which is handled as depicted in figure 2d. In this interrupt routine the next character is fetched from the message buffer and sent to the UART until all characters have been sent. Receiving messages is performed in a similar fashion.

As depicted in figure 2c, upon reception of a character by the UART, the latter will send an interrupt request to the processor. The character is then transported from the UART to an incoming message buffer, after which the UART is ready to receive the next character.

5 A Generic Sensor Interface Architecture

This section will detail the architecture used for a mobile interface to the sensor implemented on a Blackberry 'Storm' device. A modular system has been a key design goal as has attempting to keep the code base small and

² The maximum payload size is determined by the wish to send DM5 packets in order to keep energy consumption to a minimum.

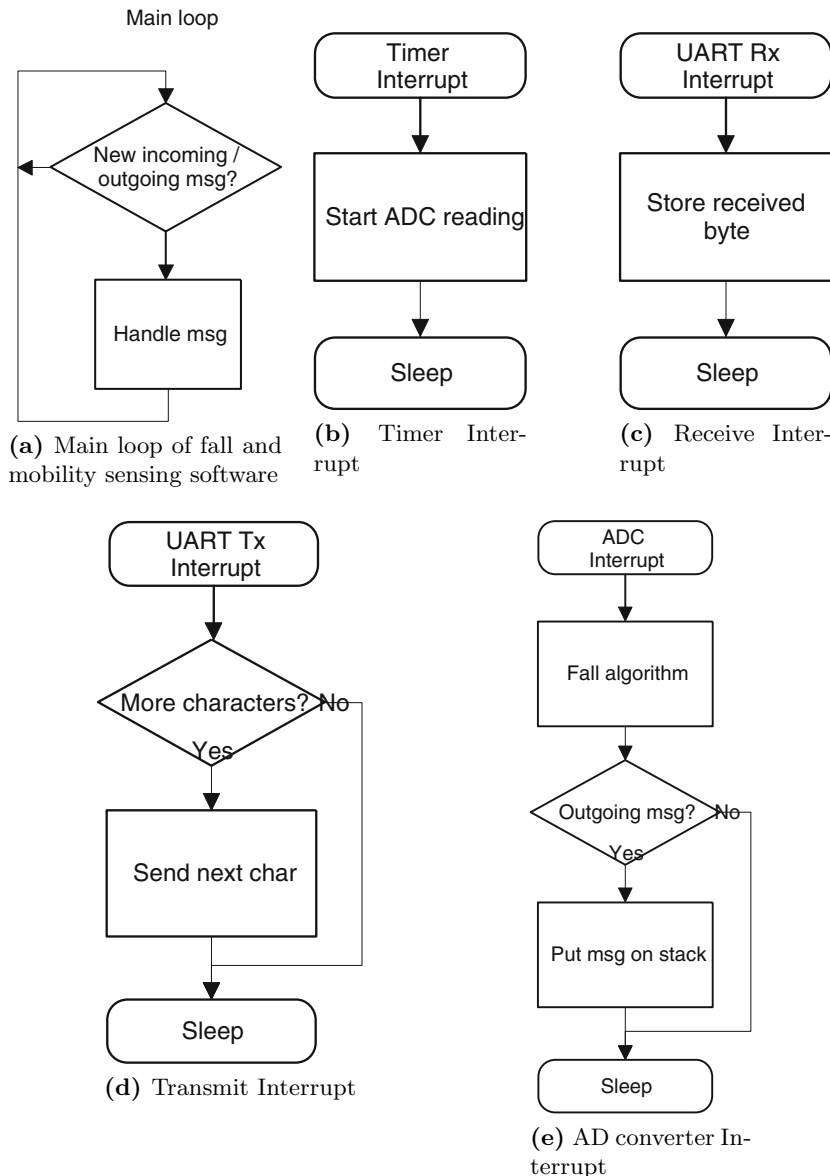


Fig. 2. Main software components of the fall and mobility sensor

efficient for use on resource constrained devices such as phones. The top level of the design consists of graphical user interfaces (GUI) and agents. The concept and function of agents will be further discussed after a discussion of the low level layers in the architecture.

In addition to the evident importance of reliable fall detection capabilities and the prompt relay of related messages to a caretaker or rescue services, an important aspect of fall and mobility monitoring is the feedback that such devices can give to the user. In many cases, the most effective means of preventing or overcoming mobility issues is frequent and sufficient exercise. The fall and mobility monitor can aid the user in complying with a set treatment programme by monitoring the user and suggesting further exercises to meet targets. This application clearly exercises one of the main benefits of using a mobile phone to interface with the sensors; the user is immediately provided with feedback which can improve treatment and this information is presented on a device that most, if not all, user groups are familiar with³. Caretakers and health professionals can access the data extracted from the users mobility patterns through any of the transport mechanisms the phone provides.

5.1 General Overview

A high-level overview of the generic sensor interface architecture is given in figure 3. The Bluetooth connection from the sensor is visible as a stream of bytes on the BlackBerry handset. The message protocol discussed in section 3.5 was used. For each sensor connection on the handset a state machine monitors the byte stream to detect when a valid message has been seen. The checksum of the message is computed, and if valid, a new SensorMessage object is created by the state machine. The state machine then resets its state ready to begin monitoring for a new message.

The SensorMessage object creates a SensorHeader object, which accesses the raw bytes stored in the SensorMessage and parses them into native data types. The SensorHeader also logs status information to the DataStore.

Using the message type information gleamed from the SensorHeader, the SensorMessage dispatches the remaining raw bytes to the appropriate message handler defined for the particular message type received. e.g. a mobility message contains information on the user's cadence so a MobilityMessage object parses the bytes according to the defined structure of a mobility message. Once parsed, these readings are stored in the DataStore.

The DataStore acts as the division between the lower and the higher layers of the interface. The lower layers need only send their readings to it. All records stored in the DataStore are interactive objects, which maintain their own value and a list of Agents who require notification when the value changes. Agents may register for updates on a record that does not yet exist, so that if the record should ever receive data from the lower layer, the agent will be immediately informed.

Agents monitor the records, such as 'step count' and may either present this data to the user in the form of a graphical screen (as in figure 4), store

³ Phones with large touch displays are currently becoming increasingly popular.

These phones offer accessible interfaces for less technologically experienced users or users with reduced motor skills.

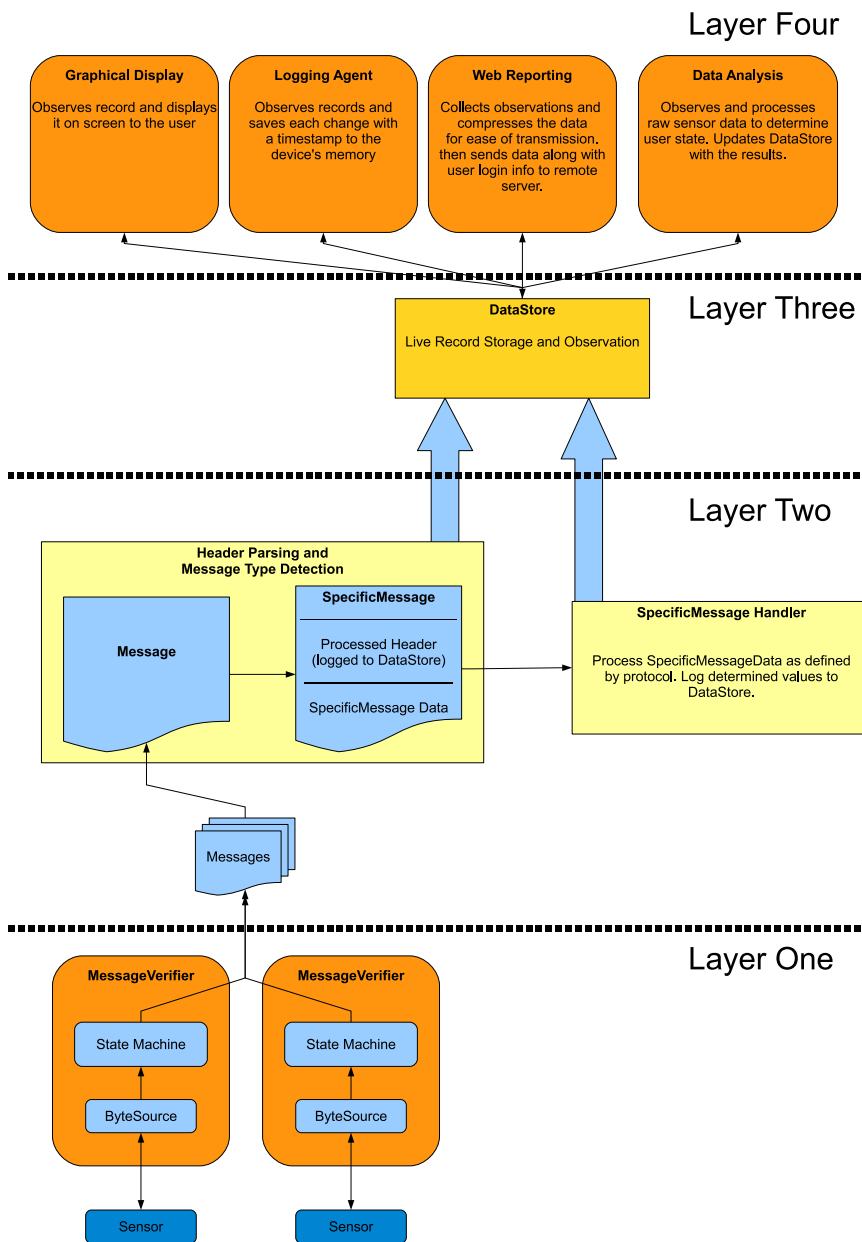


Fig. 3. High-level overview of generic sensor interface architecture



Fig. 4. Graphical Interface used to visualize information from a fall and mobility sensor

the data in the device’s flash memory, upload the data to a remote server, or in the case of an emergency, make use of the handset’s telephony features to directly contact emergency services.

5.2 ByteSources

At the bottom of the stack are the ByteSources. The function of this layer is to interact with whatever data source they are designed for, such that they may buffer data as it is received and push the individual bytes of the data one at a time into the next layer, the MessageVerifier. Each ByteSource is required to create its own instantiation of a MessageVerifier (described below). For reasons relating to the functionality of upper layers each ByteSource also passes its object (a.k.a.’this’) reference into the constructor of its personal MessageVerifier.

5.3 MessageVerifier

The MessageVerifier class models a state machine that is responsible for ensuring that the bytes passed into it from a ByteSource match an expected sequence and conform to the defined message protocol. Should a message meet these requirements it is then checksummed to ensure that no errors occurred in transit. Internally, bytes are input in a piecemeal fashion strictly from a single ByteSource and are stored in memory that is managed by the MessageVerifier. The internal state machine monitors the number and contents of the received bytes and when it has determined that enough bytes have been received that they constitute a message, it performs the checksum. Should the message pass all of the tests the MessageVerifier creates a new instance of a SensorMessage passing into its constructor the valid message as well as a reference to the ByteSource that created the message. The MessageVerifier does not hold a reference to this new SensorMessage and once it

has been created the state machine will reset and be ready to begin processing the next message. This functionality is completely opaque to the ByteSource.

5.4 SensorHeader

Though the MessageVerifier passes a valid message into a SensorMessage constructor, the very first action of the SensorMessage constructor is to pass the same valid message into a SensorHeader, for this reason it will be described first. The SensorHeader is processed much like any of the other messages, the key difference being that header data is always present regardless of the message type being received.

Three features differentiate it from other messages, firstly it is responsible for comparing the sequence number of the message against the expected sequence number. If these numbers do not match, an error is logged in the DataStore. If they do match then the next expected sequence number is updated to reflect the current sequence number plus one.

Secondly, the SensorHeader is capable of logging detailed statistics on the frequency of messages of differing lengths and types. This is controlled through a toggle value in the DataStore.

Thirdly, once the SensorHeader has fully parsed the input and determined key values such as the message type and source ID of the Sensor, it stores these values in public access members, freeing other messages to deal only with their specific message content while still retaining (simplified) access to the data stored in the message header. The message type value in particular is required by a SensorMessage and is the reason the SensorHeader is created first.

5.5 SensorMessage

As described above, the first order of business for a SensorMessage is to create a new SensorHeader and store a reference to it. Once the SensorHeader has been fully constructed, the SensorMessage can access the message type data and, using a switch statement, determine which of the various message types to create.

5.6 SensorRecords

SensorRecords represent the fundamental data storage unit within the Data-Store. At a basic level, a SensorRecord may be essentially viewed as a large wrapper for a single integer value. The most useful aspect of a SensorRecord is that it maintains a list of objects that implement the Observer interface and provides methods for additional Observer-implementing objects to be appended to this list. Classes that implement Observer provide a public access method called `update()` that takes an Observable object as a parameter. SensorRecord extends the Observable class such that when a SensorRecord

receives a new integer value to store (handled by the DataStore), should it decide that it has changed enough to warrant notifying the objects that are observing it, it will iterate over its list of Observers calling the `update()` method on each of the elements, passing itself as the only argument. The Observers can use the accessor methods defined in SensorRecord on the `this` reference they receive to find out exactly which SensorRecord it was that triggered the update. This is necessary as the same Observer may be observing a multitude of Observable objects yet each of them will call the same `update()` method of the Observer.

5.7 The DataStore

The DataStore contains only static members and methods, it is always available and no other part of the system is responsible for instantiating it. At its heart is a hash table with Strings as keys and SensorRecords as entries. DataStore provides some simple accessor methods that allow client classes to directly access a SensorRecord (`getRecord(String key)`) or to act as a proxy so that storing or retrieving the integer value associated with a particular SensorRecord is made easier due to the reduced type casting (the `Store(String key, int value)` method and the `retrieve(String key)` method).

For each of the accessor methods, DataStore will first scan the hash table to determine if the record being queried already exists. Instead of returning an error in the case of a non-existent record, DataStore will automatically create the record with the default value of zero and will carry out the rest of the request on the newly created record as normal, e.g. if the store method was called it will change the value in the SensorRecord from the default, to the specified value. The reasoning for this behaviour is an attempt to reduce the coupling between agents and SensorRecords. Should an agent attempt to access a SensorRecord that had not yet been created because the message type that creates it has yet to be received (e.g. ‘Fall Type’ from ‘FallAlertMessage’) then there would be no clear mechanism for the agent to be notified should the record be created later in the session (polling is too inefficient to consider). By registering on a non-existent record the agent is able to ensure that should this record ever receive an update, it will be alerted through its `update()` method.

5.8 Records

‘SensorRecords’ are self contained objects that can store an integer value and are observable. ‘Records’ is a single class filled with static nested classes filled with either more static nested classes or static final Strings. The reason for this seemingly mindless class is that it serves as an invaluable programming aid when accessing particular records from the DataStore. Due to the nature of the DataStore, if a non-existent SensorRecord is accessed, the DataStore

will create the record with default values and return it, this is done so that agents can register on SensorRecords that have not yet had data stored in them but are expected to do so.

The problem arises that if a programmer makes a typographical error in accessing the DataStore, there will be no indication that the record they are requesting will never receive an update. By categorising the expected records into a hierarchical system, errors such as this are averted and record selection while programming is made more intuitive.

5.9 ConfigDB

Storing observable records that represent the current state of a Sensor has immediate usefulness, but the limitation on what data can be stored (integers only) has made it difficult to use the DataStore to store anything else, such as the list of currently connected sensors or the set of user defined options that control the interface itself. For this reason a separate section of the Records tree was created which does not have the requirement to return SensorRecords when queried. In implementation, it is an entirely separate hash table to the one that is used for the SensorRecords but is still maintained by the DataStore. The ConfigDB does not allow new entries to be created dynamically as the regular DataStore does, if an attempt is made to access a record that does not exist then an exception is thrown. Valid records are listed under the ‘config’ tree in the Records file.

SourceList

The SourceList stores the list of all Sensor source IDs that have been seen by the system along with a reference to the ByteSource that is responsible for it. In SensorMessage, after the header processing but before the dispatch to the message handlers, the source ID of the message is sent to the SourceList. The SourceList is designed for agents that monitor records and may find it necessary to transmit data back to the Sensor that generated the record. Normally, the only information about the Sensor available to the Agent is the SourceID from the top of the record name but with the SourceList the agent can look up the reference to the ByteSource responsible for handling that Sensor and call its `sendToSensor` method. This functionality would be used for example for the delivery of acknowledgement messages to the fall sensor.

As SourceList extends the Observable class, agents may also register as Observers of it so that they are notified when a new Sensor becomes connected to the device. In this way an agent may determine the source ID of the new sensor and immediately begin observing records of interest that it generates, or is expected to generate.

5.10 Agents

Agents are applications that interact with the contents of the DataStore, and, based on what they find or determine through calculation, will initiate some action or write some value back to the DataStore. Agents are self-contained and conduct all of their communication through the DataStore (i.e. an agent may observe the output record of another agent). Many agents may be ‘running’ simultaneously and each may observe any number of SensorRecords or other observable objects.

Agents represent the top layer of the component stack and offer a flexible way to expand the functionality of the interface. All agents extend the ‘Agent’ abstract class which exposes start and stop control to other aspects of the system. Also provided is a wrapper function that eases the act of registering as an observer of an object; this wrapper maintains a list of Observables that the agent has registered with so that if the agent is stopped the Observables will have the agent’s entry removed from their update lists.

An example of an agent for the fall sensor interface is the FallHandler agent which monitors the `status.falldetected` record on a number of Sensor IDs and uses the BlackBerry OS integration features to place a phone call to a number defined in an Options file. A further example is the FallAlertAcknowledger which implements a protocol requirement that the Sensor receive an acknowledgement message after alerting the Handler to a fall event. Both agents also observe the SourceList and register themselves on the appropriate records anytime a new source ID becomes known to the interface.

Agents may also be used to log data to external media, to interact with a Web service, to compute user mobility patterns based on Sensor data, or implement virtually any other high-level functionality. The strength of the agent based approach is demonstrated by the potential for an agent to reprogram a Sensor with a new version of its firmware should one become available. This could for example be done by the web service agent, who can download the firmware to the device and signal the reprogramming agent which will or will not run as determined by user preferences.

Further examples of useful agents would be a high level ‘agent manager’ which would determine which agents to start at device boot time or application start time and a ‘connection manager’ agent that would ensure the Sensors are continuously connected and alert the user if a connection issue exists.

5.11 Graphical Interfaces

Graphical interfaces are implemented as a special form of agent. Their main goal is to access the DataStore and represent the information found there in a visual manner to the user. As they may observe any record, the graphical interface dynamically updates anytime new information is received from the sensor. User modifiable preferences are also exposed through a graphical agent.

6 Case Study: The CAALYX Project

In the recently successfully concluded CAALYX project (Complete Ambient Assisted Living eXperiment) funded by the European Community under the 6th Framework Programme, fall and mobility monitoring played an important role. The aim of the CAALYX project was to provide a suite of sensors for healthy elderly users to detect potential health threats at an early stage. This section will detail how the integration of the fall and mobility sensor in this platform was performed.

6.1 Project Description

As mentioned above, the aim of the project was to detect potential health threats in elderly citizens at an early stage. This approach can help to significantly reduce hospitalization and thus the cost associated with health care provision. A detailed investigation of the most dominant health issues encountered by the elderly, led to the choice of a suite of sensors. The chosen sensors were for blood pressure, weight, temperature, blood oxygen saturation, pulmonary rate, cardiac information (heart rate and full ECG) and fall and mobility information. The mobility information obtained from the fall and mobility monitor played an important role in determining whether measurements were valid (movement artifacts play a dominating role in e.g. ECGs) and to schedule measurements (measurements were scheduled to coincide with expected periods of user inactivity or rest). For this reason, an intricate integration of this sensor in the platform and its data processing functionality, was required.

Trials were performed in two phases to allow for gradual integration of the fall and mobility hardware and functionality in the wider system. Both phases will be discussed separately.

6.2 Phase 1 Trials Description

During Phase 1 of the CAALYX trials, a stand-alone fall and mobility sensor was used to reduce physical integration efforts and focus on system integration first to demonstrate the significant value of mobility information in a remote health monitoring system.

Sensor Location

In previous research [39], positive results were obtained with the fall sensor positioned on the chest as depicted in figure 5a. Hence this position was initially used to test the new fall sensor platform. After positive results the sensor was also used under the left arm, thus minimizing the influence of the device on the user. To achieve greater compliance with wearing the fall and mobility sensor located on the chest, the vest depicted in figure 5b was

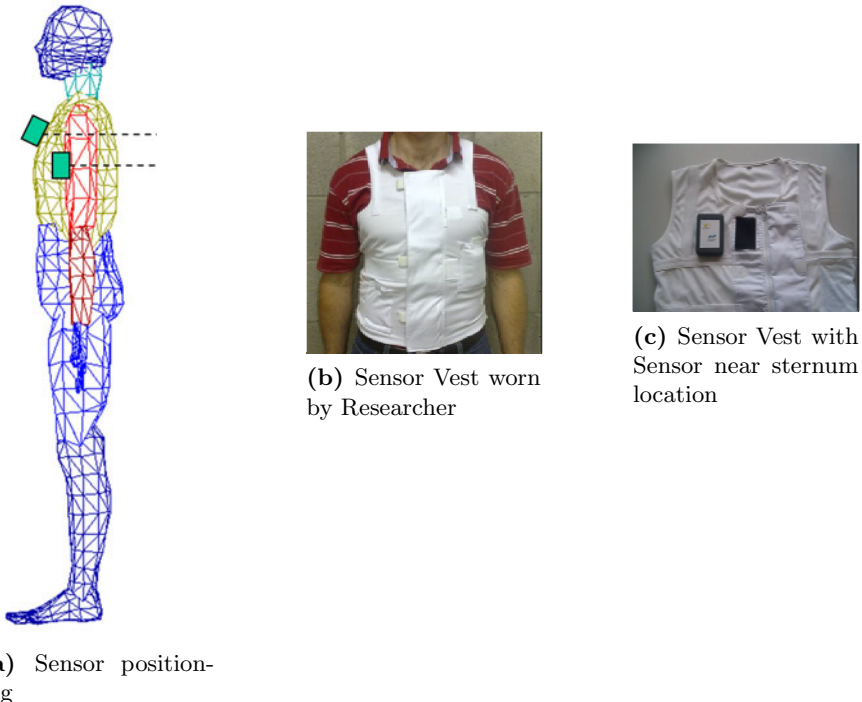


Fig. 5. Details regarding Phase 1 sensor positioning and fixation

developed as an alternative to the chest strap used in the previous study [39]. The CAALYX Fall and Mobility Monitoring Vest is a light weight garment (230g) with a zipper on the front for ease of donning and doffing of the garment. Support elastic is incorporated into the vest to ensure the sensor is held close to the body. As can be seen in figure 5c the sensor is attached to the vest using velcro and covered with a flap of material which is also closed using velcro. A pocket is located at hip level for a mobile phone which can be used for communication with the sensor. A set of vests adjustable from sizes 2XS to 3XL was designed for the trials. The size adjustment was achieved using 2 velcro adjustment strips at each side (4 in total per vest). These should be adjusted so that no gap between the subjects body and the vest existed, but should not be so tight as to restrict breathing.

Phase 1 Fall Sensor Hardware

The CAALYX system setup during the phase 1 trials dictated a stand-alone fall and mobility sensor that communicated with the wider system through a Nokia N95 mobile phone. To increase robustness of the system as a whole, the fall and mobility sensor was equipped with a 1000mAh LiIon battery. This allowed monitoring of the user including on-board high resolution recording

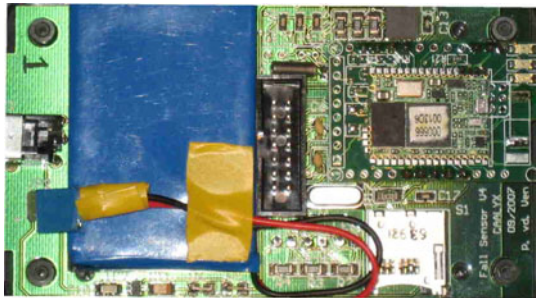


Fig. 6. Printed circuit board of Phase 1 fall and mobility sensor with battery.

of 3D accelerations for periods up to 11 hours whilst also transmitting the recorded data to the mobile phone (or a custom-built PC application) through Bluetooth. The used sensor is depicted in figure 6. The requirements for a fast prototype required the use of off-the-shelf enclosures. A suitable enclosure was found in an enclosure made by OKW with dimensions 104.5mm x 65mm x 19mm. The weight of the device is less than 150g.

Phase 1 Fall Sensor Software and Algorithms

As the phase 1 trials did not require communication of mobility information to other parts of the CAALYX system, the fall sensor software consisted of the necessary fall algorithms, software to log the measured data on a μ SD card on the fall sensor and a communication interface to notify the system of potential trip or fall incidents. The fall algorithm used is based on measuring the acceleration of the user in three degrees of freedom. These measurements are performed at a high sampling frequency such that high frequency impacts can be detected. Such impacts are the first trigger for a fall analysis, as displayed in figure 7. Upon measuring an acceleration exceeding the threshold, an algorithm is started in which the user is analyzed for his/her mobility patterns following the high impact. If the user is found to be lying for a prolonged time, the algorithm will generate a fall alert.

Stand Alone Fall Sensor Trials

Initially the wireless mobility and fall sensor was used in an experiment performed in the University of Limerick. While their movements were recorded, subjects performed a series of simulated falls and normal activities of daily living (ADL). The subjects were young (<35 years) healthy males. A total of 11 subjects were recruited for the study. The mean and standard deviation of age, height and mass of the subjects were 23.4 ± 4.6 years, 1.8 ± 0.076 m and 80.9 ± 13.3 kg respectively. The fall types were selected in order to best simulate the type of fall that may occur and cause injury to an elderly person.

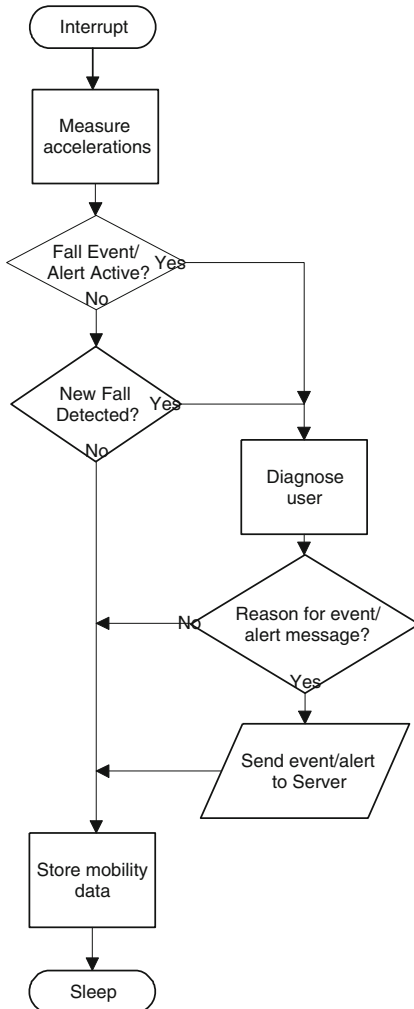


Fig. 7. Flowchart of fall algorithm

These were the same fall types that were performed in the previous study by [39]. Each fall was performed with the subject initially in a standing position. All the falls were performed onto large crash mats with a combined thickness of 0.76m. The simulated falls performed were: forward, backward and lateral falls left and right, all with both legs kept straight and with knees relaxed to allow knee flexion. Each fall was performed 3 times; a total of 264 falls were recorded. The normal activities that were performed, included sitting on a kitchen chair, sitting on a bench, sitting on a bed, lying down on a bed and walking 10m. All were repeated 3 times; a total of 165 ADL were recorded.

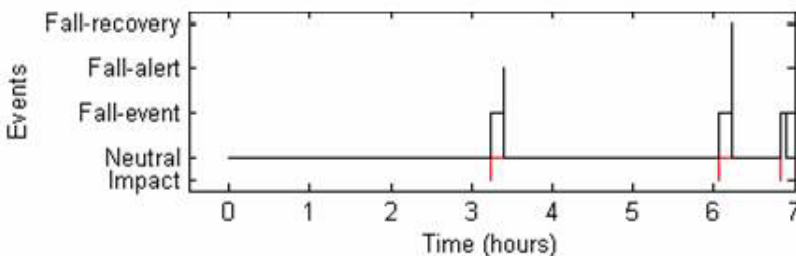


Fig. 8. Example events summary of a 7 hour trial session

After the successful completion of the trials with healthy subjects, the fall sensor was used in an experiment involving the monitoring of elderly subjects as part of the aforementioned CAALYX project. In this experiment the fall sensor was part of a suite of sensors chosen to demonstrate the feasibility of unobtrusive monitoring of elderly subjects in daily living. During four weeks, elderly people were equipped with the fall sensor for eight hours per day, but trials were often shorter as the elderly volunteers were given significant flexibility in choosing the start time and stop time of daily trials. In these four weeks, 833 hours of relevant ADL data were captured. Data were gathered in a body-area network and transmitted by a nokia N95 to a web server. Figure 8 shows the results of one 8-hour experiment with an elderly person performing ADL. Around 3:15 hours into the experiment, the sensor registers a heavy impact with consecutively a predominantly horizontal position of the user for the next ten minutes. This event is interpreted as a fall, but in reality was due to the elderly person sitting heavily onto a bed before lying down. These types of events, where the elderly person's reduction in mobility results in high accelerations are hard to distinguish from real falls with the algorithm used in these trials. After ten minutes the caretaker centre is alerted and contact is made with the elderly person. As a result of this contact the fall alert is regarded to be a false fall alert and the device resets upon an acknowledgement received from the care centre. The second high impact moment at just over six hours into the day is again due to the reduced mobility of the user. In this case, the fall sensor correctly identifies the impact as non threatening and the care centre is notified of this conclusion.

6.3 Phase 2 Trials Description

Phase 2 of the CAALYX trials further explored the opportunities identified during the phase 1 trials by further device and system integration of the fall and mobility sensor in the CAALYX remote health monitoring system. To increase user acceptance, the fall and mobility sensor was redesigned for inclusion as an add-on board in a waist worn sensor which incorporated ECG, temperature, blood oxygen saturation and breathing rate sensors.

Sensor Location

Given the type of sensors to be used, a waist worn device was found to be most appropriate. As previous fall sensors had been used in higher locations on the user's torso, the fall and mobility algorithms were adapted for use in this new location.

Phase 2 Fall Sensor Hardware

As discussed above, the phase 2 fall and mobility sensor hardware was integrated in hardware provided by one of the project partners. This device incorporated all the wearable sensors and was dubbed the Wearable Light Device (WLD). Through a shared Bluetooth interface, falls and mobility messages were reported to the CAALYX system for use in fall and mobility monitoring, health measurement scheduling and for use by the medical professionals involved in testing the CAALYX system. The hardware is shown in figure 9. As power and communication functionality were provided by the host system, it was possible to develop a smaller and thinner PCB with dimensions 44mm x 28mm x 3mm that neatly fitted into the hardware used for the other mobile sensors.

Phase 2 Fall Sensor Software and Algorithms

The CAALYX fall detection algorithm is based on measuring the accelerations of the user in three degrees of freedom. Using thresholds in acceleration, posture and time, the algorithm determines whether a fall has occurred. With these thresholds the algorithm examines both the impact received by a faller as well as examining the orientation of the subject following the impact to see if the user is lying. The magnitude of acceleration from the subject's trunk is compared to an experimentally derived threshold [39]. If the acceleration



Fig. 9. Fall Sensor Hardware for integration in the WLD

exceeds this threshold then an impact is deemed to have occurred. The subject posture is then monitored to see if the subject is lying or standing for the following 2 seconds. If the subject is lying following a large impact, then a fall-event is registered. Upon detection of a fall event, the sensor will send a fall event message to the mobile phone using a Bluetooth radio. These messages will be repeated at specified intervals until a message is received from the phone indicating that the fall event message has been received. Meanwhile, the fall sensor will be analyzing the user for a further 10 minutes. In case the user has not recovered from the fall, a long lie event will be sent to the phone, thus indicating that help is required. Again, the fall alert message will be repeated until the phone acknowledges having received the message. In case the user recovers from the fall, a fall recovery message is sent using the same message protocol. The algorithm developed for the CAALYX project incorporates many of the best and most reliable features of previously detailed fall detection algorithms. A more in-depth description of the design, development and testing of the fall detection algorithm can be found in [40, 41].

Integrated Fall Sensor Trials

The fall and mobility sensor hardware integrated in the WLD was initially used in trials performed at the University of Limerick (Ireland). Both fall trials and trials identifying ADL were performed. Fall trials were performed with young healthy subjects and ADL trials were performed with both healthy young volunteers and healthy elderly volunteers. The simulated falls study involved 10 young healthy male subjects performing simulated falls onto large crash mats. The subjects fell from a specially constructed platform under the supervision of a physical education professional. Each subject performed eight different fall types and each activity was repeated three times. The subjects ranged in age from 24–35 years (27.2 ± 3.61 years), body mass from 68 to 111 kg (84.2 ± 14.43 kg), and height from 1.65 to 1.96m (1.81 ± 0.102 m). All gave written informed consent and the University of Limerick Research Ethics Committee (ULREC) approved the protocol. The simulated falls performed were: forward falls, backward falls, lateral falls left and right all performed with both legs straight and with knee flexion similar to those performed in the study by [39]. The results of these trials showed excellent sensitivity of the fall algorithms for the various falls from a standing to a lying position. Only 1 fall out of a total of 240 was not identified as a fall by the fall and mobility sensor.

Further trials investigated the capabilities of the fall algorithms to correctly identify various ADL as non-fall events. These trials were conducted inside the University of Limerick and in the Limerick region with ethical approval of the ULREC. In addition to the 10 young healthy subjects, the study involved 10 elderly volunteers (>65 years) performing scripted ADL in their own homes. All volunteers performed 3 repetitions of 6 different ADL, thus leading to a

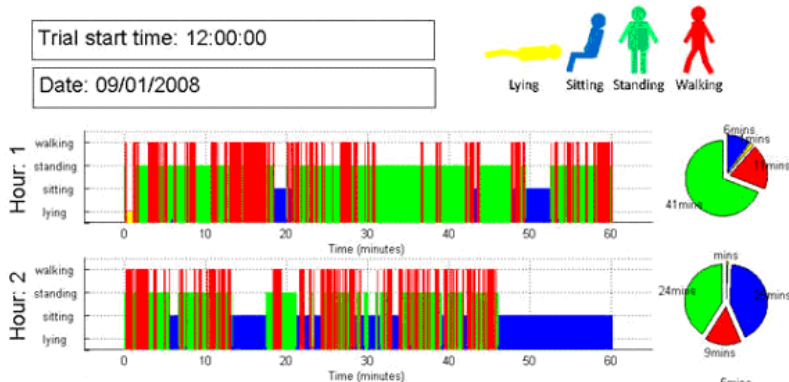


Fig. 10. Extract of results of mobility and activity trials with healthy elderly volunteers

total of 360 activities performed. Only 1 ADL was detected as a fall, which leads to an overall sensitivity of 99.7 %.

In a further experiment, elderly volunteers used the device in an unscripted trial for a period of up to 8 hours. During this period, the elderly volunteers were free to perform their normal daily routines, whilst the fall and mobility monitor detected potential falls and extracted the user's mobility patterns. An example of such a mobility pattern is shown in figure 10. In these trials it was established that the integrated device did not obstruct the elderly user significantly in carrying out his/her daily routine.

6.4 Clinical Trials in Ancona

Upon the successful completion of the trials in Limerick, the CAALYX system was deployed in Ancona (Italy) and used by both care-home based and independently living elderly citizens. In these clinical trials, which were performed over a 3 month period, 10 elderly volunteers, 4 nurses, 2 care givers and 1 general practitioner used the system. At the same time the system was used remotely by geriatricians to monitor the trial results and provide feedback to the elder or their general practitioner if necessary. The trials clearly demonstrated the impact a mobility monitor has on the validation and scheduling of vital signs measurements. For example, when an elderly person has just walked up a set of stairs and the elder's heart rate is measured directly after this activity, the measured heart rate is very likely to cause an alarm. Due to introducing the knowledge obtained from the mobility monitor these measurements can be safely discarded. In addition, the mobility monitor can be used to schedule and start measurements once the elder has been at rest for a predetermined time.

7 Conclusions

The aim of this chapter was to describe the development of a fall and mobility sensor platform and the integration of this platform in a mobile health monitoring system. The platform, which was developed in the Ambient Wireless Assisted Living (AWAL) Lab at the University of Limerick can be used as a stand-alone sensor network node or can be integrated in a mobile health measurement platform. In addition to describing this platform, a generic interface architecture for communication with the sensor from resource-constrained devices was described. To illustrate design and implementation issues and to emphasize the important role fall and mobility monitoring plays in mobile health monitoring systems, the chapter concluded with an overview of the implementation and testing of the University of Limerick fall and mobility monitoring platform in the European Communion (FP6) CAALYX project.

References

1. Recent demographic developments in Europe. Council of Europe Publishing (2004)
2. Cotter, P.E., Timmons, S., O'Connor, M., Twomey, C., O'Mahony, D.: The financial implications of falls in older people for an acute hospital. *Ir. J. Med. Sci.* 175, 11–13 (2006)
3. Lord, S.R., Sherrington, C., Menz, H.B.: Falls in Older People: Risk Factors and Strategies for Prevention. Cambridge University Press, Cambridge (2001)
4. Doughty, K.: Fall prevention and management strategies based on intelligent detection monitoring and assessment. In: New Technologies in Medicine for the Elderly, Charing Cross Hospital, London (November 2000)
5. Gannon, B., O'Shea, E., Hudson, E.: Economic consequences of falls and fractures among older people. *Ir. Med. J.* 101, 170–173 (2008)
6. Stevens, J., Corso, P., Finkelstein, E., Miller, T.: The costs of fatal and nonfatal falls among older adults. *Injury Prevention* 12, 290–295 (2006)
7. Noury, N., Rumeau, P., Bourke, A., ÓLaighin, G., Lundy, J.: A proposal for the classification and evaluation of fall detectors. *IRBM* 29, 340–349 (2008)
8. The prevention of falls in later life, pp. 1–24 (1987)
9. Lord, C., Colvin, D.: Falls in the elderly: Detection and assessment. In: Ann. Int. Conf. IEEE Eng. Med. Biol. Society (1991)
10. Díaz, A., Prado, M., Roa, L.M., Reina-Tosina, J., Sanchez, G.: Preliminary evaluation of a full-time falling monitor for the elderly. In: Proceedings of the 26th Annual International Conference of the IEEE-EMBS, San Francisco, CA, USA (September 2004)
11. Williams, G., Doughty, K., Cameron, K., Bradley, D.A.: A smart fall and activity monitor for telecare applications. In: 20th Ann. Int. Conf. IEEE Eng. Med. Biol. Society, pp. 1151–1154 (1998)
12. Hwang, J., Kang, Y., Jang, J.M., Kim, H.: Development of novel algorithm and real-time monitoring ambulatory system using bluetooth module for fall detection in the elderly. In: Proceedings of the 26th Annual International Conference of the IEEE-EMBS, San Francisco, CA, USA (September 2004)

13. Prado, M., Reina-Tosina, J., Roa, L.: Distributed intelligent architecture for falling detection and physical activity analysis in the elderly. In: Proceedings of the second Joint EMBS/BMES conference, Houston, TX, USA (October 2002)
14. Noury, N., Barralon, P., Virone, G., Boissy, P., Hamel, M., Rumeau, P.: A smart sensor based on rules and its evaluation in daily routines. In: Proceedings of the 25th Annual International Conference of the IEEE-EMBS, Cancun, Mexico (September 2003)
15. Noury, N., Herve, T., Rialle, V., Virone, G., Mercier, E., Morey, G., Moro, A., Porcheron, T.: Monitoring behaviour in the home using a smart fall sensor and position sensors. In: 1st Ann. Int. Conf. IEEE Eng. Med. Biol. Society, Lyon, France, pp. 607–610 (2000)
16. Noury, N.: A smart sensor for the remote follow up of activity and fall detection of the elderly. In: 2nd Ann. Int. Conf. IEEE Eng. Med. Biol. Society (2002)
17. Tamura, T., Yoshimura, T., Horiuchi, F.: An ambulatory fall monitor for the elderly. In: Ann. Int. Conf. IEEE Eng. Med. Biol. Society, Chigaco, IL, USA, pp. 2608–2610 (2000)
18. Doughty, K., Lewis, R., McIntosh, A.: The design of a practical and reliable fall detector for community and institutional telecare. *J. Telemed Telecare* 6, S150–S154 (2000)
19. Wu, G.: Distinguishing fall activities from normal activities by velocity characteristics. *J. Biomech.* 33, 1497–1500 (2000)
20. Nait-Charif, H., Mckenna, S.: Activity summarisation and fall detection in a supportive home environment. In: 17th International Conference on Pattern Recognition (2004)
21. Demongeot, J., Virone, G., Duchene, F., Benchetrit, G., Herve, T., Noury, N., Rialle, V.: Multi-sensor acquisition, data fusion, knowledge mining and alarm triggering in health smart homes for elderly people. *C. R. Biologies* 325, 673–682 (2002)
22. Degen, T., Jaeckel, H., Rufer, M., Wyss, S.: Speedy: a fall detector in a wrist watch. In: Proceedings of the 7th IEEE International Symposium on Wearable Computing, White Plains, NY (2003)
23. Karantonis, D., Narayanan, M., Mathie, M., Lovell, N., Celler, B.: Implementation of a real-time human movement classifier using a triaxial accelerometer for ambulatory monitoring. *IEEE Transactions on Information Technology in Biomedicine* 10, 156–167 (2006)
24. Kangas, M., Konttila, A., Lindgren, P., Winblad, I., Jamsa, T.: Comparison of low-complexity fall detection algorithms for body attached accelerometers. *Gait Posture* 28, 285–291 (2008)
25. Chao, P., Chan, H., Tang, F., Chen, Y., Wong, M.: A comparison of automatic fall detection by the cross-product and magnitude of tri-axial acceleration. *Physiological measurement* 30, 1027–1037 (2009)
26. Greenspan, S., Myers, E., Kiel, D., Parker, R., Hayes, W., Resnick, N.: Fall direction, bone mineral density, and function: risk factors for hip fracture in frail nursing home elderly. *American Journal of Medicine* 104, 539–545 (1998)
27. Hayes, W., Myers, E., Morris, J., Gerhart, T., Yett, H., Lipsitz, L.: Impact near the hip dominates fracture risk in elderly nursing home residents who fall. *Calcified Tissue International* 52, 192–198 (1993)
28. Schwartz, A., Kelsey, J., Sidney, S., Grisso, J.: Characteristics of falls and risk of hip fracture in elderly men. *Osteoporosis International* 8, 240–246 (1998)

29. Cummings, S., Nevitt, M.C.: A hypothesis: the causes of hip fractures. *Journal of Gerontology* 44, 107–111 (1989)
30. Melton, L., Riggs, B.: Epidemiology of age-related fractures. In: *The Osteoporotic Syndrome*. Grune & Stratton, pp. 54–72 (1983)
31. Veltink, P., Bussmann, H., Vries de, W., Martens, W., Lumme van, R.: Detection of static and dynamic activities using uniaxial accelerometers. *Rehabilitation Engineering* 4, 375–385 (1996)
32. Bouten, C., Koekkoek, K., Verduin, M., Kodde, R., Janssen, J.: A triaxial accelerometer and portable data processing unit for the assessment of daily physical activity. *IEEE Trans. Biomed. Eng.* 44, 136–147 (1997)
33. Culhane, K.M., O'Connor, M., Lyons, D., Lyons, G.M.: Accelerometers in rehabilitation medicine for older adults. *Age and Ageing* 34, 556–560 (2005)
34. Lyons, G., Culhane, K., Hilton, D., Grace, P., Lyons, D.: A description of an accelerometer-based mobility monitoring technique. *Med. Eng. Phys.* 27, 479–504 (2005)
35. Ni-Scanaill, C., Ahearne, B., Lyons, G.: Long-term telemonitoring of mobility trends of elderly people using sms messaging. *IEEE Trans. Inf. Technol. Biomed.* 10, 412–413 (2006)
36. Godfrey, A., Culhane, K., Lyons, G.: Comparison of the performance of the activpal professional physical activity logger to a discrete accelerometer-based activity monitor. *Med. Eng. Phys.* 29, 930–934 (2007)
37. Tay, F., Nyan, M.N., Koh, T.H., Seah, K.H.W., Sitoh, Y.: Smart shirt that can call for help after a fall. *Int. J. of Software Engineering and Knowledge Engineering* 15, 183–188 (2005)
38. Noury, N., Dittmar, A., Corroy, C., Baghai, R., Weber, J., Blanc, D., Klefstat, F., Blinovska, A., Vaysse, S., Comet, B.: Vtamm—a smart clothe for ambulatory remote monitoring of physiological parameters and activity. In: *Conf. Proc. IEEE Eng. Med. Biol. Soc.*, pp. 3266–3269 (2004)
39. Bourke, A., O'Brien, V.J., Lyons, G.: Evaluation of a threshold-based tri-axial accelerometer fall detection algorithm. *Gait Posture* (2007)
40. Bourke, A., van de Ven, P., Chaya, A., OLaighin, G., Nelson, J.: The design and development of a long-term fall detection system incorporated into a custom vest for the elderly. In: *Conference Proceedings IEEE Engineering in Medicine and Biology Society*, pp. 2836–2839 (2008)
41. Bourke, A., van de Ven, P., Chaya, A., OLaighin, G., Nelson, J.: Testing of a long-term fall detection system incorporated into a custom vest for the elderly. In: *Conference Proceedings IEEE Engineering in Medicine and Biology Society* (2008)

Smart Nano-systems for Tumour Cellular Diagnoses and Therapies

Conversano Francesco, Greco Antonio, and Casciaro Sergio

CNR-IFC, National Council of Research - Institute of Clinical Physiology, Lecce, Italy

Abstract. The rapid diffusion recently experienced by minimally invasive therapies (MIT) is currently receiving a further significant boost towards modern medicine by the introduction of new nanotechnology-based techniques in the fields of medical imaging and localized therapeutic delivery. The innovative idea of “nanomedicine” is emerging, with its potential to revolutionize the entire disease management process, from diagnosis, through therapy, to serial follow-up, influencing the entire apparatus of medical devices. Nanoparticle contrast agents, in fact, can be targeted to specific cells and tissues of human body, allowing imaging of pathologic processes at a cellular scale. Moreover, nanoparticles are being increasingly involved in the development of new therapeutic approaches (e.g., site-targeted drug delivery, localized hyperthermia, optimized employment of laser and ultrasound power). This chapter reviewes recent nanotechnological applications in the field of non-ionizing cellular imaging and “personalized” therapies, with special focus on innovative strategies for selective cancer detection and treatment. Some very recent experimental results regarding automatic detection of innovative nanoparticle contrast agents on echographic images are also presented.

Keywords: cellular imaging, non-ionizing diagnoses, minimally invasive therapies, nanoparticle contrast agents.

1 Introduction

Minimally invasive therapies (MIT) are experiencing a rapid growth and diffusion in various clinical specialties, going for instance from surgical interventions to tumour management approach. This rapid onset is essentially a consequence of two key-factors: the increasing emphasis on achieving the best survival benefit for the patient, while better preserving his quality of life, and the significant technology upgrades of recent years, that have opened new scenarios for surgery and defined innovative approaches for interventional therapy in general. The first factor, in particular, is related to the ever greater efforts made to provide the patient with short post-operative in-hospital stay, safer procedures, fast recovery, less traumatic return to normal activities, less and smaller scars on the body. These goals are being progressively reached in ever more satisfactory ways thanks to important

technological developments, including in particular robotic assistance for surgeons and the introduction of novel non-ionizing techniques for medical imaging at cellular and molecular level, allowing for earlier and safer disease diagnosis and for the improvement of therapy accuracy and effectiveness through its combination with high-resolution image-guidance.

In this context, the introduction of the emerging nanotechnology-based techniques in the fields of medical imaging and drug delivery represents a further breakthrough which extends and revolutionizes the MIT conception itself. The development of nanoscale biomedical technologies, in fact, is beginning to change the foundations of the entire disease management process, from first diagnosis until evaluation of therapy effects, leading toward the concept of “personalized medicine”, characterized by very early, even pre-symptomatic, diagnoses coupled with highly-effective “self-tailoring” targeted therapies.

The application of nanotechnology to disease diagnosis, treatment, monitoring and to the control of biological systems has recently been referred to as “nanomedicine” by the National Institutes of Health (Bethesda, MD, USA) [1,2]. The overall goal of nanomedicine is the same as it has always been for medicine: to diagnose as accurately and early as possible, to treat as effectively as possible without side effects, and to evaluate the efficacy of treatments non-invasively. The promise that nanotechnology brings is multifaceted, offering not only improvements to current techniques, but also providing entirely new tools and capabilities [3]. By manipulating drugs and other materials at the nanometer scale, in fact, fundamental properties and bioactivity of materials can be altered. So these tools can permit unprecedented control over characteristics of drugs and imaging agents such as solubility, blood pool retention times, controlled release over short or long durations, highly specific site-targeted delivery.

In particular, by virtue of their small size and by functionalizing their surface with synthetic polymers and appropriate ligands, nanoparticulate carriers can be targeted to specific cells and locations within the body after intravenous or subcutaneous routes of injection [4-12]. Such approaches may enhance detection sensitivity in medical imaging, improve therapeutic effectiveness and decrease side effects. Some of the carriers can be engineered in such a way that they can be activated by changes in the environmental pH, chemical stimuli, by the application of a rapidly oscillating magnetic field or by the application of an external heat source [5,13-15]. Moreover, some nanoparticles for specific diagnostic purposes can be also designed with the focus on “multifunctionality”: these agents can simultaneously produce signals that are detectable by more than one imaging modality, e.g. ultrasound (US) and magnetic resonance imaging (MRI) [16].

The specific pathological targets of these innovative methodologies include atherosclerotic plaques, inflammation, angiogenesis and thrombus formation, but the most exciting perspectives of nanomedicine applications are those related to the new modalities for cancer diagnosis and therapy at cellular and molecular level [1,17,18]. Cancer, in fact, is among the top three “killers” in modern society and cancer patients are not very satisfied with the currently available treatment options. In particular, many forms of cancer are treatable by the present therapy methods, including surgery, chemotherapy and radiation therapy, but sometimes

they have significant toxicities and side effects are common [1]. For instance, in the process of killing cancer cells, chemotherapeutic agents also damage healthy tissues. Thus, the first step in improving treatment effectiveness is a better exploitation of the potential of therapeutic agents (drugs or genes) by more effectively targeting them to tumor tissues.

In general, anticancer agents can be encapsulated in particles or attached to the surfaces of capsules and side effects are essentially due to toxicities to sensitive normal cells, because the therapies are not selective to target cells. Drug targeting by nanoparticles has been widely explored in recent years, by encapsulating anti-cancer agents into suitable nanocapsules or by attaching therapeutic molecules to nanoparticle surface, and it offers the following main advantages [6,19,20]: reduces drug dosage, ensures pharmaceutical effectiveness, minimizes side effects, protects drugs against degradation and enhances drug stability. Furthermore, nanoparticles can penetrate through small capillaries where are taken up by cells, allowing efficient drug accumulation at target sites: a sustained and controlled release of drugs at the specific target sites over a period of days or even weeks is possible following a single drug dose administration [1]. Anyway, the most significant breakthrough introduced by nanoparticle drug delivery is probably represented by the possibility of a real-time monitoring of therapy efficacy, since targeted nanovectors can “report back” upon their success through non-invasive signalling (i.e. imaging) to provide direct and immediate assessment of the predicted therapy effectiveness.

However, although nanocarriers may overcome solubility and stability issues for the drug and minimize the induced side-effects, there could be significant toxicity concerns associated with the nanocarriers themselves, which require attention. In fact, the superb benefits offered by nanomedicine are also accompanied by new specific, and often yet unknown, constraints. These, for the patient, are mainly related to the increased duration of the clearance mechanisms from the body: some nanoparticles might be retained not only for days but potentially for years, so the safety profile of all nanoparticle components becomes of vital significance. On the other hand, safety and drug effects are not only limited to the patient population receiving the final nanomedicine product, but, since for example standard filtering or protection equipment might not be appropriate for nanoparticle management, the entire manufacture and disposal process needs to be strictly regulated [3].

In this chapter, we will first review the recent nanotechnological applications in the field of diagnostic cellular and molecular imaging employing non-ionizing techniques and new disease-specific contrast agents. In particular, some encouraging experimental results regarding the feasibility of using silica nanospheres for echographic imaging and automatic detection of targeted tissues with conventional clinical settings will be illustrated and discussed. Then, the currently most promising ways to utilize site-targeted nanoparticles for therapeutic purposes will be presented. Finally, the future perspectives of these research topics will be outlined.

2 Cellular Imaging of Tumours

Positron Emission Tomography (PET) currently represents the reference imaging modality for early detection and monitoring of treatment outcome of most cancers, with a high discrimination power: only invasive and risky surgical procedures (biopsies) could achieve better results. PET systems can detect abnormal cellular activity at molecular level, generally before any anatomical change is visible and structural anomalies can be measured by other imaging modalities like ultrasound (US), magnetic resonance (MRI), X-rays or computerized tomography (CT). Then, the main winning feature of PET is related to the cellular nature of its detection mechanism.

However, PET examinations implies the use of highly ionizing radiation, involvement of complex systems and low intrinsic resolution images, which often oblige the combination with high resolution techniques like CT, so increasing both costs and radiation dose. These factors bring significant limitations concerning the examination repetition rate and its potentiality as a screening technique. On the other hand, cancer pathologies are still frequently diagnosed at an advanced stages and early diagnosis still remains the key factor for successful treatments.

Fortunately, recent developments in the field of nanoparticle-based cellular imaging promise to allow non-invasive detection of the molecular components of pathologic processes through non-ionizing methods, like optical imaging [21,22], ultrasound [18,23] and MRI [24].

In the next subparagraphs we will summarize the most interesting properties of novel nanoparticle contrast agents, and then we will briefly review the literature available experience about their employment with the mentioned imaging modalities for early and safe pathology characterization at cellular and molecular level, which represents the basis toward the next frontier of combining non-invasive imaging with “personalized” therapy.

2.1 Nanoparticle Contrast Agents

In recent years, several international attempts have been made to synthesize new nanoparticle contrast agents (NPCA) to be employed for cellular and molecular imaging through non-ionizing diagnostic techniques. In order to achieve a clinically effective method of diagnostic imaging, NPCA must be designed to have the following features: long circulating half-life, high extravasation rate, selective binding to the epitope of interest, prominent contrast-to-noise ratio enhancement, absence of toxicity, ease of clinical use, and compatibility with standard commercially available imaging systems [17,25].

A key issue consists in effective interaction of NPCA with molecular targets that depends among other on their own size. Generally speaking, 50 nm is the upper size threshold to penetrate the vascular endothelium and directly target tissue cells, otherwise intravascular targets are essentially reachable. Tumour vasculature instead, thanks to its peculiar physiopathology, allows effective targeting of cancer cells beyond the capillary endothelium also with bigger NPCA. In fact, a consistent difference between normal vessels and those created by tumour angiogenesis

is the tendency of the latter to be “leaky” for the EPR (enhanced permeability and retention) effect, which depends on type, location and histologic grade of tumor [26-28].

Once the endothelium barrier has been overcome, selective targeting of established cellular receptors is needed and this is obtained through “functionalization”, which consists in the NPCA surface conjugation with specific ligands to facilitate the targeting of pathological cells.

Additionally, in order to improve particle stability and to allow adequate circulation times, a polymeric coating able to increase biocompatibility and to avoid immediate sequestration by the reticuloendothelial system (RES) might be also necessary.

The array of nanomaterials that can be used as contrast agents for molecular imaging is broad, and the following description, including the main literature-reported studies, is intended to be illustrative rather than comprehensive.

Liposomes (50-700 nm) are uni- or multi-lamellar vesicles that consist of lipid bi-layer membranes surrounding an aqueous interior, whose applications as molecular imaging agents have been widely reported for both ultrasound [29] and MRI [30]. Liposomes have been also approved to enhance the efficacy and safety of various drugs, such as doxorubicin [17].

Emulsions are oil-in-water-type mixtures that are stabilized with surfactants to maintain their size and shape. Perfluorocarbon core emulsions (200-400 nm) have been used for molecular imaging with ultrasound [31] and MRI [32]. For example, when vast numbers of paramagnetic gadolinium complexes ($>50,000$) are incorporated onto emulsion particles the possible signal enhancement for each binding site is magnified by a factor of $>10^6$ over conventional paramagnetic extracellular contrast agents [33].

Polymers (40-200 nm) are being used in a variety of approaches to construct molecular imaging agents and also therapeutic delivery devices [25]. They may be linear, branched or globular, and comprise single or multiple molecular components (copolymers). Their size and shape can be tightly controlled and functionalization of their surface permits binding of myriad targeting and therapeutic moieties, for imaging as well as for drug and gene delivery. For example, dendrimers (or cascade polymers) are highly branched polymeric structures that are globular in configuration. Their cores are varied and the branches are sequentially assembled in covalent interactions that produce layers referred to as “generations”. The multivalent surface comprises a number of functional sites that can undergo reactions to add drugs, imaging agents and targeting ligands [17]. Paramagnetic poly-amidoamine (PAMAM) and diaminobutane (DAB) dendrimers have been employed for molecular MRI applications [34,35].

Metallic particles, such as iron oxide nanoparticles, comprise paramagnetic and superparamagnetic agents that can be coated with dextran, phospholipids or other compounds to inhibit aggregation and enhance stability for use as passive or active targeting agents. The iron in monocrystalline iron oxide nanoparticles (MIONs), small particles of iron oxide (SPIO, 50-500 nm) and ultrasmall particles of iron oxide (USPIO, 10-50 nm) produces strong local disruptions in the magnetic fields

of MRI scanners, which leads to increased T_2^* relaxation and hence a decrease in image intensity in areas with iron particle accumulation (“susceptibility” effects). These particles exhibits a very long circulating half-life (more than 24 hours) and may be sequestered by tissue macrophages [17]. These properties have allowed dextran-coated USPIO nanoparticles to be employed for passive targeted imaging of pathological inflammatory processes by MRI [36].

Other metal-based agents, such as gold shell nanoparticles, have been recently used for combined imaging and therapy purposes [37-39], as it will be shown in more detail in the next section. Carbon nanotubes with surfaces functionalized for tissue binding have been utilized as targeted contrast agents for optical imaging, exploiting their fluorescent properties [40-43]. Quantum dots (2-8 nm) are constructed from semiconductor materials (e.g., cadmium selenide) that manifest stable fluorescent properties at various wavelengths, depending on the exact composition of the materials [44-47]. For effective in vivo use, they must be coated with polymers to both allow solubilization and prevent leaching of the toxic heavy metals.

2.2 Non-ionizing Imaging Modalities and Methods

The role of nanoparticles in targeted imaging of selected pathologies is diverse and varies among the available imaging modalities. Herein we present a brief summary of the most significant attempts recently made to increase the feasibility of early diagnosis of several pathologies, when they are only detectable at cellular or molecular level, by employing non-ionizing radiation techniques.

2.2.1 Optical Imaging

Optical approaches for more localized detection of cancer pathologies are particularly promising: quantum dots that address vascular endothelial targets have been reported to be useful for identifying selected tissue zip-codes [44,45]; gold nanoshells have been used to evaluate tumors through optical imaging techniques and also for treatment of detected tumors with application of exogenous thermal energy [37-39]; carbon nanotubes have been also shown to emit detectable fluorescence that varies depending on the specific agent composition [40-43]. In some recent cases multifunctionality has started to be designed into nanoparticles, aiming to combine, for instance, fluorescence imaging and MRI thanks to the combination of fluorophores and iron oxide nanoparticles [48].

A common complication is represented by tissue autofluorescence that can cause absorption of most of the incident light at some wavelengths. However, optimization of near-infrared wavelength employment appears to be suitable in order to get enhanced sensitivity and specificity [49,50]. In optoacoustic imaging, in fact, tissue is irradiated with a short laser pulse that can be selected at the near-infrared region of the spectrum to enhance light penetration. Gold nanoparticles possess a tunable and exceptionally strong optical absorption due to their plasmon resonance and this results in the generation of detectable acoustic waves upon laser pulse irradiation [51].

2.2.2 Ultrasound Imaging

Ultrasound imaging probably offers the best patient tolerance but also the highest operator-dependence, coupled with the inability to image all areas of the body with the same effectiveness.

Currently available US contrast agents are essentially aqueous solutions of shell-stabilized gas-filled microbubbles, some of which have been also developed with the possibility of being targeted to vascular epitopes [18]. In the regime of smaller particles, reflective liposomes, acoustically active nanoparticle emulsions and nanobubbles have received the greatest attention [23,52,53]. Solid nanoparticles (like silica ones), instead, have not yet been fully evaluated for this kind of purposes, although they have the potential to perform better than liquid ones (because of the larger acoustic impedance), being also more time stable than nanobubbles. Some preliminary experimental results obtained by our research group through “in vitro” studies will be presented in the next section of this chapter.

Another interesting concept is that, although US is highly sensitive for detecting microbubbles both in flowing and targeted conditions, it is less so for unbound nanoparticles, given the strong size dependency of particle scattering cross-section (proportional to the sixth power of the radius) and the substantial incompressibility of liquid and solid nanoparticles, which precludes the use of available harmonic resonance-based imaging techniques that are typically applied to microbubble detection [17]. This means that nanoparticles have low acoustic reflectivity in solution, but their echogenicity increases when they are deposited in a layer, resulting in a contrast agent that is well detectable only when adherent to the target site [23].

Furthermore, US has a unique potential for precisely depositing large amounts of highly focused energy in a convenient manner that can facilitate nanoparticle-based imaging and therapies with exogenous US activation, as recently described by several groups [54,55]. Finally, the advent of mathematical models to characterize the scattering behavior of nanoparticles is raising the potential for extracting more quantitative information from the reflected signals [56,57].

2.2.3 Magnetic Resonance Imaging

Magnetic resonance imaging is characterized by high resolution, elevated anatomical contrast, high signal-to-noise ratio and widespread clinical availability. However, the relatively modest MRI contrast enhancement achievable with targeted contrast agents for molecular imaging tasks requires the delivery of higher payloads of contrast materials, which can be provided by novel nanotechnologies [17]. For example, in the case of T_1 -weighted images, it is possible to decorate the surface of paramagnetic nanoparticles with numerous copies of Gd chelates (up to 100,000), to achieve the micromolar concentration required per voxel [17,33]. Quantitative approaches have been also described for targeted paramagnetic emulsions to allow the computation of bound nanoparticle concentration under certain circumstances [58].

Imaging with superparamagnetic agents takes advantage of the fact that enough material can be packed into the core of the nanoparticle to exert a prominent T_2^* effect and produce a localized signal reduction that can be detected with potentially greater sensitivity with respect to paramagnetic agents [17].

Recent advances in imaging techniques have enabled “hot-spot” detection of iron oxide-based nanoparticles. These techniques [59,60] require specialized excitation pulses that image the water molecules in close proximity to an accumulation of nanoparticles. Once optimized, these techniques offer potential for localizing sources of extraneous magnetic dipoles (i.e., superparamagnetic particles) and, via their signal intensity, tracking their size and distribution and providing a method for relative quantification.

Alternatively, the signal generated by the fluorine atoms in the perfluorocarbon core of perfluorocarbon-based nanoparticles has been introduced as a unique signature for molecular MRI [61]. Since biological tissues contain little endogenous fluorine, measurement of the fluorine component of targeted particles may allow confirmation of actual nanoparticle deposition at the site. This approach has been demonstrated to be effective for quantifying the concentration of nanoparticle binding to a selected site based on localized fluorine spectroscopy [61] and subsequently for *in vivo* imaging of stem cells [62].

The sensitivity of MRI for detecting paramagnetic or superparamagnetic nanoparticulate imaging agents depends on the specific field strength, pulse sequence, coil sensitivities, epitope prevalence and contrast agent concentration used [17]. For instance, at clinical imaging field strengths, micromolar concentrations of paramagnetic agents are required, while for superparamagnetic agents nanomolar concentrations may suffice. Signal-to-noise ratios of 5 or better generally produce readily identifiable qualitative signal enhancement. Examples of optimization of both pulse sequences and nanoparticle concentrations to enhance sensitivity with MRI signal modeling approaches have been recently reported in literature [58,61].

3 Preliminary Experimental Results on Silica Nanoparticles for Ultrasound Molecular Imaging

As mentioned in the previous section, the use of solid NPs provides higher ultrasound signal enhancement as well as longer stability than liquid and gaseous particles of the same size. Nevertheless, ultrasound investigations of solid NPs have been until now limited to very high frequencies (30–40 MHz) [63,64], whose clinical usefulness is restricted to few highly specific applications.

We have just demonstrated the feasibility of using silica NPs as ultrasound contrast agents at common diagnostic frequencies. Actually, we performed a pilot experimental study in which we investigated the image contrast enhancement produced by varying particle diameter in a range of clinical interest for tumour targeting and subsequent automatic detection through radiofrequency (RF) signal analysis.

Diagnostic power of silica nanospheres having diameters of 160 nm, 330 nm and 660 nm was evaluated by studying ultrasound backscatter behaviour when NPs were dispersed in agarose gel samples at the constant concentration of 10^{11} part/mL. Each NP-containing gel sample was prepared into a Petri dish and immersed in water, where it was imaged employing a digital ecograph (Megas GPX,

Esaote Spa, Florence, Italy), equipped with a linear transducer operating at 7.5 MHz and linked to a prototype platform for acquisition of unprocessed RF data.

Fig. 1 shows a representative echographic image for each considered NP diameter, together with a reference image acquired on a pure gel sample: it is evident the progressive increase in image brightness with increasing NP diameter. Moreover, it is noticeable that, at the considered concentration, presence of 160-nm NP is already well detectable and this opens interesting perspectives for potential optimization of nanoparticle diameter-dose combination towards the employment of very low contrast agent concentrations.

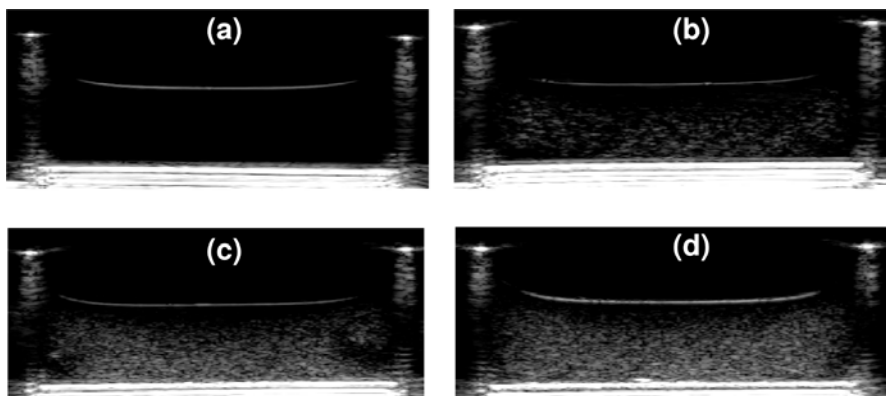


Fig. 1. Echographic images of NP-containing agarose gel samples: (a) pure agarose gel, (b) agarose gel with 160-nm NPs, (c) agarose gel with 330-nm NPs, (d) agarose gel with 660-nm NPs.

Furthermore, information available in the raw RF signal can be exploited to automatically discriminate tissue target by means of silica NPs. In fact, in our experience, a software for wavelet decomposition and spectral analysis was employed to develop a tailored colour map then applied to raw RF signals. This technique was applied on a different group of NP-containing agarose gel samples, synthesized just for this specific purpose and consisting of Petri dishes filled with a layer of agarose gel containing silica NPs placed between two different layers of pure agarose gel. One of these samples was prepared for each of the considered NP sizes.

RF acquired data were off-line processed in order to find a specific software configuration to selectively discriminate the NP-containing layer from the surrounding layers of pure agarose gel. In particular, we were able to find a different configuration for each tested NP size, with the final output being represented by the superimposition on the initial B-mode image of a specific colour map, capable of identifying the searched NPs in the echographic image.

Fig. 2 illustrates the results obtained through the described software processing, showing a reference image acquired on a “control” made of three layers of pure gel and the corresponding images of the three different NP-containing samples.

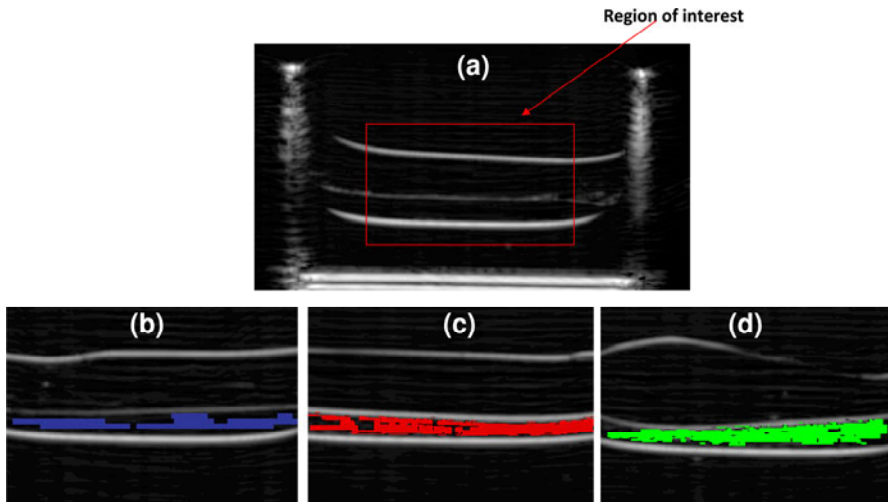


Fig. 2. Automatic software processed echographic images of three-layer agarose gel samples: (a) pure agarose gel, (b) central layer containing 160-nm NPs, (c) central layer containing 330-nm NPs, (d) central layer containing 660-nm NPs.

We can observe that sensitivity in nanoparticle detection was particularly high for both 330- and 660-nm NPs, while it was sensibly inferior for 160-nm NPs. In addition, “false positives” were absent in all the three cases.

4 New Therapeutic Approaches for Tumour Management

In the previous section we summarized the potential of new nanoparticle contrast agents to improve performances of current non-ionizing diagnostic methods. However, early and accurate diagnosis is futile if not coupled with effective therapy, so in very recent years much effort has been put in applying nanotechnology to therapeutic treatments [65-69].

Currently there is a limited number of nanomedical products on the market, with the majority being pharmaceuticals that are formulated (or re-formulated) into nanosized structures to manipulate the pharmacodynamics, biodistribution and overall effectiveness [3]. The surface addition of polyethylene glycol (PEG) of varying dimensions is a common technique used to alter chemical formulations into “stealthy” nanoparticles with increased circulating half lives [70].

However, beyond the pharmacokinetic manipulations, a more complex goal of nanotherapy is to devise agents that travel undetected within the body to deliver specific therapeutics – whether chemical, radioactive, genetic or other – to uniquely identified sites, having minimal untoward effects elsewhere [3].

The next subparagraphs will review recent advances in nanoparticle applications for simultaneous detection and treatment of cancer through site-targeted delivery therapeutic agents, hyperthermia and combined use of laser and ultrasound power.

4.1 Site-Targeted Drug Delivery

Although the delivery of anticancer therapeutic agents to solid tumors is still problematic, nanoparticles as drug carriers represent an attractive potential drug delivery system because they apparently target tumors with minimal toxicity to normal tissues [71]. Many of these innovative drug delivery approaches take advantage of the unique pathophysiology of the tumor vasculature. In contrast to normal tissues, in fact, tumors contain a high density of abnormal blood vessels that are dilated and poorly differentiated, with a chaotic architecture and irregular branching [72,73]. Subsequently, various functions of the tumor vasculature are impaired and this explains the higher concentration of plasma proteins detected in tumor tissues than in normal tissues [4]. This is due the previously mentioned enhanced permeability and retention effect. These findings support the use of nanoparticles as carriers for simultaneous tumor diagnosis and therapy, because they passively accumulate in solid tumors after their intravenous administration.

In general, the most commonly used method is antibody- or ligand-mediated targeting of anticancer therapeutics. The basic principle that underlies ligand-targeted therapeutics is that the selective delivery of antineoplastic drugs to cancer cells or cancer-associated tissues, such as tumor vasculature, can be enhanced by associating the drugs with molecules that bind to antigens or receptors that are either uniquely expressed or overexpressed on target cells compared with normal tissues. This allows the specific delivery of drugs to cancer cells [1].

In fact, it is now well-known that a major difficulty during cancer treatment is to destroy tumor cells without destroying normal tissues, since, for example, radiotherapy and chemotherapy generally cause some severe side effects. Therefore several approaches to improve the selective delivery of anticancer therapeutics are being pursued presently.

Alexiou et al. [74-76] widely showed the feasibility of “magnetic drug targeting” on animal experimental studies, employing nanoparticle carriers made of iron oxide particles and covered by starch derivatives with phosphate groups which bound a specific chemotherapeuticum. Magnetic drug targeting is a new approach to the locoregional treatment of tumors: ferrofluids (colloidal dispersion of magnetic nanoparticles) can be reversibly bound to chemotherapeutic agents and injected intra-arterially, while focused with an external magnetic field to a certain body compartment (i.e. the tumor). With only 20% or 50% percent of the regular systemic chemotherapeutic dose, it was achieved an up to 26 times higher concentration in the tumor region with this application compared to the usual systemic administration [75].

Employment of ligand-targeted liposomes containing anticancer drugs or therapeutic genes specifically directed to cell surface receptors expressed on cancer cells represents also a recognized strategy for improving the therapeutic effectiveness of conventional chemotherapeutics or gene therapeutics [77]. Liposomes have been employed with various coupling methods (e.g. covalent and noncovalent drug binding), demonstrating enhanced efficacy compared to conventional drugs [78]. In particular, specific targeting of liposome-formulated cytotoxic drugs or antigens to receptors expressed selectively on target cells represents an effective strategy for increasing the pharmacological efficacy of the delivered molecules [79].

Another very good material to generate nanoparticle drug carriers is poly(lactic-co-glycolic acid) (PLGA). These nanoparticles result biocompatible and degradable with no toxicity [1]. Cegnar et al. [80] investigated the use of PLGA nanoparticles containing cystatin, a potential anticancer drug, as a carrier system to regress tumor growth and showed that these nanoparticles are useful for a rapid delivery of protein inhibitors into tumor cells. McCarthy et al. [81] synthesized PLGA nanoparticles encapsulating a photosensitizer (meso-tetraphenylporpholactol) which, after cellular internalization, is released from the nanoparticles and becomes highly phototoxic: the subsequent irradiation with visible light resulted in a cell-specific killing of several cancer lines.

Furthermore, nanoparticle carriers could be in principle assembled in such a way to enable them, upon their success, to “report back” through non-invasive signaling (i.e. imaging), in order to provide confirmation of the predicted therapy efficacy [3]. This would greatly alter the current paradigm for treating and following patients. Many novel nanoparticle agents, currently under development, share this final goal.

Quintana et al. [82] designed and synthesized a complex nanodevice that experimentally allowed targeted intracellular drug delivery while having an imaging capability for tracking uptake of the material. The device was based on a nano-scale polymer to whose surface folic acid, fluorescein and methotrexate were covalently attached to provide targeting, imaging, and intracellular drug delivery capabilities, respectively. Targeting data in human carcinoma cell lines confirmed the modeling predictions of specific and highly selective binding: targeted delivery improved the cytotoxic response of the cells to methotrexate 100-fold over free drug.

Several efforts have also been made to design and synthesize polyamidoamine (PAMAM) dendrimer-based multifunctional cancer therapeutic conjugates [83,84]. In particular, Shukla et al. [83] reported the synthesis and targeting properties of a PAMAM dendrimer labeled with alexaFluor488 and conjugated to an anti-HER2 (human growth factor receptor-2) mAb (monoclonal antibody). The binding and internalization of the antibody-conjugated dendrimer to HER2-expressing cells was evaluated *in vitro* by flow cytometry and confocal microscopy. The conjugate demonstrated selective cellular uptake and better internalization in HER2-expressing cells as compared to free antibody. In the same study it was demonstrated that the conjugate was able to target HER2-expressing tumors also in animal models.

Roy et al. [85] published the encouraging results of an *in vitro* study involving fluorescently labeled organically modified silica nanoparticles employed as a vector for gene delivery, coupled with biophotonics methods to optically monitor intracellular trafficking and gene transfection. In this way they were able to real-time monitoring the drug action by directly tracking drug delivery and drug-cell interactions.

The same authors had previously demonstrated the potential of using similar nanoparticles as drug carriers for photodynamic therapy [86]. They synthesized ultrafine organically modified silica-based nanoparticles (diameter approximately 30 nm), entrapping a water-insoluble photosensitizing anticancer drug. The resulting

drug-doped nanoparticles were spherical, highly monodispersed and stable in aqueous systems. The entrapped drug was more fluorescent in aqueous medium than the free drug, so permitting use of fluorescence bioimaging studies. Irradiation of the photosensitizing drug entrapped in nanoparticles with light of suitable wavelength resulted in efficient generation of singlet oxygen. In vitro studies demonstrated the active uptake of drug-doped nanoparticles into the cytosol of tumor cells and significant damage to such impregnated tumor cells was observed upon irradiation with light of 650 nm wavelength.

The development of new drug delivery systems for photodynamic therapy has involved also multifunctional polymeric nanoparticles. Reddy et al. [87] synthesized new polymeric nanoparticles consisting of a surface-localized tumor vasculature targeting F3 peptide and encapsulating a photodynamic therapy agent (Photofrin) and a MRI contrast agent (iron oxide nanoparticles). These nanodevices specifically bound to the surface of MDA-435 cells in vitro and were internalized, conferring photosensitivity to the cells. Significant MRI contrast enhancement was also achieved in rat 9L gliomas following intravenous nanoparticle administration. Serial MRI was used for determination of pharmacokinetics and distribution of nanoparticles within the tumor: animals were imaged every 2 to 3 days using T2-weighted and diffusion MRI to follow changes in tumor diffusion for up to 2 weeks after photodynamic therapy. Treatment of glioma-bearing rats with targeted nanoparticles followed by photodynamic therapy showed a significant improvement in survival rate when compared with animals who received photodynamic therapy after administration of non-targeted nanoparticles or systemic Photofrin.

4.2 Gold Nanoparticles for Laser Hyperthermia of Tumours

The unique optical properties of noble metal nanoparticles are generating much enthusiasm in molecular biology and medicine for their immense potential for cancer diagnosis and therapy on account of their enhanced light scattering and absorption, due to surface plasmon resonance (SPR) [88].

For a spherical nanoparticle much smaller than the wavelength of light, an electromagnetic field at a certain frequency induces a resonant, coherent oscillation of the metal free electrons across the nanoparticle itself. This oscillation is known as the surface plasmon resonance (SPR). The resonance lies at visible frequencies for the noble metals Au, Ag and Cu [89]. The frequency and cross-section of SPR absorption and scattering is dependent on metal composition [90], nanoparticle size and shape [89,91], dielectric properties of the surrounding medium [92] and presence of inter-particle interactions [93-95]. In general, Au and Ag are the metals of choice because of their much higher stability as compared to Cu. Additionally, spherical Au colloids can easily be made in a wide range of sizes (4-80 nm) by facile chemistry involving the reduction of Au ions in solution [88].

In particular, Au nanoparticles appear biocompatible and non-cytotoxic, as supported by recent experiments on human cells [96], and their use is further motivated by their easy bioconjugation and biomodification [97]. The Au nanoparticle surface, in fact, has a strong binding affinity towards several antibodies and biomolecules that allow for selective targeting of cancer cells [88,98,99]. Moreover, theoretical calculations [88,91] showed that the magnitude of visible light

scattering by plasmon resonant 80-nm diameter Au nanoparticles is comparable to the scattering at the same wavelength from the much larger 300-nm diameter polystyrene nanospheres commonly used in confocal imaging of cells. Also, for the same light excitation intensity, the number of photons emitted by fluorescein (a fluorescent molecule commonly used in imaging) is five order of magnitudes lower than the light scattering from 80 nm Au nanospheres.

The SPR absorption of Au nanoparticles is followed by the rapid conversion (≈ 1 ps) of the absorbed light into heat [89,100]. This property of Au nanoparticles can be exploited for selective cancer photothermal therapy (or laser hyperthermia, i.e. use of optical heating for tumor ablation) [37,101-105]. Targeting of nanoparticles to biomarkers on cancer cells increases the specificity of labeling and decreases the laser dose needed to kill diseased cells, without injuring healthy ones [101-103,105]. The absorption cross-section of Au nanoparticles is five orders of magnitude larger than that of indocyanine green (a dye used in earlier demonstrations of laser photothermal tumor therapy) [88,106], thus promising effective photothermal therapy at much lower irradiation energy. Besides this, the selection of a nanoparticle configuration with optimum SPR absorption as well as SPR scattering makes possible the innovative dual approaches based on the combination of imaging and therapy.

El-Sayed et al. [101] recently showed the efficiency of immunotargeted Au nanospheres as photothermal agents in living cells *in vitro*. They used 40 nm Au nanoparticles conjugated to anti-EGFR antibodies to label two oral squamous carcinoma cell lines. Dark-field microscopy images of the SPR scattering from the nanoparticles provided visual confirmation of cancer cell surface labeling. For photothermal therapy, 514 nm excitation from a commonly available continuous-wave argon-ion laser was used to excite the nanoparticle SPR band and ensure maximum light absorption by the nanoparticles. The cancerous cells suffered photothermal damage within 4 minutes at laser energy thresholds of 19 W/cm^2 and 25 W/cm^2 respectively, which are less than half of that required to damage healthy cells that had shown some non-specific nanoparticle labeling (57 W/cm^2). None of the cell lines without Au nanoparticle treatment showed any photothermal damage up to laser energies of 76 W/cm^2 . Thus, specific targeting of Au nanoparticle bioconjugates to cancer cells, combined with the high absorption cross-section of the nanoparticle in the excitation region, facilitates selective photothermal cancer therapy at low enough laser energy to preserve benign cells.

The *in vitro* success of cancer therapy/imaging using visible light absorbing nanoparticles can be extended to skin or surface type cancers. However, *in vivo* optical imaging and photothermal therapy applications for deeper tissues require light in the near-infrared (NIR) region, where tissues have the highest transmissivity. The light penetration depth can be up to a few centimetres in the spectral region 650-900 nm, also known as the biological NIR window, depending on tissue type [107]. Thus the plasmon resonance of nanoparticles for *in vivo* applications is required to be in the NIR region. While changing the size of Au nanospheres shows limited tunability of the SPR wavelength [91], changing the Au nanoparticle shape [89,91,100] and composition [38] offers dramatic variation in SPR absorption and scattering properties. Interesting nanostructures, such as silica-Au

nanoshells [38], Au nanorods [108-110], Au nanocages [111] and Au nanoparticle assemblies [103], showed optical tunability in the NIR region suitable for in vivo applications.

Novel multifunctional magnetic gold nanocomposites have also been very recently tested for targeted cancer detection *in vitro* by MRI and synchronous therapy via therapeutic antibodies and hyperthermia effects [112]. These nanoparticles consisted of magnetic kernels (aggregates of MnFe_2O_4 magnetic nanocrystals wrapped in a polymer) as MRI contrast agents and silica-gold nanocomposites as hyperthermal therapeutic agents. A therapeutic antibody was also conjugated for specific tumor cell targeting, aiming both to localize the NIR laser beam and to image the involved molecular events through MRI. Nanoparticles selectively recognized the target cancer cell lines, as quantitatively confirmed by fluorescence images and MRI. The nanoparticles had also an excellent synchronous therapeutic efficacy as a result of the therapeutic antibody and the NIR laser-induced hyperthermia effect, emphasizing the therapeutic potential of multifunctional magnetic gold nanocomposites for simultaneous diagnosis and treatment of cancer.

4.3 Improved Employment of Ultrasound Power

It is known [113] that in vivo generated microbubbles may improve and widen numerous diagnostic and therapeutic applications in which ultrasound contrast agents are currently used. Among the applications reviewed by Kimmel [114], one may consider ultrasonically induced drug delivery [115], which is based on releasing medication from broken contrast agents at a specific location and increasing permeability of blood vessel walls for facilitated transport [116]. Also, microbubbles are essential in ultrasonically induced targeted hyperthermia [117] and diagnostic imaging of specific cells [118], as well as for increasing cell membrane permeability for gene transfection [119].

In tap water insonified at a frequency of 1 MHz, bubbles will form when a negative acoustic pressure peak of about 0.15 MPa is applied. In contrast, even much higher acoustic pressures – of up to about 4 MPa – cannot initiate bubbles *in vivo*, because of the absence of pre-existing nucleation sites for bubble generation in most tissues [114]. However, high intensity focused ultrasound (HIFU) sources of at least 4.5 MPa negative pressure peak provide enough power density to initiate bubble generation and growth *in vivo* [120]. For this reason, HIFU based medical treatments require to be coupled with on-line high resolution imaging [113].

An attractive method for generating useful microbubble nucleation sites *in vivo* without HIFU employment was suggested by Farny et al. [120] in 2005. They demonstrated that nanobubbles of about 150 nm in diameter could be obtained by exposing gold nanoparticles embedded in gel to a 532 nm laser pulse phase-synchronized with an ultrasound burst of 10 cycles, lasting about 10 μs at a frequency of 1.1 MHz. The used acoustic pressure amplitude was 0.9 MPa. They also identified the threshold at which a nanobubble, once generated by a laser pulse heating a single nanoparticle, evolves into a microbubble: the threshold occurred at acoustic pressures near 1 MPa for laser energy densities of about 5 mJ/cm^2 .

Regarding the use of microbubbles for tissue heating, it had been previously demonstrated [121] that microbubble oscillations could enhance local ultrasound energy deposition by two orders of magnitude.

In this context, a very interesting result was recently obtained by Krasovitski et al. [110]. They developed a numerical method capable of predicting laser power and acoustic pressure amplitude that are needed to produce stable microbubbles on demand at target locations by heating single nanoparticles or clusters of them. In particular, their simulations predicted that relatively low threshold values of laser and ultrasound power are required to obtain a stable microbubble from a single nanoparticle and even lower power is required when microbubbles are formed by coalescence around a cluster of nanoparticles. For instance, laser pulse energy density of 21 mJ/cm^2 is predicted together with an acoustic pressure of 0.1 MPa for a cluster of 10 nanoparticles, while 62 mJ/cm^2 are required in the case of a single nanoparticle. These values are well within the safety limits and as such are most appealing for targeted therapeutic purposes. In fact, administering suitable nanoparticles to the target cells and exposing them to laser power and ultrasound insonification enables safe microbubble generation on demand: the coupled energy may then be used for localized and well-controlled hyperthermia, enhanced drug delivery and other medical treatments.

5 Conclusion and Future Perspectives

Nanomedicine, although in its early stages of development, has the potential to revolutionize not only the conception of minimally invasive therapies, but the general idea of medicine itself.

The huge impact of the innovative medical nanodevices and associated techniques can be summarized in the mentioned concept of “personalized medicine”, which is based on a completely new disease management paradigm from diagnosis, through therapy, to serial non-invasive follow-up.

In this context, the key role is played by disease-targeted nanoparticles, each of which may be viewed as a tiny submarine that navigates vessels and capillaries searching for signature molecules expressed by the target pathology. Once selectively identified its objective, the nanoparticle anchors in some way to the corresponding site, where it can be imaged to provide accurate diagnosis at a cellular or molecular level and then, depending on specific nanoparticle design, it can release therapeutic agents in form of drugs or genetic materials, it can be heated for hyperthermia treatments or for producing microbubbles to enhance local ultrasound power deposition, it can be imaged again, maybe with a different technique, to give direct and immediate confirmation of therapy effectiveness, or it can combine more of these actions.

One of the most stimulating future perspectives of this research field involves, in fact, the achievement of newer multifunctional nanoparticles, capable of giving by themselves the whole disease treatment, from diagnosis until post-therapeutic follow-up. Multifunctional activity, in principle, can be achieved by simultaneously incorporating, into a single nanoparticle formulation, combinations of one or more targeting ligands, imaging agents and/or drugs. Materials can be covalently

or non-covalently linked to the particle surface, dissolved in the coating or carried in the particle interiors for cellular deposition and activation [17].

On the other hand, although some great achievements have been reached, many challenges still remain. For example, the low encapsulation efficiency of some drugs needs to be overcome and some nanoparticles are still toxic for clinical application [1]. Additionally, this rapid onset and drastic change in methods will create new challenges in the regulatory process [3]. However, it will also provide a fruitful ground from which many exciting, and yet unimagined, applications of nanomedicine will arise.

References

1. Liu, Y., Miyoshi, H., Nakamura, M.: Nanomedicine for drug delivery and imaging: a promising avenue for cancer therapy and diagnosis using targeted functional nanoparticles. *Int. J. Cancer* 120, 2527–2537 (2007)
2. Moghimi, S.M., Hunter, A.C., Murray, J.C.: Nanomedicine: current status and future prospects. *FASEB J.* 19, 311–330 (2005)
3. Caruthers, S.D., Wickline, S.A., Lanza, G.M.: Nanotechnological applications in medicine. *Curr. Opin. Biotechnol.* 18, 26–30 (2007)
4. Allen, T.M., Cullis, P.R.: Drug delivery systems: entering the mainstream. *Science* 303, 1818–1822 (2004)
5. Moghimi, S.M., Hunter, A.C., Murray, J.C.: Long-circulating and target-specific nanoparticles: theory to practice. *Pharmacol Rev* 53, 283–318 (2001)
6. Sahoo, S.K., Labhasetwar, V.: Nanotech approaches to drug delivery and imaging. *Drug Discov. Today* 8, 1112–1120 (2003)
7. Kramer, M., Stumbé, J.F., Grimm, G., Kaufmann, B., Kruger, U., Weber, M., Haag, R.: Dendritic polyamines: simple access to new materials with defined treelike structures for application in nonviral gene delivery. *Chem. Bio. Chem.* 5, 1081–1087 (2004)
8. Raja, K.S., Wang, Q., Gonzalez, M.J., Manchester, M., Johnson, J.E., Finn, M.G.: Hybrid virus-polymer materials. Synthesis and properties of PEG-decorated cow-pea mosaic virus. *Biomacromolecules* 4, 472–476 (2003)
9. Fenske, D.B., MacLachlan, I., Cullis, P.R.: Long-circulating vectors for the systemic delivery of genes. *Curr. Opin. Mol. Therap.* 3, 153–158 (2001)
10. Allen, T.M.: Ligand-targeted therapeutics in anticancer therapy. *Nat. Rev. Cancer* 2, 750–763 (2002)
11. Sudimack, J., Lee, R.J.: Targeted drug delivery via the folate receptor. *Adv. Drug. Deliv. Rev.* 41, 147–162 (2000)
12. Torchilin, V.P., Lukyanov, A.N., Gao, Z.G., Papahadjopoulos-Sternberg, B.: Immunomicelles: targeted pharmaceutical carriers for poorly soluble drugs. *Proc. Natl. Acad. Sci. USA* 100, 6039–6044 (2003)
13. Drummond, D.C., Zignani, M., Leroux, J.C.: Current status of pH-sensitive liposomes in drug delivery. *Prog. Lipid. Res.* 39, 409–460 (2000)
14. Panyam, J., Zhou, W.Z., Prabha, S., Sahoo, S.K., Labhasetwar, V.: Rapid endolysosomal escape of poly(DL-lactide-co-glycolide) nanoparticles: implications for drug and gene delivery. *FASEB J.* 16, 1217–1226 (2002)

15. Clark, H.A., Hoyer, M., Philbert, M.A., Kopeiman, R.: Optical nanosensors for chemical analysis inside single living cells. 1. Fabrication, Characterization, and Methods for Intracellular Delivery of PEBBLE Sensors. *Anal Chem.* 71, 4831–4836 (1999)
16. Wickline, S., Neubauer, A., Winter, P., Caruthers, S., Lanza, G.: Applications of nanotechnology to atherosclerosis, thrombosis, and vascular biology. *Arterioscler Thromb Vasc Biol.* 26, 435–441 (2006)
17. Wickline, S.A., Neubauer, A.M., Winter, P.M., Caruthers, S.D., Lanza, G.M.: Molecular imaging and therapy of atherosclerosis with targeted nanoparticles. *J. Magn. Reson. Imaging* 25, 667–680 (2007)
18. Conversano, F., Casciaro, S.: Last advances in ultrasound molecular imaging. In: Casciaro, S., Gersak, B. (eds.) *New technology frontiers in minimally invasive therapies*, Ch. 18, pp. 161–171. Lupiensis Biomedical Publications, Lecce (2007)
19. Fahmy, T.M., Samstein, R.M., Harness, C.C., Saltzman, W.M.: Surface modification of biodegradable polyesters with fatty acid conjugates for improved drug targeting. *Biomaterials* 26, 5727–5736 (2005)
20. Couvreur, P., Barratt, G., Fattal, E., Legrand, P., Vauthier, C.: Nanocapsule technology: a review. *Crit. Rev. Ther Drug Carrier Syst.* 19, 99–134 (2002)
21. Herschman, H.R.: Molecular imaging: looking at problems, seeing solutions. *Science* 302, 605–608 (2003)
22. Tsien, R.Y.: Imagining imaging's future. *Nat. Rev. Mol. Cell Biol.*, SS16–SS21 (2003)
23. Lanza, G.M., Wickline, S.A.: Targeted ultrasonic contrast agents for molecular imaging and therapy. *Curr. Prob. Cardiol.* 28, 625–653 (2003)
24. Wickline, S.A., Lanza, G.M.: Nanotechnology for molecular imaging and therapy. *Circulation* 107, 1092–1095 (2003)
25. Hawker, C.J., Wooley, K.L.: The convergence of synthetic organic and polymer chemistries. *Science* 309, 1200–1205 (2005)
26. Pasqualini, R., Arap, W., McDonald, D.M.: Probing the structural and molecular diversity of tumor vasculature. *Trends Molec. Med.* 8, 563–571 (2002)
27. Hobbs, S.K., Monsky, W.L., Yuan, F., Roberts, W.G., Griffith, L., Torchilin, V.P., Jain, R.K.: Regulation of transport pathways in tumor vessels: role of tumor type and microenvironment. *Proc. Natl. Acad. Sci. USA* 95, 4607–4612 (1998)
28. Iyer, A.K., Khaled, G., Fang, J., Maeda, H.: Exploiting the enhanced permeability and retention effect for tumor targeting. *Drug Discov. Today* 11, 812–818 (2006)
29. Demos, S.M., Alkan-Onyuksel, H., Kane, B.J., Ramani, K., Nagaraj, A., Greene, R., Klegerman, M., McPherson, D.D.: In vivo targeting of acoustically reflective liposomes for intravascular and transvascular ultrasonic enhancement. *J. Am. Coll. Cardiol.* 33, 867–875 (1999)
30. Sipkins, D.A., Cheresh, D.A., Kazemi, M.R., Nevin, L.M., Bednarski, M.D., Li, K.C.: Detection of tumor angiogenesis in vivo by alphaVbeta3-targeted magnetic resonance imaging. *Nat. Med.* 4, 623–626 (1998)
31. Marsh, J.N., Partlow, K.C., Abendschein, D.R., Scott, M.J., Lanza, G.M., Wickline, S.A.: Molecular imaging with targeted perfluorocarbon nanoparticles: quantification of the concentration dependence of contrast enhancement for binding to sparse cellular epitopes. *Ultrasound Med. Biol.* 33, 950–958 (2007)

32. Lanza, G.M., Winter, P., Caruthers, S., Schmeider, A., Crowder, K., Morawski, A., Zhang, H., Scott, M.J., Wickline, S.A.: Novel paramagnetic contrast agents for molecular imaging and targeted drug delivery. *Curr. Pharm. Biotechnol.* 5, 495–507 (2004)
33. Flacke, S., Fischer, S., Scott, M.J., Fuhrhop, R.J., Allen, J.S., McLean, M., Winter, P., Sicard, G.A., Gaffney, P.J., Wickline, S.A., Lanza, G.M.: Novel MRI contrast agent for molecular imaging of fibrin: implications for detecting vulnerable plaques. *Circulation* 104, 1280–1285 (2001)
34. Kobayashi, H., Kawamoto, S., Jo, S.K., Bryant Jr., H.L., Brechbiel, M.W., Star, R.A., Macromolecular, M.R.I.: Macromolecular MRI contrast agents with small dendrimers: pharmacokinetic differences between sizes and cores. *Bioconjug Chem.* 14, 388–394 (2003)
35. Sato, N., Kobayashi, H., Hiraga, A., Saga, T., Togashi, K., Konishi, J., Brechbiel, M.W.: Pharmacokinetics and enhancement patterns of macromolecular MR contrast agents with various sizes of polyamidoamine dendrimer cores. *Magn. Reson. Med.* 46, 1169–1173 (2001)
36. Schmitz, S.A., Coupland, S.E., Gust, R., Winterhalter, S., Wagner, S., Kresse, M., Semmler, W., Wolf, K.J.: Superparamagnetic iron oxide-enhanced MRI of atherosclerotic plaques in Watanabe heritable hyperlipidemic rabbits. *Invest Radiol.* 35, 460–471 (2000)
37. Hirsch, L.R., Stafford, R.J., Bankson, J.A., Sershen, S.R., Rivera, B., Price, R.E., Hazle, J.D., Halas, N.J., West, J.L.: Nanoshell-mediated near-infrared thermal therapy of tumors under magnetic resonance guidance. *Proc. Natl. Acad. Sci. USA* 100, 13549–13554 (2003)
38. Loo, C., Lin, A., Hirsch, L., Lee, M.H., Barton, J., Halas, N., West, J., Drezek, R.: Nanoshell-enabled photonics-based imaging and therapy of cancer. *Technol. Cancer Res. Treat.* 3, 33–40 (2004)
39. O’Neal, D.P., Hirsch, L.R., Halas, N.J., Payne, J.D., West, J.L.: Photo-thermal tumor ablation in mice using near infrared-absorbing nanoparticles. *Cancer Lett.* 209, 171–176 (2004)
40. Cherukuri, P., Bachilo, S.M., Litovsky, S.H., Weisman, R.B.: Near-infrared fluorescence microscopy of single-walled carbon nanotubes in phagocytic cells. *J. Am. Chem. Soc.* 126, 15638–15639 (2004)
41. Tsyboulski, D.A., Bachilo, S.M., Weisman, R.B.: Versatile visualization of individual single-walled carbon nanotubes with near-infrared fluorescence microscopy. *Nano Lett.* 5, 975–979 (2005)
42. Barone, P.W., Baik, S., Heller, D.A., Strano, M.S.: Near-infrared optical sensors based on single-walled carbon nanotubes. *Nat. Mater.* 4, 86–92 (2005)
43. Hertel, T., Hagen, A., Talalaev, V., Arnold, K., Hennrich, F., Kappes, M., Rosenthal, S., McBride, J., Ulbricht, H., Flahaut, E.: Spectroscopy of single and double-wall carbon nanotubes in different environments. *Nano Lett.* 5, 511–514 (2005)
44. Akerman, M.E., Chan, W.C., Laakkonen, P., Bhatia, S.N., Ruoslahti, E.: Nanocrystal targeting in vivo. *Proc. Natl. Acad. Sci. USA* 99, 12617–12621 (2002)
45. Chen, L., Zurita, A.J., Ardelt, P.U., Giordano, R.J., Arap, W., Pasqualini, R.: Design and validation of a bifunctional ligand display system for receptor targeting. *Chem. Biol.* 11, 1081–1091 (2004)
46. Gao, X., Nie, S.: Quantum dot-encoded beads. *Methods Mol. Biol.* 303, 61–71 (2005)

47. Michalet, X., Pinaud, F.F., Bentolila, L.A., Tsay, J.M., Doose, S., Li, J.J., Sundaresan, G., Wu, A.M., Gambhir, S.S., Weiss, S.: Quantum dots for live cells, in vivo imaging, and diagnostics. *Science* 307, 538–544 (2005)
48. Kelly, K.A., Allport, J.R., Tsourkas, A., Shinde-Patil, V.R., Josephson, L., Weissleder, R.: Detection of vascular adhesion molecule-1 expression using a novel multimodal nanoparticle. *Circ. Res.* 96, 327–336 (2005)
49. Chen, J., Tung, C.H., Mahmood, U., Ntziachristos, V., Gyurko, R., Fishman, M.C., Huang, P.L., Weissleder, R.: In vivo imaging of proteolytic activity in atherosclerosis. *Circulation* 105, 2766–2771 (2002)
50. Jaffer, F.A., Tung, C.H., Wykrzykowska, J.J., Ho, N.H., Hwang, A.K., Reed, G.L., Weissleder, R.: Molecular imaging of factor XIIIa activity in thrombosis using a novel, near-infrared fluorescent contrast agent that covalently links to thrombi. *Circulation* 110, 170–176 (2004)
51. Eghtedari, M., Oraevsky, A., Copland, J.A., et al.: High sensitivity of in vivo detection of gold nanorods using a laser optoacoustic imaging system. *Nano Letters* 7, 1914–1918 (2007)
52. Hamilton, A.J., Huang, S.L., Warnick, D., Rabbat, M., Kane, B., Nagaraj, A., Klegerman, M., McPherson, D.D.: Intravascular ultrasound molecular imaging of atheroma components in vivo. *J. Am. Coll. Cardiol.* 43, 453–460 (2004)
53. Morawski, A.M., Lanza, G.A., Wickline, S.A.: Targeted contrast agents for magnetic resonance imaging and ultrasound. *Curr. Opin. Biotechnol.* 16, 89–92 (2005)
54. Crowder, K.C., Hughes, M.S., Marsh, J.N., Barbieri, A.M., Fuhrhop, R.W., Lanza, G.M., Wickline, S.A.: Sonic activation of molecularly-targeted nanoparticles accelerates transmembrane lipid delivery to cancer cells through contact-mediated mechanisms: implications for enhanced local drug delivery. *Ultrasound Med. Biol.* 31, 1693–1700 (2005)
55. Zhao, S., Borden, M., Bloch, S.H., Kruse, D., Ferrara, K.W., Dayton, P.A.: Radiation-force assisted targeting facilitates ultrasonic molecular imaging. *Mol. Imaging* 3, 135–148 (2004)
56. Lanza, G.M., Trousil, R.L., Wallace, K.D., Rose, J.H., Hall, C.S., Scott, M.J., Miller, J.G., Eisenberg, P.R., Gaffney, P.J., Wickline, S.: In vitro characterization of a novel, tissue-targeted ultrasonic contrast system with acoustic microscopy. *J. Acoust. Soc. Am.* 104, 3665–3672 (1998)
57. Marsh, J.N., Hall, C.S., Scott, M.J., Fuhrhop, R.W., Gaffney, P.J., Wickline, S.A., Lanza, G.M.: Improvements in the ultrasonic contrast of targeted perfluorocarbon nanoparticles using an acoustic transmission line model. *IEEE Trans. Ultrason Ferroelectr. Freq. Control* 49, 29–38 (2002)
58. Morawski, A.M., Winter, P.M., Crowder, K.C., Caruthers, S.D., Fuhrhop, R.W., Scott, M.J., Robertson, J.D., Abendschein, D.R., Lanza, G.M., Wickline, S.A.: Targeted nanoparticles for quantitative imaging of sparse molecular epitopes with MRI. *Magn. Reson. Med.* 51, 480–486 (2004)
59. Cunningham, C.H., Arai, T., Yang, P.C., McConnell, M.V., Pauly, J.M., Conolly, S.M.: Positive contrast magnetic resonance imaging of cells labeled with magnetic nanoparticles. *Magn. Reson. Med.* 53, 999–1005 (2005)
60. Stuber, M., Gilson, W.D., Schaer, M., Bulte, J.W., Kraitchman, D.L.: Shedding light on the dark spot with IRON: a method that generates positive contrast in the presence of superparamagnetic nanoparticles. In: Proceedings of the 13th Annual Meeting of ISMRM, Miami Beach, FL, USA (2005)

61. Morawski, A.M., Winter, P.M., Yu, X., Fuhrhop, R.W., Scott, M.J., Hockett, F., Robertson, J.D., Gaffney, P.J., Lanza, G.M., Wickline, S.A.: Quantitative “magnetic resonance immunohistochemistry” with ligand-targeted ^{19}F nanoparticles. *Magn. Reson. Med.* 52, 1255–1262 (2004)
62. Ahrens, E.T., Flores, R., Xu, H., Morel, P.A.: In vivo imaging platform for tracking immunotherapeutic cells. *Nat. Biotechnol.* 23, 983–987 (2005)
63. Liu, J., et al.: Nanoparticles as image enhancing agents for ultrasonography. *Phys. Med. Biol.* 51, 2179–2189 (2006)
64. Liu, J., Li, J., Rosol, T.J., Pan, X., Voorhees, J.: Biodegradable nanoparticles for targeted ultrasound imaging of breast cancer cells in vitro. *Phys. Med. Biol.* 52, 4739–4747 (2007)
65. Cyrus, T., Winter, P.M., Caruthers, S.D., Wickline, S.A., Lanza, G.M.: Magnetic resonance nanoparticles for cardiovascular molecular imaging and therapy. *Expert Rev. Cardiovasc Ther.* 3, 705–715 (2005)
66. Farokhzad, O.C., Langer, R.: Nanomedicine: developing smarter therapeutic and diagnostic modalities. *Adv. Drug Deliv. Rev.* 58, 1456–1459 (2006)
67. Lanza, G., Winter, P., Cyrus, T., Caruthers, S., Marsh, J., Hughes, M., Wickline, S.: Nanomedicine opportunities in cardiology. *Ann. NY Acad. Sci.* 1080, 451–465 (2006)
68. Leary, S.P., Liu, C.Y., Apuzzo, M.L.: Toward the emergence of nanoneurosurgery: part III—nanomedicine: targeted nanotherapy, nanosurgery, and progress toward the realization of nanoneurosurgery. *Neurosurgery* 58, 1009–1026 (2006)
69. Pison, U., Welte, T., Giersig, M., Groneberg, D.: Nanomedicine for respiratory diseases. *Eur. J Pharmacol.* 533, 341–350 (2006)
70. Wagner, V., Dullaart, A., Bock, A.K., Zweck, A.: The emerging nanomedicine landscape. *Nat. Biotechnol.* 24, 1211–1217 (2006)
71. Vasir, J.K., Reddy, M.K., Labhasetwar, V.: Nanosystems in drug targeting: opportunities and challenges. *Curr. Nanosci.* 1, 47–64 (2005)
72. Dreher, M.R., Liu, W., Michelich, C.R., Dewhirst, M.W., Yuan, F., Chilkoti, A.: Tumor vascular permeability, accumulation, and penetration of macromolecular drug carriers. *J. Natl. Cancer Inst.* 98, 335–344 (2006)
73. Moses, M.A., Brem, H., Langer, R.: Advancing the field of drug delivery: taking aim at cancer. *Cancer Cell* 4, 337–341 (2003)
74. Alexiou, C., Schmid, R.J., Jurgons, R., Kremer, M., Wanner, G., Bergemann, C., Huenges, E., Nawroth, T., Arnold, W., Parak, F.G.: Targeting cancer cells: magnetic nanoparticles as drug carriers. *Eur. Biophys J* 35, 446–450 (2006)
75. Alexiou, C., Jurgons, R., Schmid, R., Erhardt, W., Parak, F., Bergemann, C., Iro, H.: Magnetic Drug Targeting—a new approach in locoregional tumor therapy with chemotherapeutic agents. Experimental animal studies. *HNO* 2005 53, 618–622 (2005)
76. Alexiou, C., Jurgons, R., Seliger, C., Brunke, O., Iro, H., Odenbach, S.: Delivery of superparamagnetic nanoparticles for local chemotherapy after intraarterial infusion and magnetic drug targeting. *Anticancer Res.* 27, 2019–2022 (2007)
77. Sapra, P., Tyagi, P., Allen, T.M.: Ligand-targeted liposomes for cancer treatment. *Curr. Drug Deliv.* 2, 369–381 (2005)
78. Nobs, L., Buchegger, F., Gurny, R., Allémann, E.: Current methods for attaching targeting ligands to liposomes and nanoparticles. *J. Pharm. Sci.* 93, 1980–1992 (2004)
79. Marty, C., Schwendener, R.A.: Cytotoxic tumor targeting with scFv antibody-modified liposomes. *Methods Mol. Med.* 109, 389–402 (2005)

80. Cegnar, M., Premzl, A., Zavasnik-Bergant, V., Kristl, J., Kos, J.: Poly(lactide-co-glycolide) nanoparticles as a carrier system for delivering cysteine protease inhibitor cystatin into tumor cells. *Exp. Cell Res.* 301, 223–231 (2004)
81. McCarthy, J.R., Perez, J.M., Brückner, C., Weissleder, R.: Polymeric nanoparticle preparation that eradicates tumors. *Nano Lett.* 5, 2552–2556 (2005)
82. Quintana, A., Raczka, E., Piehler, L., Lee, I., Myc, A., Majoros, I., Patri, A.K., Thomas, T., Mulé, J., Baker Jr., J.R.: Design and function of a dendrimer-based therapeutic nanodevice targeted to tumor cells through the folate receptor. *Pharm Res.* 19, 1310–1316 (2002)
83. Shukla, R., Thomas, T.P., Peters, J.L., Desai, A.M., Kukowska-Latallo, J., Patri, A.K., Kotlyar, A., Baker Jr., J.R.: HER2 specific tumor targeting with dendrimer conjugated anti-HER2 mAb. *Bioconjug Chem.* 17, 1109–1115 (2006)
84. Majoros, I.J., Myc, A., Thomas, T., Mehta, C.B., Baker Jr., J.R.: PAMAM dendrimer-based multifunctional conjugate for cancer therapy: synthesis, characterization, and functionality. *Biomacromolecules* 7, 572–579 (2006)
85. Roy, I., Ohulchanskyy, T.Y., Bharali, D.J., Pudavar, H.E., Mistretta, R.A., Kaur, N., Prasad, P.N.: Optical tracking of organically modified silica nanoparticles as DNA carriers: a nonviral, nanomedicine approach for gene delivery. *Proc. Natl. Acad. Sci. USA* 102, 279–284 (2005)
86. Roy, I., Ohulchanskyy, T.Y., Pudavar, H.E., Bergey, E.J., Oseroff, A.R., Morgan, J., Dougherty, T.J., Prasad, P.N.: Ceramic-based nanoparticles entrapping water-insoluble photosensitizing anticancer drugs: a novel drug-carrier system for photodynamic therapy. *J Am. Chem. Soc.* 125, 7860–7865 (2003)
87. Reddy, G.R., Bhojani, M.S., McConville, P., Moody, J., Moffat, B.A., Hall, D.E., Kim, G., Koo, Y.E., Woolliscroft, M.J., Sugai, J.V., Johnson, T.D., Philbert, M.A., Kopelman, R., Rehemtulla, A., Ross, B.D.: Vascular targeted nanoparticles for imaging and treatment of brain tumors. *Clin. Cancer Res.* 12, 6677–6686 (2006)
88. Jain, P.K., El-Sayed, I.H., El-Sayed, M.A.: Au nanoparticles target cancer. *Nanotoday* 2, 18–29 (2007)
89. Link, S., El-Sayed, M.A.: Optical properties and ultrafast dynamics of metallic nanocrystals. *Ann. Rev. Phys. Chem.* 54, 331–366 (2003)
90. Lee, K.S., El-Sayed, M.A.: Gold and silver nanoparticles in sensing and imaging: sensitivity of plasmon response to size, shape, and metal composition. *J Phys. Chem. B* 110, 19220–19225 (2006)
91. Jain, P.K., Lee, K.S., El-Sayed, I.H., El-Sayed, M.A.: Calculated absorption and scattering properties of gold nanoparticles of different size, shape, and composition: applications in biological imaging and biomedicine. *J. Phys. Chem. B* 110, 7238–7248 (2006)
92. Jensen, T.R., Duval, M.L., Kelly, K.L., Lazarides, A.A., Schatz, G.C., Van Duyne, R.P.: Nanosphere lithography: effect of the external dielectric medium on the surface plasmon resonance spectrum of a periodic array of silver nanoparticles. *J. Phys. Chem. B* 103, 9846–9853 (1999)
93. Jain, P.K., Qian, W., El-Sayed, M.A.: Ultrafast electron relaxation dynamics in coupled metal nanoparticles in aggregates. *J. Phys. Chem. B* 110, 136–142 (2006)
94. Sönnichsen, C., Reinhard, B.M., Liphardt, J., Alivisatos, A.P.: A molecular ruler based on plasmon coupling of single gold and silver nanoparticles. *Nat. Biotechnol.* 23, 741–745 (2005)

95. Jain, P.K., Eustis, S., El-Sayed, M.A.: Plasmon coupling in nanorod assemblies: optical absorption, discrete dipole approximation simulation, and exciton-coupling model. *J. Phys. Chem. B* 110, 18243–18253 (2006)
96. Connor, E.E., Mwamuka, J., Gole, A., Murphy, C.J., Wyatt, M.D.: Gold nanoparticles are taken up by human cells but do not cause acute cytotoxicity. *Small* 1, 325–327 (2005)
97. Katz, E., Willner, I.: Integrated nanoparticle-biomolecule hybrid systems: synthesis, properties, and applications. *Angew. Chem. Int. Ed. Engl.* 43, 6042–6108 (2004)
98. Sokolov, K., Follen, M., Aaron, J., Pavlova, I., Malpica, A., Lotan, R., Richards-Kortum, R.: Real-time vital optical imaging of precancer using anti-epidermal growth factor receptor antibodies conjugated to gold nanoparticles. *Cancer Res.* 63, 1999–2004 (2003)
99. El-Sayed, I.H., Huang, X., El-Sayed, M.A.: Surface plasmon resonance scattering and absorption of anti-EGFR antibody conjugated gold nanoparticles in cancer diagnostics: applications in oral cancer. *Nano Lett.* 5, 829–834 (2005)
100. El-Sayed, M.A.: Some interesting properties of metals confined in time and nanometer space of different shapes. *Acc. Chem. Res.* 34, 257–264 (2001)
101. El-Sayed, I.H., Huang, X., El-Sayed, M.A.: Selective laser photo-thermal therapy of epithelial carcinoma using anti-EGFR antibody conjugated gold nanoparticles. *Cancer Lett.* 239, 129–135 (2006)
102. Loo, C., Lowery, A., Halas, N., West, J., Drezek, R.: Immunotargeted nanoshells for integrated cancer imaging and therapy. *Nano Lett.* 5, 709–711 (2005)
103. Zharov, V.P., Galitovskaya, E.N., Johnson, C., Kelly, T.: Synergistic enhancement of selective nanophotothermolysis with gold nanoclusters: potential for cancer therapy. *Lasers Surg. Med.* 37, 219–226 (2005)
104. Pitsillides, C.M., Joe, E.K., Wei, X., Anderson, R.R., Lin, C.P.: Selective cell targeting with light-absorbing microparticles and nanoparticles. *Biophys J.* 84, 4023–4032 (2003)
105. Huang, X., Jain, P.K., El-Sayed, I.H., El-Sayed, M.A.: Determination of the minimum temperature required for selective photothermal destruction of cancer cells with the use of immunotargeted gold nanoparticles. *Photochem. Photobiol.* 82, 412–417 (2006)
106. Urbanska, K., Romanowska-Dixon, B., Matuszak, Z., Oszajca, J., Nowak-Sliwinski, P., Stochel, G.: Indocyanine green as a prospective sensitizer for photodynamic therapy of melanomas. *Acta. Biochim Pol.* 49, 387–391 (2002)
107. Weissleder, R.: A clearer vision for in vivo imaging. *Nat. Biotechnol.* 19, 316–317 (2001)
108. Lee, K.S., El-Sayed, M.A.: Dependence of the enhanced optical scattering efficiency relative to that of absorption for gold metal nanorods on aspect ratio, size, end-cap shape, and medium refractive index. *J. Phys. Chem. B* 109, 20331–20338 (2005)
109. Brioude, A., Jiang, X.C., Pilani, M.P.: Optical properties of gold nanorods: DDA simulations supported by experiments. *J. Phys. Chem. B* 109, 13138–13142 (2005)
110. Huang, X., El-Sayed, I.H., Qian, W., El-Sayed, M.A.: Cancer cell imaging and photothermal therapy in the near-infrared region by using gold nanorods. *J. Am Chem. Soc.* 128, 2115–2120 (2006)
111. Chen, J., Wiley, B., Li, Z.-Y., Campbell, D., Saeki, F., Cang, H., Au, L., Lee, J., Li, X., Xia, Y.: Gold nanocages: engineering their structure for biomedical applications. *Adv. Mater* 17, 2255–2261 (2005)

112. Lee, J., Yang, J., Ko, H., Oh, S.J., Kang, J., Son, J.-H., Lee, K., Lee, S.-W., Yoon, H.-G., Suh, J.-S., Huh, Y.-M., Haam, S.: Multifunctional magnetic gold nanocomposites: human epithelial cancer detection via magnetic resonance imaging and localized synchronous therapy. *Adv. Funct. Mater.* 18, 258–264 (2008)
113. Krasovitski, B., Kislev, H., Kimmel, E.: Modeling photothermal and acoustical induced microbubble generation and growth. *Ultrasoundics* 47, 90–101 (2007)
114. Kimmel, E.: Cavitation bioeffects. *Crit. Rev. Biomed Eng.* 34, 105–161 (2006)
115. Stride, E., Saffari, N.: On the destruction of microbubble ultrasound contrast agents. *Ultrasound Med. Biol.* 29, 563–573 (2003)
116. Miller, D.L., Quddus, J.: Diagnostic ultrasound activation of contrast agent gas bodies induces capillary rupture in mice. *Proc. Natl. Acad. Sci. USA* 97, 10179–10184 (2000)
117. Holt, R.G., Roy, R.A.: Measurements of bubble-enhanced heating from focused, MHz-frequency ultrasound in a tissue-mimicking material. *Ultrasound Med. Biol.* 27, 1399–13412 (2001)
118. Ashush, H., Rozenszajn, L.A., Blass, M., Barda-Saad, M., Azimov, D., Radnay, J., Zipori, D., Rosenschein, U.: Apoptosis induction of human myeloid leukemic cells by ultrasound exposure. *Cancer Res* 60, 1014–1020 (2000)
119. Price, R.J., Kaul, S.: Contrast ultrasound targeted drug and gene delivery: an update on a new therapeutic modality. *J. Cardiovasc Pharmacol. Ther.* 7, 171–180 (2002)
120. Farny, C.H., Wu, T., Holt, G., Murray, T.W., Roy, R.A.: Nucleating cavitation from laser-illuminated nano-particles. *Acoust Res. Lett. Online* 6, 138–143 (2005)
121. Fujishiro, S., Mitsumori, M., Nishimura, Y., Okuno, Y., Nagata, Y., Hiraoka, M., Sano, T., Marume, T., Takayama, N.: Increased heating efficiency of hyperthermia using an ultrasound contrast agent: a phantom study. *Int. J. Hyperthermia* 14, 495–502 (1998)

Miniature Differential Mobility Spectrometry (DMS)

Advances towards Portable Autonomous Health Diagnostic Systems

Weixiang Zhao^{1,3}, Abhinav Bhushan^{1,3}, Michael Schivo^{2,3},
Nicholas J. Kenyon^{2,3}, and Cristina E. Davis^{1,3,*}

¹ Mechanical and Aerospace Engineering

² Division of Pulmonary and Critical Care Medicine

³ Clinical and Translational Science Center, University of California Davis,
One Shields Avenue, Davis CA 95616, USA
cedavis@ucdavis.edu

Abstract. Many modern analytical instruments, such as mass spectrometry, have been developed to provide insight into the biochemical content of many different biological sample types. Typically these instruments are large bench-top machines that have very high sensitivity and specificity for the compounds they detect. However, these instruments are not mobile or autonomous, and they require highly trained personnel to operate. There have been many developments in the area of miniature chemical sensors that can maintain performance levels observed in large traditional bio-analytical instruments, but are low-power and potentially mobile and autonomous in function. Miniature differential mobility spectrometry (DMS) is a small instrument that can potentially be used in point-of-care diagnostic applications. This chapter will review the significant advances in this emerging research area, and provide insight as to how these systems could be further improved and adapted for use in autonomous health monitoring and sensing systems.

Keywords: differential mobility spectrometry (DMS), non-invasive disease diagnostics, breath analysis, chemometrics, breath analysis.

1 Introduction to Miniature Differential Mobility Spectrometry (DMS)

Differential Mobility Spectrometry (DMS) or high Field Asymmetric Waveform Ion Mobility Spectrometry (FAIMS) or simply Field Ion Spectrometry is a technique for gas phase ion separation and detection. The DMS is a novel detector,

* Corresponding author.

and has recently been used for chemical and biological sensing and detection in field trials as well as being used as a gas chromatography (GC) detector. This category of devices hold much promise due to several desirable properties, including: on-site near-real-time analysis, small size, low cost, and high sensitivity and analyte specificity.

The DMS has been used in many application areas, such as the detection of explosives, environmental pollution, and biological materials. The device has been shown to detect chemical species at lower concentrations than traditional mass spectrometers [1], although the operating principal is different than the MS device. Differential mobility spectrometry relies on the nonlinear mobility of charged species or ions of chemical compounds in an asymmetric RF field. Chemical compounds of interest can be ionized in variety of different ways, including photoionization, radioactive Ni⁶³ sources or through more advanced methods such as electrospray. Charges are imparted both directly and indirectly onto the chemical species of interest, and are then carried by a carrier gas into what is known as the “drift tube” region of the device. This drift tube region is composed of a set of parallel electrodes that is modulated by two electric fields – the time-dependent, asymmetric RF voltage, which is superimposed by a DC compensation voltage that guides the ions through the electrodes to a detector and deflector electrode [2]. Figure 1 illustrates the operational concept of the device and detection technique. When coupled with a gas chromatograph (GC) front end device, a GC/DMS produces a three-dimensional output – retention time, compensation voltage, and intensity for both positive and negative ions that contains useful information to discern between complex chemical mixtures.

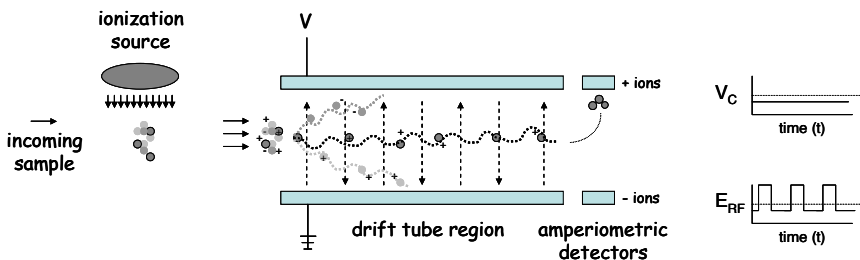


Fig. 1. Ionized analytes are separated under an RF electric field superimposed with linear a compensating electric field.

2 Mathematical Models of DMS

As DMS has become a more widely studied and utilized analysis technique, it has become more important to have adequate models of the device function. A correct understanding of the DMS principles can help the user to design a proper experiment protocol for sample analysis, and may facilitate a deeper understanding of fundamental underlying sensing and detection mechanisms. This section provides a brief review of the mathematical models of DMS operation principle to help

grasp the core part of DMS operation mechanism. A complete description of DMS mathematical models can be referred to in the literature [3].

Basically, DMS is an electric field driven ion spectrometer instrument. Assuming an electric field of strength E causes trace amounts of ions to move through a dilute gas media of density D , and the ion mobility coefficient k can be expressed as Eq. (1):

$$k\left(\frac{E}{D}\right) = k(0)\left[1 + \beta\left(\frac{E}{D}\right)\right] \quad (1)$$

where, $k(0)$ is the mobility coefficient under a very low field condition, $\beta\left(\frac{E}{D}\right)$ is a normalized function to describe field-mobility dependence, which is a unique feature for ion separation in differential mobility spectrometry. The ion mobility coefficient is a major factor that determines the ion drift velocity, which is shown in Eq. (2)

$$v = k\left(\frac{E}{D}\right)[S \cdot f + C] \quad (2)$$

where, S is the separation voltage, C is compensation voltage (CV), and f is a function that describes the electrical field waveform. By applying a low strength constant CV to the electrodes, particular ions can be kept in the center of two electrodes. CV is superimposed on the separation field to allow ions to stay in equilibrium and pass through the electrodes. Setting the drift velocity in Eq. (2) to be zero, we can estimate the required CV that can keep a specific ion in equilibrium by subsequently integrating Eq. (1) with Eq. (2) and expanding the polynomial via Taylor first order approximation:

$$C = \frac{S\langle\beta \cdot f\rangle}{1 + \langle\beta\rangle + S\langle\beta' \cdot f\rangle} \quad (3)$$

where, β is the ion field-mobility dependence described in Eq. (1) and β' the first order derivative of β .

We can estimate the location of a chemical peak through Eq. (3). Meanwhile, according to ion diffusion factor, ion focusing factor, DMS carrier gas flow rate and ion residence time in electrode field, we can also estimate peak height. The detailed process is clearly described in the literature [3]. After scanning each CV point in a pre-defined CV span range, we can obtain a spectrum of ion mixture, which is the fundamental of DMS operation [3-5]. These mathematical models provide us with a platform to have a simulation study of the DMS separation process. A correct understanding of these mathematical models can eventually help us design proper experiment protocols, and can lead to detection hardware advances in next-generation devices.

3 Miniature DMS for Chemical and Biological Sensing Applications

Over the last decade, many uses of the DMS have been widely explored [6, 7]. Specifically, the detector has been extremely useful for both chemical and biological applications, which have helped lead towards new uses that are proposed in the clinical biomedical arena. As a new sensor modality, the DMS is quiet well suited for diagnostic applications.

Initially, the planar microfabricated miniature DMS was considered mostly for chemical detection methods, especially nitro-organic explosives compound detection [8, 9] and homeland security applications [10]. Subsequently these techniques and devices have proven to be extremely useful as portable and mobile detection platforms, and have been widely commercialized for chemical detection [5]. This detection method was also used for environmental detection of chlorocarbons [11], halogenated compounds [12], surrogate compounds of chemical weapons [13], and ground water contaminants such as benzene [14]. In most of the early cases, the detector was used primarily to sense one specific chemical or class of chemicals at a time; however, it soon became clear that the sensor could easily function to monitor for specific compounds within complex mixtures as well.

In addition to the chemical detection applications, the sensor has been frequently used to monitor for biologically-relevant materials. By coupling unique sample introduction modules to the sensor, it becomes possible to introduce biological samples that are either in solid or liquid phase. For example, pyrolysis (Py) is a technique that uses heat to thermally decompose materials into small component molecules and usually results in vapour compounds that can be sensed by a variety of gas phase detection sensors. In 2004, Eiceman's research group initially demonstrated that a combined Py/GC/DMS sensor could achieve very good differentiation of different bacteria cultures based on the combination of chemicals that resulted from the pyrolysis process [15]. Subsequently, this technique has proven extremely useful in bacterial strain identification [16-19], especially when coupled with advanced algorithms to recognize biomarker features within the detector output spectra [18, 19]. This method has also been used to distinguish different viruses within liquid mixtures [20], and to detect various strains of *Bacillus* endospores [13, 21, 22].

While all the above methods of bacteria detection relied on converting liquid samples into the gas phase, another study in 2005 demonstrated that it was possible to monitor for vegetative bacteria metabolites produced as the cultures proliferated and grow [23]. A gas chromatographic column is interfaced with the miniature DMS to facilitate compound differentiation. In this report, four different closely-related bacteria strains (*Escherichia coli*, *Bacillus subtilis*, *Bacillus thuringiensis*, and *Mycobacterium smegmatis*), were differentiated with accuracies as high as 84% by observing clusters of points in the spectra that were unique to each species (Figure 2).

The miniature DMS has also been successfully connected to various miniature front end sample introduction modules, that allow for the entire sample analysis system to be reduced in size. A microfabricated gas chromatograph (GC) column

allows for good gas phase pre-separation of complex chemical mixtures [24, 25], and a thermal desorption system has proven useful for solid-phase microextraction filters to be used in pre-concentrating gas phase compounds for later DMS analysis [26]. A polymeric sampling device for absorbing and concentrating environmental pollutants has also been employed [14]. A nanoelectrospray sample introduction method allows for separation and identification of peptides and oligosaccharides [27-29], and electrospray of other proteins and biological materials [30]. The GC/DMS system has most recently been used to monitor for volatile compounds that emanate from other biological sources such as plants and trees [31], for specific compounds such as putrescine and cadaverine [32], and for detecting and separating ignitable liquids and fuel sources [33-35].

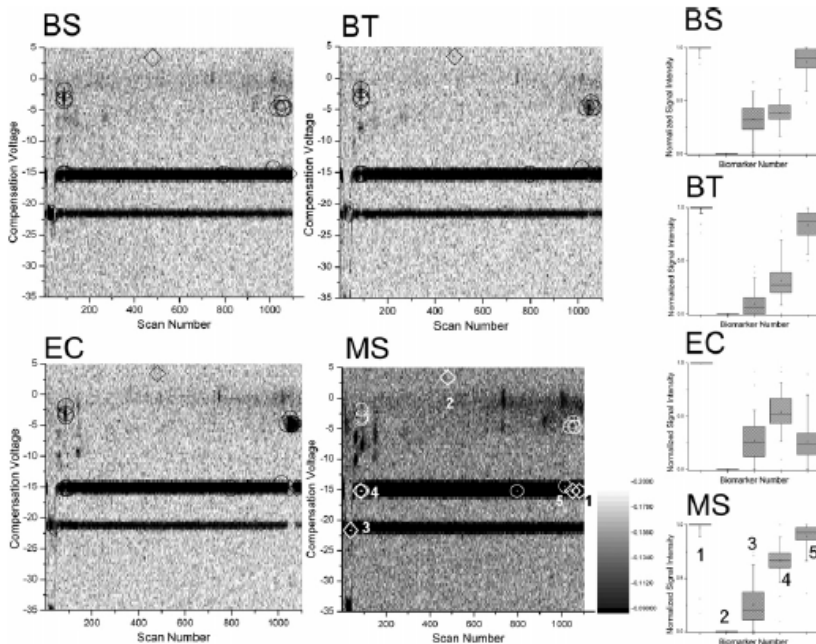


Fig. 2. GC/DMS spectral traces illustrate biomarker differences between closely-related bacterial strains (BS: *Bacillus subtilis*, BT: *Bacillus thuringiensis*, EC: *Escherichia coli*, MS: *Mycobacterium smegmatis*). (reprinted with permission from [23])

4 Clinical Applications for DMS

Several reports to date have illustrated how the DMS could be useful for potential biomedical and clinical applications, from bacterial detection that could be applied to human effluents [13, 15-19, 21, 23], to protein detection [27-30], and virus detection [20]. In particular, exhaled human breath contains many physiological metabolites compounds that are very important for clinical diagnostics, and the DMS

has also been tailored to potentially be used in breath analysis applications [4, 36–39]. All of these methods have the potential to reduce the DMS sensor system to scalable sizes that are appropriate for mobile diagnostic platforms.

Two sample introduction methods appear to be very well suited to introduce exhaled breath into the DMS sensor for clinical analysis: thermal desorption of compounds from a solid phase microextraction (SPME) fiber into a GC/DMS system, and electrospray ionization. Both have benefits and potential uses that could aid in mobile diagnostics. In the first case, volatile compounds from exhaled breath can be immobilized onto polymeric absorptive substrates. This allows for concentration of the compounds, which can then be desorbed into the DMS for chemical analysis. Electrospray ionization is a “soft” ionization technique that is very useful for analysis of biological materials. Briefly, a liquid that contains biological material of interest is used to generate aerosol particles, which are then charged. As the solvent in the aerosol particles evaporates, this leaves charges behind on the biological material that we seek to analyze. The charged species can then be monitored using technologies, such as the miniature DMS [37]. Figure 3 shows a schematic of an ESI/DMS analysis system, which can be used to generate dispersion plots characteristic for a particular biological material being analyzed (Figure 4). These dispersion plots enable researchers to potentially identify specific compounds of interest, even in the presence of interfering background chemicals (discussed in further detail in section 5.3).

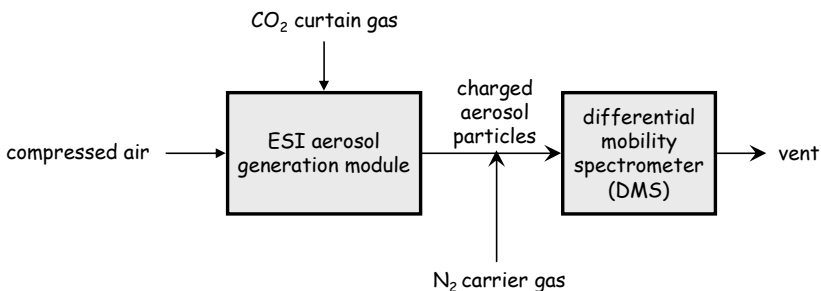


Fig. 3. System level configuration for ESI/DMS. (adapted from [37])

Sensor technologies such as the miniature DMS hold great promise for clinical medicine. The individual sensor and sample introduction methods each can be further reduced in size, and ultimately included into a hand-held or wearable sensor system that can perform routine health monitoring via breath diagnostics.

An ideal clinical diagnostic tool is sensitive without sacrificing specificity, is easy for to use and interpret, provides reproducible data, and allows for meaningful interpretation and decision-making. One area where the DMS has significant potential is in diagnostics and monitoring in lung disease. Heterogeneous diseases such as asthma, chronic obstructive pulmonary disease (COPD), and pulmonary fibrosis are all examples of common lung diseases that are caused and triggered by a variety of environmental and infectious agents. A sensor that could allow a clinician to determine whether a patient with new onset cough and

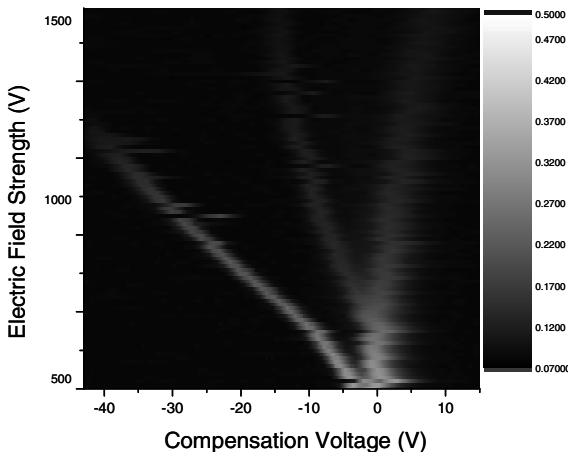


Fig. 4. Example of an ESI/DMS dispersion plot. (adapted from [37])

shortness of breath has a bacterial bronchitis related to COPD or a pulmonary embolism would be highly advantageous. Given the wide spectrum of compounds that have been measured in human breath, it is likely that the DMS would have diagnostic and monitoring capabilities for systemic diseases also. Furthermore, it is not unreasonable to consider that a DMS system could be inserted into a mechanical ventilator to provide real-time diagnostic information regarding infection or metabolic status. Finally, the problem of determining response to medications could be addressed with the DMS system, suggesting this type of technology could be the cornerstone for “personalized medicine” in the future.

One reality with biomedical diagnostic sensors is that a plethora are and will be available in the next decade. The DMS will compete in this difficult market with other sensors based on usability and accuracy. One such sensor is the electronic nose (eNose). eNoses are a collection of nanosensor arrays which react with different components of volatile organic compounds in breath and generate high-density “breathprints” [40, 41]. Studies have shown that eNoses can differentiate airway disease in 90 subjects with asthma, chronic obstructive pulmonary disease (COPD), and active smokers [42]. Principle component analysis allowed the investigators to separate subjects with asthma from those with COPD (accuracy 96%) and controls (accuracy 95% nonsmoking, 92.5% smoking). Another study used eNoses to differentiate subjects with non-small cell lung cancer (NSCLC) from subjects with COPD [43]. Last, subjects with chronic rhinosinusitis were compared to controls using exhaled breath and eNose technology. The resulting breath signatures accurately predicted whether a subject had chronic rhinosinusitis or not in 72% of the samples using principle component analysis and a machine learning algorithm [44]. Emerging clinical applications of breath nanosensors include the identification of bacterial infections in intubated and mechanically ventilated patients [45] and screening for tuberculosis [46] in at-risk populations. While the DMS does not yet have a well-established track-record in clinical studies to date, this will change soon.

The potential of the DMS can only be realized if it is brought to the clinics and usable as a handheld or easily-portable device. Only when such a device is easy to use, can be incorporated into the daily work flow of a busy physician's office, and provides important and clinically relevant information that can be acted on immediately, will it be adopted. There is recent precedent with exhaled nitric oxide measurements that can now be performed with a handheld technology, and has become increasingly utilized.

5 Advanced Data Analysis Methods

Signal processing and adaptive learning methods have increasingly played an important role in how novel sensor data can be effectively interpreted [47], and this is especially true for DMS data given that the sensor outputs a multi-dimensional signal for both positive and negative ions that are measured. Early on, simple peak amplitude and peak area analysis were sufficient to interpret the data systems; however, newer data analysis methods have recently been reported using DMS that could provide an avenue towards autonomous real-time diagnostics.

5.1 Simple Peak Detection and Interpretation

Initial DMS reports in the literature used relatively simple peak detection and interpretation methods to attempt to identify and quantify compounds present from the samples being analyzed [8, 9, 11, 13, 15]. In these cases, points in the spectra were located that appeared to correlate to specific chemicals and then analogous locations in new spectra were observed to determine if a compound is present in a new unknown sample. This process can clearly be very effective, especially when one knows the identity of the compounds that are being sought.

One problem that can occur with DMS data, especially GC/DMS data, is that some portions of the signal may be slightly misaligned in time. This occurs in many types of hyphenated GC analysis methods (such as GC/MS). This can be compounded if there are also small deviations in the compensation voltage measured for specific chemical peaks. This type of two-dimensional misalignment can make it particularly difficult to enable higher level data analysis, such as pattern recognition methods. One promising method to overcome this limitation is by using a step-wise linear interpolation algorithm to align portions of the GC/DMS spectra to referenced markers within the data sets [48]. This data pre-processing can occur off-line or in near-real time, if sufficient training data is available to compare to new incoming unknown data samples.

5.2 Pattern Recognition, Machine Learning, and Advanced Statistical Analysis Methods

Briefly, feature extraction and machine learning strategies provide a powerful tool for us to concentrate information, prevent possible disturbance from noise contamination and unrelated variables, and establish a model to uncover complex system mechanisms. There have been many reported progresses in these fields

[49-51], but we still face substantial challenges to efficiently apply machine learning and feature extraction approaches to large data systems, such as those seen in DMS sensor outputs. Both sample number and sample dimension can significantly delay or even derail a knowledge discovery process. Particularly, an overly large sample dimension number can cause a “curse of dimensionality” problem in data mining and machine learning field.

5.2.1 Genetic Algorithms (GA)

The GA is a powerful optimization method that mimics natural evolution principle. One significant advantage of GA over traditional optimization methods is its ability to optimize any type of function (continuous or discontinuous, derivable or non-derivable). The evolution process of GA consists of three major operators: selection, crossover, and mutation. Through the selection operator, a proportion of members are selected to develop a new generation based on a fitness related process. In the crossover step, members are grouped in pair to generate their two children that contain the genes from their both parents. The mutation operator is used to maintain the genetic diversity of the population members in each generation and also to prevent possible local optima (i.e., premature solutions) during the evolution process. GA has become a most powerful optimization strategy, and was effectively used in DMS analysis to analyze *Bacillus* endospores [21], viruses [20], and off-gassed metabolites from vegetative bacteria [23].

One of the GA studies reported on DMS data to date was to detect the most distinguishable feature (biomarkers) from the Pyrolysis Gas Chromatography Differential Mobility Spectrometry (Py/GC/DMS) data to separate proteins and viruses [20]. In this study, two types of biological samples were tested using the PY/GC/DMS system: proteins and viruses. Each sample was composed of composed of $2 \times 3,553$ (retention time dimension) $\times 100$ (compensation voltage dimension) = 710,600 pixels of the signal, each with the potential to serve as a biomarker and distinguish our data sets. Therefore, each chromosome during the evolution process is a 710,600 dimensional binary vector in which “1” or “0” denotes whether or not the corresponding signal is selected to build a classifier. Using principal component analysis and back-propagation neural network to evaluate the quality of the selected features, the GA eventually selected ten features (biomarkers) to separate protein from virus. Employing principal component analysis (PCA) coupled with a backward propagating neural network (PCA-BPNN) based classifier, the 10 selected biomarkers yielded a separation accuracy of 94% to this two-class classification problem.

The GA technique was also recently combined with a technique called wavelet analysis [5]. In that report, the authors applied GA to the wavelet coefficients of the GC/DMS spectral data of pure chemicals to establish a chemical family classification model. In total, 390 spectra from six chemical families were employed for this study, which were 70 spectra from 7 cycloalkane samples; 90 spectra from 9 alkane samples; 60 spectra from 6 alcohol samples; 47 spectra from 5 ketone samples; and 83 spectral form 8 substituted ketone samples; and 40 spectra from 4 substituted benzene samples. Each spectrum was composed of GC/DMS data, but only the DMS data vector was used for analysis. First, the wavelet transformation

packet was used to de-noise and de-convolute the DMS data by decomposing each spectrum into its wavelet coefficients. In the next step, GA was employed to identify wavelet coefficients for chemical family classification through a supervised machine learning process. Acting as a spectral signal filter, the GA selected the separable wavelet coefficients for machine learning methods to generate an accurate chemical family identification model.

5.2.2 Fuzzy Logic Analysis

Fuzzy logic data analysis has been widely used for pattern recognition and signal processing [52-54]. Fuzzy rule building expert system (FuRES) is a typical fuzzy logic data analysis method which essentially is a multivariate classification algorithm for data classification. Basically, FuRES builds a collection of membership functions to form an inductive classification tree, each branch of which is a multivariate fuzzy rule to minimize classification entropy [33]. Because of the membership of fuzzy functions, overlapping data can be accommodated without forcing the classifier into wrong solutions. The advantage of fuzzy classification trees over conventional neural networks is that they afford a simple and straightforward inductive structure that is amenable to interpretation. There have been several successful applications of FuRES to DMS data [33, 34].

One application was in a forensic study where gas chromatography differential mobility spectrometry (GC/DMS) was used for the classification of ignitable liquids from fire debris [33]. In this study, a variety of ignitable liquids including gasoline, diesel, mineral spirits, paint thinner, paint remover, lighter fuel, and turpentine were analyzed with GC/DMS. Different from some studies where only the data from one dimension of GC/DMS were retained for analysis, this study employ both dimensions and convert the data matrix of each sample into a long vector. Both FuRES and PLS were used to create a separation model. The results indicated that both methods presented good classification accuracies: $99.07\pm0.04\%$ (FuRES) and $98.00\pm0.04\%$ (PLS), but FuRES was a more adaptive and self-adjusting model. This study presented a promising onsite detection method for arson investigation [33]. FuRES along with the two-way data converting method was also successfully applied to classify the GC/DMS data of different fuel samples [34]. The classification accuracy of fuel samples was up to $95.00\pm0.3\%$, clearly indicating the feasibility of using GC/DMS to identify fuel type. This functionality bodes well for distinguishing biological metabolites for clinical diagnostics.

5.2.3 Projected Difference Resolutions (PDR)

Recently, a novel method called project difference resolutions (PDR) was applied to examine the seperability of DMS samples [35]. Briefly, the data of a spectral sample is projected onto the difference vector between two class centers to calculate the score of this spectrum. Then, the scores of all the samples are used to examine the resolution of two classes. Experientially, in general a resolution value larger than 1.5 indicates two classes are well resolved. This straightforward but effective testing method has been successfully applied to compare the seperability of GC/DMS and GC/MS data of seven kind of ignitable liquids. Both GC/DMS

and GC/MS data were converted into two data structures: summarizing signal across one single dimension and concatenating all the row/column vectors of 2-D original sample data into one dimension. The results indicated that the latter data conversion method was more efficient on classifying ignitable liquids and GC/MS showed smaller prediction errors than GC/DMS [35].

5.2.4 Principle Component Analysis (PCA)

PCA is a widely used method that employees a linear transformation of a set of original high dimensional data onto a new coordinate system. In the new coordinate system, the data with the greatest variance lie on the first coordinate, which is called the first principal component. The second greatest variance then lies on the second coordinate, and so this process continues onward. In other words, PCA converts correlated variables into a much fewer independent variables called principal components. With the ability to concentrate information, reduce data dimension, provide a visual observation of data space distribution and remove possible noise, PCA is almost the most widely used data analysis method for high dimensional data, including DMS output data.

PCA was used for a pyrolysis-gas chromatography/differential mobility spectrometry (Py/GC/DMS) based bacterial and analysis [16]. In this study, eight vegetative bacterial strains and two spores were characterized by Py/GC/DMS, presenting topographic plots of ion intensity, retention time, and compensation voltage simultaneously for ions in positive and negative polarity. Each original file from Py/GC/DMS were composed of 1,105 rows, covering the GC retention time dimension (33 min) and 150 columns for the DMS compensation voltage dimension (-5 to 20 V). The whole CV chromatograms were made for locating the reactant ion peaks in both polarities. The vectors at compensation voltages of -1, 1, 3, and 5 V were extracted for chemometric analysis. The results indicate that the Py/GC/DMS allows a rapid characterization of the biochemical information from whole cell bacteria and PCA performs a good discrimination of bacteria.

PCA was also applied for another bacteria discrimination study [19]. Three *Bacillus* strains, *B. subtilis* (B0014), *B. subtilis* (B1382), *B. megaterium* (B0010) were analyzed using Py/GC/DMS. The 2-D GC/DMS data of each sample was converted into 1-D DMS chromatograms by summing the data across the compensation voltage (CV) axis (negative: from -5 to +5 CV and positive: from -6 to +6 CV). Working on the 1-D converted chromatograms, PCA provided a visually separation between *B. megaterium* and two *B. subtilis* strains and indicated the separation of two *B. subtilis* strains needs more sophisticated machine learning methods. In this study, partial least square based discrimination analysis (PLS-DA) was employed for this supervised learning process. Two thirds of the samples were used for training and the remaining one third for testing. The classification results of the whole study demonstrate that the separation between different species can be readily observed by PCA but the strain discrimination for the same species requires more powerful chemometric methods and supervised classifiers [19]. PCA has been also successfully applied to the DMS data for the study of the constituents of bacterial growth [17, 18].

5.2.5 Design of Experiments (DOE) Approach to DMS System Parameter Optimization

Given that a GC/DMS or ESI/DMS system may have multiple parameters that can be optimized, it can be extremely useful to utilize a statistical method to determine the most effective parameter values for optimum sample analysis.

This was recently demonstrated using a SPME/GC/DMS system to analysis exhaled breath condensate [36]. With ability to measure small (even trace) amount of chemicals in complicated chemical and biological samples, analytical instruments have become a powerful diagnostic tools. However, the heterogeneous and variant background and complex composition of the test samples make it a challenging job to analyze and characterize the samples, which require us to design a good experiment protocol by optimizing the instrument parameters. In this study, the authors selected four major factors (parameters) that would influence chemical analysis and set two experimental levels for each factor. They were the RF voltage of the DMS sensor (1200 or 1400 V), nitrogen carrier gas flow rate through the DMS (250 or 500 mL min^{-1}), solid phase microextraction (SPME) filter type (polyacrylate or PDMS–DVB), and GC cooling profile (cryogenic and non-cryogenic). The corresponding dependent variables were the number of total chemical peaks in the GC/DMS plots and the amplitude of acetone. The objective was to find the best parameters that present the highest acetone peak while preserving the largest number of chemical peaks in the spectra. Using a traditional 2^4 factorial design, the best parameter set was determined and the significance of each parameter to analysis quality were also extensively discussed. For example, carrier gas flow rate proved to be the most significant single factor for acetone peak amplitude and also a significant factor for peak number. SPME polymer type also significantly affected the breath analysis measurements. The results demonstrate that design of experiment (DOE) is a powerful method to systematically optimize the parameters and the strategies in this study can be generalized and applied to the analysis of other sample types [36].

Recently, another statistical experiment design method, called the Box-Wilson central composite design (CCD), was introduced for DMS parameter optimization [32]. In brief, a Box-Wilson CCD, commonly just called CCD, consists of an response surface model based imbedded factorial or fractional factorial design. In a study which aimed to optimize the parameters of thermal desorption-GC/DMS for putrescine and cadaverine analysis, CCD was employed to find the best dispersion field strength and DMS cell temperature [32]. The optimal values for these two factors were estimated to be 16.22 kVcm^{-1} and $116\text{ }^\circ\text{C}$ for putrescine and 14.78 kVcm^{-1} and $112\text{ }^\circ\text{C}$ for cadaverine. The results also indicated that the sample mass at the limit of detection was estimated to be 3ng for putrescine and cadaverine. The interactive functions between these two factors were also examined. Elevated temperatures will enhance the de-clustering effect of the high-field segment of the RF dispersion field and will tend to increase the dispersion velocity. CCD has clearly proven to be a efficient tool for GC/DMS experiment protocol design and trace chemical analysis [32].

5.3 Dispersion Plots for Chemical Identification

DMS spectra can be displayed as spectra of detector current versus compensation voltage or as topographic plots scanned in both compensation and separation voltages. The latter option creates dispersion plots presenting ion transformations with changes in RF voltage [55]. Extending the spectral data to a new dimension, dispersion plot has been used for chemical identification and instrumentation quality analysis.

Using dimethyl methyl phosphonate (DMMP) as a standard chemical, dispersion plots were employed to examine the pressure effect on differential mobility spectrometry [55]. Comparing the spectra at different pressure shows that low pressure provides higher separation between the dimmer and monomer peaks and decreases the dimmer fraction for the same sample concentration. It is summarized that operating DMS instruments at pressures below 1 *atm* can provide reduced clustering, good monomer intensities, high CV values, lower risks of electrical breakdown, and reduced power consumption [55].

DMS dispersion plots were also successfully applied for the rapid separation and quantitative analysis of the peptides [27]. In this study, DMS was coupled with mass spectrometry (MS) to have potential advantages such as increased signal-to-noise ratio of mass spectral, orthogonal/complementary ion separation to mass spectrometry, enhanced ion and complexation structural analysis, and rapid analyte quantization. First, the DMS dispersion plots and the mass spectra at the selected compensation voltage (CV) points were collected to determine the ideal CV points for the maximum ion signal of the fragment. The dispersion plots provide a complete view of DMS based ion separation for a given sample. And also, the observed bands (tracts) in the dispersion plots demonstrate unique differences in DMS ion separation for the different sample conditions. More importantly, the results of the dispersion plots demonstrated that under optimized drift gas modifier conditions, DMS would be capable of selectively separating peptide ions of interest [27].

In addition to these reported studies, DMS dispersion plots or radio frequency (RF) voltage plots have also been used for a variety of DMS based chemical analysis studies. These include a study that aimed to increase analytical space in gas chromatography-differential mobility spectrometry with dispersion field amplitude programming [4], a miniature DMS based investigation of the field dependence of ion mobilities of isomeric hydrocarbons [56], and a comparative study that examined the efficiency of time-of-flight ion mobility spectrometry and differential mobility on halogenated compounds [12].

5.4 Applications of Signal Processing Methods

Most recently, wavelet analysis has been explored as a useful method to aid in DMS data analysis [31]. Conventional methods for 2-D GC/DMS data are to convert 2-D data into 1-D data, either by summing signal across one dimension or simply concatenating column/row vectors into a long vector. This paper [31] was the first study to apply 2-D wavelet analysis to the GC/DMS data, considering

GC/DMS spectrum as an image, and examine the classification effect of the extracted wavelet coefficients.

The fruit sample set in this study contained sixteen tissue samples obtained from fruit with a particular disorder and twenty-two tissue samples obtained from healthy control fruit from the same species and variety. Two typical machine learning methods, principal component regression (PCR) and support vector machine (SVM), were employed to compare the feature extraction effects of four data processing methods including retention time (RT) based vector, compensation voltage (CV) based vector, original data and wavelet coefficients. A 3-fold cross validating method was used to demonstrate the system seperability.

The machine learning results show (1) using PCR, the wavelet coefficients present the highest classification accuracy, (2) employing SVM can increase the classification accuracy based on the RT and CV based sample vectors, but the wavelet coefficients still show the best separation result, and (3) the classification based on the extracted wavelet coefficients does not need to be coupled with a specific machine learning process. In sum, showing the classification accuracy of 93.3%, this study demonstrated 2-D wavelet analysis is a very efficient feature extraction method for 2-D GC/DMS data, keeping the original data topological structure [31]. Although demonstrated in fruit samples, this metabolomics based approach to diagnostics translates very well to human samples as well.

6 Future Trends

In addition to techniques that have already been applied to various types of DMS data sets, there are emerging numerical methods that may be able to aid in transforming this sensing technique so that it may function autonomously for health diagnostics. Two methods that are particularly notable are: (1) various swarm intelligence methods, such as the ant colony algorithm; and (2) the artificial immune system.

Various types of biological learning processes have been mimicked in machine learning. The ant colony algorithm (ACA) is an optimization strategy, mimicking group social behaviour or swarm intelligence. The basic concept of ACA is to use a large number of simple artificial agents (ants) to find the best numerical solution to a problem. Real ants collaborate during their food searching process, by depositing pheromones (a chemical that triggers a collective response of other members in the same colony) on the paths they selected towards a food source. A path which is selected by more ants has more pheromone deposited and consequently this path is more likely to be selected in the next searching step. Eventually, all the ants will choose the same path which usually is the shortest path from their nest to food. In an artificial ant colony based optimization process, a “path” is a candidate solution and the “score” of a selected “path” is determined by a user defined objective function. Generally, a “path” selected by all the artificial ants theoretically would be the optimal solution of this optimization problem. Recently, this technique was used along with wavelet analysis for biomarker selection from SELDI-TOF mass spectrometry data sets on human clinical samples [57]. This

mathematical learning technique may also be useful for DMS data analysis, and would be very interesting to try in future studies.

Another mathematical algorithm that could be very useful for DMS data analysis is the Artificial Immune System (AIS). AIS was recently developed as an artificial intelligence technique which mimics human immune systems that protect our bodies from infectious agents such as viruses and bacteria [58]. There are two types of immunity, innate and adaptive. Innate immunity is directed against any pathogens in the body, so it is called non-specific immunity. Adaptive immunity is for specific invaders and is modified by repeated exposures to such invaders [58, 59]. In brief, when a pathogen invades the body, B cells produce a large number of antibodies to fight against the antigen. Once antibodies are generated that have sufficient affinity to the antigen, B cells rapidly clone and also mutate themselves to have an even closer match to the antigen. This is a rapid proliferation process in which the successive generations of immune cells present an increasingly better match to the antigen. Once the body has successfully defended against a pathogen, a small number of memory cells remain in the body for very long time. In future, they can recognize new antigens that are similar to those that caused immune system responses, so the body response to a future invasion of the same or similar pathogen will be much more efficient than before [59]. A machine learning version of this process would be useful to adapt and analyze real-time DMS clinical data for autonomous detection.

To some extent, most spectral data including DMS data can be considered as a time series data, so digital signal processing methods can be a potential feature extraction and modelling method for spectral data. Auto-regressive (AR) model is a typical feature extraction method for time series data, revealing signal changing trend or pattern. Recently, AR model has been successfully applied to the feature extraction of the GC profiles [60, 61]. Employing a bacterial species classification study in which the headspace of bacterial culture was analyzed using GC/MS, AR model not only presented its feasibility to the normal GC profiles but also showed its advantage over conventional feature extraction methods for the GC profiles with time shifts [60]. As signal shift is also a common problem for GC/DMS data, so we expect AR model would also presents its advantage in the feature extraction of GC/DMS data. By converting GC/DMS data to either retention time or compensation voltage based data, AR model can be easily applied to the output data of GC/DMS to extract pertinent and robust features for data classification or quantitative correlation.

7 Conclusions

DMS systems have seen rapid technology advances over the last decade to reduce their size and increase the sensor performance. The most promising route forward will be continued development of miniature sensor system components, but this almost certainly will need to be done with advanced algorithm development. Together this hardware/software approach is likely to yield small continuously monitoring biomedical diagnostic systems that can be effectively used for autonomous health diagnostics. The DMS holds promise as a powerful diagnostic tool in the

clinical setting. The technology's portability, enormous sensitivity, and potential accuracy make it an attractive modality for office-based clinicians. Once acceptable miniaturization and reproducibility occur, it could replace and improve upon more expensive and laborious diagnostics. More clinical studies with the DMS need to be done in order to understand its potential and competitive advantage over other new sensors. Future studies with the DMS likely will focus on both normal healthy populations and complex disease patients to understand and document endpoint variability through repeated measures over time.

Author Acknowledgements

This work was partially supported by grant number UL1 RR024146 from the National Center for Research Resources (NCRR), a component of the National Institutes of Health (NIH), and NIH Roadmap for Medical Research [NK, CD]. The authors would also like to acknowledge financial support from the Defense Threat Reduction Agency [CD], Gilead Sciences, Inc. [CD], the California Citrus Research Board [CD], Florida Citrus Production Research Advisory Council [CD] and the California Industry-University Cooperative Research Program [CD]. Partial support was also provided by the Mentored Clinical Research Training Program (MC RTP) for trainees [AB, MS].

The contents of this manuscript are solely the responsibility of the authors and do not necessarily represent the official views of any funding agencies.

References

1. Miller, R.A., et al.: A MEMS radio-frequency ion mobility spectrometer for chemical vapor detection. *Sensors and Actuators A: Physical* 91(3), 301–312 (2001)
2. Nazarov, E.G., et al.: Miniature differential mobility spectrometry using atmospheric pressure photoionization. *Analytical Chemistry* 78(13), 4553–4563 (2006)
3. Krylov, E.V., Nazarov, E.G., Miller, R.A.: Differential mobility spectrometer: Model of operation. *International Journal of Mass Spectrometry* 266(1-3), 76–85 (2007)
4. Basanta, M., et al.: Increasing analytical space in gas chromatography-differential mobility spectrometry with dispersion field amplitude programming. *Journal of Chromatography A* 1173(1-2), 129–138 (2007)
5. Eiceman, G.A., et al.: Pattern recognition analysis of differential mobility spectra with classification by chemical family. *Analytica Chimica Acta* 579(1), 1–10 (2006)
6. Kolakowski, B.M., Mester, Z.: Review of applications of high-field asymmetric waveform ion mobility spectrometry (FAIMS) and differential mobility spectrometry (DMS). *Analyst* 132(9), 842–864 (2007)
7. Shvartsburg, A.A., et al.: Ultrafast Differential Ion Mobility Spectrometry at Extreme Electric Fields in Multichannel Microchips. *Analytical Chemistry* 81(15), 6489–6495 (2009)
8. Eiceman, G.A., et al.: Separation of ions from explosives in differential mobility spectrometry by vapor-modified drift gas. *Analytical Chemistry* 76(17), 4937–4944 (2004)
9. Eiceman, G.A.: Detection of explosives by differential mobility spectrometry and GC DMS. *Abstracts of Papers of the American Chemical Society- ANYL* 230, 320 (2005)

10. Morgan, J.T.: Differential mobility spectrometry applications in homeland security, clinical diagnostics and drug discovery. In: ASME International Mechanical Engineering Congress and Exposition, ASME, Chicago (2006)
11. Eiceman, G.A., et al.: Differential mobility spectrometry of chlorocarbons with a micro-fabricated drift tube. *Analyst* 129(4), 297–304 (2004)
12. Borsdorf, H., Nazarov, E.G., Miller, R.A.: Time-of-flight ion mobility spectrometry and differential mobility spectrometry: A comparative study of their efficiency in the analysis of halogenated compounds. *Talanta* 71(4), 1804–1812 (2007)
13. Krebs, M.D., et al.: Detection of biological and chemical agents using differential mobility spectrometry (DMS) technology. *IEEE Sensors Journal* 5(4), 696–703 (2005)
14. Kanu, A.B., Thomas, C.L.P.: The presumptive detection of benzene in water in the presence of phenol with an active membrane-UV photo-ionisation differential mobility spectrometer. *Analyst* 131(9), 990–999 (2006)
15. Schmidt, H., et al.: Microfabricated differential mobility spectrometry with pyrolysis gas chromatography for chemical characterization of bacteria. *Analytical Chemistry* 76(17), 5208–5217 (2004)
16. Prasad, S., et al.: Analysis of bacterial strains with pyrolysis-gas chromatography/differential mobility spectrometry. *Analyst* 131(11), 1216–1225 (2006)
17. Prasad, S., et al.: Analysis of bacteria by pyrolysis gas chromatography-differential mobility spectrometry and isolation of chemical components with a dependence on growth temperature. *Analyst* 132(10), 1031–1039 (2007)
18. Prasad, S., et al.: Constituents with independence from growth temperature for bacteria using pyrolysis-gas chromatography/differential mobility spectrometry with analysis of variance and principal component analysis. *Analyst* 133(6), 760–767 (2008)
19. Cheung, W., et al.: Discrimination of bacteria using pyrolysis-gas chromatography-differential mobility spectrometry (Py-GC-DMS) and chemometrics. *Analyst* 134(3), 557–563 (2009)
20. Ayer, S., Zhao, W.X., Davis, C.E.: Differentiation of Proteins and Viruses Using Pyrolysis Gas Chromatography Differential Mobility Spectrometry (PY/GC/DMS) and Pattern Recognition. *IEEE Sensors Journal* 8(9-10), 1586–1592 (2008)
21. Krebs, M.D., et al.: Novel technology for rapid species-specific detection of *Bacillus* spores. *Biomolecular Engineering* 23(2-3), 119–127 (2006)
22. Davis, C.E.: Spore biomarker detection using a MEMS differential mobility spectrometer. In: *IEEE Transducers Proceedings* (2003)
23. Shnayderman, M., et al.: Species-specific bacteria identification using differential mobility spectrometry and bioinformatics pattern recognition. *Analytical Chemistry* 77(18), 5930–5937 (2005)
24. Lambertus, G.R., et al.: Silicon microfabricated column with microfabricated differential mobility spectrometer for GC analysis of volatile organic compounds. *Analytical Chemistry* 77(23), 7563–7571 (2005)
25. Lambertus, G.R., et al.: Rapid determination of complex mixtures by dual-column gas chromatography with a novel stationary phase combination and spectrometric detection. *Journal of Chromatography A* 1135(2), 230–240 (2006)
26. Rainsberg, M.R., Harrington, P.D.B.: Thermal desorption solid-phase microextraction inlet for differential mobility spectrometry. *Applied Spectroscopy* 59(6), 754–762 (2005)
27. Levin, D.S., et al.: Rapid separation and quantitative analysis of peptides using a new nanoelectrospray-differential mobility spectrometer-mass spectrometer system. *Analytical Chemistry* 78(15), 5443–5452 (2006)

28. Levin, D.S., et al.: Characterization of gas-phase molecular interactions on differential mobility ion behavior utilizing an electrospray ionization-differential mobility-mass spectrometer system. *Analytical Chemistry* 78(1), 96–106 (2006)
29. Levin, D.S., et al.: Using a nanoelectrospray-differential mobility spectrometer-mass spectrometer system for the analysis of oligosaccharides with solvent selected control over ESI aggregate ion formation. *Journal of the American Society for Mass Spectrometry* 18(3), 502–511 (2007)
30. Shvartsburg, A.A., et al.: Ultrafast Differential Ion Mobility Spectrometry at Extreme Electric Fields Coupled to Mass Spectrometry. *Analytical Chemistry* 81(19), 8048–8053 (2009)
31. Zhao, W., et al.: Two-dimensional wavelet analysis based classification of gas chromatogram differential mobility spectrometry signals. *Analytica Chimica Acta* 647(1), 46–53 (2009)
32. Awan, M.A., Fleet, I., Thomas, C.L.P.: Optimising cell temperature and dispersion field strength for the screening for putrescine and cadaverine with thermal desorption-gas chromatography-differential mobility spectrometry. *Analytica Chimica Acta* 611(2), 226–232 (2008)
33. Lu, Y., Harrington, P.B.: Forensic application of gas chromatography - Differential mobility spectrometry with two-way classification of ignitable liquids from fire debris. *Analytical Chemistry* 79(17), 6752–6759 (2007)
34. Rearden, P., et al.: Fuzzy rule-building expert system classification of fuel using solid-phase microextraction two-way gas chromatography differential mobility spectrometric data. *Analytical Chemistry* 79(4), 1485–1491 (2007)
35. Lu, Y., Chen, P., Harrington, P.B.: Comparison of differential mobility spectrometry and mass spectrometry for gas chromatographic detection of ignitable liquids from fire debris using projected difference resolution. *Analytical and Bioanalytical Chemistry* 394(8), 2061–2067 (2009)
36. Molina, M.A., et al.: Design-of-experiment optimization of exhaled breath condensate analysis using a miniature differential mobility spectrometer (DMS). *Analytica Chimica Acta* 628(2), 155–161 (2008)
37. Davis, C.E., et al.: Volatile and non-volatile analysis of biomarkers in human breath using differential mobility spectrometry. *IEEE Sensors Journal* 13(1), 1–9 (2010)
38. Sankaran, S., et al.: Microfabricated differential mobility spectrometers for breath analysis. In: *IEEE Sensors*, Atlanta, GA, pp. 16–19 (2007)
39. Frank, M., et al.: Modular sampling and analysis techniques for real-time analysis of human breath. In: *IEEE Sensors*, Atlanta, GA, pp. 10–13 (2007)
40. Lewis, N.S.: Comparisons between mammalian and artificial olfaction based on arrays of carbon black-polymer composite vapor detectors. *Accounts of Chemical Research* 37(9), 663–672 (2004)
41. Friedrich, M.J.: Scientists Seek to Sniff Out Diseases Electronic “Noses” Someday Be Diagnostic Tools. *Jama-Journal of the American Medical Association* 301(6), 585–586 (2009)
42. Fens, N., et al.: Exhaled Breath Profiling Enables Discrimination of Chronic Obstructive Pulmonary Disease and Asthma. *American Journal of Respiratory and Critical Care Medicine* 180(11), 1076–1082 (2009)
43. Dragonieri, S., et al.: An electronic nose in the discrimination of patients with non-small cell lung cancer and COPD. *Lung Cancer* 64(2), 166–170 (2009)
44. Thaler, E.R., Hanson, C.W.: Use of an electronic nose to diagnose bacterial sinusitis. *American Journal of Rhinology* 20(2), 170–172 (2006)

45. Thaler, E.R., et al.: Use of an electronic nose for detection of biofilms. *American Journal of Rhinology* 22(1), 29–33 (2008)
46. Fend, R., et al.: Prospects for clinical application of electronic-nose technology to early detection of *Mycobacterium tuberculosis* in culture and sputum. *Journal of Clinical Microbiology* 44(6), 2039–2045 (2006)
47. Zhao, W., et al.: Machine learning: a crucial tool for developing sensors. *Algorithms* 1(2), 130–152 (2008)
48. Krebs, M.D., et al.: Two-dimensional alignment of differential mobility spectrometer data. *Sensors and Actuators B-Chemical* 119(2), 475–482 (2006)
49. Liu, Y.H.: Wavelet feature extraction for high-dimensional microarray data. *Neurocomputing* 72(4-6), 985–990 (2009)
50. Akaho, S.: Conditionally independent component analysis for supervised feature extraction. *Neurocomputing* 49, 139–150 (2002)
51. Gualdrón, O., et al.: Variable selection for support vector machine based multisensor systems. *Sensors and Actuators B-Chemical* 122(1), 259–268 (2007)
52. Ochoa, M.L., Harrington, P.B.: Chemometric studies for the characterization and differentiation of microorganisms using *in situ* derivatization and thermal desorption ion mobility spectrometry. *Analytical Chemistry* 77(3), 854–863 (2005)
53. Walczak, B., Wu, W.: Fuzzy warping of chromatograms. *Chemometrics and Intelligent Laboratory Systems* 77(1-2), 173–180 (2005)
54. Alsberg, B.K., et al.: Classification of pyrolysis mass spectra by fuzzy multivariate rule induction-comparison with regression, K-nearest neighbour, neural and decision-tree methods. *Analytica Chimica Acta* 348(1-3), 389–407 (1997)
55. Nazarov, E.G., et al.: Pressure effects in differential mobility spectrometry. *Analytical Chemistry* 78(22), 7697–7706 (2006)
56. Borsdorf, H., Nazarov, E.G., Miller, R.A.: Atmospheric-pressure ionization studies and field dependence of ion mobilities of isomeric hydrocarbons using a miniature differential mobility spectrometer. *Analytica Chimica Acta* 575(1), 76–88 (2006)
57. Zhao, W., Davis, C.E.: Swarm intelligence based wavelet coefficient feature selection for mass spectral classification: an application to proteomics data. *Analytica Chimica Acta* 651(1), 15–23 (2009)
58. Timmis, J., Neal, M., Hunt, J.: An artificial immune system for data analysis. *Biosystems* 55(1-3), 143–150 (2000)
59. Watkins, A.B., Boggess, L.C.: A resource limited artificial immune classifier. In: Proceedings of the, Congress on Evolutionary Computation. CEC 2002, vol. 1/2, vol.xxxvi+2034, pp. 926–931 (2002) (Cat. No.02TH8600)
60. Zhao, W., Davis, C.E.: Autoregressive model based feature extraction method for time shifted chromatography data. *Chemometrics and Intelligent Laboratory Systems* 96(2), 252–257 (2009)
61. Zhao, W., Morgan, J.T., Davis, C.E.: Gas chromatography data classification based on complex coefficients of an autoregressive model. *Journal of Sensors* 1(1), 1–8 (2008)

A Distributed Telemedical System for Monitoring of the Respiratory Mechanics by Enhanced Interrupter Technique

Ireneusz Jabłoński and Janusz Mroczka

Chair of Electronic and Photonic Metrology,
Wrocław University of Technology, Wrocław, Poland

Abstract. The chapter presents the development of a telemedical system. Works have been focused on algorithmic, applied hardware, software and transmission solutions. Modification of classical interrupter method, dedicated to the respiratory mechanics evaluation, has been postulated as a starting point for the whole project. It assumes exploitation of post-occlusional transients states in indirect measurement of physiological properties by solution of the inverse problem, where pressure and flow signals are pre-processed and then fitted to the outputs of reduced model in the time and/or frequency domain. The system consists of a base unit managing users and other devices as well as data transmission, processing, storage and presentation. It co-operates with home-based patient units capable of performing occlusional manoeuvres, tests. All the elements communicate via the Internet, wire or mobile telephony.

Keywords: respiratory mechanics, airflow interrupter technique, telemedical system.

1 Introduction

Ongoing advances in hardware and software technologies, including wireless and mobile communication, lead to the emergence of a new type of healthcare services as telemedicine. Home monitoring of chronically ill patients shows increasing significance within the space of several years to traditional care. Patients using home-based monitoring units experience fewer hospitalizations, acute exacerbations, urgent calls, emergency room visits and lost time from work. Simultaneously, telemedical systems reduce costs of treatment, improve the management of disease and the quality of life. Especially Internet and cellular network based approaches become popular, offering a broad spectrum of data transfer and storage, two-way messaging as well as visualizations, including interactive displays.

Contemporary medical diagnostics in the area of respiratory measurements is before the challenge of proposing the minimal invasive technique for multi-function evaluation of physiological characteristics connected with various

aspects of respiration, e.g. respiratory mechanics, gas exchange, sleep disorders, etc. [10,36,44]. Formal indexing of such properties and processes can be conducted in an on-line or off-line procedure, more or less complicated in hardware and algorithmically. Propositions of the mobile diagnostic devices need the assurance of simplicity both of them, which finally results in easy operation and service by user.

A particular group of patients suitable for home monitoring are those suffering from respiratory diseases as asthma and chronic obstructive pulmonary disease (COPD) [4,7,12,13,19]. The both chronic respiratory diseases comprise a major public health problem: COPD is the fourth leading cause of chronic morbidity and mortality, and is expected to rank fifth worldwide in 2020, whereas the asthma causes the one-third of older people experience significant breathlessness. The popular solution for early detection and managing the breathing problems connected with such changes in respiratory mechanics is spirometry [4,8,37,38]. Nevertheless, there are also other conceptions of concluding about lung function on the basis of pressure and flow measurements, e.g. forced oscillation technique (FOT), impulse oscillometry (IOS) or interrupter technique (IT). They use different excitations, set-up configurations and different regimes of experimental data exploitation [21,32,34,48,51,52,54]. The airflow interruption method is especially interesting in this group, first of all, because of simple measurement assumptions, both algorithmic and hardware, as well [29,33,35,50]. There have been proposed also some modifications of the basic version of IT, renaming the method the enhanced interrupter technique (EIT) [24-26,28], which use more sophisticated and better calibrated theoretical tools to the analysis of standard occlusional data. Introduced changes makes it possible to design a set of portable modules functioning in distributed telemedical system.

The chapter reports in an introductory way the construction of a telemedical system dedicated to the respiratory mechanics monitoring by enhanced interrupter technique. It includes the basics of a classical and enhanced interrupter experiment, issues of mathematical modeling of the respiratory system, software and hardware demands and configurations for the measurement set-up, as well as the first simulation and experimental outcomes.

2 Airflow Interrupter Techniques

Introduced by von Neergard and Wirz [39], the airflow interrupter technique (IT) consists of short-term interruption (about 100 ms; by valve closure) of the airflow at the mouth (Fig.1).

During the occlusion, when the volume flow (Q_{ao}) is falling to zero, there is a rising pressure (P_{ao}) measured simultaneously at the mouthpiece. In this way, based on the most straightforward interpretation [3], the interrupter resistance $R_{int} = \Delta P_{ao}/Q_{ao}$ (Fig. 2) was understood to be the measure of resistance in the airways (R_{aw}). Subsequent analysis [3,29,35,40] showed errors in this approach but has not eliminated the high inaccuracy and significant dispersion in the R_{aw} measurement – the only quantity estimated by this technique.



Fig. 1. A stationary, multi-method system with the option of interrupter measurements (Jaeger, Germany)

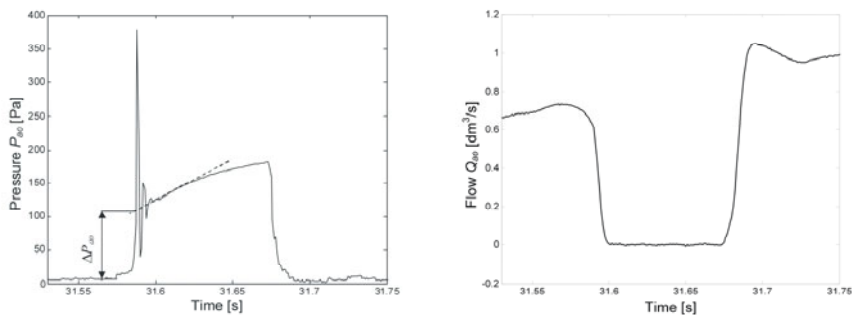


Fig. 2. Pressure (P_{ao}) and flow (Q_{ao}) measured at the mouth during interruption

In spite of unclear interpretation of R_{int} and its limited repeatability, numerous utilitarian advantages still makes the airflow interrupter technique the subject of interests [1,6,31,49]. Simplicity of assumptions finds expression in:

- small invasiveness,
- short time of measurement,
- low hardware requirements,
- minimal requirements regarding patient co-operation,
- small failure frequency,
- low costs of manufacturing,
- easy operation and cheap maintenance.

But there are also the weaknesses of the occlusional procedure, the most important of which are poor and uncertain information about respiratory mechanics evaluated during interrupter experiment. These arguments motivate physician and technician to further work in the domain of postocclusional data exploration. To date, some innovative attempts have been proposed as regards diagnostic factor/-s calculation and standardisation [5,9,18,20,52], but especially interesting are the results of Romero et al. [45] and Frey et al. [14-17] who postulated frequency description of pressure transients observed during flow interruption at the mouth. These research point at possible spreading of diagnostic insight, as the dynamical changes in acquired signals are the symptoms of existing properties and interactions in respiratory system when valve operating.

Incorporation of the transient states observed in postocclusional pressure and flow data (see Fig. 2) has become the leading idea in revision the occlusional methodology applied to the respiratory mechanics measurements. The question is how can we enhance diagnostic power of the interrupter technique without breaking the basic assumptions on non-invasiveness and small hardware requirements? Firstly, the procedure of indirect conclusion about the dynamical properties of the system can be introduced. It involves new, more advanced (and thus reliable) physical-mathematical description (forward complex model and inverse analog) of the physiological object and the measurement equipment and solution of the inverse problem, i.e. elaboration of an identification algorithm for concluding quantitatively about respiratory mechanics with acquired and prepared data set. Secondly, as there is no systematic analysis on experimental occlusional data preparation and processing, both in the time and frequency domain, some metrological conditions and properties of the algorithms should be evaluated and optimised in the future. Above-mentioned arguments are a schedule for construction of the enhanced interrupter technique (EIT), which exploits dynamical changes of pressure and flow during occlusion for conclusion about the system by inverse model identification.

A complex physical-mathematical equivalent of the respiratory system for the interrupter technique has been proposed to enable analysis of the processes during occlusional measurements and then facilitate objective transition to the reduced analog [27,28,43], which hasn't been the subject of investigations so far. Implemented in the Matlab-Simulink environment (The MathWorks, USA), the complex physical-mathematical model consists of six dynamic, lumped parameter submodels representing successive components of the system and a model of the interrupter (Fig. 3).

The well-known analogies between electrical and mechanical/pneumatic systems has been used during modeling, where resistance R is an equivalent of mechanical resistance, capacitance C is analogous to compliance ($C = 1/E$, where E is elastance) and inductance L – inertance in a pneumatic sense is a measure of mass inertia proportional to acceleration. Voltages and currents in that system can be comprehended as pressures (P) and flows (Q), respectively. Detailed description of model creation together with applied values of parameters can be found in [28,43].

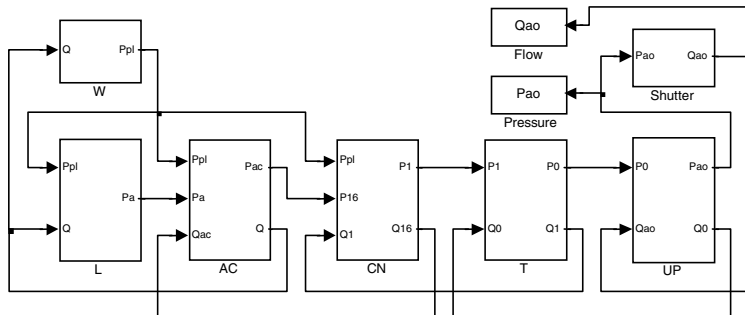


Fig. 3. A Simulink complex model for the respiratory system during airflow interruption, including the chest wall (W), the lung (L), the acinar airways (AC), the convective airways (CN), the trachea (T), the upper airways (UP) and the interrupter (Shutter)

Proposed complex structure of physical-mathematical equivalent has been tested in a full range of conditions, proper for normal, quiet breathing and occlusion at the mouth, both in the time and frequency domain. Example plots of pressure (P_{ao}) and flow (Q_{ao}) outputs were presented in Fig. 4, and Fig. 5 is an exemplification of a theoretical impedance Z_{th} calculated in the model for the parameter values representing normal state in humans.

Measured signals of P_{ao} and Q_{ao} , or their some combination for a chosen time range, can be direct inputs for the identification procedure in the time domain after preliminary preprocessing (e.g. filtering, detrending etc.) [24]. It is not the case in the frequency regime, where the solution of inverse problem needs earlier reconstruction of spectral characteristics of the respiratory system. First proposals for the interrupter technique used a power spectrum density as an indication of transient behaviour of the object in response to a pseudo-step excitation by valve [45]. But then, analogously to the forced oscillation technique, Frey et al. [14,15] have proposed an input impedance (Z_{in}) to be the frequency representative of postocclusional system manifestation. Additionally, experimental findings from [14-17] have revealed preliminarily the potential for spreading the diagnostic insight of IT to the higher frequency range, where some resonant phenomena (proper for the conductive airways) can be observed. On the other hand, Jabłoński and Mroczka have showed in computer simulations [26], that using the complete information from real and imaginary parts of measured Z_{in} improves the quality of model identification in the frequency domain.

In these circumstances, studying and standardisation of the conditions for interrupter impedance reconstruction from measured pressure and flow data seems to be one of the critical points in designing the telemedical system dedicated to the respiratory mechanics measurement. Precise aspects of such analysis in the class of linear systems can be found in (together with the comments on directions for future research) [28,43]. Effectiveness of the algorithms worked out there and applied to the synthetic data simulated in the model from Fig. 3 is depicted in Fig. 5 and Fig. 6.

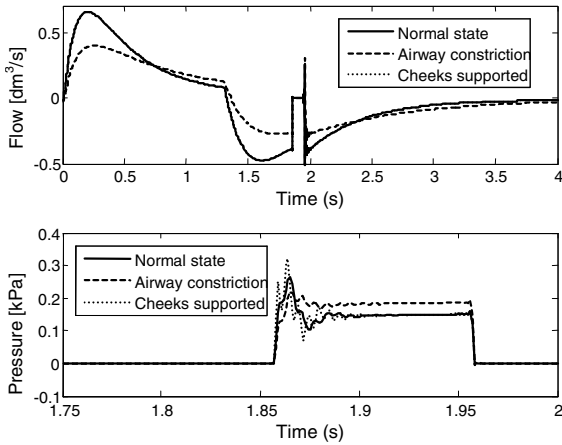


Fig. 4. Synthetic data of flow and pressure generated with the model of the respiratory system during airflow interruption

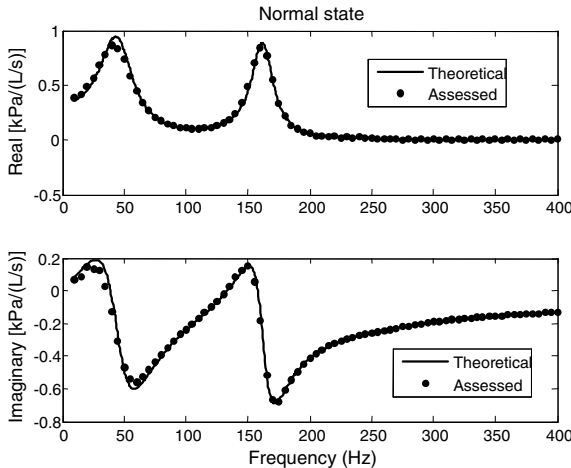


Fig. 5. Comparison of calculated interrupter impedance Z_{int} to theoretical input impedance Z_{th} for normal state of respiratory mechanics

As the complex model usually is elaborated for precise imitation of the real system properties and behaviour it can be a starting point for the procedure of its reduction to the inverse form, which is demanded by identification algorithm. Such reduced, inverse analogue is based on structural and parametrical aggregation of the chosen subsystems and its properties, very often conducted intuitively. It is worth to note here, that there have been used only one- or two-element representations of the respiratory system during the interrupter measurements [3,20,39,41]. The objectivation of the complex model reduction can be ensured by calculation

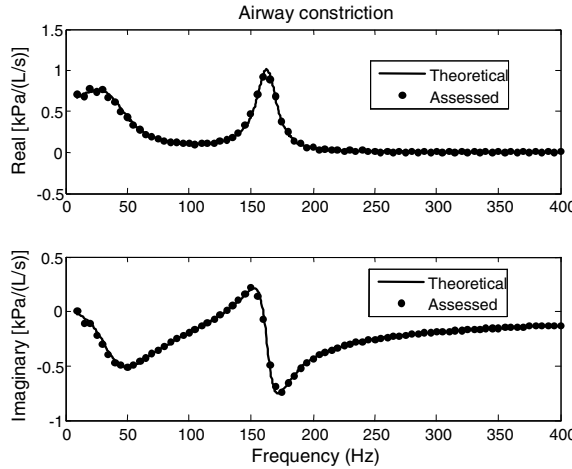


Fig. 6. Comparison of calculated interrupter impedance Z_{in} to theoretical input impedance Z_{th} for the mild constriction of intrathoracic convective airways

its sensitivity (structural and/or parametrical) [23,47]. Analytically, the functions (vectors) of sensitivity \mathbf{x}_k are defined according to (1). Numerically, this operation consists in modification of values of consecutive parameters in the model and registering the changes in output signals (2), which enable to calculate the sensitivity matrix for undertaken object (4). Because absolute values of parameters can differ each other in a real system by some orders, calculation of the relative, normalised sensitivity of output to the parameter values is legitimated and more effective – \mathbf{S}_y matrix (3).

$$x_k(t) = \frac{\partial y(t)}{\partial \theta_k}, \quad \mathbf{x}_k = \frac{\partial \mathbf{y}}{\partial \theta_k} \quad (1)$$

$$x_k = \lim_{\Delta \theta_k \rightarrow 0} \frac{y_m(\theta_k + \Delta \theta_k) - y_m(\theta_k)}{\Delta \theta_k} \approx \frac{y_m(\theta_k + \Delta \theta_k) - y_m(\theta_k - \Delta \theta_k)}{2\Delta \theta_k} \quad (2)$$

$$\begin{aligned} s_y(i, j) &= \frac{\partial y_i}{\partial \theta_j} \theta_j, \\ \mathbf{S}_y^{n \times p} &= \mathbf{X} \operatorname{diag}(\boldsymbol{\theta}), \end{aligned} \quad (3)$$

where the sensitivity matrix for the value of parameters:

$$\mathbf{X}^{n \times p} = \frac{\partial \mathbf{y}}{\partial \boldsymbol{\theta}} = [\mathbf{x}_1 \quad \mathbf{x}_2 \quad \dots \quad \mathbf{x}_p] = \begin{bmatrix} x_{11} & \cdots & x_{p1} \\ \vdots & \ddots & \vdots \\ x_{1n} & \cdots & x_{pn} \end{bmatrix}. \quad (4)$$

In a case of reduction of the complex model for the airflow interruption technique we can place the subjective level of importance of succeeding parameters at different levels in displayed sensitivity output changes. This decides about diversity of ranges in model aggregation, which means that the resulting inverse equivalents can offer various insights into the physiological system properties and behaviour. Sensitivity functions calculated for the structure depicted in Fig. 3 provide the two candidates for the inverse models of airflow interruption (Fig. 7), more or less precise in reality projection.

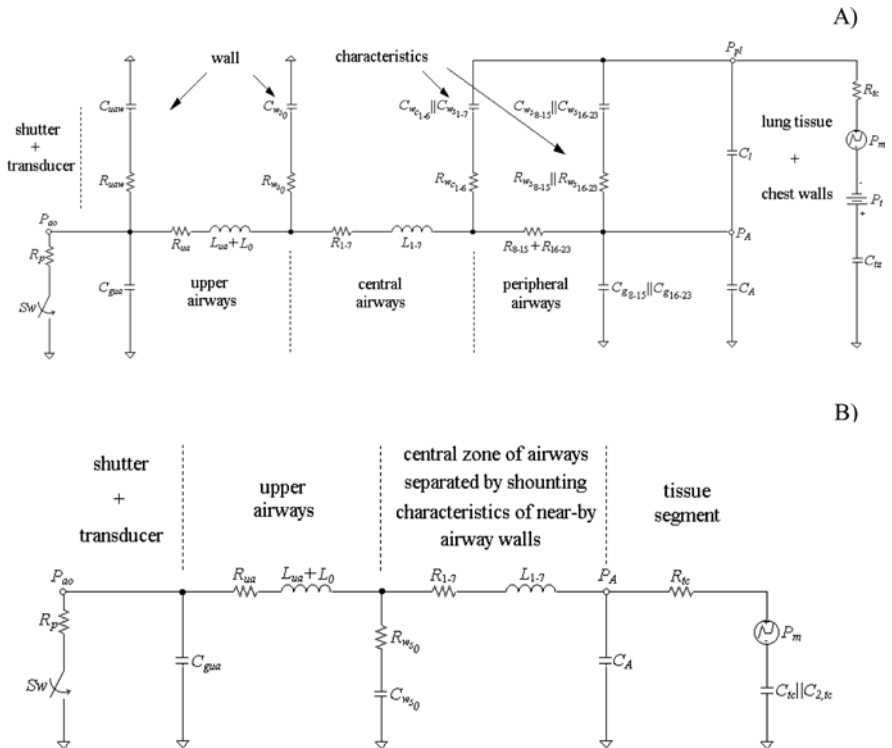


Fig. 7. Reduced inverse models for the respiratory system during airflow interruption with described parameter aggregations [23]

Resulting electrical analogues (Fig. 7 A and B) correspond to the propositions of simplified descriptions of the respiratory system for the other techniques, e.g. to the models used by Rotger et al. [46] and DuBois et al. [11], respectively. They were also used during author's verifications of the conceptions proper for the occlusional algorithms [24-26]. Summarising their expressions it can be stated that some detailed properties in a range of consecutive segments of the complex model are now represented by cumulative ones, characteristic of the tissue compartment, central and peripheral zones of the bronchial tree, upper airways plus the equivalent of interrupter.

The next question is the identifiability of the inverse models. As the enhanced interrupter technique is designed as a fusion-like algorithm, where there are some influences of information from each of the time and frequency domain, various arguments and rules can be used during inference, finally. For example, it is possible to construct mixed parametric-nonparametric, time-frequency identification algorithm based on the time (P_{ao} , Q_{ao}) and frequency (input interrupter impedance – Z_{int}) outputs. Such procedure stands for the area of future research in the undertaken topic. At this level, the minimisation of the criterion function is proposed, where the chosen outputs from the inverse model (\mathbf{y}_m) and measured experimentally (\mathbf{y}) are fitted:

$$\hat{\boldsymbol{\theta}} = \arg \min_{\boldsymbol{\theta}} (\mathbf{y} - \mathbf{y}_m)^T \mathbf{R}_y (\mathbf{y} - \mathbf{y}_m), \quad (5)$$

where \mathbf{R}_y represents covariant matrix of output signal disturbances.

In a case of nonlinear models, it can be boiled down to the application of iterative algorithm, which is typical also for the respiratory mechanics measurements [34,53]. There are certain methods designed for searching minimum of the criterion function, whose directions can be defined generally as:

$$\begin{aligned} \hat{\boldsymbol{\theta}}^{(i+1)} &= \hat{\boldsymbol{\theta}}^{(i)} - \mu_i \mathbf{M}_i^{-1} \nabla_{\boldsymbol{\theta}} V^{(i)}, \\ \nabla_{\boldsymbol{\theta}} V^{(i)} &= \frac{\partial V(\hat{\boldsymbol{\theta}}^i)}{\partial \boldsymbol{\theta}}, \end{aligned} \quad (6)$$

where: $\boldsymbol{\theta}$ – vector of the unknown parameters, μ – the step size, \mathbf{M} – matrix modifying of the search direction and V – the criterion function. As was showed exemplarily in [24,26], both of the structures from Fig. 7 can be identified quite reliably, which makes the indirect interrupter measurement possible in the time and frequency domain. Some dedicated tools can be helpful in such inverse problem solution, i.e. combining parameter selection with ridge regression [42].

3 Architecture of Telemedical System

A telemedical system dedicated to the interrupter measurements is devoted to patients suffering from chronic diseases as asthma, chronic obstructive pulmonary disease (COPD) etc. The special groups of users establish persons whose physiological limitations or consciousness can't afford important co-operation with the medical staff or forced expiration manoeuvres. Practical application of the device in newborns and early childhood is additional motivation for the innovative works in this area.

Designed system consists of home-based economical patients units cooperating with a base medical unit (Fig. 8).

Each of the home units is equipped with an interrupter set as an standard accessory, enabling time (P_{ao} , Q_{ao} , airway resistance (R_{int})) as well as frequency (input respiratory impedance - Z_{int}) characteristics measurements. Additionally, the home unit can also act as a digital recorder of parameters coming from external

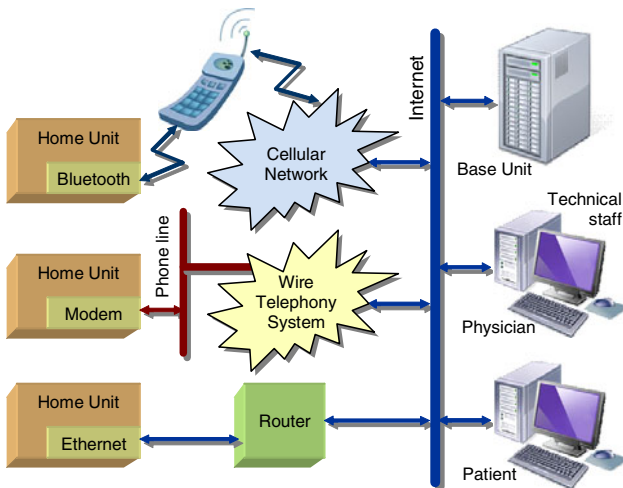


Fig. 8. A block diagram of the telemedical system structure

instruments, as e.g. a pulsoximeter. The base unit serves for managing the whole system, interchanging information and receiving data from the home units, storing test results in a database, automatic data analyzing, and generating required visualizations. The home units make contact with the base unit via the Internet. However, taking into account the diversity of telecommunication media available in different regions of East European countries still developing their infrastructures, the data can be sent using either Ethernet, wire telephony line or a cellular network. The system works under control of software applications with user-friendly, interactive graphical interfaces. The users as patients, physicians and technical staff can exploit the system resources via own computers connected to the Internet using web browsers. Additionally, the system should comply with appropriate standards as IEC60601.

4 Home-Based Patient Unit

The home unit is built with a low-cost embedded development system (NGW100, Atmel) as a core part (Fig. 9). It includes, among others, a 32-bit AVR processor running at 140 MHz, 32MB SDRAM, 16MB on-board flash, memory expandable by memory cards, USB connection and Ethernet controller.

The system has been supplemented with three groups of peripheral devices fulfilling functions of a user interface, additional communication controllers, and interfaces for medical transducers. The user interface includes an LCD alphanumerical display and a simple keyboard. These components, together with some other peripherals, run under control of an additional 8-bit AVR microprocessor. A patient can interact with the unit using a context menu, reading short messages from the LCD, and pressing appropriate buttons.

Two additional communication modules have been integrated with the system, enabling connection between the home and base units by wire telephone line or a mobile phone. In the former case an analog modem mediates between the home unit and the wire telephony system, and in the latter one a short-range Bluetooth link is used to couple the unit with the phone connected to a cellular network by a GPRS/EDGE service.

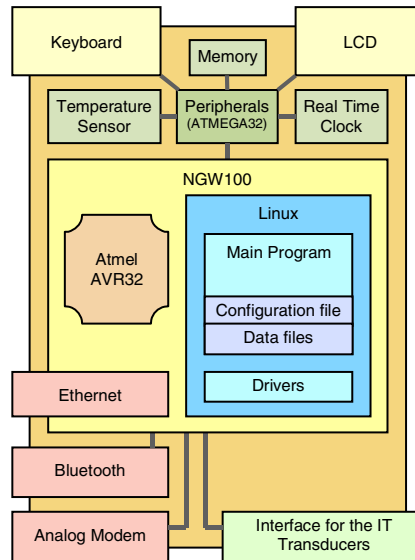


Fig. 9. A block diagram of the home unit

The home unit is adapted to cooperate with an interrupter set. It consists of a shutter combined with flow and pressure transducers. The shutter interrupts expiratory flow producing the change of pressure, and both the signals are sampled by 12-bit A/D converter at 500, 1000 or 5000 Hz (depending on user preferences). Sample frequency can be optional in the test version, but to facilitate the exploitation of final home unit one option will be applied (the best for diagnostic inference – according to the trial observations, e.g. 1000 Hz). The samples are analyzed online and placed in a memory via a DMA controller. The data are labeled with a number and a current time.

The home unit works under control of the Linux operating system. All the firmware components have been written in the C programming language. They include, among others, drivers for the additional peripheral devices, the main program and its procedures, as well as a configuration file. Measurement data from the medical examinations are stored in the internal memory (up to 100 complete tests) and sent on patient's request to a database located in the system base unit via the Internet.

The prototype version of the home unit was shown in Fig. 10. Additional peripherals (e.g. flow transducer) and dedicated software were supplied in this case

for author's research, which is important for final optimisations of hardware-software set-up and work modes, according to the new procedures of enhanced interrupter technique. In this trial version commercially available IT transducers were used (interrupter head produced by Micro Medical Ltd., United Kingdom). As the question of valve speed and leakage is important for interrupter observations [30], joining of other solutions of shutter heads to the test version of home unit is currently considered.



Fig. 10. A prototype of the home unit

It is plenty of unsolved issues connected with occlusional measurement of the respiratory mechanics, which need to be analysed and explained currently. Many of them concern the hardware properties and their influence on experimental observations. These issues trigger and shape the schedule of the works, and strictly apply to the arranged control procedures of prototype device (Fig. 11).

Apart from the physical-mathematical representations of the respiratory system, very important issue for a reliable medical diagnostics is to reconstruct the whole measurement path of designed experiment. It concerns the nature of the physiological system, properties of the measurement set-up and peculiarity of the theoretical tools used for signal processing, as well. Engineer endeavour to acquire raw data, without any in-between stages of processing of information contained in the signal/-s (e.g. filtration, constant trend removing, compensation, etc.), is an adequate direction in fulfilling the condition. The research module of home-based patient unit with its control panel is an example of such attempt (Fig. 11). It is possible to monitor and control in it many of the basic components influencing the observations in interrupter strategy. Finally, we can also write in file and export the state variables to the other programming environments (to further processing), both in nominal basic units (electrically, in LSB) and after transformation according to the physiological nomenclature. The construction of the research module enables testing the valves and transducer properties (mechanical and electrical) in diagnostic findings, establish optimal measurement protocol for the enhanced

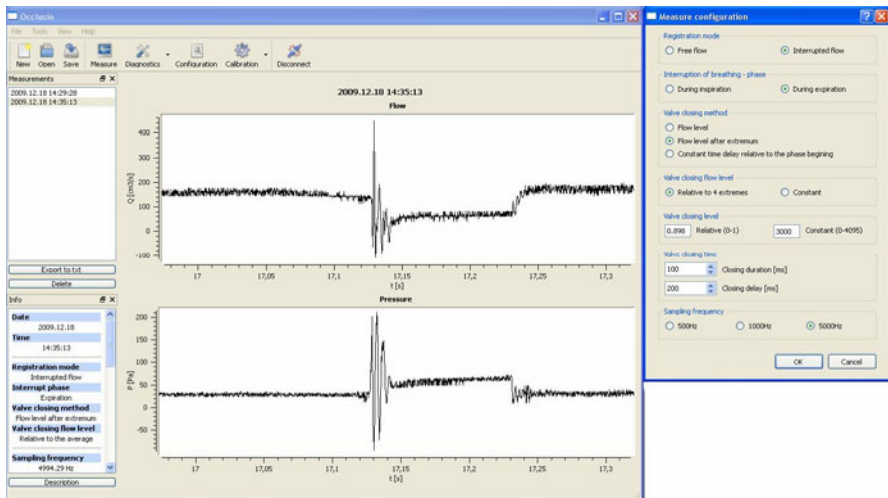


Fig. 11. The main control panel of the prototype of interrupter device designed for a wide-range experimental research

interrupter technique by studying various modes of occlusional valve work: airflow interruption during inspiration or expiration [5], duration time of occlusional manoeuvre, relation between sample frequency and the quality of model identification. General diagnostics concerning the level of energy in battery used for valve operation or pressure and flow sensors testing and calibration is also possible. Configuring the measurement mode, we can analyse character of relations between respiratory airflow and diagnostic parameters evaluations, which is the vivid question for the airflow interrupter technique. The outcomes, i.e. raw pressure (P_{ao}) and flow (Q_{ao}) data are invaluable and objective source of recording of interaction manifestation between the physiological system and measurement set-up.

5 Base Unit System

The base unit system is responsible for communication with the home units, medical data acquisition, storage of the data, processing raw measurements, graphical presentation of the system resources to the users, as well as management of patients, physicians and home units.

Generally, it consists of four main layers: acquisition, data, processing and presentation ones (Fig. 12). The system communicates with the Internet using the secure HTTPS protocol.

A. Acquisition layer

The acquisition server exchanges information with the home units sending configuration files and receiving medical data, and then places the test results in the central database. A created servlet makes a preliminary validation of packets

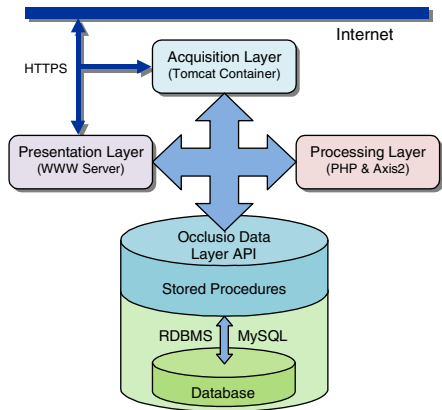


Fig. 12. A block diagram of the base unit system

coming from the home units, parameterizes data and sends them to the *Occlusio Data Layer Application Programming Interface (API)*. The acquisition layer has been implemented using the Tomcat Servlet/JSP Container (Apache).

B. Data layer

The data layer governs information covering patients, physicians, technical staff and home units data as well as the results of medical tests (spirometry and interrupter data). Specific patients are coupled with a given home unit and each of physicians is associated with the patients she/he takes care of. A special interface *Occlusio Data Layer API*, consisting of a few dozens of procedures, has been defined for the maintenance of the layer by applying the stored procedures mechanism. Additional programs provide other functionalities, as e.g. patient or home unit registration by separate Java-based applications. The database has been created using the open source Relational Database Management System (RDBMS) MySQL. It is also supplied with the PHP interface for the web applications.

C. Presentation layer

The presentation layer is organized as a WWW service. Its role consists in making the database information available to the three types of entitled users, defined in the database: patients, physicians and members of technical staff. The exploitation of the service is possible after the authentication of a user by login procedure. The patients are allowed to browse only their own examination results and the physicians have access merely to their patients' data. The entitled members of the staff may administrate the system or/and register and modify patients' and home units' data. Beside these dedicated functions, the service presents a general information about the *Occlusio* system accessible for all web users.

The service offers four types of graphical, interactive documents: general, patient, physician and technical staff ones. All the documents have the same structure consisting of four elements: header, menu, basic content and footnote.

Depending on the menu selection, in the basic content display the user can e.g. browse through a list of registered medical tests, choose and watch the results of specific examination, or access the visualization of trends.

The service has been built using HTML documents created dynamically by PHP scripts running on the WWW server. Simultaneously some JavaScript scripts built in the documents are executed at the client side by applying AJAX technology that allows asynchronous communication with the server, enhancing the interactivity of the WWW pages.

D. Processing layer

Only raw results of the medical tests are held in the database, reducing its size. Once a page displaying a specific examination is called, adequate indices characterizing this test are calculated according to their definitions using PHP scripts and web services deployed on the Axis2 core engine (Apache), visualized and kept on the WWW server to the end of a session.

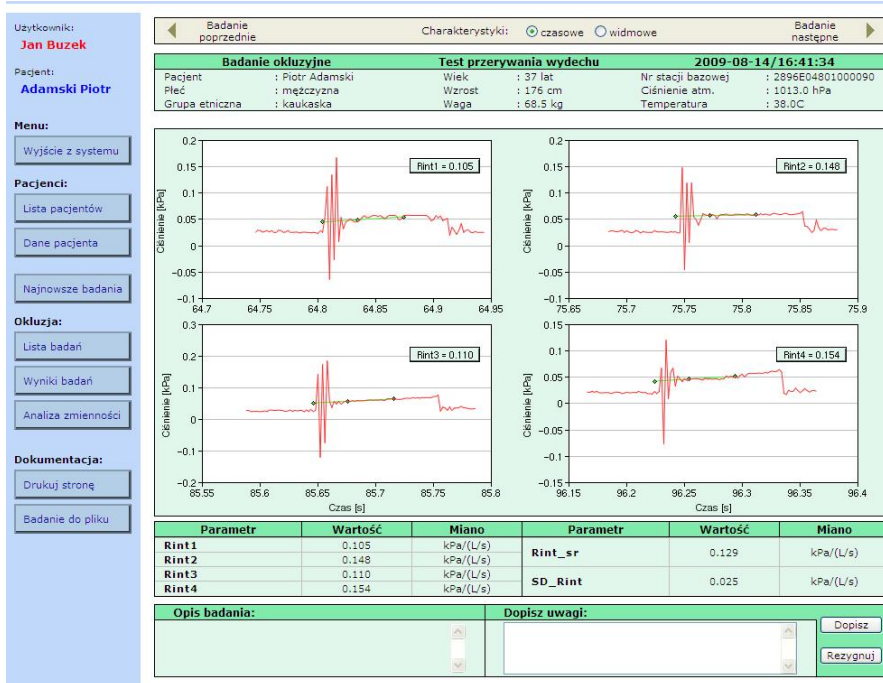


Fig. 13. Example results (patient and measurement set-up characteristics, P_{ao} pressure plots, numerical data) for the classical interrupter procedure obtained in the telemedical system; the time domain $Rint_1 \dots Rint_4$ were evaluated for the four consecutive interruptions and sampling frequency $f_s = 500$ Hz and then averaged to $Rint_{sr}$ (standard deviation SD_{Rint} was also calculated for such measurement)

6 Example Results

The presentation interface designed in the project enables data inspection according to the status of the user. Communication in Polish language used at this level is justified to the preferences of national medical environments (patients, technical staff and doctors), where the system will be tested. Consecutive measurements can be listed in a time range defined by the user or considered individually. This opens the possibility to follow time trends in diagnostic indexes (look through the history and development of disease) or look into the physiological system state at the moment (Fig. 13–Fig. 15).

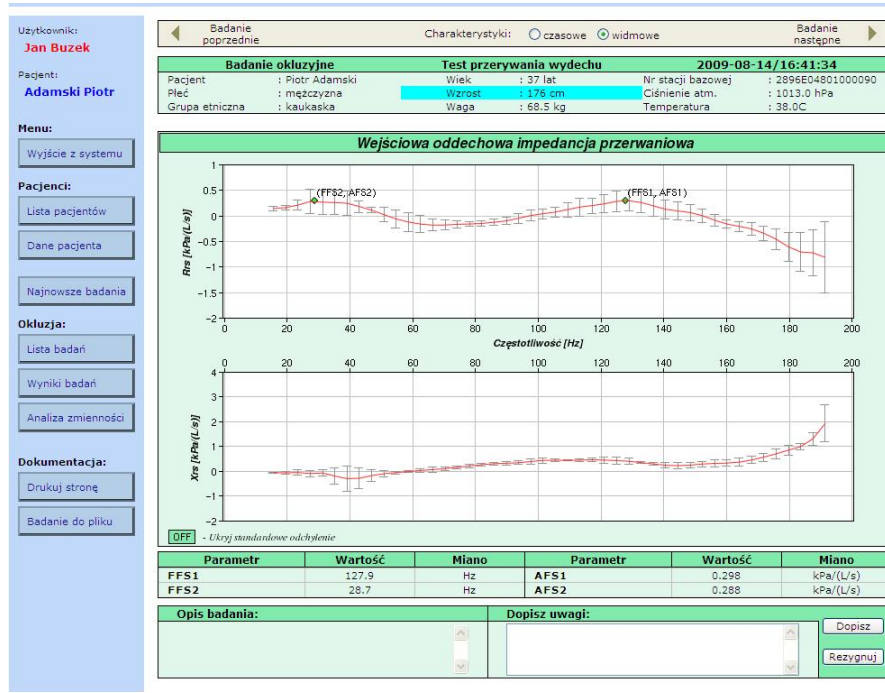


Fig. 14. Example plots of real (R_{rs}) and imaginary (X_{rs}) parts of input interrupter impedance Z_{int} with characteristic quantities (FFS1, AFS1, FFS2 – frequencies and amplitudes of dominant and secondary antiresonances, respectively) measured with the telemedical system

Graphical interface has been divided into three parts. Left, vertical panel gives information about names of user and patient and enables managing the menu of the presentation layer (patient list, patient's data, the latest results of measurement, list of measurements, results of measurements, variability of diagnostic indexes in time, printing the page, writing results to the ASCII file). The choice between time and frequency analysis is possible by diodes placed in heading frame; there is also

possible to skip forward and back here in consecutive measurements. Beneath upper information frame (short list of actual patient data: name, gender, race, age, height, weight, the number of home-based patient unit and atmospheric conditions: temperature, atmospheric pressure), there are the plots of characteristic trends and list of values for calculated diagnostic indexes. At the bottom, a section for writing down physician comments is placed.

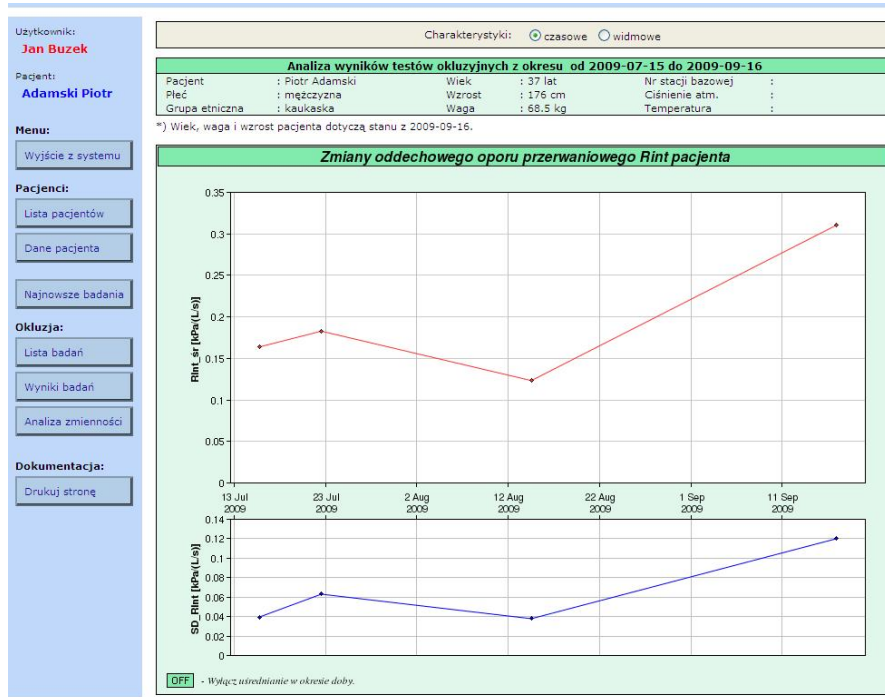


Fig. 15. Example plots of Rint and SD_Rint variability in time observed with the telemedical system

Presented example results are only demonstrative as regards the possibility of respiratory mechanics exploration in the time and frequency domain during enhanced interrupter experiment. Calculated indexes ought to be comprehended as the part of wider analysis proposed by the enhanced interrupter technique, where even more precise parametric description is offered.

At present, advanced works on construction of the whole telemedical system are at the level of optimal identification experiment design, which would exploit parametric and nonparametric, time and frequency characteristics measured in occlusional protocol [2,22]. The diagnostic potential of the basic enhanced interrupter algorithm, reliability and security of data transfer in the system are tested in the meantime. The separate issue will be to interpret the diagnostic factors measured in EIT. It requires additional studies in the future, combining technical

solutions with medical knowledge. These all circle the general directions for indispensable work to finalise the project on construction the distributed telemedical system for monitoring the respiratory mechanics by the enhanced interrupter technique. Unsolved issues include theoretical and practical questions from various areas of knowledge and determine the development in a wide range of disciplines of science.

7 Conclusion

New technologies are very useful in the remote care for patients at their homes, reducing costs, improving the management of disease and the quality of life. We have developed a telemedical system for monitoring patients suffering from chronic respiratory diseases, achieving the main objectives as lung test self-performing, transmitting patient data, processing, storage and presenting the test results, as well as remote managing of the overall system. The adaptation of microcontroller-based, relational database and web technologies enhances easy interaction between the system and the users, including both patients and physicians.

There are the two question depicted in the chapter: algorithmic (the occlusional methods) and straightly connected with the telemedical system designing. Advances in the interrupter technique diagnostics concern the exploitation of transient states in enhancing the information about the respiratory system, deduced in classical IT experiments. This algorithm is easy in hardware-software implementation and offers many advantages, e.g. easiness in device operation, which is especially important in telemedical solutions. Finally, our work postulates the two-sided practical good – independent, wearable diagnostic unit, which can work in the tele-/medical system architecture as home-based patient unit. Project of both, the prototype of diagnostic interrupter device and the telemedical system supported by it, has been reported. Each component needs to be still developed and optimized.

In the next stage we plan to validate separately the prototype of interrupter device (home-based patient unit) and the whole system. Such procedure assumes performing adequate tests of the all components, beginning from medical signal acquisition and electromedical safety, through communication correctness, to the efficiency of database and system management. Produced the portable interrupter device can be also a source of new facts on the interrupter measurement, and to explore this question we supplied the prototype version with many functionalities, which make future considerations more flexible. The gained experiences will be utilized to improve the system before it can be finally put into practice in a real-life healthcare environment.

References

1. Adams, A.M., Olden, C., Wertheim, D., Ives, A., Bridge, P.D., Lenton, J., Seddon, P.: Measurement and repeatability of interrupter resistance in unsedated newborn infants. *Pediatric Pulmonology* 44, 1168–1173 (2009)

2. Akçay, H., Ninnnes, B.: Rational basis functions for robust identification from frequency and time-domain measurements. *Automatica* 34, 1101–1117 (1998)
3. Bates, J.H.T., Baconnier, P., Milic-Emili, J.: A theoretical analysis of interrupter technique for measuring respiratory mechanics. *Journal of Applied Physiology* 64, 2204–2214 (1988)
4. van den Bemt, L., Schermer, T., Smeele, I., Bischoff, E., Jacobs, A., Grol, R., van Weel, C.: Monitoring of patients with COPD: a review of current guidelines' recommendations. *Respiratory Medicine* 102, 633–641 (2008)
5. Bridge, P.D., McKenzie, S.A.: Airway resistance measured by the interrupter technique: expiration or inspiration, mean or median? *European Respiratory Journal* 17, 495–498 (2001)
6. Bridge, P.D., Wertheim, D., Jackson, A.C., McKenzie, S.A.: Pressure oscillation amplitude after interruption of tidal breathing as an index of change in airway mechanics in preschool children. *Pediatric Pulmonology* 40, 420–425 (2005)
7. Bruderman, I., Abboud, S.: Telespirometry: novel system for home monitoring of asthmatic patients. *Telemedicine Journal* 3, 127–133 (1997)
8. Celli, B.R.: The importance of spirometry in COPD and asthma: effect on approach to management. *Chest* 117, 15S–19S (2000)
9. Child, F., Clayton, S., Davies, S., Fryer, A.A., Jones, P.W., Lenney, W.: How should airways resistance be measured in young children: mask or mouthpiece? *European Respiratory Journal* 17, 1244–1249 (2001)
10. Corbishley, P., Rodriguez-Villegas, E.: Breathing detection: towards a miniaturized, wearable, battery-operated monitoring system. *IEEE Transactions on Biomedical Engineering* 55, 196–204 (2008)
11. DuBois, A.B., Brody, A.W., Lewis, D.H., Burgess Jr., B.F.: Oscillation mechanics of lungs and chest in man. *Journal of Applied Physiology* 8, 587–594 (1956)
12. Finkelstein, J., Cabrera, M.R., Hripcak, G.: Internet-based home asthma telemonitoring: can patients handle the technology? *Chest* 117, 148–155 (2000)
13. Finkelstein, J., O'Connor, G., Friedmann, R.H.: Development and implementation of the home asthma telemonitoring (HAT) system to facilitate asthma self-care. *Studies in Health Technology and Informatics* 84, 810–814 (2001)
14. Frey, U., Kraemer, R.: Oscillatory pressure transients after flow interruption during bronchial challenge test in children. *European Respiratory Journal* 10, 75–81 (1997)
15. Frey, U., Schibler, A., Kraemer, R.: Pressure oscillations after flow interruption in relation to lung mechanics. *Respiration Physiology* 102, 225–237 (1995)
16. Frey, U., Silverman, M., Kraemer, R., Jackson, A.C.: High-frequency respiratory input impedance measurements in infants assessed by the high speed interrupter technique. *European Respiratory Journal* 10, 148–158 (1998)
17. Frey, U., Suki, B., Kraemer, R., Jackson, A.C.: Human respiratory input impedance between 32 and 800 Hz, measured by interrupter technique and forced oscillations. *Journal of Applied Physiology* 82, 1018–1023 (1997)
18. Gappa, M., Colin, A.A., Goetz, I., Stocks, J.: Passive respiratory mechanics: the occlusion techniques. *European Respirator Journal* 17, 141–148 (2001)
19. Gibson, P.G.: Outpatient monitoring of asthma. *Current Opinion in Allergy and Clinical Immunology* 2, 161–166 (2002)
20. Goetz, I., Hoo, A.F., Loom, S., Stocks, J.: Assessment of passive respiratory mechanics in infants: double versus single occlusion. *European Respiratory Journal* 17, 449–455 (2001)

21. Green, J., Chiang, S.T., Yang, Y.C.: Improved computation of respiratory resistance as measured by transiently increased resistance. *Medical & Biological Engineering & Computing* 28, 50–53 (1990)
22. Inanc, T., Sznaier, M., Parrilo, P., Sanchez Pena, R.S.: Robust identification with mixed time/frequency-domain experiments and parametric/nonparametric models: theory and an application. *IEEE Transaction on Control Systems Technology* 9, 608–617 (2001)
23. Jabłoński, I.: A metrological analysis of the airflow interrupter technique for properties characterisation of the respiratory system. Wroclaw University of Technology, Poland, PhD thesis (in Polish) (2004)
24. Jabłoński, I., Mroczka, J.: Computer-aided evaluation of a new interrupter algorithm in respiratory mechanics measurement. *Biocybernetics and Biomedical Engineering* 26, 33–47 (2006)
25. Jabłoński, I., Mroczka, J.: Interrupter valve kinematics in the issues of parameter estimation of the respiratory system model. *Metrology and Measurement Systems* 14, 339–350 (2007)
26. Jabłoński, I., Mroczka, J.: Frequency-domain identification of the respiratory system model during the interrupter experiment. *Measurement* 42, 390–398 (2009)
27. Jabłoński, I., Polak, A.G., Mroczka, J.: A complex mathematical model of the respiratory system as a tool for the metrological analysis of the interrupter technique. In: *IMEKO XIX World Congress: fundamental and applied metrology*, Lisbon, Portugal (2009)
28. Jabłoński, I., Polak, A.G., Mroczka, J.: A preliminary study on the accuracy of respiratory input impedance measurement using the interrupter technique. *Computer Methods and Programs in Biomedicine* (submitted, 2010)
29. Jackson, A.C., Milhorn Jr., H.T., Norman, J.R.: A reevaluation of the interrupter technique for airway resistance measurement. *Journal of Applied Physiology* 36, 264–268 (1974)
30. Kessler, V., Mols, G., Bernhard, H., Haberthür, C., Guttmann, J.: Interrupter airway and tissue resistance: errors caused by valve properties and respiratory system compliance. *Journal of Applied Physiology* 87, 1546–1554 (1999)
31. Kivastik, J., Talts, J., Primhak, R.A.: Interrupter technique and pressure oscillation analysis during bronchoconstriction in children. *Clinical Physiology and Functional Imaging* 29, 45–52 (2009)
32. Lausted, C.G., Johnson, A.T.: Respiratory resistance measured by an airflow perturbation device. *Physiological Measurement* 20, 21–35 (1999)
33. Liistro, G., Stănescu, D., Rodenstein, D., Veriter, C.: Reassessment of the interruption technique for measuring flow resistance in humans. *Journal of Applied Physiology* 67, 933–937 (1989)
34. Lutchen, K.R., Giordanella, C.A., Jackson, A.C.: Inability to separate airway from tissue properties by use of human respiratory input impedance. *Journal of Applied Physiology* 68, 2403–2412 (1990)
35. Mead, J., Whittenberger, J.L.: Evaluation of airway interruption technique as a method for measuring pulmonary air-flow resistance. *Journal of Applied Physiology* 6, 408–416 (1954)
36. Menzies, D., Nair, A., Lipworth, B.J.: Portable exhaled nitric oxide measurement: Comparison with the “gold standard” technique. *Chest* 131, 410–414 (2007)

37. Morlion, B., Knoop, C., Paiva, M., Estenne, M.: Internet-based home monitoring of pulmonary function after lung transplantation. *American Journal of Respiratory and Critical Care Medicine* 165, 694–697 (2002)
38. Morlion, B., Polak, A.G.: Simulation of lung function evolution after heart-lung transplantation using a numerical model. *IEEE Transactions on Biomedical Engineering* 52, 1180–1187 (2005)
39. Neergaard, J., von, W.K.: Die Messung der Strömungswiderstände in den Atemwegen des Menschen, insbesondere bei Astma und Emphysem. *Zeitschrift für Klinische Medizine* 105, 51–82 (1927)
40. Otis, A.B., Proctor, D.F.: Measurement of alveolar pressure in human subjects. *American Journal of Physiology* 152, 106–112 (1948)
41. Phagoo, S.B., Watson, R.A., Pride, N.B., Silverman, M.: Accuracy and sensitivity of the interrupter technique for measuring the response to bronchial challenge in normal subjects. *European Respiratory Journal* 6, 996–1003 (1993)
42. Polak, A.G.: Indirect measurements: combining parameter selection with ridge regression. *Measurement Science and Technology* 12, 278–281 (2001)
43. Polak, A.G., Jabłoński, I., Mroczka, J.: Measurement of respiratory input impedance using the interrupter technique – a model study. In: Proc. 7th IFAC Symposium on Modelling and Control in Biomedical Systems, Aalborg, Denmark (2009)
44. Polak, A.G., Wysoczański, D., Mroczka, J.: A multi-method approach to measurement of respiratory mechanics. *Metrology and Mesurement Systems* 13, 3–17 (2006)
45. Romero, P.V., Sato, J., Shardonofsky, F., Bates, J.H.T.: High frequency characteristics of respiratory mechanics determined by flow interruption. *Journal of Applied Physiology* 69, 1682–1688 (1990)
46. Rotger, M., Peslin, R., Duvivier, C., Navajas, D., Gallina, C.: Density dependence of respiratory input and transfer impedances in humans. *Journal of Applied Physiology* 65, 928–933 (1988)
47. Saltelli, A., Chan, K., Scott, E.M.: Sensitivity analysis. John Wiley & Sons, New York (2000)
48. Schmidt, M., Foitzik, B., Hochmuth, O., Schmalisch, G.: In vitro investigations of jet-pulses for the measurement of respiratory impedance in newborns. *European Respiratory Journal* 14, 1156–1162 (1999)
49. Seddon, P., Wertheim, D., Bridge, P., Bastian-Lee, Y.: How should we estimate driving pressure to measure interrupter resistance in children? *Pediatric Pulmonology* 42, 757–763 (2007)
50. Sly, P.D., Lombardi, E.: Measuerment of lung function in preschool children using the interrupter technique. *Thorax* 58, 742–744 (2003)
51. Sobol, B.J.: A simple rapid technique for assessing airway resistance during quiet breathing. *The Americal Review of Respiratory Disease* 102, 970–974 (1970)
52. Sobol, B.J.: A simplified approach to the measurement of total respiratory impedance. *The American Review of Respiratory Disease* 102, 280–281 (1970)
53. Suki, B., Yuan, H., Zhang, Q., Lutchen, K.R.: Partitioning of lung tissue response and inhomogeneous airway constriction at the airway opening. *Journal of Applied Physiology* 82, 1349–1359 (1987)
54. Vogel, J., Schmidt, U.: Impulse oscillometry: analysis of lung mechanics in general practice and the clinic, epidemiological and experimental research. pmi-Verl.-Gruppe, Frankfurt am Main (1994)

Nonlinear Dynamics, Materials and Integrated Devices for Energy Harvesting in Wearable Sensors

Bruno Andò¹, Salvatore Baglio¹, Marco Ferrari², Vittorio Ferrari²,
Luca Gammaitoni³, and Carlo Trigona¹

¹ DIEES, Engineering Faculty, University of Catania, V.le A. Doria, 6, Catania, Italy

² Department of Information Engineering, University of Brescia,
Via Branze 38, Brescia, Italy

³ INFN Sezione di Perugia, Via A. Pascoli, 1 – 06100 Perugia, Italy

Abstract. Several kinds of energy are available in the environment such as sunlight power, thermal gradients, wind, rain, tides, acoustic, and mechanical vibrations. This energy can be exploited to power electronic devices by means of suitable conversion mechanisms. Specifically, in the case of wearable device the need for onsite energy production emerges for the sake of both battery recharge and powering of sensors and electronics.

In this chapter a review of power harvesting methodology is presented along with two examples of devices implementing advanced energy harvesting.

Keywords: energy harvesting, kinetic energy, piezoelectric, non linear mechanism, MEMS.

1 Introduction to Devices for Energy Harvesting

Energy harvesting materials, renewable power sources, scavenging techniques and autonomous sensor nodes that save energy from the environment, have emerged as a prominent research area and continues to grow at rapid pace. Sources of power generation have the potential to significantly augment and, in the longer term, supplant electricity generating systems (based on fossil fuels and nuclear power). However, the interest to save energy from the environment is highly felt also in small and integrated scale: self powered integrated systems, autonomous MEMS transducers and batteryless sensor node represent a set of devices that adopt the harvested energy to sustain or to supply an electronic device. Other examples include embedded and implanted sensor nodes [1], batteries rechargers [2], self powered sensors [3], unmanned vehicles powering [4], human powered energy harvesting [5] and smart systems [6]. Different kinds of energy can be harvested from renewable natural sources, such as: sunlight power, thermal gradients, wind, rain, tides, acoustic and mechanical vibrations. In particular, the latter mechanism can be exploited to produce a reasonable amount of energy by earth's vibration,

seismic vibrations, naturally noise source, but of course also as induced oscillations, vehicle motion, thermal noise, multi tone vibrating system and more generally all noisy environments and equipments. In [7,8] the authors present characteristics of various energy sources available in the environment. Vibration energy can be converted into electrical power through electromagnetic, electrostatic transducers and piezoelectric materials applied in resonators and oscillators [9]. The case of MEMS devices including harvesters based on thin film Lead Zirconate Titanate (PZT) are investigated in [10-11].

Many vibration energy harvesters are based on a mechanically resonant device that is, hopefully, matched to the single tone vibration of the source. However, in the vast majority of cases the ambient mechanical vibrations come in a vast variety of forms and the energy is distributed over a wide spectrum of frequencies, typically confined in a maximal bandwidth of few thousands of Hz [12].

Several ways to optimize the amount of harvested energy have been explored in literature, as regards the conversion and extraction mechanisms. Recently, a resonance frequency tunable energy harvester based on a magnetic force technique and a variable beam stiffness system [13,14] has been proposed in order to obtain a wide spectrum response by using a vibration source. Another approach is based on a piezoelectric multi-frequency converter array [15] which combines multiple linear converters with different frequencies responses to obtain a wider equivalent bandwidth. A similar approach based on the electromagnetic principle is presented in [16], where power is generated by means of electromagnetic induction using a magnet and serially connected coils on resonating multi length cantilever beams. Examples of novel approaches presented in the literature are: energy harvester based on a magnetic levitation principle which has been designed to tune the resonance frequency of the oscillator [17] and frequency up conversion based on piezoelectric bimorph cantilever [18]. In [19] the authors present the use of magnetic arrays to rectify the incoming frequency to a higher frequency combined with piezoelectric energy conversion. In [20], an energy harvester, that combines piezoelectric and magnetic materials with a tuning system to compensate small and slow variations of temperature, has been proposed. The common point is to optimize the energy recovery capability of the system.

The rest of this chapter will focus on a novel methodology to perform energy harvesting which exploits features of nonlinear oscillators. For these oscillators, it is not possible to define an intrinsic resonant frequency while one or more well defined peaks are achievable in the frequency domain. Furthermore a wider spectrum is predicted for the nonlinear system with respect to the linear oscillator. The latter is a crucial feature in the perspective of a single harvester system collecting energy from the environment.

In order to implement the nonlinear oscillator for energy harvesting applications, different materials can be considered and several technologies can be adopted. In the following two examples will be presented: a macro-cantilever based on piezoelectric bimorph converters realized by screen printing low-curing-temperature PZT films; a micro-cantilever developed in BESOI (Bulk and Etch Silicon On Insulator) technology. Experimental results are also presented, which confirm the expected behavior predicted by numerical simulation of devices under investigation.

2 Advanced and Innovative Solutions for Energy Harvesting

2.1 Introduction

Powerful computers as small as shirt buttons, micro-sensors invisibly dispersed in the natural environment, human and animal health control devices that can be ingested or implanted; all these scenarios have something in common: the need for a reliable, cheap, durable, efficient powering. For this reason ambient energy harvesting has been the object of a large research efforts aimed at providing an autonomous solution to the powering of small electronic mobile devices. As pointed out before vibration harvesting is an interesting option due to the almost universal presence of mechanical vibrations. In fact, ambient vibrations come in a vast variety of forms from sources as diverse as wind induced movements, seismic noise, car motion, micro and nano-scale vibration induced by thermal noise[21]. Present working solutions for vibration-to-electricity conversion are based on oscillating mechanical elements that convert kinetic energy via capacitive, inductive or piezoelectric methods.

The standard approach is illustrated in Fig. 1 where a scheme of the energy-harvesting device is presented, consisting of three main components: the vibrating body, the oscillator and the transducer. The vibrating body represents the vibration energy source and is a generic element that is contacted to the device in order to transmit the vibrational energy to be converted. It is supposed to have large mechanical impedance so that the contact does not significantly alter the dynamic features of the vibration source itself. For the oscillator part, the traditional approach is based on the resonant tuning of a linear oscillator with the region of the vibrational spectrum that is rich in energy. This idea is not new. In fact the first to exploit vibrations as an energy source was probably Abraham-Louis Perrelet, a

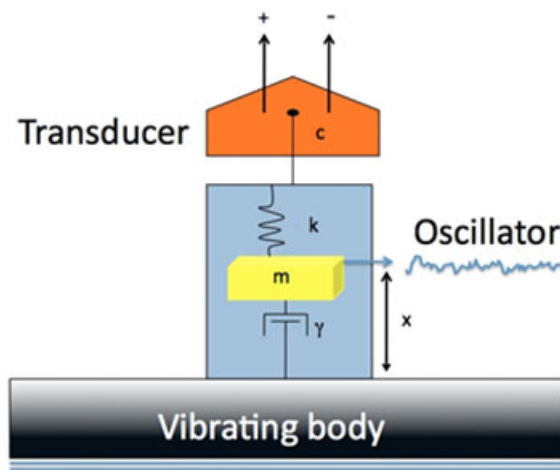


Fig. 1. A standard approach to convert mechanical vibration to electricity

Swiss watchmaker that in 1770 invented a mechanism capable of compressing a spring thanks to the “random” movement of the human wrist. Specifically, this mechanism is designed to wind the spring as the owner walks, using an oscillating weight inside the watch that moves up and down. As it is easy to grasp the mechanism is particularly efficient when the walking (or the wrist motion) is resonant with the ups and downs of the moving weight. Such a need for tuning the motion to some resonance of the device oscillator is still a major feature of present day vibration energy harvesters. However, difficulties arise both because the tuning of the oscillator is constrained by geometrical factors and because the energy spectrum of the available vibration is commonly spread in a wide frequency range, with the prevalence of low frequency components, where tuning is more difficult.

To overcome such a difficulty it has been recently proposed a new method based on the exploitation of the dynamical features of stochastic nonlinear oscillators[22]. Cottone et al. have shown that a bistable oscillator can outperform a linear oscillator in the presence of a wide vibration spectrum. Moreover in a recent paper[23] this result has been extended showing that the bistable configuration represents a special case of a more general behavior and that the increased performances of nonlinear oscillators can be found, also in monostable/multistable nonlinear dynamics. In refs [22] and [23] the authors focused on the functioning of a piezoelectric energy harvesting device[24], thought most of the considerations presented there are applicable also to other energy conversion mechanisms based on dynamical oscillators.

2.2 Physical Modeling and Simulations

In order to discuss the advanced scheme of energy harvesting techniques based on the exploitation of nonlinear oscillator let's fix our attention on piezoelectric vibration harvesters.

Strain in a piezoelectric material causes charge separation and produces a voltage V proportional to the stress applied. The piezoelectric oscillator is usually realized with a cantilever beam structure with a mass at one end of the lever and is acted on by the vibration applied to the other end. The voltage produced varies with the strain that is a function of the applied vibrations. The electric energy production can be accounted for by introducing a dynamical description that takes into account both the mechanical energy part of the oscillator and the conversion mechanism, as follows. Let's consider a one-dimensional oscillator with a mass m that is characterized by a potential energy $U(x)$ and a frictional viscous force with viscous coefficient γ . This oscillator is acted on by an external vibrational force represented by a stochastic term ξ . The oscillator is connected to an energy conversion mechanism that produces a voltage output V via a coupling function $c(x, V)$. The dynamic equations for such an oscillator can be written as:

$$m\ddot{x} = -\frac{dU(x)}{dx} - \gamma\dot{x} - c(x, V) + \xi_z \quad (1)$$

$$\dot{V} = F(\dot{x}, V) \quad (2)$$

where the second equation represents the dynamics of the voltage quantity. V is obtained here via a conversion mechanism represented by the function F . F and c represent two generic functions that need specification once the motion-to-electricity conversion mechanism is selected. As an example, in the piezoelectric conversion mechanism we have[22]:

$$c(x, V) = -K_V V \quad (3)$$

$$F(\dot{x}, V) = K_c \dot{x} - \frac{1}{\tau_p} V \quad (4)$$

and thus

$$m\ddot{x} = -\frac{dU(x)}{dx} - \gamma \dot{x} - K_V V + \xi_z \quad (5)$$

$$\dot{V} = K_c \dot{x} - \frac{1}{\tau_p} V \quad (6)$$

Here K_V is the coupling coefficient that relates the oscillation to the voltage. The random force ξ_z (a stochastic process that might assume with Gaussian distribution, zero mean, standard deviation σ and exponential autocorrelation function with correlation time τ) represents the action of the vibration. K_c is the coupling constant of the piezoelectric material. The second equation assumes here the characteristic of a linear dynamics with a time constant, τ_p set by the coupling between the energy harvesting device and the electric part. In fact $\tau_p = RC$, where C is the coupling capacitance and R is the resistive load. Quite notably the power obtained from the energy-harvesting device is given by V^2/R .

The oscillator dynamics is defined by the potential $U(x)$. The traditional approach based on resonant tuning assumes that the potential is linear, i.e.:

$$U(x) = a \frac{1}{2} x^2 \quad (7)$$

where the resonance frequency ω_0 depends on a through:

$$\omega_0 = 2\pi\nu_0 = \sqrt{\frac{a}{m}} \quad (8)$$

However, as discussed before, it is sometime difficult to change a in order to match a specific frequency, because a is connected to geometrical and physical properties of the oscillator (e.g. its stiffness). It is interesting to consider a more general potential of the form[22]:

$$U_q(x) = -a \frac{1}{2} x^2 + b \frac{1}{4} x^4 \quad (9)$$

with $b > 0$. This is the case of the so-called Duffing oscillator [25], extensively studied in the literature in the presence of noise both in the classical [26] and in the quantum domain [27]. The potential $U_q(x)$ is bistable when $a > 0$ with $x_{\pm} = \pm\sqrt{a/b}$ and $\Delta U_q = a^2/4b$ and monostable when $a < 0$. We are interested in solving the coupled differential equations

$$m\ddot{x} = ax - bx^3 - \gamma\dot{x} - K_v V + \zeta_z \quad (10)$$

$$\dot{V} = K_c \dot{x} - \frac{1}{\tau_p} V \quad (11)$$

in order to compute the quantity $V(t)$. This can be done by digital simulation of the stochastic nonlinear dynamics, i.e. by a numerical solution of the corresponding stochastic differential equations[28].

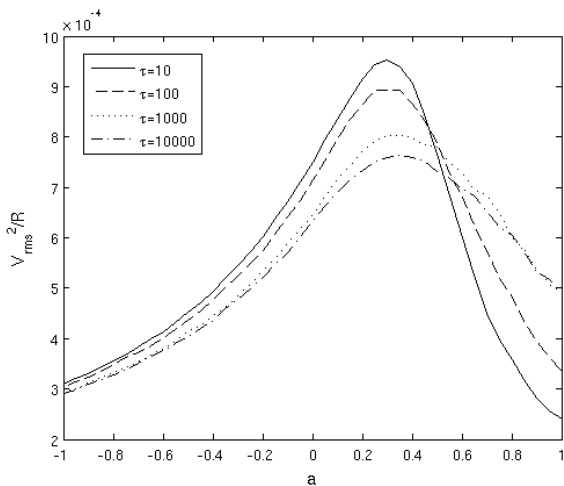


Fig. 2. Power output computed from the output voltage V . V is obtained via a simulation of the relevant dynamics. The numerical solution of the system of equations above is obtained for the following parameter values: $b = 0.5$, $\sigma = 0.6$, $\gamma = 0.5$, $\tau_p = 10^3$, $R = 50$. In the figure t is measured in terms of the integration step $\Delta t = 10^{-2}$, thus $\tau = 10$ means $\tau = 10 \Delta t$. All numbers are in arbitrary units.

In fig. 2 it is presented the power obtainable, computed as V^2/R , as a function of the parameter a , for four different values of the random force correlation time τ and same standard deviation σ . As it is well apparent the power goes through a maximum when a grows from negative to positive values. Three distinct regimes can be identified: (1) $a \ll 0$. The potential is monostable and the dynamics is characterized by quasilinear oscillations around the minimum located at $x = 0$. (2) $a \gg 0$. The potential is bistable with a very pronounced barrier between the two

wells. The dynamics is mainly trapped inside one minimum. (3) In between, for $a > 0$ there is a range of values where the power reaches a maximum and the dynamics is characterized by frequent jumps between the two wells. For a fixed value of b , the power shows a pronounced maximum as a function of a , located in the $a > 0$ region, i.e. in the strongly nonlinear bistable regime. Quite remarkably, if a is fixed, the power shows a maximum, as a function of b also, only if $a > 0$ [23]. In general, two conditions have to be met in order to have a maximum in the produced power: *i*) the oscillation amplitude has to be as large as possible, and; *ii*) the oscillation amplitude has to be transduced into voltage with minor losses and this can happen if $V(t)$ can follow closely the evolution of $x(t)$. Clearly, the condition *ii*) is constrained by the form of the dynamical equation of the voltage that acts as a high-pass filter for $x(t)$, with cut-on frequency determined by $\omega_p = 1/\tau_p$.

It is interesting to note that on increasing the correlation time τ the power amplitude decreases and the peak of the curve moves slightly toward larger values of a . This can be interpreted as a consequence of the high-pass filter effect of the voltage dynamics. A higher τ for the same σ , implies that less and less energy is located at high frequencies and thus above the cut-on represented by $\omega_p = 1/\tau_p$.

As a consequence less oscillation amplitude can be transduced into electric power.

The advantage of the nonlinearity has been experimentally documented in [22] where an inverted pendulum (see Fig.3) has been used in order to realize a typical

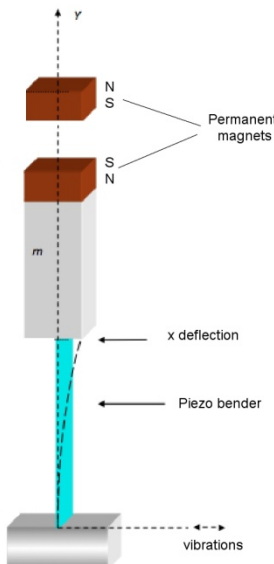


Fig. 3. Schematic of the inverted pendulum employed to show the advantage of the nonlinear dynamics over the linear one in terms of power extracted for a wide spectrum vibration.

cantilever vibration energy harvester. Under the action of the excitation the pendulum oscillates, bending the piezoelectric beam and thus generating a measurable voltage signal. The dynamics of the inverted pendulum can be controlled with the introduction of an external magnet conveniently placed at a certain distance and with polarities opposed to those of the tip magnet.

The external magnet introduces a force dependent from the distance that opposes the elastic restoring force of the bended beam. As a result, the inverted pendulum dynamics can show two different types of behaviours as a function of the distance between the magnets: A) when the external magnet is far away, the inverted pendulum behaves like a linear oscillator whose dynamics is resonant with a resonance frequency determined by the system parameters. This situation accounts well for the usual operating condition of traditional piezoelectric vibration-to-electric energy converters. On the other hand, B) when the distance between the magnets is small enough, two new equilibrium positions appear. The random vibration makes the pendulum swing in a more complex way with small oscillations around each of the two equilibrium positions and large excursions from one to the other. This dynamics is well reproduced by the discussion of the bistable potential presented above. The experimental results in terms of electric power obtained from the experiment, well accounted by the digital simulation, show unequivocally that the power reaches a maximum when the two magnets are at a finite distance and the dynamics of the swing, far from being linear, is characterized by a marked bistable character[22].

3 A Miniaturized Energy Harvester: Design and Experiments

For validation of the principle described in section 2.2, piezoelectric converters for power harvesting from environmental vibrations were designed and tested. The nonlinear behaviour is obtained by properly exploiting a repulsive magnetic force [29].

For validation at the macroscale, different sets of piezoelectric bimorph converters were realized by depositing lead zirconate titanate (PZT) films on steel cantilevers. To create nonlinearity and bistability, a permanent magnet was fixed on the cantilever tip while an external permanent magnet, with opposite polarity, was placed in front of the cantilever tip, in a configuration similar to that shown in Fig.3.

3.1 Experimental Results on Macroscale Devices

A first set of piezoelectric bimorph converters were initially used for the principle validation by focusing on the mechanical behaviour of the devices and measuring the tip displacement caused by excitation at the base.

The piezoelectric bimorph converters were realized by screen printing low-curing-temperature PZT films on steel cantilevers with dimensions of (40x5x0.5) mm³ [30].

The prepared piezoelectric ink is a compound of PZT milled powder ($\varepsilon_{33} = 4100$, $d_{31} = -260 \cdot 10^{-12}$ C/m², $\rho = 7.5$ g/cm³) and a polymeric vehicle-binder mixed in ratio of 2:1 wt. The obtained compound after mixing is homogenized in an ultrasonic bath which limits heating and consequent binder evaporation.

The PZT ink was screen printed on both faces the cantilever along most of its length using a 325 mesh screen, dried for 1 hour at room temperature and then cured at 150°C for 10 minutes. By repeating these three print-dry-fire steps, a PZT film with a final thickness of about 75 μm on each face of the converter was realized. The density in both wet and cured conditions was measured by weighting known volumes of ink and fired film, obtaining values of $\rho_{\text{wet}} = 1 \text{ g/cm}^3$ and $\rho_{\text{cured}} = 4 \text{ g/cm}^3$ respectively. Top and bottom electrodes were screen printed and fired at low temperature using a conductive Ag based polymeric ink. A cross-section diagram of the cantilever and a picture of one completed device are shown in Fig. 4a and 4b respectively.

The films were poled by applying a field of 5 MV/m between the electrodes and the steel bulk at 130°C for 10 minutes. Since the piezoelectric films are poled along their thickness with the poling axis 3 normal to the cantilever surface, and considering that the mechanical strain induced by bending is mostly along the axis 1 parallel to the beam length, then the piezoelectric elements work predominantly in the mode 31, i.e., with electric field and strain axes that are mutually perpendicular.

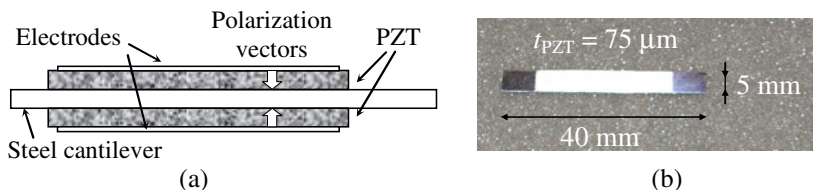


Fig. 4. Cross-section diagram of the cantilever (a) and a picture of the completed device (b).

A permanent magnet was fixed on the cantilever free end while an external permanent magnet was positioned on a micrometric stage so that vertical alignment could be adjusted and the distance d between the magnets could be varied, as shown in Fig. 5. The magnets were mounted with opposed polarities, so that the resulting magnetic force was repulsive. According to this setup, decreasing the distance d implies an increase of the values of the coefficients a and b in Eq. (9).

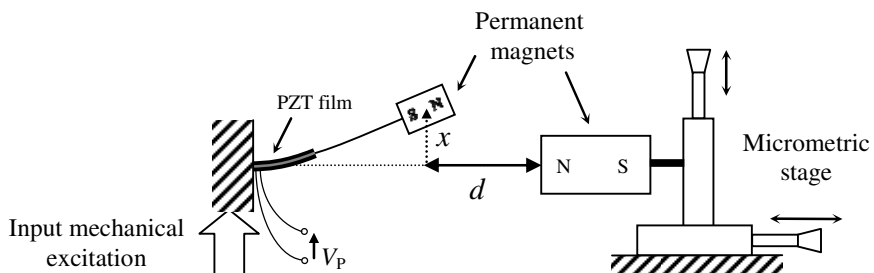


Fig. 5. Nonlinear system formed by a piezoelectric cantilever beam and two permanent magnets.

The converter was excited at the base by vertical mechanical vibrations generated by an electrodynamic shaker. A custom designed optical triangulator, based on the reflective sensor OPB705, was clamped to the converter base and used to measure the cantilever deflection, i.e. the displacement relative to the base, which corresponds to $x(t)$ in Fig. 1. A view of the complete setup is shown in Fig. 6.

The shaker was driven by a band-pass filtered white-noise voltage whose normalized spectrum is shown in Fig. 7.

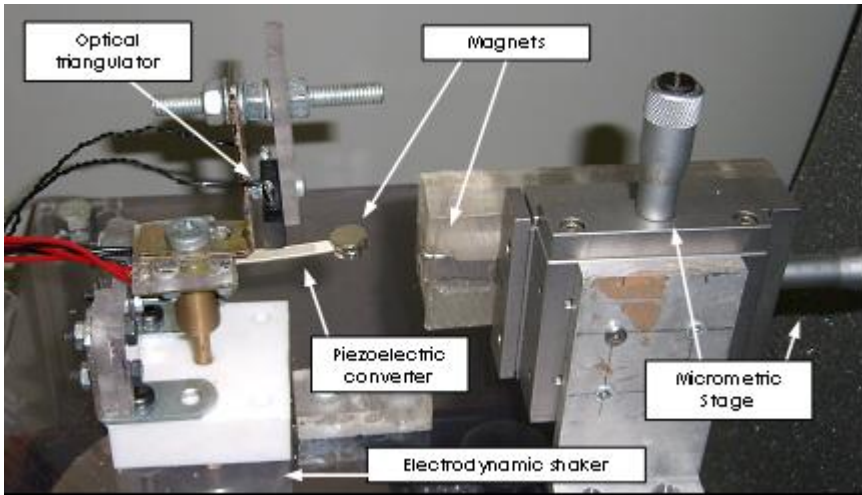


Fig. 6. Experimental setup for the characterization of the nonlinear piezoelectric converter.

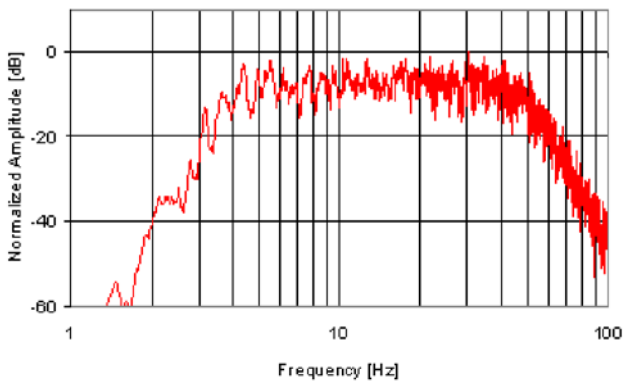


Fig. 7. Frequency spectrum of the input mechanical vibration used for the excitation of the converter.

Fig. 8 shows the measured time records of the cantilever deflection under an applied excitation from the shaker with a rms acceleration $a_{\text{rms}} = 0.3 \text{ g}$. As it can be observed by comparing the three signal plots, when the distance d is decreased starting from a comparatively large value (top plot, $d = 25 \text{ mm}$), the system initially maintains a monostable behaviour (middle plot, $d = 5 \text{ mm}$) with a decrease in the resonance frequency as long as the coefficient a is negative, corresponding to a positive equivalent stiffness.

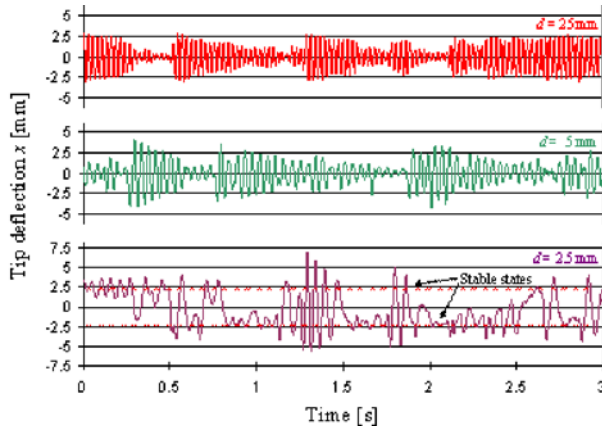


Fig. 8. Measured deflections of the converter for different values of the distance d between the two magnets, under random vibration excitation with an acceleration $a_{\text{rms}} = 0.3 \text{ g}$.

At the same time, this produces an increase in the displacement at parity of excitation due to the increased equivalent compliance. As expected, when the magnets are adequately close (bottom plot, $d = 2.5 \text{ mm}$), the coefficient a becomes positive, thereby making the system bistable. In this condition, switching between the two stable states occurs and the cantilever deflection significantly increases.

A second set of piezoelectric converters, having the same dimensions of the first set, was used to verify and measure the performances of the nonlinear converters in terms of open-circuit output voltage, in comparison with the linear case. The same setup shown in Fig. 6 was used. The system was excited by means of the electrodynamic shaker with mechanical vibrations having the same spectrum of Fig. 7 used in the previous experiment on the measurement of deflection. In this case, the open-circuit output voltage V_P generated by the piezoelectric converter was measured together with the deflection x , at different values of the distance d between the magnets. The output voltage V_P was obtained by the series connection of the top and bottom piezoelectric films of the bimorph converter.

A suitable condition to force the system into a bistable behaviour was $d = 2.5 \text{ mm}$. Fig. 9 shows the typical results obtained in such case, which are consistent with those of Fig. 8. Due to the intrinsic high-pass function between the output voltage V_P of the piezoelectric converter and the deflection x , when a switching in the deflection x occurs, a voltage pulse is generated in V_P .

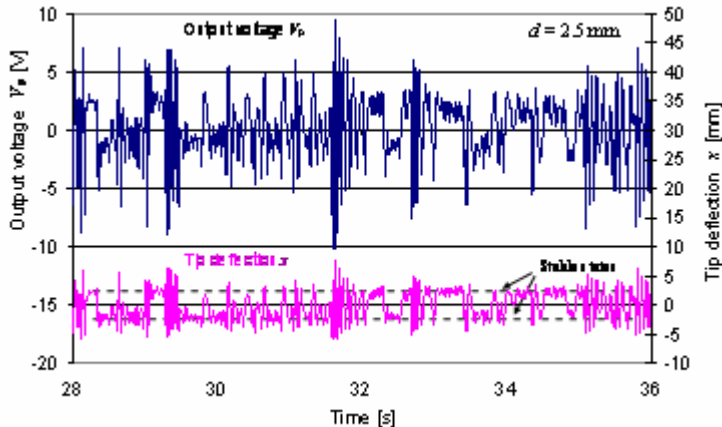


Fig. 9. Output voltage V_p and deflection x of the piezoelectric converter under a nonlinear condition, with an acceleration of the input vibrations $a_{\text{rms}} = 0.3 \text{ g}$.

As a consequence of the nonlinear behaviour, an increase in the open-circuit voltage and power from the converter is produced, as demonstrated by the computed rms voltage values at different distances d that result respectively $V_{d=25.0\text{mm}} = 4.27 \text{ V}$, $V_{d=5.0\text{mm}} = 6.11 \text{ V}$, and $V_{d=2.5\text{mm}} = 7.99 \text{ V}$.

Also the frequency spectra of the open-circuit voltage V_p generated by the converter were measured, as shown in Fig. 10.

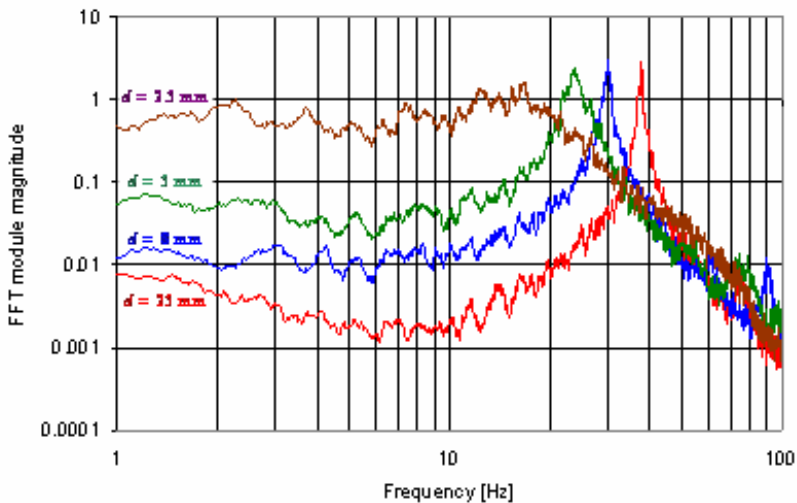


Fig. 10. Frequency amplitude spectra of the output voltage V_p , measured for different values of the distance d , with an acceleration of the input vibrations $a_{\text{rms}} = 0.3 \text{ g}$.

It can be observed that decreasing the distance d the system initially remains monostable and quasi linear, and at the same time the resonance frequency decreases due to the increase in the equivalent compliance. When d is small enough, i.e. lower than a threshold that was estimated to be around 4 mm in this condition, the equivalent stiffness becomes negative and the system toggles into nonlinear bistable behaviour. As expected, the bistable system evidences a wider spectrum with respect to the linear case.

Such a change in the system dynamic behaviour when d is varied is represented in a different way in Fig. 11, where the converter resonance frequency is plotted versus the distance d .

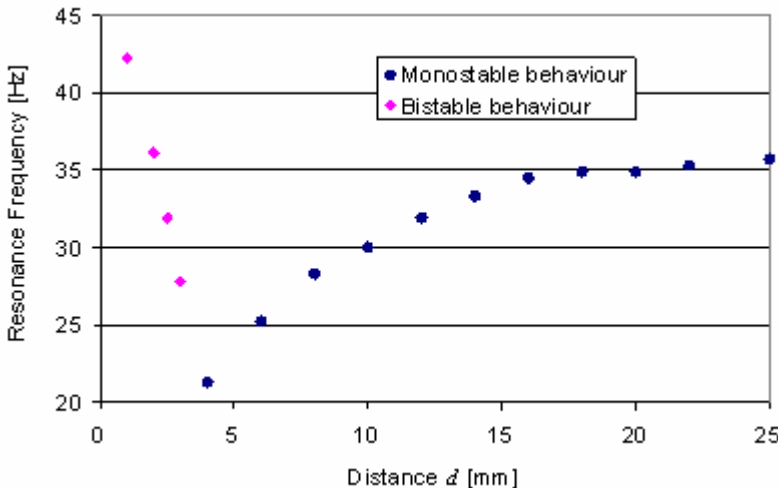


Fig. 11. Frequency of resonance of the converter for different values of the distance between the two magnets.

When the distance between the magnets is decreased starting from large values, a decrease in the resonance frequency occurs as long as the system maintains a quasi linear monostable behaviour. When d decreases below 4 mm, the system switches to the bistable behaviour. In this region, provided that the excitation is low enough, the system can sit in either equilibrium states and behave as locally linear. The closer are the magnets, the higher is the confinement and the equivalent stiffness, which in turn causes the resonance frequency to increase with decreasing the distance d .

4 A MEMS Energy Harvester: Design and Experiments

In order to implement an integrated prototype of the nonlinear oscillator for energy harvesting applications the custom MEMS process, named BESOI [31, 32] (Bulk and Etch Silicon On Insulator), was adopted. As shown in Figure 12, it is based on a Silicon On Insulator substrate having two layers of silicon (450 μ m and

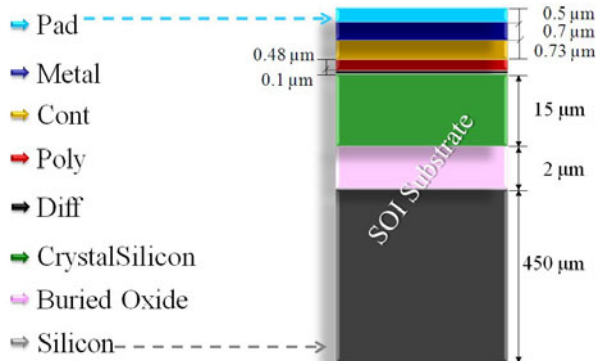


Fig. 12. Cross sectional area of the Bulk and Etch Silicon on Insulator (BESOI) technology.

15 μm of thickness respectively) and 2 μm of buried oxide; a front and back side DRIE etching technique has been adopted. A polysilicon and a metal layer have been used to realize integrated strain gauges and electrical routing, while a final oxide (PAD) has been considered as protection layer increasing also the stoutness of the MEMS device.

The proposed device is an U-shaped cantilever composed of two parallel cantilever beams having a length of 2500 μm and width of 700 μm , connected at their free extremity by a ‘linking arm’ (3400 μm x 700 μm , the thickness of the device is 15 μm). The bistable principle was implemented by using a permanent magnet deposited onto the top surface by a dedicated post-processing. A fixed magnet was placed in front of the cantilever tip at a distance A to produce a repulsive magnetic force.

The designed structure provides a large area in view of the magnetic stack deposition and the need for implementing a piezoresistive readout strategy. To this aim two strain gauges have been designed at the clamped end of each cantilever to obtain the best sensitivity, the metal layer has been neglected. Figure 13 shows the layout of the U-shaped device; two masks were conceived to etch the substrate from the bottom and from the top, whereas a lithography mask has been used for the polysilicon etching.

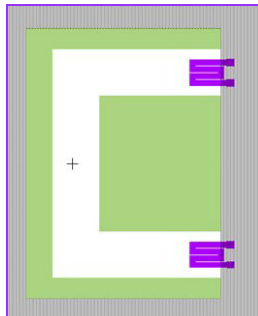


Fig. 13. Layout of the conceived U-shaped device.

4.1 Simulations of the Device Behavior

The designed structure was simulated by implementing the physical modeling previously studied through a MATLAB® routine based on Euler-Maruyama method. A Gaussian white noise was used as the vibration source. Figure 14 shows the spectral response of the cantilever in both the nonlinear case and the linear one, corresponding respectively to finite and exceedingly large distance between the cantilever and the external magnet. Simulation parameter values are indicated in the figure.

It must be observed that the nonlinear case provides a wider spectrum compared to the resonant behaviour of the linear case. This is expected to produce an improved effectiveness in converting wide-spectrum vibrations.

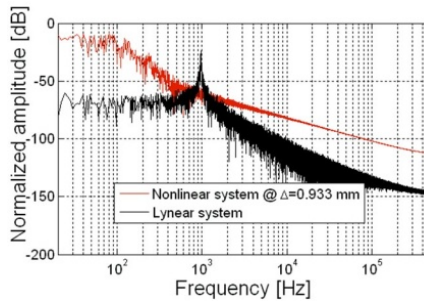


Fig. 14. Spectral response in linear case and in the nonlinear condition. Simulation parameters obtained through numerical estimations are: input noise standard deviation, 20 μN , device mass, $\sim 0.203\mu\text{g}$, spring constant, $\sim 12.7 \text{ kg/s}^2$.

4.2 Some Experimental Results

Tests on the U-shaped prototype have been performed by a dedicated setup. The experimental setup consists of an external permanent magnet stack and a translator system, performed to modulate the distance between the two magnets (the first deposited onto the U-shaped tip and the latter is the movable stack), a shaker used to stimulate the structure, a Wheatstone bridge used as conditioning circuit and a LabVIEW™ tool to manage the experiment. Figure 15a shows the U-shaped device with the permanent magnet deposited on the tip. The system dynamic was analyzed using a noisy stimulus with a standard deviation of $\sim 20 \mu\text{N}$. Figure 15b shows a typical output signal obtained through the piezoresistive readout of the active bridge.

As can be observed, the device oscillates between its mechanical stable states thus confirming the expected behavior. Deep measurement on the devices have evidenced an improvement of the performances as respect to a linear oscillator. As future trend different MEMS geometries will be considered also performing a complete custom SOI technology improved with other functional and structural materials including PZT and magnetic stacks.

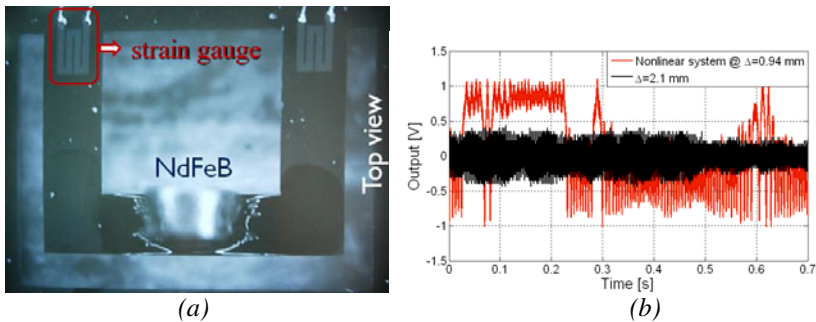


Fig. 15. (a) Microscope picture of the MEMS U-shaped cantilever BESOI-based. (b) Output signal of the readout electronic.

References

1. Raghunathan, V., Kansal, A., Hsu, J., Friedman, J., Srivastava, M.: Design considerations for solar energy harvesting wireless embedded systems. In: IEEE International Symp. on Information Processing in Sensor Network (2005) ISBN 0-7803-9202-7
2. Sodano, H.A., Inman, D.J., Park, G.: Comparison of Piezoelectric Energy Harvesting Devices for Recharging Batteries. *Journal of Intelligent Material Systems and Structures* 16(10), 799–807 (2005)
3. Torah, R., Jones, P.G., Tudor, M., O'Donnell, T., Roy, S., Beeby, S.: Selfpowered autonomous wireless sensor node using vibration energy harvesting. *Meas. Sci. Technol.* 19 (2008) ISSN 1361-6501
4. Anton, S.R., Inman, D.J.: Energy harvesting for unmanned aerial vehicles. In: Proceeding of SPIE (2008)
5. Kuo, A.D.: Harvesting Energy by Improving the Economy of Human Walking. *Science* 309, 1686–1687 (2005)
6. Guyomar, D., Jayet, Y., Petit, L., Lefevre, E., Monnier, T., Richard, C., Lallart, M.: Synchronized Switch Harvesting Applied to Self-Powered Smart Systems: Piezoactive Microgenerators for Autonomous Wireless Transmitters. *Sensors and Actuators A* 138(1), 151–160 (2007)
7. Vullers, R.J.M., Van Schaijk, R., Doms, I., Van Hoof, C., Mertens, R.: Micropower energy harvesting. *Solid-State Electronics* 53, 684–693 (2009)
8. Roundy, S., Wright, P.K., Rabaey, J.: A study of low level vibrations as a power source for wireless sensor nodes. *Computer Communications* 26, 1131–1144 (2003)
9. Elfrink, R., Kamel, T.M., Goedbloed, M., Matova, S., Hohlfeld, D., van Andel, Y., van Schaijk, R.: Vibration energy harvesting with aluminum nitride-based piezoelectric devices. *J. Micromech. Microeng.* 19 (2009)
10. Lee, B.S., Lin, S.C., Wu, W.J., Wang, X.Y., Chang, P.Z., Lee, C.K.: Piezoelectric MEMS generators fabricated with an aerosol deposition PZT thin film. *J. Micromech. Microeng* 19 (2009)
11. Choi, W.J., Jeon, Y., Jeong, J.H., Sood, R., Kim, S.G.: Energy harvesting MEMS device based on thin film piezoelectric cantilevers. *J. Electroceram.* 543–548 (2006)
12. Roundy, S., Wright, P.K., Rabaey, J.M.: Energy Scavenging for Wireless Sensor Networks with Special Focus on Vibrations. Kluwer Academic Publishers, Dordrecht (2003) ISBN 978-1-4020-7663-3

13. Challa, V.R., Prasad, M.G., Shi, Y., Fisher, F.T.: A vibration energy harvesting device with bidirectional resonance frequency tenability. *Smart Mater. Struct.* 17 (2008)
14. Peters, C., Maurath, D., Schock, W., Manoli, Y.: Novel electrically tunable mechanical resonator for energy harvesting. In: Proceeding of Power MEMS 2008, pp. 253–256 (2008)
15. Ferrari, M., Ferrari, V., Guizzetti, M., Marioli, D., Taroni, A.: Piezoelectric multifrequency energy converter for power harvesting in autonomous Microsystems. *Sensors and Actuators A* 142, 329–335 (2008)
16. Sari, I., Balkan, T., Kulah, H.: A Wideband Electromagnetic Micro Power Generator for Wireless Microsystems. In: Proceeding of Transducers, pp. 275–278 (2007)
17. Mann, B.P., Sims, N.D.: Energy harvesting from the nonlinear oscillations of magnetic levitation. *Journal of Sound and Vibration* 319, 515–530 (2009)
18. Lee, D.G., Carman, G.P., Murphy, D., Schulenburg, C.: Novel Micro Vibration Energy Harvesting Device using Frequency Up Conversion. In: Proceeding of Transducers, pp. 871–874 (2007)
19. Chung, T.K., Lee, D.G., Ujihara, M., Carman, G.P.: Design, Simulation, and Fabrication of a Novel Vibration Based Magnetic Energy Harvesting Device. In: Proceeding of Transducers, pp. 867–870 (2007)
20. Carlioz, L., Delamare, J., Basrour, S.: Temperature threshold tuning of a thermal harvesting switch. In: Proceeding of Transducers, pp. 1385–1388 (2009)
21. Wang, Z.L., Song, J.: Piezoelectric nanogenerators based on zinc oxide nanowire arrays. *Science* 312(5771), 242–246 (2006)
22. Cottone, F., Vocca, H., Gammaitonni, L.: Nonlinear Energy Harvesting. *Phys. Rev. Lett.* 102, 080601 (2009)
23. Gammaitonni, L., Neri, I., Vocca, H.: Nonlinear oscillators for vibration energy harvesting. *App. Phys. Lett.* 94, 164102 (2009)
24. Anton, S.R., Sodano, H.A.: A review of power harvesting using piezoelectric materials (2003–2006). *Smart Materials & Structures* 16(3), R1–R21 (2007)
25. Duffing, G.: Braunschweig, Erzwungene Schwingungen bei Veränderlicher Eigenfrequenz, p. 134 (1918)
26. Rahman, M.: Stationary solution for the color-driven Duffing oscillator. *Phys. Rev. E Part B* 53(6), 6547–6550 Part B (1996)
27. Dittrich, T., Oelshlagel, B., Hanggi, P.: Driven Tunnelling with Dissipation. *Europhysics Letters* 22(1), 5–10 (1993)
28. Kloeden, P.E., Platen, E.: Numerical Solution of Stochastic Differential Eq. Springer, Berlin (1999)
29. Ferrari, M., Ferrari, V., Guizzetti, M., Marioli, D.: Piezoelectric Low-Curing-Temperature Ink for Sensors and Power Harvesting. In: Malcovati, Baschirotto, D’Amico, Di Natale (eds.) *Sensors and Microsystems, AISEM 2009 Proceedings*, vol. 54, pp. 77–81. Springer, Heidelberg (2010)
30. Ferrari, M., Ferrari, V., Guizzetti, M., Andò, B., Baglio, S., Trigona, C.: Improved Energy Harvesting from Wideband Vibrations by Nonlinear Piezoelectric Converters. In: Proceedings of the Eurosensors XXIII conference Procedia Chemistry, vol. 1(1), pp. 1203–1206 (August 2009)
31. Andò, B., Baglio, S., Trigona, C.: Nonlinear MEMS mechanism for Energy harvesting from mechanical vibrations. In: Associazione Italiana Sensori e Microsistemi. Proceeding of AISEM 2010 (2010)
32. Andò, B., Baglio, S., Dumas, N., Latorre, L., Nouet, P., Trigona, C.: Nonlinear behaviour of a micromachined SOI device for energy harvesting application. In: Proceeding of DTIP 2010, Design, Test, Integration & Packaging of MEMS/MOEMS (2010)

Wearable Sensors for Foetal Movement Monitoring in Low Risk Pregnancies

Luís M. Borges¹, Pedro Araújo², António S. Lebres³, Andreia Rente⁴, Rita Salvado⁴, Fernando J. Velez^{1,5}, J. Martinez-de-Oliveira⁶, Norberto Barroca¹, and João M. Ferro¹

¹ Instituto de Telecomunicações – Departamento de Engenharia Electromecânica

² Instituto de Telecomunicações – Departamento de Informática

³ Unidade de Detecção Remota – Departamento de Física

⁴ Unidade de Materiais Têxteis e Papeleiros – Departamento de C. T. Têxteis
Universidade da Beira Interior

Rua Marquês d' Ávila e Bolama, 6201-001 Covilhã, Portugal

⁵ Centre for Telecommunications Research, King's College London,
Strand, London WC2R 2LS, UK

⁶ School of Health Sciences, University of Beira Interior
Department of Child and Mother Health
Centro Hospitalar Cova da Beira
6200-251 Covilhã, Portugal

lborges@lx.it.pt, paraujo@di.ubi.pt, lebres@ubi.pt,
rente.andreia@gmail.com, rita.salvado@ubi.pt, f JV@ubi.pt,
jmo@fcsaude.ubi.pt, nbarroca@lx.it.pt, ferro@lx.it.pt

Abstract. In low risk pregnancies, the continuous monitoring of the foetal health is based on traditional protocols for counting the foetal movements felt by the mother. Although the maternal perception is a relevant characteristic for the evaluation of the foetal health, this kind of monitoring is hard to accomplish and being subjective can induce into errors due to mother's anxiety and lack of concentration. Furthermore, the majority of foetal fatalities occur during the last weeks of low risk pregnancies. Therefore, it is important to obtain a universal electronic obstetric tracing, allowing for the identification of sudden changes in the foetus health, by continuously monitoring the foetus movements. The Smart-Clothing project aim has been the development of easy-to-wear belts with a telemedicine system for this purpose. One of the tried solutions is the Flex sensor belt system, which guarantees real-time and continuous foetal monitoring while creating effective interfaces for querying sensor data and store all the medical record (which can later be accessed by health professionals). Another developed belt has piezoelectric sensors incorporated onto it. The piezoelectric sensor belt has shown a high capacity to detect foetal movements, isolating them from external interferences.

Keywords: smart textiles, hierarchical wireless communications, WSAN, telemedicine, foetal healthcare.

1 Introduction

Technological innovation applied to healthcare is making the use of new materials and tiny communication systems embedded into textiles. The development of smart textile belts prototypes, such as those proposed by the Smart-Clothing project, combines investigation in functional textiles materials, data acquisition and processing, and wireless communication networks in the context of human body monitoring and statistical methods for the data analysis and treatment. The data extracted from the Wireless Body Area Network (WBAN) attached to pregnant women may be made available to the health professionals through a hierarchical communication system. Research on WBANs is already being conducted considering WBAN Medium Access Control (MAC) and routing schemes, as well as different remote monitoring architectures, namely “On-body” and “In-body” ones, as mentioned by the authors from [1].

The interest in the coexistence among several wireless communication systems is increasing because of the possibility of using unlicensed frequency bands. In Europe, there are two unlicensed frequency bands specifically available for wireless networks: i) The Industrial Scientific and Medical (ISM) band, which includes the 433 MHz, 900 MHz, 2.4 GHz and 5.8 GHz frequency bands; ii) the Unlicensed National Information Infrastructure (UNII) band, which includes the 5.2 GHz frequency band. It is nevertheless important to note that users of unlicensed bands can equally affect the quality and the use of the frequency spectrum. Hence, one of the principal disadvantages of unlicensed frequency bands is frequency sharing and resulting interference.

The remaining of the Chapter is organized as follows. Section 2 presents the overview of the Smart-Clothing project. Section 3 describes its main area in detail and presents the associated scenario. Section 4 describes the experimental layout for the project, presenting two versions of the Flex sensor belt, as well as the piezoelectric sensor belt and a belt with conductive fabrics. Section 5 presents the experimental results for the flex sensor belt and piezoelectric sensor belt. Finally, Section 6 presents the conclusions and suggestions for further work.

2 Smart-Clothing

The Smart-Clothing project is an iCentro project approved by CCDR-C with FEDER funding. The methodological specifications applied in this project enables to quantify the precision of the experimental measurement with a new device for signal acquisition, develop algorithms to extract the parameters that show clinical relevance and to establish strategies for efficient data mining in the context of medical diagnostic of foetal health in pregnant women. From the conventional sensor and data acquisition and storage circuit’s point of view, the objective is to develop a set of electronic microcircuits associated with textile materials that enable to measure relevant biomedical and biomechanical parameters through an easy-to-use telemedicine gear, e.g., a belt. One example of how the theme of pregnancy monitoring is gaining importance in the research community is mentioned

by the authors from [2], which describes an innovative, remote monitoring decision support system, employed in the early diagnosis of pregnancy complications, through the effective and non-invasive monitoring of maternal and foetal electrocardiograms.

A hierarchical communication system, Fig. 1, is needed to deliver the data from the WBAN that is attached to pregnant woman. Note that, although the main focus of the Smart-Clothing is to produce the sensors integrated into the clothes and to integrate them into the WBAN, the consideration of aspects of data aggregation, routing and MAC protocols were also important, as they facilitate the integration of wireless sensor networks (WSNs) into the hierarchical network.

New algorithms and protocols were developed to optimize the trade-off between energy consumption/processing and communication capabilities, namely in the MAC layer [3]. Hierarchical communications can be a solution to obtain a network of networks, e.g., by using internet protocol (IP). A bottom-up architecture formed by i) WSNs, ii) Wi-Fi, and iii) Ethernet (or WiMAX) was explored to facilitate healthcare monitoring anyway, anywhere and anytime.

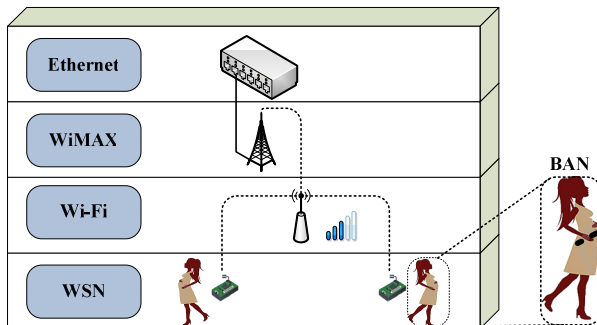


Fig. 1. Hierarchical network considering the WBAN and other communication networks

3 Field of Study

A. Main Area

The majority of foetus fatalities in the end of pregnancy occur in the low risk pregnancies group. The main area addressed by the Smart-Clothing project is obstetric tracing, enabling to identify sudden changes in the foetus health, by monitoring its movements and the foetal heart rate (FHR). In low risk pregnancies, in the periods between medical sessions (that occur weekly during the last five weeks of pregnancy), the objectively monitoring of the foetal health based in traditional protocols for counting the foetal movements felt by the mother is very important [2, 4]. Although the maternal perception is a relevant characteristic for the evaluation of the foetal health, the monitoring is hard to accomplish and may induce into error, e.g., due to the mother's anxiety or lack of concentration.

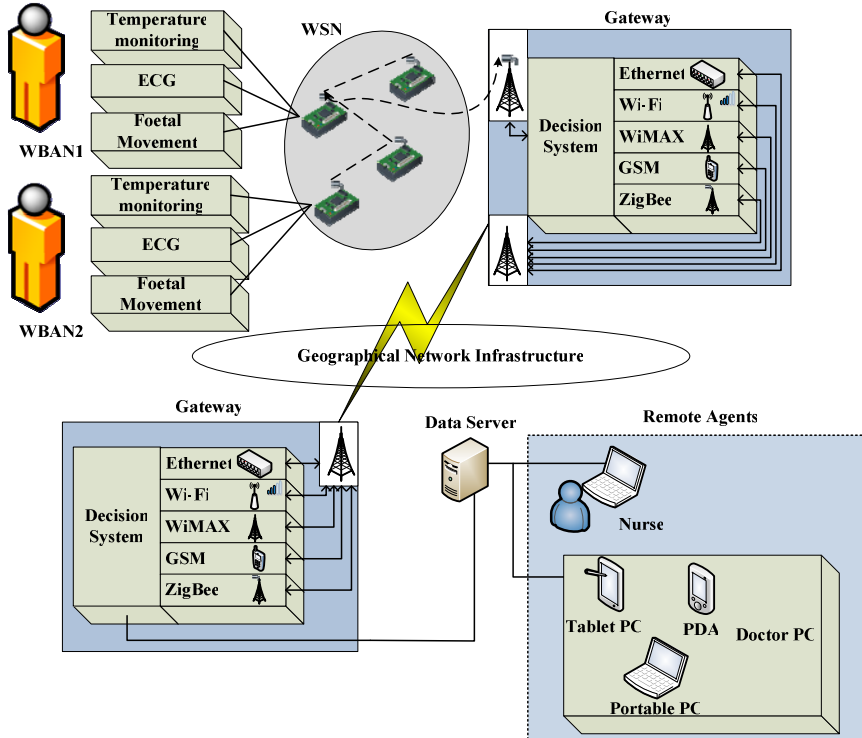


Fig. 2. Smart-Clothing main healthcare scenario

In the Hospital, the foetal monitoring is done by using a Cardiotocograph, which records the FHR and the uterine contractions. The FHR is determined by means of an ultra-sound Doppler sensor (operating at a frequency $f = 1$ to 3 MHz), while the uterine contractions are detected with a pressure sensor (dynamometer). The foetal monitoring can be done by the pregnant woman at home, counting the foetus movements (the pregnant woman feels 80% of them), which should be registered by herself in a form for posterior analysis of the physician. There is in the market low cost portable equipments based on the Doppler technology, which allow for foetal heart sounds hearing and the foetal movements detection, to be performed by a pregnant woman [6]. They can be used beyond the 12 weeks of pregnancy and allows for recording the cardiac sounds. The possible effects over the foetus due to the use of equipments based on the ultra-sound technique raise some concerns but their effects, although not well known, are probably unimportant when applied intermittently.

Frequently pregnant woman does not show the same accuracy in detecting the foetus movements as it is done by the health services. Smart-Clothing is motivated by the need to conceive an automatic harmless remote monitoring device to the purpose of foetal movement monitoring.

B. Project Scenario

The main Smart-Clothing scenario is presented in Fig. 2. It consists of four main actors: the WBANs, WSN, gateway and remote agents. Each WBAN is attached to the pregnant woman and collects the data from the electrocardiographic (ECG) and the foetal movement sensors. The WSN is itself responsible by the aggregation of the data collected by the WBAN, and its accurate delivery to the gateway. The gateway has got a decision system that chooses the better way to deliver the data to the gateway located in the Hospital. The Hospital gathering system has the same decision system and is used for the interconnection of a WSN with remote agents through a geographical network, to collect, aggregate and eventually pre-process data received by the WSN.

Finally, the remote agents can be either a collector of information (through a server where the information is stored and could be accessed later on) or a nurse that monitors the foetus in the pregnant women as well as a doctor that closely monitors the foetus by using his/her personal digital assistant (PDA), or his/her laptop or even his/her tablet PC or Ultra-mobile PC (UMPC).

4 Experimental Apparatus

A. Belt with Flex Sensor

After the application scenarios had been defined [6], the next step was to identify which types of sensors would be incorporated into the Smart-Clothing belt. To achieve this goal, several belts were made, tested and compared to see which sensors were capable of better detecting the foetal movements [6]. One of the Smart-Clothing belt prototypes is based on the Flex sensor, while another one incorporates a piezoelectric sensor.

The first version of the Flex sensor belt incorporates eight Flex sensors, as shown in Fig. 3. A simple voltage divider, associated to a temperature compensated voltage reference, generates the input signal. The manufacturer proposes a correspondence of standard values of the flexion angle to a certain value of resistance.



Fig. 3. Flex sensor belt

The acquisition system diagram is presented in Fig. 4. For the sake of simplicity just one Flex sensor is presented. Besides the Flex sensor a button was incorporated in the system to be pressed by the pregnant woman (when she feels or detects foetal movement). The recording of these events is very useful for comparison purposes, as they enable a comparison of personal detected movements with the movements automatically detected by the belt.

A microcontroller was used for data acquisition and communication. For practical reasons, in a preliminary experimental context, we supplied the V_{cc} voltage to the voltage divider by using external pin from the MSP430 microcontroller (MSP430-F449STK2 module) and read the voltages from the voltage dividers using the Analog-to-Digital Converter (ADC) inputs from the microcontroller.

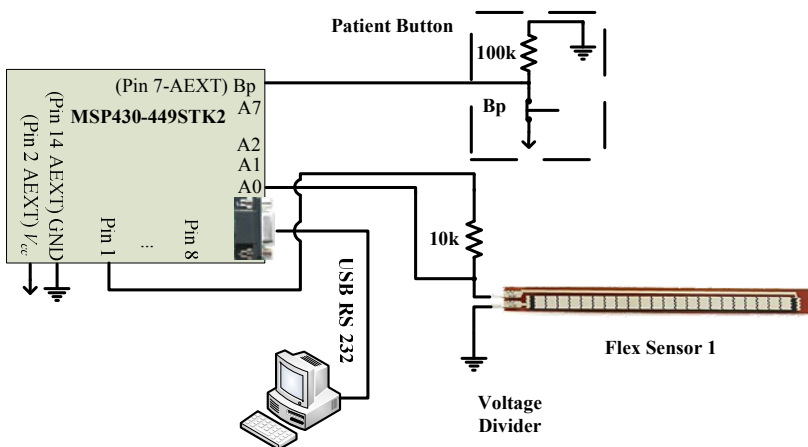


Fig. 4. Flex sensor belt acquisition system diagram

To compute the resistance value from the Flex sensor one uses the voltage divider formula as follows

$$R_{Flex1} = R_1 \times V_{out} / (V_{in} - V_{out}) \quad (1)$$

where R_{Flex1} is the resistance value, R_1 is equal to 10 kΩ, V_{in} is the V_{cc} value supplied to the voltage divider, and V_{out} is the voltage value from the voltage divider. The V_{cc} voltage supplied to the voltage divider is measured periodically by a routine that is located in the microcontroller, in order to compensate the battery losses during the system operation. This enables a better accuracy for the values extracted from the Flex sensors.

Two formulas were used for the conversion of the resistance value to the angle value, as follows

$$\theta_1 [^\circ] = (R_{Flex1} - 10 \times 10^3) / 44.44 \quad (2)$$

$$\theta_2 [^\circ] = (R_{Flex1} - 6001) / 88.88 \quad (3)$$

where θ_1 and, θ_2 are the angles for the corresponding Flex sensor resistance value. This enables to extrapolate the angle values.

Equation (2) is used when the resistance value is between 10 kΩ and 14 kΩ while equation (3) is used when the resistance value is between 14 kΩ and 22 kΩ. We have made a calibration curve to identify the broad range resistance characteristic for the sensor. The Flex sensor manufacturer states that a resistance value of 10 kΩ matches an angle of 0° while values of 14 kΩ and 22 kΩ match angles of 90° and 180°, respectively.

These formulas were based on the theoretical and calibration curves for the Flex sensor, as shown in Fig. 5. The theoretical line is based on the resistance values and corresponding deflection angle supplied by the flex sensor manufacturer. The calibration curve is results from an experiment where the flex sensor was bent from 0° to 90° and the resistance value measured with a protractor was registered at each 10° of bending increment.

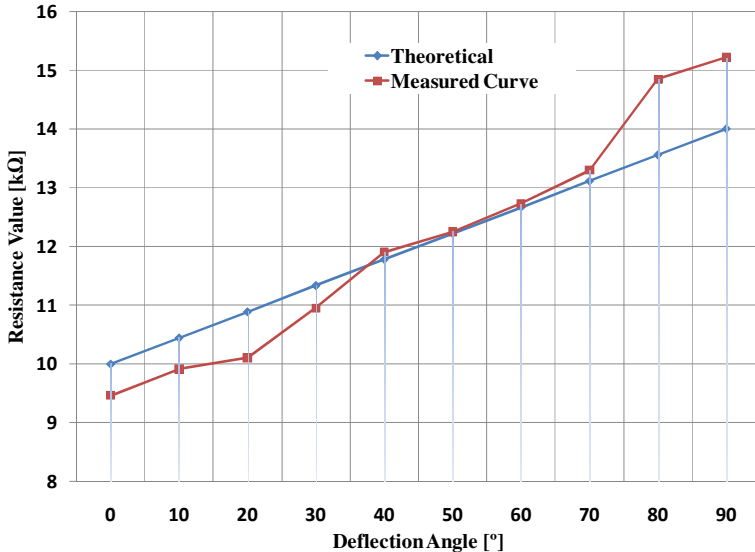


Fig. 5. Theoretical and calibration curves for the Flex sensor

The MSP430-F449STK2 module, after acquiring the values for each Flex sensor, sends all the data to the computer (where several values for the correspondence between resistance and angles are presented), and automatically counts the movements above a preset threshold.

The algorithm from Fig. 6, used in the acquisition module, begins with the reset option, (applied to all system). If the reset option is not chosen then the algorithm

will measure the voltage from the power supply, in order to compute later the corresponding voltage to a flexion angle. Then if button B1 (located in the acquisition module) is pressed a timer (of 100 ms) is set. After 100 ms, the algorithm starts reading all Flex sensors. First, the Flex sensor 1 voltage divider is powered up. Then, the algorithm waits 10 ms so that the ADC can read properly the voltage value from the voltage divider. Then, it computes the flexion angle depending on the read voltage value and extracts the state of the patient button (if the patient pressed the button it records the time and add one unit to the counter). This procedure is repeated for the other seven Flex sensors. However, in the last one the data from all the Flex sensors and patient counter is aggregated enabling to build the data packet while sending it to the computer. The Flex Sensor View program running presents the values of the different angles for each Flex sensor.

The final version of the standalone Flex sensor belt uses only one data packet to transmit the deformation angles of the eight Flex sensors, according to the packet protocol established between the computer and the acquisition module. This data packet is sent at the end of the routine controlled by a timer in the microcontroller only, in order to maintain a constant data flow between the acquisition module and the computer. Besides, a calibration routine was implemented in the microcontroller. Each calibration packet is sent from the program running in the computer to the acquisition module and has the ability to calibrate all the (eight) Flex sensors (or only one).

Considering the preliminary work performed in the first version of the Flex sensor belt, a belt with only five Flex sensors was integrated with a WSN device. Each of the five Flex sensors is connected to an ADC channel, in order to convert the voltage (given by each Flex sensor voltage divider) to the corresponding deformation angle.

This device consists of an IRIS mote from Crossbow, a small battery and a set of Flex sensors. A hybrid communication system is employed in order to deliver the data through the WSN. The system detects the foetal movement based on the flexion angle of the sensors while the IEEE 802.15.4 network delivers all the data collected by the motes to our Centralised Management of Resources (CMR) identity.

An application that manages the WSN (and saves the information) was developed and is located at the CMR, by using a Structured Query Language (SQL) database. Fig. 7 shows a simplified block diagram for the monitoring system. The WSN management application is also responsible to present the data to the user (nurse/doctor). As an option, it is possible to transmit the data via Wi-Fi. The information can be shared or accessed by other authorized users. The foetal movements are monitored while data is being transmitted wirelessly to a Mote Interface Board (MIB) directly connected to our CMR, as shown in Fig. 7. The CMR is formed by a personal computer, an application which displays and saves the measured data into the database, and a Wi-Fi module to transmit data through the Wireless Local Area Network (WLAN) [7, 8].

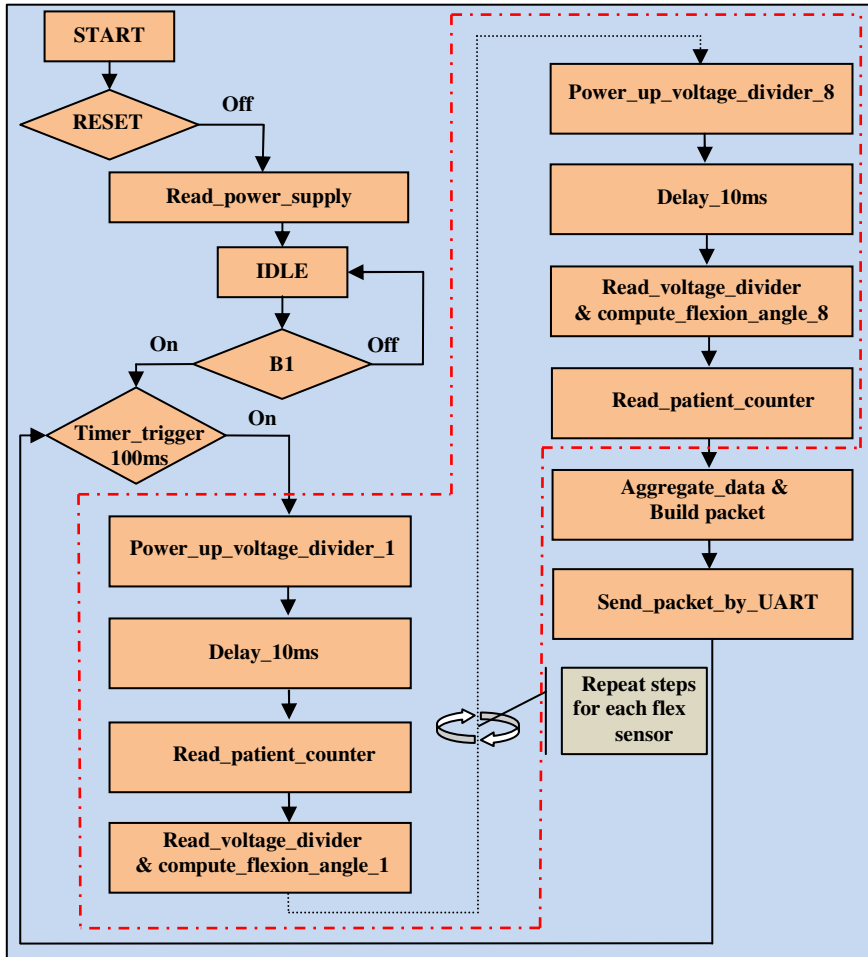


Fig. 6. Algorithm diagram for the flex sensor acquisition system

There are two different possibilities to receive and send information. One uses an IEEE 802.15.4 network, while the other one considers two protocol layers (IEEE 802.15.4 and 802.11 ones). If the priority is to collect as much data as possible from the patient, some questions like energy consumption arise. Trade-offs between energy consumption and processing and communication capabilities are relevant [3].

The IEEE 802.15.4 standard was chosen because of its unique characteristics that lead to energy-efficient MAC protocols. It also facilitates the development of our application according to the patient needs, while ensuring an integrated and complete solution for sensor networking based applications, including analog-to-digital conversion. One possible scenario for this small scale wireless flex sensor belt network is a waiting room of the health centre or clinic, where pregnant women wait to visit the obstetrician.

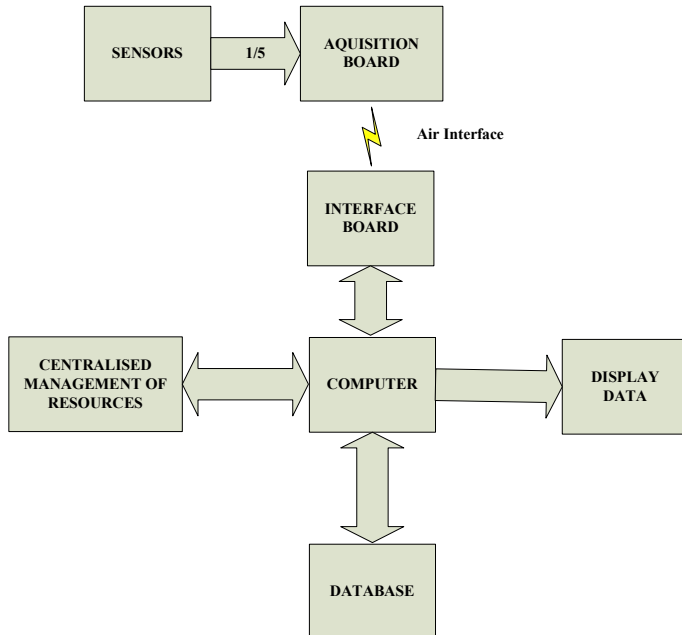


Fig. 7. Block Diagram for the acquisition system

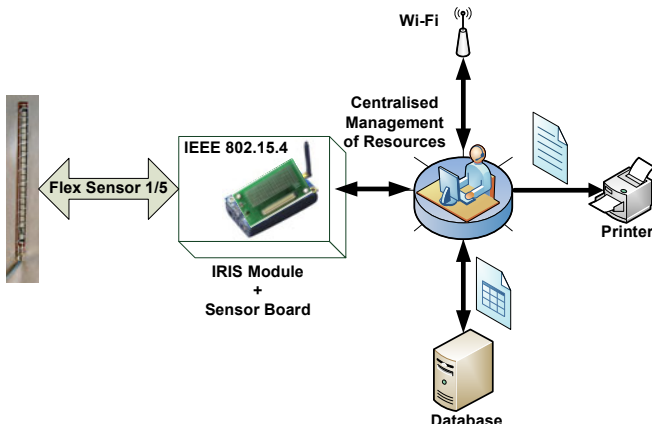


Fig. 8. Patient monitoring and IEEE 802.15.4 wireless networking

In the second solution for this belt, another communication layer was considered that allows for sending and receiving information that was collected from the IEEE 802.15.4 network through an IEEE 802.11 wireless network, as shown in Fig. 8. This solution was chosen because it constitutes a practical and interesting solution for network connectivity while offering some mobility, flexibility, and low cost of deployment. An example is transmitting the data from our CMR to any

computer that is in its range and has an IEEE 802.11 (Wi-Fi) connection capability. In this scenario the CMR identity may be controlled and monitored by a nurse that looks up for anomalies in the Flex sensor belt data.

B. Belt with Piezoelectric Sensors

We developed a belt incorporating piezoelectric sensors. This type of sensor transduces the force to voltage (and vice-versa) and present high sensitivity. They proved to be an appropriate choice to detect mechanical movements such as those originated from foetus in a pregnant woman. Furthermore, the sensors could be very small, they respond to a broad frequency range, do not react to static forces and are cheap.

In this belt, we used plastic pre-encapsulated piezoelectric sensors with a BNC connector (to drive the electrical voltage signal to the signal processing circuit). This type of sensor, Fig. 9, is used by PowerLabs data acquisition system from ADInstruments [9], at Health Science Faculty from Universidade da Beira Interior.



Fig. 9. Piezoelectric sensor MLT1010 (ADI Instruments)

Other healthcare monitoring devices are based in piezoelectric film sensors, as the one shown in Fig. 10, commonly used for the detection of biological signals. This sensor is placed against the abdomen of the pregnant woman in order to detect slight surface deformations caused by the movements of the foetus. Compared with other sensors this one presents a high sensibility, reduced dimensions and does not need power supply to operate.

Fig. 11 shows the signals captured by the sensor above, during an experiment where the pregnant woman also holds a pressure switch that should be pressed when perceiving a foetal movement. In this experiment, only one sensor was used several times, placed in several positions in order to detect the foetal movements. Besides the detection of the foetal movement, the mother's breath movement is also as well as the movements due to the displacement of the sensor (motion artefacts). These movements represent an interference signal that should be eliminated [10], and are represented upon the curve in Fig. 11.



Fig. 10. A piezoelectric film sensor used in a preliminary Smart-Clothing belt

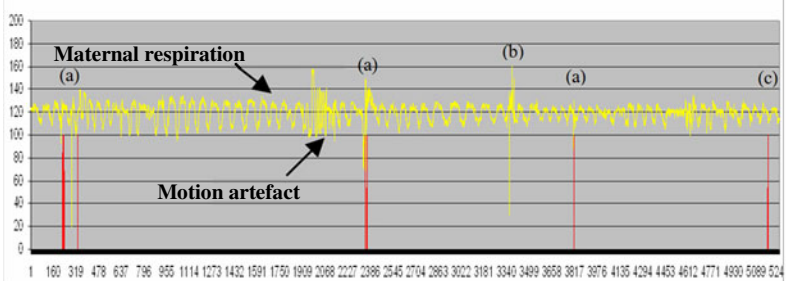


Fig. 11. Foetal movement curves (upper=belt, lower=mother): (a) detected by mother and belt, (b) detected by belt only, and (c) detected only by the mother

C. Other Techniques

Another belt is based on pressure sensors. It was built up with conductive and semi-conductive fabrics. The pressure sensor belt shown in Fig. 12 is made with two different types of conductive fabrics: one is conductive in the entire surface while the other is conductive only in some zones.

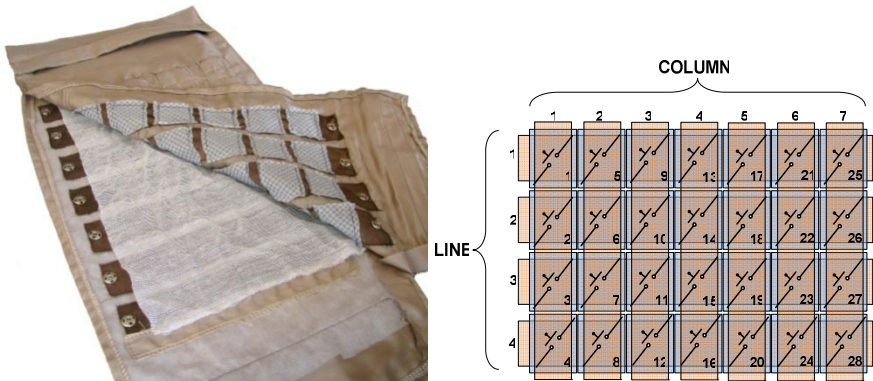


Fig. 12. Smart-Clothing On-Off belt with fabric pressure sensor

Fabrics are deployed in layers so that the fabric (with square shaped conductive areas) stays between the other layers. This will act as a switch when the outer fabric layers are pressed, letting the current traverse from one to the other, according to the value of its resistance. By observing Fig. 12, while the orange stripes are conductive fabric, the blue squares are the semi-conductive fabric which forms the switch.

The system diagram is presented in Fig. 13, where the lines and columns from the belt are connected to MSP430 based acquisition module.

As presented in Figs. 12 and 13, the Smart-Clothing On-Off sensor belt is based on a matrix of 28 fabric squares. Each of these fabric square acts like a switch that closes the circuit if it is pressed and leave the circuit open if it is not pressed.

Besides the On-Off belt, a button (or a patient counter) was incorporated into the system, to be pressed by the pregnant woman when she feels or detects the foetus moving. These events will be very useful for comparison purposes, as they enable a comparison with the movements detected automatically by the belt. One idea was to connect each individual fabric square (a switch) to the power supply and the other connector of the switch to a port in the acquisition module and detect if there was any signal entering in the port of the microcontroller. This possibility was abandoned due to hardware restrictions. To further develop this idea, twenty eight inputs of the acquisition module would be needed but the chosen microcontroller did not have so many inputs available. To overcome this difficulty, the final and definitive proposal to read the switches was to connect the seven columns and the four lines to input/output ports.

The algorithm to scan all the switches uses only eleven ports and has the following sequence:

- It places a signal at the first column and reads if there is any signal at the first line;
- It places a signal at the first line and reads the first column to detect any signal;
- It puts a signal at the first column and reads if there is any signal at the second line;
- It feeds a signal at the second line and reads if there is any signal at the first column;
- A signal is applied at the first column and the algorithm reads if there is any signal at the third line;
- It places a signal at the third line and reads if there is any signal at the first column;
- It places a signal at the first column and reads if there is any signal at the fourth line;
- It puts a signal at the fourth line and read if there is any signal at the first column.

When it reaches the last line verification for a column it checks if the patient pressed the button. The procedure for the other columns is the same. The data packet is built and sent to the computer when these iterations are finished for all the switches from the last column.

Some tests have been made with this belt in a pregnant woman and the results have shown that the belt was too sensitive to allow for a discrimination of movements. The belt detected some foetal movements but it was quite difficult to understand if the detection was due to a foetus movement or to the woman movement.

Note that the conductive fabrics from the On-Off belt may be washed after disconnecting all the electronics associated to the belt.

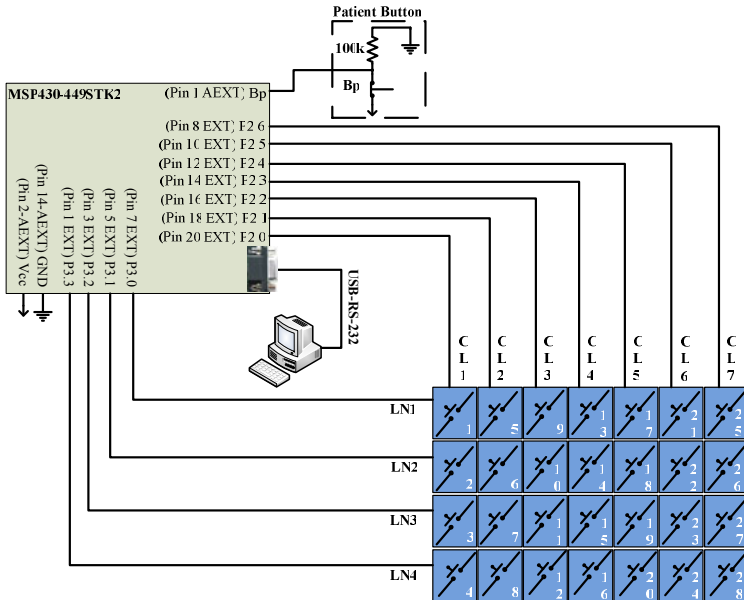


Fig. 13. System diagram for the On-Off belt

5 Experimental Results

A. Flex Sensor Belt

Some initial results were extracted from the Flex sensor belt with a patient that was not a pregnant woman. The objective of this test was to verify if the respiratory movements or other type of motion artefact influence the angles of each Flex sensor in the belt. It was verified that the respiration movements were slightly felt. Besides, if the patient moves quickly the sensors may detect the deformation from the belt.

After these preliminary tests, the Flex sensor belt was tested in a pregnant woman, in order to detect foetal movements and compare these occurrences with those signalled when the pregnant woman presses the button. A good idea that can be extracted from these initial tests is to implement a routine which automatically defines the value for a detection threshold-trigger whose values will be tuned.

The Flex Sensor View software was incorporated and its final version is presented in Fig. 14. Examples are the capability to simultaneously show eight angles from the Flex sensor, the patient counter and the option to save the data in a log file (for later treatment). This version enables the communication between the computer and the acquisition module by using a single interface a packet for all Flex sensors.

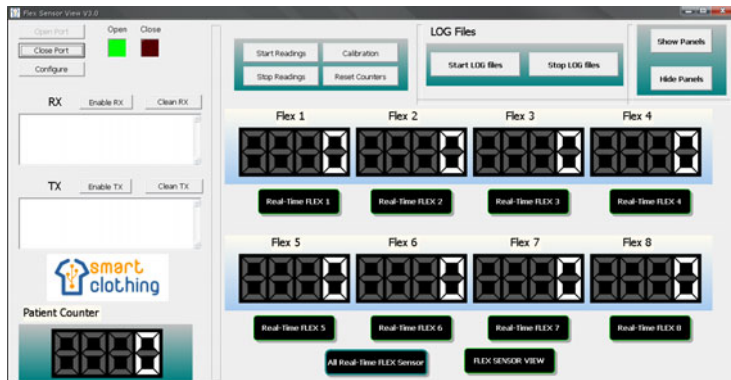


Fig. 14. Main window for Flex Sensor View application

Fig. 15 presents the real-time view chart plot for the Flex sensor, extracted from the application to display the deformation angles. For each sensor, an independent threshold trigger can be defined individually or a unique threshold value can be defined (as a whole) for all the sensors.

When considering this threshold-trigger, even if the sensor detects some motion artefact, a boundary can be established in order to tune when the application should count the deformation angle as a foetal movement.

In Fig. 15, the value used for the global threshold is equal to 15° (angle deformation). This threshold was established by analysing the experimental data. This means that the automatic counter from each Flex sensor counts a flexion as a movement when the instant value of the Flex sensor angle is larger than the threshold value at one time instant and smaller at the next time instant. As an example of how the automatic counter works, considering Flex sensor 8 in the view chart at time instant t_1 , the angle value is equal to 28° . Hence, the counter will count a foetal movement if this value decreases at the next time instant. In time instant t_2 the angle value is equal to 8° ; so, the automatic counter will add one unit to the counter of the Flex sensor 8.

Some tests were made in a pregnant woman. During the test, the patient was sitting in a chair most of the time. A calibration of the flex sensors is made in the belt circuit before any test. A test was also made on how curves vary if a sudden change of the pregnant woman position happens, as shown in Fig. 16.

One may verify that the change of position occurred approximately at the time instant 190 s. There was a lot of artefact movement detected during the change of position, which causes the loss of the initial calibration.

Another test was made while the patient was sitting in a chair. Two different foetal movement occurrences were detected. In this case, instead of presenting all the flex sensors in the same window we enabled the software option to show separate windows for each flex sensor. The movements were detected in the flex sensor 1, at time instants ≈ 420 s and ≈ 460 s, as shown in Fig. 17. A motion artefact was detected after the time instant 500 s, probably due to the mother respiration movements.

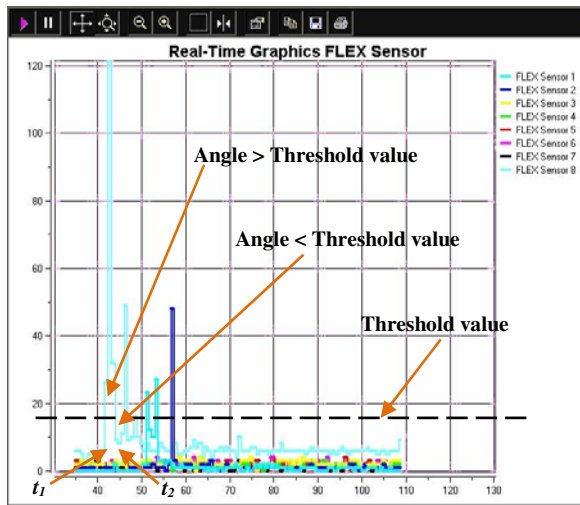


Fig. 15. Real-time view chart plot for the Flex Sensor

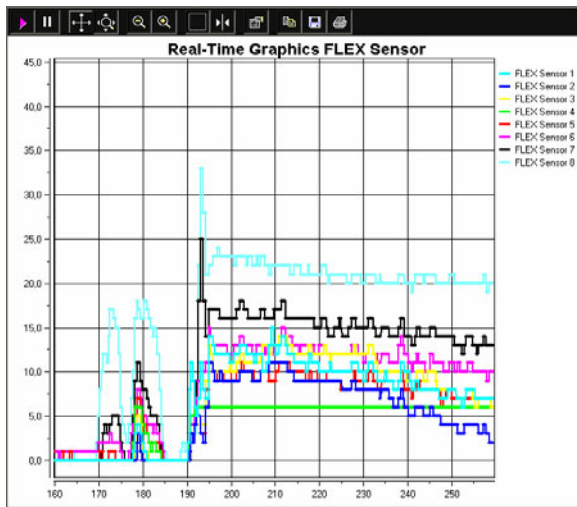


Fig. 16. Results when patient stands up at time $t = 190$ s

Simultaneously, the window that monitors the Flex sensor 2 shows two peaks, whose amplitude is larger than the other peaks in the chart, one at the time instants ≈ 420 s and another at time instant ≈ 460 s, as shown in Fig. 18. The movements detected by Flex sensor 1 caused a deformation angle larger than the one from flex sensor 2. Hence, because the Flex sensors are placed side by side (and separated by 8 cm) we may conclude that the movements detected were nearer Flex sensor 1.

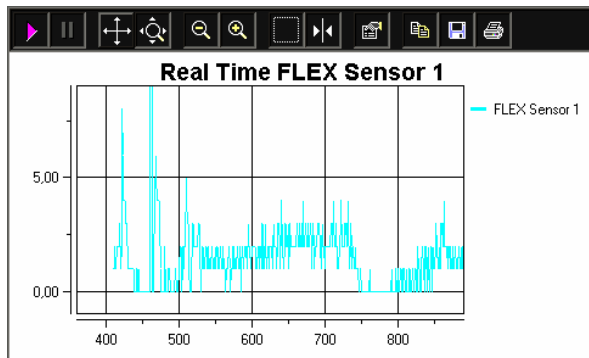


Fig. 17. Results from Flex sensor 1 when patient is sited

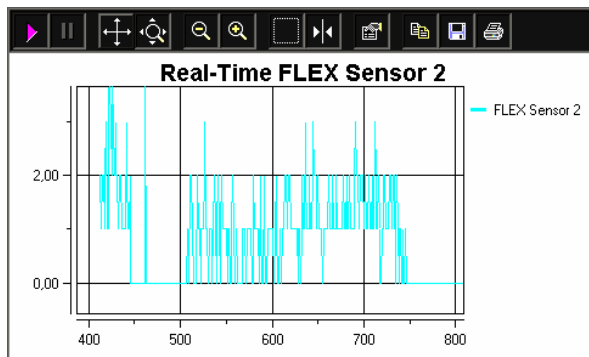


Fig. 18. Results from Flex sensor 2 (Patient sited)

Another test was made when the patient was sitting in a chair, as presented in Fig. 19. A movement was detected by the system, while the patient claims to have detected two foetal movement occurrences. The time instant when the system and the patient detected the foetus movement simultaneously was ≈ 910 s. The system detected the movement at the Flex sensors 1, 2, 3, 4, 5 and 6, with a stronger intensity in the Flex sensor 3. The other movements the pregnant woman claimed to have felt a foetus movement was at time instant ≈ 895 s. However, the system did not detect any foetal movement. At the instant ≈ 925 s the system detected a foetus movement but it was considered a false positive, as the patient did not feel it.

B. Piezoelectric Sensor Belt

All the tests of the piezoelectric sensor belt were performed in Centro Hospitalar da Cova da Beira. A woman in her 38th week of pregnancy wore a belt that incorporates three piezoelectric sensors (one central sensor and two on both sides), adjusted to the abdomen by an elastic belt. The signals obtained from the sensors were combined into only one signal, amplified, filtered and applied to an ADC

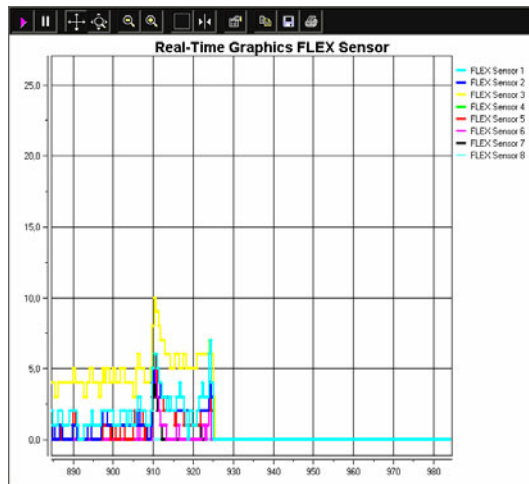


Fig. 19. Results when patient is sited

converter, and then sent to the computer via USB. At the computer, the signals were processed and graphically presented to the medical team. The pregnant woman had a manual event marker (patient button) to mark the foetal movements when she felt it, for redundancy purposes. Another device was also used, called Respisense [11] and usually applied to detect the baby breathing. The signals of the event marker and Respisense were compared with those extracted from piezoelectric sensors. Fig. 20 shows a block diagram of the circuit to acquire the signals from the sensors.

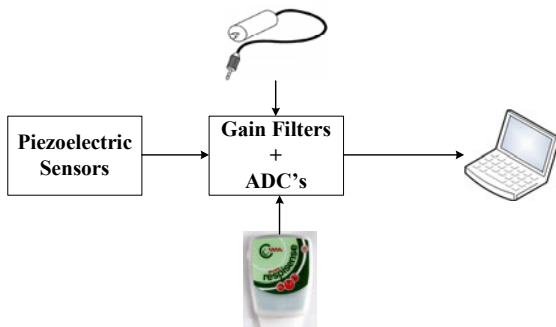


Fig. 20. Diagram for the circuit to acquire the signals from the sensors

Fig. 21 shows the Hospital environment in which the tests were performed, as well as the pregnant woman. The belt covers only a small part of the pregnant patient belly, contributing for non-ideal results. We plan to use more piezoelectric sensors in a future version of the belt.



Fig. 21. Field tests for foetal movements' detection

Fig. 22 shows the experimental results. Different signals can be observed, distinguished by different colours:

- Red – original signal (piezoelectric sensors);
- Blue – filtered signal (finite impulse high-pass response filter);
- Brown – event marker;
- Green – detected foetal movements.

Fig. 22 presents a screenshot from the program developed to display the signals from the sensors. It shows the a) multiple foetal movements simultaneously detected by the mother and sensors, as well as b) some discrepancies caused by

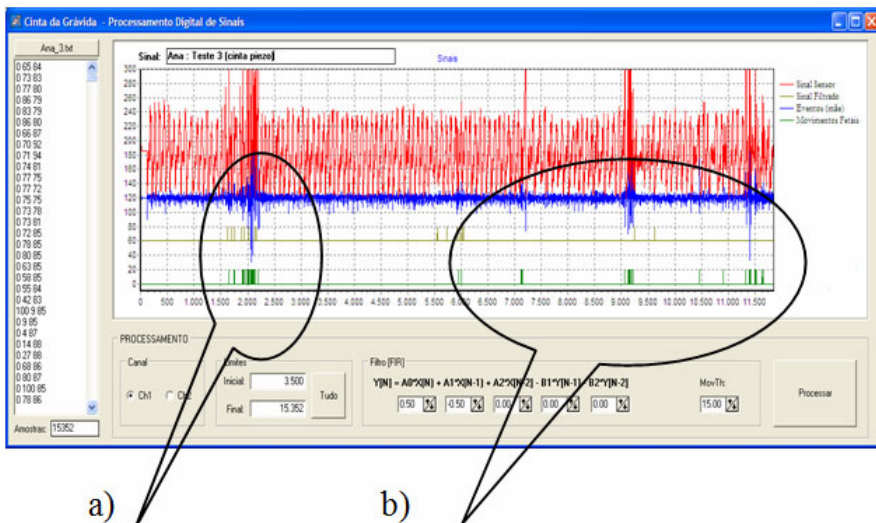


Fig. 22. Test results for foetal movements' detection

patient movements (like speaking, tossing), by the event marker detection forgotten by the patient, and due to the reduced number of piezoelectric sensors included.

From the experimental results, we can conclude that the system has a high potential to detect foetal movements, isolating them from external interferences. However, weak foetal movements are easily hidden by signals with larger amplitude, such as maternal walking, speaking and even breathing.

Filtering and interference reduction will be important topics that need further research. Also, using more piezoelectric sensors inside of the belt, to cover a broader area of the pregnant woman abdomen, is one suggestion for future developments. As a suggestion, it may be possible to use sensors built with polymer films (Polyvinylidene Fluoride) [12] in the future.

6 Conclusions

This paper presents two main versions of prototype sensor belts produced within the Smart-Clothing Project, which aim at counting the movements of the foetus in a pregnant woman. Besides the standalone solution for the Flex Sensor belt, where data can be saved into a memory card, we developed a wireless Flex sensor belt network based on the IEEE 802.15.4 standard. A hierarchical wireless network with a Wi-Fi layer on top of the sensor network will allow for extra flexibility in data communication. The system guarantees real-time and continuous foetal monitoring while creating effective interfaces for querying sensor data and store all the medical record (which can later be accessed by health professionals). Another developed belt has piezoelectric sensors incorporated onto it. The system has a high capacity to detect foetal movements, isolating them from external interferences.

As future work, we propose to implement other types of communication systems that may work together with the existing ones. For example, create a web-page where we can scroll through all the data produced in real time while sharing the information with other medical institutions. Another proposal is to implement algorithms for signal source separation, noise and motion artefact signal suppression, as well as to implement advanced algorithms for data treatment and aggregation.

Further work is needed to upgrade the signal conditioning circuitry, the processing software (to accomplish a real time filtering) and statistical techniques to detect the foetal movements in the piezoelectric belt. The data collected from the belt contains signals from the mother and foetus. An alternative approach to distinguish the different signals detected with the belt may be based on a spectral analysis instead of time domain analysis, facilitating the separation of the different signals, such as the mother respiration, foetus movements, mother's heart beat and motion artefacts. Other techniques may be based on the Fast Fourier Transform (FFT), which detects a peak from a signal composed by signals with different frequencies, or blind source separation.

Acknowledgements

This work was supported by UDR (Unidade de Detecção Remota), Department of Physics from University of Beira Interior, by IST-UNITE, by Fundação Calouste Gulbenkian, by the PhD FCT (Fundação para a Ciência e Tecnologia) grant SFRH / BD / 38356 / 2007, SFRH/BD/36742/2007, SFRH/BD/66803/2009, by the Smart-Clothing Project, by Marie Curie Intra-European Fellowship OPTIMO-BILE (Cross-layer Optimization for the Coexistence of Mobile and Wireless Networks Beyond 3G, FP7-PEOPLE-2007-2-1-IEF), and by the programmatic budget from Instituto de Telecomunicações, as it enabled to make Wireless Sensor Network hardware and software available to our work. Norberto Barroca acknowledges the MSc grant assigned to him by Instituto de Telecomunicações. Norberto Barroca and Andreia Rente acknowledge the grant assigned by Universidade da Beira Interior in the context of the Smart-Clothing project. We sincerely thank to Magda Henriques, Sandra Roque and Ana Palmeira, our patients during the tests presented in this work.

References

1. Cao, H., Leung, V., Chow, C., Chan, H.: Enabling Technologies for Wireless Body Area Networks: A Survey and Outlook. *IEEE Communications Magazine* 47(12), 84–93 (2009)
2. Evaggelos, C., Karvounis, E., Papaloukas, C., Tsipouras, M., Bougia, P., Dimitrios, I., Naka, K.: Remote maternal and fetal health monitoring during pregnancy. In: Proc. Information Technology Applications in Biomedicine - ITAB 2006, Ioannina, Greece (2006)
3. Barroca, N., Velez, F.J., Lebres, A.S. (2009) Energy-Aware Medium Access Control Protocols for Wireless Sensor Network Applications, MSc thesis, Universidade da Beira Interior (September 2009)
4. Gribbin, C., James, D.: Assessing fetal health. *Current Obstetrics & Gynaecology - Elsevier* 15(4), 221–227 (2005)
5. [http://www.hibaby.co.uk/acatalog/](http://www.hibaby.co.uk/acatalog/Angelsound_Fetal_Doppler.html)
Angelsound_Fetal_Doppler.html, Angelsound Fetal Doppler (September 2009)
6. Borges, L.M., Rente, A., Velez, F.J., Salvado, L.R., Lebres, A.S., Oliveira, J.M., Araújo, P., Ferro, J.: Overview of Progress in Smart-Clothing Project for Health Monitoring and Sport Applications. In: Proc. 1st International Symposium on applied Sciences in Biomedical and Communication Technologies - ISABEL 2008, Aalborg, Denmark, pp. 160–166 (2008)
7. [http://www.e-projects.ubi.pt/smartclothing/](http://www.e-projects.ubi.pt/smartclothing/photo_galley.html)
photo_galley.html / Smart-Clothing Project (September 2009)
8. Sohraby, K., Minoli, D., Znati, T.: Wireless Sensor Networks Technology, Protocols, and Applications. John Wiley & Sons, Hoboken (2007)
9. [http://www.adinstruments.com/products/hardware/](http://www.adinstruments.com/products/hardware/research/product/MLT1010D/)
research/product/MLT1010D/ ADInstruments (September 2009)

10. Vullings, R., Peters, C., Mischi, M., Sluijter, R., Oei, G., Bergmans, J.: Artifact reduction in maternal abdominal ECG recordings for fetal ECG estimation. In: Proc. 29th Annual International Conference of the IEEE - EMBS, Lyon, France, pp. 43–46 (2007)
11. <http://www.respisense.com/en/index.php> Respisense (September 2009)
12. <http://www.meas-spec.com/searchresults.aspx?search=Polyvinylidene%20Fluoride#> Measurement Specialities (September 2009)

An Embedded System for EEG Acquisition and Processing for Brain Computer Interface Applications

A. Palumbo¹, F. Amato^{1,*}, B. Calabrese¹, M. Cannataro¹, G. Cocorullo²,
A. Gambardella^{3,4}, P.H. Guzzi¹, M. Lanuzza², M. Sturniolo³,
P. Veltri¹, and P. Vizza¹

¹ School of Computer and Biomedical Engineering, University of Catanzaro Magna Graecia, Viale Europa, Campus “Salvatore Venuta”, 88100 Catanzaro, Italy

² Department of Electronics, Computer Science and Systems, University of Calabria, 87036, Rende, Italy

³ Institute of Neurological Sciences, National Research Council, Piano Lago, 87050 Mangone, Cosenza, Italy

⁴ Institute of Neurology, University of Catanzaro Magna Graecia, viale Europa, Campus “Salvatore Venuta”, 88100 Catanzaro, Italy
amato@unicz.it

Abstract. A new research methodology named Brain Computer Interface (BCI) studies novel human-computer interactions; by means of BCI electronics devices, paralyzed patients are able to interact with the environment using no muscular contractions. This technique provides an external electronics support to all persons with severe motor disabilities, by acquiring in continuous mode the electroencephalogram (EEG) signals and operating some processing to control a computer or other domotics devices. Patients are so allowed to control external devices or to communicate simple messages through the computer, just concentrating their attention either on codified movements or on a letter or icon on a digital keyboard. The use of a customized and optimized spatial filtering technique embedded in the BCI system, based on the detection of the Electroencephalographic activity, improves the accuracy of BCI system itself, thanks to the explicit separation of the signal activity of interest from artefact signals. In this chapter, after an overview of the state-of-the-art research on BCI systems, the spatial filtering problem in EEG signals acquisition will be illustrated. In particular, a spatial filtering algorithm, known as ICA (Independent Component Analysis) and its application will be discussed. Finally, the design and implementation of an embedded system for EEG signals acquisition and real-time processing for BCI applications will be presented. The system is based onto a very performing and reconfigurable hardware platform. Moreover ICA algorithm has been implemented for noise reduction and artifacts removal.

Keywords: BCI, signal processing, software and algorithms, embedded systems.

* Corresponding author.

1 Introduction

People with severe motor diseases require technologies that allow them to interact with the external environment. These people may also be completely paralyzed as, for example, in the case of neuro-degenerative diseases such as Amyotrophic Lateral Sclerosis (ALS), or trauma due to serious accidents. In these cases, the patients are unable to communicate in a traditional way, since this basic function requires muscles control. In the past decades, many studies have shown the ability to recover in these people partial communicative and control capabilities through the acquisition and processing of brain activity [1, 2, 3]. These systems are called Brain Computer Interfaces (BCI).

A first definition of BCI was given during the First International Meeting on BCI systems held in June 1999 at the Rensselaerville Institute, Albany, New York [4]. BCI is defined as a system that allows to communicate or control without the use of muscles or peripheral nerves.

In general, the architecture of a BCI system (Figure 1) consists of the following hardware and software sections [5]:

- Signal Acquisition: The signal can be acquired either by invasive or non-invasive systems [6]. Invasive systems allow acquisition with a signal to noise ratio higher than non-invasive systems; however they may present stability problems for long-term monitoring. The electroencephalography (EEG) is the most used non-invasive method. It is based on the detection of the electrical activity of cortical neurons extended below the electrode surface. Other non-invasive methods of acquisition are described in [7].
- Signal Conditioning: the signals coming from the sensors are amplified and conditioned to enhance the signal dynamic range [8].
- Pre-processing: this stage is aimed to reduce the effects of the artefacts (e.g. ocular, muscular or cardiac potentials) and to improve the spatial resolution of the signals, with appropriate digital signal processing techniques [9].
- Features extraction: at this stage, features of interest are extracted. These features consist of signal variations linked to the patient's underlying neurological mechanisms which control the system. The features of interest can be extracted in the time, frequency or time/frequency domain. There are several extractors used [10]; the most common are:
 - Estimation of the power spectral density using either the Welch's method or the autoregressive model;
 - Time/frequency analysis using either the Short Time Fourier Transform (STFT) or the Wavelet Transform;
 - Coherence analysis of the EEG signals.
- Features classification: the vector of features extracted at the previous stage is given as input to the classifier, which associates it to a particular class related to a control signal [11].
- Control of the device: the control signals can be used in the context of smart home, word processing or neuroprostheses applications.

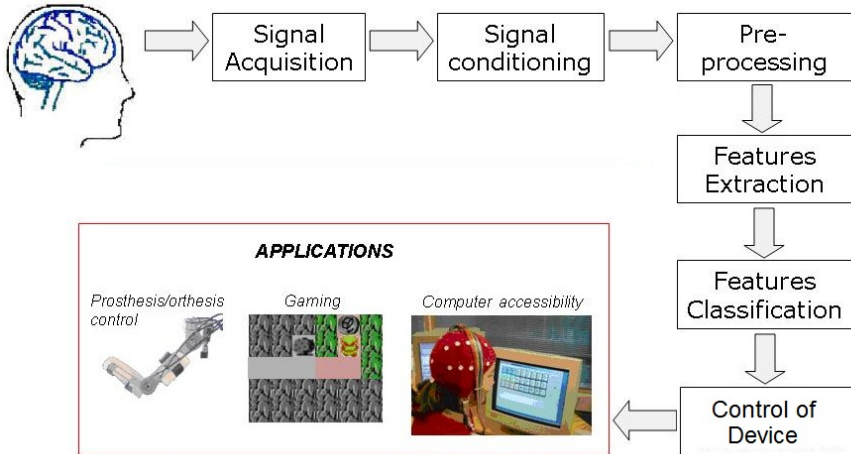


Fig. 1. Architecture of a BCI system

Some of the major limitations of the EEG-based BCIs currently under development are briefly reported following:

- they are bulky and not portable systems because they are based on the use of commercial EEG amplifiers connected to personal computers to elaborate and generate control signals;
- the brain signals detected by EEG-based systems are relatively weak and affected by several artefacts.

This work addresses to these issues. In particular a novel embedded system design and implementation for BCI application will be described. The system features a portable and reconfigurable architecture for signal acquisition and real time processing. Furthermore spatial filters have been implemented for a more accurate EEG signals detection.

The chapter starts with a description of BCI technology. Section 4 introduces the spatial filtering problem in the context of the EEG acquisition. The description will focus on a specific spatial filtering procedure, known as Independent Component Analysis (ICA). Finally, an embedded system for the acquisition, conditioning and processing of EEG signals for BCI applications is proposed.

2 State-of-the-Art in BCI Technology

The number of research groups working on BCI has increased remarkably in recent years (Figure 2) [12]. The skills required are multidisciplinary. In this paragraph the state of the research of some of the principal BCI laboratories will be described.

The beginning of research on BCI dates back to the Seventies. At that time, Jacques Vidal identified a BCI as a computer-based system capable of producing

detailed information on the functions of the brain. He also built a first BCI system based on the detection of visual evoked potentials [13].

Farwell and Donchin [14] have used the P300 evoked potential to achieve a BCI system such that the user is able to select letters for word processing operations. In particular, a matrix which contains the letters of the alphabet is displayed on the computer monitor and user is asked to select the letters (that he/she wants) counting the number of times that the column or row containing the letter are blinking. Letters flash at a low frequency of 10 Hz and the P300 component is identified by assessing the mean response for each row and each column. After a long phase of training, users are able to achieve a rate of 2.3 characters per second with an accuracy of 95%. Unfortunately the system is slow because stimulus must first be presented and then the collected signals have to be mediated.

Pfurtscheller and his group have started the project "Graz Brain Computer Interface" in 1991 at the University of Technology of Graz in Austria. Several prototypes have been realized over the Nineties. Generally these prototypes detect event-related de-synchronization (ERD) and synchronization (ERS) during the task of movement imagination and translate them into control signals [15]. The control outputs are used for experiments in virtual reality (VR) with tetraplegic patients, for control of neuroprostheses and for functional electrical stimulation (FES) used to restore motor functions.

One of the major laboratories involved in BCI research is located at the Wadsworth Center in Albany, near New York. Jonathan Wolpaw and his colleagues began their research at the Wadsworth BCI Center in 1986. They focused on the use of μ -rhythm (8-12 Hz) and β -rhythm (13-28 Hz) [16]. Using these rhythms, generated in correspondence of the sensorimotor cortex, subjects learn to move the cursor on a computer screen as feedback.

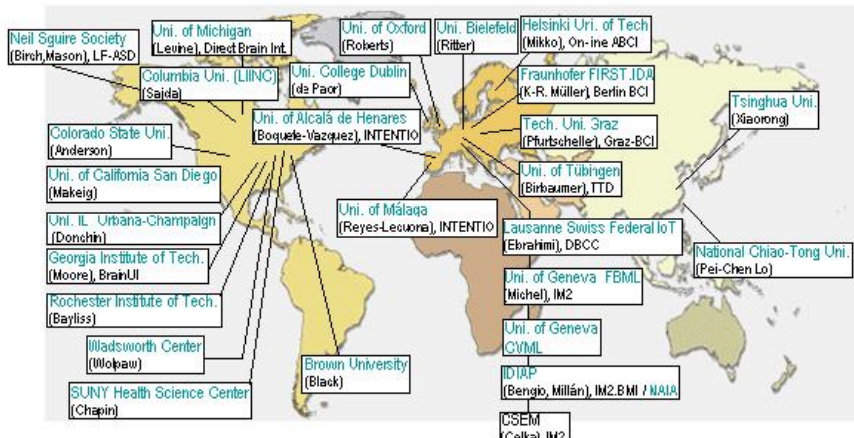


Fig. 2. Some BCI research laboratories.

The Laboratory of Neuroelectrical Imaging and BCI at Santa Lucia Foundation in Rome has started the development of an assistive system for motor impaired individuals (Assistive System for Patient's Increase of Communication, ambient control and mobility in absence of muscular Effort, ASPICE project). The aim is to allow these subjects to control domotic appliances and a small robot [17].

At the Wadsworth Center in recent years a software platform called BCI2000 has been developed and tested [18]. It has been provided to several laboratories around the world.

3 Characteristics of EEG Signals

The features used as input of EEG-based BCI systems include slow cortical potentials [19], event-related potentials (ERPs) (such as evoked potentials or visual evoked potentials) [20, 21] and rhythmic activity [22].

Slow cortical potentials are slow oscillations of cortical activity with frequency between 0 and 2 Hz. Healthy and pathological subjects can learn to control voluntarily these changes. To develop this capability they must perform appropriate training.

The ERPs are variations of the EEG signal caused by a particular event or stimulus. They can be divided into exogenous and endogenous. Potential exogenous occurs 100ms after the onset of the stimulus, while potential endogenous occurs after 100 ms from the beginning of the stimulus. The most studied ERP is the P300 component. It is given by a positive variation of the EEG signal that appears approximately 300-400 ms after a stimulus. It is located on the central parietal region and no training is required.

Evoked potentials are a subset of the ERP occurring as a result of a physical stimulus (visual, auditory). A typical evoked potential is the visual evoked potential (VEP). Other features are the steady-state visual evoked potentials (SSVEPs). They occur when a visual stimulus is presented repeatedly at a frequency of 5 - 6 Hz or greater.

The rhythmic activity of the EEG signal varies according to the state of consciousness and age of the patient [23]. The frequency and the amplitude of EEG waves are the two main parameters under which the fundamental rhythms are distinguished:

- Delta: frequency 1-4 Hz and amplitude up to 200 μ V; delta rhythm consists of waves at low frequency and high voltage. In the state of sleep delta waves are physiological; in other cases they take a clear pathological significance, as when recorded from a limited area of the cerebral cortex during wakefulness. In this case there can be the suspect of a pathological lesion that, by altering the normal structure of the brain, prevents the appearance of alpha or beta rhythm.
- Theta: frequency 5-7 Hz and amplitude up to 100 μ V; theta rhythm can be recorded physiologically from the temporal and parietal lobes of young subjects. In the first weeks after birth, the EEG shows only theta and delta activities.

- Alpha: frequency 8-14 Hz and amplitude 20-50 μ V; alpha waves occur after 18 months of the child's life and their presence increases with age. In the adult at rest, lying with closed eyes, the EEG is characterized by the presence of alpha rhythm, which is evident especially on the occipital lobes and adjacent temporo-parietal areas. If the subject is asked to focus the attention or if suddenly opens his/her eyes the alpha rhythm disappears.
- Beta: frequency 15-30 Hz and amplitude 5-20 μ V; this rhythm appears in conditions of wakefulness and in a particular phase of sleep: despite the individual is sleeping, an electrical rhythm is exhibited as if he/she was awake. The beta rhythm is detected in the central and frontal areas.
- Gamma: frequency >30 Hz and amplitude <10 μ V; waves range are usually associated with sensory and cognitive activities.
- Mu: frequency 8-12 Hz and amplitude up to 80 μ V; it is similar to the alpha rhythm but is recorded in the central areas and may appear even in parietal derivations. It is observed only in 19% of healthy adults. It is recorded in subjects relaxed with open eyes and vanishes with motor activity.

3.1 Electrode Placement: The International 10-20 System

To register an EEG, several electrodes are placed on the surface of the skull. To allow comparison with measurements in the same subject or the comparison of measures in different subjects, in the late '40s, the International Federation of Electroencephalography and Clinical Neurophysiology has developed a universal system, known as the International System 10-20 (Figure 3), that describes the exact location of each electrode [24].

Lines are measured, using as a starting point precise anatomical locations:

- nasion (upper attachment of the nose),
- inion (bump at the base of the occipital bone),
- preauricular point (depression bone immediately in front of tragus).

These lines draw a grid on the surface of the skull; the electrodes are positioned at the intersection points of the grid. The distance between an electrode and the other is always 10% or 20% of the total length of the line.

Each location of an electrode is named using a letter and a number (or sometimes a second letter). The letter takes its name from the underlying brain lobe (Fp = frontopolar, F = frontal, T = temporal, P = parietal, O = occipital), except for the electrodes C (central). The number is even (2, 4, 6, 8) for the right side and odd (1, 3, 5, 7) for the left, with lower values in the medial position. The position on the midline is denoted by the letter Z. A1 (left) and A2 (right) identify regions electrically neutral as reference (ear lobe or mastoid).

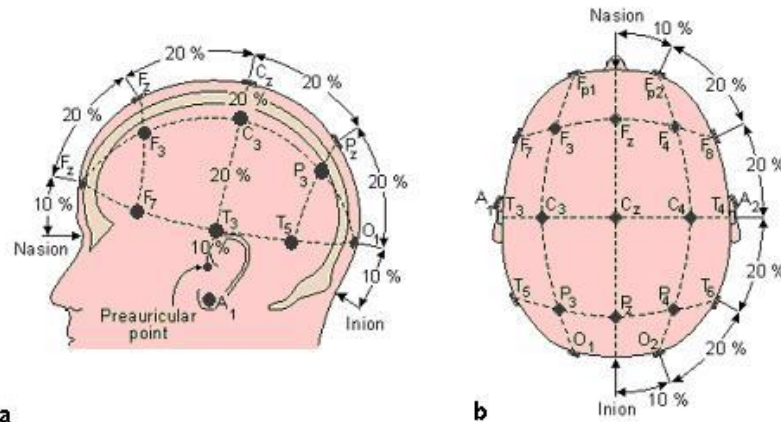


Fig. 3. The International 10-20 System of electrode placement

4 Spatial Enhancement of EEG-Data

EEG signals acquired through the scalp are characterized by a low signal to noise ratio, due to three principal aspects: (i) non physiological artefacts, (ii) physiological artefacts and (iii) mixture of EEG potentials.

Non-physiological artefacts are due to the external noise which is coupled to the EEG signals. They usually can be avoided through an appropriate filtering stage and/or appropriate shielding techniques.

Physiological artefacts are electrical signals coming from inside the human body; among these, the EEG signals are mainly affected by muscle, electrocardiographic and ocular potentials. Moreover, even breathing can cause artefacts by introducing rhythmic activity synchronized with the respiration's movements. Furthermore, the sweating can modify the impedance of the electrodes corrupting the EEG signals.

Another problem related to the accuracy of EEG acquisition is represented by the mixture of EEG potentials localized into the cerebral cortex [25].

In a BCI system, a filtering pre-processing stage is needed in order to improve the signal to noise ratio; in particular, this stage is aimed to reduce the effects of the artefacts and to improve the spatial resolution of the signals, by using spatial filtering techniques [26, 27].

Different spatial filtering techniques are developed with respect to EEG signals separation. In this chapter we present the implementation onto a novel and compact data acquisition embedded architecture of an algorithm for EEG spatial filtering, based on the Independent Component Analysis (ICA) technique.

4.1 Fundamentals of the ICA Technique

The ICA technique is based on the fact that physiological EEG signals, arising from different cortical areas, are temporally independent [28]. This means that the

EEG activity, generated at a given moment in a specific cortical domain, is not linked to the EEG generated in other areas at the same time. The idea that the EEG signals are originated from processes temporally independent or nearly is consistent with what has been observed on the functional specialization of different cortical areas.

Different studies have demonstrated that the ICA succeeds in separating the EEG activity from the artefacts [29, 30]. Some attempts have been made in selecting the different rhythmic components belonging to the neurological signals through this algorithm [31]. As a result, the ICA algorithm appears suitable to be efficiently used in the pre-processing stage of a BCI system.

In order to individuate the signals generated by different sources, the ICA algorithm exploits the following generative model

$$\underline{x}(t) = \underline{\underline{A}}\underline{s}(t) \quad (1)$$

where $\underline{x}(t)$ are the signals acquired by the sensors, $\underline{s}(t)$ are the signal sources and $\underline{\underline{A}}$ is the mixing matrix, whose coefficients depend on both the characteristics of the propagation medium and the distance between sources and sensors. It is assumed that the number of hidden sources (n) is less or equal than the number of measured channels (m). In particular, the number of statistically independent components is not generally known. For the EEG activity, if the acquisitions are performed by a low number of electrodes, the actual number of sources will be greater than the available number of electrodes and therefore in this case all the sources will not be established. In the case of measures with a high density of electrodes, however, the algorithm will extract the components that do not actually contain any physical information and, therefore, it is necessary to select the subset of independent real components. The number of independent sources is very important for the quality and accuracy of the algorithm.

The aim of ICA is to recover the original signals only from the observations and therefore it is necessary to build a de-mixing matrix W , i. e. the inverse of the mixing matrix,

$$\underline{s}(t) = \underline{\underline{W}}\underline{x}(t) \quad (2)$$

where $\underline{s}(t)$ are the estimates of the independent components.

Estimating the independent sources without knowing the de-mixing matrix and without making any assumption on these sources is, from a mathematical point of view, an untractable problem. Therefore, it is necessary to make some assumptions; in particular, to solve this problem, one approach is to exploit the information on the statistical properties of the signals to estimate the coefficients of the mixing matrix. The first assumption is that the sources are statistically independent. A second hypothesis is that the sources have a distribution of amplitudes of a non-Gaussian type. Finally, another assumption is that the mixing process is linear and instantaneous. In the biomedical field, this means that sources are linearly superimposed and that the delays of propagation of the signals from the sources to the electrodes can be neglected. This assumption is valid for EEG signal features

of interest within the BCI, as for example the rhythmic activity. Indeed, the EEG signals are placed in the low frequency range, so it is reasonable to assume that there are no time delays between signals coming from different sources and the point of sensing. Furthermore, the mixing of independent components is considered stationary, because it is assumed that the mixing matrix does not change its structure over time. For the detection of EEG signals, the sources have fixed locations and orientations, but a time-varying amplitude. Thus, the coefficients of the mixing matrix are constant.

A criterion used in the search for independent components is based on the Central Limit Theorem, which states that the probability density of the sum of random variables, independent each other and with equal probability density, tends towards a Gaussian distribution when the number of variables increases. Therefore, the sum of two random variables has a distribution that is more similar to a Gaussian than the individual distributions. Considering the ICA generative model of data, a typical mixture of independent components is closer to a Gaussian distribution than the original signals. The estimate of the independent variables can be obtained through the inversion of the generative model.

In the BCI, few attempts have been made to use this algorithm [32]. Reference [33] presents the results of an initial study on the EEG signals related to the movement for BCI. These signals are contaminated by muscle artefacts and therefore it is difficult to analyze and to use them in BCI systems. The authors submit the EEG signals recorded during the flexion of the finger at the stage of pre-processing carried out with the ICA. The analysis is conducted with the software EEGLAB. By using topographical maps and the power computation in specific ranges, it is possible to distinguish artefacts from neurological components.

Different ICA methods to separate signal components have been developed (Infomax, JADE, SOBI). The most common ICA method is FastICA. The FastICA algorithm is a computationally highly efficient method for performing the estimation of ICA [34]. This method adjusts the separating matrix (or de-mixing matrix, W) to maximize the *negentropy*. The FastICA method is implemented according to the following steps:

- Calculates negentropy:* Negentropy measures non-gaussianity of a time series. For each independent component, it is computed according to the following equation:

$$J(s_i) = [E\{G(s_i)\} - E(v)]^2, i = 1, \dots, n \quad (3)$$

where n is the number of independent components, s_i represents the i -th independent component, v is a Gaussian variable of zero mean and unit variance, and $G(\cdot)$ is any non-quadratic function specified within the chosen method (Table 1).

- Maximizes negentropy:* Each independent component s_i can be computed by an input time series $x(t)$ multiplied by coefficients in the separating matrix. It is possible to obtain the maximum value for negentropy by adjusting the coefficients in the separating matrix by the Newton optimization method.

Table 1. Gaussianity function for each method

Method	Gaussianity Function
Square	$G(u) = \frac{1}{3}u^3$
Cube	$G(u) = \frac{1}{4}u^4$
Tanh	$G(u) = \log \cosh u$
Gaussian	$G(u) = -\exp\left(\frac{-u^2}{2}\right)$

5 The Design and Implementation of an Embedded System for BCI Applications

The EEG-based BCI systems described in the section 2 remain at the stage of laboratory demonstration. They are neither compact nor portable systems because the EEG signals are amplified and conditioned through commercial EEG amplifiers and then the algorithms for features extraction and classification run on personal computers [35]. So they cannot be used conveniently in hospitals or at home. Instead, to make the BCI system an effective assistive communication and control device, parameters such as size, robustness, portability and power consumption should be considered.

There are some studies regarding the design of portable BCI devices. In [36] an environmental controller using a BCI technique based on steady-state visual evoked potential is described. The system is composed of a stimulator, a digital signal processor (DSP) and a trainable infrared remote-controller. Edlinger et al. [37] have developed a portable pocket PC-based BCI. The eight-channels system with its compact dimensions allows the usage outside the research laboratory for patient training and also for implementing sophisticated applications. However, these systems mainly focused on the monitoring hardware, rather than on real-time analysis. Lin et al [38] propose a novel BCI system that can acquire and analyze EEG signals in real-time. The BCI system consists of a four-channels bio-signals acquisition/amplification module, a wireless transmission module, a dual core signal processing unit and a host system for displaying and storage. This system was implemented for real-time driver's drowsiness detection and warning.

In the following section a novel embedded real-time system for EEG acquisition and processing for BCI applications is presented [39]. The system has been developed on a commercial platform, named CompactRIO, produced by National Instruments (NI) lab. The proposed approach is based on the use of a system which performs better than that one described in [38]. It is based on the use of a reconfigurable embedded control and data acquisition system with Field Programmable Gate Array (FPGA) technology. In particular, the system shows the following advantages: it is modular, portable, with low power consumption and hardwired algorithm on FPGA matrix. Moreover, ICA and spatial filters are employed for noise reduction and artefacts removal.

5.1 Compact-RIO Architecture

The NI CompactRIO is a complete, reconfigurable embedded control and data acquisition system; it exhibits a flexible and open architecture for ultrahigh performance and customization [40]. CompactRIO consists of a low-power consumption embedded real-time processor, a high-performance FPGA for reliable stand-alone embedded or distributed applications and I/O modules (Figure 4).

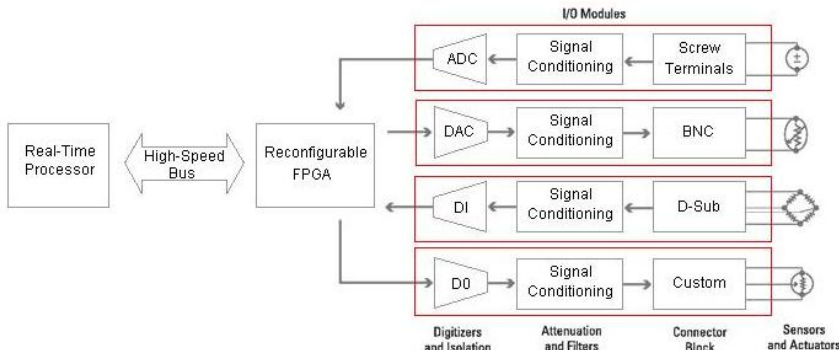


Fig. 4. Compact-RIO Architecture

These modules include built-in connectivity for direct connection to sensors and actuators, signal conditioning, conversion circuitry (such as ADC or DAC) and an optional isolation barrier. Each I/O module is connected directly to the FPGA which in turn is connected to the embedded real-time processor via a high-speed PCI bus. In the modular configuration, the embedded controller chassis containing the FPGA are sold separately. The design represents a low-cost architecture with open access to low-level hardware resources.

The CompactRIO embedded system features an industrial 400 MHz Freescale MPC5200 processor that deterministically executes LabVIEW Real-Time applications on the reliable Wind River VxWorks real-time operating system. The real-time processor also consists of a dual 11 to 30 VDC supply inputs, a user DIP switch, LED status indicator, a real time clock, watchdog timers and other features for high reliability.

5.1.1 Reconfigurable I/O (RIO) Technology

NI reconfigurable I/O (RIO) technology allows to define own custom measurement hardware circuitry using reconfigurable FPGA chips and LabVIEW graphical development tools [41]. The FPGA chip and surrounding circuitry in RIO core enable LabVIEW to automatically synthesize a highly optimized electrical circuit implementation of input/output, control and/or communication applications. The chip can be programmed with the LabVIEW FPGA tool, which is a graphical tool to program and customize FGPAs more simply than the traditional complex design languages, such as VHDL.

FPGA devices are widely used because of their reconfigurability, high-performance, small size and low engineering development costs.

5.1.2 Description of FPGA Technology

A FPGA is an integrated circuit designed to be configured by the customer or designer even after the product has been installed in the field — hence the name “field-programmable” [42, 43]. FPGAs contain programmable logic components, called “logic blocks”, and a hierarchy of reconfigurable connections that allow the blocks to be “wired together”. Logic blocks can be configured to implement any logical function, like AND and XOR, and/or to perform complex functions. In particular, libraries of predefined complex functions and circuits, called IP cores, are available to simplify the design of complex systems in FPGAs. Often the logic blocks also include memory elements, as simple flip-flops or complete blocks of memory.

The most common FPGA architecture consists of an array of configurable logic blocks (CLBs), I/O pads and routing channels. Each logic block consists of a four-input lookup table and a flip-flop, as shown in Figure 5.

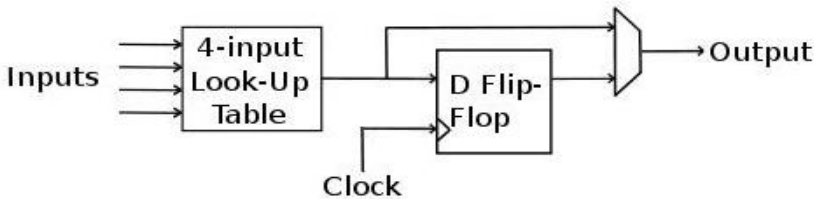


Fig. 5. Typical FPGA logic block

Modern FPGA families include higher level functionality fixed into the silicon. Examples of these include multipliers, generic DSP blocks, embedded processors, high speed I/O logic and embedded memories. This reduces the area required and increases the computational speed.

The FPGA configuration is generally specified by using a hardware description language (HDL) or a schematic design. The HDL form might be recommended when working with large structures to avoid to draw every piece by hand but just specify them numerically. Instead, schematic entry can be used for easier visualization during the design phase. The most common HDLs are VHDL (Very Hard Description Language) and Verilog.

Then, a technology-mapped net list is generated by using an electronic design automation tool and it is fitted to the actual FPGA architecture performing a place-and-route process. The user will validate the map, place and route results via timing analysis, simulation, and other verification methodologies. After the design and validation process, the binary file is generated and it is used to (re)configure the FPGA.

5.2 A Compact RIO-Based System for EEG Acquisition and Processing for BCI Applications

5.2.1 Description of System Architecture and Functionalities

As reported in the previous section, traditionally most BCI systems use bulky equipments to measure brain activity. These systems are unsuitable for patients because they limit mobility. We have developed a novel stand-alone embedded system for EEG signals acquisition and processing for BCI applications [39]. The system is based on the use of a Compact-RIO platform, whose features and architecture have been outlined in the previous section. In particular, its size and weight features allow to realize a wearable and comfortable BCI device.

Our system provides a wide variety of I/O connections and a high channel density. This is an important feature because it renders the platform flexible and adaptable to different EEG experiments for final target applications. Also the I/O modules allow an high accuracy concerning the EEG signal acquisition. Specifically, the FPGA chip manages the I/O resources of the system, determining the number of analog channels of acquisition and the sampling rate; furthermore, the FPGA performs a first pre-processing stage. A digital filters bank is synthesized on the FPGA hardware, in order to enhance the EEG signals elaboration performances; filtered signals are then transmitted to the controller through a FIFO DMA.

The PowerPC section controls in real-time the whole system and executes the processing algorithms. A pre-processing stage is implemented; in particular, the digitized signals are spatially filtered through the ICA technique. The algorithm executed by the PowerPC is the FastICA; after pre-processing, the features of interest for BCI applications are extracted in the frequency domain through spectral analysis. The EEG signals power is evaluated in various pre-defined bands. Power spectra are estimated through a non-parametric method based on the Fast Fourier Transform.

It is worth pointing that our system represents an interesting novelty in BCI research since it is a stand-alone platform managed in real-time. Indeed signal processing of existing BCI systems is often performed off-line using personal computers; a real-time signal analysis is needed to realize an effective BCI system.

Moreover, the proposed system enables high speed of acquisition and elaboration of the EEG signals thanks to the high-performance I/O hardware section and the embedded PowerPC microprocessor. The modular configuration provides the most flexibility in system configuration and performance selection. All these characteristics render the proposed system suitable for real-time BCI applications.

5.2.2 Testing Results

In this section the results relative to ICA processing and spectral analysis implemented on a Compact-RIO based system are reported. For testing purposes, we analyzed the EEG activity from three signals acquired by electrodes that were spatially close each other and these signals were processed through the ICA technique. Figure 6 shows the signals acquired by electrodes Fp2 (Fig. 6a), F4 (Fig. 6b) and F8 (Fig. 6c) (the electrodes are set on the right frontal lobe) and the signal components extracted by the FastICA algorithm, which succeeds in separating

beta rhythmic activity (14-30 Hz) from different types of artefact (ocular and cardiac signals). Indeed the algorithm that we have implemented on the Compact-RIO platform individuate a component due to the ocular activity (IC1, Fig. 6d), a cardiac artefact of mechanic type (known as wrist artefact) (IC2, Fig. 6e) and the beta rhythmic activity (IC3, Fig. 6f) typical of the frontal lobes. As reported in the above sections, different papers outline the efficiency of ICA algorithms in separating rhythmic activity from biological artefacts, but all these studies are off-line. Instead, this pre-processing stage is performed in real-time.

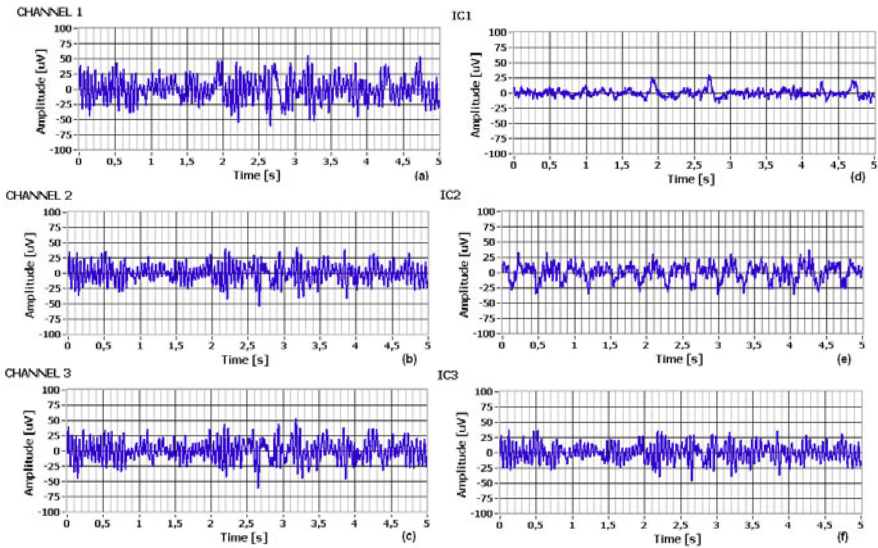


Fig. 6. The signals acquired by the Fp2 (a), F4 (b) and F8 (c) electrodes. The corresponding extracted signal components (d, e, f).

The origin of these components is also confirmed by the analysis of the power spectrum, obtained through the FFT algorithm. The power spectrum of the mixed signals (Figure 7) turns out to be very similar, whereas much less similarity is evident in the power spectrum of the independent components. More precisely, the power spectrum of the component IC1 shows a remarkable activity in the band below 4 Hz, which is the typical band of the ocular artefacts. The component IC3 shows evident components in the range of frequencies between 15 and 25 Hz. The latter are in the band of the beta rhythmic activity (15-30 Hz).

In summary, the implemented system is able to effectively increase the spatial resolution of the acquired EEG and to detect important artifacts present in the EEG. Such platform is thus a first step toward a more accurate and precise BCI systems and applications.

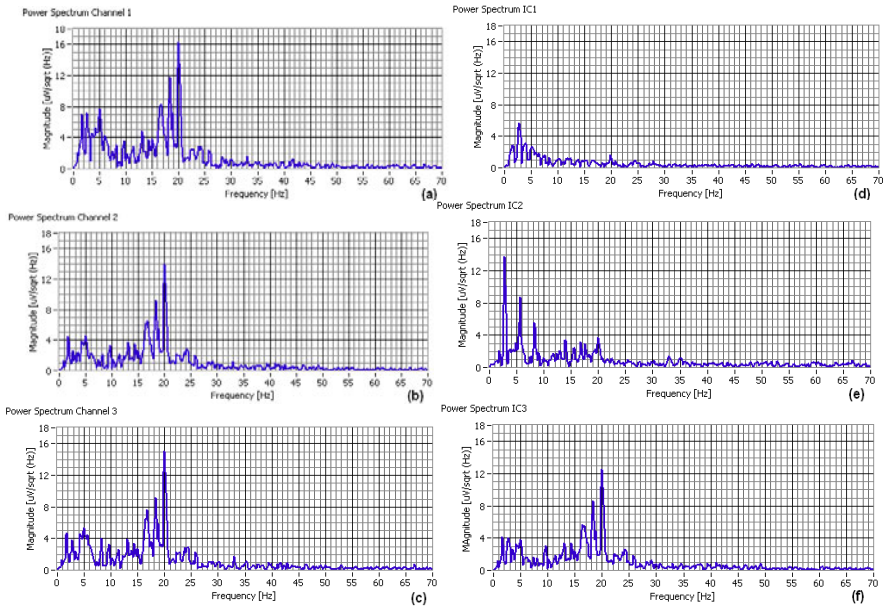


Fig. 7. The power spectrum of the signals acquired by the Fp2 (a), F4 (b) and F8 (c) electrodes and those of the extracted signal components (d, e, f).

6 Conclusions

Brain computer interface is an important research topic in the field of neural engineering, rehabilitation and cognitive neurosciences. BCI systems enable the acquisition and analysis of brain activities in order to establish a direct communication channel between the brain and an external device. Most of the BCI systems acquire and process EEG signals by means of non-invasive detection of cerebral activity with a good temporal resolution but poor spatial resolution. In literature several spatial filtering algorithms for EEG analysis, useful to improve signal to noise ratio and spatial resolution, are provided.

Most of BCI designs were realized for real applications, such as domotic. So, in the last years, there has been an increasing need to develop stand-alone wearable BCI devices, capable of high-fidelity recording and online signal processing. In this chapter a novel embedded system for EEG acquisition and processing for real time and portable BCI applications has been presented. A first set of interesting results are reported to demonstrate the effectiveness of the proposed approach.

References

1. Mason, S.G., Bashashati, A., Fatourechi, M., Navarro, K.F., Birch, G.E.: A comprehensive survey of brain interface technology designs. *Annals of Biomedical Engineering* 35(2), 137–169 (2007)

2. Donoghue, J.P.: Connecting cortex to machines: recent advances in brain interfaces. *Nature Neuroscience* 5, 1085–1088 (2002)
3. Wolpaw, J.R., Birbaumer, N., McFarland, D.J., Pfurtscheller, G., Vaughan, T.M.: Brain-computer interfaces for communication and control. *Clinical Neurophysiology* 113(6), 767–791 (2002)
4. Wolpaw, J.R., Birbaumer, N., Heetderks, W.J., McFarland, D.J., Peckham, P.H., Schalk, G., Donchin, E., Quatrano, L.A., Robinson, C.J., Vaughan, T.M.: Brain-Computer Interface Technology: A Review of the First International Meeting. *IEEE Transactions on Rehabilitation Engineering* 8(2), 164–173 (2000)
5. Mason, S.G., Birch, G.E.: A general framework for brain-computer interface design. *IEEE Transactions on Neural Systems and Rehabilitation Engineering* 11(1), 70–85 (2003)
6. Wolpaw, J.R., Loeb, G.E., Allison, B.Z., Donchin, E., Nascimento, O.F., Heetderks, W.J., Nijboer, F., Shain, W.G., Turner, J.N.: BCI meeting 2005: Workshop on signals and recording methods. *IEEE Transactions on Neural Systems and Rehabilitation Engineering* 14(2), 138–141 (2006)
7. Ortiz, S.J.: Brain-Computer Interfaces: Where Human and Machine Meet. *IEEE Computer* 40(1), 17–21 (2007)
8. Cincotti, F., Bianchi, L., Birch, G., Guger, C., Mellinger, J., Scherer, R., Schmidt, R.N., Yáñez Suárez, O., Schalk, G.: BCI Meeting 2005-Workshop on Technology: hardware and software. *IEEE Transactions on Neural Systems and Rehabilitation Engineering* 14(2), 128–131 (2006)
9. Bashashati, A., Fatourechi, M., Ward, R.K., Birch, G.E.: A survey of signal processing algorithms in brain – computer interfaces based on electrical brain signals. *Journal of Neural Engineering* 4, R32–R57 (2007)
10. McFarland, D.J., Anderson, C.W., Müller, K.R., Schlögl, A., Krusienski, D.J.: BCI Meeting 2005–workshop on BCI signal processing: feature extraction and translation. *IEEE Transactions on Neural Systems and Rehabilitation Engineering* 14(2), 135–138 (2006)
11. Lotte, F., Congedo, M., Léchner, A., Lamarche, F., Arnaldi, B.: A review of classification algorithms for EEG-based brain computer interfaces. *Journal of Neural Engineering* 4, R1–R13 (2007)
12. International Assessment, International Assessment of research and development in brain computer interfaces. WTEC Panel Report (2007)
13. Vidal, J.: Towards Direct Brain-Computer Communication. *Annual Review of Biophysics and Bioengineering* 2, 157–180 (1973)
14. Farwell, L.A., Donchin, E.: Talking off the top of your head: a mental prosthesis utilizing event-related potentials. *Electroencephalography and Clinical Neurophysiology* 70, 510–523 (1988)
15. Pfurtscheller, G., Neuper, C., Guger, C., Harkam, W., Ramoser, H., Schlögl, A., Obermaier, B., Pregenzer, M.: Current Trends in Graz Brain-Computer Interface (BCI) Research. *IEEE Transactions on Rehabilitation Engineering* 8(2), 216–219 (2000)
16. Wolpaw, J.R., McFarland, D.J., Vaughan, T.M.: Brain Computer Interface Research at Wadsworth Center. *IEEE Transactions on Rehabilitation Engineering* 8(2), 222–226 (2000)
17. Aloise, F., Cincotti, F., Babiloni, F., Marciani, M.G., Morelli, D., Paolucci, S., Oriolo, G., Cherubini, A., Sciarra, F., Magnola, F., Melpignano, A., Davide, F., Mattia, D.: ASPICE: An interface system for independent life. In: Proc. of 4th International Conference on Smart Homes and Health Telematics, ICOST (2006)

18. Schalk, G., McFarland, D.J., Hinterberger, T., Birbaumer, N., Wolpaw, J.R.: BCI2000: a general-purpose brain-computer interface (BCI) system. *IEEE Transactions on Biomedical Engineering* 51, 1034–1043 (2004)
19. Birbaumer, N., Ghanayim, N., Hinterberger, T., Iversen, I., Kotchoubey, B., Kübler, A., Perelmouter, J., Taub, E., Flor, H.: Spelling device for the paralyzed. *Nature* 398, 297–298 (1999)
20. Serby, H., Yom-Tov, E., Inbar, G.F.: An improved P300-Based Brain Computer Interface. *IEEE Transactions on Neural Systems and Rehabilitation Engineering* 13(1), 89–98 (2005)
21. He, Q., Wu, B., Wang, H., Zhu, L.: VEP Feature Extraction and Classification for BCI. In: Proc. of 8th International Conference on Signal Processing (2006)
22. Pfurtscheller, G., Neuper, C.: Motor Imagery and Direct Brain–Computer Communication. *Proc. of The IEEE* 89(7), 1123–1134 (2001)
23. Nyedermeyer, E., Lopes da Silva, F.: *Electroencephalography: Basic Principles, Clinical Applications and Related Fields*. Williams & Wilkinsfourth Edition (1999)
24. American Clinical Neurophysiology Society Guidelines, <https://www.acns.org/>
25. Nunez, P.L.: *Electric Fields of the Brain: The Neurophysics of EEG*. Oxford University Press, New York (1981)
26. Fatourechi, M., Bashashati, A., Ward, R.K., Birch, G.E.: EMG and EOG artefacts in brain computer interface systems: a survey. *Clinical Neurophysiology* 118(3), 480–494 (2007)
27. McFarland, D.J., McCane, L.M., David, S.V., Wolpaw, J.R.: Spatial filter selection for EEG-based communication. *Electroencephalography and Clinical Neurophysiology* 103(3), 386–394 (1997)
28. James, C.J., Hesse, C.W.: Independent Component Analysis for biomedical signals. *Physiological Measurement* 26, R15–R39 (2005)
29. Hyvärinen, A., Karhunen, J., Oja, E.: *Independent Component Analysis*. John Wiley & Sons, Chichester (2001)
30. Jung, T.P., Humphries, C., Lee, T.W., Makeig, S., McKeown, M.J., Iragui, V., Sejnowski, T.J.: Removing Electroencephalographic Artefacts: Comparison between ICA and PCA. *Neural Networks for Signal Processing VIII*, 63–72
31. Onton, J., Westerfield, M., Townsend, J., Makeig, S.: Imaging human EEG dynamics using independent component analysis. *Neuroscience and Biobehavioral Reviews* 30, 808–822 (2006)
32. Kachenoura, A., Albera, L., Senhadji, L., Comon, P.: ICA: a potential tool for BCI systems. *IEEE Signal Processing Magazine* 25(1), 57–68 (2008)
33. Ruckay, L., Stastny, J., Sovka, P.: Movement-related EEG decomposition using Independent Component Analysis. In: Proc. of International Conference on Applied Electronics, pp. 149–152 (2006)
34. Hyvärinen, A.: Fast and Robust Fixed-Point Algorithms for Independent Component Analysis. *IEEE Transactions on Neural Networks* 10(3), 626–634 (1999)
35. Lin, C.T., Ko, L.W., Chang, M.H., Duann, J.R., Chen, J.Y., Su, T.P., Jung, T.P.: Review of Wireless and Wearable Electroencephalogram Systems and Brain-Computer Interfaces – A Mini-Review. *Gerontology* (2009), <http://content.karger.com/produktedb/produkte.asp?typ=pdf&file=000230807>

36. Gao, X., Xu, D., Cheng, M., Gao, S.: A BCI-Based Environmental Controller for the Motion-Disabled. *IEEE Transactions on Neural Systems and Rehabilitation Engineering* 11(2), 137–140 (2003)
37. Edlinger, G., Krausz, G., Laundl, F., Niedermayer, I., Guger, C.: Architectures Of Laboratory-Pc and Mobile Pocket Pc Brain-Computer Interfaces. In: Proc. of the 2nd International IEEE EMBS Conference on Neural Engineering (2005)
38. Lin, C.T., Chen, Y.C., Huang, T.Y., Chiu, T.T., Ko, L.W., Liang, S.F., Hsieh, H.Y., Hsu, S.H., Duann, J.R.: Development of Wireless Brain Computer Interface With Embedded Multitask Scheduling and its Application on Real-Time Driver's Drowsiness Detection and Warning. *IEEE Transactions on Biomedical Engineering* 55(5), 1582–1591 (2008)
39. Palumbo, A., Calabrese, B., Cocorullo, G., Lanuzza, M., Veltri, P., Vizza, P., Gambardella, A., Sturniolo, M.: A novel ICA-based hardware system for reconfigurable and portable BCI. In: Proc. of MEMEA 2009, International Workshop on Medical Measurement and Application, pp. 95–98 (2009)
40. National Instruments, CompactRIO Developers Guide (May 2009),
<http://www.ni.com/compactriodevguide/>
41. <http://www.ni.com>
42. Rabaey, J.M., Chandrakasan, A., Nikolic, B.: Digital Integrated Circuits, 2nd edn. Prentice Hall, Englewood Cliffs (2003)
43. <http://www.xilinx.com>

Micro Systems for the Mechanical Characterization of Isolated Biological Cells: State-of-the-Art

Denis Desmaële¹, Mehdi Boukallel¹, and Stéphane Régnier²

¹ CEA LIST, Interactive Robotics Unit, 18 Route du Panorama, BP 6,
92265 Fontenay-aux-Roses, France

² Institute of Intelligent System and Robotics, University of Pierre
and Marie Curie/ CNRS UMR 7222, 4 Place Jussieu, 75005 Paris, France

Abstract. Historically, biological cells tended to be considered as entities governed exclusively by biochemical reactions. Nonetheless, physical constraints are ubiquitous in the cell environment, and it is nowadays widely recognized that mechanical factors also play a vital role in the regulation of the cell state. Indeed, early studies conducted on muscular tissues already showed few decades ago that an applied mechanical stress was able to alter the structure and functions of cells. However, one criticism usually granted about such historical investigations was that the properties of a particular cell could not be easily decoupled from the properties of the entire population. Furthermore, by probing such multicellular organisms, the heterogeneity among cell properties was largely ignored, even though this cellular heterogeneity rapidly appeared crucial to thoroughly grasp various cellular mechanisms. Accordingly, the research community has mainly focused on the study of individual microbial cells in the course of the last years. In particular, the constant progress made in the manufacturing of sophisticated micro devices have spawn very promising methods for probing the mechanical properties of single cells. In this chapter, the authors review the *Micro Electro Mechanical Systems* (MEMS) that have been recently reported in literature for the mechanical testing of individual cells.

Keywords: Cell mechanics, cell mechanical stimulation, cell force measurement, cell stiffness, cell viscoelasticity, MEMS.

1 Introduction

Numerous experiments have highlighted the fact that mechanical and biochemical cues occurring at the cell level prove to be intimately correlated through reciprocal mechanochemical conversion pathways. Thereby, an external stress sensed by a cell may elicit a cell biochemical signal, which in turn may provoke morphological changes and hence induce modifications of the intrinsic mechanical properties of the cell. Such a mutual interaction is often referred in literature as cellular *mechanotransduction*.

In the last decades, mechanics applied in the context of cell analysis has progressively turned to be indissociable from conventional cell biology, and a thorough understanding of the mechanotransduction processes has now become a priority in life sciences. If the research community appears so interested by the mechanical aspect of cells, it is mainly because achievements in cell mechanics might lead to novel breakthroughs as well as fruitful applications in medicine:

- In a broad and long term perspective, *mechanical stimulation* might constitute an alternative technique in the cure of cellular degenerative diseases such as cancer. This ultimate scientific quest is mainly motivated by the fact that mechanotransduction studies conducted on certain types of cells have reported that precisely controlled forces applied upon cells were able to successfully activate cell reparative functions. Meanwhile, several research teams presently try to control the differentiation of stem cells via appropriate mechanical stimuli. Even though the results reported so far are still solely at a preliminary stage, one might envision that mechanical stimulation could offer accurate and localized treatments, avoiding thereby unwanted side effects caused by the pharmaceuticals currently used.
- Cell mechanics may also be used as a efficient *diagnostic tool* for the prevention of cellular degenerative diseases. Indeed, it has been observed that cell mechanical properties, such as the cell membrane stiffness, can give access to precious indications on the cell life or state. By way of example, cancerous cells become stiffer than healthy cell. In the same way, the compliance of red blood cells (RBCs) infected by malaria parasites is also altered. Integrated into *Lab On Chip* or *Micro Total Analysis System* (μ TAS), the accurate estimation of such information could allow an early and painless diagnosis of various diseases.

Considering the stakes involved, many solutions aiming at fulfil the above expectations have been suggested by the research community. In particular, and considering their microscopic size, MEMS devices show great potential as versatile miniature units that could be used as compact diagnostic tools by probing the mechanical properties of cells.

As in the case of macroscale materials, the mechanical characterization of biological entities is indissociable from the notion of **stress-strain** (i.e. **force-deformation**). Therefore, a micro system intended for such purposes must somehow encompass an actuation mean in order to exert a mechanical stress upon a cell **as well as** a mean to **monitor the corresponding cell reaction**. Accordingly, this chapter is structured as follows: Section 2 lists the micro actuation means identified by the authors in order to mechanically stimulate cells. Section 3 enumerates the associated measurement techniques permitting the extraction of various cell mechanical properties. At last, Section 4 concludes the chapter by summarizing the strengths and weaknesses of the MEMS approaches devoted to the mechanical characterization of cells.

2 Actuation Means of MEMS Used for the Mechanical Characterization of Isolated Cells

This section outlines the main actuation principles exploited by MEMS in order to apply a mechanical stimuli upon a cell membrane. Two principal types of mechanical stresses for cell stimulation are often encountered in literature: **compression** and **elongation**. Compression and elongation stimuli are usually favoured because they allow to mimic in a simple way a large variety of mechanical constraints that a wide class of cells naturally undergo in their physiological environment. One will note that these two mechanical stimuli can be preferably generated either by the way of a controlled **force** or a controlled **displacement**. It is also worth to note that due to their highly intrinsic structure, cells prove to be highly heterogeneous and anisotropic entities. Thereby, depending on the type of studies conducted, analysis can be preferably carried out either at the cell level (i.e. the entire cell is stimulated) or at the subcellular level (i.e. only a specific cellular region is excited). Hereafter, the features of micro devices able to generate mechanical stimuli either at the local/global level and based on both force/displacement control are indifferently reported.

- Actuation based on microtranslation and micropositioning stages

Micropositioning stages turn to be common actuators used in conjunction with micro structures dedicated to cell mechanical characterization. By way of example, compression as well as elongation of an entire adherent fibroblast was proposed by Thoumine et al. [40, 41], who made use of a pair of flexible and rigid microplates manufactured from borosilicate bars (see Fig. 1). Compression and stretching steps up to **12 μ m** were applied by translating the rigid microplate along the vertical axis thanks to a **piezoelectric translator**. Quasi static as well as dynamic stimulations were investigated. In the latter case, the periodicity of the steps applied ranged from **4 to 4000s**. A similar platform was also conceived by Micoulet et al. [23].

A variant of the microplates approach was suggested by Girot et al. [5, 12, 13] who utilized an Atomic Force Microscope (AFM) tipless cantilever to globally load an Epithelial Hela (EpH) cell anchored at the bottom of a Petri dish (see left image of Fig. 2). Tipless cantilever was favoured to avoid irreversible damages

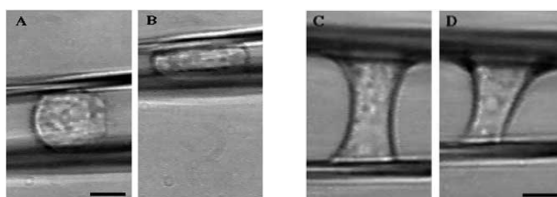


Fig. 1. Microplates used by Thoumine et al. to compress and stretch a chicken fibroblast [40, 41]

that could be caused to the external lipid biomembranes by a sharp tip. Thanks to the use of **micropositioning stages** offering a submicrometer resolution (**0.1 μm**), the authors applied compression steps up to **8 μm** with a resolution of **200nm**.

Polesel-Maris et al. [26] proposed an enhancement of the above tipless microcantilever approach by proposing a 4x4 matrix (right picture in Fig. 2). Each cantilever integrated piezoresistive (PZR) gauges to avoid the need of multiple lasers and photodiodes as conventionally used in AFM, and hence to avoid misalignment difficulties. Although no experiment was directly validated on cells, this array was however able to work in liquid environments. One may thus envision that such cantilever array could have been used to squeeze up to 16 adherent cells simultaneously.

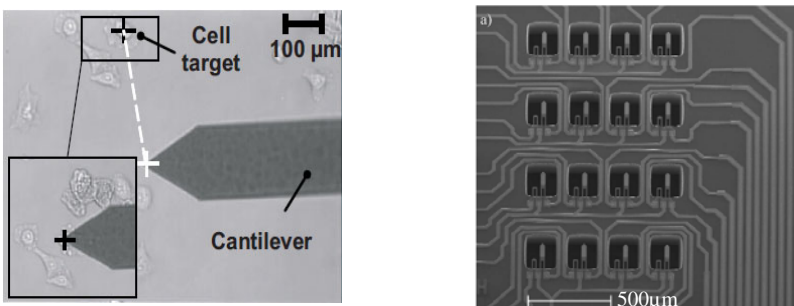


Fig. 2. Left: AFM tipless cantilever used by Girot et al. to load EpH cells [5, 12, 13]. Right: 4x4 matrix of tipless cantilever integrating PZR gauges as reported in [26]

An *off-chip* (i.e. distant) manipulator was also required to actuate the MEMS-based cell puller of Serrel et al. [32]. Fig. 3 illustrates the microfabricated structure which was based on a circular platform split in two parts, one of them being movable. After proper adhesion of an adherent cell manually deposited in the centre of the disk, the movable part was translated along one direction. In [31], an improved configuration of this cell tener was put forward by the authors. Thanks to a new piezoelectric stage, the maximum travel range of the movable plate reached **50 μm** , with a displacement resolution of **0.4nm** and a bandwidth of **520Hz**.

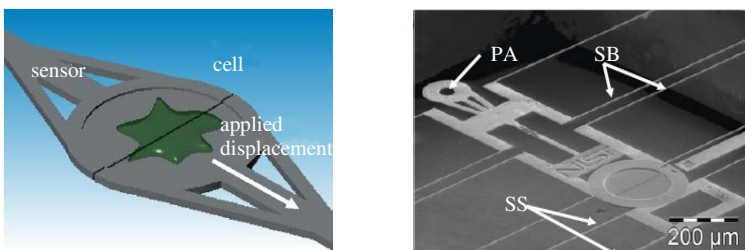


Fig. 3. Concept of the MEMS-based cell puller manufactured by Serrell and co-workers [31, 32]

In [28, 29], Sasoglu et al. suggested an array of compliant microposts for stretching multiple neurons axons aligned in a regular pattern. Again, this array was attached and moved via a distant micromanipulation station (see Fig. 4) which offered a precision of **40nm**, whereas each microbeam featured a diameter of **40 μm** , a length of **120 μm** , a standard deviation **0.2 μm** and an elastic modulus of about **1MPa**. Via this configuration, the authors claimed that tensile forces as small as **250 +/- 50nN** and as great as **25 +/- 2.5 μN** could be exerted on the specimen under investigation.

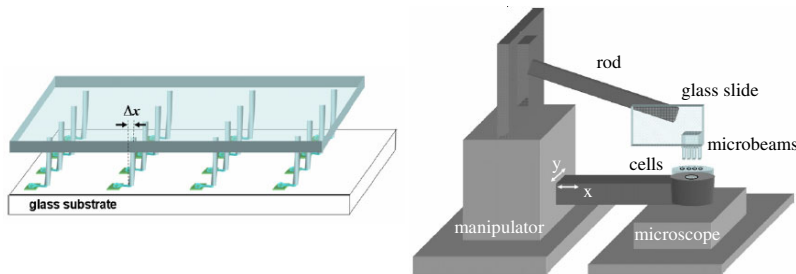


Fig. 4. Microposts array of Sasoglu et al. [28, 29] for the stretching of neuron axons. Left: the neurons are attached between a glass substrate and the extremity of a micropost. Right: the displacement of the entire array is controlled by a micromanipulator

Because unidimensional stimulation may appears simplistic in the sense that it does not reflect the real and complex multidimensional nature of the mechanical forces and geometrical constraints that cells undergo *in vivo*, Yang and Saif [44] manufactured two micro backbone structures in order to apply large stretches to adherent fibroblasts in three dimensions (Fig. 5). The probes, ended by extremities of different shapes, were functionalized by fibronectin to promote extracellular matrix adhesion. Thanks to a **x-y-z micromanipulation** stage actuated by **piezoelectric (PZT) actuators**, fibroblasts were alternatively subjected to stretches up to **50 μm** , which was about twice of the cell initial size.

- Actuators exploiting magnetic fields

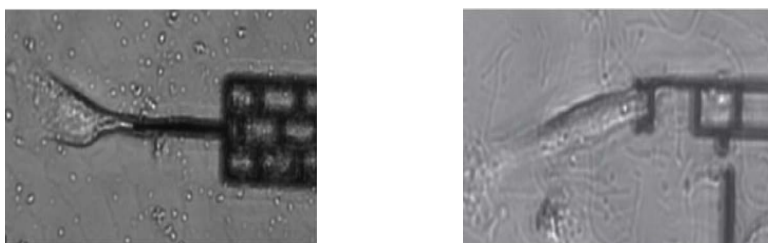


Fig. 5. Microstructures allowing the stretching of fibroblasts in three dimensions (images from [44])

Similarly to the work conducted by Sasoglu et al., Sniadecki and co-workers also designed a dense bed of micropillars [33, 34]. Soft pillars of **1.5µm** radius, **10µm** high and a low stiffness of **32nN/µm**, were arranged in a pattern array with spatial resolution of **9µm**.

However here, instead of using a micromanipulation station, the authors provided local stimulation to adherent cells lying on the surface of this bed of micropillars through the use of a horizontal uniform **magnetic field** generated by external **NdFeB magnets** which controlled the bending of certain pillars.

Indeed, the authors employed a novel and innovative way to actively move the pillars thanks to the incorporation of magnetic cobalt nanowires (**350nm** diameter **5-7µm** long) among some pillars during the fabrication process of the pillars array (1 nanowire per 200 pillars). Attracted magnetic wires enabled a bending of the magnetized pillars up to **15°** relative to the pillar's longitudinal axis. Such bending corresponded to a pillar displacement ranging from **100nm** to **1µm**. When a cell lain at the top of a magnetic pillar, this displacement transferred a punctual force to the focal adhesion site of the cell. The magnitude of this force was function of the pillar as well as the nanowire dimensions, in accordance with the formula:

$$F_{\text{Mag}} = \frac{3\mu_{\text{perp}} B(L + L_w)}{2(L^2 + L_w L + L_w^2)} \quad (1)$$

where L and L_w are the length of the post and the length of the embedded nanowire respectively, and μ_{perp} is the component of the dipole moment perpendicular to the magnetic field B . For a nanowire of length **Lw=5µm**, a magnetic field **B=0.31T** created a torque of **µ.B=210nN/µm** and a maximum force of **27nN** was experimentally validated by the authors.

- Actuators exploiting electrothermal effects

If an external actuation means may represent a convenient solution for laboratory prototypes, such *off-chip* actuators remain cumbersome and hence prevent the use of the actuated MEMS as an autonomous and portable device. To bridge this gap, physical principles showing high integration potential have been obviously

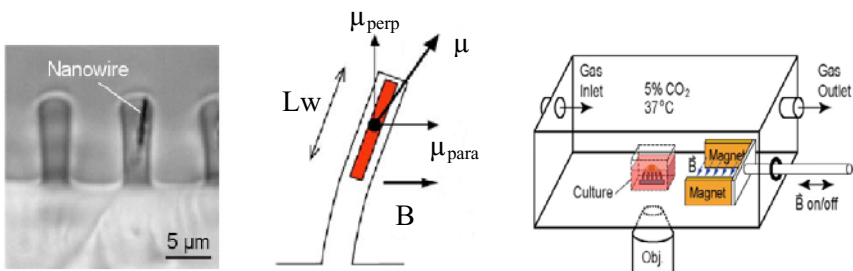


Fig. 6. Magnetic nanowires incorporated in micropillars to control their bending via the application of an external magnetic field as proposed by Sniadecki et al. [33, 34]

considered in order to conceive micro actuators that might be directly implemented in *Lab on Chip* devices.

For instance, Zhang et al. [45] designed a miniature cell loading system (see left picture of Fig. 7) in order to estimate the compliance of a cell. This MEMS was actuated by a **polymer electrothermal V-shaped actuator array**. Despite the severe restrictions usually encountered in liquids, the authors claimed that such electrothermal actuator was all the same able to operate in electrolytic solution (e.g. cell medium allowing to maintain cell alive during manipulation). However, tests were exclusively validated in ambient conditions. In air, the V-shaped array could translate in one direction with a maximal displacement of **9 μ m**.

The electrothermal effect also proved to be an appropriate mean to control the opening of microgrippers intended for the manipulation of cells in liquid media, as reported for instance by Kim et al. [18] (see right image of Fig. 7), Chronis and Lee [6], or Solano and Wood [35]. In the latter reference, the authors reported a displacement of the active gripping arms as large as **265 μ m** for input voltage as low as **1.94V (78mw power)**.

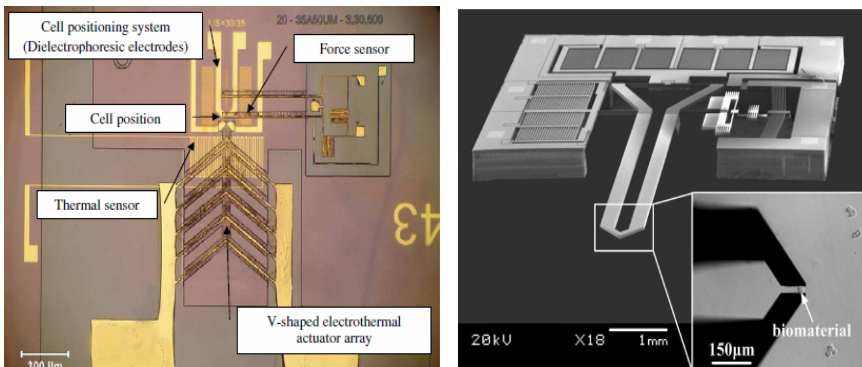


Fig. 7. Illustration of electrothermal MEMS. Left: MEMS cell loader of Zhang et al. for cell compliance measurement [45]. Right: Microgripper of Kim et al. for the manipulation of cells/biomaterials in liquids [18].

- Electrostatic actuators and electrical fields

Interdigitated comb fingers exploiting electrostatic phenomena constitute another well known actuation principle of micro mechanisms. By way of example, a multidimensional approach based on a single **linear electrostatic** structure was put forward by Scuor et al. [30] who conceived a micro in-plane biaxial cell stretcher (see left image of Fig. 8). The quadrants of a sliced circular plate were actuated in mutually-orthogonal directions (the quadrants moved on horizontal and vertical directions simultaneously). Since the force developed by a comb drive actuator is:

$$F = N \left(\frac{\epsilon t}{g} \right) V^2 \quad (2)$$

where N is the number of comb electrodes, ϵ is the permittivity constant, t is the comb thickness, g is the comb electrode gap and V is the driving voltage; a nominal voltage of **100V** theoretically permitted this electrostatic structure to provide an actuation force of **60μN**. In practice, a power supply of **100V** led to a maximum space between the quadrants of **3.4μm** in ambient conditions (i.e. air).

The right picture of Fig. 8 illustrates another micro mechanical testing platform based on an **electrostatic comb drive actuator** which was proposed by Eppell et al. to stretch thin collagen fibril along one dimension [10]. In this reference, monotonic as well as cyclic stretches (maximum amplitude **6μm**) were imposed to the fibril under test at fixed frequencies (**1, 10 and 100Hz**).

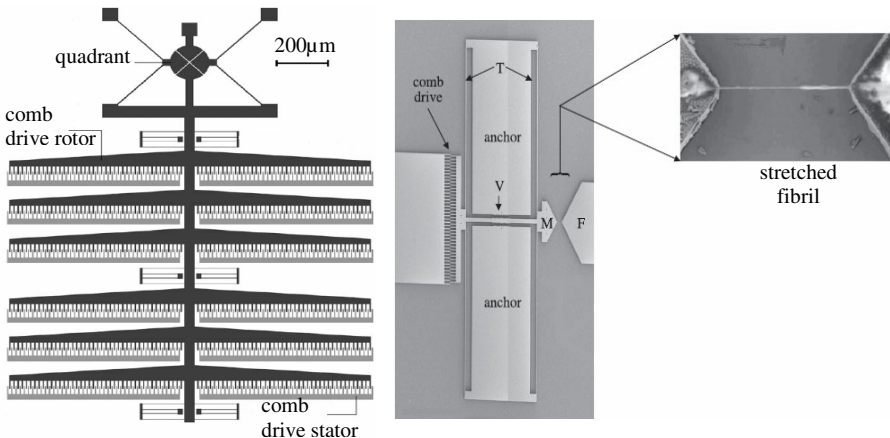


Fig. 8. Bi-axial cell stretcher of Scuor et al. [30] (left) as well as the unidimensional cell tenser of Eppell et al. [10] (right). Both devices were actuated by a electrostatic comb drive system

Bao et al.[2] exploited the phenomena of cell **electroporation** to indirectly provoked cell stimulation via an electrical field. Electroporation occurs when cells experience an external **electrical field** with an intensity beyond a certain threshold. During electroporation, the electrical field opens up pores in the cell membrane that allow material exchange across the membrane. Thereby, cells can swell if they are flowing across a microchannel (as illustrated in Fig. 9). Here the authors applied an electric field intensity of **200V/cm**, **400V/cm** and **600V/cm** across the narrow section of a microchannel (32μm deep, 58μm wide). A liquid level difference imposed a constant flow rate of **0.1-0.25 cm/s** in the narrow channel. With this approach, the authors serially stressed individual human breast cells at a throughput of **5 cells/s**.

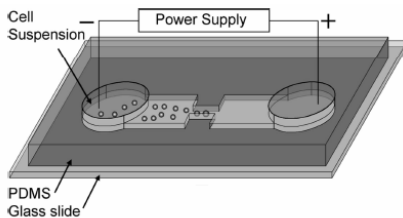


Fig. 9. Microfluidic electroporative flow cytometer developed by Bao et al. [2]

- Actuation means based on laser beams and optical gradients

If optical traps created by laser beams focused through microscope objectives are well known scientific instruments for the manipulation of biological entities, Guck et al. [14, 15] embedded two **optical fibers** into a microfluidic chip in order to trap and stretch non adherent cells flowing through a microchannel (see illustrations Fig. 10). In this all fiber optical stretcher, the two divergent laser beams were shone on diametrically opposite portions of the cell. This favourably allowed the cancellation of the scattering forces at the centre of the cell, whereas the net stretching forces at the surfaces doubled in magnitude. As well explained and detailed by Van Vliet et al. in [42], the net stretching force F_s exerted by such configuration on a single cell can be expressed by the following equation:

$$F_s = [n_m - (1-R)n_c + R n_m] \left[\frac{P}{c} \right] + [n_c - (1-R)n_m + R n_c] \left[(1-R) \frac{P}{c} \right] \quad (3)$$

where n_m and n_c are the refractive indices of the surrounding media and cell, respectively, R is the fraction of reflected light, c is the speed of light in vacuum, and P is total light power.

This approach allowed Guck and co-workers to generate uniaxial stretching forces up to **400pN** in aqueous media with a **500mW** laser. The authors even predicted that maximum force could even exceed **1nN** with higher power lasers.

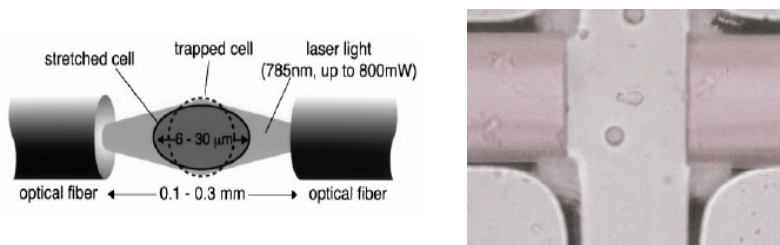


Fig. 10. Left: schematic of an all fiber optical stretcher as conceived by Guck et al. [14, 15]. Right: microscope image of the optical stretcher of Lincoln et al. [21] used in combination with a microfluidic channel for the fast stretching of suspended cells

Indeed, high power lasers could be used without damaging the cell since, as the divergent laser beams are necessarily unfocused on the cell, the light intensity transmitted to the cell - and hence the risk of radiation damage - is reduced.

3 Measurement Techniques Associated to MEMS Devices for Extracting the Mechanical Properties of Isolated Cells

As already mentioned at the beginning of this chapter, the mechanical characterization of a cell is indissociable from the notion of **force-deformation** (or **stress-strain**). Therefore, once a controlled force (or displacement) has been applied upon a cell through one of the actuation principle previously presented, the mechanical behaviour of the cell has then to be monitored. In the following paragraphs, one hence enumerates some of the different instruments and/or methods coupled to MEMS devices that have been found by the authors in the literature to extract various mechanical properties of a cell.

- Measuring the elastic parameters of single cells

As a matter of fact and as confirmed by several authors (e.g. [7, 17]), certain cells appear to behave as solids or rigid structures. Assuming that a cell can be roughly approximated as a passive material, cell elastic parameters (i.e. stiffness, Young's modulus) can thus be identified. In particular, estimating the cell stiffness turns to be of paramount importance since, as already underlined, it can be affected by different cellular diseases (e.g. cancer, malaria). Stiffness may hence be utilized as a precious indicator of the cell state. Micro biomedical diagnostic instruments aiming at detecting and sorting malignant cells must then encompass somehow a mean for determining the cell stiffness.

To this end, Sun et al. proposed several types of MEMS-based **capacitive force sensors**. In particular, the differential tri-plate comb drive configuration reported in [37] (see Fig. 11) significantly improved the linearity between an axial force applied on the probe extremity and the resulting capacitance changes. Thereby, the displacement of the comb plates Δ_d was simply estimated via the relationship:

$$\Delta_d = d_0 \left(\frac{V_{out}}{V_s} \right) \quad (4)$$

where d_0 is a constant representing the nominal position of the comb structure (i.e. no force applied, plates equally spaced), V_s is the voltage supply of the device, and V_{out} is a measured voltage.

Two springs of given stiffness then allowed to convert the displacement estimated into a force. The springs being modelled as two fixed-fixed beams with a load point applied in the middle, the force-deflection relationship was given by:

$$F = \Delta_d \left(\frac{4E\omega^3 t}{l^3} \right) \quad (5)$$

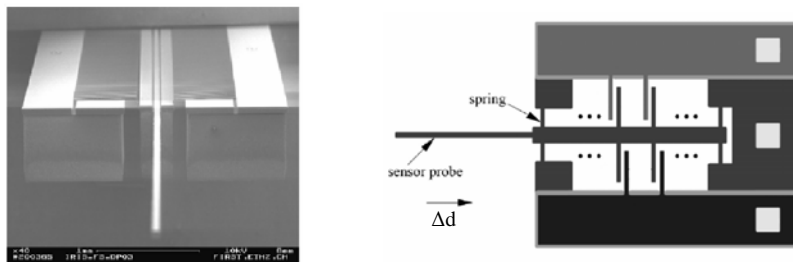


Fig. 11. Microscope view of the uniaxial capacitive force sensor proposed by Sun et al. [37]

where F is the force applied upon the probe, E is the average Young's modulus of P-type silicon ($E=100\text{GPa}$), and l , ω , and t are the spring length, width, and thickness respectively. A force resolution of $0.68\mu\text{N}$ with a sensitivity of $1.35\text{mV}/\mu\text{N}$ and a measurement range of 1mN was reported for this particular sensor. Other variants, sometimes with multiaxial capabilities, can also be found in [36, 4, 9, 18].

In [38], Sun et co-workers then proposed to exploit such capacitive sensor integrated to a micropipette tip in order to determine the elastic modulus (i.e. Young's modulus) of the zona pellucida (extracellular biomembrane envelope) of mouse oocytes and mouse embryos ($\sim 25\text{-}50\mu\text{m}$ radius). The force sensor was coupled to a microscope and a charge coupled device (CCD) camera. An advanced load point model (illustrated in Fig. 12), explained in details in the original article with step by step demonstrations, was also specifically developed. In particular, this analytical model led to the following equation:

$$F = \frac{2\pi h w_d^3}{a^2(1-v)} \left[\frac{3 - 4\zeta^2 + \zeta^4 + 2\ln(\zeta^2)}{(1-\zeta^2)(1-\zeta^2 + \ln(\zeta^2))^3} \right] \quad (6)$$

where $\zeta = \frac{c}{a}$, c being the pipette radius, a and w_d being the radius and the depth of the dimple created by the biomembrane deformed under pipette indentation, respectively. Here, the Poisson's ratio of the biomembrane was assumed to be $v = 0.5$.

The force F applied upon the cell was measured by the way of a capacitive sensor, such as the one introduced above (Fig. 11). The geometric parameters a and w_d were measured from the analysis of frame sequences captured during the experiments. With this approach, the Young's moduli of the zona pellucida of mouse oocytes and mouse embryos were calculated to be $E = 17.9\text{kPa}$ and $E = 42.2\text{kPa}$ respectively.

Vision based techniques were also used by Liu et al. In [22], the authors presented a platform where a zebrafish embryo ($\sim 1.2\text{mm}$) was placed in the centre of a Polydimethylsiloxane (PDMS) cell holding device (ring a microposts **280μm** diameter, **420μm** long see Fig. 13). When poking the embryo with a micropipette, deflections of the surrounding low-stiffness posts occurred and were visually

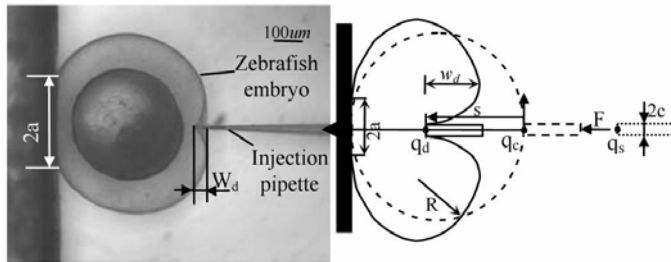


Fig. 12. Microscope image of a mouse embryo indented by an injection pipette. The latter is attached to a capacitive force sensor (not visible on this view). The geometric parameter a and w_d of Equation (6) are estimated from video frames sequences. The equivalent load point model developed by Sun et al. [38] for the calculation of the embryo's elastic modulus is drawn next to the microscope view

tracked thanks to a **sub-pixel visual tracking algorithm**. After the experimental determination of the posts stiffness, material deflections were subsequently transformed into forces. Experimental results validated a minimum resolution of this vision-based force sensing system of **3.7 μ N** (with 10x microscope objective). Meanwhile, a vision sensor followed the deformations of the cell cytoplasm under indentation, and hence allowed the authors to trace the force-deformation curve of the indented zebrafish embryo. Slope of the force-deformation curve reported revealed a stiffness **K~2.75 N/m** for the embryo tested.

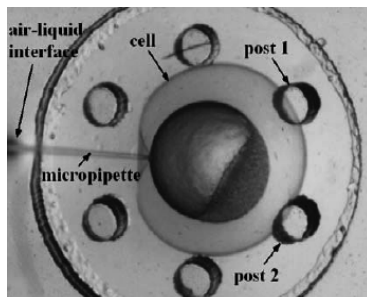


Fig. 13. Vision based platform of Liu et al. [22] where a zebrafish embryo is surrounded by a ring of PDMS microposts

In [3], Barret et al. conducted experiments to determine the stiffness of stereociliary bundles on hair cells of the inner ear with a miniature glass whisker whose deflections were locally monitored thanks to an Extrinsic Fabry Perot Interferometer (EFPI¹) composed of two optical fibers (see Fig. 14). With a coherent laser source centred around a wavelength of 1310nm, this interferometric measurement

¹ As it will go beyond the scope of this review to explain the physics underlying EPFI, the reader is invited to consult [3][27] for further details.

method enabled to detect a minimum displacement of the whisker of **30nm**. Thanks to an a priori knowledge of the whisker stiffness, the measurement of the whisker bending permitted the determination of the bundle stiffness k_b via the simple equation:

$$k_b = k_w \left(\frac{\Delta_{xP}}{\Delta_{xB}} - 1 \right) \quad (7)$$

where k_w is the whisker stiffness, and Δ_{xP} , Δ_{xB} are the pipette and bundle displacement respectively (see Fig. 14). Via this approach, the authors measured an average stiffness of vertebrate hair cells spanning $\sim 3 \cdot 10^{10} \text{ N/m}$.

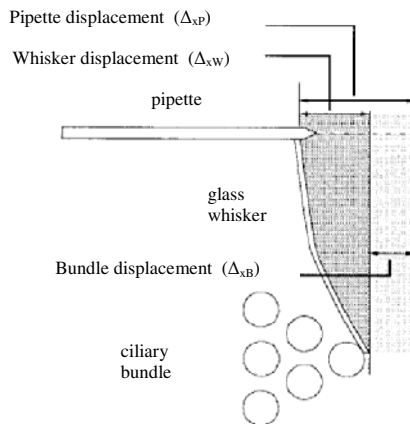


Fig. 14. Deformation of a fine glass pipette whisker measured by an EPFI allowing the determination of the stiffness of a vertebrate hair cells as reported by Barrett et al. [3] (fiber interferometers do not explicitly appear on the scheme)

- Measuring cellular traction forces

Although the consideration of cells as passive materials can effectively lead to relevant applications, one should always keep in the back of the mind that cells are above all living entities of incredible complexity, able to adapt themselves to environmental changes as well as to generate a multitude of dynamic forces. In particular, various MEMS devices have been conceived in order to measure and analyse such time-dependent forces.

For instance, traction forces are developed by the motility mechanisms of adherent cells. They are thus involved during migration phases of the cell and can be detected during cell movements. Soft silicon substrates have constituted a first mean to detect and analyse such cellular forces. For instance, in the continuity of the precursory works initiated by Harris et al. [16] as well as Munevar et al. [24], Balaban and co-workers [1] proposed a thin deformable substrate which integrated **regular micropatterned array of dots** (diameter **0.8µm**, grid pitch **2-30µm**) within **transparent elastomers** (Fig. 15).

Because the traction forces exerted by a cell anchored to this substrate caused elastic deformation of the latter and hence a displacement of the embedded dots, cellular traction fields could be quantified. Indeed, by knowing the initial position of the dots as well as the stiffness of the substratum, local forces generated by the cell could be computed thanks to the Hooke's law:

$$F = k_s x_d \quad (8)$$

where k_s is the substrate's stiffness and x_d the displacement of the dots measured by a time-lapse **video microscopy system** associated to **images analysis algorithms**. With such compliant substrates, Balaban et al. reported traction forces ranging from **10nN** to **70nN**.

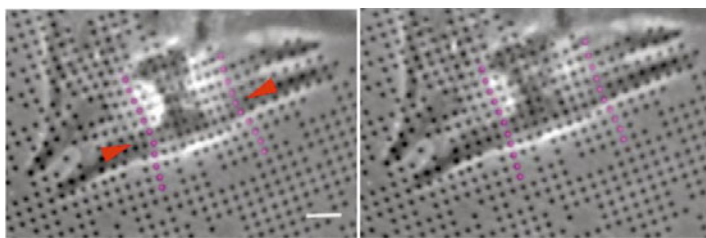


Fig. 15. Phase contrast images of a contracting cardiac myocyte plated on elastomer with embedded photoresist pattern of dots as proposed by Balaban et al. [1]. The arrowheads and the magenta dots underlined the pinching action of the contraction on the elastomer (bar=6μm)

Similarly, passive arrays of compliant micropillars (see images in Fig. 16) were extensively used in order to study interactions between cells and their substrate. In all the references consulted by the authors [8,46,39,25,43], the pillars dimensions typically spanned **3-50μm** in length with a diameter **2-10μm**. The pillars were also closely spaced (typical pitch of **2-10μm**) in order to allow subcellular spatial resolution in force measurements as well as to avoid spreading of the cells between pillars. Pillars deflected independently in response to local tractions. This deflection x imposed by the cells was also measured by **optical microscopy** and then related to the force F via the standard linear elastic beam theory:

$$F = \frac{3EI}{L^3} x \quad (9)$$

where E , I and L are the time-independent elastic modulus, the moment of inertia and the length of the pillar, respectively. Knowing the stiffness of the pillars (typically **0.47** to **1600nN/μm**), **image analysis** of each pillar yielding an independent force vector. Combined, these force vectors formed a map of subcellular traction forces. Such a technique allowed Du Roure et al. [8] to measure a minimum force as low as **1nN**.

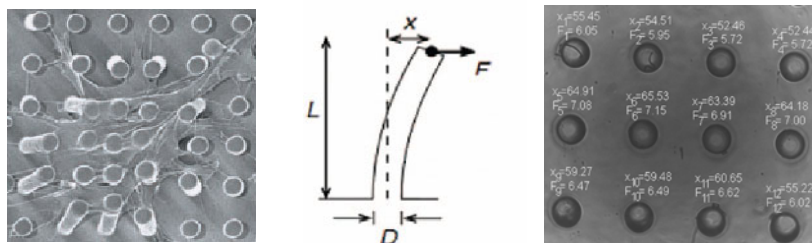


Fig. 16. Microposts array detector for the mapping of cell traction forces. Deviations of the pillars are monitored in real-time via dedicated image analysis algorithms. Local forces are then estimated via standard beam theory (illustrations from [39,29])

Another devices exploiting the deflections of microscopic levers to make dynamic measurements of subcellular tractions was proposed in [11]. Here, Galbraith et al. proposed a micromachined device where a chicken fibroblast was able to locomote over one of the **5904 pads** which made up the surface of the micro device. Each pad, whose surface ranged in area from **4 to 25mm²**, rested on a pedestal at the free end of one of the cantilever levers of various lengths that were buried beneath the surface (see Figure 17).

The forces that the cells exerted on the pads were determined by measuring the displacement of the pads and calculating the product of the pad displacement and the stiffness of the cantilever lever. Accordingly, a **microscope** associated to **frame grabbing system** monitored the centroid of the pads. The minimum spatial resolution reported was **20nm**. Traction forces **<1nN** and up to **100nN** were measured for different regions of the cell. However, only vertical (1D) forces developed by the cell could be detected by this system.

- Measuring contraction forces

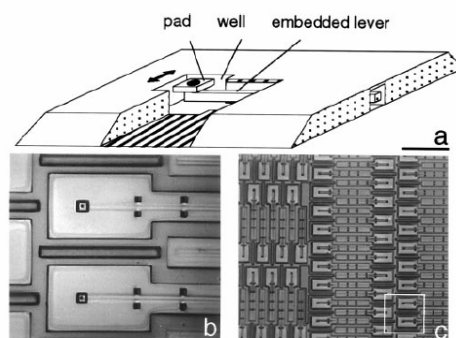


Fig. 17. Different magnifications of the micromachined substrate designed by Galbraith et al. [11]. Above (a), a cut-away drawing shows a lever, a pad and a well (bar=10μm). Below, (c) shows 0.18mm long levers (bar=1mm). Inset (b) corresponds to the white square area visible in (c)

Contraction forces represent another class of relevant dynamic forces which are exclusively generated by living heart muscle cells. In particular, measuring such cellular twitches is highly requested by the science community since it may significantly contribute to the understanding of the pathophysiology of heart failure and hence can help for gene therapy of cardiac diseases.

To this end, Lin et al. [20] proposed a MEMS force transducer system (volume <1mm³) composed of two free-standing polysilicon clamps, the latter allowing to hold the ends of a heart cell under investigation. As shown in Fig. 18, each clamp was suspended by a pair of microbeams. Cell contractions then provoked the bending of the beams, and the force was determined from the measured deflection and the spring constant of the beams. The **optical system** (microscope coupled to a **CCD camera**) and a **PC-based frame grabber** offered a minimum image resolution of **0.3μm**. With this system, an average contraction force of ~12 μN was quantified for several rat cardiac myocytes.

Lin et al. also put forward an evolution of this concept in [19]. This time, instead of monitoring the deflections of the beams via a video system, **PZR strain gauges** were implemented at the base of the beams. With the PZR gauges connected to a Wheatstone bridge and amplification electronics for electrical readout, the force generated by a cardiac cell could be estimated by measuring the output voltage V_{bridge} of the bridge in accordance to the following formula:

$$\frac{dV_{\text{bridge}}}{dF} = \frac{3 V_{\text{in}} G L}{2 a^2 b E} \quad (10)$$

where V_{in} was the input voltage of the Wheatstone bridge, F was the input force deforming the piezoresistive gauges, G was the gauge factor of the piezoresistors

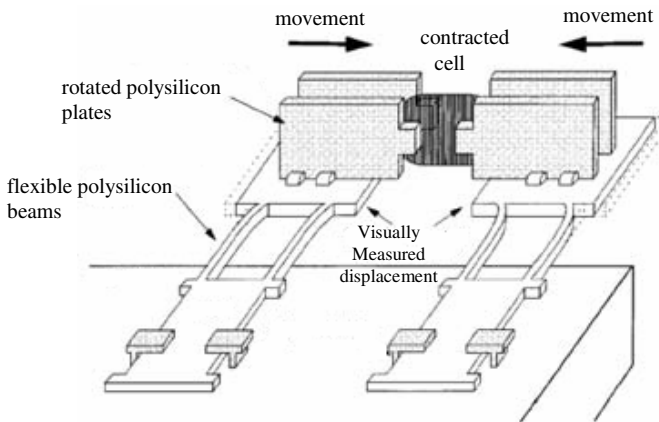


Fig. 18. Compliant micro arms clamping a cardiac myocyte as proposed by Lin et al. Left: contractile force is extracted from image analysis monitoring beams deflections [20]. Right: Evolution of the system implementing PZR strain gauges [19]

and a , b , L , E were the thickness, width, length and elastic modulus of the beams respectively. Theoretically, this new configuration could offer a sensitivity of $2.6\text{mV}/\mu\text{N}$. In experimental conditions, the authors were able to measure contractile forces spanning a range from **100nN** to **50μN**.

4 MEMS Devices for the Mechanical Characterization of Biological Cells: Strengths and Limitations

It is indisputable that the emergence of micro technologies have incomparably facilitated assays conducted on individual cells. Indeed, with the recent possibility to manufacture sophisticated micro actuators and/or sensors, MEMS have enabled tremendous breakthroughs in helping to elucidate how a cell receives and processes extracellular mechanical signals. Indeed, many studies involving MEMS have provided invaluable data and information on the mechanisms of cellular deformation and mechanotransduction pathways. Accordingly, MEMS have thus legitimately become indissociable from the mechanical testing of cells. However, and without reconsidering the evident benefits of MEMS in the mechanical characterization of cells, several limitations remain.

First of all, it is worth noting that many of the MEMS introduced in the course of this chapter involve delicate and time consuming processes for placing the cell targeted. Functionalization of probes are required to guarantee a firm bonding with the cell under test, whereas long curing time ensuring a sufficient adhesion usually remain *a sine qua non* condition to successfully conduct experiments. For instance in [10], the authors used small drops of epoxy in order to attach a fibril between two pads. However, one might assume that some of these "gluing" chemicals may somehow interact with the living cell, having a certain impact and locally alter the intrinsic cell mechanical properties. Furthermore, such long protocols aiming at properly preparing the cell before experiment prevent a high rate analysis. Currently, several hours may still be needed in order to characterize just few cells. However, it is widely recognized that the mechanical properties of cells can significantly vary from cell to cell, even for a given cell line. Meanwhile, high throughput devices, able to quickly provide quantitative and accurate data based on the characterization of thousands of cells appear indispensable for efficient biomedical diagnosis.

Moreover, the majority of the MEMS devices aforementioned finally remain dependent on bulky peripheral equipments. For instance, most of them are actuated via a micropositioning stage and/or must be combined with an optical measurement systems for the extraction of the cell mechanical parameters. Such measurement set-ups are usually composed of a microscope associated with a CCD camera, a frame grabber system and specific image processing programs running on a computer. Unfortunately, it goes without saying that such equipment totally prevent the use of the MEMS device as a portable and autonomous system.

By way of example, and as seen in Section 2, electrostatic as well as electro-thermal micro actuators offering high integrability capabilities have been proposed to partly overcome these limitations. Nevertheless, the mechanical characterization

of cells should be imperatively conducted in a cell medium guaranteeing optimum environmental conditions for their survival during experiments. In the mean time, the micro actuators based on electrostatic as well as electrothermal effects inherently cope with complex and challenging phenomena in liquid media. For the former type, the hydrophobic nature of the silicon wafer interface usually causes air trapping between the comb drive fingers and the ground plane of the structure. The enhanced conductivity in liquids also drastically reduce the displacement capabilities of such devices: typically, the translation magnitude of an electrostatic actuator in liquids is approximately lowered by a factor two when compared to the initial performances reached in ambient conditions. This is mainly why studies conducted with such actuators have usually reported data for cells characterized only in air. Nonetheless, cells prove to be particularly sensitive to the humidity rate. Considering the fact that their mechanical properties can be drastically impacted, one might reasonably assume that the results of these studies could have been perhaps partly biased and could have possibly led to some misinterpretations. Complex problems and performance limitations also arise as soon as electrothermal actuators are immersed in liquid environments. In addition, one must pay particular attention to the temperatures that can be generated by such actuators. Indeed, excessive temperatures may be harmful and cause irreversible damages to a living entity as delicate as a cell.

Nevertheless, and even if such technical difficulties remain challenging to solve, they should not be considered as insurmountable restrictions. Indeed, and as already highlighted, tremendous breakthroughs have already been accomplished. As a matter of fact, and although the MEMS presented in this chapter still solely constitute a first step, their dimensions comparable to the size of the cells under investigation have already paved the way for miniaturized and autonomous biomedical platforms. Thereby, they should be seen as the preliminary components of novel tools which will undoubtedly revolutionize medicine as well as biomedical research in the near future.

References

1. Balaban, N.Q., Schwarz, U.S., Riveline, D., Goichberg, P., Tzur, G., Sabanay, I., Mahalu, D., Safran, S., Bershadsky, A., Addadi, L., Geiger, B.: Force and focal adhesion assembly: a close relationship studied using elastic micropatterned substrates. *Nature Cell Biology* 3, 466–472 (2001)
2. Bao, N., Zhan, Y., Lu, C.: Microfluidic electroporative flow cytometry for studying single-cell biomechanics. *Analytical Chemistry* 80(20), 7714–7719 (2008)
3. Barrett, M., Peterson, E., Grant, J.: Extrinsic fabry-perot interferometer for measuring the stiffness of ciliary bundles on hair cells. *IEEE Transactions on Biomedical Engineering* 46(3), 331–339 (1999)
4. Beyeler, F., Nelson, B.: Design and calibration of a microfabricated 6-axis force torque sensor for microrobotic applications. In: *IEEE International Conference on Robotics and Automation*, Kobe, Japan, pp. 520–525 (2009)
5. Boukallel, M., Girot, M., Regnier, S.: Characterization of cellular mechanical behavior at the microscale level by a hybrid force sensing device. *Journal of the Mechanical Behavior of Biomedical Materials* 2(3), 297–304 (2009)

6. Chronis, N., Lee, L.P.: Polymer MEMS-based microgripper for single cell manipulation. In: 17th IEEE International Conference on MEMS, Maastricht, The Netherlands, pp. 17–20 (2004)
7. Daoudi, M., Lavergne, E., Garin, A., Tarantino, N., Debre, P., Pincet, F., Combadiere, C., Deterre, P.: Enhanced adhesive capacities of the naturally occurring Ile²⁴⁹-Met²⁸⁰ variant of the chemokine receptor CX₃CR₁. *Journal of Biological Chemistry* 279(19), 19649–19657 (2004)
8. Du Roure, O., Saez, A., Buguin, A., Austin, R.H., Chavrier, P., Silberzan, P., Ladoux, B.: Force mapping in epithelial cell migration. *Proceedings of the National Academy of Sciences* 102(7), 2390–2395 (2005)
9. Enikov, E., Nelson, B.: Three-dimensional microfabrication for a multi-degree-of-freedom capacitive force sensor using fibre-chip coupling. *Journal of Micromechanics and Microengineering* 10(4), 492–497 (2000)
10. Eppell, S., Smith, B., Kahn, H., Ballarini, R.: Nano measurements with micro-devices: mechanical properties of hydrated collagen brils. *Journal of The Royal Society Interface* 3(6), 117–121 (2006)
11. Galbraith, C.G., Sheetz, M.P.: A micromachined device provides a new bend on fibroblast traction forces. *Proceedings of the National Academy of Sciences*, 9114–9118 (1997)
12. Girot, M., Boukallel, M., Regnier, S.: An hybrid micro-force sensing device for mechanical cell characterization. In: IEEE Instrumentation and Measurement Technology Conference, Sorrento, Italy, pp. 501–506 (2006)
13. Girot, M., Boukallel, M., Regnier, S.: Modeling soft contact mechanism of biological cells using an atomic force bio-microscope. In: 2006 IEEE/RSJ International Conference on Intelligent Robots and Systems, Beijing, China, pp. 1831–1836 (2006)
14. Guck, J., Ananthakrishnan, R., Cunningham, C.C., Käs, J.: Stretching biological cells with light. *Journal of Physics: Condensed Matter* 14, 4843–4856 (2002)
15. Guck, J., Ananthakrishnan, R., Mahmood, H., Moon, T.J., Cunningham, C.C.: The optical stretcher: a novel laser tool to micromanipulate cells. *Biophysical Journal* 81, 767–784 (2001)
16. Harris, A., Wild, P., Stopak, D.: Silicone rubber substrata: a new wrinkle in the study of cell locomotion. *Science* 208(4440), 177–179 (1980)
17. Hochmuth, R.: Micropipette aspiration of living cells. *Journal of Biomechanics* 33(1), 15–22 (2000)
18. Kim, K., Liu, X., Zhang, Y., Sun, Y.: Micronewton force-controlled manipulation of biomaterials using a monolithic MEMS microgripper with two-axis force feedback. In: IEEE International Conference on Robotics and Automation, Pasadena, CA, USA, pp. 3100–3105 (2008)
19. Lin, G., Palmer, R., Pister, K., Roos, K., Inc, S., Verdes, R.: Miniature heart cell force transducer system implemented in MEMS technology. *IEEE Transactions on Biomedical Engineering* 48(9), 996–1006 (2001)
20. Lin, G., Pister, K., Roos, K.: Surface micromachined polysilicon heart cell force transducer. *Journal of Microelectromechanical Systems* 9(1), 9–17 (2000)
21. Lincoln, B., Erickson, H., Schinkinger, S., Wottawah, F., Mitchell, D., Ulwick, S., Bilby, C., Guck, J.: Deformability-based flow cytometry. *Cytometry* 59(2), 203–209 (2004)
22. Liu, X., Sun, Y., Wang, W., Lansdorp, B.: Vision-based cellular force measurement using an elastic microfabricated device. *Journal of Micromechanics and Microengineering* 17(7), 1281–1288 (2007)

23. Micoulet, A., Spatz, J., Ott, A.: Mechanical response analysis and power generation by single-cell stretching. *Chem. Phys. Chem.* 6(4), 663–670 (2005)
24. Munevar, S., li Wang, Y., Dembo, M.: Traction force microscopy of migrating normal and h-ras transformed 3t3 fibroblasts. *Biophysical Journal* 80, 1744–1757 (2001)
25. Petronis, S., Gold, J., Kasemo, B.: Microfabricated force-sensitive elastic substrates for investigation of mechanical cell-substrate interactions. *Journal of Micromechanics and Microengineering* 13(6), 900–913 (2003)
26. Polesel-Maris, J., Aeschimann, L., Meister, A., Ischer, R., Bernard, E., Akiyama, T., Giazzon, M., Niedermann, P., Staufer, U., Pugin, R.: Piezoresistive cantilever array for life sciences applications. *Journal of Physics: Conference Series* 61(1), 955–959 (2007)
27. Pullteap, S.: Development of an Extrinsic dual-cavity Fiber Fabry-Perot interferometer: Applications to periodic and non-periodic vibration measurements. PhD thesis, Institut National Polytechnique de Toulouse (2008)
28. Sasoglu, F.M., Bohl, A.J., Layton, B.E.: Design and microfabrication of a high-aspect-ratio PDMS microbeam array for parallel nanonewton force measurement and protein printing. *Journal of Micromechanics and Microengineering* 17(3), 623–632 (2007)
29. Sasoglu, F.M., Bohl, A.J., Allen, K.B., Layton, B.E.: Parallel force measurement with a polymeric microbeam array using an optical microscope and micromanipulator. *Computer Methods and Programs in Biomedicine* 93(1), 1–8 (2009)
30. Scuor, N., Gallina, P., Panchawagh, H., Mahajan, R., Sbaizer, O., Sergo, V.: Design of a novel MEMS platform for the biaxial stimulation of living cells. *Biomedical Microdevices* 8(3), 239–246 (2006)
31. Serrell, D., Law, J., Slifka, A., Mahajan, R., Finch, D.: A uniaxial biomems device for imaging single cell response during quantitative force-displacement measurements. *Biomedical Microdevices* 10(6), 883–889 (2008)
32. Serrell, D., Oreskovic, T., Slifka, A., Mahajan, R., Finch, D.: A uniaxial biomems device for quantitative force-displacement measurements. *Biomedical Microdevices* 9(2), 267–275 (2007)
33. Sniadecki, N.J., Anguelouch, A., Yang, M.T., Lamb, C.M., Liu, Z., Kirschner, S.B., Liu, Y., Reich, D.H., Chen, C.S.: Magnetic microposts as an approach to apply forces to living cells. *Proceedings of the National Academy of Sciences* 104(37), 14553–14558 (2007)
34. Sniadecki, N.J., Lamb, C.M., Liu, Y., Chen, C.S., Reich, D.H.: Magnetic microposts for mechanical stimulation of biological cells: Fabrication, characterization, and analysis. *Review of Scientific Instruments* 79, (044302) 1–8 (2008)
35. Solano, B., Wood, D.: Design and testing of polymeric microgripper for cell manipulation. *Microelectronic Engineering* 84, 1219–1222 (2007)
36. Sun, Y., Nelson, B.J.: MEMS capacitive force sensors for cellular and flight biomechanics. *Biomedical Materials* 2(1), 16–22 (2007)
37. Sun, Y., Potasek, D., Bell, D., Fry, S., Nelson, B.J.: Characterizing fruit fly flight behavior using a microforce sensor with a novel comb drive configuration. *Journal of Microelectromechanical Systems* 14(1), 4–11 (2005)
38. Sun, Y., Wan, K., Roberts, K., Bischof, J., Nelson, B.: Mechanical property characterization of mouse zona pellucida. *IEEE transactions on nanobioscience* 2(4), 279–286 (2003)
39. Tan, J.L., Tien, J., Pirone, D.M., Gray, D.S., Bhadriraju, K., Chen, C.S.: Cells lying on a bed of microneedles: An approach to isolate mechanical force. *Proceedings of the National Academy of Sciences* 100(4), 1484–1489 (2003)

40. Thoumine, O., Ott, A.: Time scale dependent viscoelastic and contractile regimes in fibroblasts probed by microplate manipulation. *Journal of Cell Science* 110(17), 2109–2116 (1997)
41. Thoumine, O., Ott, A., Cardoso, O., Meister, J.: Microplates: a new tool for manipulation and mechanical perturbation of individual cells. *Journal of Biochemical and Biophysical Methods* 39(1-2), 47–62 (1999)
42. Van Vliet, K., Bao, G., Suresh, S.: The biomechanics toolbox: experimental approaches for living cells and biomolecules. *Acta Materialia* 51(19), 5881–5905 (2003)
43. Wang, N., Ostuni, E., Whitesides, G., Ingber, D.: Micropatterning tractional forces in living cells. *Cell motility and the cytoskeleton* 52(2), 97–106 (2002)
44. Yang, S., Saif, T.: Reversible and repeatable linear local cell force response under large stretches. *Experimental Cell Research* 305, 42–50 (2005)
45. Zhang, W., Gnerlich, M., Paly, J.J., Sun, Y., Jing, G., Voloshin, A., Tatic Lucic, S.: A polymer V-shaped electrothermal actuator array for biological applications. *Journal of Micromechanics and Microengineering* 18, 8, 075020 (2008)
46. Zhao, Y., Zhang, X.: Cellular mechanics study in cardiac myocytes using PDMS pillars array. *Sensors and Actuators A: Physical* 125(2), 398–404 (2006)

On-Body Chemical Sensors for Monitoring Sweat

Shirley Coyle, Fernando Benito-Lopez, Robert Byrne, and Dermot Diamond

CLARITY: Centre for Sensor Web Technologies, National Centre for Sensor Research,
Dublin City University, Dublin 9, Ireland

Abstract. In this paper, we discuss the challenges of performing on-body chemical analysis of body fluids. Wearable chemosensors are a relatively novel implementation, bringing new challenges to the field of wearable sensor technology and body sensor networks. Integration of chemical sensors into a textile substrate is a challenging task, as a chemical reaction must happen for these devices to generate a signal. Furthermore, they often require mixing samples and reagents, which results in waste generation. Therefore a wearable chemosensor must be capable of controlling the movement of these substances for a reaction to occur before generating a signal that can be measured. In this paper, we present the design and development of platforms to collect and analyse sweat *in-situ* and provide real-time feedback to the wearer. Two approaches are described, the first a textile based approach developed during the EU BIOTEX project. The second improves on this design through miniaturisation of the device by using a micro-fluidic platform. The performance of the developed systems is presented and the relevance of these wearable lab-on-a-chip devices is discussed for personalised healthcare and sports performance.

Keywords: sweat analysis, pH sensor, wearable chemo-sensor, interactive textiles, microfluidic device, lab-on-a-chip.

1 Introduction

Wearable chemical sensors in principle have the ability to continuously monitor the physiology of the wearer and also the chemistry of their surrounding environment. This means that the wearer is kept informed of their well-being and they can be actively involved in their own health. This is important for preventative healthcare and early diagnosis of disease. It is also of huge potential benefit for athletes, through customisation of their training regimes and nutrition plans. Most of the existing wearable technologies are based on physical sensors, such as electrocardiograph (ECG) electrodes, thermistors and accelerometers. [1] These sensors respond to physical changes in their environment e.g. heat, movement and light. Wearable chemo-sensors have the potential to measure many more variables relating to the person's well-being and safety. This is an emerging research

concept that brings another dimension to the field of wearable sensors. The potential to perform on-body chemical measurements of body fluids opens new opportunities for medical science and healthcare delivery by providing valuable real-time information about the wearer's health status. In the case of those working in hazardous and demanding environments, wearable chemical sensors may be used to augment the capability of the normal human senses to rapidly identify potential dangers and hazards. [2] PROTEX is an EU project which focuses textile based sensors to improve the safety and efficiency of emergency workers. Part of this work involves the integration of carbon monoxide and carbon dioxide sensors into garments for the safety of fire-fighters. [3] Wearable sensors combined with wireless communications allow others to be notified immediately of dangerous situations and for appropriate actions to be taken, for example by staff at disaster co-ordination centres.

However, wearable sensors have certain requirements in terms of wearability and comfort. They must not restrict the activities of the wearer and ideally be integrated fully within a garment. The sensors must therefore be robust, non-invasive, low-power and straightforward to use. Unlike physical sensors, chemical sensors have the added complexity of having an active surface, which must be exposed to a sample in order for a reaction to occur and a signal to be generated. Chemical and biological sensors must also be regularly calibrated, meaning that the sensing surface is exposed to standards and any baseline drift or change in sensitivity compensated. [4] This increases the system complexity by introducing the need for multiple reagents and their controlled delivery to the sensor. The overall assembly of sensor must be safe for the wearer's health, and the use of toxic or hazardous reagents should obviously be avoided. A major issue in this type of measurement is sensor placement and sample delivery. This will depend on the type of sample being analysed, whether it is in liquid phase or gaseous phase, and where the source of the sample lies. Wearable sensors in principle may have access to multiple samples from the wearer and also from the environment surrounding the wearer. If the wearable sensor is monitoring the external environment, the sample is likely to be volatile (e.g., presence of hazardous/toxic gas). In this case the sensor could be positioned on an outer garment to optimise contact between the sensor and the sample. If the sensor is monitoring the body's physiology by analysing body fluids then a fluidic system is needed to deliver the liquid sample to the sensor. Urine, saliva, sweat and tears are possible samples that may be acquired non-invasively from the body. [5] Breath analysis is also possible and has the potential to be a diagnostic tool. [6] However up to now this has been developed as in a portable rather than wearable format. [7, 8]

For wearable chemosensors, obtaining a sample should ideally happen naturally. Sweat is the most accessible specimen to be collected by a garment. The textile industry has developed many high performance textiles with fluid-handling materials to keep sweat away from the body surface in order to maintain the wearer's comfort. [9] Moisture management textiles are designed to move sweat away from the skin to the outer layers of the textile for faster evaporation. These materials possess inherent fluid transport capabilities that can be harnessed by

appropriately located chemosensors and delivery of fluidic samples may be performed using moisture wicking textiles placed in contact with the skin.

The first section of this paper discusses the current techniques that are being employed for sweat analysis to highlight the challenges involved in collecting and analysing sweat. Two approaches to analyse the pH of sweat in real-time using a wearable device are presented, the first of which is work carried out as part of the EU BIOTEX project. The aim of the BIOTEX project was to integrate chemical sensors into a textile substrate for monitoring body fluids. This involved the development of a fabric-based platform to collect and analyze sweat. Following on from that work the system has evolved into a miniaturised platform, which is based around a micro-fluidic systems approach to wearable sensing. Finally we consider the applications and impact of these sensors and discuss the future challenges to commercialisation and broad adoption of these technologies.

2 Sweat Analysis

Sweat analysis has the advantage of being a non-invasive measurement technique while presenting valuable physiological information. Sweat is secreted by two types of sweat glands, namely eccrine and apocrine glands. These two types of glands have quite different characteristics and functions. Eccrine sweat glands play an essential role in the regulation of the body temperature. There are 2-4 million eccrine sweat glands in the adult skin and they are distributed over nearly the entire body surface. The apocrine glands are bigger but less numerous and are thought to be the source of chemical signals (pheromones) that play an important role in the reproductive biology of mammals. Apocrine sweat composition is still not well known and there is limited literature regarding eccrine sweat. Eccrine sweat is a clear, hypotonic, odourless fluid containing mainly sodium and chloride but also potassium, urea, lactate, amino acids, bicarbonate, and calcium. [10] The composition of sweat can vary extensively between different people. Age, emotional state, diet, exercise and a variety of hereditary factors influence the composition.

The sweat test is the gold standard technique for the diagnosis of Cystic Fibrosis(CF).[11, 12] This is a once-off test that is performed in newborns and the diagnosis is based on sodium and chloride concentration levels. Individuals with Cystic Fibrosis have higher than normal levels of sodium chloride in their sweat. A typical approach in carrying out this type of test is to use filter paper to collect sweat from the skin. In order to induce sweating a process called iontophoresis using pilocarpine is used. This involves applying an electrical current to the skin in order to deliver the pilocarpine through the skin surface to stimulate the sweat glands. The sodium and chloride are subsequently eluted from the filter paper and measured by a technique such as flame photometry or anion exchange chromatography. Wescor Inc. has simplified this test by developing a system to collect and analyse sweat samples. A collection device (Macrodust®/Nanoduct®) in the form of a coiled capillary tube is placed on the wrist following pilocarpine iontophoresis. The collected samples of sweat are then extracted from the collection device by syringe and analysed using a SweatChek™ conductivity analyser. Lynch *et al*

used miniaturised solid-state ion-selective electrodes to analyse sweat samples for sodium, potassium and chloride simultaneously. [13] The micro-sensor array was incorporated into a miniature flow cell as a small, portable, analytical instrument. Such a device could be developed into a complete package for sample collection and analysis as a wearable system with integrated wireless connectivity features.

The most widely used methods of sweat analysis to date involve the collection of sweat by using patches or pouches and then analysis afterwards using a standard measurement technique. A collection pocket using parafilm has been proposed by Brisson *et al.* [14] Parafilm is attached to the skin by an adhesive dressing and a small opening is created to allow a dull needle to extract samples at various time intervals. The opening is sealed during the time between sampling events. The parafilm patch creates a capsule on the skin surface for sweat collection but this configuration may change the sweat composition by preventing water evaporation. This arises because the sweat gland ducts become blocked, and this leads to a progressive fall in sweating rates. [15] There is also evidence that there are regional variations in sweat composition [16], so multiple on-body sampling sites are needed. An alternative to the sweat patches is to use whole-body sweat collection techniques. In this case the total sweat loss is generally estimated from change in body mass. In early studies to measure electrolyte losses subjects were washed before exercise, the body and the clothes worn were washed after exercise with distilled water, and the electrolyte content of that water was measured. [17] More recently a “wash-down” approach has been taken which involves exercising within a plastic enclosure to collect sweat and then washing down the body within the enclosure using de-ionised water at the end of the exercise trial. [15, 18] This approach has been used for trials involving indoor cycling with a friction-braked ergometer which was also washed down with a power hose. This approach is quite complex and is limited to exercises that can be performed within the plastic enclosure. In the field, the most practical way for athletes to monitor their sweat loss is to measure changes in body weight pre- and post-exercise [13]. The purpose of these studies has been to monitor fluid and electrolyte loss during exercise. These methods are obviously unsuitable for long-term, real-time measurements outside of a laboratory setting. Therefore it is clear that a method is needed to collect and analyse sweat in an unobtrusive way in normal settings, at home, in the gym or on the sports track to provide real-time analysis of sweat composition.

Sweat analysis has also been used to monitor illicit drug use by sweat patches such as the PharmChek® patch. Drugs enter sweat by passive diffusion, which allows for a cumulative estimate of drug exposure over several days. [19] The sweat patch comprises a white absorption pad, covered with a unique polyurethane dressing. The absorption pad of the patch is protected from the environment by a film composed of polyurethane coated with adhesive. The polyurethane film is a semi-permeable membrane, which allows the transfer of water vapour and gases. Drugs excreted in sweat are trapped by this polyurethane dressing and retained on the white absorption pad. The testing procedures used for the analysis of sweat are the same well established procedures used for the analysis of urine specimens. The specimens are initially screened using an enzyme immunoassay technique, and positive specimens are confirmed using liquid chromatography/mass spectrometry

(LC/MS/MS). A similar patch is available from Pacific Biometrics called the Os-teopatch™ which can help to identify those at risk for rapid bone loss and possible osteoporosis. [20] The patch is worn continuously for 2 to 5 days to accumulate the non-volatile components of sweat and is then peeled off and posted to a laboratory for processing where the samples are tested using a quantitative assay for detecting biochemical markers of bone loss in sweat.

Another application of sweat analysis is in alcohol testing. SCRAM® (Secure Continuous Remote Alcohol Monitor) is a continuous alcohol monitoring technology. The SCRAM® bracelet captures transdermal alcohol readings by sampling the insensible perspiration collected from the air above the skin. The bracelet stores the data and, at pre-determined intervals, transmits it via a wireless radio-frequency (RF) signal to the SCRAM® modem. It is a tool that helps courts and agencies continuously monitor their alcohol offenders to ensure that they are not drinking.

Hence, sweat can clearly offer valuable physiological information coupled with the advantage of being a non-invasive method of assessment. However, up to now there has been limited research into the characteristics of sweating functions and sweat composition. This is because collection and measurement techniques for analysis can be awkward. As previously mentioned sweating can be induced by iontophoresis of pilocarpine, or sweat may be generated naturally by putting the subject in a heated environment or exercising. In the following sections we present our approach to overcome issues related to sweat sampling. The sampling and analysis functions are combined in-situ and the signals presented in real-time to the wearer to give immediate information regarding their physiological status.

3 Sensor Design and Development

3.1 Textile Patch

The initial prototype for sweat collection and analysis was developed as part of the EU-funded BIOTEX project. A textile based platform was designed to control fluid sampling and delivery of sweat to sensors integrated within the system. The design of the fabric based fluidic system used to collect and manage distribution of the sweat samples is shown in Fig. 1. The system employed a passive (i.e. power free) pumping mechanism, controlling fluid flow through a fabric substrate through the use of the moisture wicking properties of a nylon/lycra® knit fabric. The fabric-based fluidic system was developed by masking a channel in the fabric and coating the remaining regions with an acrylic hydrophobic substance on both sides of the fabric. The device was designed with an inlet on one side of the fabric at the beginning of the fabric channel, where sweat can enter from the skin. The sweat samples flowed through the fabric by capillary action along the channel. At the opposite end of the channel a super-absorbent material was placed provide the driving force for continuous wicking and to store the collected sweat. This superabsorbent material maintained a constant flow of sweat through the device. Absortex®, produced by Texsus, is a non-woven textile containing superabsorbent materials that is suitable for this purpose. A layer of this material was enclosed within an envelope of another non-woven Acquitex® which makes contact with

the fluidic channel and functions as an acquisition and distribution layer. To maximise sweat delivery to the fabric patch an acquisition layer of moisture wicking fabric (COOLMAX®) was stitched in place at the inlet. The acquisition layer was placed in contact with the skin and its purpose was to increase the collection capacity of the device.

To analyse the sweat sample, sensors were integrated along the length of the fabric channel. This is shown in Fig. 2, in which a pH sensitive dye was immobilised at the beginning of the fabric channel. pH sensitive dyes are colorimetric sensors that respond to changes in pH. There are a number of different dyes that respond at different pH ranges, depending on the pKa of the dye. Sweat pH can range from pH 4-8, and therefore a suitable dye for this range of pH values is bromocresol purple (BCP, pKa = 6.2). BCP changes colour from yellow in its acidic form, with an absorption peak at 430 nm, to purple in its basic form, with an absorption peak at 590 nm. To obtain quantitative data while still maintaining a very low power, compact and light format, a paired emitter-detector LED configuration was used to monitor the changes in colour accompanying transformations between the acid/base forms of the dye. A reflectance configuration was implemented in which the LEDs were positioned over the fabric channel at a 45° angle. The LEDs were encased in silicone to prevent the condensation of sweat on the surface of the components. The encased LEDs were held in place by a protective black PMMA cover which blocks the effects of ambient light. The cover was kept at a fixed height above the fabric channel by a silicone gasket which was attached to the fabric layer. A custom built Bluetooth system fabricated by CSEM for the BIOTEX project was used to wirelessly control the LEDs, sample the data and transmit to a nearby laptop. Earlier studies used a Mica2dot Crossbow Mote with a Mica2 base-station connected to a laptop. In both cases, the implementation of the optical detection was the same, employing the digital I/O pins of the microcontroller. The detector LED was reverse-biased at +5 V, which charges the capacitance across it. This was discharged by the photocurrent generated upon exposure to incident light, and the discharge rate was proportional to the intensity of the light reaching the detector. A digital output was obtained by using a basic detection/timer circuit, which measures the time it takes the photocurrent to discharge the voltage from +5 V (logic 1) to +1.7 V (logic 0).

In order to test the sensors and fabric patch on-body, the sensors were enclosed in a waistband, custom made by Smartex srl, which ensured the fabric patch maintained good contact with the skin. It was also used to reduce motion artefacts during exercise and block ambient light, which may affect the operation of the pH sensor. The waistband and the position of the fabric patch are shown in Fig. 3. A reference patch was also included in the design. This patch was used to make pH measurements using a Skincheck™ pH meter. This is a portable hand-held device designed to measure skin surface pH. As it does not allow for continuous real-time measurements, at 5 minute time intervals, it was pressed against the reference patch to validate the measurements taken by the textile based pH sensor. The waistband was positioned on the subject's back so that both the fabric patch and the reference were to the right of the spine. This was done to avoid collecting sweat which had run from the top to the bottom of the back along this hollow. The experimental setup is shown in Fig. 4.

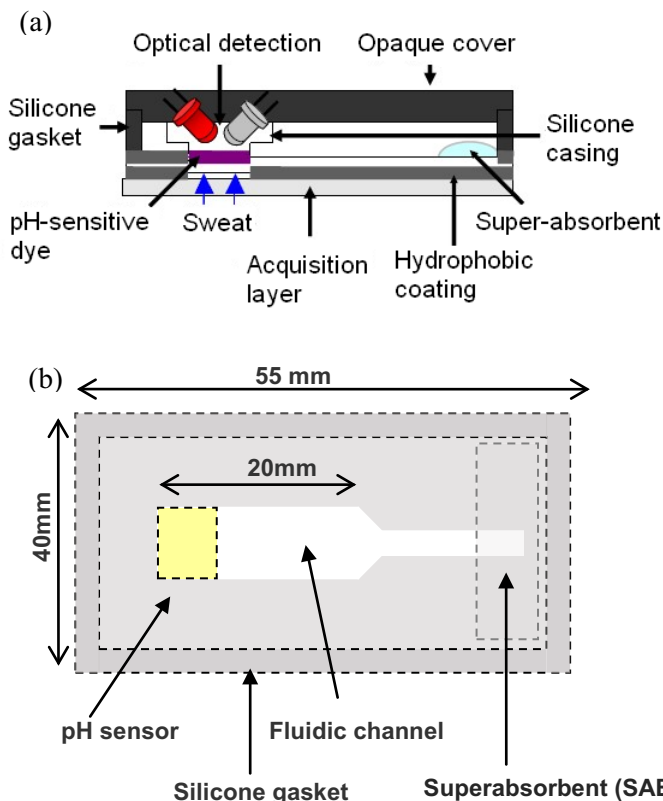


Fig. 1. (a) Fabric patch for sweat pH analysis (b) Textile based fluidic handling system

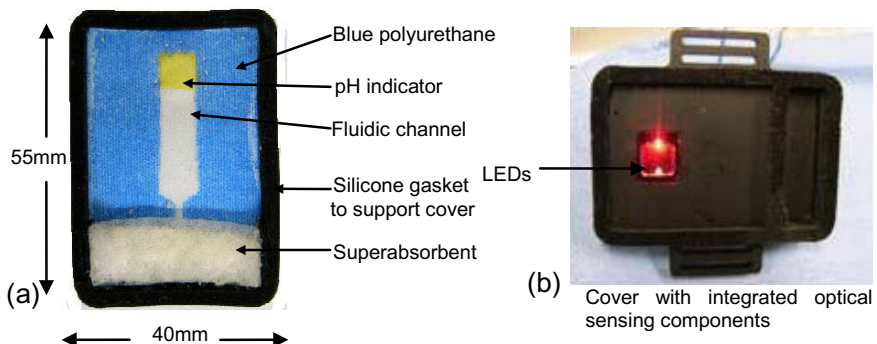


Fig. 2. (a) Photo of the fabric patch for sweat pH analysis (b) Cover of the device with integrated paired LED optical sensing configuration



Fig. 3. Waistband containing Fabric Patch and Sensors for On-body Trials.

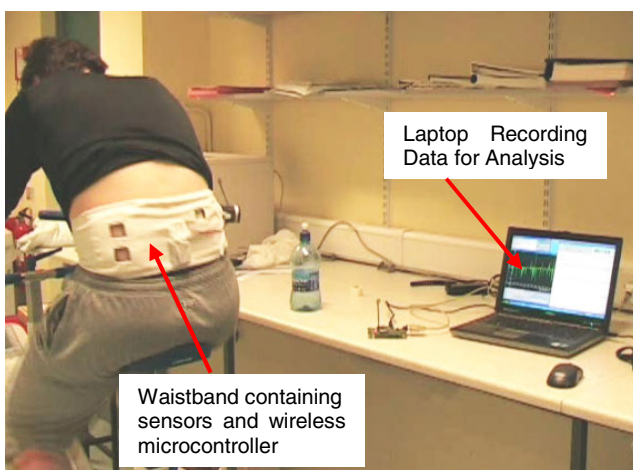


Fig. 4. Experimental set-up during exercise trial

The ability of the textile based pH sensor to measure real time changes in sweat pH during exercise was assessed by comparing the results of the sensor to those obtained using the Skincheck™ pH meter. A priming time is involved before the pH measurements are valid. This involves the time it takes for the subject to start sweating and for the sweat to enter the fluidic channel and reach the sensors. This varies between individuals and depends on fitness levels and environmental conditions. The priming time is also indicated by the reference measurements as these measurements are taken once there was adequate sweat on the reference patch to wet the reference electrode. For the trial depicted in Fig. 5 it takes 20 minutes before valid readings can be taken. This was also the stage at which there was enough sweat present on the reference patch to take a measurement using the reference pH meter. In order to reduce the priming time, the size of the device and therefore the sample size need to be reduced. This is important not only to ensure a faster response time but also to make the device suitable for all populations

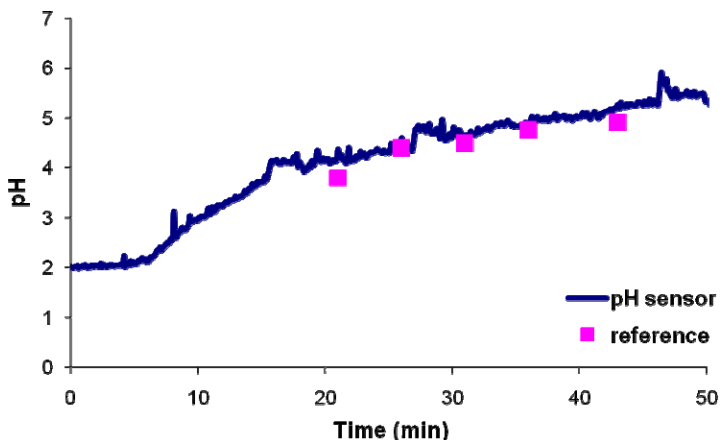


Fig. 5. Sweat pH sensor response and reference measurements during an exercise trial

including those with low sweat rates. In order to do this, a micro-fluidic device has been developed which requires much smaller samples of sweat.

3.2 Micro-fluidic Device

Several features of micro-fluidic devices suggest that they would be ideal for wearable body systems. These include their ability to process very small samples using small quantities of reagents, to exploit the physics of low-Reynolds-number environments (capillary forces), miniaturization of the whole system by integration of small electronic components and potential to include multiple separation stages and sensors. [21] Therefore, the requirements for wearable chemo-sensing point to micro-fluidic devices as the key tools for future development. Bearing this in mind, further development of the above system has been carried out by miniaturizing the system, through the generation of an autonomous micro-fluidic device capable of measuring real-time pH changes. By miniaturizing the system smaller quantities of sweat are needed for analysis making the device suitable for users with low sweat rate and also decreasing the priming time of the system. The device is designed to be incorporated into a simple adhesive plaster format which can be easily attached to the skin, thereby causing little or no discomfort during training.

Fig. 6(a) shows the fabrication of the microchip structure and Fig. 6(b) a picture of the final microchip. The micro-chip ($2 \times 3\text{cm}$) was easily fabricated using extra thin poly(methyl-methacrylate) ($50\text{ }\mu\text{m}$) and pressure-sensitive adhesive ($80\text{ }\mu\text{m}$) in three layers using a CO_2 ablation laser. The inlet had a drop shape for efficient sweat collection when in contact with the skin. The sensing area was a small patch of pH sensitive fabric, which varied in colour depending on the acid/base nature of the sweat moving along the micro-fluidic channel. The patch was made from moisture wicking fabric with bromocresol purple dye immobilized on it. The

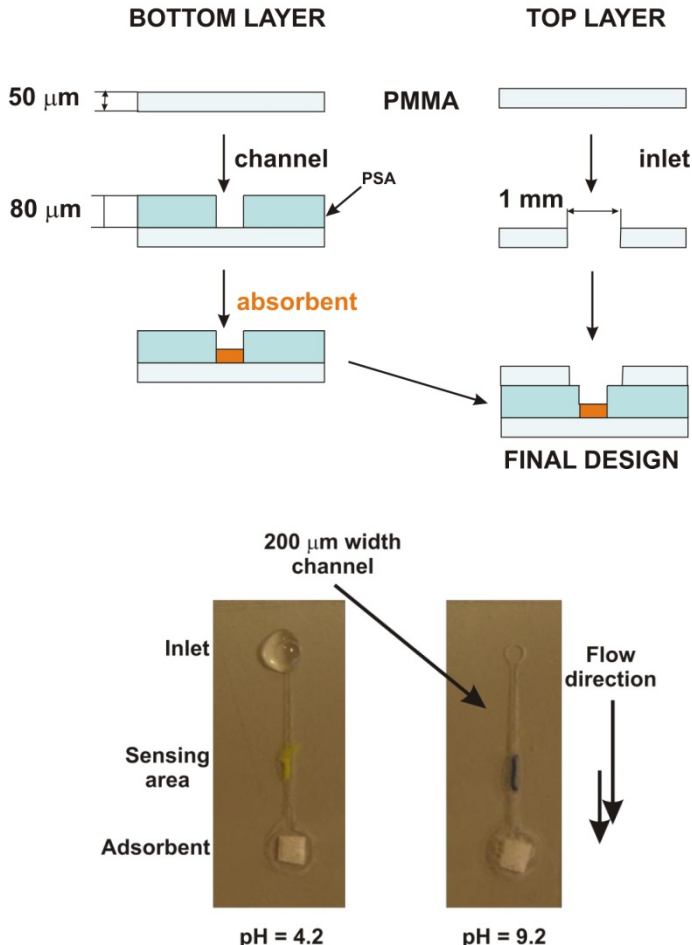


Fig. 6. (a) Schematic representation of the micro-chip fabrication; (b) Picture of the micro-chip at pH: 4.2 and pH: 9.2, with the colour change in the sensing area easily visible.

sweat was drawn into the sensing area by a piece of superabsorbent (Absortex®) placed at the end of the channel. The final device (180 μm thick) was flexible and could adapt easily to contours of the body.

The colour change of the pH sensitive material was detected using an optical configuration. This is shown in Fig. 7. A surface mount (SMT) LED and surface mount photodiode module were used for this purpose. 30 awg wire leads were soldered to the pins of the components and the devices subsequently coated in silicone (Dow Corning, Sylgard 184). This was to protect the components and also to prevent short circuits between the pins. The optical components were selected based on the absorption properties of the pH sensitive dye, Bromocresol Purple (BCP). A yellow LED (KINGBRIGHT - KP-2012SYC) with peak wavelength of

590nm was used as the light source. The LED was protected by a current limiting resistor. The value of the resistor controlled the current flowing to the LED, thereby controlling the light output. The photodiode (Avago Technologies, APDS-9004) had peak sensitivity at 620nm. The output pin of the photodiode module was connected to the analogue pin of the microcontroller. A capacitor was used as a low pass filter to remove high frequency noise, and a load resistor was used to control the current to voltage output signal of the photo-sensor. The circuit diagram is shown in Fig. 8.

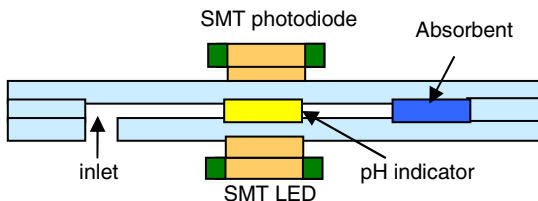


Fig. 7. Wearable micro-fluidic pH sensor with optical sensing configuration

The LED and photodiode were placed on either side of the pH sensing region of the micro-fluidic chip. This is a transmission configuration, where the light passes directly through the sensing material. Light is attenuated as it passes through the sensing region, with the degree of attenuation depending on the pH of the sample.

The detected light signal was sampled by a 10-bit analog to digital (A/D) channel of an Arduino microcontroller at a rate of 2Hz. Data was transferred to a laptop for analysis via a RS232 serial link. This link could be easily replaced by a wireless connection by attaching a Bluetooth® modem (BlueSMiRF silver) to the microcontroller. This modem works as a serial (RX/TX) pipe, transferring a serial data stream at a baud rate of 9600bps, which is passed seamlessly to a laptop up to 30m away. Alternatively an Xbee module (Digi International Inc.) which uses the IEEE 802.15.4 networking protocol could be deployed. These are low-power devices suitable for wearable sensor technology.

Calibration on the device has been carried out using artificial sweat solutions. These solutions were prepared based on the standard ISO 3160-2 (20 g/L NaCl, 17.5 g/L NH₄OH, 5 g/L acetic acid and 15 g/L lactic acid), in which the pH is adjusted by adding NaOH. Fig. 9 shows the response of the micro-chip to artificial sweat solutions at pH values from pH 1 to pH 14. From this graph it can be seen that the measurement range of the sensor is between pH 5 and pH 9. According to the literature bromocresol purple has an acid dissociation constant (pKa) of 6.2. [22] A best-fit sigmoid curve was fitted to the data and the pKa of the developed sensor was calculated to be 6.8. The reason for the difference is that the dye is in solid form as it is immobilized on a textile while the literature reports the pKa in solution. The response of the sensor is therefore suitable for the analysis of human sweat which is typically between pH 5-7. [16]

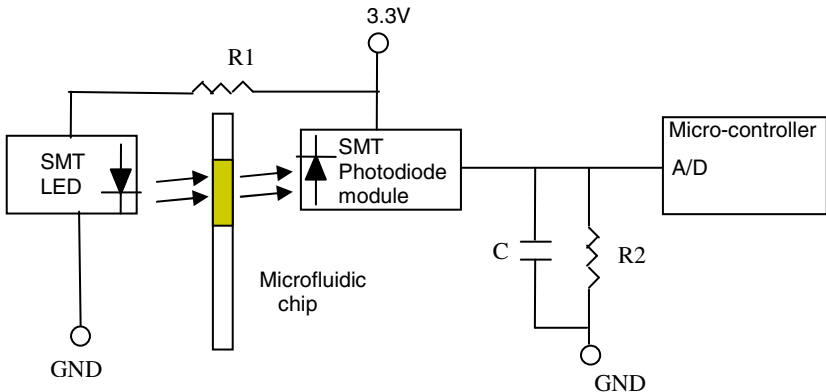


Fig. 8. Circuit diagram for micro-fluidic pH sweat sensor

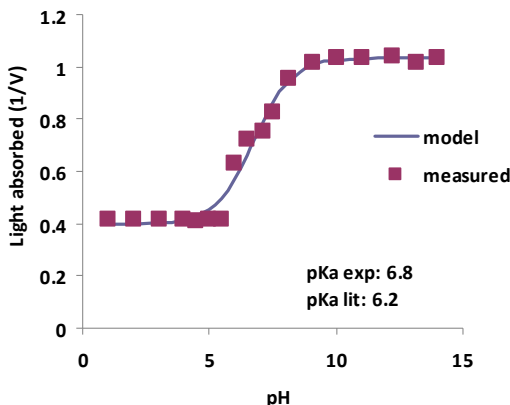


Fig. 9. pK_a determination of the dye bromocresol purple in the micro-chip

The micro-fluidic structure ensures fresh sweat flowing through the active sensing region throughout an entire training period. A schematic representation of the micro-fluidic performance is presented in Fig. 10. In this experiment, dyed sweat (brown colour), was collected in the inlet of the micro-chip and driven through the channel until it came in contact with the pH sensitive fabric. Then, the sweat reached the second chamber and it was drawn by the absorbent which acts as a passive valve. The sweat flow was calculated using snap-shots pictures of the channel over time and it was $6.4 \pm 2 \mu\text{L min}^{-1}$ ($n = 12$). Once the sweat reached the absorbent the sweat flow decreased significantly to an approximately $1.1 \pm 0.8 \mu\text{L min}^{-1}$ ($n = 12$) and it was drawn until the absorbent reached its maximum loading capacity, $278 \pm 2 \mu\text{L}$ ($n = 20$) of sweat. This gives the device a functional time of ca. 63 minutes. Nevertheless, since the device is easy to fabricate and tens of them can be prepared in a single batch, this period could be extended by replacing

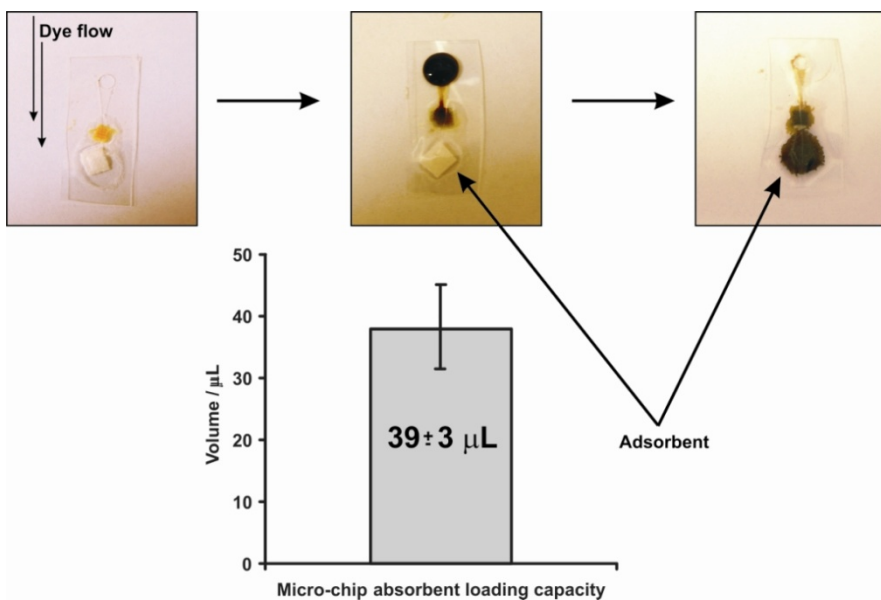


Fig. 10. Maximum sweat sampling capacity of the micro-fluidic chip

the initial device, reducing the flow rate through the micro-fluidic manifold (e.g. by constricting the channel dimensions, or by increasing the capacity of the adsorbent material).

4 Discussion

Changes in the composition of sweat can be used to provide information on a person's physiological condition. In addition, prolonged exercise can lead to dehydration and a change in the electrolyte concentrations in sweat. For elite athletes, a noticeable reduction in performance will occur for a 2 % drop in body weight due to dehydration. Further fluid loss can lead to symptoms such as irritability, headache, dizziness, cramps, vomiting, increased body temperature and heart rate, increased perceived work rate, reduced mental function, slower gastric emptying. [23] At the other extreme, drinking too much water can lead to hyponatremia, which is characterized by low levels of sodium ions. This results in symptoms such as headache, nausea, vomiting and muscle cramps. Where there is a quick onset of hyponatremia, for example during prolonged exercise, it can lead to more severe complications such as seizures, coma, brain damage and death. [24] Therefore, it can be seen that real-time knowledge of the variation in sweat composition during exercise can be useful in developing individualized rehydration strategies to maximize performance of elite athletes and to protect amateur sports people from developing potentially fatal conditions. The field of sports science and human performance involves the study of exercise and sports physiology. This area

of study examines the scientific basis for understanding how the body responds to single and multiple bouts of exercise. For sports applications, the development of wearable sensors that are non-obtrusive will allow the assessment of an athlete's performance in the field. Naturally this would provide a better assessment of performance abilities than trials carried out in a laboratory setting.

In addition to monitoring the electrolyte balance, knowledge of sweat pH can be useful. It has been shown that sweat pH during exercise will change with the onset of metabolic alkalosis. Therefore, pH measurements may also provide a non-invasive method of relating the build-up of acid muscle cells during exercise. Physiological testing can serve as a valuable tool for athletes and coaches to check the athlete's health and develop individualised training strategies. While laboratory testing may be increasingly widespread, there is a great demand for wearable sensors to be used in the field. Optimum rehydration depends on the individual, and on the type of sport and whether it is during competition or training. While there are guidelines regarding fluid intake, the personalisation of rehydration for each athlete is only in its infancy.[25]

In the approach presented here we have overcome the issue of calibration by using a disposable sensing layer for the sensor. These layers could be calibrated prior to and after experimental trials using standard reference pH solutions. In the case of the textile patch the fabric layer is disposable while the cover, which contains the optical components, and the associated electronics are re-useable. Similarly for the micro-fluidic device, the PMMA microchip layer is disposable. Hence, this is a low-cost device which could be mass-produced at a cost of a few euro cents. It has been designed to be used during an exercise session and will function for several hours depending on the sweating characteristics of the wearer and the characteristics of the absorbent. For instance, a 4 x 4 mm absorbent of the chip is able to retain more than 36 µL of sweat, which is approximately one hour of exercise period. Therefore it is easy to extrapolate that a larger amount of absorbent material will reach to higher loading capacity and so longer exercise periods. Moreover, the channel dimensions can be varied to reduce the sweat flow rate.

For the textile fluid handling approach we have demonstrated that the absorption and wicking capabilities of appropriate textile and fabric structures may be used to enable and control fluid movement, and perform sophisticated analytical operations without an external power source. In previous work we have investigated the use of low power actuators to gate fluid movement and control flow characteristics. The gated textile device has been shown to provide an excellent means of controlling fluid movement for sampling, delivery of reagents and calibrants, reagent/calibrant/sample mixing, and on-textile chemical analysis.[26] The same passive pumping concept has been implemented on a micro-fluidic chip which gives greater flexibility and expands the capabilities of the system. Micro-fluidic processes (e.g. separation, isolation, and chemical and biological reactions) are being applied to point-of-care, clinical, and medical diagnostics. Laboratory analysis that previously required laborious hours of work is now more easily performed in few minutes or even in seconds. [27]

5 Conclusions

A textile based platform has been developed using the inherent fluid handling properties of textiles that were previously developed by the textile industry to maintain wearer comfort by wicking moisture away from the body. Using a combination of moisture wicking fabric and a superabsorbent a textile based passive pump was developed. The textile pump can successfully collect sweat from human subjects during exercise and deliver the sweat to pre-defined channel where it reacts with a sensor, i.e. a pH sensitive material. Real time information regarding sweat pH was harnessed using optical detection techniques. The sweat was stored by an absorbent in such a way as to allow for a continuous flow of fresh sweat. The textile sensor system provides a straightforward, real-time measurement system which may prove to be a valuable tool for medical research and particularly sports physiology. The system offers real-time analysis of sweat using a wearable device that is straightforward to use unlike current measurement techniques which are impractical for day to day use outside of a laboratory setting. The device responds over the typical pH range of sweat and has been tested during exercise trials and validated with reference measurements. In order to improve the system performance a micro-fluidic chip has been developed. The reason for this was to reduce the sample size needed and also to reduce the reaction time of the sensor. This chip functions on the same principle as the textile platform. Capillary action draws the sweat sample through to a pH sensitive fabric enclosed in the microfluidic channel and an absorbent stores the waste. To detect the colour change of the fabric a miniature surface mount LED and photodiode are attached to either side of the chip. Miniaturization of the system has the added advantage of creating a smaller, lighter and more comfortable device. Therefore this is an unobtrusive and non-invasive method for the analysis of sweat during exercise. The integration of a wireless microcontroller allows sweat analysis to be taken outside of a laboratory environment and applicable to many forms of activity. Here the focus is on the pH of sweat however there are multiple markers of interest in sweat that may be measured by adapting the platform. The device is configured to perform colorimetric analysis so it is capable of utilizing other colorimetric reagents, e.g. to detect sodium. [28] The great advantage here is that it can give immediate feedback to the user regarding their physiology so that they can take the necessary action to maintain their health and improve sports performance.

References

1. Axisa, F., Schmitt, P.M., Gehin, C., Delhomme, G., McAdams, E., Dittmar, A.: Flexible Technologies and Smart Clothing for Citizen Medicine, Home Healthcare, and Disease Prevention. *IEEE Transactions on Information Technology in Biomedicine* 9(3), 325–336 (2005)
2. Schreuder-Gibson, H.L., Truong, Q., Walker, J.E., Owens, J.R., Wander, J.D., Jones, W.E.J.: Chemical and Biological Protection and Detection in Fabrics for Protective Clothing. *MRS Bulletin*, 574–578 (August 2003)

3. Radu, T., Fay, C., Lau, K., Waite, R., Diamond, D.: Wearable sensing application-carbon dioxide monitoring for emergency personnel using wearable sensors. In: Proc. ICESE 2009 - International Conference on Environmental Systems Engineering, Venice, Italy, October 28-30 (2009)
4. Byrne, R., Diamond, D.: Chemo/bio-sensor networks. *Nature Materials* 5, 421–424 (2006)
5. Brady, S., Dunne, L., Lynch, A., Smyth, B., Diamond, D.: Wearable Sensors? What is there to sense? *Studies in Health Technologies and Informatics* 117, 80–88 (2006)
6. Di Francesco, F., Fuoco, R., Trivella, M.G., Ceccarini, A.: Breath analysis: trends in techniques and clinical applications. *Microchemical Journal* 79, 405–410 (2005)
7. Pizzimenti, S., Bugianib, M., Piccionib, P., Hefflera, E., Carossoa, A., Guidaa, G., Rolla, G.: Exhaled nitric oxide measurements: Correction equation to compare hand-held device to stationary analyzer *Respiratory Medicine*, vol. 102(9), pp. 1272–1275 (2008)
8. Zuba, D.: Accuracy and reliability of breath alcohol testing by handheld electrochemical analysers. *Forensic Science International* 178(2), 29–33 (2008)
9. Braddock Clarke, S.E., O’Mahony, M.: *Techno Textiles*, vol. 2. Thames & Hudson Ltd. (2005)
10. Kreyden, O.P., Scheidegger, E.P.: Anatomy of the Sweat Glands, Pharamacology of Botulinum Toxin, and Distinctive Syndromes Associated With Hyperhidrosis. *Clinics in Dermatology* 22, 40–44 (2004)
11. Massie, J., Gaskin, K., Van Asperen, P., Wilcken, B.: Sweat testing following newborn screening for cystic fibrosis. *Pediatric Pulmonology* 29(6), 452–456 (2000)
12. Gibson, L.E., Cooke, R.E.: A test for concentration of electrolytes in sweat in cystic fibrosis of the pancreas utilizing pilocarpine by iontophoresis. *Pediatrics* 23(3), 545–549 (1959)
13. Lynch, A., Diamond, D., Leader, M.: Point-of-need diagnosis of cystic fibrosis using a potentiometric ion-selective electrode array. *The Analyst* 125, 2264–2267 (2000)
14. Brisson, G.R., Boisvert, P., Péronnet, F., Parrault, H., Boisvert, D., Lafond, J.S.: A simple and disposable sweat collector. *European Journal of Applied Physiology* 63, 269–272 (1991)
15. Shirreffs, S.M., Maughan, R.J.: Whole body sweat collection in humans: an improved method with preliminary data on electrolyte content. *Journal of Applied Physiology* 82, 336–341 (1997)
16. Patterson, M., Galloway, S., Nimmo, M.A.: Variations in regional sweat composition in normal human males. *Experimental Physiology* 85(6), 869–876 (2000)
17. Dill, D.B., Jones, B.F., Edwards, H.T., Oberg, S.A.: Salt economy in extreme dry heat. *The Journal of Biological Chemistry*, 755–767 (1933)
18. Lemon, P.W., Yarasheski, K.E.: Feasibility of sweat collection by whole body wash-down in moderate to high humidity environments. *International Journal of Sports Medicine* 6(1), 41–43 (1985)
19. Kidwell, D.A., Holland, J.C., Athanaselis, S.: Testing for drugs of abuse in saliva and sweat. *Journal of Chromatography B* 713, 111–135 (1998)
20. Rianon, N., Feeback, D., Wood, R., Driscoll, T., Shackelford, L., LeBlanc, A.: Monitoring sweat calcium using skin patches. *Calcified Tissue International* 72(6), 694–697 (2003)
21. Sorger, P.K.: Microfluidics closes in on point-of-care assays. *Nature Biotechnology* 26(12), 1345–1346 (2008)
22. Green, F.J.: *The Sigma Aldrich Handbook of Stains, Dyes and Indicators* (1990)

23. Casa, D., Armstrong, L.E., Hillman, S., Montain, S.J., Reiff, R., Rich, B.S.E., Roberts, W.O., Stone, J.: National Athletic Trainers' Association Position Statement: Fluid Replacement for Athletes. *Journal of Athletic Training* 35(2), 212–224 (2000)
24. Maughan, R.J., Shirreffs, S.M.: Development of individual hydration strategies for athletes. *International Journal of Sport Nutrition and Exercise Metabolism* 18(5), 457–472 (2008)
25. Maughan, R.: Nutrition in sport. *Encyclopedia of sports medicine*; v.7. Oxford, Malden (2000)
26. Wallace, G., Diamond, D., Lau, K., Coyle, S., Wu, Y., Morris, D.: Flow Analysis Apparatus and Method, U.S Patent Application No. 20080213133 (2008)
27. Ohno, K., Tachikawa, K., Manz, A.: Microfluidics: Applications for analytical purposes in chemistry and biochemistry. *Electrophoresis* 29, 4443–4453 (2008)
28. O'Neill, S., Conway, S., Twellemeyer, J., Egan, O., Nolan, K., Diamond, D.: Ion-selective optode membranes using 9-(4-diethylamino-2-octadecanoatestyril)-acridine acidochromic dye. *Anal Chim Acta* 398, 1–11 (1999)

A Wearable Measurement System for the Risk Assessment Due to Physical Agents: Whole Body Mechanical Vibration Injuries

Rosario Morello and Claudio De Capua

Dept. of Computer Science and Electrical Technologies,
University “Mediterranea” of Reggio Calabria, Reggio Calabria, Italy

Abstract. Whole Body Vibration (WBV) is caused by vibration transmitted to human body through the seat or the feet. Typical causes are motor vehicles and machines. So high levels of whole-body vibration affect people who drive vehicles over rough surfaces as part of their job, for example off-road vehicles such as tractors, excavators, pallet-trucks and dumper trucks. Exposure to high levels of vibration can risk the health and safety of the worker. Typically vibration transmitted to body may be cause of back injuries and may aggravate pre-existing pathologies affecting the lumbar spine. The risks are greatest when the vibration magnitudes are high, or if the exposure time is long. Moreover frequent and regular exposure to severe shocks or jolts can increase the resultant effects. So syndromes and diseases affect backbone and cardio-vascular system. The European Directive 2002/44/EC deals with the minimum health and safety requirements regarding the exposure of workers to the risks arising from physical agents. The “Vibration Directive” sets minimum standards for reducing the risks from whole-body vibration, so that daily exposure limits are fixed.

The present paper proposes a wearable measurement system for the whole-body vibration risk assessment. The system is a portable device based on a Pocket PC, a DAQ card and a set of accelerometers. It is able to estimate and to process the vibration exposure levels according to the guidelines of ISO Standards. The purpose is to check the exposure of workers to physical agents and to prevent risks during the use of driving vehicles.

Keywords: whole body vibration, health injuries, medical instrumentation, vibration measurements, risk assessment.

1 Introduction

Working activities entailing the use of motor vehicles or in general of means of transport, like excavator, cranes, bulldozer, tractor, bus, train, helicopters, lorry, expose the human body to shakes and vibrations. With the term of “Whole Body Vibration” (WBV), it is meant the vibration transmitted to the human body due to

physical agents. The propagation depth depends on the exposed body surface and on the position of the person (seated or standing). Several studies show that the vibration exposure is cause of health harms like spine pathologies, abdominal and chest pains, problems to motion and balance. Health risks depend on the duration, intensity, frequency and direction of the vibration transmitted to the body. The ISO 2631-1 Standard defines methodologies for the measure of human exposure to whole-body vibration, [1]. Moreover it provides guidelines for the estimation of the effects on the human health. Nevertheless it is important to notice that no quantitative relationship exists between the vibration exposure and health risks. Therefore risk probabilities can be defined with difficulty referring to the time and intensity of exposure. Anyway caution criteria induce laws and regulations to fix specific limits for the daily amount of vibration exposure, [1-2]. In fact the repeated exposure to high vibration levels is correlated with an increasing risk of onset of ailments and injuries to the lumbar spine, [3-4]. Specific studies show even the occurrence of possible problems to the circulatory system and digestive apparatus (gastroenteritis, ulcer) or sprain to neck. However there is a clear epidemiological evidence proving a causal relationship between the WBV exposure and pathologies involving the lumbar spine. The propagation of vibration depends on body posture, consequently the effects are really complex. The main risk is to aggravate pre-existing back injuries. In detail, vibration in the range 3-10 Hz may be cause of lesions of the muscular-skeletal apparatus of the spine because of resonance effects, affecting also neck and shoulders. It is cause of structural injuries involving discs (herniated disc) and inter-vertebral joints. Lumbar hernia or muscular pains are further consequences. Statistical studies have shown that such pathologies are typical for drivers of motor vehicles and farm machines. The seriousness of the effects depends on the vibration intensity and on the exposure time. The body posture, the type of torsion affecting the lumbar spine, previous trauma and habits have further influence on the possible effects. So there are not specific models able to define the effective risk because of the different parameters of influence involved (working posture, physical workload, muscle tone, individual susceptibility, anthropometric characteristics). Anyway, even if such models are not available, the onset of specific illnesses is a clear symptom of the WBV exposure. For such reason, World Health Organization suggests the application of preventive actions to use at workplace in order to prevent and diagnose rapidly any disorders correlated with exposure to mechanical vibration. The WBV exposure may be assessed by means of specific measures, which require the use of suitable instrumentation and appropriate methodologies, [5-6]. The availability of health records about the vibration exposure may be an useful information in order to diagnose timely the onset of pathologies affecting the lumbar spine. On this issue, the authors propose a wearable measurement system in order to keep the vibration exposure under control, checking the observance of the law requirements. A Pocket PC, by a data acquisition card, collects and computes acceleration levels measured by three orthogonal accelerometers. Embedded decisional rules perform the comparison between acquired data and law limits, so to assess possible health hazards. Measurement uncertainty information is used in order to qualify

the processing algorithms. The aim of the projected system is to safeguard the health of persons exposed to vibration during working activities.

2 Whole Body Vibration

Whole-body vibration is the term used to indicate the mechanical vibration that, when transmitted to the whole body, entails risks to the health and safety of workers. In particular it is cause of lower-back ailment and trauma of the spine. Such mechanical stress is due to oscillatory shakes which involve the whole body. The vibration is typically transmitted to the body by means of vibrating surfaces or means of transport like motor vehicles or farm machines.

By using human body models, scientific studies have shown the different response of the body according to the vibration frequency. Vibration below 2 Hz have effects on the whole body which shakes in a homogeneous way with the vibrating surface. For vibration with frequency in the range 2-20 Hz the main effects concern the lumbar spine. Vibration over 20 Hz affects limited parts of the body, in fact the shakes are typically transmitted to the zone touching the vibrating surface. About this topic, the European Directive 2002/44/CE, [2], fixes the following Action Values and Exposure Limits to vibration:

- i) the daily exposure action value (*EAC*) standardised to an eight-hour reference period shall be 0.5 m/s^2 or, at the choice of the Member State concerned, a vibration dose value (*VDV*) of $9.1 \text{ m/s}^{1.75}$;
- ii) the daily exposure limit value (*ELV*) standardised to an eight-hour reference period shall be 1.15 m/s^2 or, at the choice of the Member State concerned, a vibration dose value (*VDV*) of $21 \text{ m/s}^{1.75}$.

In this way it is possible to characterize three zones:

- i) the security zone: the vibration exposure level is below the action value, so no risk for the health has been singled out;
- ii) the warning zone: the vibration exposure level is below the limit value and above the action value, so corrective actions have to be taken;
- iii) the alert zone: the vibration exposure level is above the limit value, in this case the vibration exposure has to be stopped.

The two values has a different meaning. In fact, if the *EAC* value or the corresponding *VDV* value are exceeded, the employer shall establish and apply a program of suitable actions. The aim is to reduce to a minimum the exposure to mechanical vibration and the attendant risks. Moreover the employer is responsible to define and carry out suitable health check-up. Otherwise, if the *ELV* value or the corresponding *VDV* value are exceeded the employer should immediately take actions to reduce exposure below the limit value. He shall identify the reasons why the maximum value has been exceeded. So protection and prevention actions have to be taken in order to prevent that limit is exceeded again.

Nevertheless, it has to be said that the Standard ISO 2631-1, [1], fixes further zones for the root mean square (rms) vibration level and the *VDV* value: a caution zone and a likely health risk zone. According to these zones different limits are

obtained with reference to 8-hour exposure. For the caution zone 0.43 m/s^2 (rms value) and $8.5 \text{ m/s}^{1.75}$ (VDV value); for the likely health risk zone 0.86 m/s^2 and $17 \text{ m/s}^{1.75}$ respectively. Anyway in the present application the limits of the European Directive have been considered.

The requirements of the “Vibration Directive” shall apply to activities in which workers are or are likely to be exposed to risks from mechanical vibration during their work.

In order to have quantitative information on the vibration typically transmitted to the human body during the use of common motor vehicles, the Table 1 reports data concerning the main characteristics of farm machines.

Table 1. Maximum vibration exposure time for specific machines.

Vehicle Type	$a_v [\text{m/s}^2]$	Freq. [Hz]	Max exposure time [hour]
tractor	0.5-1.6	2-5	8-0.74
caterpillar	0.6-1.2	10-20	5-1.38
combine harvester	0.4-0.8	2.5-5	11.7-2.8
lawnmower	0.4-1.6	2.5-5	11.7-0.74

The table refers to the typical vibration levels generated, the corresponding working frequency values, and the maximum exposure time according to the caution limits, [2].

However specific derogations are allowed about the limit overcoming. So if the vibration exposure is usually below the exposure action value, occasionally it can exceed the exposure limit value. But the exposure value averaged over 40 hours must be less than the exposure limit value. Regarding the employer duties, vibration records shall be kept so as to permit any consultation to the competent authority on request.

3 The Measurement System

The proposed measurement system is a wearable and portable device that is able to acquire and process acceleration levels due to WBV exposure. Since the most serious effects concern the muscle/skeletal system of the back, the present application focuses the attention on the vibration affecting the lumbar spine. In order to describe the system’s functioning, we have to single out the hardware section from the data processing algorithms. The system is compliant with the requirements of the Standard ISO 8041, [5]. According to the Dir. 2002/44/CE and the ISO 2631-1, the device assesses the risk due to the WBV and the observance of the maximum tolerable levels of vibration exposure. The system represents an useful tool for workers during the use of motor vehicles and machines in workplaces. In fact the vibration absorption for the lumbar spine is monitored, so to control the possible occurrence of risks for the health.

A. The Data Acquisition System

The hardware equipment in Fig. 1 consists of a Pocket PC (*HP iPAQ h2210*), a CompactFlash data acquisition card (*National Instruments CF-6004 DAQ*), and an isotropic vibration sensor (*n.3 PCB Piezotronics INC. 393B04*).

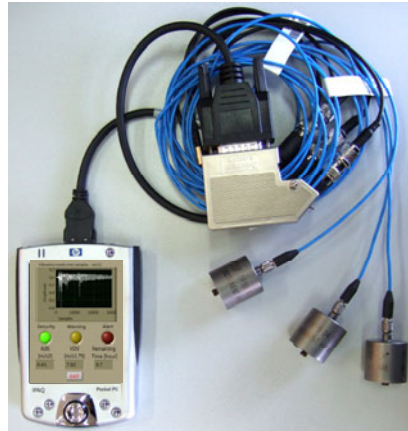


Fig. 1. Measurement system

An executable program, developed by using the *LabVIEWTM PDA Module*, allows the communication between the Pocket PC and the DAQ card. The sensing unit has been obtained by means of three ceramic accelerometers placed along the axes of a Cartesian system (x , y and z), [7], see Fig. 2 for reference. The z axis has the same direction of the lumbar spine, so it represents the reference axis for the assessment of the vibration effects on the back.

The sensor has to be worn from the worker by means of a belt. The single transducer has a small size, so the movement freedom is not reduced. A set of cables connects the sensor with the DAQ card. The Table II shows the main characteristics of the sensor.



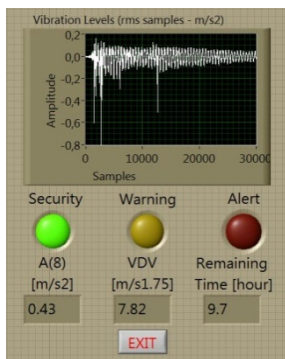
Fig. 2. Sensors orientation

Table 2. Sensor characteristics.

Characteristic	Value
Sensitivity	102 mV/(m/s ²)
Measurement Range	± 49 m/s ² pk
Frequency Range	0.06 to 450 Hz
Resonant Frequency	≥ 2.5 kHz
Resolution	0.00003 m/s ² rms
Non-Linearity	≤ 1 %

The data acquisition card has four analog input channels with 14-bit resolution (successive approximation ADC) and a sampling rate up to 132 kS/s for channel.

The analog voltage signals of the three accelerometers are acquired by means of the DAQ card with 100 kS/s sampling frequency. Data are stored in the internal memory of the Pocket PC. Subsequently the embedded algorithms process data and available information. So the acquired levels are filtered using a second order Hanning digital filter with a low-pass cut off of 100 Hz and a high-pass cut off of 0.5 Hz. As a result, the system estimates the daily vibration exposure value and through visual tools it displays the computational results. In detail, a set of digital led and a graph allow the worker to keep under control the vibration absorption, see Fig. 3. According to the “Vibration Directive”, a green led has the task to check if the vibration exposure is in compliance with the security zone; so the led lights up when vibration exposure level is below the action value. A yellow led lights up if the exposure value is within the warning zone. In this case corrective actions have to be taken. While a red led checks if the WBV absorption is within the alert zone. In such an occurrence the red led lights up, and the worker must stop the working activity. On the screen of the Pocket PC, text boxes show the estimated values of the daily vibration exposure $A(8)$ and VDV of which meaning is described in the following subsection. A further text box allows the worker to estimate the remaining time period in order to continue the use of the machine without risking his health according to the European Directive guidelines.

**Fig. 3.** Pocket PC's Screen and Tools

In the end the worker has to launch the executable file, so the program starts the acquisition and executes atomically the embedded algorithms.

The system every 30 s updates the screen's information. Whereas, a 'stop' button allows user to exit from the program when the vibration exposure or the use of the motor vehicle is finished.

B. The Computing Algorithms

After the acquisition of the acceleration signals, data are appropriately processed by the built in algorithms. In order to estimate the daily vibration exposure value, information on the frequency, direction and intensity of the acceleration has to be considered. In fact, the propagation of the vibration in the body happens by means of the feet, the gluteus or back according to the position (seated or erected) of the person exposed to vibration. The lumbar spine represents surely the organ more at risk. The sensor provides information on the vibration absorbed from the spine along the three directions x , y and z (see Fig. 2). The direction and frequency of the shakes transmitted to body represent therefore two important factors of influence, which contribute to characterize the effects of vibration on the human body. In fact, the body response changes with the vibration frequency, see Table 3 as example.

Table 3. Effects on human body Vs vibration frequency value.

Frequency	Possible Ailment
<0.5 Hz	movement sickness
4-8 Hz	troubles of cochlea or digestive apparatus
3-10 Hz	lumbar spine troubles
40-55 Hz	female reproductive organ ailments
4-80 Hz	skeletal-muscle sickness

So the Standard ISO 2631-1 suggests to use filters for weighting the vibration levels according to the frequency value. In this way it is possible to single out the vibration components having more impact on the body. In fact the several components are weighted according to the risk of injury. In detail, different filters have to be applied for the three axes in order to distinguish the diverse effects of the vibration on the human body with reference to the z axis that is the spine direction, see Table 4.

The "Vibration Directive" suggests two methods for the vibration exposure assessment as mentioned in the previous Section. Consequently the system is able to estimate the daily exposure value $A(8)$ and the vibration dose value VDV . The former represents the acceleration normalised to an 8 hour day. In other words it is expressed as equivalent continuous acceleration over an eight-hour period. The estimation is made by the root-mean-square averaging of the acceleration signal and has units of m/s^2 . The latter is a cumulative dose based on the 4th root-mean-quad of the frequency-weighted acceleration signal with units of $m/s^{1.75}$. Both parameters are defined in compliance with the guidelines of the ISO 2631-1. Therefore in detail, the system first calculates the rms acceleration values for each i -th axis:

$$a_{wi} = \sqrt{\frac{1}{T} \int_0^T a_{wi}^2(t) dt} \quad (1)$$

where $a_{wi}(t)$ is the instantaneous value of the frequency-weighted acceleration along the i-th axis. In fact since the risk of damage is not equal at all frequencies, a frequency-weighting filter has been used. So the rms acceleration values are frequency-weighted in the range 0.5-80 Hz, see Table 4 for reference. Two different frequency weighting curves have been used. The first curve (W_d weighting) is applied to the signals acquired along the x and y axes. The second curve (W_k weighting) weights the vertical vibration along the z axis.

Table 4. Frequency Weightings, ISO 2631-1.

Frequency Hz]	W_d	W_k
0.1	0.0624	0.0312
0.2	0.243	0.121
0.4	0.713	0.352
1	1.011	0.482
2	0.89	0.531
5	0.409	1.039
10	0.212	0.988
20	0.1	0.636
40	0.0494	0.314
50	0.0388	0.246
80	0.0211	0.132
100	0.0141	0.0887
125	0.00863	0.054
160	0.00455	0.0285

According to the Table 4, specific filters allow the frequency-weighting to be performed. It is possible to notice that the weighted acceleration decreases when the frequency increases in the range from 0.5 Hz to 80 Hz.

In addition, in order to take into consideration the different effects on the lumbar spine due to the three acceleration components, additional multiplying factor have to be applied to the frequency-weighted vibration values. Consequently the total value of body exposure to vibration is got by:

$$a_v = \sqrt{(k_x \times a_{wx})^2 + (k_y \times a_{wy})^2 + (k_z \times a_{wz})^2} \quad (2)$$

where for seated exposure the used factors are $k_x=k_y=1.4$ and $k_z=1$ for the three axes respectively.

This vector sum of the weighted rms accelerations provides a quantitative information about the total vibration absorbed from the body. In order to estimate the daily vibration exposure standardised to an eight-hour reference period, the $A_i(8)$ value has to be calculated for each i-th axis by:

$$A_i(8) = k_i a_{wi} \sqrt{T_e / 8} \quad [\text{m/s}^2] \quad (3)$$

where T_e is the total daily vibration exposure time expressed in hour units. According to the ISO 2631-1, the daily vibration exposure value $A(8)$ is the highest value between $A_i(8)$. If the person is exposed to more vibration contributions during the day, due to different activities or to the use of more vehicles, the total daily vibration exposure $A_T(8)$ has to be estimated. The frequency-weighted rms acceleration values (a_{j-wx} , a_{j-wy} and a_{j-wz}) are estimated for each j-th contribution by (1). For the single i-th axis we can estimate the daily vibration exposure value $A_i(8)$ by a sum of the partial vibration exposure values due to any contribution j-th:

$$A_i(8) = \sqrt{\sum_{j=1}^n (k_j a_{j-wi} \sqrt{T_{j-e}/8})^2} \quad [\text{m/s}^2] \quad (4)$$

where n is the number of exposure contributions, T_{j-e} the vibration exposure time of the single j-th contribution expressed in units of hour. The total daily vibration exposure value $A_T(8)$ is the highest value between $A_i(8)$.

An alternative method for the vibration exposure estimation is provided. In fact the previous equations could underestimate the effect due to transient or impulsive vibrations. So in presence of abrupt shakes, the ISO Standard suggests to estimate the vibration dose value VDV . Consequently daily exposure to vibration may be assessed using either or both of the two exposure measures $A(8)$ and VDV . The first method provides the 8-hour energy equivalent total vibration value in meters per second squared (m/s^2), it includes all whole-body vibration exposures during the day. Nevertheless the VDV estimation has to be preferred in order to get a better indication of the risks from vibration that includes repeated shocks. It is a cumulative value with units of $\text{m/s}^{1.75}$, and is obtained by the fourth root of the fourth power of the acceleration signal. Therefore in a similar way we obtain that:

$$VDV_{wi} = \sqrt[4]{\int_0^T (a_{wi}(t))^4 dt} \quad [\text{m/s}^{1.75}] \quad (5)$$

$$VDV_i = k_i VDV_{wi} \sqrt[4]{T_e/T_m} \quad [\text{m/s}^{1.75}] \quad (6)$$

where T_e is the total daily vibration exposure time, and T_m is the measurement time. The daily vibration dose value is the highest value between VDV_i .

If the vibration exposure is due to several contributions during the daily activity, the total daily vibration dose value VDV_T has to be estimated. If VDV_{j-wi} is the partial vibration dose value estimated by (5) and due to the single j-th contribution, the total vibration dose value for each axis is estimated by:

$$VDV_i = \sqrt[4]{\sum_{j=1}^n (k_j VDV_{j-wi} \sqrt[4]{T_e/T_{j-m}})^4} \quad [\text{m/s}^{1.75}] \quad (7)$$

where T_{j-m} is the measurement time of the single vibration exposure contribution. The daily vibration dose value is the highest value between VDV_i .

Measurements should be made over periods of at least 20 minutes in order to get meaningful information. If shorter measurements are unavoidable, they should

normally be at least three minutes long with a total measurement time of more than 20 minutes, [8]. Measurements of 2 hours or more are preferable.

Several factors affect the measurement uncertainty of vibration exposure estimation. The main contribution to uncertainty is due to the used instrumentation. Other sources of uncertainty are attributable to the accuracy of available data and to environmental factors.

The system uses the available information on measurement uncertainty in order to optimize the decision-making process. So the $A(8)$ and VDV values are put in comparison with the respective European Directive limits taking into account the uncertainty influence. The used decision-making procedure has been previously developed from the authors in [9]. It permits to determine the most reliable decision about the conformity or non-conformity of vibration exposure values with the control limits. The procedure minimizes costs and risks associated to a possible wrong decision.

4 Experimental Results

Tests have been executed by using a shaking table in order to check the sensor response. In this way the functioning of a machine working on a rough terrain has been simulated. In fact, by means of numerical models, vibrations with specific intensity and frequency values have been generated. The computing results of the measurement system have been compared with the expected values. The system response was compliant with the results obtained by means of a numerical analysis of the generated vibration. Deviation from the expected values was below 1%. Such a behaviour can be reasonably attributed to the measurement uncertainty effect. During the tests the digital filtering has shown one fault occurrence. The error has been compensated by means of corrective factors used in the computing algorithms. Anyway the results have shown a significant accordance with the numerical data. Further experimental results have been obtained by using the measurement system during the driving of two motor vehicles. In detail a worker has worn the system during his working activity involving the use of a tractor and a caterpillar. The total exposure time was equal to 500 minutes. The sensor has measured a vibration peak along the z axis equal to 17.8 m/s^2 . The total daily vibration exposure value was $A_T(8)=0.54 \text{ m/s}^2$. Whereas the estimated total daily vibration dose value was $VDV_T=12.58 \text{ m/s}^{1.75}$. The estimated values belong to the warning zone since the whole body vibration absorption has exceeded the action values of the European Directive. Consequently, the yellow led of the system screen lighted up in order to alert worker to have a break in the use of the motor vehicle. Nevertheless, during the use of the caterpillar, abrupt and repeated shakes along the direction of the lumbar spine have been measured. In this case the vibration dose value estimation has permitted to characterize better such effects due to transient and impulsive vibrations. In fact repeated experimentations have shown a more capability of the VDV parameter to single out information and to get a better indication about the risks due to vibration that includes repeated shocks. In detail, with reference to the previous experimentation, the analysis of the measured data has shown different results for the two parameters. In fact during the driving of the

caterpillar, after a measurement time of 450 minutes, the system has detected a vibration dose value above the action value. In detail, the daily vibration exposure value $A(8)$ was equal to 0.46 m/s^2 whereas the estimated daily vibration dose value was $VDV = 10.2 \text{ m/s}^{1.75}$. The considered case represents a clear proof of the more reliability of the second parameter for the characterization of health risk. As a matter of fact, medical studies have demonstrated a more influence of impulsive vibration on the lumbar spine rather than a continuous exposure to low vibration levels. So when abrupt and repeated shakes occur, the VDV value allows a timely detection of the warning zone to be made; differently the $A(8)$ parameter underestimates such occurrences so to risk the health of the exposed worker.

So experimental data have highlighted the capabilities of the proposed system to assist the worker exposed to vibration during his working activity. Moreover the experimentation has allowed the authors to make further improvements and corrections on the embedded algorithms optimizing the computational features.

5 Conclusion

In the paper the authors propose a wearable and portable system able to assess the risks due to whole-body vibration exposure. The system assists the worker during the driving of motor vehicles or machines in order to check the conformity of vibration absorption with the requirements of the European Directive 2002/44/CE. A Pocket PC, mounting on board a DAQ card and an isotropic vibration sensor, shows on screen the processing results. In this way the worker gets control on his vibration exposure, and by means of visual tools he has information about warning or alert occurrences. The embedded processing algorithms are compliant with the ISO 2631-1 guidelines. So when the maximum tolerable limits are exceeded, the system alerts worker to stop his working activity. The developed device is a safety tool, of which task is to safeguard the worker health from possible risks due to vibration transmitted to whole body. In this application, attention has been focused on the possible hazardous effects to lumbar spine. The experimental results have allowed the authors to check the reliability of the measurement system. The built-in algorithms have been optimized in order to minimize fault occurrences. Besides, information on measurement uncertainty has been used so to improve the decision-making procedures.

References

1. ISO 2631-1, Mechanical vibration and shock – Evaluation of human exposure to whole-body vibration-Part 1: General requirements (1997)
2. Dir. 2002/44/CE of European Parliament and Council, On the minimum health and safety requirements regarding the exposure of workers to the risks arising from physical agents, vibration (2002)
3. Paddan, G.S., Griffin, M.J.: Effect of seating on exposures to whole-body vibration in vehicles. Journal of Sound and Vibration 253(1), 215–241 (2002)

4. Seidel, H., Bluethner, R., Hinz, B.: Effects of sinusoidal whole-body vibration on the lumbar spine: the stress-strain relationship. International Archives of Occupational and Environmental Health Journal, Springer Journal, 207–223 (2004) ISSN 0340-0131
5. ISO 8041, Human response to vibration-Measuring instrumentation (2005)
6. Koenig, D., Chiaramonte, M.S., Balbinot, A.: Wireless Network for Measurement of Whole-Body Vibration. Sensor Journal, 3067–3081 (2008) ISSN 1424-8220
7. ISO 5348, Mechanical vibration and shock - Mechanical mounting of accelerometers (1998)
8. EN 14253, Mechanical vibration - Measurement and evaluation of occupational exposure to whole-body vibration with reference to health- Practical Guidance (2003)
9. De Capua, C., Morello, R., Pasquino, N.: A Fuzzy Approach to Decision Making About Compliance of Environmental Electromagnetic Field with Exposure Limits. IEEE Trans. on Instrumentation and Measurement 58(3), 612–617 (2009)

A Measurement System Design Technique for Improving Performances and Reliability of Smart and Fault-Tolerant Biomedical Systems

Rosario Morello and Claudio De Capua

Dept. of Computer Science and Electrical Technologies,
University “Mediterranea” of Reggio Calabria, Reggio Calabria, Italy

Abstract. The present Chapter intends to provide a practical guide for designers in planning smart measurement systems to be used in critical applications like medical ones. The authors propose an original approach to the design of measurement instrumentation with high performances. The procedure allows the designer to characterize the best measurement uncertainty that the system must have. The main purpose is to project a system with appropriate performances, so that suitable accuracy and reliability levels are guaranteed for the resulting measurements. The used approach starts from the consideration that typically the measured data are used during the processing stage in order to make decisions. In example, medical diagnoses are based on measurements which are put in comparison with reference limits. Therefore the measurement uncertainty can affect the reliability of the final results so to be source of mistaken decisions. Consequently high values of measurement uncertainty may be cause of unreliable data and inaccurate diagnoses. In the Chapter, a statistical model is used in order to characterize the functional relationship between the measurement uncertainty and the probability to make mistaken decisions because of the same uncertainty. Consequently the designer can characterize the best uncertainty value for the measurement system to be projected. So suitable reliability can be guaranteed during the decision-making stage by assuring a tolerable probability of mistaken decision. Furthermore the Chapter describes the architecture used in order to design smart and patient-adaptive biomedical systems. In detail the use of specific memory devices is shown. Information concerning the metrological characteristics of system and the patient data are so made available. In detail, information on measurement uncertainty and calibration curve is stored in a first memory device in order to estimate the reliability of measurement results. Whereas a further writable and readable storage device stores private and medical data of the specific examined subject. Such memory is a personal data-logger replaced for each patient and updated with the passing of time according to the current clinical conditions of the subject. In this way the computing algorithm fits the patient by means of the available information so to qualify the final diagnosis. In fact the available data allow the system to adapt and configure itself according to the patient features and to his health state so to get fault-tolerant diagnoses. In this way it is possible to project a biomedical system

which is updateable and configurable according to the specific subject. Experimental results concerning the project of an ECG measurement system are added.

Keywords: biomedical measurement system, design and prototyping, measurement uncertainty, patient-adaptive system, fault-tolerant diagnosis.

1 Introduction

Measurement instrumentation nowadays is widely used in medical applications. Biomedical systems allow doctors to get information on patient health state, consequently measured data are used in order to make diagnoses. Often smart systems are able to make automated data processing, so to diagnose timely the onset of pathologies or occurring diseases. Therefore, the reliability of the used measurement instrumentation represents a basic requirement to be guaranteed. Diagnoses are commonly based on reference values and models. In fact the estimation of a specific pathology or disease is made by comparing the measured data with fixed threshold values. In example the diagnosis of cardiac pathologies is made by putting in comparison the electrocardiogram (ECG) signal of the patient with a reference model. Typically such reference models are classified according to age, sex, physical constitution and life habits. They are obtained by means of an average of normal ECG waveforms of healthy persons. So a pathology occurrence is singled out if specific parameters exceed fixed reference levels. Unfortunately such models do not represent a reliable reference for different patients having varied health conditions. Therefore computational criteria have to be fitted according to patient and his state of health. Moreover during the diagnosis, further faults are frequently due to an erroneous characterization of the measurement system or to its poor accuracy. So measurement uncertainty plays a leading role during data processing. In example a parameter can apparently seem compliant with the reference threshold because of the uncertainty, so to entail mistakes. The underestimation of such aspects is the main cause of inaccurate or erroneous clinical diagnoses. The present issue requires the design of accurate and patient-adaptive systems, which are able to adapt themselves according to information on patient or to historical data about his health. Though several models concerning system design techniques have been proposed in literature, the state of art is lacking in applicable guidelines and practical tools. So several questions concerning project, prototyping and implementation of smart systems are still open. In the Chapter the authors present an original technique for the design of smart and fault-tolerant biomedical systems. The used approach focuses on the analysis of the correlation between the metrological characteristics of the measurement system and the reliability of the data processing results. In detail, the measurement uncertainty is cause of data inaccuracy. Consequently decisions based on such measurements may be unreliable. The matter is more critical in medical field, where measured data are used in order to make diagnoses. Therefore unsuitable metrological characteristics of the measurement system can affect the final results. As a result, an erroneous diagnosis may put the patient health at risk. In fact the reliability of decision-making process is strongly influenced from the system performances. Starting from this view, the

authors propose an original methodology for improving the performances of measurement instrumentation. The procedure has the aim to characterize the best measurement uncertainty value for the system to be designed. Consequently, since the decision-making process is based on the measured data, in this way it is possible to optimize the reliability of the relating decisions or diagnoses. Such an approach permits to correlate the design of the measurement system with the specific application in order to guarantee suitable levels of reliability for the decisions taken. Various authors have developed models of system design, [1-5], but few of them offer a practical method about how to correlate the metrological features of system with the final purpose of the measurement process. The objective of the proposed technique is to provide a procedure for designing suitable medical instrumentation which is compliant with fixed specifications. In this way it is possible to obtain desired performances during the decision-making process for fault-tolerant diagnoses. The main contribution of the present research is due to the characterization of the functional relationship between the measurement uncertainty and the system's project. In detail, the used Statistical Model correlates the reliability of decision with the measurement uncertainty value. As a result the procedure allows designer to obtain quantitative information about the allowed uncertainty that can affect the measurement system so to have a desired decision reliability during data processing.

In order to improve the performances of the system being projected, in the Chapter the authors propose moreover the use of memory devices storing information on the system specifications and patient data. In this manner the availability of such information allows the system to optimize the computing algorithms. In fact data concerning patient health are used for adapting the system to the examined subject. So diagnoses may be fitted according to patients health state for fault-tolerant results.

2 The Decision-Making Approach

Medical diagnoses are mainly based on comparison between experimental data and specific reference levels or specification limits. So if such limits are exceeded it may be due to an occurring pathology or disease. However measurement results are affected from uncertainty which may be cause of wrong diagnoses. In fact measured data could incorrectly seem above the specification limit because of the uncertainty, diagnosing an unreal disease. As an alternative during the comparison procedure, data could be considered erroneously compliant with the limit, underestimating an occurring pathology. Appropriate decision-making algorithms are therefore indispensable for a suitable characterization of the uncertainty effect. The authors propose an original Statistical Model [6] in order to estimate the maximum tolerable value of measurement uncertainty assuring a desired reliability level for the decision-making process. Let be x_m a continuous random variable associated with the considered medical parameter. It represents also the measurand of the measurement system to be projected. Let be moreover x_a the expected value for the parameter and δ the reference limit used in order to diagnose the pathology occurrence. The variable x is the random variable associated with the

realizations of measurand around the expected value. The latter variable represents the randomness of each measurement and its standard deviation σ_x is the measurement uncertainty of the system. On this assumption the probability of wrong decision P_α is obtained by the following expression:

$$P_\alpha = P(x_m \in [x_a - \delta, x_a + \delta] \cap |x + x_m - x_a| > \delta) \quad (1)$$

It represents the probability to assert that the measured parameter is beyond the limit δ (because of the measurement uncertainty) when instead the measurand is within the limit.

The previous equation is obtained by the joint probabilities of the events:

$$A_1 = \{x_m \in [x_a - \delta, x_a + \delta]\} \quad \text{and} \quad A_2 = \{|x + x_m - x_a| > \delta\} \quad (2)$$

Where the event A_1 asserts that the parameter is really compliant with the reference limit, instead the event A_2 asserts that the parameter is non-compliant with the limit because of the measurement uncertainty. If the interval $[x_a - \delta, x_a + \delta]$ is divided in N disjoint sub-intervals Δ_i with $i=0\dots N-1$, it can be written that:

$$P_\alpha = \sum_i P(x_m \in \Delta_i \cap |x + x_m - x_a| > \delta) \quad (3)$$

for the conditional probability definition, it follows that:

$$P_\alpha = \sum_i [P(|x + x_m - x_a| > \delta \mid x_m \in \Delta_i) * P(x_m \in \Delta_i)] \quad (4)$$

for $N \rightarrow \infty$ we can assert that:

$$P_\alpha = \int_{x_a - \delta}^{x_a + \delta} P(|x + x_m - x_a| > \delta \mid x_m = x') * f_{X_m}(x') dx' \quad (5)$$

where x' is an occurrence of x_m and $f_{X_m}(x)$ is the probability density function of the random variable x_m . If $F_X(x)$ is the cumulative distribution function of the variable x we can write:

$$\begin{aligned} P(|x + x_m - x_a| > \delta \mid x_m = x') &= \\ P(x + x_m - x_a < -\delta \mid x_m = x') + P(x + x_m - x_a > \delta \mid x_m = x') &= \\ P(x \leq -\delta - (x_m - x_a) \mid x_m = x') + 1 - P(x \leq \delta - (x_m - x_a) \mid x_m = x') &= \\ F_X(-\delta - (x' - x_a)) + 1 - F_X(\delta - (x' - x_a)) \end{aligned}$$

Consequently if $\tilde{x}' = x' - x_a$, the equation (5) turns into:

$$P_\alpha = \int_{-\delta}^{+\delta} [1 - F_x(\delta - \tilde{x}') + F_x(-\delta - \tilde{x}')] * f_{\tilde{x}_m}(\tilde{x}') d\tilde{x}' \quad (6)$$

In the same way, we can define the probability of wrong decision P_β as:

$$P_\beta = \int_{\tilde{x}_m - [-\delta, \delta]} [F_x(\delta - \tilde{x}') - F_x(-\delta - \tilde{x}')] * f_{\tilde{x}_m}(\tilde{x}') d\tilde{x}' \quad (7)$$

It represents the probability to assert that the measured parameter is within the limit δ (because of the measurement uncertainty) when instead the measurand is beyond the limit. The previous probabilities P_α and P_β may be expressed by means of normalized diagrams, in which the measurement uncertainty σ_x and the reference limit δ are normalized with respect to the standard deviation of the measured data σ_y : $P_\alpha = P_\alpha(\delta/\sigma_y, \sigma_x/\sigma_y)$ and $P_\beta = P_\beta(\delta/\sigma_y, \sigma_x/\sigma_y)$. In this way it is possible to get a mathematical relationship between the measurement uncertainty and the risk to make a wrong diagnosis. As an example, the Fig. 1 and the Fig. 2 show the three-dimensional trend of $P_\alpha\%$ and $P_\beta\%$ for a specific case study. In detail it is possible to observe that an increase of the reference limit value δ is cause of a decrease of the two probability values. Whereas an increase of the measurement uncertainty value σ_x is responsible of a corresponding increase of the probabilities of wrong decision according to the expected behaviour. The two relationships provide an original approach to the choice of the best measurement uncertainty value for the projected system.

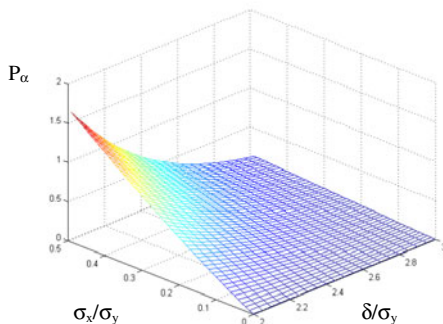


Fig. 1. Diagram of $P_\alpha\%$ versus a/σ_y and δ/σ_y

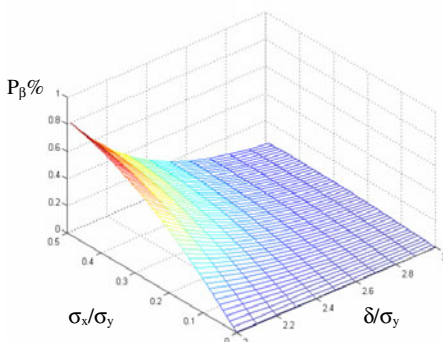


Fig. 2. Diagram of $P_\beta\%$ versus a/σ_y and δ/σ_y

The proposed procedure consists in two simple steps. Once that the reference limit δ is fixed for the considered parameter to monitor, the designer has to choose the desired values of probability of wrong decision P_α and P_β . In this way it is possible to fix a priori the maximum tolerable risk to make a wrong diagnosis, so to guarantee a suitable reliability of the decision making process. In other words by setting P_α and P_β we can fix the most suitable thresholds of error for the specific application case. Consequently by means of the mathematical functions, the maximum measurement uncertainty value is estimated according to the requirements of project. Typically low values of probability of wrong decision imply low values of measurement uncertainty, and therefore more reliability of data processing stage. Consequently the system can be projected so to assure a suitable risk level to make wrong diagnoses because of the measurement uncertainty. Such an approach permits to design measurement instrumentation with high performances with reference to the processing reliability. Decision making aspects are so taken into account in order to qualify the system design. In this way it is possible to choose the best reliability for medical instrumentation according to the purpose of the final diagnosis. The procedure can be used even during the prototyping in order to adjust the specifications of the instrument according to the needs. Therefore if the obtained decision reliability is sufficiently compliant with the desired level, then the measurement system project can be confirmed, otherwise it needs to redesign the initial features of project, changing, in example, the desired probabilities of wrong decision so to obtain greater performances.

3 Smart and Patient-Adaptive Systems

The previous model provides a practical and methodical procedure for improving the project of a measurement system during the design and prototyping stages. The used approach allows designer to adjust the system's reliability according to the desired performances and specifications. It represents an original model for projecting reliable and accurate instrumentation. In this way it is possible to guarantee a suitable accuracy for instrumentation. The aim of the proposed procedure is to minimize errors due to measurement uncertainty when measured data are compared with specification limits. A further important aspect concerns the optimization of the computing algorithms used for making diagnoses and tests. In this view, the authors propose further guidelines for the optimization of the data processing algorithms in order to guarantee smart and fault-tolerant diagnoses. Smart systems with automated data analysis need reliable data processing procedures in order to reduce the occurrence of erroneous diagnoses. The suggested system architecture is based on the use of memory devices able to store information on the system's metrological characteristics and on the examined patient. The idea is to take advantage of the built-in information in order to improve the computational algorithms of the system. In detail, as it has been described, a first problem regards the influence of the measurement uncertainty on the final diagnosis. Typically the performances of any measurement system change with time, so a measurement system may seem erroneously in a tolerance state when really it is out of

tolerance. Therefore the system's reliability has to be checked periodically in order to verify its current performances. The availability of data regarding the metrological characterization of the measurement system like its measurement uncertainty, range, calibration interval and reliability curve can represent an useful information in order to qualify the processing stage. So a first memory device (*Metrological Status Memory*) is used to store information on the system characteristics with regard to its uncertainty, calibration and reliability. Such data can be used during the data processing in order to get trace on the current operating status of the system. So information on measurement uncertainty can be used during the computing stage in order to qualify the final results. In this way in fact it is possible, by the previous model, to estimate the probabilities of mistaken decision P_α and P_β . Such values permit to get information about the reliability of computational result and about the accuracy of the final diagnosis. Moreover the embedded data regarding the calibration interval and the reliability curve allow the system to get control on the changes of its reliability with time. So the measurement uncertainty can be kept within acceptable levels, according to specific tolerable values. In detail by means of information on calibration interval, the smart system gets knowledge about its state and the risk of possible malfunctions. Typically, with the passing of time, the probability of a malfunction event increases. Therefore, when the system reliability level goes down the minimum desired tolerable value, the system has to be recalibrated since his performances are declining. In this way, during the computational stage, the measurement system can periodically check its functioning and its current reliability. Consequently information on the integrity of the acquired data is got, and it is possible to assure for the measurement system a suitable operating state with the passing of time.

According to the authors experience about the present issue, now the attention has to be focused on a second problem which characterizes the common medical instrumentation. Typically diagnoses are made by comparing acquired data with reference models. Often such models are averaged values referred to healthy people, so they are not fit for all patients. Often it is cause of wrong diagnoses due to faulty detection occurrences. In fact data concerning life habits (sporting activities, diets, etc.) and clinical conditions (congenital diseases, existing pathologies, heart status, past records), or simply information about age, sex, physical constitution, are needed in order to get a clear and complete outline of the medical condition of the patient. Such information can allow the smart system to adapt the computational algorithms to the examined subject in order to make fault-tolerant diagnoses. In this view, the measurement system design can be improved by using a second memory device (*Patient Memory*) in order to store information on the health state of the patient. It is a personal data-logger replaced with the patient, which has to be updated according to the current clinical conditions of the subject. Medical data can be so used from the system for optimizing the computing results. The aim is to improve the computational algorithms by adapting the system to the patient. Generic information, like age, sex and physical constitution, are so used in order to identify a first reference model. Typically such information is used during clinical diagnoses in order to single out a first averaged model. Otherwise information about historical data and medical records can allow the system to

characterize in detail the reference model, which can be adapted to the specific patient. In this way it is possible to single out the fittest reference model according to the subject health state. The purpose is to project patient-adaptive medical systems able to make reliable diagnoses according to the past clinical history of the examined subject.

4 The Design of an ECG Measurement System

In the present paragraph an application case of the proposed measurement system design technique is discussed. In detail the project of a smart and patient-adaptive ECG measurement system is described. The system is able to acquire and analyze the electrical activity of heart in order to characterize possible abnormalities of its regular working. The system has been designed according to the guidelines of the IEC and ANSI Standards for assuring the safety requirements, [7-10]. The system consists of a sensor (electrodes and conditioning circuit) and of a digital processing section for the data analysis, see Fig. 3.

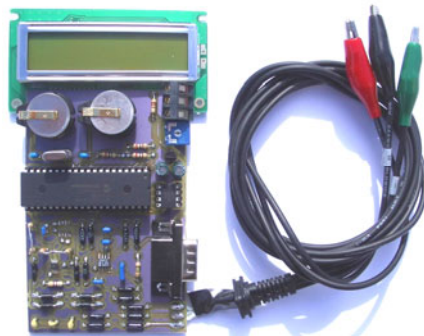


Fig. 3. Prototype of the system

During the system design and according to the proposed Statistical Model the probabilities of mistaken decision have been chosen equal to $P_\alpha=0.1$ and $P_\beta=0.1$. The estimated measurement uncertainty value was $\sigma_x\% = 0.13\%$. During the prototyping the obtained measurement uncertainty was compliant with the maximum tolerable value. Consequently the performances of the designed measurement system comply with expected mistaken decision probabilities. In detail the system architecture is based on a preliminary acquisition circuit. The ECG waveform is recorded by means of $\text{Ag}^+/\text{Ag}^+\text{Cl}^-$ electrodes. A typical ECG signal ranges from -2 mV to 2 mV with a bandwidth about equal to [0.5 100] Hz. The analog input signal is first conditioned by a pre-processing circuitry. Leakage currents are lower than 10 μA . The needed power supply is equal to ± 5 V. A band-pass filter with a 3dB attenuation at 135 Hz has been added in order to minimize the noise contributions and interferences. The signal is so digitalized by a 12-bit AD converter. A DSP unit has the task to process the acquired data by the embedded computing

algorithms. The system is besides compliant with the guidelines of the IEEE 1451 Standard about the project of smart sensors, [11]. A display shows the result of the final diagnosis.

The designed ECG measurement system is able to configure the computational algorithms according to the available information about patient to be tested. In detail, a removable and updatable memory device is used to store the clinical and personal patient data. Whereas an additional internal and read-only memory stores information on the metrological characteristics of the measurement system. The system checks the cardiac muscle activity by acquiring the heart electrical impulses. The regular heart functioning is characterized by specific voltage waves which are measured by the skin electrodes placed at designated locations of the patient body in limbs and chest. An ECG waveform consists of six component waves labeled with progressive alphabet letters from P to U, see Fig. 4.

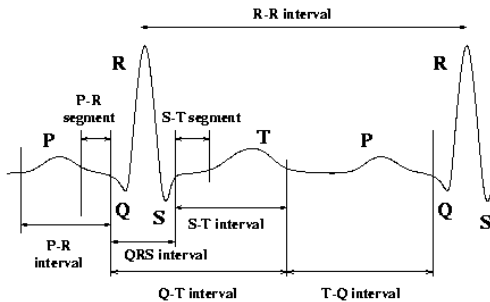


Fig. 4. ECG Waveform

Each wave describes a specific phase of the rhythmic heart activity. The system is able to diagnose specific cardiac arrhythmias (*sinus tachycardia, sinus bradycardia, ischemia and myocardial infarction*). The computing algorithm is based on a pattern recognition procedure in order to characterize the amplitude and the time duration of the single waves. Consequently specific parameters are estimated and put in comparison with the values of a reference model. The occurrence of an arrhythmia is diagnosed when specific parameters exceed the corresponding threshold levels. The systems uses the personal data and historical medical information of patient in order to adapt itself. In this way the fittest ECG model is singled out as reference, so to optimize the computing algorithm. The chosen model takes into account the real health state of the patient and the occurrence of previous cardiac diseases. In order to highlight the importance of such feature of the system, we have to focus the attention on specific aspects regarding the considered application case. So in example, medical studies have shown that previous heart diseases, like infarction or ischemia, are often cause of permanent marks in the heart. They are due to the presence of scar tissue which alters the heart working. Therefore the cardiac muscle keeps trace of previous happened infarctions. As a consequence, the associated effects may be even visible on the ECG waveform. The analysis of such a record could be cause of an erroneous diagnosis. So the marks of a previous

infarction may be confused with the effects of an occurring heart attack. As a result, the availability of historical ECG records, stored in the *Patient Memory*, allows the system to reduce the happening of faults during the diagnosis.

The information on the measurement uncertainty, stored in the *Metrological Status Memory*, is moreover used in order to improve the reliability of the final diagnosis. In this way the DSP unit can check the current system's reliability keeping trace on its metrological characterization. By means of the measurement uncertainty, the computing algorithm can get information on the consistency level of the final result in order to have knowledge on its reliability.

Tests and numerical analyses have been executed in order to check the system performances. The response of the system has been analyzed by using several ECG records of healthy and sick persons. Further experimental results have permitted to test the capability of the system to detect properly the occurrence of the four pathologies. For this aim, simulations have been made by applying ECG waves generated by means of a waveform generator. The databases have been created starting from a normal ECG waveform and altering the parameters involved in the different diagnoses. The tests have shown a good sensitivity of the measurement system with an optimal agreement with the expected behavior. The proposed patient-adaptive architecture has permitted moreover to improve the diagnosis capabilities of the common medical instrumentation. In fact the system is able to reject typical problems of detection that are observed in practice and due to an erroneous pattern recognition. In addition, information on the system's metrological characteristics is used to get useful information on the consistency of diagnosis so qualifying the system response. In this way the system provides on display not only the diagnosis result but also its reliability level.

5 Conclusion

The proposed procedure consists of a set of guidelines for a methodological project of a medical measurement system. A first Statistical Model allows the designer to estimate the best measurement uncertainty for the system. The aim is to assure suitable probabilities of mistaken decision during the comparison of measured data with specific limits or thresholds. In order to improve the performances of the system, memory devices are used to store information on the system's metrological characteristics and on patient health state. Such information is used during the processing stage in order to guarantee fault-tolerant diagnoses by estimating the influence of measurement uncertainty in the final response. In this way the smart system gets knowledge on its current state and on the reliability of the acquired data. The used patient-adaptive approach allows the system to configure its computing algorithms in order to adapt itself to the examined subject. Therefore the same instrument can be employed for different patients by replacing the memory device. The design of a smart and fault-tolerant ECG measurement system has been proposed. Experimental results and numerical analyses have shown a good agreement with the expected behaviour. The pattern detection capabilities have been improved and optimized by means of the embedded computational algorithms.

References

1. Leinonen, M.: A Survey on Performance Measurement System Design and Implementation, Tampere University of Technology, Finland
2. Neely, A., et al.: Performance Measurement System Design: Developing and Testing a Process-Based Approach. *International Journal of Operations & Production Management* 20(10), 1119–1145 (2000)
3. Joseph, E., Bronzino, D.: The Biomedical Engineering HandBook. In: Berbari, E.J. (ed.) *Principles of Electrocardiography*, 2nd edn., ch. 13. CRC Press, Boca Raton (2000)
4. Prutchi, D., Norris, M.: Design and Development of Medical Electronic Instrumentation. Wiley Book, Chichester (2004)
5. Oberg, P.A., Togawa, T., Spelman, F.A.: Sensors in Medicine and Health Care, Vol, vol. 3. Wiley Book, Chichester (2004)
6. De Capua, C., De Falco, S., Liccardo, A., Morello, R.: A Technique Based on Uncertainty Analysis to Qualify the Design of Measurement Systems. In: IEEE International Workshop AMUEM, Niagara Falls, Ontario-Canada, vol. 1, pp. 97–102 (2005)
7. IEC 60601-2-47, Particular Requirements for the Safety, Include Essential Performance, of Ambulatory Electrocardiographic Systems, International Electrotechnical Commission, Geneva, Switzerland (2001)
8. IEC 60601-2-25, Medical Electrical Equipment - Particular Requirements for the Safety of Electrocardiographs, International Electrotechnical Commission, Geneva, Switzerland (1999)
9. ANSI/AAMI ES1, American National Standard, Safe Current Limits for Electromedical Apparatus, Association for the Advancement of Medical Instrumentation (1993)
10. ANSI/AAMI EC11, Voluntary Standard for Diagnostic Electrocardiographic Devices, Association for the Advancement of Medical Instrumentation (1984)
11. IEEE 1451, Smart Transducer Interface Standards

A Self-controlled Master-Slave Robot and Its Application for Upper Limb Rehabilitation

Tao Liu, Chunguang Li, Yoshio Inoue, and Kyoko Shibata

Kochi University of Technology, Japan

Abstract. In order to motivate the activity of patients in rehabilitation training, bimanual limb training has been applied widely in rehabilitation systems. Based on this point, we propose a self-controlled master-slave robot for upper limb rehabilitation. The system contains two identical motors with a wired-connection. Under the action of the external forces from the two limbs that attached to the master and slave sides, the motor exerted with a larger force works in generating state and acts as the master, while the other motor works in electro-motion state and acts as the slave. A certain amount of compensated energy, together with the recycled energy from the master, enables the slave to reproduce the master's movements accurately. The system realizes bilateral force sensing and supports different operating modes. Subjects coordinate the force of the two limbs based on visual feedback, further, controlling the handles in the two terminals to accomplish the predefined motion. Preliminary tests on different operating modes were conducted. The results confirm that the motion of the slave is precisely consistent with that of the master, and verify that the subjects can learn how to accomplish movements by practice.

Keywords: force sensing, self-controlled operation, visual feedback, energy recycling.

1 Introduction

With the increasing in the number of hemiplegic patients and aged persons, many kinds of robots have been developed to provide rehabilitation training for hemiplegic patients, or to implement strength enhancement exercise for aged persons. In the last few years, the development of robots, with which patients can actively participate in the rehabilitation training, has become a new tendency. Viorel [1] presented a PC-based rehabilitation system for carrying out virtual-reality exercises at home. It also allowed clinic to tele-monitor patients' training process and perform evaluations after training routines. A multipurpose haptic control interface and a RM-II glove were adopted to test patient's hand positions and to apply resistive forces on the patient's fingertips, respectively. However, no experimental results were presented. Colombo and Pisano introduced two robots [2, 3] for upper

limb rehabilitation training. Particularly, a new evaluation metrics was proposed for observing the rate of improvement and selecting targeted rehabilitative strategies. The exercise was carried out with the patient controlling the handle of the device to move towards a target position repeatedly. The experimental results demonstrate the validity of their rehabilitation technique both in recent and in chronic post-stroke patients.

The above robots only supported unilateral training, in which the impaired limb started movement tasks actively, while the robot provided an assisted or a resisted force for the impaired limb. Recently, the development of robot-assisted systems requiring bilateral limbs involved in exercises has attracted much more attention. One common strategy is that the healthy limb provides a reference trajectory and the impaired limb imitates the movements symmetrically. The representative device is MIME [4-6], which supported unilateral training in passive, active-assisted, and active-constrained modes. Furthermore, it can assist the affected limb to move with the same manner of motion as the contra-lateral limb, with the two limbs performing bilateral mirror image movements. Clinical tests with MIME suggest that combining the unilateral and bilateral training modes produced larger improvements on a motor impairment scale compared with conventional unilateral therapies. In addition, movements with reduced hypertonia and abnormal synergies were achieved. BATRAC [7, 8] is another robotic device that can deliver bilateral arm therapy for stroke patients. Clinical tests on BATRAC were conducted with 21 patients and the results verify that bilateral movements improved arm function by inducing reorganization of brain regions involved in motor control. A virtual reality-based hand motion assist robot [9] was presented for self-performing rehabilitation therapies. The healthy hand produced the reference motions for the exercise, while the robot assisted the disabled hand to reproduce the motions symmetrically. The system could enhance the motivation of patients in rehabilitation training. However, the recent results were not enough to show the effectiveness of the system statistically.

In order to further activate the cognitive processing of patients, some robots that utilize the healthy limb to offer assisted force for the impaired one were introduced. Hesse [10] designed an assisted robot for training bilateral forearm and wrist of hemiparetic patients. The device supported bimanual passive and active exercise, including forearm pronation and supination and wrist flexion and extension. Preliminary experimental results indicate that the device has potential for training severely affected stroke patients. The system introduced by Guo and Song [11] realized self-assisted rehabilitation training and had a compact structure, whereas it was only suitable for training mildly affected limbs. Michelle presented another self-assisted device for bilateral arm training in [12], which also obtained positive results.

The research carried out by Mudie and Matyas [13] proved that bimanual practice can encourage the active movement of the impaired limb, resulting in a better recovery effect. However, in general, self-controlled training is realized with the healthy limb/hand providing assisted force for the impaired one. Few self-controlled rehabilitation systems achieved active-constrained training. Even though the robot presented in [10] supported active-constrained training, the

resisted force is provided by the robot rather than the patient himself/herself. Based on this point, this chapter introduces a new self-controlled robot for upper limb rehabilitation. The robot realizes bilateral force sensing and supports different training modes. No matter in which mode, the required driving force, assisted force, or resisted force for the impaired limb to accomplish movement is provided by the healthy limb. Furthermore, the system provides visual feedback for operators during the training tasks. Operators coordinate the force of the two limbs to accomplish the predefined movements. In order to verify the feasibility of the proposed system, preliminary experiments were performed and the corresponding results are presented.

2 System Description

2.1 Overview of the System

The proposed system consists of components for manipulating, visual feedback, and real-time data processing. The schematic diagram of upper limb rehabilitation training is shown in Fig. 1. Two handles are mechanically connected with two DC motors, which are wired connected directly and are the major components of the master and the slave units. During operation, the operator controls the two handles with the two limbs and senses the force of each other. Based on the visual feedback displayed in the desktop PC, the operator coordinates the force of the two limbs to accomplish the predefined movements.

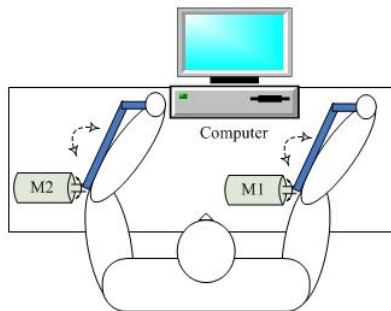


Fig. 1. Schematic diagram of upper limb rehabilitation training

2.2 Operational Principle

The operator controlled the reaction forces on the two handles with the two limbs. The directions of the two forces are determined from the operating modes (passive, active-assisted, and active-resisted), the expected movement direction (upward or downward), and the side of the impaired limb. If the left limb is impaired or possesses weak motor function, the relation between the force directions of the two limbs and the movement direction are described as Table 1. For the case that the right limb is impaired, the reverse cases will be achieved.

Table 1. Relationship between the force directions of the two limbs and the movement direction when the left limb is impaired

Limb Operating mode \	Left	Right
Passive	Produces a resistance	Provides a force with the same direction as the trajectory
Active-assisted	Provides a force with the same direction as the trajectory	Provides a force with the same direction as the trajectory
Active-resisted	Provides a force with the same direction as the trajectory	Provides a force with a different direction as the trajectory

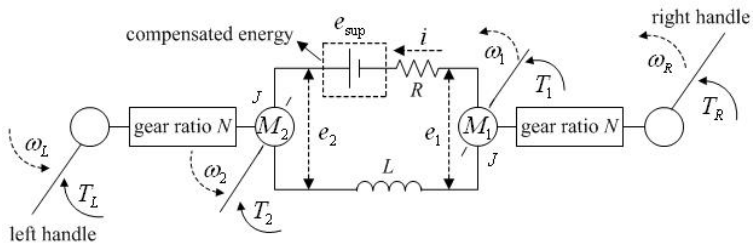


Fig. 2. Equivalent circuit of the master-slave system

The working states of the two motors depend on the magnitudes of the attached forces in the two sides. The motor exerted with a larger force works in the generating state and behaves as the master motor; while, the other motor works in the electro-motion state and behaves as the slave motor. The master motor powers the slave motor, which in turn balances the force on the other side and drives the contra-lateral limb in movement imitation.

In order to acquire a symmetric mechanism, the master and slave sides are configured with identical motors and gearboxes. An equivalent circuit of the master-slave system is shown in Fig. 2, in which M_1 and M_2 denote the two DC motors, T and ω stand for the torque and angular velocity. In this chapter, variables with the subscripts $_R$ and $_L$ represent the parameters in the right and left terminals, while variables with the subscripts $_1$ and $_2$ denote the parameters of the motors in the right and left sides, respectively. e_1 and e_2 are the armature voltages of the motors; i is the closed-loop current. R and L denote the armature resistance summation and the inductance summation of the two motors, respectively; and e_{sup} is the compensated energy provided by an H-bridge driver for matching the movements of the master and the slave terminals. Based on the dynamics mechanism, the motion equations are written as (1) when the motor 1 works as the master and the motor 2 works as the slave. When the working states of the two motors are reversed, the motion equations are re-written as (2).

$$\begin{cases} \frac{T_R}{N} = T_1 = C_T i + T_{01} + J \frac{d\omega_1}{dt} \\ \frac{T_L}{N} = T_2 = C_T i - T_{02} - J \frac{d\omega_2}{dt} \end{cases} \quad (1)$$

$$\begin{cases} \frac{T_R}{N} = T_1 = C_T i - T_{01} - J \frac{d\omega_1}{dt} \\ \frac{T_L}{N} = T_2 = C_T i + T_{02} + J \frac{d\omega_2}{dt} \end{cases} \quad (2)$$

where $C_T i$ denotes the motor electromagnetic torque, the two motors possess identical electromagnetic torque since the same torque constant C_T and the shared closed-loop current; T_{01} and T_{02} are motor unload torques caused by unload losses including mechanical loss, magnetic core loss, and additional loss in the motors; J is equivalent inertial moments; The relationship between the torques produced in the two terminals are expressed as (3) and (4) for the above two cases, respectively.

$$T_R - T_L = N(T_{01} + T_{02} + J \frac{\omega_1}{dt} + J \frac{\omega_2}{dt}) \quad (3)$$

$$T_L - T_R = N(T_{01} + T_{02} + J \frac{\omega_1}{dt} + J \frac{\omega_2}{dt}) \quad (4)$$

which indicate that the torques at the two sides correspond to each other. This is realized owing to the closed-loop current in the two motors. When the force exerted at one side increases, the current and the electromagnetic torques of the two motors increase as a result, then the operator can sense this variation and regulate the force at the contra-lateral side accordingly to achieve a balanced state. That is, the torque at each side can be fed back to the contra-lateral side. This indicates that the system is capable of bilateral force sensing without any mechanical force sensor.

In addition, the electric energy generated by the master motor is transmitted to the slave motor. Then, the slave motor is driven to move and mirror the movement of the master motor. Thus, a kind of energy recycling is realized.

However, the energy losses in the resistance and inductance make it impossible to acquire a consistent motion behavior for the two terminals completely. Especially when large resistance is attached to the slave side, the current and the resultant energy losses in the circuit will be large; further, resulting in a big difference in the velocities and positions of the two motors/terminals. In order to realize good master-slave motion tracking performance, a certain amount of energy is compensated for the circuit to offset the inside energy losses. Based on the electrical mechanism, the dynamic voltage balance equation of the circuit can be written as (5) and (6) corresponding to the above two cases expressed in Eqs. (1) and (2):

$$Ri + L \frac{di}{dt} = e_1 + e_{\text{sup}} - e_2 \quad (5)$$

$$Ri + L \frac{di}{dt} = e_2 + e_{\text{sup}} - e_1 \quad (6)$$

in which $e_1 = C_T N \omega_R$, $e_2 = C_T N \omega_L$. The energy generated by the master motor, together with the supplementary energy, enables the slave/gear unit to reproduce the movement of the master/gear unit accurately.

3 Experiments Study

3.1 System Equipments

The designed experimental system was composed of master and slave motor/gear units (motor 3863012C, combined with Planetary Gearhead 38/2 A, and Encoder IE2-512, Faulhaber Group, Germany), an H-bridge driver (LMD18200, National Semiconductor, U.S.A), a dSPACE control platform (CLP1104, dSPACE, Germany), two torque transducers (TP-20KCE, Kyowa, Japan) and a strain gage signal amplifier. Master and slave units were fixed to a table. Two torque transducers were connected to the gearbox shafts. And two handles were connected to the transducer shafts. The torque transducers and torque signal amplifier were used to verify the force sensing capability whereas they are not required in future applications. The gear ratios of the gearboxes were 66. The corresponding maximum output torque of the motor/gear unit was 5.082 Nm. When the elbow of the upper limb and the motor/gear unit are coaxially positioned, the torque caused by the gravity of a forearm was estimated for a human person with a weight of 65 kg and height of 175 cm [14], and the result was 1.519 Nm. That is, the master-slave system had enough output torque to drive a forearm to perform elbow flexion/extension movement passively. During operation, an unhealthy limb may produce impedance except the gravity due to the residual motor capacity and the movement position. Therefore, gearboxes with larger driving power were selected. The length of the two handles was 14 mm, thus the maximum allowable force actively exerted on the handles was 36.3 N, which was sufficient to verify the feasibility of the system working in different operating modes.

The experimental platform is shown in Fig. 3. The left limb was restrained to reduce motion agility and imitated an impaired limb with weak motor function. The left limb was selected because its motion agility is relative weak compared to the right limb. In training tasks, the operator coordinated the two limbs to complete the predefined round trip motion trajectory according to the sensed force and the visual feedback.

Information flow in the experimental system is explained with Fig. 4. The torque information for verification tests is displayed with dashed lines because it is not required in future applications. This information was collected through the ADC modules of the CLP1104 for verifying the force sensing capability of the

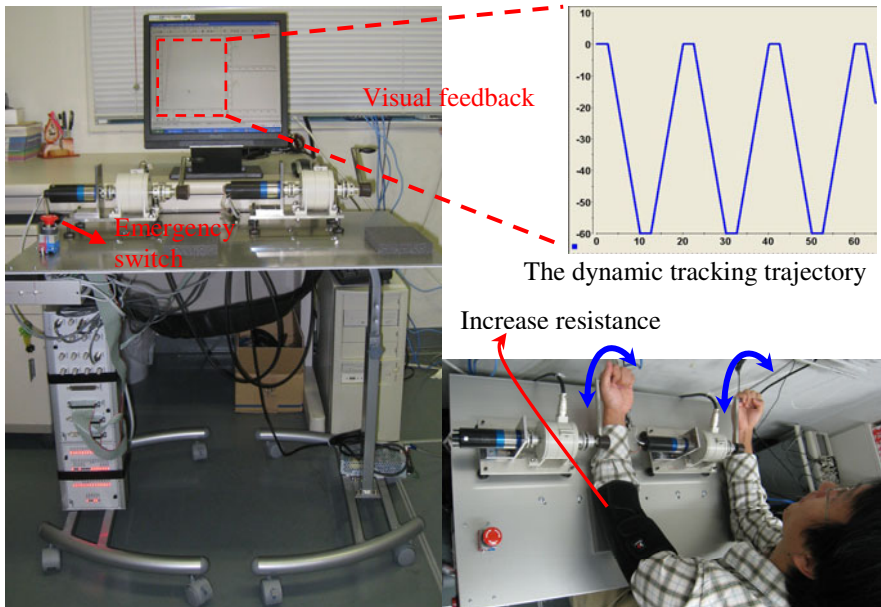


Fig. 3. Experimental platform and schematic diagram of the experiments

system and testifying the relationship between the forces in the two terminals for different operating modes. The CLP1104 collected the velocity and position information through incremental encoder interfaces. The motion tracking controller, which was realized in the CLP1104, worked out the duty cycles of the pulse-width-modulated signal (PWM, 20 kHz) and the direction of the compensation voltage based on the sampled motion information. The direction signal and the PWM signal were outputted to the H-bridge driver through a DAC module and a PWM generator module, respectively. Under the control of the motion tracking controller, the H-bridge driver supplied compensation energy for the master-slave circuit. The energy generated by the master motor, along with the supplementary energy, powered the slave motor to overcome the impedance on the corresponding side and to move the connected limb in the same manner as the contra-lateral limb. All the information mentioned above is sampled every 1 microsecond. In addition, the motion information was transmitted to the PC through CLP1104 and was displayed in the PC in the format of curves. Based on the real-time curves and the predefined motion tracking trajectory, which was also varying dynamically, the operator regulated the forces of the two limbs accordingly to achieve a force balance state and accomplish the target movements.

3.2 Control Method

The hardware connection of the H-bridge driver and the master-slave circuit is given in Fig. 5. The control inputs of the H-bridge driver are a PWM signal and a direction control signal, which are used to regulate the magnitude and direction of

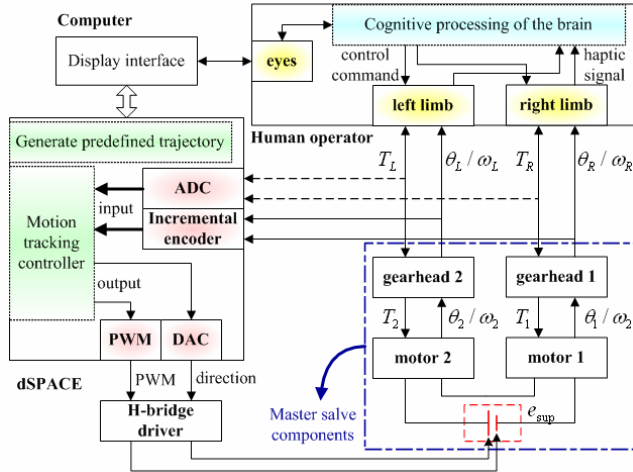


Fig. 4. Information flow of the experimental system

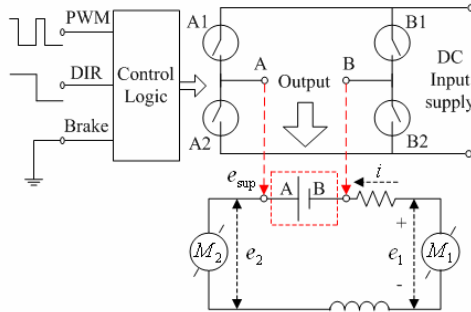


Fig. 5. Connection of the H-bridge driver and the master-slave circuit

the supplementary voltage. Based on the velocity difference and the position difference between the two terminals, the motion tracking controller regulates these control signals with a PID (proportional-integral-differential) control method.

In passive mode, the movement is completely controlled by the healthy limb, thus the motion of the healthy limb is the tracking objective; in active-assisted or active-constrained mode, the movement is started by the impaired limb, and then the motion of the impaired limb is the tracking objective. No matter which operating mode is active, the initial velocity of the motor (the tracking objective) attached with an actuating force is larger than that of the follower on the contralateral side. Therefore, the motion tracking direction is decided based on the initial velocities in the controller. The motion control equations are given as:

$$\left\{ \begin{array}{l} \alpha = \alpha^\omega + \alpha^\theta \\ \alpha^\omega = K_P^\omega ((\omega_R - \omega_L) + K_I^\omega \int (\omega_R - \omega_L) - K_D^\omega \frac{d\omega_f}{dt}) \\ \alpha^\theta = K_P^\theta ((\theta_R - \theta_L) + K_I^\theta \int (\theta_R - \theta_L) - K_D^\theta \frac{d\theta_f}{dt}) \\ \omega_f = \begin{cases} \omega_L, & |\omega_R^0| > |\omega_L^0| \\ -\omega_R, & |\omega_L^0| > |\omega_R^0| \end{cases} \\ \theta_f = \begin{cases} \theta_L, & |\omega_R^0| > |\omega_L^0| \\ -\theta_R, & |\omega_L^0| > |\omega_R^0| \end{cases} \end{array} \right. \quad (7)$$

where K_P , K_I and K_D denote the proportional, integral and differential coefficients, respectively; the superscripts ω and θ mean the velocity and the position; the variables with the subscript f represent the following velocity or position; and ω_R^0 and ω_L^0 denote the initial velocities in the corresponding terminals. In order to avoid overshoot and fluctuation of the system, a differential forward PID operation is applied in the design. For the experimental system, the adopted control parameters in the motion tracking controller is given in Table 2.

Table 2. Control parameters in the motion tracking controller

K_P^ω	K_I^ω	K_D^ω	K_P^θ	K_I^θ	K_D^θ
0.096	40	0.006	2	50	0.0048

3.3 Experimental Purpose and Methods

In order to verify the performance of the system and confirm the training effect of different operating modes, the experiment are divided into three tests: (1) The left limb controlled the movements singly; (2) The left limb provided an active force while the right limb exerted an assisted force; (3) The left limb provided an active force while the right limb exerted a resisted force. The second and the third tests are used to imitate the active-assisted and active-resisted operating modes. The first test provides a comparison baseline for the other two tests. It is also considered as the passive mode test, whereas the load in the slave side was only the handle in the right terminal, that is, the load is very small. There were four subjects participated in the experiment. For each test, the subjects controlled the handles to follow the desired motion trajectory 15 times, and each tracking task lasted one minute. The motion information (angular position and velocity) and the torque

information were collected every three tracking tasks, that is, five times for each test. The master-slave motion tracking performance is evaluated with the standard deviations of the position and velocity errors between the two terminals:

$$\delta_\theta = \sqrt{\frac{\sum_{i=1}^{5N} (\theta_m^i - \theta_s^i)^2}{5N}} \quad (8)$$

$$\delta_\omega = \sqrt{\frac{\sum_{i=1}^{5N} (\omega_m^i - \omega_s^i)^2}{5N}} \quad (9)$$

Here N represents the number of the sampled data in one task. $5N$ means that the standard deviations are calculated with all the data collected in each test, which includes 15 tracking tasks.

In order to describe the motion tracking capability of the subjects and observe its variation during the tracking tasks for the three tests, the standard deviations of the position and velocity errors between the actual and the desired values are calculated for each data collection. The errors are obtained by subtracting the predefined position/velocity information into the actual position/velocity information. The corresponding calculation formulas are written as:

$$\delta'_\theta = \sqrt{\frac{\sum_{i=1}^N (\theta_{ref}^i - \theta_m^i)^2}{N}} \quad (10)$$

$$\delta'_\omega = \sqrt{\frac{\sum_{i=1}^N (\omega_{ref}^i - \omega_m^i)^2}{N}} \quad (11)$$

The corresponding average standard deviations in each test are calculated as:

$$\overline{\delta'_\theta} = \frac{\sum_{i=1}^5 \delta'_\theta}{5} \quad (12)$$

$$\overline{\delta'_\omega} = \frac{\sum_{i=1}^5 \delta'_\omega}{5} \quad (13)$$

which are used to compare the trajectory tracking performances in different operating modes for all the subjects.

In addition, the average torques produced on the two terminals are also calculated for all the collected data in each test, and the values are used to confirm torque relationship between the two terminals for different operating modes. The average torque is calculated as:

$$\left\{ \begin{array}{l} \bar{T} = \frac{\overline{T_{pos}} + \overline{T_{neg}}}{2} \\ \overline{T_{pos}} = \frac{\sum T_{pos}}{N_1}, T_{pos} \geq 0 \\ \overline{T_{neg}} = \frac{\sum T_{neg}}{N_2}, T_{neg} < 0 \\ N_1 + N_2 = 5N \end{array} \right. \quad (14)$$

Since the average torque is calculated for one test, the sum number of the positive and the negative torques equals to the multiplication of the number of the sampled data in each task (N) and the number of the tasks with the corresponding data being collected in one test (5).

4 Experiment Results

4.1 Representative Results of One Subject

The representative motion tracking curves obtained in a task performed with only the left limb of subject 1 is shown in Fig. 6. It can be seen that the positions and the velocities in the two terminals are almost same. Besides, the two terminals are controlled to track the predefined dynamic trajectory with small errors. However, the actual velocity has a relatively large difference with the desired velocity, which is corresponding to the predefined dynamic trajectory. The reason is that the subject was concentrated on trajectory tracking rather than velocity tracking in the test.

For different operating modes, the average standard deviations of the position and velocity errors between the master and the slave terminals are listed in Table 3. It can be concluded that the slave can reproduce the movements of the master symmetrically with a high precision.

The standard deviations of the position and the velocity errors between the actual values and the desired values are calculated with the sampled data every three tracking task. That is, five results were obtained in each test. The corresponding results in different operating modes of subject 1 are described in Fig. 7. We can see that the standard deviations of the positions and the velocities have a decline trend. This indicates that the subject learned how to accomplish the tasks with training practice.

Table 3. Standard deviations of the position and velocity errors between the master and the slave terminals of subject 1

	The left limb singly	Active-assisted	Active-resisted
δ_θ (Degree)	0.0952	0.3126	0.1875
δ_ω (Degree/s)	0.0059	0.0094	0.0223

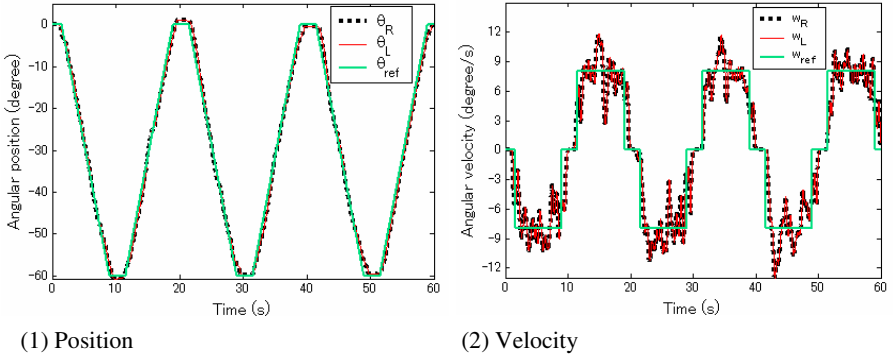


Fig. 6. The representative motion tracking curves of a task performed with only the left limb of subject 1

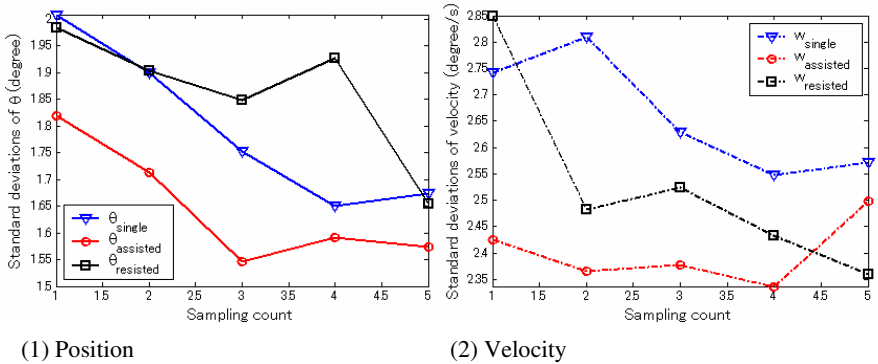


Fig. 7. Standard deviations of the position and velocity errors between the actual values and the desired values of subject 1

4.2 Torque Comparison in Different Operating Modes

In the three tests, three representative torque relation curves between the two terminals of subject 1 are shown in Fig. 8, where T_L denotes the torque exerted by the left limb, T_R represents the attached torque caused by the gravity effect of the right handle in Fig. 8 (1) and represents the torque exerted by the right limb in Fig. 8 (2) and (3). In Fig. 8 (1), the force provided by the left limb is about 0.6 Nm when the motion direction is upward (arm flexion) and is about 0.3 Nm when the motion direction is downward (arm extension). The former is larger than the latter because the left limb should overcome the gravity effect of the two handles for the upward movements. For the active-assisted operation, the force of the left limb for the upward and downward movements were about 0.4 Nm and 0.2 Nm, which are smaller than the corresponding values in the task performed with only the left limb. This is because that the right limb provided an assisted force to reduce the

burden on the left limb. Thus the active-assisted operating mode can be applied for training patients whose impaired limb has a weak motor function. For the active-resisted operation, the force of the left limb for the upward and downward movements were approximately 0.83 Nm and 0.61 Nm, which are larger than the corresponding values in the task performed with only the left limb. This is because that the right limb provided a resisted force to increase the burden on the left limb. Therefore, the active-resisted operating mode can be applied to carry out strength enhancement training for patients whose impaired limb has a certain motor capacity. The calculated average torques with Eq. (14) is shown in Fig. 9, in which the torque variation of the two terminals can be observed obviously.

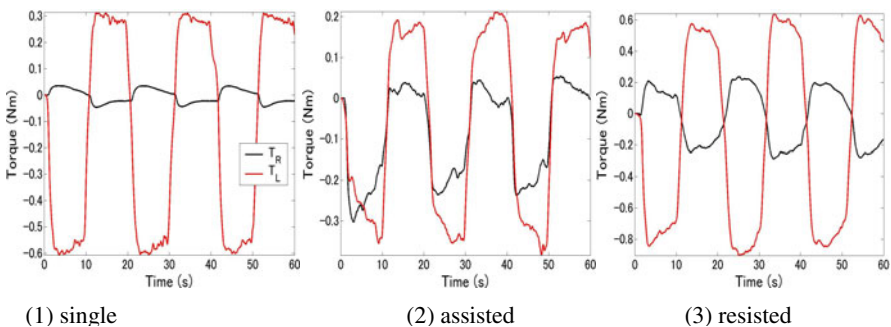


Fig. 8. Torque relationship between the two terminals in different operating modes of subject 1

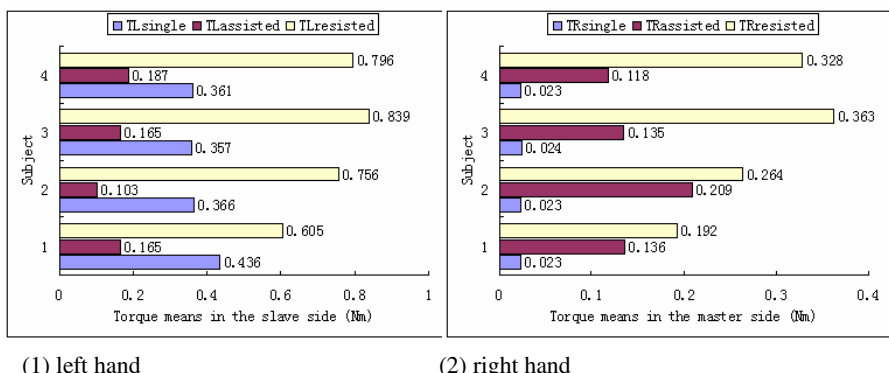


Fig. 9. Average torque comparison among different operating modes for all the subjects

4.3 Comparison of the Motion Performances in Different Operating Modes

The average standard deviations of the position and velocity errors between the actual and the desired values are shown in Fig. 10. It can be concluded that when the tracking tasks were performed with the two limbs, the motion performance

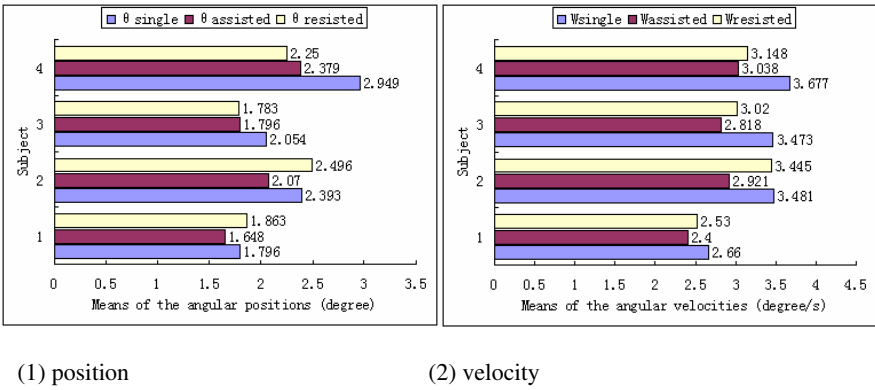


Fig. 10. Motion performance comparison among different operating modes for all subjects

was better than the case that the tasks were performed with the left limb singly (except the results of the subjects 1 and 2 in active-resisted operating task). This demonstrates that coordinating the two limbs is beneficial to achieve a better trajectory tracking performance.

5 Discussion

The experimental results verify that the slave can reproduce the movements of the master accurately in different operating modes. As well, the subjects can coordinate the two limbs to accomplish the predefined dynamic trajectory no matter in which operating mode. In addition, movement performance was improved through certain trajectory tracking tasks, that is, the subjects learned how to finish the movement with practice. This indicates that the motor capacity and the agility of the limbs can be improved by performing intensive tracking training. However, there are some defects in the proposed system:

(1) Referring to the torque relation between the two terminals for the task performed with the left limb singly (Fig. 10 (1)), it can be seen that the driving torque (T_L) was much larger than the load torque (T_R). This was mainly caused by the working efficiency of the gearboxes. In the real application, when the left limb controls the movements singly, the motion equation (2) should be rewritten as:

$$\begin{cases} \frac{T_R}{N\eta_1} = T_1 = C_T i - T_{01} - J \frac{d\omega_1}{dt} \\ \frac{T_L\eta_2}{N} = T_2 = C_T i + T_{02} + J \frac{d\omega_2}{dt} \end{cases} \quad (15)$$

Thus, the new torque relation can be expressed as (16) instead of Eq. (4):

$$T_L = \frac{1}{\eta_1\eta_2} T_R + \frac{N}{\eta_2} (T_{01} + T_{02} + J \frac{\omega_1}{dt} + J \frac{\omega_2}{dt}) \quad (16)$$

As well, when the right limb provides an active force and drives the load in the left side, Eq. (3) can be re-expressed as:

$$T_R = \frac{1}{\eta_1 \eta_2} T_L + \frac{N}{\eta_1} (T_{01} + T_{02} + J \frac{\omega_1}{dt} + J \frac{\omega_2}{dt}) \quad (17)$$

The new torque relations show that a larger control force is required for driving the same load and realizing the same motion velocity.

(2) Even though the system has bilateral force sensing capability, the torque relationship in the two terminals is not fixed since the working efficiency of the gearboxes is not constant in real applications. The operating modes and the magnitudes of the attached forces will influence the working efficiency. Otherwise, the torque transmission direction of the gearboxes is not fixed. It depends on the magnitudes of the forces in the two terminals and control direction (right to left or left to right), which further relies on the operating modes and the side of the impaired limb. The different cases are listed in Table 4. This indicates that the force sensing resolution is unfixed for different training modes and different force magnitudes.

Table 4. Torque relation between the mechanical torques in the motor shafts and the external acting torques

Impaired limb Operating mode	left	right
Passive	$T_1 = \frac{T_R \eta}{N}$	$T_1 = \frac{T_R}{N \eta}$
	$T_2 = \frac{T_L}{N \eta}$	$T_2 = \frac{T_L \eta}{N}$
Active-assisted	$T_1 = \frac{T_R \eta}{N}$ or $T_1 = \frac{T_R}{N \eta}$	$T_1 = \frac{T_R}{N \eta}$ or $T_1 = \frac{T_R \eta}{N}$
	$T_2 = \frac{T_L}{N \eta}$ or $T_2 = \frac{T_L \eta}{N}$	$T_2 = \frac{T_L \eta}{N}$ or $T_2 = \frac{T_L}{N \eta}$
Active-resisted	$T_1 = \frac{T_R \eta}{N}$ or $T_1 = \frac{T_R}{N \eta}$	$T_1 = \frac{T_R \eta}{N}$
	$T_2 = \frac{T_L \eta}{N}$	$T_2 = \frac{T_L \eta}{N}$ or $T_2 = \frac{T_L}{N \eta}$

(3) Considering the second items in Eqs. (16) and (17), the variations of velocities also affect the force requirement for the healthy limb even though the force produced by the impaired limb is a constant. And this also happens to the other operating modes. Thus, the subjects are required to regulate the forces accordingly based on the variation of the velocities, which may increase control difficulty slightly. Therefore, during the training tasks, subjects should try to control the movements with an almost constant velocity.

6 Conclusion

The proposed master-slave robot has a compact structure by utilizing two DC motors with a wired connection. During operation, the recycled energy from the master and the compensated energy enable the slave to reproduce the master's movements accurately. Besides, the system can realize bilateral force sensing without any mechanical force sensor based on the closed-loop current, and a force controller is not required as a result. Bilateral force sensing capability enables the system to support different operating modes for patients no matter which limb is impaired. In addition, visual feedback makes the training tasks involve cognitive processing of operators and make the operators pay much attention to the accuracy of the movements, which has been certified that is beneficial to the rehabilitation of motor function. All the above characteristics make the proposed robot favourable to realize self-controlled rehabilitation training in the home environments. The self-controlled exercise enable the patients to adjust the force of the healthy limb timely or stop the movement whenever according to the state of the impaired limb, thus avoiding pain or discomfort and increasing the reliability of the system. Home-based rehabilitation training can reduce economic burden of patients to a great extent.

As well, the features of force sensing without a force sensor and master-slave motion consistency make the proposed control scheme has a great potential in micro-manipulation applications.

Motion tracking task should be modified for increasing interests of the participants, and experiments should be carried out on more participants to further verify the feasibility of the system.

References

- Popescu, V.G., Burdea, G.C., Bouzit, M., Hentz, V.R.: A Virtual-Reality-Based Tele-rehabilitation System with Force Feedback. *IEEE Transactions on Information Technology in Biomedicine* 4(1), 45–51 (2000)
- Colombo, R., Pisano, F., Mazzone, A., Delconte, C., Minuco, G., Micera, S., Carrozza, M.C., Dario, P.: Motor Performance Evaluation to Improve Patient's Compliance During Robot-Aided Rehabilitation. In: Proc. 2006 the First IEEE/RAS-EMBS International Conference on Biomedical Robotics and Biomechatronics, BioRob, pp. 1090–1094 (2006)
- Colombo, R., Pisano, F., Micera, S., Mazzone, A., Delconte, C., Chiara Carrozza, M., Dario, P., Minuco, G.: Robotic Techniques for Upper Limb Evaluation and Rehabilitation of Stroke Patients. *IEEE Transactions on Neural Systems and Rehabilitation Engineering* 13(3), 311–324 (2005)
- Lum, P.S., Burgar, C.G., Shor, P.C.: Evidence for improved muscle activation patterns after retraining of reaching movements with the MIME robotic system in subjects with post-stroke hemiparesis. *IEEE Transactions on Neural Systems and Rehabilitation Engineering* 12(2), 186–194 (2004)

5. Lum, P.S., Burgar, C.G., Van Der Loos, M., Shor, P.C., Majmundar, M., Yap, R.: MIME robotic device for upper-limb neurorehabilitation in subacute stroke subjects: A follow-up study. *Journal of Rehabilitation Research and Development* 43(5), 631–642 (2006)
6. Lum, P.S., Burgar, C.G., Van Der Loos, M., Shor, P.C., Majmundar, M., Yap, R.: The MIME robotic system for upper-limb neuro-rehabilitation: results from a clinical trial in subacute stroke. In: Proc. 2005 IEEE 9th International Conference on Rehabilitation Robotics, pp. 511–514 (2005)
7. Whitall, J., Waller, S.M., Silver, K.H.C., Macko, R.F.: Repetitive bilateral arm training with rhythmic auditory cueing improves motor function in chronic hemiparetic stroke. *Stroke* 31(10), 2390–2395 (2000)
8. Luft, A.R., McCombe-Waller, S., Whitall, J., Forrester, L.W., Macko, R., Sorkin, J.D., Schulz, J.B., Hanley, D.F., et al.: Repetitive Bilateral Arm Training and Motor Cortex Activation in Chronic Stroke. *Journal of the American Medical Association* 292(15), 1853–1861 (2004)
9. Kawasaki, H., Ishigure, Y., Nishimoto, Y., Aoki, T., Mouri, T., Sakaeda, H., Abe, M.: Development of Virtual Reality Exercise of Hand Motion Assist Robot for Rehabilitation Therapy by Patient Self-Motion Control. In: Proc. 2007 IEEE 10th International Conference on Rehabilitation Robotics, Netherlands, pp. 234–240 (2007)
10. Hesse, S., Schulte-Tigges, G., Konrad, M., Bardeleben, A., Werner, C.: Robot-Assisted Arm Trainer for the Passive and Active Practice of Bilateral Forearm and Wrist Movements in Hemiparetic Subjects. *Archives of Physical Medicine and Rehabilitation* 84(6), 915–920 (2003)
11. Guo, S., Song, Z.: VR-based a Novel Active Rehabilitation System for Upper Limbs. In: Proc. 2008 IEEE International Conference on Mechatronics and Automation, pp. 230–235 (2008)
12. Johnson, M.J., Van Der Loos, H.F.M., Burgar, C.G., Shor, P., Leifer, L.J.: Experimental results using force-feedback cueing in robot-assisted stroke therapy. *IEEE Transactions on Neural Systems and Rehabilitation Engineering* 13(3), 335–348 (2005)
13. Mudie, M.H., Matyas, T.A.: Upper extremity retraining following stroke: effects of bilateral practice. *Journal of Neurorehabilitation and Neural Repair* 10(3), 167–184 (1996)
14. Zatsiorsky, V.M., Seluyanov, V.N.: Mass and Inertia Characteristics of the Main Segments of the Human Body. *International Series on Biomechanics* 4B, pp. 1152–1159 (1983), <http://www.dh.aist.go.jp/bodyDB/m/k-05.html>

Advanced Wearable Sensors and Systems Enabling Personal Applications

Andreas Lymberis

European Commission, Information Society and Media Directorate-General*,
Beaulieu Avenue 31, 1160 Brussels, Belgium

Abstract. The last decade has witnessed a rapid increase of interest in new sensing and monitoring devices including wearable wireless devices and sensor networks for several personal applications such as healthcare, well being & lifestyle, protection and safety. Smart Wearable Systems (SWS) are sensor-based integrated systems on body-worn platforms offering pervasive personalized solutions for continuous, non-invasive monitoring of body and external parameters, including feedback to the user. Several wearable solutions based on perimetric fixing using the body segments and the circular body part (e.g. head, arm, wrist and leg) are available today either in R&D prototype (the majority) or commercial products. Furthermore, new developments emerging from the miniaturization of electronics and materials processing have been leading to the integration of multiple smart functions into textiles without being a burden. The paper presents and discusses the main issues involved in the development of the area i.e. user requirements, technologies, research and development of integrated systems as well as future challenges to be met in order to reach a market with reliable and high value-added products.

Keywords: wearable systems, microsystems, body sensors, smart textile, Information & Communication Technologies.

1 Introduction

Body worn systems, endowed with autonomous sensing, actuation, processing, communication and energy harvesting and storage, are emerging as a solution to the challenges of monitoring people anywhere and at anytime in applications such as healthcare, wellbeing and lifestyle, protection and safety [1, 2, 3, 4]. Such systems, commonly called *Smart Wearable Systems (SWS)*¹ are integrated systems in contact with or near to the body able to sense and/or actuate, process & communicate body (e.g. physiological, biochemical, cognitive, emotional and physical) and

* The views developed in this article are that of the authors and do not reflect necessarily the position of the European Commission.

¹ http://en.wikipedia.org/wiki/Smart_Wearable_Systems

environmental parameters (e.g. temperature, pressure, gases or radiation). The great amount of interest and activities attracted by this area is mainly due to the remarkable progress in sciences and technologies, e.g. in micro-nano technologies (MNT), information and communication technologies (ICT), materials and bio-medicine but also to the shift of interest/investments of the healthcare community more towards early detection of diseases, health status monitoring, healthy lifestyle and overall quality of life, than therapy and treatment. For example, health monitoring and feedback to the user have shown significant contribution to the enhancement of disease prevention, early diagnosis, disease management, treatment and home rehabilitation.

Several such wearable solutions are available today like, independent sensors and devices, perimetric fixing using the body segments and the circular body part, e.g. head, arm, wrist, leg and ankle, as well as networked body sensors.

In the beginning of this decade, great effort of research in IWS worldwide was put on the enhancement of system functionality and autonomy with embedded decision support, as well as user-friendliness and multi-parameter monitoring capabilities. Significant investment, mainly from public funding agencies and some large companies, empowered interdisciplinary research and development towards proof of concepts and integrated wearable prototype systems. More than 35 projects, with an approximate total funding of 60 M€, have been supported between 2000 and 2006 by the European Union within its R&D funding programs, in the area of ambulatory and wearable ICT-based health monitoring systems and medical devices. Representative examples of such prototypes are:

- Continuous measurement and control of glucose concentration in subjects with type 1 diabetes, enabling the provision of better adjustment of insulin dosage [5].
- Personal ECG monitor [6] for early detection and management of cardiac events, including recording, storage and synthesis of standard 12-lead ECGs, self-adaptive data processing, decision support and alarms generation.
- Wrist multisensor device for continuous monitoring of health status and alert, integrating biomedical sensors for heart rate, I-lead ECG, blood pressure, O₂ blood saturation and skin temperature measurement [7].
- Personal mobile health service platform for vital signs monitoring based on a body area network, utilising public 3G wireless networks [8].
- Smart glove [9] for non-invasive multi-parametric measurements of autonomous nervous system enabling the study of cognitive and physical status, the response to odour, speech & vision and mental training.

Furthermore, the symbiosis of textile material with wearable computing, media and interface design and the collaboration between established electronics and textile engineering led to a totally new class of large-area, flexible, conformable and interactive wearable systems, so called Smart Fabrics and Interactive Textile, SFIT or e-textile² [10]. The advantages of this integration are obvious: a) about 90% of the skin can be in contact with textile which is the most "natural" interface to body; b) fabrics are flexible and fit well with human body; c) it removes the

² In this paper "Smart Fabrics and Interactive textile – SFIT" and "e-textile" will be used indifferently except if indicated otherwise.

task of placing the sensors by a professional, and can be also cheap and disposable. Research and development is being strongly supported worldwide and in particular under the Information Society Technologies (IST) activities in the 6th (2002-2006) and currently the 7th Framework Program³ (2006-2013) for R&D of the European Commission (EC). These activities led to significant results in wearable smart systems, integrated multifunctional smart textiles, body sensor networks and context aware sensor systems for enabling several applications in healthcare & health, protection, leisure and life style management [2, 10].

2 Wearable Systems: Users' Requirements

Developing SWSs requires multidisciplinary research and integration of various components and technologies like adaptable materials, sensors, actuators, wireless communications, encapsulation, power supplies, control and processing units, user interfaces, as well as intelligent algorithms for decision support.

One of the most important phases in the development of a wearable sensor-based system is the analysis of the users' needs. These issues are numerous and complex. Among the major ones are usability & wearability, sensing platform (s), data storage and transmission, power supply, embedded decision support, interoperability and personalized services.

The most demanding requirements for wearable components are posed to energy harvesting systems and sensing devices.

While today's technologies related to energy harvesting systems do not seem to be, despite growing research interest, even near to the order of magnitude which is demanded, major advances in wearable sensors technologies have provided viable, although still far from ideal, solutions to continuous monitoring of several crucial variables of biomedical interest. When dealing with wearable sensing, under safe and unobtrusive conditions, one is limited to non-invasive measurement techniques. Non invasive sensors present usually a high complexity of principle and of system design, due to the difficulty to measure deep phenomena from the surface of the skin. The choice of the localization has to satisfy several criteria and limitations e.g. obtaining the best signal/noise ratio, fixing and ergonomy, but also unobtrusiveness. Several solutions are available today however very few are in use, due mainly to reliability, comfort, regulatory and economic reasons. To date neither new sensing principle has been devised to develop wearable sensors, different from those currently used in the clinic or in the sport environment nor new methodologies have been developed as an aid to diagnosis or to therapy administration based on the availability of continuous, ubiquitous data; this opportunity should arise in the near future.

Despite these facts, the very demanding requirements proper of wearable devices have already led to clever designs of various innovative sensor configurations. Several tutorial treatments are available in the literature describing biomedical sensors and electrodes principles and operations [11, 2]; the discussion here will be limited to sensing systems purposely devised and designed for maximum compatibility with body worn platforms.

³ <http://cordis.europa.eu/ist/home.html>

So far, a limited number of biomedical parameters are accessible to measurement through wearable systems. Vital signs, biomechanical variables (muscle activation through EMG reading, motion, posture and gesture) and biochemical sensing systems analysing sweat are nowadays available, although at different stages of development. Each specific application requires an appropriate set of sensors and sensory fusion algorithms to provide significant data for assessing training and performance (wellbeing and sport), for monitoring and alert in secondary prevention (healthcare), for providing objective data in rehabilitation and for monitoring risks of professionals working under harsh conditions. Wearable sensors are further discussed in the next section.

Other major issues to be addressed in the user requirements analysis of a SWS are a) manufacturability, maintainability and connectivity, b) field trials and validation, including use of standards; for the emerging area of SFIT, standardization and certification methods for testing integrated systems is key; and 3) legal and ethical issues, e.g. liability, personal data protection, user confidentiality and risk analysis.

Finally, any possible exploitation of research results rely on the early consideration of use scenarios, cost effectiveness, market analysis and business models.

Overall, the ambitious goal of SWSs is to enable an “affordable and interactive service, anywhere, anytime for anyone”.

3 Sensors and Bioelectrodes for Wearable Systems

There are essentially two different kinds of approach in designing body worn sensing platforms: one based on body area networks [12] of local sensing units using silicon based sensors and processors at the nodes, thus fully exploiting the intrinsic characteristics of miniaturization; the second approach makes use of electronic textiles (e-textiles) to fully benefit of comfort and large area coverage offered by this technology. A separate issue relates to the design and implementation of wearable electrodes for biopotential recordings; here the need of “dry electrodes” for long term monitoring, showing low susceptibility to motion artefacts, has driven intensive research activity leading to some useful results, still far however from providing a truly motion-artefact free solution.

In this section we will first briefly describe work which has been reported related to microelectronics sensing devices and body sensor networks aimed at collecting, processing and transmitting physiological data and motion tracking. Then sensing solutions proposed and adopted based on e-textiles or being compatible with them will be discussed. Finally, current efforts aimed at developing dry bioelectrodes will be briefly reported and analysed.

3.1 Body Worn Sensors

An overall low number of biomedical variables are nowadays accessible to measurement through wearable sensing devices⁴. Taking apart electrodes for

⁴ <http://www.toumaz.com>

biopotential recordings (see next paragraph) the following parameters have been recorded: heart and respiration rate, blood pressure, oxygen saturation, temperature, 3D acceleration and joint angles. More limited solutions have been proposed to non-invasively monitoring of biochemical indicators in body fluids such as eye tears, saliva and sweat.

While the classical methods to record heart rate and heart rate variability rely upon the use of bioelectrodes for ECG recordings, a few alternative solutions have been proposed which may offer some advantages in wearable applications.

A multimodal piezoelectric wearable transducer, working over a very large frequency bandwidth, being capable of recording low frequency apex-cardiogram and high frequency M-mode through ultrasounds which both detect heart and respiratory rate has been described to be used in emergency situations [13].

A promising sensing device which monitors heart and respiratory rates through non-contact operation has been reported under development, based on UWB radar on a chip [14]. Continuous monitoring of respiratory rate in wearable applications would appear, at first sight, a simple task. However, detection of the respiratory waveform by ad hoc algorithms is not so trivial since no special features (like the QRS complex in ECG) are present in the signal; drift and motion artefacts may heavily plague this determination. Several methods and devices, however, exist to provide continuous, wearable monitoring of thoracic and abdominal respiration rates. A comparative evaluation in respect to susceptibility to motion artefacts of the most commonly used systems, e.g. inductive plethysmography, electrical impedance, piezoresistive and piezoelectric strain gauges, has been reported, using spirometry as gold standard [15].

Blood arterial pressure is undoubtedly the most important cardiopulmonary variable to be monitored, crucial in the management of hypertension. The classic inflated cuff devices in their portable versions are bulky, energy consuming, they cause discomfort and they are not suited for wearable, long term monitoring. Alternative solutions have been proposed [16] based on the method of “pulse transit time”, using peripheral pulse sensors and dedicated algorithms for identification and calibration of arterial blood pressure. Difficulties related to patient individuality and to accurate calibration still plague these methods, otherwise being fully compatible with wearable sensing specifications.

Pulse oximetry arterial oxygen saturation (SPO_2) has become one of the parameters of paramount importance to monitor in assessing cardiopulmonary conditions. However, the traditional method of transmission pulse oximetry has several limitations, particularly when intended for wearable applications. Typical measurement sites at the ear lobe or at the fingertip are not appropriate and motion artefacts strongly affect this type of measurement. Reflectance pulse oximeters with improved signal amplitude and linearity have been proposed [17] to detect the signal from various part of the body. Progresses in the development are promising although still reliability and applicability problems need to be solved.

Core body temperature is a physiological parameter whose continuous monitoring would be very valuable in several applications. Monitoring should be performed in a totally unobtrusive way. Although skin temperature is easily monitored using tiny thermocouples or thermistors, a unique correlation with core

temperature does not exist. Some methods and techniques, potentially inferring core temperature from surface temperature gradients generated by local heat sources have been proposed, but their correctness is questionable.

The possibility of non-invasively and continuously monitoring relevant biochemical markers would be of great importance, in particular in professional sport and healthcare. Parameters such as electrolytes concentration, glucose, cortisol and drugs level are just few examples. This task is extremely challenging. Beside the availability of glucose monitoring in tears through instrumented eye contact lenses [18] and some tests in saliva [19] not much exist. EU funded BIOTEX⁵ project [20] has pioneered efforts in wearable technology for sweat analysis using a combination of discrete components for fluid handling & sensing and e-textile solutions. Much more activity has to be performed along these lines but a first step has been taken.

A totally different set of variables to be monitored using wearable systems pertains to the field of biomechanics and motion analysis. Several applications are currently explored mostly related to sport, rehabilitation and videogames. Actigraphy, motion capture, posture and gesture recognition are all important fields of research and development. Being limited here to wearable techniques, there is no doubt that the recent availability of cheap, miniaturized solid state multiaxial accelerometers [21], has revolutionised the field. Instrumented body suits are nowadays commercially available⁶ offering a new dimension to the field of motion analysis. Problems still exist in slow motion recording and gesture recognition using inertial devices.

Smart fabrics and interactive textiles (or e-textile) devices to be discussed next, offer complementary solutions and a synergistic approach with inertial sensors will definitely lead to very advanced and efficient systems for monitoring body kinematics. Sensorized shoes have also been developed and described [22] which complete the set of parameters to be monitored.

3.2 e-Textiles Based Sensors

Almost 10 years ago e-textiles realizations made their appearance in the field of wearable technologies for recording vital signs [23] and biomechanical parameters [24]. Since then many realizations have been shown and the field is now well established.

Concerning fabric-made sensing devices most of the work has been performed on textile bioelectrodes (see next paragraph). However, few textile-based sensors have been reported using the fabric material itself as the primary transduction element. Several textile sensors, as reported to date, have been implemented by exploiting the following transduction principles: chemoresistivity, piezoresistivity, piezoelectricity and piezocapacitive effects.

Textile fibers coated with different conductive polymers have been shown to possess chemoresistive or piezoresistive properties leading to gas sensing and strain gauge devices. Polypirrole coated cotton-Lycra fabrics have been used to

⁵ <http://www.biotex-eu.com/>

⁶ <http://www.xsens.com>

sense toxic or noxious gases [25]. Conducting polymer coated fabrics [26] and carbon loaded thermoplastic elastomer fibers have been utilized to sense joint angles changes [27] or variations in chest diameter during respiratory activity to record respiratory rate [28]. Strain sensor arrays based on smeared piezoresistive rubber onto fabric substrates have been described, being used to capture and classify posture and gesture [29] and currently utilized in upper limb neuro-rehabilitation [30]. Contact pressure sensors have also been developed [31] based on piezocapacitive effects where a capacitor made of textile electrodes and a compliant dielectric varies its capacitance in response to mechanical stress. Electromechanical sensors which use piezoelectric polymers such as polyvinylidene fluoride have also been developed using thin films or hollow fibres configurations. Their use is intended for measurements such as detection of carotid or radial artery pulses, recording apex-cardiogram and cardiac sounds.

3.3 Wearable Bioelectrodes

The integration into skin-adherent clothes of several kinds of bioelectrodes would enable several applications such as continuous, personalized, and self-made detection of vital signs and physiological variables. This is considered a crucial point, for instance, in the diagnosis and treatment of cardiovascular diseases.

Bioelectric functional monitoring (including vital signs detection), would considerably benefit from the implementation of wearable sensorized systems using proper electrodes either for biopotential recording (e.g. ECG, EEG and EMG) and for current injection to perform electric impedance sensing and imaging, functional electrical stimulation, electro therapy and other bioelectric procedures. Biopotentials recording requires the use of electrodes designed to register electrical activity generated by excitable organs or parts of them located inside the body.

Dry electrodes are highly desirable for long term monitoring applications and, in particular, for wearable systems. Wet electrodes are generally used for clinical monitoring mostly employing Ag/AgCl electrodes and (hydrophilic) gels. These electrodes however suffer several limitations and drawbacks in long-term monitoring [32]:

- The performance regarding power line interference is limited by electrodes/skin contact impedance.
- The use of an electrolyte for chronic use leads to reduced signal quality as the gel dehydrates and the re-application of gel may not be feasible; in addition, it is unpleasant for the user and time consuming for the care giver.
- There are toxicological concerns with electrolyte gels in particular regarding dermatological response.
- Movement artifacts are caused by mechanical disturbances of the electrode/skin interface and by the signals generated from the intrinsic mechano-electric response of the skin.
- High input impedance of the amplifiers causes effects of charged bodies near electrodes.

Dry electrodes aim to remove paste or gel-coupling which is incompatible with wearable applications. Common problem of both dry and wet electrodes, however,

resides in their susceptibility to motion induced artefacts, which is usually more severe for dry electrodes. Current means to reduce motion artefacts mostly consist in a) preparation (stratum corneum abrasion) of the skin to reduce its impedance/mechano-electric contribution to the signal [33], b) the use of integrated electrode/high input impedance amplifiers and dedicated correction algorithms [34], c) the use of needle-like electrode arrays perforating the stratum corneum [35]. Existing dry electrodes are still far from having acceptable performances, in particular in terms of motion artefact rejection. Minimizing electrical contact impedance between the electrode and the skin, maximizing adhesive properties without the use of covalent bonding and mechanically stabilizing the ionic-electronic interface are crucial interventions needed to improve dry electrode performances in term of signal-to-noise ratio, motion artefact and power line interference rejection. In the literature several dry electrodes have been disclosed in an attempt to overcome above mentioned shortcomings such as dry electrodes are made of e.g. conductive rubber, integrated into garments [36], but they do not yet offer an optimal solution, despite the fact that they are easily made and cheaply fabricated. Other arrays have been developed and disclosed with the intent to provide better signal recording through skin penetration or adherence with consequent contact impedance reduction arrays of silicon micromachined spikes (e.g. needles) [36]. More recently, flexible arrays fabricated using soft lithography [37] and carbon nanotubes arrays (CNT) [38] have been reported. These electrodes however may cause discomfort; they are intrinsically fragile and can cause irritation. In the case of CNT electrodes potentially toxic effects can be caused as they disperse into the epidermal layer and subcutaneous tissue.

Non-contact capacitive (insulating) electrodes have also been developed and disclosed in particular for EMG recording [39] but their susceptibility to motion artefact and power line interference is high. The use of active electrodes which implies the integration of a buffer amplifier (impedance converter) to suppress noise is also well known and recently developed in the form of a wearable non-woven fabric and screen printed thick-film forms [40]. Although this solution is effective in terms of the front end electronic it provides very little in terms of addressing the crucial problem of electrode/skin interface. Other solutions which envisage means for an integrated electrode/skin abrasion element have been disclosed. This solution is effective in term of reducing skin contact impedance but it is complex, it may provide irritation and potential infections.

Textile based electrodes made of weaved or knitted conductive yarns have received considerable attention in recent times [41, 42]. The direct coupling of fabric with the skin provides good conformity to the subject anatomy but the susceptibility to motion artefacts is still high and considerable problems exist in recording good signal or injecting adequate currents when the skin is dry. This is particular true for non-sweating or elderly subjects. Recent efforts aiming at decorating fibres with Ag-AgCl nanoparticles to enhance transduction in ionic media have still to demonstrate resistance to environmental factors and washing.

4 Current R&D and Expected Results

4.1 State of the Art

This section will focus on the state of the art of R&D in smart wearable systems. This includes development of new sensorised garments and integration of networked mobile devices for personal health management, protection & safety, emergency, sport and healthy life style support. In addition, on going research and expected results in specific application cases will be reported.

As mentioned above, a wearable electronic system is made by different components, that may be summarized in the following types: sensors, i.e. devices that detect parameters coming from the human body and/or from the area surrounding the body; signal processing and transmission circuits, for the transduction and transmission of data generated by sensors; power storage and harvesting, possibly actuators. These classes of components are indeed mutually dependent in the system. For instance, the sensor must be put in contact with the human body (and this drives the choice of materials and technologies), the generated signals require "ad hoc" designed signal processing units (for interference tolerance) and the whole system should be energetically autonomous (so this drives the overall architecture of the system and the energy constraints of each sensor).

This underlines the need to consider the wearable device as a system, i.e. a collection of interacting elements with common constraints given by the application. Thus, the major effort required for building an efficient wearable system consists in the integration of the different elements, while respecting the constraints given by the application and the main request of wearable devices, i.e. the fact that the system, being embedded in an object that normally has a different use, like the garment, must not be perceived by the user thus improving his/her comfort and the efficacy of the measurements.

SFIT wearable systems for biomedical applications, so called "Intelligent Biomedical Clothing" [43] have been initiated almost 10 years ago and achieved the first successful prototypes 3-4 years later [44]: for instance, the European Project Wealthy⁷ has provided a t-shirt able to acquire, simultaneously and in a natural environment, a set of physiological parameters like electrocardiogram, respiration, posture, temperature, movement index by integrating textile sensors and connections with non-textile sensors (as the temperature sensors) embedded in the fabric. Other advanced textile-integrated prototype monitoring systems have been developed and tested under European and USA initiatives such as MyHeart project [45], MagIC system [46] and "SmartShirt" [47].

More recent R&D supported by the EU under the ICT (Information and Communication Technologies) program addresses smart fabrics and interactive textile for wearable personal systems through integration of sensors/actuators, energy

⁷ <http://www.smartex.it/wealthy>

sources, processing and communication within the clothes in order to enable health applications but also personal protection and emergency management. The cluster of EC-funded projects on "smart fabrics, interactive textile, and flexible systems"⁸ regroups project activities along an R&D roadmap presented in figure 1. It includes:

- Body contact garments for physiological and physical sensing (projects Wealthy, MyHeart)
- Biosensing textiles for diabetes, obesity, sport, and wound healing management (BIOTEX) [20].
- Contactless sensors for body monitoring incorporated in textiles (CONTEXT) [39].
- Integration of optical fiber-based sensors into functional textiles (OFSETH) [48].

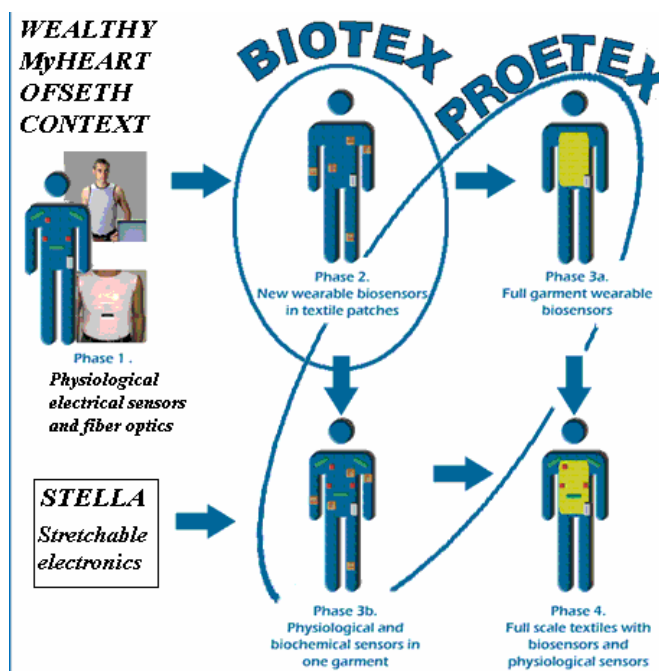


Fig. 1. R&D roadmap of the SFIT cluster of EC-Funded projects: from physiological and physical electrical sensors to wearable biosensors in patches, to full garment wearable biosensors, to physiological, physical and biochemical sensors in one garment Final goal is the full scale sensing textiles with embedded conformable electronic units for power (scavenging and storage), data processing and communication.

⁸ <http://www.csem.ch/sfit>

- Protective textiles system (PROETEX)⁹ integrating physiological, biochemical and environmental sensing.
- Stretchable electronic "motherboard" in textiles (STELLA)¹⁰, targeting substrate technology and electronics components & packages.

In the following, a more detailed description of such an integration effort is given considering the work performed in PROETEX (on going project started in February 2006), dedicated to the development of a smart uniform for fire fighters and civil protection rescuers [49].

4.2 A Concrete Example of IWS: Protective Textiles Systems for Emergency Disaster Wear

This uniform consists of 3 main components: an inner garment, in contact with the body, that collects physiological data as cardiac beat, respiration rate and internal temperature; an outer garment that collects data concerning the user position and posture and data concerning the external environment, and a pair of shoes collecting data concerning the user's posture and the possible presence of dangerous gases in the external environment. In addition to sensors, the outer garment also hosts Body Area Network (BAN) transmission components (such as a couple of textile antennas) and the electronic box to which all data are collected and transmitted to a remote station that provides the global monitoring of the operation.

The ProeTEX prototypes consist of three uniforms addressing civil protection', urban and forest fire-fighters' requirements, integrating sensors and electronics inside a T-shirt or Inner Garment (IG), a jacket or Outer Garment (OG) (see Fig. 2) and a pair of sensorised boots.

Data collected from sensors of the IG and OG are transmitted real-time to a self-powered Professional Electronic Box (PEB), hosted in the OG, through a serial RS485 protocol. In the meanwhile data coming from the sensors in the boots are transmitted wirelessly by means of a Zigbee protocol. Finally all data are sent out to the local coordinator of the operations, far away from the disaster area (Operation Area Network). This communication can be performed with a Remote Transmission System working with a Wi-Fi protocol. A monitoring software visualizes real-time all sensors' data at the coordinator's side, automatically activating alarms when dangerous contexts are detected. Similarly, a Victim Patch (VP) module has been conceived to be placed on the chest of victims in order to allow medical personnel to monitor in real-time their physiological parameters.

- Sensor Modules

Since many sensors are placed inside the ProeTEX garments and a minimum number of wires is desired, each sensor unit has a dedicated electronic module that contains the sensor analog front-end and a low power microcontroller which operates A/D conversion, on line processing and communication with the PEB. In this way, only processed data are sent to the PEB. Communication between each IG,

⁹ <http://www.proetex.org>.

¹⁰ <http://www.stella-project.de/>

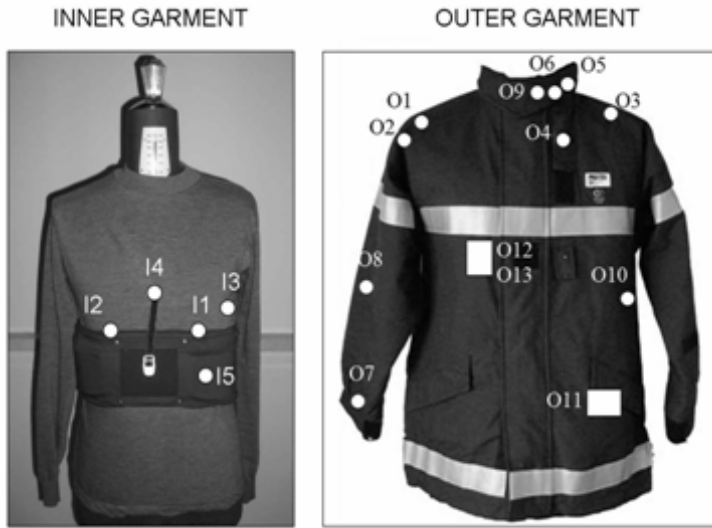


Fig. 2. Overview of the second ProeTEX Prototype: A. Inner Garment: I1: textile electrodes for HR monitoring (under the Vital Signs Board housing); I2: piezoelectric sensor for BR monitoring; I3: thermocouple for BT monitoring; I4: SPO2 sensor; I5: Vital Signs Board. B. Outer Garment: O1: external temperature sensor; O2: Heat flux sensor; O3: GPS module; O4: front visual alarm; O5: Acoustic alarm; O6-O7: Collar and Wrist accelerometers; O8: Textile motion sensor; O9: CO sensor; O10: Zigbee module; O11: Professional Electronic Box; O12: Wi-Fi module; O13: communication antenna (under the pocket layer, over the Wi-Fi module).

OG module and PEB is guaranteed by a RS485 bus, except for the GPS module, which owns a dedicated connection. The Boots module is instead interfaced with the PEB through a wireless Zigbee connection. Each module has a port for updating on board the firmware (i.e. algorithms and transmission protocols).

- Inner Garment

The IG is the subsystem devoted to monitor health status of the emergency operators without interfering with their activities.

Textile electrodes and fabric piezo-resistive sensors have been integrated in a one step process in a comfortable shirt to reveal cardiopulmonary parameters (i.e. heart rate and breathing rate), whereas non-textile sensors have been embedded in the shirt for body temperature and oxygen saturation monitoring (see Fig. 2). The textile electrodes and the piezo-resistive sensor have been realized along the following process: stainless steel based yarns have been knitted together to a ground yarn by using a tubular intarsia technique to get a double face, whereas the external part is not conductive in order to insulate the electrodes from the environment. As ground yarn a fire resistant yarn was used.

The architecture of the IG prototype is based on a T-shirt having two main areas devoted to specific tasks: an elastic region including all the sensors and a

region containing a detachable on-board electronics. The textile sensors and electrodes are connected to the electronic modules through textile conductive cables integrated in a one step process in the shirt. Dedicated textile compatible connectors are encapsulated in the fabric and allow the physical connection between the cables and the electronic components. In the second IG prototype the vital signs board has been connected to the PEB (placed in the OG) by means of an external cable, whereas a wireless connection has been foreseen for the final release.

Heart Rate Sensor - Heart Rate (HR) is detected by acquiring an ECG lead through three textile electrodes integrated in the IG. An algorithm extracts HR value from the raw ECG signal. Specific textile solutions have been adopted to improve the contact electrodes-skin without hydrogel membranes.

Breathing Rate Sensor – Two different approaches have been followed to monitor the respiratory activity at a first step: a) a fabric piezoresistive sensor that changes its electrical resistance when stretched, being sensitive to the thoracic circumference variations that occur during respiration; b) impedance pneumography monitoring: it consists on injection of a high frequency (50 kHz) and low amplitude current by means of the outer electrodes and measuring the impedance changes on the thorax by the inner ones; a relationship between the air flow through lungs and the impedance variation allows the respiratory cycles monitoring. In the second version of IG prototype a new piezoelectric sensor in wire form has been implemented (replacing the impedance pneumography device), showing a higher signal to noise ratio together with low sensitivity to motion artefact.

Body Temperature Sensor - A LM92 temperature sensor¹¹ has been sealed in a polyamide foil and then has been embedded in the shirt in a proper pocket at the left armpit level. Insulation textile layers shield the body temperature measurement from the effects of the environmental temperature.

SpO2 Sensor - An optical transducer, made of several couples of optical emitters and receivers has been integrated in a unit at breastbone level. A built-in processor triggers the best located transmitters to dynamically select the highest signal levels; a processor selects samples, stores values in memory and sends them to PEB through the RS485 bus.

- Outer Garment

The OG is the subsystem devoted to protect the rescuer, monitoring his/her activity and surrounding environment. It has been produced in three different configurations, depending on the application: civil protection, urban and forest fire-fighters. All OG configurations include two tri-axial accelerometers, an external temperature sensor, a newly developed textile motion sensor and a commercial carbon monoxide monitoring sensor. Forest fire-fighters and civil protection operators have also an integrated GPS module, whereas urban fire-fighters do not, since they operate inside buildings where reliable GPS signals are rarely available. Moreover a heat flux sensor has been included both in urban and forest fire-fighters OG, in order to prevent operators from skin burn when facing flames.

¹¹ <http://www.datasheetcatalog.org/datasheet/nationalsemiconductor/LM92.pdf>

Regarding data transmission, all OGs incorporate a long range transmission module. The civil protection system has also an alarm module, that is a subsystem launching visual and acoustic warnings when one or more sensors detect operator dangers beforehand.

Even if electronics and all cabled sensors are powered by an embedded Lithium-Ion Polymer (LiPo) battery inside the PEB, a flexible battery allowing a working time over two hours with a nominal voltage of 3.8 V., has been experimented in urban fire-fighter OG in order to increase functionality and ergonomics of garment.

External Temperature & Heat Flux Sensors- the external temperature sensor is placed under the OG external coating at shoulder operator level; this set-up avoids environmental disturbances and optimizes higher temperature detection. A 5.9x2.1x0.9 mm Atexis platinum sensor¹² with a -70°C to +500°C range and platinum coated nickel wires has been chosen. The heat flux sensor is placed in the proximity of the platinum sensor, inside the third comfort layer of the OG at shoulder level as well. The sensor has a 50 mm diameter, 420 µm thickness and a sensitivity of 75 µV/W/m2. The presence of the heat flux sensor is necessary because the very efficient protection provided by the OG textile equipment makes difficult the recording of thermal environment.

GPS Module - An active GPS Antenna¹³ was chosen. It provides an accurate measure of the absolute position of the user in open space. The sensor performances drastically decrease when approaching or entering into buildings. Nevertheless this information is considered important by rescuers working in large operative areas, where they can't be directly visually monitored.

Alarm Module - The alarm module consists of a power red led driven by a microcontroller which makes the led flashing at different frequencies depending on the type of alarm. It includes also an audio alarm board with a buzzer control. Two self-powered alarm modules have been integrated in the civil protection OG on the front side of the trunk and in the back face at shoulder level. Redundancy guarantees higher visibility in case of structure collapse or flooding.

Accelerometers - Motion sensors have been designed to detect posture, accidental falls to the ground and immobility of the operator. They are realized by means of two accelerometer modules, one placed in the jacket collar (for monitoring trunk movements) and the other in the right sleeve (to achieve more accuracy in activity detection since an operator can move his arm while not moving trunk). Each module is based on a tri-axial accelerometer (ADXL330¹⁴) and a low power microprocessor (Texas Instruments) for A/D conversion, real time signal processing and transmission of the extracted information to the PEB.

Textile Motion Sensor - It is applied to the external part of the OG insulation layer, and it is used to detect immobility. The transducer is made of conductive elastomeric strip (200x20 mm wide) printed on an elastic fabric and integrated in the sleeve's elbow region. Since the elastomer shows piezo-resistive properties, movements can be detected by analyzing sensor signal.

¹² <http://www.atexis.fr>.

¹³ <http://www.u-blox.com>

¹⁴ <http://www.analog.com>

CO sensor – A Carbon monoxide sensor is placed in the OG lapel near the user's mouth and nose. The sensor is integrated in the outer shell layer of the OG, while electronics is protected from the heat by fixing it under the insulated layer. A waterproof and gas permeable coating protects the sensor. The device (CO-D4¹⁵) is selective and sensitive for CO range between 0 and 1000 ppm; its output is fed through a transimpedance amplifier to convert current to voltage so that it can be read by the analog port of a microprocessor (Texas Instruments). The working range is 0-410 ppm: the microcontroller performs data conversion, extracts CO concentration and implements the protocol routines required to send the information through the RS485 bus.

-Boots

Boots prototypes have been developed and tested both for Civil Protection and Fire-Fighter brigades. The prototypes respect UE standards for protection shoes and are already arranged for integrating sensors in the sole. The heel zone is wide to guarantee stability of users, the upper part is made with leather and materials resisting to fire and heat, elastic flex points have been inserted in the upper part to allow high flexibility and a new lacing system have been realized to improve functionality. Furthermore, to avoid abrasion and increase comfort, breathable and waterproof lining have been inserted inside.

CO2 Sensor - The Boots have been equipped with a CO2 transducer, which enables faster detection of toxic gas before it reaches the respiratory tract. A specific housing has been created in the upper part of the boot, able to maintain the sensor in contact with air. A CO2 D1 sensor¹⁶ has been chosen and tested. Power supply is furnished by a rechargeable battery whereas communication with PEB is realized by means of a Zigbee module connected with the sensor: finally, the whole system – sensor, electronics, battery and Zigbee module – is hosted in a 58 x48 x16 mm box inserted in the boot pocket.

- Remote Transmission and Monitoring

Besides wearable technologies for sensing and data processing, a remote communication infrastructure, between the rescuers and the local coordinator, has been developed within the project. This is realized by means of a software interface and a long range communication system.

Monitoring Software - It manages data received by PEB; data detected by sensors and collected by PEB are wireless transmitted to the remote software. Data exchange is based on “query-answer” protocol.

Remote Transmission System: communication between the PEB and the PC is set up by means of a Wi-Fi based communication system, allowing the communication of data up to 1 Km far from the operator. Wi-Fi protocol was selected as a good compromise between portability, lightness and performance. Wide planar textile antennas (placed in the front and back sides of the jacket) [50] are used to transmit the signal from the OG. The bandwidth of the antennas is more than 280 MHz, whereas return loss and influence of humidity have been analyzed; the

¹⁵ <http://www.alphasense.com>

interaction between electromagnetic field radiation and operator body was investigated too, and it was found below SAR limits as requested by EU regulations. In order to cover a communication range of more than 1 Km, a 13.5 dBi sector antenna¹⁶ with a 3 dB pattern equal to 90° x 15° is adopted between the farthest nodes.

5 Challenges and Future R&D

The huge interest for wearable and smart textile systems led to the establishment of an interdisciplinary academic and industrial community and critical mass of R&D and collaborative activities worldwide. The engineering community has been particularly active. For example, IEEE Engineering in Medicine and Biology Society (EMBS) established, in 2004, a technical committee for wearable biomedical sensors and systems (WBSS) to raise awareness, promote excellence and encourage collaboration to progress R&D.

However, the current status of developing integrated, reliable, cost-effective and user-friendly smart wearable systems is far from the "affordable, any time, any place" final concept (e-textiles).

The market for wearable monitoring solutions for health care and fitness/well-being applications is estimated at \$460 million in 2006, the majority of which is comprised of strap-based solutions for fitness applications (e.g. Polar belts and bras). This market is expected to grow by over 16% annually to reach almost \$1 billion by 2011¹⁷. However, the niche markets are not yet identified, in particular when the cost has to be reimbursed by a third party. Several issues, technical as well user and business related, remain to be solved.

The current market size of SFIT is also relatively modest, estimated today between 700 m€ and 800m€. This includes SFIT enabling technologies such as materials, nanotechnologies, enabling components (e.g. electronic and fabric components), SFIT based modules (fabrics or textile) and SFIT complete solutions. However the future outlook is extremely strong (VDC Study¹⁸) with major opportunities in sensing and monitoring, actuation & response, computing & communication, heating and energy management, lighting, location and position.

A survey that has been carried out within the "European Technology Platform for the Future of Textiles and Clothing"¹⁹, aimed to identify new markets to be explored and to find out research priorities. The information collected from 27 textile industries (from 9 EU countries) in order to prioritize the developments regarding the attractiveness of the application classification for the specific end-users and the availability of the technology showed that medical, sport/civil, industrial and military sectors have both high economic relevance (high market

¹⁶ <http://www.stelladoradus.com>

¹⁷ Wearable Electronics Systems Global Market Demand Analysis: Health Care Solutions, Research Report # VDC6520, November 2007, VDC Research Group.

¹⁸ Smart fabrics, interactive textiles and related enabling technologies; market opportunities and requirements analysis, third edition, November 2007, VDC Research Group.

¹⁹ <http://textile-platform.eu/textile-platform/>

demand) as well as high need for research. The study concerning new materials, functionalities and research included 12 research centres and 2 companies from 11 EU countries. The conclusion confirms the outstanding scientific and technological challenges of textile based smart wearable systems and the need to fuse the research work and consumer insights to create multidisciplinary teams of product designers and engineers.

The important areas for future R&D are related with:

- Sensors & actuators, data processing/electronics e.g. pre-processing, diagnostics, context awareness, self learning tools and prioritisation;
- Energy storage (electrochemical, electrical), transmission (e.g. textile antenna) and generation (e.g. thermal, kinetic, magnetic and chemical);
- Communication i.e. functions to be performed by textile or structures compatible with it; interconnection is a critical aspect and industrial manufacturing is a key issue.

Longer development time is expected for biological and chemical sensors, for skin sensors, biological actuators, self learning data processing and storage tools, as well as harvesting energy from elastic, magnetic and chemical mechanisms.

The main barriers for reaching a higher market with high added value products and diversified application fields are:

- Textile and clothing industries are not sufficiently engaged and research community is fragmented.
- There is lack of critical mass in new and multidisciplinary supply chain such as, missing standards and certification for smart textiles; SFIT industry is immature despite a well established textile manufacturing industry; There is an urgent need of investment for more innovation.
- Core modules and core technologies are not sufficiently developed neither tested nor certified, namely connectivity and connectors, microelectronics encapsulation, power supply and storage, washability and durability.

Other issues such as data management (security, privacy-encryption), data transfer, extrapolation of parameters and statistical analysis need further research and optimisation.

Finally the use of neural networks for “event prediction” and consequent generation of alert signals, as well as the need for predictive cognitive model are recognised as essential for delivering an integrated communication wearable system.

Additional knowledge on biophysical issues such as biophysical expertise on skin-sensor interaction models, electrochemical aspects and skin physical-chemical properties (age, gender, race, etc.) is also an outstanding issue today.

Finally, major roadblocks constitute also the lack of strategic analyses such as commercial opportunities, market competition analysis, technologies trends and markets.

Microsystems and smart system integration significantly contribute to further enhancement of the development of SWS and in particular SFIT systems through R&D of smart & functional systems that can be embedded in or fully transformed into textile structures, e.g.

- Integration of regular electronics into textiles, including interconnect and robust attachment, stretchable conductive patterns and soft-touch substrates (important route to commercialize available intelligent textiles).
- Integration of fibred devices (e.g. piezoelectric fibers, transistors on yarns) into textile and fabric to drive a transition between present purely passive components to integrated passive/active components and systems.

In emerging application areas like mobile/ambulatory and biomedical systems a flexible/stretchable interconnect technology is a promising approach for packaging and system integration. Specifically for demands like conformability, free form shapes, biocompatibility and high reliability, it holds a high application potential. Flex-stretch technology is considered to be a key component for the realization of new ranges of on-the-body wearable systems. A strong co-development of systems and applications, with the integration technology is of utmost importance.

Acknowledgments

The author thanks Prof. Danilo De Rossi (University of Pisa) for his contribution on *sensor technologies overview* and Prof Annalisa Bonfiglio (University of Cagliari) & PROETEX consortium for their contribution on *protective textiles systems for emergency disaster wear*.

References

1. Lymberis, A., De Rossi, D.: Wearable eHealth Systems for Personalized Health Management, State of the art and future challenges. *Studies in Health Technology and Informatics*, vol. 108. IOS Press, Amsterdam (2004)
2. Lymberis, A., Dittmar, A.: Advanced wearable health systems and applications - Research and development efforts in the European Union. *IEEE Engineering in Medicine and Biology Magazine* 26(3), 29–33 (2007)
3. Bonato, P.: Wearable sensors/systems and their impact on biomedical engineering. *IEEE Engineering in Medicine and Biology Magazine*, 18–20 (May/June 2003)
4. De Rossi, D., Lymberis, A. (guest eds.): *IEEE Transactions on Information Technology in Biomedicine*, Special Section on New Generation of Smart Wearable Health Systems and Applications, vol. 9(3), pp. 293–294 (2005)
5. Hovorka, R., et al.: Closing the Loop: The Adicol Experience. *Diabetes Technology & Therapeutics* 6(3), 307–318 (2004)
6. Rubel, P., Gouaux, F., Fayn, J., Assanelli, D., Cuce, A., Edenbrandt, L., Malossi, C.: Towards Intelligent and Mobile Systems for Early Detection and Interpretation of Cardiological Syndromes. In: Murray, A. (ed.) *Computers in Cardiology 2001*, vol. 28, pp. 193–196. IEEE Computer Society Press, Los Alamitos (2001)
7. Lukowicz, P., Anliker, U., Ward, J., Tröster, G., Hirt, E., Neufelt, C.: AMON: A Wearable Medical Computer for High Risk Patients. In: Proc. ISWC 2002, 6th International Symposium on Wearable Computers, pp. 133–134 (2002)

8. Van Halteren, A., Bults, R., Wac, K., Dokovsky, N., Koprinkov, G., Widya, I., Konstantas, D., Jones, V.: Wireless body area networks for healthcare: the mobihealth project. In: Lymberis, A., De Rossi, D. (eds.) *Wearable eHealth Systems for 19 Personalised Health Management, Studies in Health Technology and Informatics*, vol. 108, pp. 181–193. IOS Press, Amsterdam (2004)
9. Dittmar, A., Axisa, F., Delhomme, G.: Smart clothes for the monitoring in real time and conditions of physiological, emotional and sensorial reactions of human. In: Proc. 25th Annual International Conference IEEE-EMBS 2003, vol. 4, pp. 3744–3747 (2003)
10. Lymberis, A., Paradiso, R.: Smart fabrics and interactive textile enabling wear-able personal applications: R&D state of the art and future challenges. In: 30th Annual International Conference of the IEEE Engineering in Medicine and Biology Society, August 20-25, pp. 5270–5273 (2008)
11. Guang-Zhong, Y., Magdi, Y. (eds.): *Body sensor networks*, Springer Verlag London Ltd (2006)
12. Jovanov, E., Milenkovic, A., Otto, C., De Groen, P.C.: A wireless body area network of intelligent motion sensors for computer assisted physical rehabilitation. *J. Neuroengineering Rehab.* 2(6), 1–10 (2005)
13. Lanatà, A., Scilingo, E.P., De Rossi, D.: A multi-modal transducer for cardiopulmonary activity monitoring in emergency. *IEEE Transaction on Information Technology in Biomedicine* (in press)
14. Zito, D., Pepe, D., Neri, B., Zito, F., De Rossi, D., Lanatà, A.: Feasibility study and design of a wearable system-on-a-chip pulse radar for contactless cardiopulmonary monitoring. *International Journal of Telemedicine and Applications* (2008)
15. Lanatà, A., Scilingo, E.P., Nardini, E., Loriga, G., Paradiso, R., De Rossi, D.: Comparative evaluation of susceptibility to motion artifact in different wearable systems for monitoring respiratory rate. *IEEE Transactions on Information Technology in Biomedicine* (accepted for publication)
16. Poon, C.C.Y., Zhang, Y.T.: Cuff-less and non-invasive measurements of arterial blood pressure by pulse transit time, in *Engineering in Medicine and Biology Society*. In: 27th Annual International Conference of the IEEE-EMBS 2005, January 17-18, pp. 5877–5880 (2006)
17. Nogawa, M., Kaiwa, T., Takatani, S.: A novel hybrid reflectance pulse oximeter sensor with improved linearity and general applicability to various portions of the body, *Engineering in Medicine and Biology Society*. In: *Proceedings of the 20th Annual International Conference of the IEEE*, October 29 - November 1, vol. 4, pp. 1858–1861 (1998)
18. Badugu, R., Lakowicz, J.R., Geddes, C.D.: Ophthalmic glucose monitoring using disposable contact lenses. *Journal of Fluorescence* 14(5) (2004)
19. Aardal-Eriksson, E., Karlberg, B.E., Holm, A.C.: Salivary cortisol—an alternative to serum cortisol determinations in dynamic function tests. *Clin. Chem. Lab Med.* 36(4), 215–222 (1998)
20. Coyle, S., Wu, Y., Lau, K.-T., Wallace, G.G., Diamond, D.: Fabric-based fluid handling platform with integrated analytical capability. In: 29th Annual International Conference of the IEEE Engineering in Medicine and Biology Society, August 22-26, p. 6450 (2007)
21. Bouten, C.V.C., Koekkoek, K.T.M., Verduin, M., Kodde, R., Janssen, J.D.A.: A triaxial accelerometer and portable data processing unit for the assessment of daily physical activity. *IEEE Transactions on Biomedical Engineering* 44(3), 136–147 (1997)

22. Morris, S.J., Paradiso, J.: Shoe-integrated sensor system for wireless gait analysis and real-time feedback, Engineering in Medicine and Biology. In: Proceedings of the Second Joint 24th Annual Conference and the Annual Fall Meeting of the Biomedical Engineering Society, EMBS/BMES Conference, October 23-26, vol. 3, pp. 2468–2469 (2002)
23. Park, S., Gopalsamy, C., Rajamanickam, R., Jayaraman, S.: The wearable motherboard: An information infrastructure or sensate liner for medical applications. *Stud. Health Technol. Informatics* 62, 252–258 (1999)
24. De Rossi, D., Della Santa, A., Mazzoldi, A.: Dressware: Wearable hardware. *Material Science & Engineering C* 7, 31–35 (1999)
25. Collins, G.E., Buckley, L.J.: Conductive polymer-coated fabrics for chemical sensing. *Synthetic Metals* 78, 93–101 (1996)
26. Scilingo, E.P., Lorussi, F., Mazzoldi, A., De Rossi, D.: Strain-Sensing fabrics for wearable kinaesthetic-like systems. *IEEE Sensors Journal* 3(4) (2003)
27. Mattmann, C., Clemens, F., Troester, G.: Sensor for measuring strain in textile. *Sensors* 8, 3719–3732 (2008)
28. Paradiso, R., Loriga, G., Taccini, N.: A wearable health care system based on knit-ted integrated sensors. *IEEE Transactions on Information Technology in Biomedicine* 9(3), 337–344 (2005)
29. Lorussi, F., Rocchia, W., Scilingo, E.P., Tognetti, A., De Rossi, D.: Wearable, redundant fabric-based sensor arrays for reconstruction of body segment posture. *IEEE Sensors Journal* 4(6), 807–818 (2004)
30. Tognetti, A., Lorussi, F., Bartalesi, R., Quaglini, S., Tesconi, M., Zupone, G., De Rossi, D.: Wearable kinesthetic system for capturing and classifying upper limb gesture in post-stroke rehabilitation. *Journal of NeuroEngineering and Rehabilitation* 2(8) (2005)
31. Sergio, M., Maranesi, N., Tartagni, M., Guerrieri, R., Canegallo, R.: A textile based capacitive pressure sensor. *Proc. IEEE Sensors* 2, 1625–1630 (2002)
32. Searle, A., Kirkup, L.: A direct comparison of wet, dry, and insulating bioelectric recording electrodes. *Physiol. Meas.* (21), 271–283 (2000)
33. Tam, H.W., Webster, J.G.: Minimizing electrode motion artefact by skin abrasion. *IEEE Transaction on Biomedical Engineering* bme-24(2), 134–139 (1977)
34. Zipp, P., Ahrens, H.: A model of bioelectrode motion artefact and reduction of artifact by amplifier input stage design. *J. Biomed. Eng.* 1, 273–275 (1979)
35. Griss, P., Enoksson, P., Tolvanen-Laakso, H.K., Meriläinen, P., Ollmar, S., Stemme, G.: Micromachined electrodes for biopotential measurements. *Journal of Microelectromechanical Systems* 10(1), 10–16 (2001)
36. Mühlsteff, J., Such, O.: Dry electrodes for monitoring of vital signs in functional textiles, Engineering in Medicine and Biology Society. In: IEMBS 2004. 26th Annual International Conference of the IEEE, September 1-5, vol. 1, pp. 2212–2215 (2004)
37. Baek, J., An, J., Choi, J., Park, K., Lee, S.: Flexible polymeric dry electrodes for the long-term monitoring of ECG. *Sensors and Actuators A* 143, 423–429 (2008)
38. Ruffini, G., Dunne, S., Farrés, E., Pallarés, J., Ray, C., Mendoza, E., Silva, G.C.: A dry electrophysiology electrode using CNT arrays. *Sensors and Actuators A* 132, 34–41 (2006)
39. Langereis, G., de Voogd-Claessen, L., Spaepen, A., Siplia, A., Rotsch, C., Linz, T.: ConText: Contactless Sensors For Body Monitoring Incorporated. In: IEEE International Conference on Textiles, Portable Information Devices, Portable 2007, May 25–29, pp. 1–5 (2007)

40. Kang, T., Merritt, C.R., Grant, E., Pourdeyhimi, B., Nagle, H.T.: Non-woven fabric active electrodes for biopotential measurement during normal daily activity. *IEEE Transaction on Biomedical Engineering* 55(1), 188–193 (2008)
41. Scilingo, E.P., Gemignani, A., Paradiso, R., Taccini, N., Ghelarducci, B., De Rossi, D.: Performance evaluation of sensing fabrics for monitoring physiological and biomechanical variables. *IEEE Transaction on Information Technology in Biomedicine* 9(3), 345–352 (2005)
42. Ctrysse, M., Puers, R., Hertleer, C., van Langenhove, L., van Egmond, H., Matthys, D.: Towards the integration of textile sensors in a wireless monitoring suit. *Sensors and Actuators A* 114(2-3), 302–311 (2004)
43. Lymberis, A., Olsson, S.: Intelligent Biomedical Clothing for Personal Health and Disease Management: State of the Art and Future Vision. *Telemedicine Journal and e-Health* 9(4), 379–386 (2003)
44. Lymberis, A.: Research and development of smart wearable health applications: the challenge ahead. In: *Wearable eHealth Systems for Personalised Health Management: State of the Art and Future Challenges*, pp. 155–161. IOS Press, Amsterdam (2004)
45. Lauter, J.: MyHeart: Fighting cardiovascular disease by preventive and early diagnosis. In: Lymberis, A., De Rossi, D. (eds.) *Wearable eHealth Systems for Personalised Health Management. Studies in Health Technology and Informatics*, vol. 108, pp. 34–42. IOS Press, Amsterdam (2004)
46. Di Renzo, M., Rizzo, F., Parati, G., Brambilla, G., Ferratini, M., Castiglioni, P.: MAGIC System: a New Textile-Based Wearable Device for Biological Signal Monitoring. In: *27th Annual Conference Applicability in Daily Life and Clinical Setting, Engineering in Medicine and Biology Society*, pp. 7167–7169 (2005)
47. Marculescu, D., Marculescu, R., Zamora, N.H., Stanley-Marbell, P., Khosla, P.K., Park, S., Jayaraman, S., Jung, S., Lauterbch, C., Weber, W., Kirstein, T., Cottet, D., Grzyb, J., Troster, G., Jones, M., Martin, T., Nakad, Z.: Electronic textiles: a platform for pervasive computing. *Proc. of the IEEE* 91(12), 1995–2018 (2003)
48. : OFSETH: Optical Fibre Embedded into technical Textile for Healthcare, an efficient way to monitor patient under magnetic resonance imaging. In: *9th Annual International Conference of the IEEE Engineering in Medicine and Biology Society, EMBS 2007*, August 22–26, pp. 3950–3953 (2007)
49. Curone, D., Dudnik, G., Loriga, G., Luprano, J., Magenes, G., Paradiso, R., Tognetti, A., Bonfiglio, A.: Smart Garments for Safety Improvement of Emergency/Disaster Operators. In: *29th Annual Conference of the IEEE Engineering in Medicine and Biology Society*, August 22–26, pp. 3962–3965 (2007)
50. Hertleer, C., Rogier, H., Vallozzi, L., Van Langenhove, L.: A Textile Antenna for Off-Body Communication Integrated into Protective Clothing for Firefighters. *IEEE Transactions on Antennas and Propagation Part 1* 57(4), 919–925 (2009)

Fall Detection of Patients Using 3-Axis Accelerometer System

Petar Mostarac, Hrvoje Hegeduš, Marko Jurčević, Roman Malarić,
and Aimé Lay-Ekuakille

University of Zagreb, Faculty of Electrical Engineering and Computing

Abstract. Triaxial accelerometers are used as a low cost solution in wide areas of patient care. This paper describes the use of triaxial accelerometer together with ZigBee transceiver to detect fall of patients. The system, including calibration of accelerometers and measurement is explained in detail.

Keywords: accelerometers, ZigBee standard, fall detection.

1 Introduction

The micro machined inertial sensors (accelerometers and gyroscopes) are used for many different applications including navigation, impact detection, position, tilt, inclination, shock, vibration, motion detection, etc... They are also used for human movement tracking. The human body has a posture control that enables humans to move and maintain stability. The measurement of human posture and movement is valuable for many different medical applications and diagnostics [1]. This paper will present an easy and simple method to detect fall detection of patients using accelerometer together with ZigBee transceiver to communicate with PC wireless.

The average age of the population around the world is increasing due to decline in birth rate and increase in the average life span of the last 60 years. Owing to a number of factors it is expected that world population will reach 7 billion in 2012 and outstrip 9 billion people by 2050 [1].

The number of persons with older ages increase faster the higher the age is considered. In Europe, that currently has the oldest population, median age is nearly 40 years and is expected to reach 47 years in 2050. In the developed regions of the world population aged 60 or over is growing at 1.9% annually and is expected to increase by 50% during period between 2010 and 2040 (Fig. 1) [2]. Over the same period, the population aged 60 or over in the developing regions of the world is expected to rise from 475 million in 2009 to approximately 1.6 billion in 2050

(at rates more than 3% annually). Global life expectancy will increase from 68 years in 2005-2010 to 76 years in 2045-2050 [1].

The constant growing number of older adults increases demands on the medical and social services and also poses the challenge for personal and family resources. Diseases which affect older population contribute to reduced life quality and physical or social disabilities. Public health system must now respond to the challenges posed by growing number of injuries, chronic illnesses and disabled population implicating increasing health-care costs.

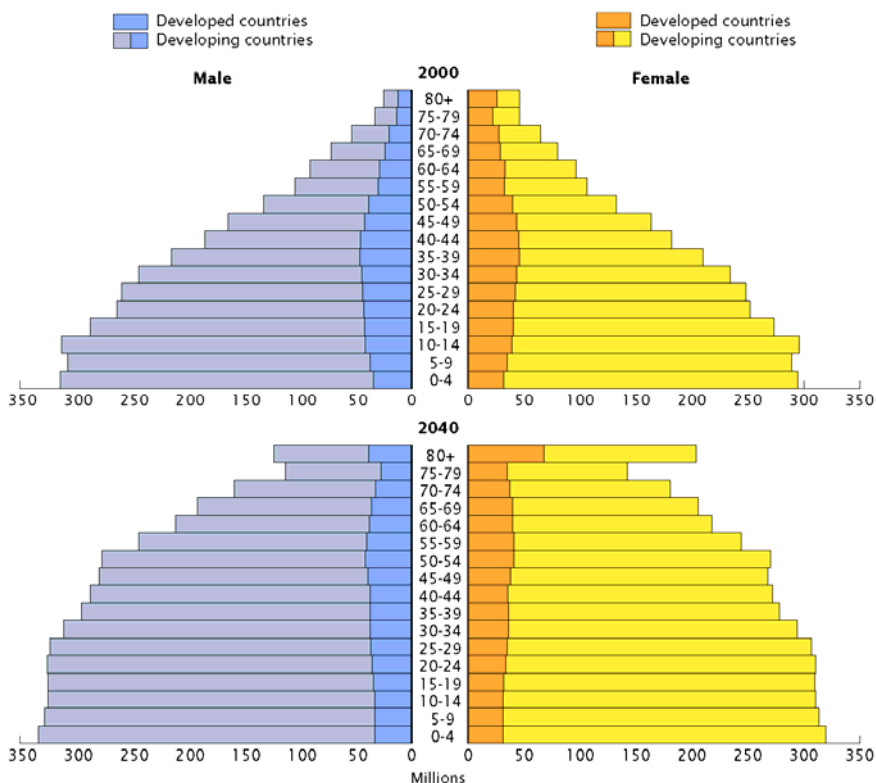


Fig. 1. Population in developed and developing countries by age and sex, 2000 and 2040 [1]

Falls are one of the leading health problems in the elderly community. They can occur in home as well as in hospitals or in the long-term care institutions [3]. The consequences of falls on elderly population and health care system are vastly. Falls increase risk for serious injuries in which case medical care and

rehabilitation is needed, morbidity, chronic pain, long-term disability, and loss of independence, psychological and social limitations due to institutionalization. Nearly 50% of older adults hospitalized for fall-related injuries are discharged to nursing homes or long-term care facilities [4]. A fall can cause psychological damage even if the person did not suffer a physical injury. Those who fall often experience decrease activities of daily living and self-care due to fear of falling again. This behavior decreases their mobility, balance and fitness and leads to reduced social interactions and increased depression. The mortality rate for falls increases progressively with age. Falls caused 57% of deaths due to injuries among females and 36% of deaths among males, age 65 and older [5].

Majority of falls result from an interaction between multiple long-term and short-term factors in person's environment [6]. Common risk factors include problems with balance and stability, arthritis, muscle weakness, multiple medications therapy, depressive symptoms, cardiac disorders, stroke, impairment in cognition and vision [7,8].

The Centers for Disease Control and Prevention estimates that approximately one third of elder people (65 years of age and older) is likely to fall at least once per year. Older adults are hospitalized for fall-related injuries five times more often than they are for injuries from other causes [9]. Of those who fall, up to 25% suffer severe injuries, such as fracture or a sprain, that make it hard for them to live independently and increase their chances of early death [5].

In 2000, the annual total costs of insurance companies for treating fall-related injuries of people aged 65 and older exceeded \$19 billion. By 2020 the annual cost of fall injuries is expected to reach \$55 billion (in 2007 dollars), not counting costs related to long-term treatment and recovery from a fall injury [9].

There are three levels of fall outcome mitigation:

- primary – fall prevention;
- secondary – early fall detection and fall injury mitigation;
- tertiary – reducing consequences from fall-related injuries.

A number of fall risk reduction and prevention approaches exists, that range from medication interventions, modification of environmental hazards, evaluation and treatment of blood pressure, balance exercises to usage of physical restraints and fall protection systems [7]. Some of these systems are costly and have limited range of protection, but they also did not indicate reduction in number of fatal falls [10].

Regardless of the fact that falls are a common event, they are rather difficult to reliably define. There are various types of falls, but they are usually characterized by larger acceleration compared to person's usual daily activities and the difference in the body orientation before and after the impact.

Detection of a fall possibly leading to injury in timely manner is crucial for providing adequate medical response and care. Present fall detection systems can be categorized [11,12,13] under one of the following groups:

- user activated alarm systems (wireless tags),
- floor vibration-based fall detection,
- wearable sensors (contact sensors and switches, sensors for heart rate and temperature [14], accelerometers, gyroscopes),
- acoustic fall detection,
- visual fall detection.

User activated alarms require person to activate button on body wearable tag with wireless transmitter in the event of a fall. The alarm system installed in the house then calls emergency center and alerts medical personnel. This fall alert principle requires a person to wear the tag all the time and also be conscious and able to manually press the alert button in a case of a fall. Sometimes, the fall can result in loss of consciousness or severe injuries resulting in inability of alarm activation.

Floor vibration-based detection systems are basically passive monitoring systems and are rather unobservable, compared to other fall detection methods. When a human body falls, it impacts with the ground (floor) and generate vibrations that are transmitted throughout the floor. Piezoelectric sensors are used to detect vibration patterns (frequency, duration, amplitude, succession). Some experiments showed that this principle has a high rate of successful fall detection [15].

The acoustic based detection systems detect a fall using audio processing. This method is not precise enough and is used as assistant method to the other fall detection methods.

Another approach is related to visual detection of a fall. Various detectors are used for this method. Camera vision equipment, lasers or infrared sensors are required to be placed in all the rooms where fall detection should be present. The video system captures the images or other movement information and determines whether a fall occurred [16]. This method can be divided into two sub-groups [11]:

- visual detection without posture reconstruction and
- visual detection with posture reconstruction.

The first technique is based on extracting useful data from images or video, but human posture is not reconstructed explicitly. The second approach is based on 3D locations of markers places on a human body. In this way it is possible to reconstruct the locations of markers from video information by applying computer vision techniques and extracting information about the human posture.

The most common method for fall detection is using a tri-axial accelerometers or bi-axial gyroscopes. Accelerometer is a device for measuring acceleration, but is also used to detect free fall and shock, movement, speed and vibration. Using the threshold algorithms while measuring changes in acceleration in each direction, it is possible do detect falls with very high accuracy [17].

Some authors suggest placing sensor at the head to track movement during daily activities and falling or using accelerometers embedded in modern cell phones [12] [13].

Using two or more tri-axial accelerometers and combining them with gyroscopes at different body locations it is possible do recognize several kinds of postures (sitting, standing, etc.) and movements, thereby detecting falls with much better accuracy [18].

2 Accelerometers

Accelerometer is a device for measuring acceleration, but is also used to detect free fall and shock, movement, speed and vibration.

There are many different accelerometers defined by way of working, such as: capacitive, piezoelectric, hall-effect or heat transfer. Most common type of accelerometer, and also used in this application is the one detecting internal capacitor's change of capacitance. The change of capacitance is caused by reducing or expanding the plate distance. One plate is still on accelerometer case, and the other is mobile under the influence of acceleration. In one accelerometer there can be several capacitors serially connected or in bridge. Principle of changing capacitance is shown in Fig. 2. The most essential features of accelerometer are range, sensitivity, number of axis and output signal's independence of supply voltage.

Range is defined with earth's gravity g ($1g = 9.80665 \text{ m/s}^2$), and in today's accelerometers it can be from $\pm 1.5g$ to more than $\pm 100g$. Sensitivity is defined as ratio of output voltage and gravity on sensor. With high sensitivity it is possible to detect very small acceleration fluctuation, small vibration and motion.

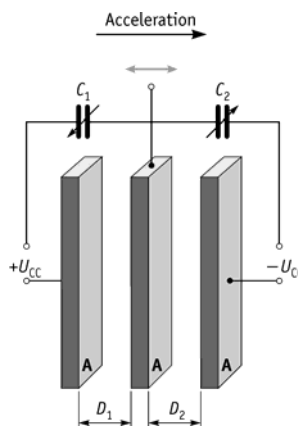


Fig. 2. Change of capacitance in accelerometer.

Accelerometers used in this application are micro electromechanical sensors (MEMS). MEMS is the name used for technology which combine mechanical parts, usually sense, and electronics circuits necessary to drive mechanical parts

and give output signals dependent of sense activity, all integrated in one device. MEMS technology is widely used, from robotics to agriculture. It is small in dimension, and usually low cost.

MEMS accelerometers can be found with 1 axis, 2 axis or 3-axis detection of acceleration. For applications of three-dimensional (3D) positioning it is necessary to use 3-axis accelerometer. In this application MMA7260Q MEMS accelerometer from Freescale™ is used as a measuring device. It is an accelerometer that can change the sensitivity programmatically to enable wide variety of applications. The sensitivity can be changed from ± 1.5 g to ± 6 g in four steps. It is a low cost, low power consumption device, and also low profile device measuring 6 mm x 6 mm x 1.45 mm. These characteristics make it ideal for high accuracy applications to measure vibration, motion, position, and tilt of objects.

For example, this accelerometer is widely used in applications for protection of electro-mechanical parts and devices such as hard disk drives, mobile phones, or laptop computers. It is also used for human monitoring in health care institutions, for fall detection of old and infirm persons [6]. Free fall detection can be perceived by monitoring all three output signals from accelerometer axis X, Y and Z. If they all give values for zero g acceleration then accelerometer is experiencing free fall.

The Freescale™ ZSTAR wireless sensing triple axis board is used in this application. It is a low power, small and portable device (board size is 56 mm x 27 mm) using MMA7260Q triple-axis accelerometer together with 8-bit MC9S08QG8 microcontroller unit and MC13191 wireless ZigBee low power transceiver for sending measurement data to USB stick board. USB stick board has MC13191 transceiver, together with HC908JW32 USB enabled microcontroller (Fig. 3.). The transceiver is working on 2.4 GHz industrial, scientific, and medical (ISM) band. It is ideal for low power, long battery life application such as this. Both boards have integrated 2.4 GHz Loop antennas on board [19].

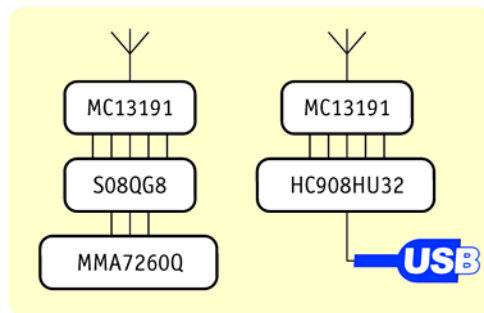


Fig. 3. Wireless ZSTAR accelerometer sensing board

The microcontroller MC9S08QG8 measures the three axis sensor data from the MMA7260QT accelerometer with integrated 8 - channel, 10-bit analog to digital converter, then creates a data packet and sends it with the SMAC (Simple Media Access Controller) to the MC13191 Transceiver. The sensor board needs current in the range of 1 mA, and only 1 μ A in standby mode which is provided from the CR2032 Lithium battery located on the bottom of the board. The simple ZSTAR RF protocol also transfers the calibration data. These data are stored in non-volatile Flash memory and are transferred on request [9]. The sensor board has been evaluated and it has been shown that the distance over which the USB stick will receive the data from sensor board is over 20 meters in buildings. The distance is lower if there are some obstacles, but the boards successfully communicated even in rooms divided by brick walls. The HC908JW32 microcontroller belongs to the family of 8-bit microcontrollers that offer the Universal Serial Bus (USB) full speed functions. The software in the USB stick board converts the data from the transceiver to the USB connection, and places it in USB stick memory. The data are transferred to the PC through the simple serial protocol communication (virtual serial port). The user can communicate with it from LabVIEW using Virtual Instrument Software Architecture (VISA). It is a standard for configuring, programming, and troubleshooting instrumentation systems comprising GPIB, VXI, PXI, Serial, Ethernet, and/or USB interfaces, and it can provide the programming interface between the hardware and development environments such as LabVIEW. The sensor is capable of measuring all three axes approximately 30 times per second providing nearly a real-time response from the Sensor. The measurement data are packed to a special data frame 10 bytes long which is then decoded in the LabVIEW program. The program communicates with the sensor board using simple set of commands. For example, to receive data, command 'V' is used, to establish handshake command 'Z', and to select g-level command 'G'.

The data frame, besides accelerometer data, also includes information on temperature and bandgap voltage, which is used to calculate battery voltage. The accelerometer MMA7260QT provides three separate analog levels for 3-axis. These outputs are ratiometric which means that the output offset voltage and sensitivity will scale linearly with applied supply voltage. This characteristic is essential as it provides system level cancellation of supply induced errors in the analog to digital conversion process [19].

3 Fall Detection Using Two Accelerometers

Setup for accelerometer fall detection (Fig. 4.), consists of the measuring sensor with transmitter, receiver and personal computer for data processing and fall detection.

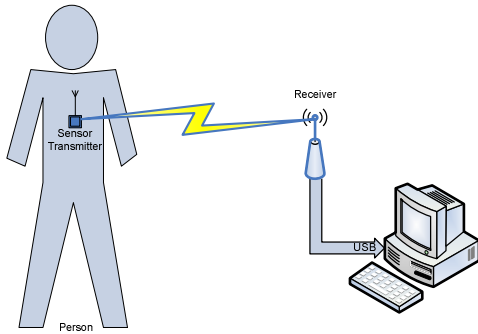


Fig. 4. Wireless ZSTAR accelerometer sensing board

The problem of fall detection is the problem of defining the fall and to make it distinct from various everyday activities. Everyday activities fall under the safe activity and are defined as walking, mastering stairs, lifting, sitting and other activities. Undesirable actions, such as falls, can be difficult to differentiate from the daily activities, especially with sensors that react to changing accelerations.

Figures 5. shows accelerations of accelerometer during walking. Oscillations are periodic and have relatively small magnitude. Red, green and white are X, Y and Z axis of accelerometer. Figure 6. shows the Euclidean norm of measurement on Fig. 5.

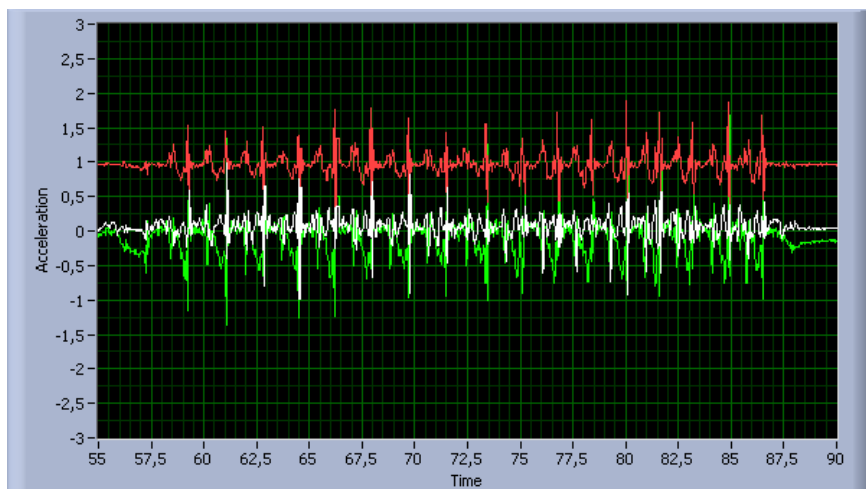


Fig. 5. Walking measured with accelerometer.

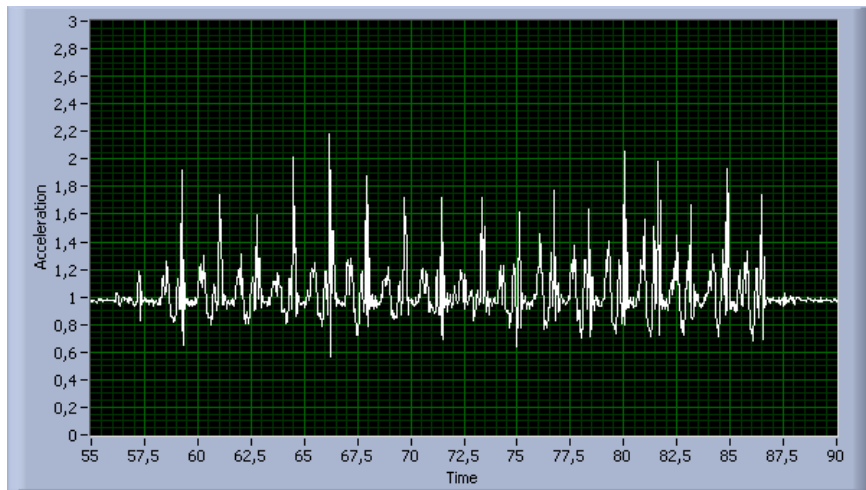


Fig. 6. The length of the vector computed with the Euclidean norm.

The purpose of such system is to detect every fall, because the speed of assistance depends on the system reliability. Everyday activities such as going up or down stairs, and running or jumping which can cause acceleration change equal and even greater than the acceleration recorded in the fall of the body. Because of this fall can not be defined easily and only with the magnitude of measured accelerations.

As stated in the Introduction there are several methods to detect the fall with accelerometers. One method to detect the fall [20] is defined by changing the orientation before and after detecting large fluctuations in measured values (Fig. 7.). Common zone is defined with everyday activities and lying zone is the position when the body falls down.

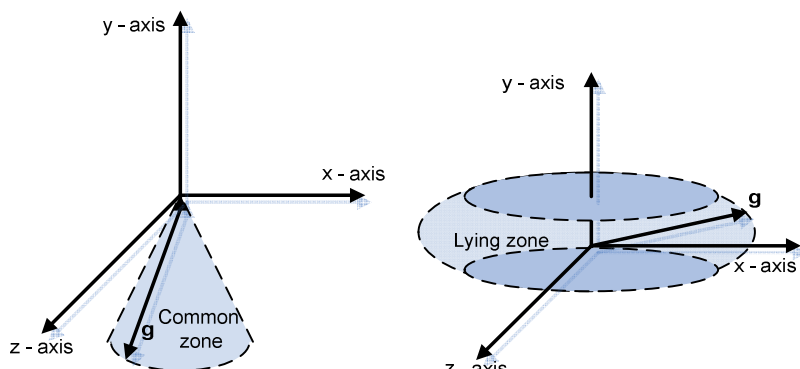


Fig. 7. The position of g before and after impact

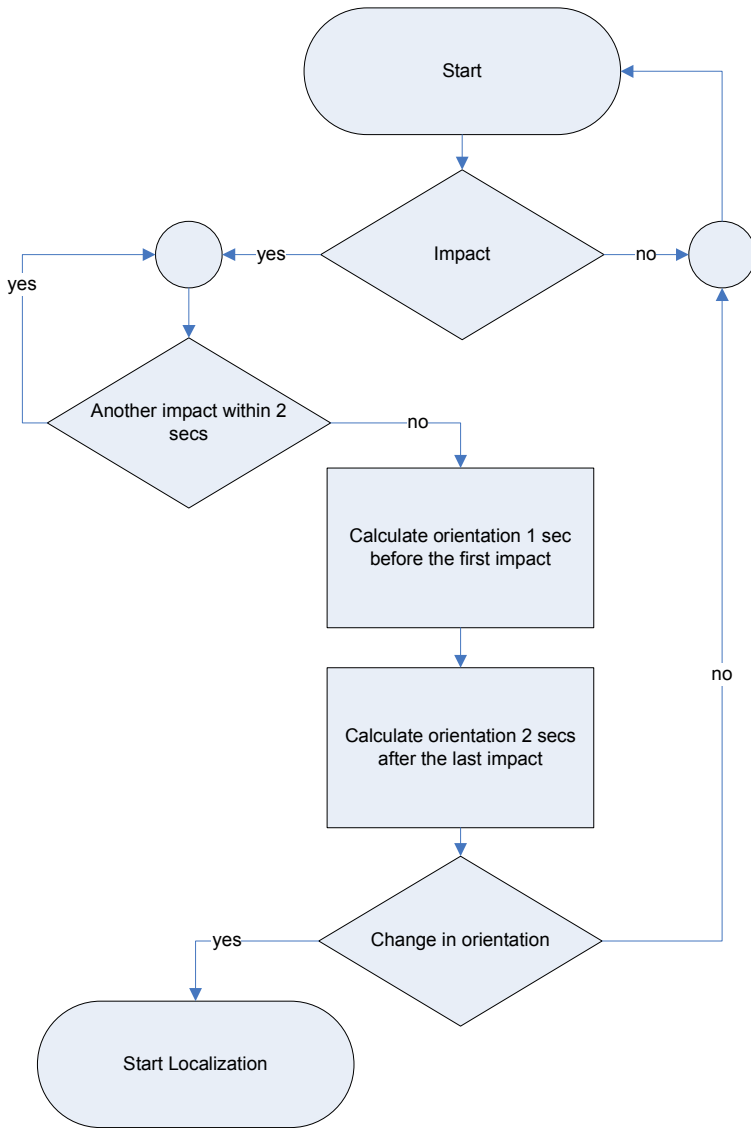


Fig. 8. Fall detection algorithm from [20].

This algorithm (Fig. 8.) detects the impact and then checks for another impact in some defined time after the first impact. If the impact did not happen then we can talk about an isolated impact. However, such an isolated impact can be a part of everyday activities, such as ending of walking or sitting.

The algorithm shown in Fig. 8. and similar methods have difficulty in detecting backward falls. In this case there is a strong fluctuation of acceleration, but if only one accelerometer is mounted on the chest there is no change of orientation. We

can then detect different situations such as a jump or going down stairs, but situations like sitting down or backward fall will be very difficult to detect, and we can only hope that the change of acceleration will be greater than usual. One solution is to install additional accelerometer on the leg thighs (Fig. 10.).

Therefore, the algorithm should be modified to check the orientation of both sensors (Fig. 9.).

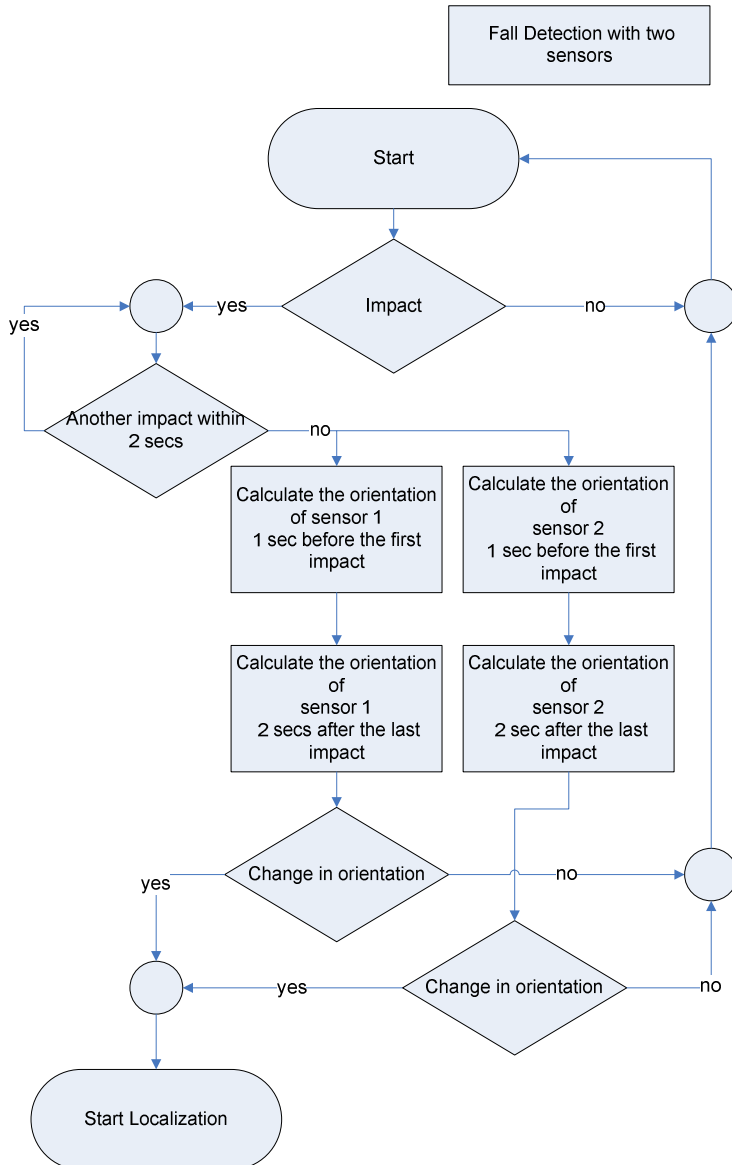


Fig. 9. Algorithm for fall detection with two accelerometers.

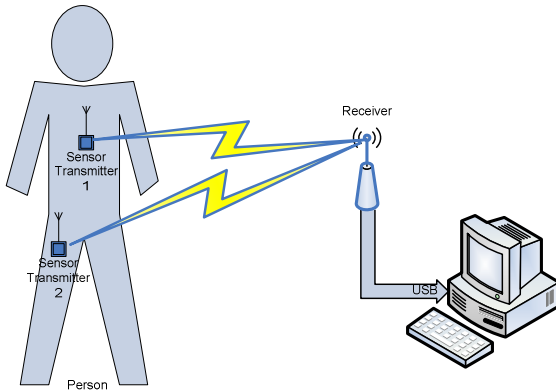


Fig. 10. Improved system for better detection of backward fall

If at least one of the sensors changed its orientation then we can determine that there has been a fall. Orientations in the standing position are shown on Fig. 11.

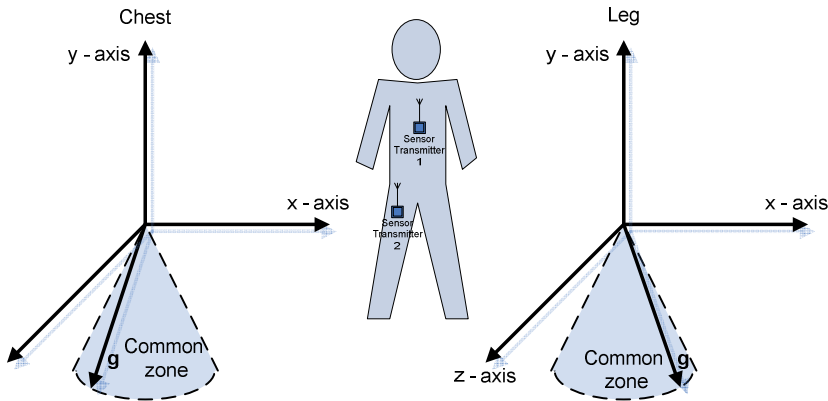


Fig. 11. The body orientation and sensors before impact

Both sensors are worn on the body. After the fall it is possible that only one changes orientation, as shown in Fig. 12. And that is the case in backward fall or fall in to the chair.

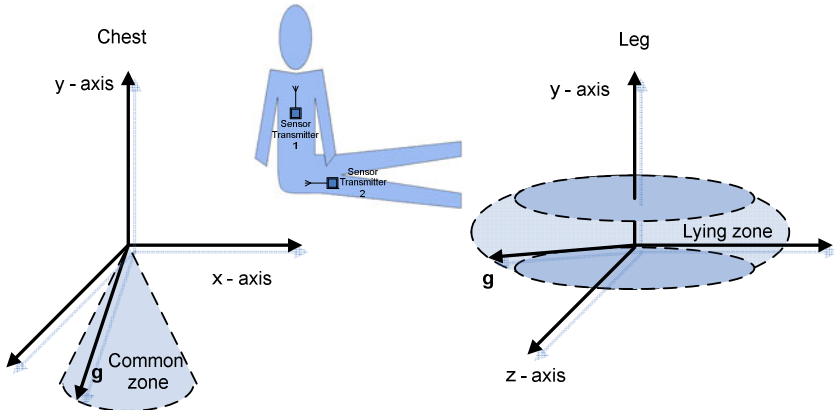


Fig. 12. Body orientation and sensors after impact

Fig. 12. shows the orientation of the body after the fall. We can see that the sensor 1 remained in its normal position, although there has been an impact. In the case with only one sensor on the body, this situation would be characterized as a jump. However, the position of other sensors shows the changed position of the body, and with detecting an isolated impact, we can say with certainty that there was a fall. Real measurements are shown on Figures 13. and 14.

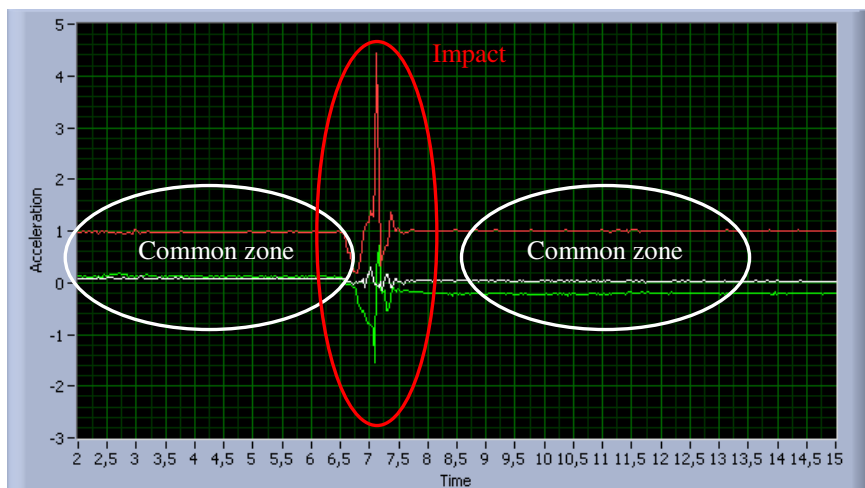


Fig. 13. Backward fall measured with accelerometer mounted on chest.

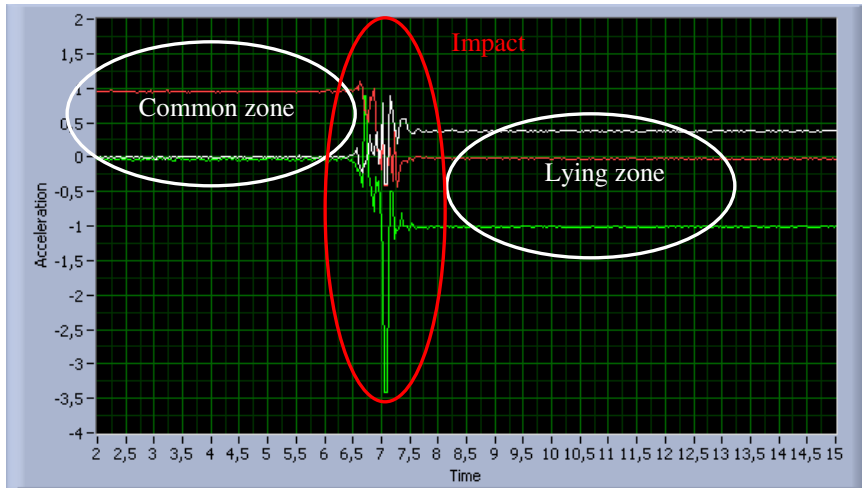


Fig. 14. Backward fall measured with accelerometer mounted on leg.

4 ZSTAR Accelerometer Board Applications for Fall Detection

ZSTAR accelerometer board transmits the so-called raw data (voltages) for each of the three-axis accelerometer, which are proportional to the measured accelerations in the three axes. To calibrate the accelerometer, it is necessary to average acceleration of each axis in two points, namely 1 g when the accelerometer axis is parallel



Fig. 15. ZSTAR calibration application

to the Earth's gravity, and 0 g when accelerometer axis is perpendicular to the earth's gravity. After accelerometer is calibrated in two points for each measured value of raw data, other values can be interpolated to calculate acceleration in units of g. For calibration of accelerometers, a special application (Fig. 15.) has been developed for easy calibration process. The operator first selects the serial COM port to which the ZSTAR accelerometer is connected. Accelerometer is placed in three characteristic mutually perpendicular positions. Each position is confirmed by pressing the button below the picture. After the calibration, the results are saved and stored on the hard disk in order to use them during measurement.

Application for detecting fall is using two ZSTAR boards at the same time and calibration process needs to be repeated for each of the two accelerometers. To run the measurement process, the operator first needs to open SETUP windows for each accelerometer to select COM port, measuring range and calibration data. After that the application is ready to monitor patients (Fig. 16.).

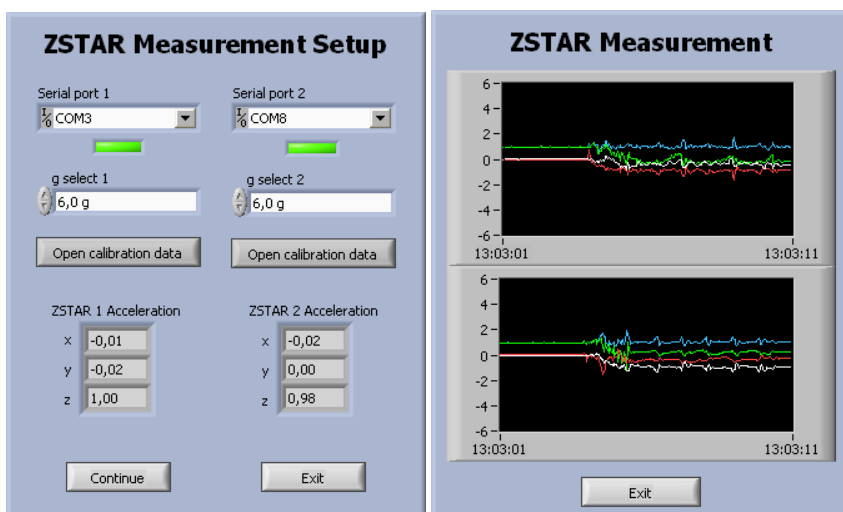


Fig. 16. ZSTAR setup and measurement

5 Conclusion

Triaxial accelerometers can be used for detecting fall of patients. They offer low cost solution, and together with wireless connectivity solutions such as ZigBee provide efficient solution for both patients and medical personnel. This paper describes the use of triaxial accelerometer together with ZigBee transceiver to detect fall of patients. The system, including calibration of accelerometers and measurement procedure is explained in detail. The use of two accelerometers on patient's body as explained in this paper can be used to detect difficult to detect falls such as backward fall and sitting in the chair, which is difficult to accomplish with only one accelerometer.

References

- [1] Kinsella, K., He, W., U.S. Census Bureau: An Aging World, vol. P95/09-1. U.S. Government Printing Office, Washington (2008) (June 2009)
- [2] Statistics in Focus; Ageing characterises the demographic perspectives of the European societies, (72) (August 26, 2008)
- [3] Benceković, Ž.: Analiza indikatora kvalitete zdravstvene njegе na Internoj klinici (2. dio); Hrvatski časopis za javno zdravstvo; Vol 4, Broj 14, 7. travanj (2008)
- [4] Shumway-Cook, A., Ciol, M.A., Hoffman, J., Dudgeon, B.J., Yorkston, K., Chan, L.: Falls in the Medicare Population: Incidence, Associated Factors, and Impact on Health Care. *Physical Therapy* 89(4), 324–332 (2009)
- [5] British Columbia Ministry of Health Planning Office of the Provincial Health Officer, Prevention of Falls and Injuries Among the Elderly: A Special Report From the Office of the Provincial Health Officer (January 2004), <http://www.health.gov.bc.ca/library/publications/year/2004/falls.pdf>
- [6] Tinetti, M.E.: Preventing Falls in Elderly Persons. *The New England Journal of Medicine* 348, 42–49
- [7] Fuller, G.F.: Falls in the Elderly. *American Family Physician* 61, 2159–2168 (2000), <http://www.aafp.org/afp/2000/0401/2159.html>
- [8] Weir, E., Culmer, L.: Fall prevention in the elderly population, *Public Health. Canadian Medical Association* 171(7), 724 (2004), <http://www.cmaj.ca/cgi/reprint/171/7/724.pdf>
- [9] Centers for Disease Control and Prevention, Costs of Falls Among Older Adults, Department of Health and Human Services, Injury Center, August 28 (2008), <http://www.cdc.gov/NCIPC/factsheets/fallcost.htm>
- [10] Wu, G.: Distinguishing fall activities from normal activities by velocity characteristics. *Journal of Biomechanics* 33, 1497–1500 (2000)
- [11] Luštrek, M., Kaluža, B.: Fall Detection and Activity Recognition with Machine Learning. *Informatica* 33, 205–212 (2009)
- [12] Lindemann, U., Hock, A., Stuber, M., Keck, W., Becker, C.: Evaluation of a fall detector based on accelerometers: a pilot study. *Medical & Biological Engineering & Computing* 43, 548–551 (2005)
- [13] Zhang, T., Wang, J., Liu, P., Hou, J.: Fall Detection by Embedding an Accelerometer in Cellphone and Using KFD Algorithm. *IJCSNS International Journal of Computer Science and Network Security* 6(10), 277–284 (2006)
- [14] Yazaki, S., Matsunaga, T.: A Proposal of Abnormal Condition Detection System for Elderly People Using Wireless Wearable Biosensor. In: SICE Annual Conference The University Electro-Communications, Japan, August 20-22, pp. 2234–2238 (2008)
- [15] Alwan, M., Rajendran, P.J., Kell, S., Mack, D., Dalal, S., Wolfe, M., Felder, R.: A Smart and Passive Floor-Vibration Based Fall Detector for Elderly. *Information and Communication Technologies, ICTTA 2006* 1, 1003–1007 (2006)
- [16] Huang, B., Tian, G., Li, X.: A Method for Fast Fall Detection. In: Proceedings of the 7th World Congress on Intelligent Control and Automation, Chongqing, China, June 25 - 27, pp. 3619–3623 (2008)
- [17] Kumar, A., Rahman, F., Lee, T.: Fall Detection Unit for Elderly. In: Proceedings ICBME 2008, vol. 23, pp. 984–986 (2009)

- [18] Barth, A.T., Qiang, L., Gang, Z., Hanson, M.A., Lach, J., Stankovic, J.A.: Accurate, Fast Fall Detection Using Gyroscopes and Accelerometer-Derived Posture Information. In: Sixth International Workshop on Wearable and Implantable Body Sensor Networks, BSN 2009, June 3-5, pp. 138–143 (2009)
- [19] Lajšner, P., Kozub, R.: Wireless Sensing Triple Axis Reference Design, Designer Reference Manual, ZSTARRM, Rev. 3 (January 2007)
- [20] Chen, J., Kwong, K., Chang, D., Luk, J., Bajcsy, R.: Wearable Sensors for Reliable Fall Detection. In: Proceedings of the 2005 IEEE Engineering in Medicine and Biology 27th Annual Conference Shanghai, China, September 1-4, pp. 3551–3554 (2005)

Unobtrusive and Non-invasive Sensing Solutions for On-Line Physiological Parameters Monitoring

Octavian Postolache, Pedro Silva Girão, Eduardo Pinheiro,
and Gabriela Postolache

Instituto de Telecomunicações, Instituto Superior Técnico
Av. Rovisco Pais 1, 1049-001 Lisbon, Portugal
Tel.: +351 21 841 84 54; Fax: +351 21 841 84 72,
eduardo.pinheiro@lx.it.pt

Abstract. Demographic developments, social changes, and the rising costs of health and social care due to people with chronic disease, people with mobility limitations and elderly population make necessary to rethink care delivery. A practical way to improve care and cut healthcare costs is to develop integrated electronic health (e-health) solutions that permit monitoring of physiological parameters and motor activities of the users in their homes.

The unobtrusiveness and non-invasiveness of biomedical measuring devices are key factors on acceptance and satisfaction from the subjects in e-health context. This is justified taking into account that through unobtrusive and non-invasive measurements the data on user's health status may be obtained with or without interactions between subject and biomedical monitoring system.

Unobtrusive cardiac and respiratory activity monitoring remains a challenging task. This chapter is dedicated to a review of unobtrusive biomedical sensing solutions with higher capability in integration on ubiquitous healthcare systems. Elements of signal processing associated with health status measuring channels are included in this chapter.

Keywords: e-health care, unobtrusive biomedical sensors, capacitive coupled ECG, contact ballistocardiography, radar ballistocardiography.

Introduction

The Greek Aesop, around 600 B.C., stated that "Necessity is the mother of invention". Before and since Aesop's time, necessity has indeed often evoked the unique type of problem solving that we humans engage in when helping to meet, through design and special tools, the challenges caused by disability and limitations of ourselves, our families or our community.

Nowadays, in many European countries, demographic developments, social changes, and the rising costs of health and social care due to people with chronic disease, people with mobility limitations and elderly population make necessary to rethink care delivery. A practical way to improve care and cut healthcare costs has been shown to be the integration of telemedicine in hospitals, clinic centres, homes and communities. In the last 20 years, in many European countries, videoconference,

tele-consulting or tele-prescription have shown to improve availability of the right information and to reduce inefficient, costly and sometimes the wrong care of the patients. However, only a few projects have already a more comprehensive approach like the implementation of electronic health records (EHR) in a unobtrusive and ubiquitous context. This is important because this technology can increase the efficiency of disease prevention, prediction of disease and personalization of healthcare, which enables improvements to the quality of health care while driving down costs and benefits both the people and the health system. We focus the present review on electrocardiogram (ECG) monitoring based on the usage of dry and capacitive coupled electrodes, and contact and contactless ballistocardiography as technique and methods that allow non-invasive, non-obtrusive, remote, in real-time and at a lower price diagnosis and monitoring of the cardiac and respiratory function and autonomic nervous system balance.

1 Electronic Health Records Based on ECG/BCG for Homeostasis and Allostasis Monitoring in e-Health Context

It is widely agreed (e.g. by the World Health Organisation - WHO and the European Commission - EC) that is necessary a shifting away from today's reactive model of care to an integrated approach that enables, encourages and supports individuals and communities to continuously monitor and manage their health from the comfort of their homes, work place, etc., to ensure a smooth health examination, without unnecessarily repeated examination or search for relevant information, avoiding costly acute intervention. The European Commission was one of the first international funding agencies to support research and development (R&D) in e-health (e-health is defined as healthcare practice which is supported by electronic processes and communication), investing more than €1 billion in e-health research projects during the last 20 years [1]. In the High Level e-health Conference 2006 in Malaga, Spain, it was emphasized that "*Europe can benefit from e-health that focuses on ensuring better: prevention disease, prediction of disease, personalization of healthcare, participation of Europe's citizens in their own healthcare improvement, increased patient safety throughout all stages of the healthcare process, productivity and performance of Europe's healthcare systems, and of Europe's third healthcare industrial pillar, monitoring of indicators and productions of regular data and reports on health status*" [2].

Since 1993, when Khalid Mahmud, M.D., F.A.C.P., and American TeleCare's founder performed the first implementation of a Tele-Health Care system, an increasing number of projects and implementations in this area are reported. Thus, original devices realization, patenting and production of non-invasive wearable or portable devices with capabilities of warning the patient about disorders in basic bodily functions are reported. It is predicted that successful implementation of the EHR will be at the core of creating effective, safe, and efficient healthcare systems worldwide. However, most initiatives cover yet only certain aspects of healthcare, and various barriers and challenges inducing lack of interoperability prevented widespread implementation of telemedicine. Lack of information or lack of coordination in health systems has serious impact resulting in medical error, injuries or

even loss of life, and staggering economic costs [3,4]. Also, WHO estimates that one in ten patients is affected by some type of preventable medical mistake, under-scoring the importance of Information Technology (IT) as a solution to improve the situation [5]. IT is able to integrate complex information from different sources that can facilitate providers' access to relevant public health data as well as enabling patients to be better involved in personal health decisions. Telemedicine can provide support to health professionals by: making up to date information available on disease prevention and management; cross-border health care purchasing and provision; creating interaction and organizational links among various health communities, and health impact assessment network realisation (see figure 1).

Telemedicine

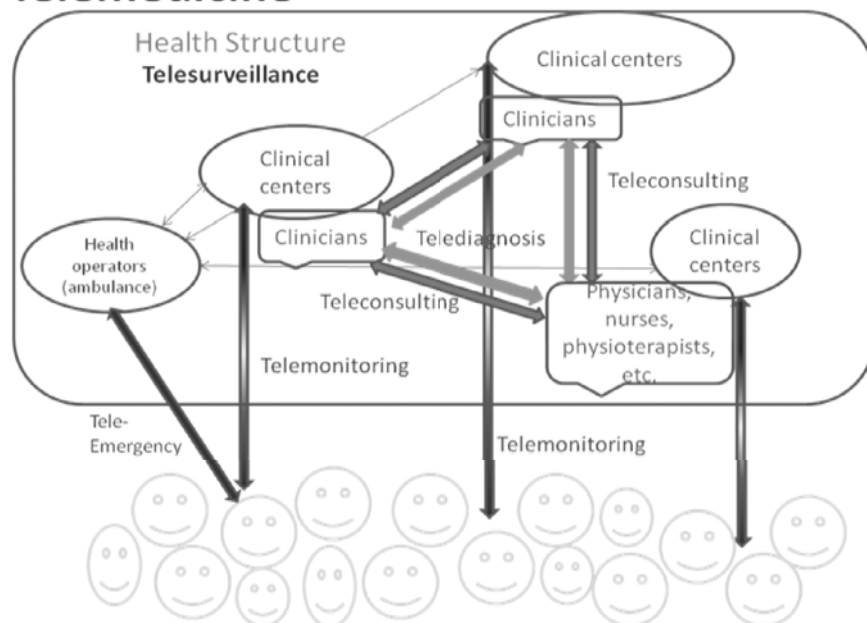


Fig. 1. Health subject healthcare provider interactions in telemedicine

Monitoring requires frequent and regular checks of vital signs to predict homeostasis or near term progression of the disease. Non-invasive monitoring of heart rate, respiratory function, body mass index, blood pressure, glucose, heart rate variability and blood pressure variability associated with autonomic nervous system outflow to the body, give information on subject homeostasis - a process by which physiologic self-regulatory mechanisms maintain steady states in the body through coordinated physiological activity (see figure 2).

The homeostatic mediators discussed by McEwen [6] and McEwen and Wingfield [7] are changes in behaviour, changes in the central nervous system, mediators of immune function, mediators of the hypothalamic-pituitary-adrenal axis,

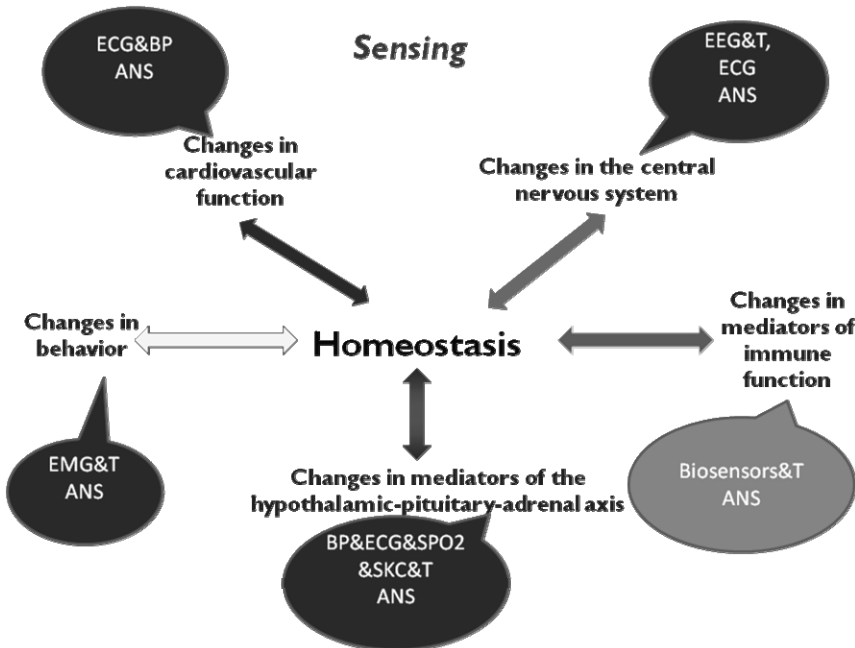


Fig. 2. Homeostasis and sensing block diagram

and changes in cardiovascular function. Usually, only few and simple parameters, like heart rate or respiratory function, can give information on changes in homeostasis, indicating if the subject needs to be admitted at clinical centres or can continue a largely normal life. This is important mainly for subject with chronic diseases, elderly people or other people with elevated disease risk.

Devices that acquire, analyse, and remotely communicate relevant information on vitals signals, as heart rate, respiratory rate, blood pressure, temperature, and oxygen saturation, were implemented and introduced in various EHR contexts. These devices acquired a variety of physiological measurements via several on-body sensors, mainly related with the cardiac function (as electrodes for electrocardiography, ballistocardiography, pulse rate sensors, etc.) and process and fuse those measurements in order to derive an estimation of the patient's overall health condition. Communication modules give access to health information for patients, clinical assistants like nurses, general physicians or specialists. The information provided by the e-Health portal can be subsequently converted into medical actions.

In the future, EHR systems can be leveraged to create knowledge. All of the information available in a patient's electronic record captured over a lifetime, together with images and test results, genetic history and analysis of medical knowledge data bases can help to predict allostatic load and to prevent a disease. Allostasis, literally “maintaining stability through change” [8] characterize the physiological reactions developed in an adaptive manner in order to maintain

homeostasis, when the body is challenged by unexpected or threatening events. In contrast with homeostatic systems characterized by the need of tight physiological regulation to maintain survival of the organism (e.g., body temperature, pH balance, or oxygen tension), allostatic systems are those where normal resting points vary according to dynamic biological processes whose variability is a healthy adaptive mechanism to environmental challenge (e.g., heart rate). The allostatic state allows the organism to cope physiologically, behaviourally, and emotionally with specific environmental challenges while maintaining regulatory control of the homeostatic systems that operate within narrow parameters [7]. These dynamics include the structure and function of the hypothalamo-pituitary-adrenal (HPA) axis, the autonomic nervous system (ANS), and the immunity system. The construct of allostasis was first developed in an effort to understand the physiological basis for disparate patterns of morbidity and mortality unexplained by socioeconomic status, access issues, or lifestyle choices [8]. The concept has great promise in understanding some human diseases and is currently a leading model for understanding the etiology of diseases such as diabetes, obesity, and neurological diseases [9,10].

Physiologic health appears nowadays to be a function of both classical concepts of homeostasis and a combination of specific feedback mechanisms and spontaneous properties of complex interconnected networks and nonlinear interactions that characterized allostasis. To obtain information on allostasis and to prevent disease before it occurs or at an early stage, different subject assessment methods can be used. Thus, are mentioned: long term monitoring of heart rate variability (HRV), through the usage of electrocardiography or ballistocardiography, long term monitoring of blood pressure variability (BPV), cardiovascular response to stress, and long term monitoring of body temperature. Even if a disease is already installed, data from the above mentioned methods can be used to assure an optimal treatment with better outcome.

Combining all available information from multiple diagnostic modalities, the most accurate diagnosis and the selection of the most efficient therapy for every individual patient can be done. This will contribute to achieve the goals of cost-effectiveness and quality outcomes.

2 Non-contact Electrocardiography

Electrocardiography (ECG) is one of the most important diagnostic methods of cardiac activity. In order to obtain the ECG specific signals, different kind of sensors are used. In the classical way, for ECG measurement, a set of conductive electrodes are directly attached to the skin. Thus, surface potentials due to heart currents are measured in different locations of the body, common systems providing the possibility to measure the potentials in 3, 12 or even 64 locations. Using extended number of electrodes, the potential variations caused by cardiac activity is recorded and can be used to construct a body-surface potential map (BSPM). The quality of BSPM depends on the number of ECG electrodes and on the quality of the galvanic contact. The usage of the galvanic electrodes method requires the necessity of maintaining low-resistance contact with the skin, which is

obtained using high-conductivity electrolytic paste. The method is characterized by high repeatability and accuracy. However, it is known in clinical studies as a stress inducing method caused by the wet electrodes fixed on the body, which becomes critical when the number of electrodes is increased to obtain the BSPM. In order to reduce the mechanical and biomedical stress for the dermal tissue and the psychological stress and to facilitate high acceptance by the patients and reliable results, non-intrusive electrodes (e.g., dry conductive electrodes based on electronic textile (e-textiles) [11][12] and exclusively capacitive coupling electrodes can be used and represent promising solutions [13][14]. Long term monitoring of cardiac activity can be implemented with this kind of solutions.

2.1 Unobtrusive Solution for Biopotential Measurement Using Dry Electrodes with Conductive Contact

Dry electrodes use an impedance transformation at the sensing site via active electronics and present a metallic or an e-textile surface in direct contact with parts of the body of the subject under test. This electrodes impose resistive and capacitive coupling to the local skin potential [15][16]. The commercial electrodes use electrolytes [17] that establish a reliable dermal tissue-electrode connection characterized by low values of resistance without significant variation of this parameter during long term monitoring processes. Dry electrodes have the advantage of unobtrusive measurement over the commercial wet electrodes.

ECG dry electrodes latest developments are strongly related to the conductive material evolution and the necessity to develop wearable and unobtrusive solutions for physiological signals continuous monitoring. In the 1990s, different e-textiles were developed and systems based on the usage of carbon fibres from Toray [18] or based on metal plated fibres from Electrofibers Technologies [19] reached the market of ECG recording. Ishijima [20] developed a system characterized by textile electrodes for in bed monitoring ECG. The electrodes in this case were placed on a pillow (negative pole) and on the lower part of the bed sheet (positive pole) where the feet are positioned (Figure 3). In order to assure the shielding against 50Hz line frequency interference a conductive plate is placed on the bottom of the bed sheet.

Taking into account the capacitive and resistive coupling corresponding to the usage of dry electrodes, the conditioning circuit requires the use of a high impedance instrumentation amplifier. A good choice for the instrumentation amplifier can be an OPA124 characterized by an input differential impedance of $10^{13} \Omega$ and a common mode rejection ration (CMRR) of 100dB.

Various wearable solutions for vital signs monitoring have been described and commercialized in the last years. Some examples: SmartLife (UK, 2003); ECG shirt GEOView and FALKE KG (Germany, 2004); VTAM (France, 2004); WEALTHY (FP6 EU project); ECG Shirt (Finland, 2006); Sensatex (USA, 2007); MyHeart (FP6 EU project); Philips ECG body vest (2009); SMART VEST (India, 2008), Proetex (FP5 EU project, 2008); VitalJacket, Biodevices (Portugal, 2009); Smartex ECG (Italy, 2009); ECG, EMG, breathing rate and muscular activity (Swedish hi-tech clothing, 2009). In the ECG and electromiogram (EMG) monitoring system based on dry electrodes embedded in the t-shirt [21], the ECG was

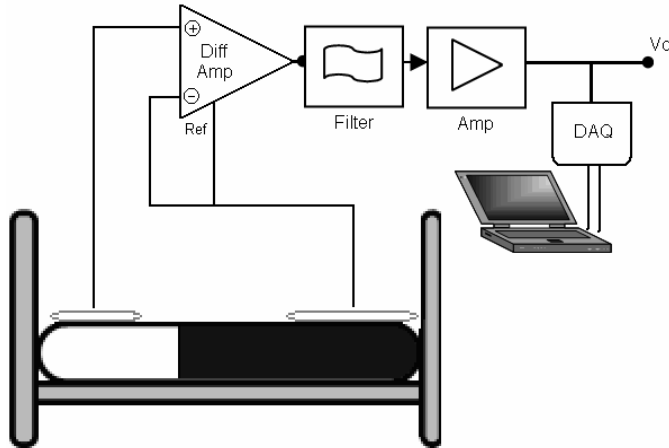


Fig. 3. ECG recording system architecture based on e-textiles electrodes

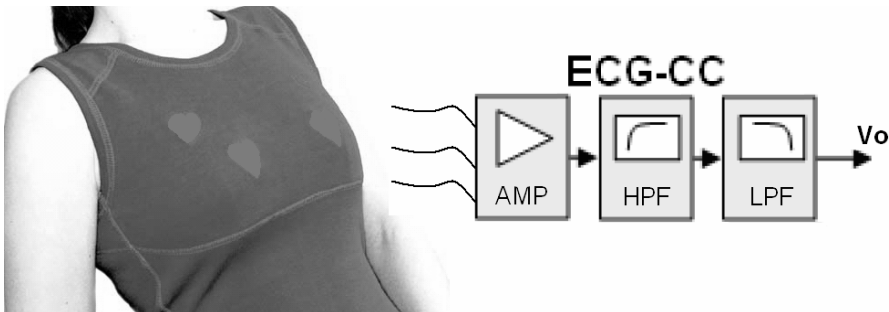


Fig. 4. Example of a prototype T-shirt housing smart textile based ECG electrodes (ECG-CC – electrocardiogram conditioning circuit, AMP- amplifier, HPF – high pass filter, LPF - low pass filter).

measured bipolarly using textile electrodes that were located on the chest. The smart t-shirt allows EMG acquisition capabilities using additional dry electrodes (Roessingh Research and Development dry electrodes). The t-shirt developed by the Swedish team and a basic signal conditioning block diagram are shown in Figure 4.

Wearable solutions, characterized by high degree of mobility, continue to have some drawbacks regarding the discomfort that can cause when are daily used. The usage of washing machine to clean the used T-shirt can change the characteristics of the conductive textile fibre and in this case the conditioning system associated to the ECG dry electrodes will require adjustments or even major changes. Referring to the possibility of using the ECG dry electrodes based on e-textile embedded in furniture (e.g. chairs or bed) as part of ubiquitous healthcare systems [22] that is not a proper solution taking into account the inexistence of direct contact

between the subject skin and the electrodes. Systems based on contactless capacitive-coupled electrodes (CCEs) are the best solution in this case and different authors report good results of CCE usage in ubiquitous home healthcare context [23] and also as wearable mobile solutions [21,24].

2.2 Unobtrusive Solution for Bio-potential Measurement Using Capacitive Electrodes

Capacitive ECG sensing is based on the use of an insulated electrode, which is an electrode without direct contact to the body assuring the possibility to use this kind of electrodes as part of wearable solutions for vital signal monitoring but also to be embedded in furniture objects such as bed or chairs for fully unobtrusive solutions. Very adequate for long-term monitoring the capacitive electrodes are affected by the variation of the distances between electrodes and the body reflected on capacitive electrode impedance variations.

The idea of ECG without conductive contact or with capacitive coupling, also named indirect or contactless, dates back to the end of the 1960s and first years of the 1970s. Lopez et. al. [25] proposed an insulated anodized electrode based on the usage of a 2N3022 N channel MOSFET transistor. The obtained ECG signal amplitude was comparable with the ECG obtained with conventional wet electrodes. Later, Potter [26] developed a double insulated electrodes unit with shield that was applied for EMG signal monitoring. New implementations regarding the capacitive active electrodes for biomedical applications will be reported in the 80s and 90s. In this architectures, the MOSFET transistor was replaced by high impedance low noise operational amplifiers (e.g. MAX405) used in follower schemes where a high value resistor ($R_B > 10^9 \Omega$) is used for the bias current of the operational amplifier [27]. The diagram of the ECG capacitive coupling active electrode is presented in Figure 5. In the equivalent electrical scheme of the capacitive-coupled ECG electrodes R_A and C_A represent the resistive and capacitive components of the high impedance operational amplifier, R_B represents the bias resistor that assures a path for the amplifier's input bias current, C_{Shield} is the shield capacitance, i.e., the capacitance between the electrode face and the circuit ground, and C_s is the capacitance between the skin and non contact electrode. This capacitance is a component of a very high impedance ($> 10^9 \Omega$) of non conductive contact electrodes. For ECG wet conductive contact electrodes the associated impedance is of the order of 10Ω .

The dependence of active capacitive-coupled electrode (CCE) voltage output V_o versus electrical potential V_{ECG} from a heart is expressed by:

$$V_o(\omega) = \frac{C_s \cdot R_B \cdot j\omega}{1 + (C_A + C_{\text{shield}} + C_s)R_B \cdot j\omega} \cdot V_{ECG}(\omega) \quad (1)$$

which underlines the high influence of C_s and R_B on the body potential reading. Several results concerning V_o versus C_s for different high input impedance operational amplifiers are presented in Figure 6.

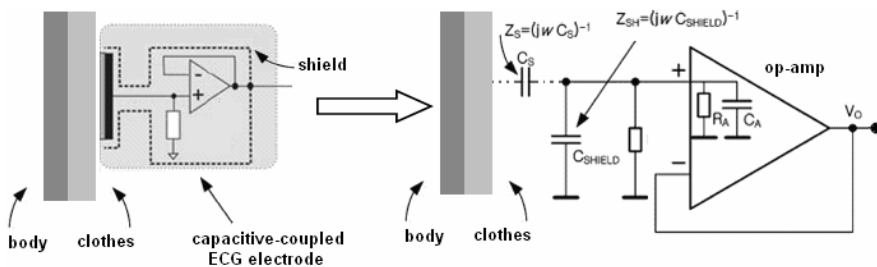


Fig. 5. Block diagram of capacity coupled ECG active electrode

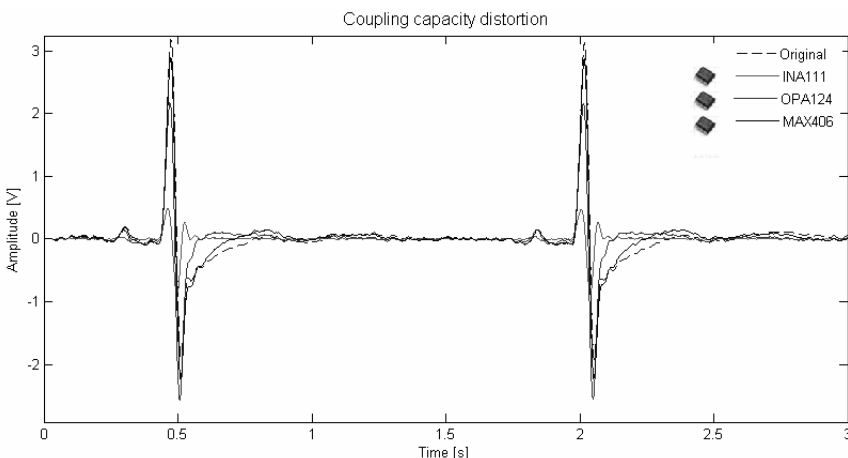


Fig. 6. The evolution of V_o versus C_S variations for different high input impedance operational amplifiers

Capacitive-coupled ECG electrodes became nowadays not only a research object but also useful devices in the implementation of unobtrusive systems for cardiac activity assessment in contact less wearable versions [28] or in pervasive versions [29]. Quasar [24] is one of manufacturers that provide small-size wearable capacitive-coupled electrodes for cardiac activity (Fig. ECG6). The results published by Quasar relative to a young subject with no cardiac problems and reproduced in figure 7, show that the electrocardiogram signal ($V_{CCE}(t)$) obtained using capacitive-coupled electrodes is basically the same of the one obtained using wet electrodes (V_{WE}).

An original implementation of capacitive-coupled electrodes is reported by Nakamura [30]; the electrodes are embedded in a wrist band, the signal conditioning including a voltage follower based on TL071 from Texas Instruments connected to copper plate and copper-polyimide layered sheet electrodes.

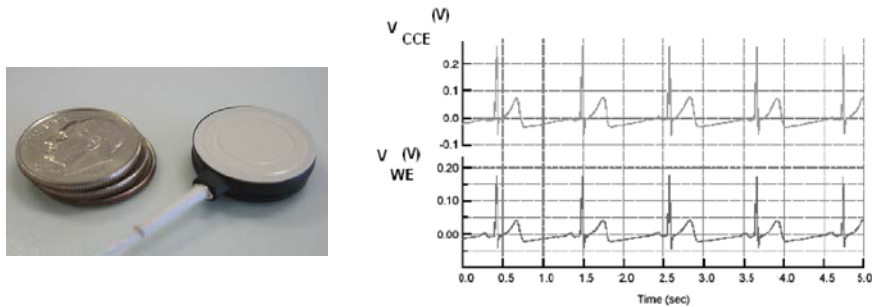


Fig. 7. Quasar electrodes and signals

A non-contact ECG measurement system for pervasive cardiac activity monitoring using CCE embedded in the bed was presented by Da-Huan Zhu et. al [29]. The system architecture includes two contactless electrodes and a ground sheet. The implemented solution includes two primary conditioning circuits expressed by voltage followers based on OPA2277 and bias resistors concentrated in a signal conditioning and acquisition unit connected to the e-textile electrodes by wires whose length highly influences the signal-to-noise ratio (SNR) value. In order to increase the SNR, analogue signal processing is performed before signal acquisition. The corresponding circuit includes active high pass, low pass and notch filters that are connected to the output of the instrumentation. The high pass filter performs the baseline wandering removal (0.05Hz cut-off frequency) while the low pass filter is used to extract ECG relevant information removing the noise generated by muscle contraction (120Hz cut-off frequency). The notch filter is used for 50Hz power supply noise removal [31].

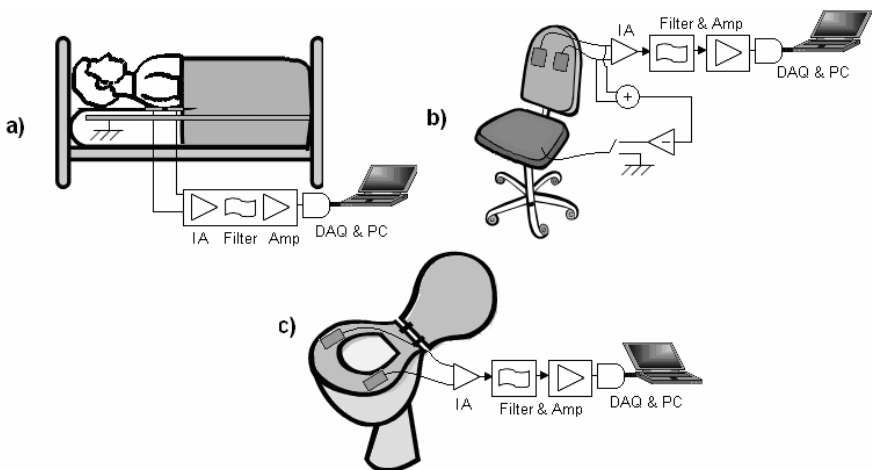


Fig. 8. Unobtrusive ECG monitoring based on CCE a) “in bed” version, b) “in chair version”, c) “in toilet seat version”

ECG monitoring using capacitive-coupled electrodes embedded in house daily used objects is specially associated with chairs, wheelchairs, beds and even toilet seats [32] (Figure 8).

An interesting implementation of CCE is reported by Kim [33]. He proposes an ECG recording system on a toilet seat. Using a proper active grounding [34] and ECG specific analogue filters, the obtained ECG signal can be easily used to extract the heart rate through the R-wave usage. However, this implementation shows limitations regarding the Q-R-S-T complex identification. Regarding the active grounding it reduces the common mode noise in the body by negative feedback of sum of the signals coming from insulated electrodes (Figure 9).

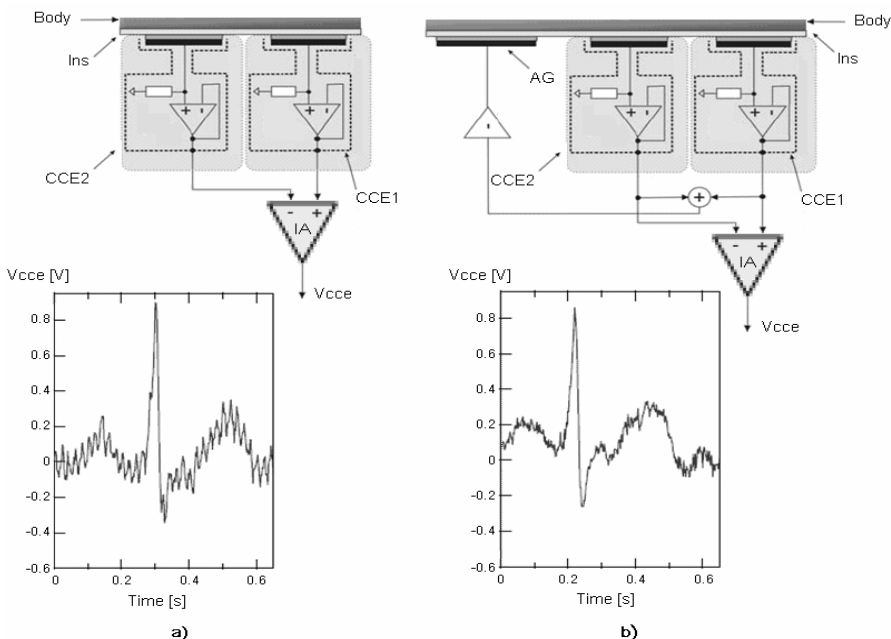


Fig. 9. The block diagram of ECG measurement using the capacitive-coupled electrodes (CCE1 & CCE2) a) non-active grounded scheme, b) active grounded scheme

Figure 9 represents the advantage of active ground usage for noise removal. An important drawback of ECG long term monitoring using CCE is related to the values of coupling capacitances of the active electrodes imposed by the distance between the subject body and the metallic part of the electrodes. If the distances between the electrodes and subject body surface are the same, the transfer functions associated with capacitive coupled ECG measuring channels are the same and no distortion is introduced in the ECG signal. In practical implementations of the ECG monitoring using CCEs embedded in furniture factors such as the subject motion or the wrong mounting of CCEs will conduct to mismatches of the coupling capacities C_{S1} and C_{S2} distorting the acquired ECG signal.

Another inconvenient of subject movement is the triboelectric charge generation [35], which will also introduce differences between the electrical potentials sensed by the electrodes.

The work developed by the authors in the area of capacitive coupled active electrodes for ECG recording shows that good results can be obtained for and embedded active electrodes in a wheelchair (Figure 10.a). The ECG signal acquired with 1kS/s sampling frequency is presented in Figure 10.b.

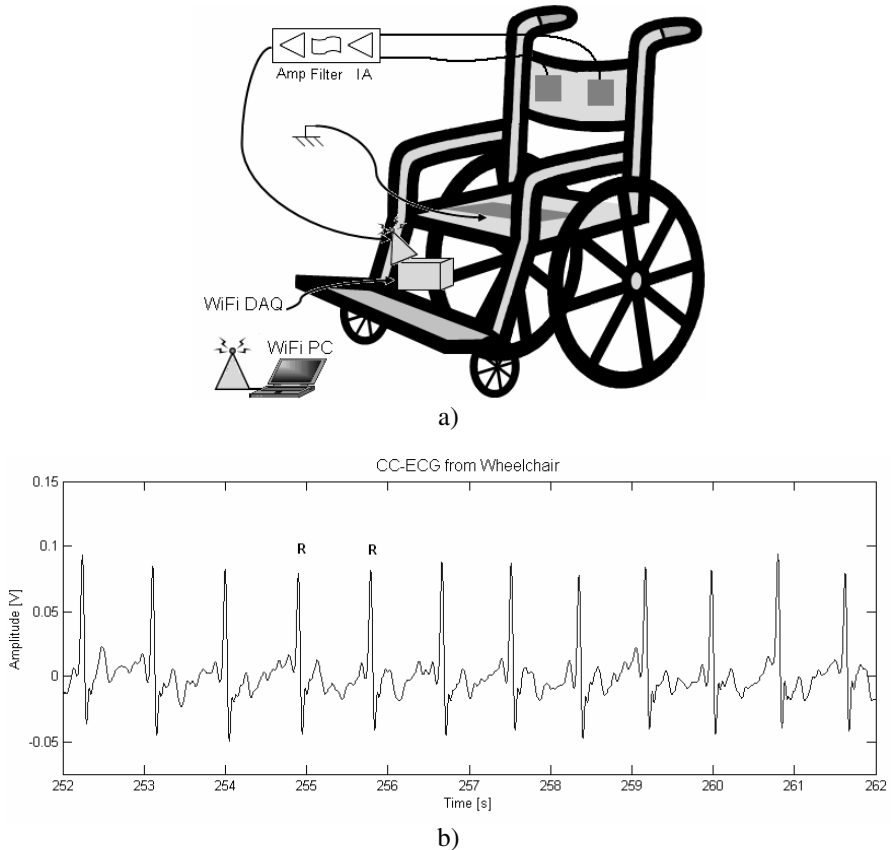


Fig. 10. A non-conductive ECG long term monitoring system embedded in a wheelchair: a) system architecture b) 10s acquired ECG signal

Applying a peak detection procedure, the subject tachogram expressed by the time sequence of ECG R-R time intervals can be obtained and used to estimate the heart rate variability (HRV) of the monitored subject. Several elements concerning heart rate variability concepts and the work of the authors on HRV , that can be considered as output of the virtual measurement channel associated with unobtrusive cardiac assessment systems are following presented.

The term heart rate variability in most instances refers solely to the variability of cardiac cycles, the beat-to-beat variation that has an intrinsic oscillation, and not the variability of heart rate that is being measured, as the term suggests. It reflects a complex interplay between ionic membrane currents responsible for sinus node automaticity, the regulatory influences of the autonomic nervous system, respiration, circadian rhythm, humoral control, and genetic expression [36].

Because of the nonlinear inverse relationship between heart rate and cardiac periods, some complex measurements of HRV derived from cardiac cycles signals (tacogram) do not parallel those derived from heart rate samples.

The first study concerning variability of cardiac cycles was published more than four decades ago [37]. The number of published studies dealing with measurement, physiological interpretation, and clinical use of heart rate variability is increasing all the time (search result in PubMED show a number of 81 studies published in 1980, 246 in 1990, 846 in 2000, 2293 in 2008, and 2757 in 2009). Heart rate variability tool for diagnosis and prediction of health status is still expanding and of interest to a number of disciplines beyond physiology, bioengineering or cardiology.

Various approaches of spectral analysis of HRV have increased the understanding of the modulator effect of neural mechanisms on the heart sinus node. The Fourier Transform has been the most used algorithm for analysis of sympathetic and parasympathetic autonomic control of cardiac function. In human trials, in traditional spectral calculation of recorded 5 minute ECG signals, were identified three main spectral components, classified as; very low frequency (VLF) ranging from 0.003 to 0.004 Hz, low frequency (LF) ranging from 0.04 to 0.15 Hz and high frequency (HF) ranging from 0.15 to 0.4 Hz components. In addition, for long time recording of R-R intervals (24 hours or 48 hours) an ultra low frequency (ULF) was defined as spectral components with frequencies less than 0.003 Hz. The relative contribution of vagal and sympathetic modulation of the heart rate was attributed to the distribution of spectral power in these bands [38].

However, the Fourier transform is suitable for frequency analysis of stationary signals. The limitations of power spectral analysis of heart signal in Fourier domain include non-stationarity and the presence of singular-type of oscillation within the sequence.

To measure time-frequency contents in transient signal one tends to use linear time-frequency transforms that correlate the signal with a family of waveforms that are well concentrated in time and in frequency. Windowed Fourier Transform (WFT) and wavelet transforms (WT) are two important classes of local time-frequency decompositions. In Windowed Fourier Transform, the signal is divided into small enough segments, where these segments of the signals can be assumed to be stationary. For this purpose, a window function is chosen. The width of this window must be equal to the segment of the signal where its stationarity is valid. The problem with the Windowed Fourier transform has something to do with the width of the window function that is used. What gives the perfect frequency resolution in the FT is the fact that the window used in the FT is its kernel, which lasts at all times from minus infinity to plus infinity. In windowed Fourier transform the window is of finite length, thus it covers only a portion of the signal, which causes

the frequency resolution to get poorer, that is, we no longer know the exact frequency components that exists in the signal, but we only know a band of frequencies that exist. The narrower we make the window, the better the time resolution, and better the assumption of stationarity, but poorer the frequency resolution. In addition, the finite data set makes it necessary to make assumption. Sometimes not realistic, about the data outside the recording window: commonly, they are considered to be zero. Different windows, that smoothly connect the side samples to zero, are most often used in order to solve this problem, but they introduce a reduction in frequency resolution. The Wavelet Transform can detect and characterize transients with a zooming procedure across scales. Singularities are also detected by following across scale the local maxima of the Wavelet Transform.

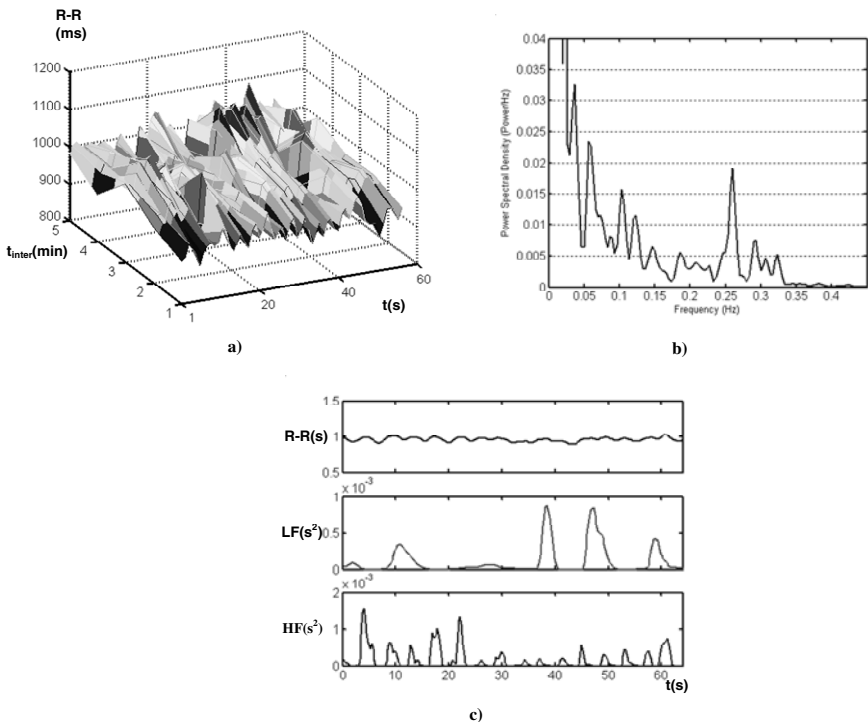


Fig. 11. Figure. Geometrical and spectral representation of R-R signal. a). R-R signal obtained from 5 minute acquired ECG represented in order to observe the R-R variation in each 60s. b). FFT representation of 60s R-R signal. The spectral component associated with sympathetic branches of autonomic nervous system can be observed LF:0.05-0.15 Hz band. High frequency component HF:0.15-03Hz correspond to parasympathetic branches of autonomic nervous system control of heart. c). DWT decomposition of 60s R-R signal. Dynamic changes in low frequency (detail d6 of daubechies discrete wavelet transform decomposition) and high frequency component (detail d4 and d5) of beat-to-beat oscillation can be better observed in this type of time-frequency representation.

The zooming capability of the wavelet transform not only locates isolated singular events, but can also characterize more complex multifractal signal having non-isolated singularities.

The authors applied Daubechies wavelets [39] to characterize low frequency and high frequency components presented in beat-to-beat signal extracted from ECG or from BCG devices embedded on chairs or wheelchairs.

In figure 11 are represented the time domain, frequency domain and time-frequency beat-to-beat variability recorded on a healthy subject sited on a chair. More information on dynamic of autonomic nervous system control on the heart associated with low frequency oscillation (LF; 0.05-0.15 Hz) and high frequency component (HF; 0.15-0.5 Hz) represented in detail 6 and respectively detail 4 and 5 of db4 decomposition is obtained using wavelet transform decomposition. [40].

3 Ballistocardiography: Historical Note: An Appraisal of Technical and Physiological Principles

Ballistocardiography (BCG) is a technique used to measures small movements of the body, imparted by the ballistic forces (recoil and impact) associated with cardiac contraction and ejection of blood and with the deceleration of blood flow through the large vessels informing about the overall performance of the circulatory system[41-43]. The term ballistocardiography comes from the Greek, $\betaάλλω$ (*ballō*) “throw” + $\kappaρδία$ (*kardia*) “heart” + $\gammaραφία$ (*graphia*) “description”).

As a physiological parameter measurement method, ballistocardiography was first introduced in the 19th century and is one of the first clinical methods for non-invasive and non-obtrusive evaluation of the cardiac activity. The first experimental work in the area is reported by Gordon in 1877 [44]. Later, in the first decades of 20th century, important results are reported by Henderson [45] and Isaac Starr [46-48] that also develops the BCG terminology. Isaac Star is considered by the Cardiovascular System Dynamics Society, USA, the founder of the modern ballistocardiography, taking into account that, in 1936, he built a new type of bed BCG measurement device that allowed accurate recordings of the BCG waves.

The development of BCG measuring instruments was always a big challenge considering the low amplitude of the mechanical oscillations [49] caused by cardiac activity comparing with the mechanical oscillations associated with subject breath and the amplitudes of the artefacts related to the subject motion during the BCG recording [50][51]. The first architectures were represented by suspended rigid platforms using elastic ropes, a mechanical system recording the small oscillations of the human body lying on a bed (Figure 12).

Sophisticated mechanical devices were developed during the 1940s, one of them being reported by Nickelson et. al [52]. Using the mechanical device presented in Figure 12, an accurate BCG signal was recorded (Figure 13).

The 1950s and 1960s are characterized by important developments in the area of BCG devices especially regarding the BCG recording. However, compared with electrocardiography (ECG) that became a method well studied and frequently applied in the physiological phenomena context, BCG research teams did not

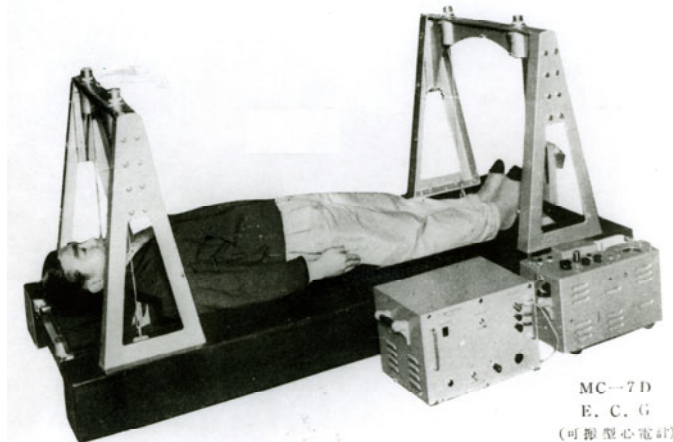


Fig. 12. Ballistocardiograph device MB-1, produced by Nihon Kohden in 1953. Image courtesy of Nihon Kohden

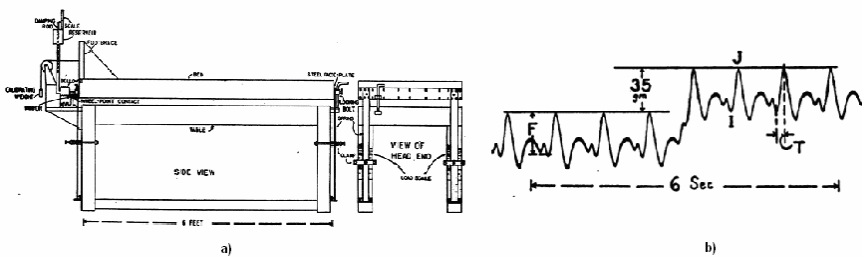


Fig. 13. Ballistocardiography system and signal

obtain important results regarding the interpretation of the BCG waves and the correlation between the BCG profiles and the cardiac diseases.

Even in the periods with substantial developments of BCG devices, clinical applications of the BCG were reduced. This fact was mainly related to the complexity of the sensing and recording systems and to the difficulties to analyse the complex BCG waveform. Then, the BCG was maintained in competition with the ECG assuming a position in the cardiac assessment of the patient. Later, in 1970s, the usage of BCG decreased, even at the research level. After three decades, the developments in sensors and in the area of acquisition and signal processing transformed the BCG from an obsolete method into a promissory one as part of in home fully health monitoring systems or ubiquitous home healthcare systems.

Thus, BCG can be considered nowadays as an alternative to ECG with conductive contact electrodes and even of the ECG based on the capacitive coupled electrodes and of the impedance cardiogram (ICG) [27][53].

As new devices used to sense the cardiac activity through the BCG are mentioned piezoelectric sensors [54], light weight and flexible electromechanical films [55] [56] [57], MEMS (micro-electro-mechanic systems) accelerometers [58][59] and microwave radar [60] [61]. The latest developments in the area of data acquisition devices and systems, of embedded processing using DSP [62] or FPGA [63] and of wireless communications create the possibility to implement robust, accurate and unobtrusive BCG measurement systems [64].

3.1 BCG Classification

Taking into account the mechanical connection between the BCG sensors and the patient body, BCG monitoring systems can be classified in two classes: 1). BCG monitoring system requiring *mechanical connection* between the sensor and subject's body, 2). BCG monitoring system *without mechanical connection* between the sensing unit and human body. A BCG monitoring systems classification diagram is presented in Figure 14.

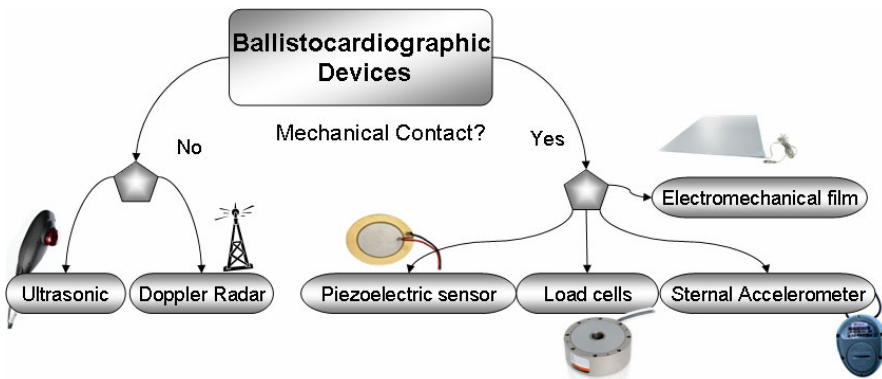


Fig. 14. BCG monitoring system classification diagram

The main ballistocardiographic devices of the mechanical contact class are the piezoelectric sensors, the load cells, the electromechanical film sensors and the accelerometers. Different systems, with implementation of different architecture of ballistocardiography that uses these kind of sensors have been reported in the last decades [54] [58] [60] [65-68].

Regarding the robustness and the number of implementations, BCG monitoring system based on electromechanical film (EMFi) sensors represent the state of the art in this area. The authors have been working in the past years to develop multi-sensor systems based on EMFis for cardiac activity and stress monitoring embedded in chairs and wheelchair, in an intelligent environment context, for home TeleCare applications. The work is developed considering that computing technology continues to become increasingly pervasive and ubiquitous and long-term monitoring of subject physiological parameters as well as the motor daily activities using ubiquitous sensing is nowadays an important research area. A brief

description of several architectures designed, implemented and tested by the authors is presented in the next paragraph.

3.2 Some Contributions from the Authors to Ballistocardiography

Two independent systems were developed to monitor a person's vital signs based on multi-BCG acquisition, one embedding the sensors in a regular office chair [51][56][69][70], characterized by limited mobility, and a second one for the acquisition of the BCG in a wheelchair [64][71] without restraining neither the user's neither the wheelchair's mobility. Figure 15 presents an implemented architecture developed for BCG recording using two EMFi sensors (EMFi-S1, EMFi-S2) embedded on the backrest and the seat of an office chair. The subject seated on the chair corresponds to the application of a set of forces F_{hx} and F_{hy} on the chair, forces that are characterized by static and dynamic components. The static components (F_{hxS} , F_{hyS}) are mainly caused by the gravity imposed by the mass of the user seated on chair but also by different postures of the user while the dynamic components (F_{hxD} , F_{hyD}) are originated by the ballistic forces associated with cardiac activity and the respiration. Additionally, the dynamic components are strongly influenced by user's motion on the chair.

$$F_{hx} = F_{hxS} + F_{hxD} \quad F_{hy} = F_{hyS} + F_{hyD} \quad (2)$$

The main advantage of the EMFi sensor, which consists of several polypropylene layers separated by air voids, is its high sensitivity to the dynamic forces exerted on the film's surface. These forces will change the thickness of the air voids (10-100um wide and 1-5 um high) [72]. The charges residing on the polypropylene/void interfaces will then move in respect to each other and, as a result, a mirror charge proportional to the applied dynamic forces applied on the film is generated on the electrodes (ΔQ_x and ΔQ_y),

$$\Delta Q_x = k \cdot F_{hxD} \quad \Delta Q_y = k \cdot F_{hyD} \quad (3)$$

where k represents the sensitivity factor expressed in CN^{-1} and whose value is included in the 100pC/N and 600pC/N interval. The sensitivity values are influenced by the static forces known also as the preloaded forces. Using known values of forces the direct model and inverse model of the EMFi sensor characteristics can be obtained [73].

To perform the charge-to-voltage conversion, a charge amplifier (QA) scheme including a digital potentiometer was usually used on different BCG measurement implementation developed by the authors. A simplified representation of the QA scheme is presented in Figure 16. The values of $R1$ and C were chosen to assure a proper time constant according to the frequency characteristics of the physiological monitored signals (e.g. respiration for an adult resting on the chair, $f_{resp}=0.2Hz-0.3Hz$; heart beat signal, $f_{HB}=0.9-3Hz$). Good results were obtained for $R1= 10M\Omega$ and $C= 200pF$. Considering the level of V_{BCG} signal obtained at the QA output, a

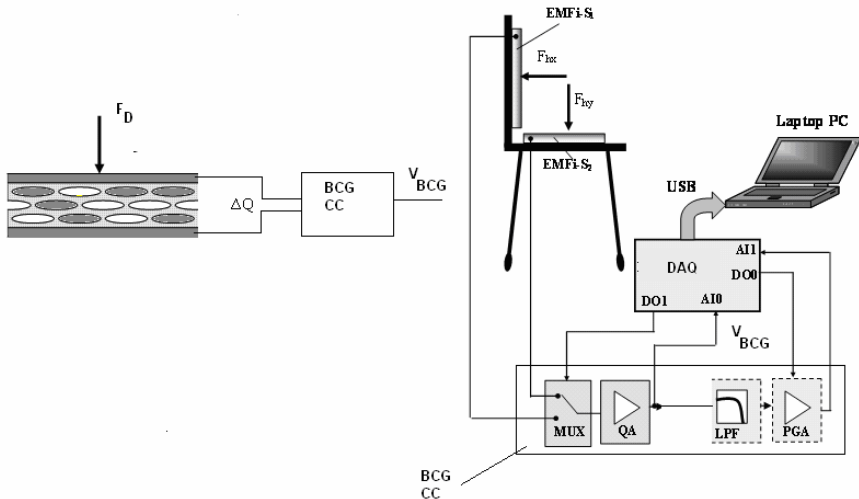


Fig. 15. Multi-EMFi based measuring system, for heart rate and respiratory rate assessment (QA – charge amplifier, NF-notch filter, LPF-low pass filter, PGA – programmable gain amplifier), and example of a BCG signal obtained with it.

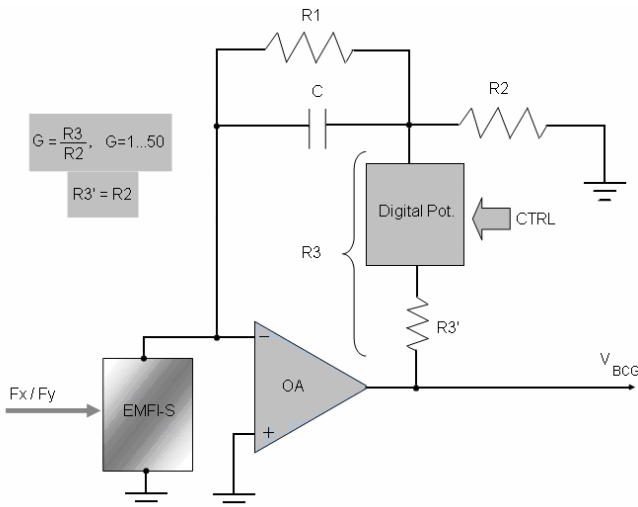


Fig. 16. Charge amplifier scheme with automatic gain control capabilities

programmable gain amplification scheme (PGA) materialized by a set of resistors R2 and R3 and a digital potentiometer (e.g. Xicor X9C104) is used as part of the conditioning scheme. Using a digital output line of a multifunction board (e.g. NI USB 6008) associated with the BCG monitoring system, the digital potentiometer is controlled to obtain a V_{BCG} adapted to the analogue input range (e.g. -5 to +5V)

assuring accurate conversion for an optimal usage of the ADC characteristics (12-bit represents the recommended resolution).

To improve the signal-to-noise ratio (SNR) of the ballistocardiography signal in the presence of noise mainly due to power line interference and to muscles' activity, additional filtering is required. Thus, a low pass active filter (LPF) characterized by $f_c=15\text{Hz}$ was employed [64]. For low level of the noise superposed on the BCG, the analogue filters can be replaced by digital filter algorithms. Figure 17 shows the ballistocardiography signals obtained by EMFI sensors placed in the seat and backrest of the chair of figure 15 acquired at 1kHz/s sampling rate, amplified and digital filtered using a Butterworth 5 order low pass filter.

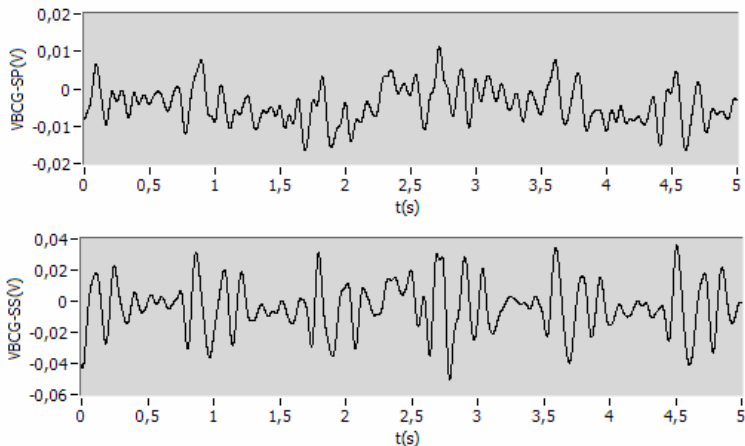


Fig. 17. BCG waves corresponding to the EMFI sensors embedded on the chair (BCG-S1 and BCG-S2) after digital filtering

In figure 17 can be observed that, for a healthy male subject, V_{BCG}^{SS} , signal obtained for a subject seated on the chair at rest, behaves well according to expected caused by voluntary pressure applied by the body on the backrest (F_{hx}). One of the component of the F_{hx} conducts to diminishing of the F_{hx} . Low preloaded forces means low sensitivity of EMFI sensor which conduct to low quality of the acquired V_{BCG}^{SP} . When the subject is seated passively on the chair the literature [75][76] reports that accurate BCG signals are coming from the BCG-SP embedded in the seat.

Processing the acquired BCG, the respiration (Resp) and heart beat (HB) signals are obtained. One of the methods used is based on the Discret Wavelet Transform (DWT) decomposition [51][64]. The separation between the Resp and HR signals done using DWT corresponds to the implementation of a digital filter bank that consists of pairs of digital high-pass (HPF) and low-pass (LPF) filters organized in a tree structure [74] as depicted in figure 18.

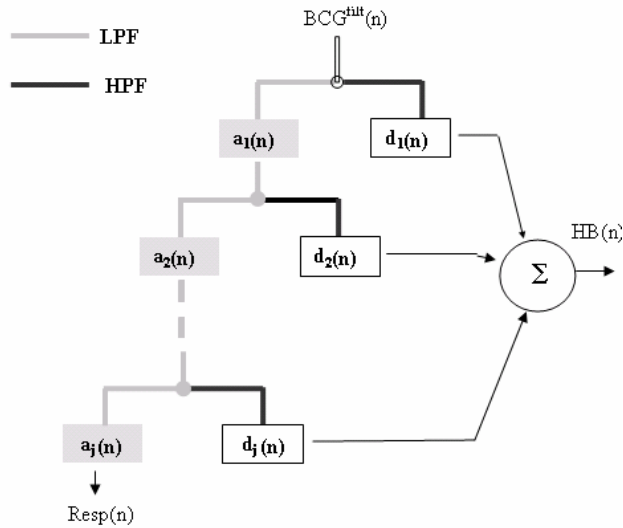


Fig. 18. The wavelet decomposition diagram (LPF – low pass filter, HPF- high pass filter, $a_i(n)$ – approximations, $d_i(n)$ – details, $Resp(n)$ – respiration signal, $HB(n)$ – heart beat signal)

In Figure 18 shows that the digital filtered ballistocardiography ($BCG^{filt}(n)$) is decomposed at each scale, j , into details coefficients (d_j) as the HPF output and approximation coefficients (a_j) as the LPF output. The coefficients are expressed by the following inner products:

$$d_j(k) = \langle x(l), \Psi_{j,k}(l) \rangle \quad (4)$$

$$a_j(k) = \langle x(l), \phi_{j,k}(l) \rangle \quad (5)$$

where $\Psi_{j,k}(l)$ and $\phi_{j,k}(k)$ are scaled and dilated versions of the basis functions associated with HPF and LPF impulse response:

$$\Psi_{j,k}(l) = 2^{-j/2} \Psi(2^{-j}l - k) \quad (6)$$

$$\phi_{j,k}(l) = 2^{-j/2} \phi(2^{-j}l - k) \quad (7)$$

The respiratory and heart signals are obtained combining the products between the decomposition coefficients and the basis functions. Thus, the respiratory signal samples $Resp(n)$ are calculated using the following relation:

$$Resp(n) = \sum_{k \in Z} a_j(k) \phi_{j,k}(n) \quad (8)$$

Regarding the heart beat signal, it is obtained as the sum of the selected details (e.g. m and p) from the total number of decomposition details,

$$HB(n) = \sum_{k \in Z} d_m(k) \Psi_{m,k}(n) + \sum_{k \in Z} d_p(k) \Psi_{m,k}(n) \quad (9)$$

For the wavelet decomposition using Daubechies mother functions and 8 level of decomposition, the respiration and cardiac signals evolutions are presented in Figure 19 together with the BCG signal from which they were obtained.

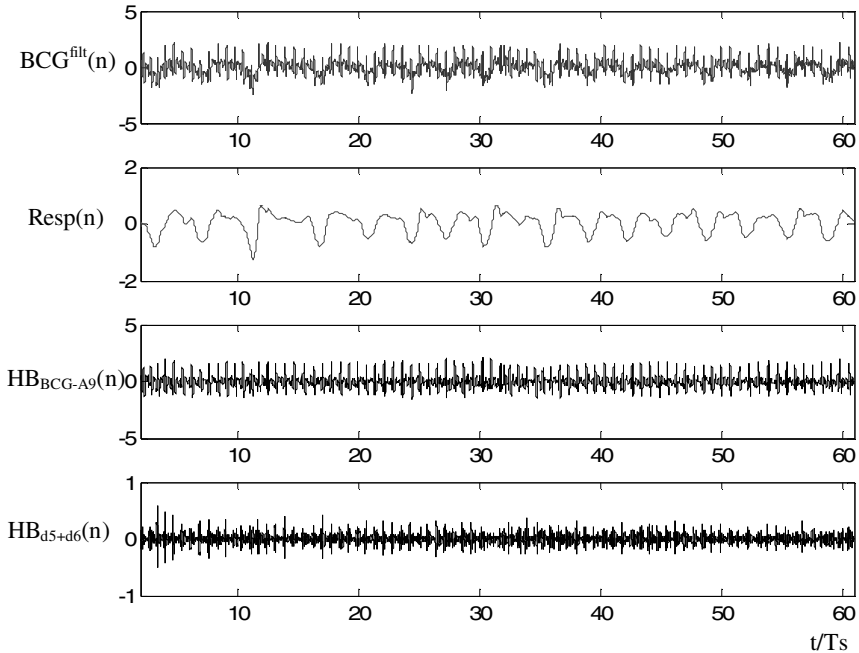


Fig. 19. BCG(n) processing using DWT: a) original BCG signal, b) respiration signal (8^{th} level approximation of the BCG signal decomposition) c) heart beat signal as the difference between the original signal and the 8^{th} level approximation, d) heart beat signal as the sum of decomposition d_5 and d_6 details

To obtain the respiration rate and the heart rate a peak detection procedure for 60s BCG time segments was implemented. The results obtained by BCG signal processing using wavelets were validated with reference instruments and methods (respiratory belt and heart beat extracted from the 3 electrodes ECG, from ADI instrument).

To improve the mobility of the BCG measurement system and to extend the usage of this kind of system to long-term cardiac activity monitoring for people with motor disabilities, a “smart wheelchair” architecture was implemented by the authors. The main sensing components embedded in the wheelchair are two large

area electromechanical film sensors (L-3030 from EMFIT) and two MEMS accelerometers (LIS3LV02DQ 3D from Sparkfun). The signal conditioning scheme mentioned of figures 13 and 14 was used to obtain a voltage BCG signal that is acquired by a data acquisition board with Wi-Fi data communication capabilities [64]. Different architectures of this kind of system is also reported in [75][76].

One of the big challenges associated with the usage of these smart devices is related to the possibility of accurate measurement of the BCG in dynamic conditions, that is to say, when the wheelchair is moving or even when the user moves in the chair. Using the signals from the EMFi sensors (Figure 20) and from 3D accelerometers mounted also on the seat and backrest of the wheelchair, the authors designed and implemented an Independent Component Analysis (ICA) algorithm to remove the noise and especially the low amplitude artefacts that occurs during the wheelchair motion [64][70]. Some results concerning the BCG profile during the wheelchair motion and the ICA based signal processing are presented in Figure 21. Artefacts were removed according to a pre-defined value of the kurtosis of ICA components.

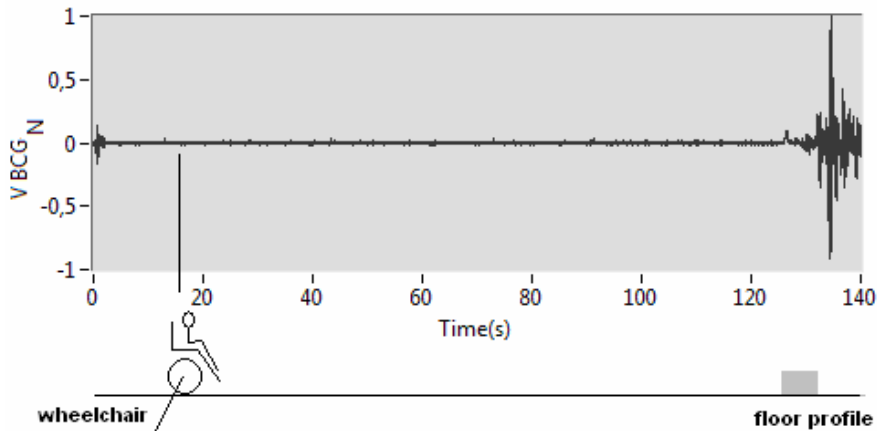


Fig. 20. Evolution of the BCG signal recorded from the EMFi sensor mounted on the wheelchair seat for a particular floor profile

3.3 Non-contact Ballistocardiography

Mechanical contact ballistocardiography proves to be an interesting solution that is used for unobtrusive cardiac function assessment. However, there are an important number of situations where an optimal mechanical contact is difficult to be obtained, namely, when the BCG sensors are embedded in other furniture than the bed. A high difference among the BCG signals according to the localization of the sensors in the systems that acquires the ballistocardiography in unobtrusive way was identified by our team [70]. For the particular case of embedding EMFi sensors in the seat and the backrest of the wheelchair, the different levels of the BCG signal are due to different values of the static forces (subject weight) and to

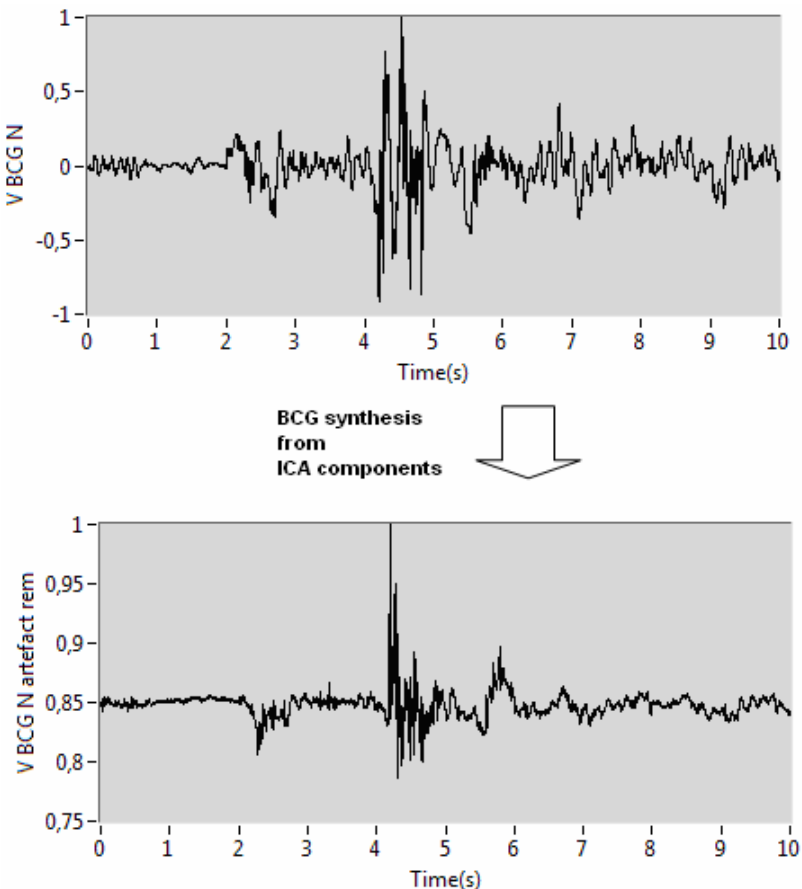


Fig. 21. The BCG signal reconstruction from ICA components for a 10s signal segment

different positions of the body on the backrest. An important problem of BCG measurement systems based on mechanical contact is the difficulty to acquire reliable values from persons unable to voluntary maintains contact with the BCG sensor (e.g. people with motor disabilities). Imposing pre-defined positions for people lying on a bed or seated on a chair with BCG sensors requiring mechanical contact conducts to the increase of the stress level of the patient during the clinical exam or long time monitoring.

Acquiring BCG signals with devices without mechanical contact with the subject still represents an important challenge. Implementation of non-mechanical contact ballistocardiography appeared during the last decades with the developments in the area of microwave Doppler radar [77][78], particularly in the area of frequency modulated continuous waves (FMCW) radar [79][80]. Comparing with ultrasonic Doppler, which was commonly used for breath assessment [81][82] and even heart rate monitoring - based on Doppler shift resulting from the movements

of the hearth [83] - the microwave Doppler radar is an appropriate device to monitor the low amplitude movements particularly related with a person's breath and cardiac activity. The capability to penetrate through an obstacle eliminating the reflected microwaves from stationary objects around the antennas and measuring only the small reflected waves from the subject's body taking into account the applied modulation based on subject's body motion is the main strength of Doppler radars.

In the last years have been reported microwave Doppler radar applications in the area of search and rescue operations [84] but also the usage of this kind of

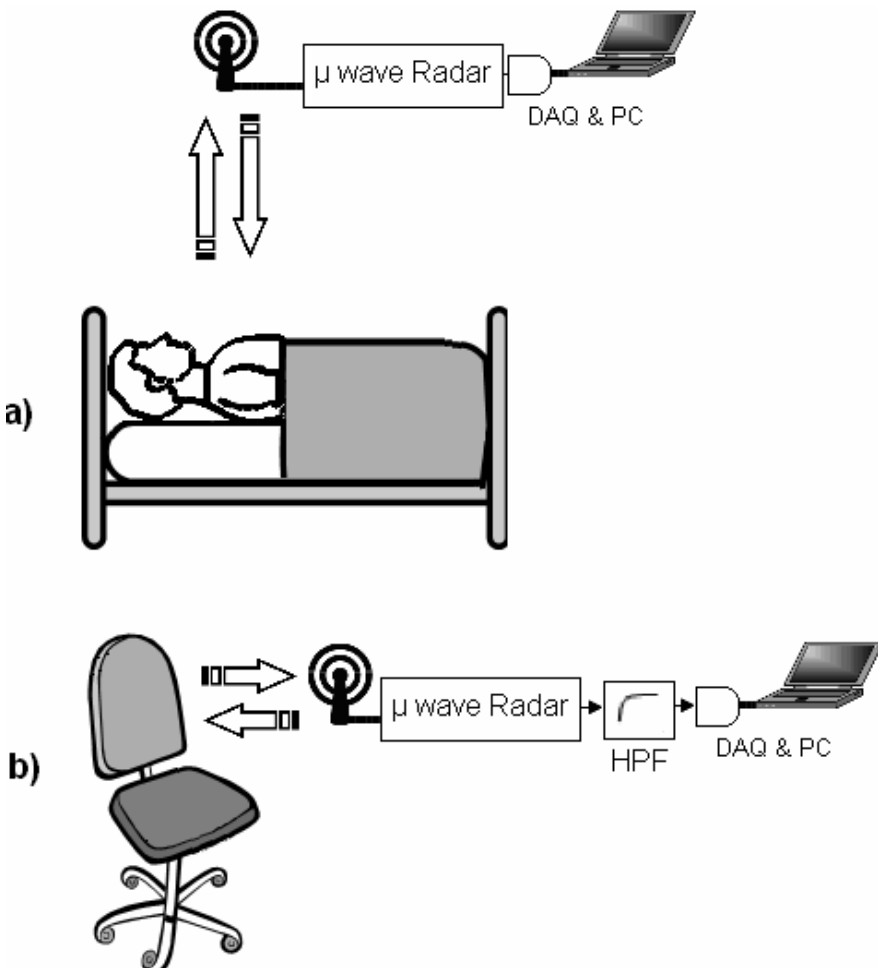


Fig. 22. Vital signs monitoring system block diagram: a) respiratory monitoring system designed for a subject lying on a bed; b) heart rate monitoring system designed for a subject sitting on a chair

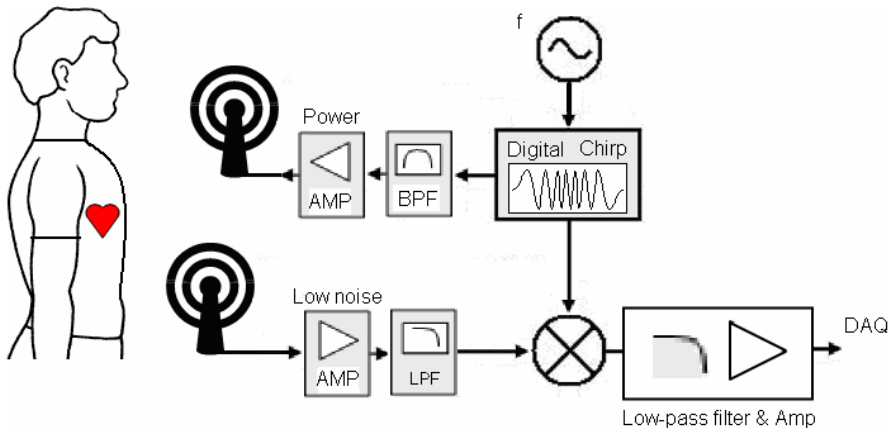


Fig. 23. Block diagram of the microwave radar (DAQ – data acquisition board, BPF- band pass filter, LPF- low pass filter)

sensor in the area of non-contact ballistocardiography as part ubiquitous health care systems. In the area of vital signs monitoring, Matsui et al. report an interesting work related to non-contact measurement of heart rate variability using microwave Doppler radar[85]. The general architecture associated with vital signs monitoring using microwave Doppler antenna is described in Figure 22.

The main elements of the above presented architectures are a microwave signal generator, RF splitters, RF mixers, low pass filters and integrated patch antennas for emitting and receiving the microwave signal (Figure 23).

The microwave signal generator provides the tuning signal whose frequency and shape play an important role on the Doppler radar measurement technique. For the CW Doppler radar, a constant frequency (with respect to time) waveform is transmitted, which allows breath speed to be measured using the Doppler principle. Accordingly, the frequency of the received signal decreases during the subject expiration (target is moving away from the radar antenna) and increases during the subject inspiration (target moving toward the radar antenna) Figure 24.

The relation between the Doppler frequency (frequency shift by Doppler Effect) and the transmitted signal frequency (constant in CW Doppler radar case) is given by:

$$f_D = 2 \cdot f \cdot \frac{v}{c} \cdot \cos \alpha \quad (10)$$

where:

f_D - frequency shift by Doppler effect,

c - speed of light

v – velocity associated with respiratory motion

α - angle of the direction of subject chest motion with the direct connecting straight line between antenna and subject's chest

f - transmitted frequency

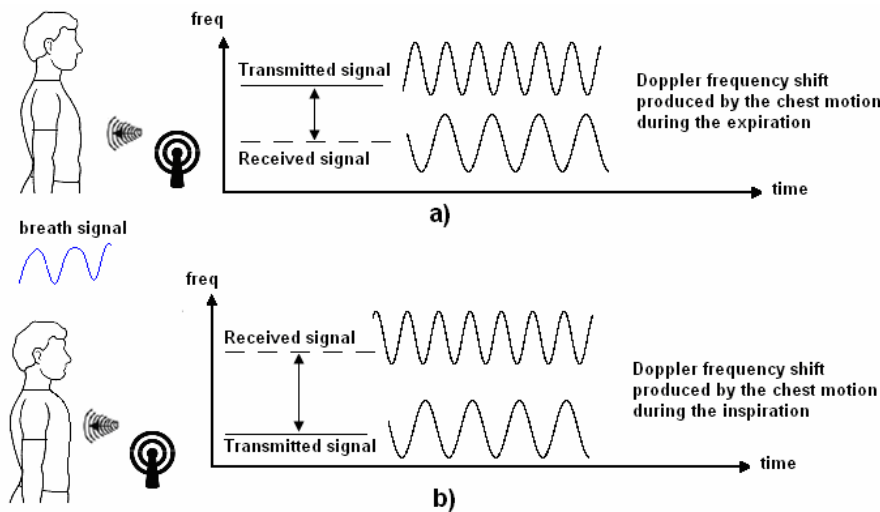


Fig. 24. The relation between the frequencies of the transmitted and received signals during a subject's respiration

In the practical case the frequency of the received signal, f_R , is given by:

$$f_R = f \pm f_D \quad (11)$$

In what concerns the operating microwave frequency, f , it was reported the usage of 1215 MHz by Matsui group [60][85] that use Tau Giken, LDR-1 microwave Doppler radar model; others report the usage of 2.4GHz or even 10.587 GHz Doppler radars [86].

In order to obtain the range and velocity of a target, frequency modulated continuous wave Doppler radar is used. Common applications of this kind of radar are vehicle localization and speed measurement; also, military applications were published [80]. The main difference between FMCW radar and pulse and CW Doppler radar is the usage of time variable transmitted frequency versus fixed

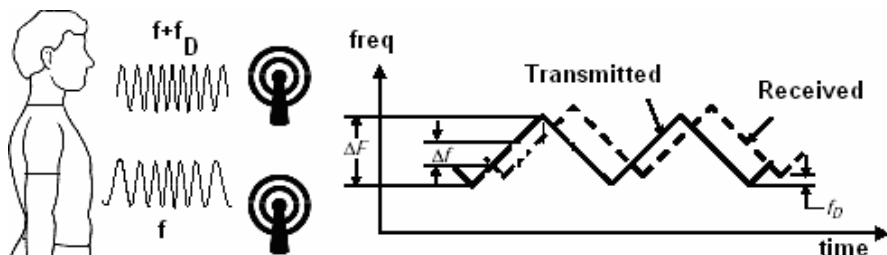


Fig. 25. Transmit and receive signal frequencies of triangular modulated FMCW Doppler radar

frequency as it is presented in Figure 25. This make of FMCW Doppler radar a presence sensor detecting the motionless subject and at the same time permits to detect small motions caused by breath and of the body imparted to it by the heart beat. These small motions originate the ballistocardiography signal, turning FMCW Doppler radar into a non-mechanical contact ballistocardiography sensing device.

The position of a subject, also known by range, R, is given by the following relation:

$$R = \frac{c \cdot \Delta f}{4 \cdot \Delta f \cdot f_m} \quad (12)$$

where

Δf = instantaneous difference in frequency, in Hz, of the transmitter at the times the signal is transmitted and received,

ΔF = radio frequency (RF) modulation bandwidth in Hz

f_m = RF modulation frequency in Hz,

c - light velocity

Thus, using the FMCW Doppler radar, the subject is localized by processing the signal delivered by the radar IF output (e.g. output of Innosent IVS-162 used by our group). Small motions caused by subject breath and heart beat are expressed by fluctuation of the IF signal provided by the radar. In order to separate the respiration and the heart beat signal a low pass filter (LPF: $f_c=0.3\text{Hz}$, 3 poles) and a high pass filter (HPF: $f_{1c}=0.5\text{Hz}$, 2 poles) can be used. The evolution of the signals obtained at the LPF and HPF outputs are presented in Figure 26.

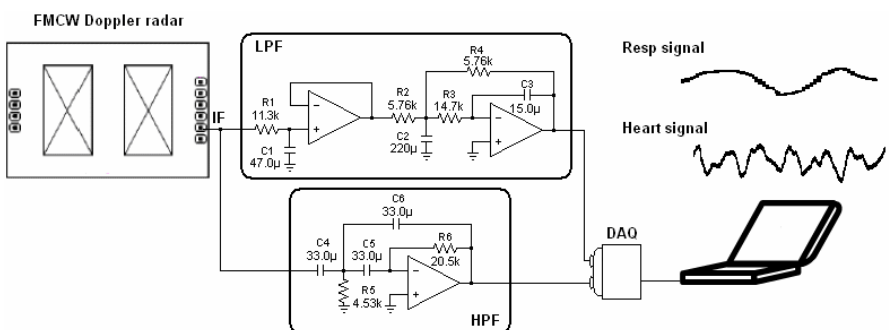


Fig. 26. Radar ballistocardiography system block diagram

In Figure 26 are represented the FMCW Doppler radar (162-IVS-162 from Innosent) and a filtering scheme based on the LM324. The obtained respiration and heart beat signals are amplified and acquired using the analogue inputs of a multifunction board (e.g. NI USB-6009). The sampling frequency is normally

considered in the 200Hz-1 kHz [31] interval, which permits to establish good correlations between non-contact BCG processing and ECG processing, where ECG is considered as reference measurement method for cardiac activity.

Because of the high correlation ($r = 0.98$, $P < 0.0001$) between the J-J intervals between J peaks of the BCG wave measured using the radar sensor and R-R time intervals of the 3 electrodes ECG signal using and ECG measurement device (e.g. Medlab P-OX 100), the heart beat signal can be used to estimate the heart rate variability. The Matsui team [86] presents some results concerning the use of the Fast Fourier Transform applied to J-J signal, where J-J are successive peaks of the heart beat signal. Good results are reported also by Postolache et. Al [31][39][59][64] on the use of the heart beat signal obtained from ballistocardiography to estimate the HRV through FFT and also DWT processing.

Nowadays, taking into account the miniaturization and the low power consumption achieved for this kind of sensors, FMCW Doppler radar is an interesting solution for vital signs monitoring in the in-home ubiquitous healthcare context. The above presented Doppler radar (CW and FMCW) represents a reliable solution for long term monitoring of the vital signs in subjects in ambulatory conditions [60], in residence for continuous healthcare, embedded in furniture (e.g. bed, chair), in Home TeleCare context. At the same time, the microwave radar can be part of the sensing system of a smart wheelchair replacing the mechanical contact ballistocardiographic [88]. Regarding this challenge, the authors embedded a FMCW Doppler radar (162-IVS-162 from Innosent) in a wheelchair for respiration and heart activity assessments through on-line non-contact ballistocardiography analysis. The system setup, which includes ballistocardiography obtained from EMFi sensor as reference BCG, is presented in Figure 27.

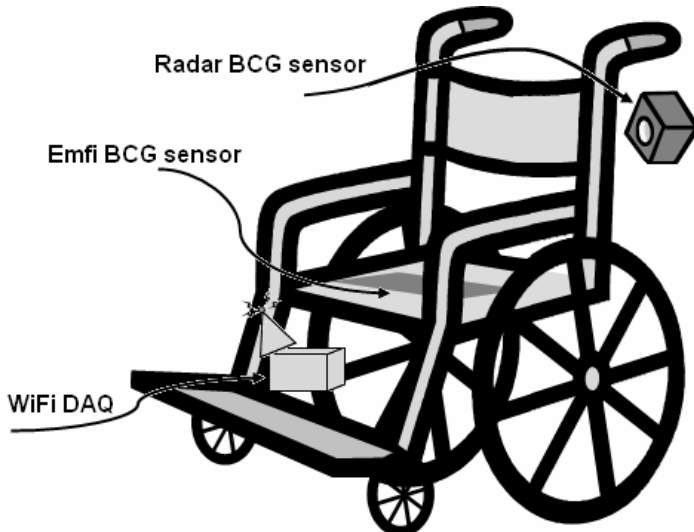


Fig. 27. Vital signs long-term monitoring based on EMFI BCG and Radar BCG sensors embedded in a wheelchair

Related to radar BCG signal processing after analogue filtering, the signals corresponding to the respiration and heart beat (Resp and HB) are acquired using a Wi-Fi DAQ NI-WLS-9163 -NI DAQ-9215 using 1kS/s sampling rate. Two IIR Butterworth digital filters are implemented using LabVIEW filtering functions. A LPF digital filter characterized by 8th order and fc=15Hz is applied to the acquired signal obtained from the EMFi sensor (EMFIT L-3030) that is taped on the wheelchair seat. The BCG signal obtained with the EMFi sensor from a young male user is presented in Figure 28.

Analyzing the evolution of I and J peaks can be observed a light variation of the amplitude during the time caused by the modulation effect of the respiration activity. The respiration influence is stronger highlighted in the radar ballistocardiography signal obtained after acquisition and digital filtering. Using a 5th order IIR

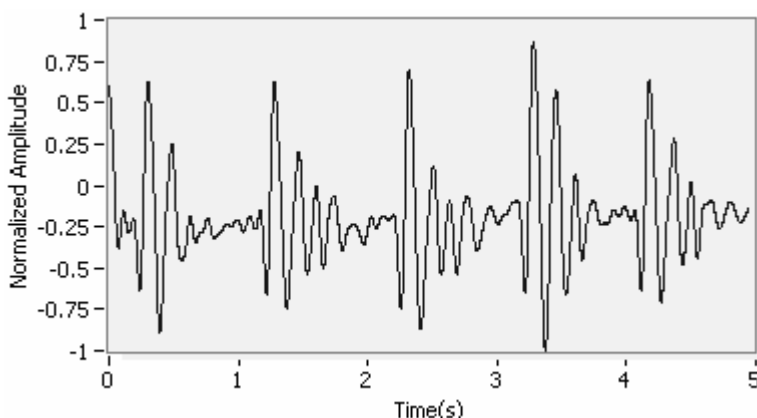


Fig. 28. Ballistocardiogram reference signal for a mechanical contact BCG sensor (EMFi sensor taped on the seat of the wheelchair)

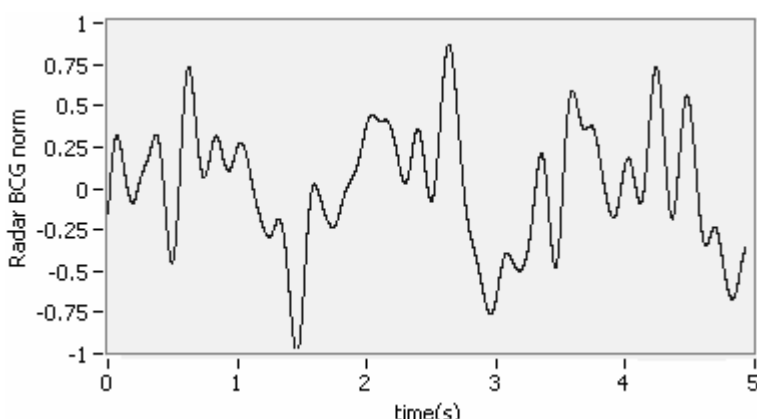


Fig. 29. Band pass filtered radar BCG signal

Butterworth band-pass filter, a heart beat signal characterized by low frequency modulation component is obtained (Figure 29).

To calculate the heart rate, the signals peaks must be better underlined and in this case a detrend procedure based on DWT was implemented by the authors using the “WA detrend” function from LabVIEW Advanced Signal Processing Toolkit. The designed procedure was applied to the radar BCG signal considering different types of mother wavelets. Good results were obtained for Coiflets (coif2), and Symmlets (sym4) mother wavelets.

The heart beat signal represented in Figure 29 after application of wavelet de-trend procedure for 5s acquisition time is presented in Figure 30.

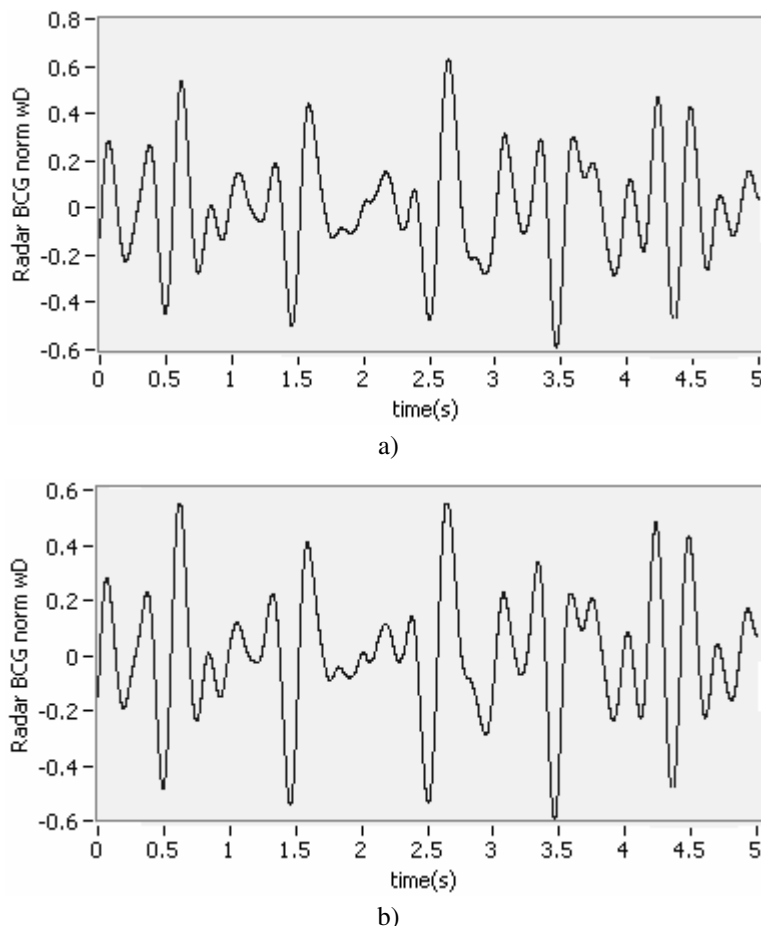


Fig. 30. Radar BCG signal after wavelet detrending a) detrending using coif2 mother wavelet; b) detrending using sym4 mother wavelet

The results presented in Figure 28 and Figure 30 emphasize the robustness of the radar ballistocardiograph usage for accurate detection of the heart beat signal.

4 Conclusion

Ubiquitous healthcare is one of the promising issues in our society and an important challenge for the biomedical sensing area. As part of ubiquitous healthcare systems, non-invasive and unobtrusive measurement devices permit to obtain health information from subjects without any notice, allowing painless and stress free online patient monitoring without the important constraints that characterize classical devices needing wired connections and complex monitoring procedures. Taking into account these paramount advantages, in the last century, many research groups developed non-invasive solutions for homeostasis monitoring. However, the pervasive characteristics of vital signs monitoring systems appear in the last decades as result of the developments in the areas of microelectronics, embedded processing and data communications.

In this context, and considering the research work developed by the authors in the area of unobtrusive bio-sensing as well as in the area of intelligent processing of the vital signs, the present chapter presented elements of theory and practical implementation of several sensing solutions that are state of the art in cardiac and respiratory activity monitoring.

It has been described specific implementations of ECG monitoring devices characterized by the usage of dry contact electrodes and capacitive coupled electrodes as part of ubiquitous systems. New materials as carbon fibbers associated with e-textile, are been used as part of new sensors.

If the ECG is still considered as a gold standard for cardiac activity monitoring, the ballistocardiography is a promissory method to evaluate both respiration and cardiac activity and represents an actualization of an “old fashion” method. A description of ballistocardiography sensors and systems with and without contact between the sensing part and the subject under test as well as the signal processing including wavelets decomposition were included in the chapter. Ballistocardiography monitoring system prototypes including a brief description of the hardware and software components permit the reader to understand the practical aspects related with the sensing component implementation, highlighting some of the drawbacks and the challenges for developers and users of this kind of systems.

From ECG and BCG acquired signals in unobtrusive way additional parameters related with the health status of a person, such as heart rate variability, autonomic nervous system, homeostasis and allostasis assessment can be done and a reference to this new challenge was also made here.

Given the harsh signal-to-noise ratio encountered in uninhibited environments, as the homecare scenario, and the impact of automatically measure the important features of the ballistocardiogram, renewing efforts in developing robust ballistocardiographic systems is a promising high-risk high-payoff task. Different solutions concerning SNR improvement removing noise and artefacts were mentioned.

Because one of the central challenges from a practical point of view remains movement related changes on ballistocardiographic signal, we are continuing to expand our study with new sensors and filters to make our system more robust.

When operational, unobtrusive monitoring systems of homeostasis and allostasis should generate large amounts of high quality physiological data in natural situations with the potential of great reduction of health care costs.

References

- [1] Iakovidis, I., Purcarea, O.: EHealth in Europe: from vision to reality. In: Blobel, B., Pharow, P., Nerlich, M. (eds.) EHealth: Combining health telematics, telemedicine, biomedical engineering and bioinformatics to the edge: Global Experts Summit Textbook. Studies in health technology and informatics, vol. 134, pp. 163–168 (2008)
- [2] Draft final Conference conclusions- High level Conference 2006, Malaga, Spain (2006), <http://www.ehealthconference2006.org/images/stories/conclusions.pdf>
- [3] Kohn, L.T., Corrigan, J.M., Donaldson, M.S. (eds.): Institute of Medicine (IOM). Committee on Quality of Health Care in America. To Err is human: Building a safe Health System. National Academy Press, Washington (2000)
- [4] Flum, D.P., Koepsell, T.: The clinical and economic correlates of misdiagnosed appendicitis. *Archives of Surgery* 137, 799–804 (2002)
- [5] Zhang, J., Patel, V.L., Johnson, T.R.: Medical error: Is the solution medical or cognitive? *Journal of the American Medical Informatics Association* 6 (Suppl.1), 75–77 (2008)
- [6] McEwen, B.S.: Interacting mediators of allostasis and allostatic load: towards an understanding of resilience in aging. *Metabolism* 52(10 Suppl. 2), 10–16 (2003)
- [7] McEwen, B.S., Wingfield, J.C.: The concept of allostasis in biology and biomedicine. *Hormones and Behavior* 43, 2–15 (2003)
- [8] Sterling, P., Eyer, J.: Allostasis: A new paradigm to explain arousal pathology. In: Fisher, S., Reason, J. (eds.) *Handbook of Life Stress, Cognition and Health*. John Wiley & Sons, New York (1988)
- [9] Golay, A., Ybarra, J.: Link between obesity and type 2 diabetes. *Best Practice & Research: Clinical Endocrinology&Metabolism* 19(4), 649–663 (2005)
- [10] McEwen, B.S.: Sleep deprivation as a neurobiologic and physiologic stressor: Allostasis and allostatic load. *Metabolism* 55, S20–S23 (2006)
- [11] Yoon, S.W., Min, S.D., Yun, Y.H., Lee, S., Lee, M.: Adaptive Motion Artefacts Reduction Using 3-axis Accelerometer in E-textile ECG Measurement System. *Journal of Medical Systems* 32(2), 101–106 (2008)
- [12] Gruetzmann, A., Hansen, S., Müller, J.: Novel dry electrodes for ECG monitoring. *Physiological Measurement* 28, 1375–1390 (2007)
- [13] Kim, K.K., Lim, Y.G., Kim, J.S., Park, K.S.: Capacitive-Coupled ECG Measurement and Its Applications for Ubiquitous Healthcare. In: Proc. 2007 International Conference on Convergence Information Technology, November 21-23, 2007, pp. 811–814 (2007)
- [14] Lim, Y.G., Kim, K.K., Park, K.S.: ECG Measurement on a Chair Without Conductive Contact. *IEEE Transactions on Biomedical Engineering* 53(5), 956–959 (2006)

- [15] Wu, K.F., Chan, C.H., Zhang, Y.T.: Contactless and Cuffless Monitoring of Blood Pressure on a Chair Using E-Textile Materials. In: Proc. 3rd IEEE-EMBS International Summer School and Symposium on Medical Devices and Biosensors, September 4-6, pp. 98–100 (2006)
- [16] Ruffini, G., Dunnea, S., Farrés, E., Marco-Pallarés, J., Ray, C., Mendoza, E., Silva, R., Grau, C.: A dry electrophysiology electrode using CNT arrays. Sensors and Actuators A 132, 34–41 (2006)
- [17] Hoffmann, K.P., Ruff, R.: Flexible dry surface-electrodes for ECG long-term monitoring. In: Proc. of the 29th Annual International Conference of the IEEE EMBS, August 23-26, 2007, pp. 5739–5742 (2007)
- [18] Toray Inc: Fundamentals of carbon fiber technology and their application to Torayca products on-line at, <http://www.toraycfa.com/about.html> (2005)
- [19] Electro Fiber Technologies: Metal-plated carbon from Electro Fiber Technologies. In: Advances in Textiles Technology February 1 (2008)
- [20] Ishijima, M.: Monitoring of Electrocardiograms in Bed Without Utilizing Body Surface Electrodes. IEEE Transactions on Biomedical Engineering 40(6), 593–594 (1993)
- [21] Stefan Karlsson, J.S., Wiklund, U., Berglin, L., Östlund, N., Karlsson, M., Bäck-lund, T., Lindecrantz, K., Sandsjö, L.: Wireless Monitoring of Heart Rate and Electromyographic Signals using a Smart T-shirt. In: Proceedings of International Workshop on Wearable Micro and Nanosystems for Personalised Health, Valéncia, Spain (2008), <http://www.phealth2008.com/Events/papers/p7.pdf>
- [22] Lee, Y.D., Chung, W.Y.: Wireless sensor network based wearable smart shirt for ubiquitous health and activity monitoring. Sensors and Actuators B: Chemical 140(2), 390–395 (2009)
- [23] Kim, K., Gyu Lim, Y., Soo Kim, J., Suk Park, K.: Capacitive-Coupled ECG Measurement and Its Applications for Ubiquitous Healthcare. In: IEEE International Conference on Convergence Information Technology, pp. 811–814 (2007)
- [24] Matthews, R., McDonald, N., Hervieux, P., Turner, P., Anumula, H., Woodward, J.: Nonintrusive, Wearable Bioelectrodes for Monitoring the Heart and Brain. Sensors Magazine (2007)
- [25] Lopez, A., Richardson, P.C.: Capacitive electrocardiographic and bioelectric electrodes. IEEE Transactions on Biomedical Engineering 16, 99 (1969)
- [26] Searle, A., Kirkup, L.: A direct comparison of wet, dry and insulating bioelectric recording electrodes. Physiological Measurement 21, 271–283 (2000)
- [27] Zhu, D., Wang, L., Zhang, Y.: A Non-contact ECG Measurement System for Pervasive Heart Rate Detection. In: Proceedings of IEEE 2nd International Symposium & Summer School on Biomedical and Health Engineering, pp. 518–519 (2008)
- [28] Park, C., Chou, P., Bai, Y., Matthews, R., Hibbs, A.: An Ultra-Wearable, Wireless, Low Power ECG Monitoring System. In: Proc. IEEE BioCAS, pp. 241–244 (2006)
- [29] Ishida, S., Shiozawa, N., Fujiwara, Y., Makikawa, M.: Electrocardiogram measurement during sleep with wearing clothes using capacitively-coupled electrodes. In: Conference Proceedings IEEE Engineering in Medicine& Biology Society, pp. 2647–2650 (2007)
- [30] Nakamura, H., Shimada, K., Tatsuro, F.: A Comparative Evaluation Between Conditions of the Wrist Band Capacitive-Coupled ECG Recording through Signal-to-Noise Ratio. In: Proc. of the 29th Annual International Conference of the IEEE EMBS, August 23-26, 2007, pp. 5886–5889 (2007)

- [31] Postolache, O., Postolache, G., Girão, P.S.: Non-invasive Mobile Homeostasis Instrument. In: Proc. 2006 IEEE International Workshop on Medical Measurement and Applications, April 20-21, pp. 94–97 (2006)
- [32] Prance, R.J., Debray, A., Clark, T.D., Prance, H., Nock, M., Harland, C.J., Clippingdale, A.J.: An ultra-low-noise electrical-potential probe for human-body scanning, IOP Science. Measurement Science and Technology 11, 291–297 (2000)
- [33] Kim, K.K., Lim, Y.K., Park, K.S.: The Electrically Non-contacting ECG Measurement on the Toilet Seat Using the Capacitively-coupled Insulated Electrodes. In: Proc. of the 26th Annual International Conference of the IEEE EMBS, September 1-5, 2004, pp. 2375–2378 (2004)
- [34] Steffen, M., Aleksandrowicz, A., Leonhardt, S.: Mobile Noncontact Monitoring of Heart and Lung Activity. IEEE Transactions on Biomedical Circuits And Systems 1(4), 250–257 (2007)
- [35] Casas, O., Pallàs-Areny, R.: Electrostatic Interference in Contactless Biopotential Measurements. In: Proc. of the 29th Annual International Conference of the IEEE EMBS, August 23-26, 2007, pp. 2655–2658 (2007)
- [36] Malik, M., Camm, J.: Heart Rate Variability. Futura Publishing, Armonk (1995)
- [37] Welford, N.T., Sontag, L.W., Phillips, W., Phillips, D.: Individual differences in heart rate variability in the human fetus. American Journal Obstetrics&Gynecology, 1 98(1), 56–61 (1967)
- [38] : Task Force of the European Society of Cardiology and the North American Society of Pacing and Electrophysiology. Heart rate variability: standards of measurement, physiological interpretation and clinical use. Circulation, 1 93(5), 1043–1065 (1996)
- [39] Postolache, O., Postolache, G., Silva-Girão, P.: Non-invasive mobile homeostasis instrument. In: Proceedings of IEEE International Workshop on Medical Measurements and Applications, Benevento, Italy, vol. I, pp. 94–98 (2006)
- [40] Rajendra, A.U., Paul, J.K., Kannathal, N., Lim, C.M., Suri, J.S.: Heart rate variability: a review. Medical& Biological Engineering &Computing 44(12), 1031–1051 (2006)
- [41] NASA: Ballistocardiography – A Bibliography. SP-7021 (1965)
- [42] Scarborough, W.R., Baker, B.M.: Ballistocardiography: appraisal of current status. Circulation 16, 971–975 (1957)
- [43] Gubner, R.S., Rodstein, M., Ungerleider, H.E.: Ballistocardiography – an appraisal of technic, physiologic principles, and clinical Value. Circulation 7, 268–286 (1953)
- [44] Gordon, J.W.: On certain molar movements of the human body produced by the circulation of the blood. Journal of Anatomy & Physiology 11, 533–536 (1877)
- [45] Henderson, Y.: The mass-movements of the circulation as shown by a recoil curve. American Journal of Physiology 14, 287–298 (1905)
- [46] Starr, I., Rawson, A.J., Schroeder, H.A.: Apparatus for recording the heart's recoil and the blood's impacts in man (Ballistocardiograph). Experiments on the principles involved, records in normal and abnormal conditions. In: Proceedings of American Physiology Society 50th Ann. Meeting, American Journal of Physiology, vol. 123, pp. 1–223 (1938)
- [47] Starr, I., Rawson, A.J., Schroeder, H.A., Joseph, N.R.: The estimation of cardiac output and the determination of the blood's impacts (Ballistocardiogram). In: Proceedings of American Society of Clinical Investigation, 30th Ann. Meeting, Journal Clinical Investigation, vol. 17, p. 506 (1938)

- [48] Starr, I., Rawson, A.J., Schroeder, H.A., Joseph, N.R.: Studies on the estimation of cardiac output in man, and of abnormalities in cardiac function from the heart's recoil and the blood's impact; The Ballistocardiogram. *American Journal of Physiology* 127, 1–28 (1939)
- [49] Holcik, J., Moudr, J.: Mathematical model of seismocardiogram. *Springer World Congress on Medical Physics and Biomedical Engineering* 14(22), 3415–3418 (2007)
- [50] Koivistoinen, T., Junnila, S., Varri, A., Koobi, T.: A new method for measuring the ballistocardiogram using EMFi sensors in normal chair. In: *Proceedings of the 26th Annual International Conference of the IEEE EMBS 2004*, September 1-5, pp. 2026–2029 (2004)
- [51] Postolache, O., Girão, P.S., Postolache, G., Dias Pereira, J.M.: Vital signs monitoring system based on EMFi sensors and wavelet analysis. In: *Proceedings 2007 IEEE Instrumentation and Measurement Technology Conference*, vol. I, pp. 1–4 (2007)
- [52] Nickerson, J.L., Warren, J.V., Brannon, E.S.: The cardiac output in man: Studies with the low frequency, critically-damped ballistocardiograph, and the method of right atrial catheterization. *Journal of Clinical Investigation* 26(1), 1–10 (1947)
- [53] Zhang, Y., Qu, M., Webster, J.G., Tompkins, W.J., Ward, B.A., Bassett, D.R.: Cardiac output monitoring by impedance cardiography during treadmill exercise. *IEEE Transaction on Biomedical Engineering* 33, 1029–1041 (1986)
- [54] Baevskiĭ, R.M., Funtova, I.I.: Ballistocardiographic studies during the 4th expedition on the Saliut-6 orbital station. *Kosm. Biol. Aviakosm Med.* 16(5), 34–37 (1982)
- [55] Rauhalaa, E., Virkkala, J., Himanena, S.: Periodic limb movement screening as an additional feature of Emfit sensor in sleep-disordered breathing studies. *Journal of Neuro-science Methods* 178, 157–161 (2009)
- [56] Postolache, O., Postolache, G., Girão, P.S.: New Approach on Cardiac Autonomic Control Estimation Based on BCG Processing. In: *Proc. 2007 IEEE Canadian Conference on Electrical & Computer Engineering*, pp. 875–879 (2007)
- [57] Park, K.S., Jeong, D.U., Choi, B.H., Shin, J.H., Kim, K.K., Lim, Y.G.: Non-intrusive monitoring of heart rate variability during sleep. *Telecommunications Review* 17(2), 277–287 (2007)
- [58] Castiglioni, P., Faini, A., Parati, G., Di Renzo, M.: Wearable seismocardiography. In: *Proc. of the 29th Annual International Conference of the IEEE EMBS*, August 23–26, pp. 3954–3957 (2007)
- [59] Geoffrey, H.: The digital ballistocardiograph. *US Cardiology* 6(2), 115–119 (2009)
- [60] Uenoyama, M., Matsui, T., Yamada, K., Suzuki, S., Takase, B., Suzuki, S., Ishi-hara, M., Kawakami, M.: Non-contact respiratory monitoring system using a ceiling-attached microwave antenna. *Medical& Biological Engineering Computing* 44, 835–840 (2006)
- [61] Mohammad-Zadeh, F., Taghibakhsh, F., Kaminska, B.: Contactless heart monitoring. In: *IEEE Proceedings of CCECE*, pp. 583–585 (2007)
- [62] Such, O., Muehlsteff, J., Pinter, R., Aubert, X., Falck, T., Elixmann, M., Reiter, H., Cohen-Solal, E., Raju, B., Petruzzello, J., Brauers, A., Thijs, J., Igney, C.: On-body sensors for personal healthcare. *Advances in Health care Technology Care Shaping the Future of Medical – Springer Netherlands* 6, 463–488 (2006)
- [63] Yu, X., Dent, D.: Neural networks in Ballistocardiography (BCG) using FPGAs. In: *IEE Colloquium on Software Support and CAD Techniques for FPGAs*, April 13, pp. 7/1–7/5 (1994)

- [64] Postolache, O., Girão, P.S., Mendes, J., Postolache, G.: Unobtrusive heart rate and respiratory rate monitor embedded on a wheelchair. In: Proc. 2009 IEEE International Workshop on Medical Measurements and Applications, May 29-30, pp. 83–88 (2009)
- [65] Tavakolian, K., Ngai, B., Akhbardeh, A., Kaminska, B., Blaber, A.: Comparative analysis of infrasonic cardiac signals. In: Proc. Computers in Cardiology, vol. 36, pp. 757–760 (2009)
- [66] Su, J., Zhu, X., Zhang, X., Tang, J., Liu, L.: Ballistocardiogram measurement system using three load-cell sensors platform in chair. In: Proceedings 2nd International Conference on Biomedical Engineering and Informatics, October 17-19, pp. 1–4 (2009)
- [67] Hun Choi, B., Sung Chung, G., Lee, J.S., Jeong, D., Suk Park, K.: Slow-wave sleep estimation on a load-cell-installed bed: a non-constrained method 30, 1163–1170. IOP Publishing Physiol. Meas. (2009)
- [68] Tavakolian, K., Kaminska, B., Vaseghi, A., Kennedy-Symonds, H.: Respiration analysis of the sternal ballistocardiograph signal. Computers in Cardiology 35, 401–404 (2008)
- [69] Postolache, O., Postolache, G., Girão, P.: New device for assessment of autonomic nervous system functioning in psychophysiology. In: Proc IEEE International Workshop on Medical Measurements and Applications, vol. I, pp. 95–99 (2007)
- [70] Pinheiro, E.C., Postolache, O., Girão, P.S.: Theory and developments in an unobtrusive cardiovascular system representation: ballistocardiography. The Open Biomedical Engineering Journal (2010) (to be published)
- [71] Postolache, O., Girão, P., Mendes, J., Pinheiro, E., Postolache, G.: Physiological parameters measurement based on wheelchair embedded sensors and advanced signal processing. accepted for publishing IEEE Transaction on Instrumentation and Measurement (2010)
- [72] Lekkala, J., Paajanen, M.: EMFi - New electret material for sensors and actuators. In: Proc. 10th IEEE International Symposium on Electrets, September 22-24, pp. 743–746 (1999)
- [73] Paajanen, M., Lekkala, J., Valimaki, H.: Electromechanical modelling and properties of the electret film EMFI. IEEE Transactions on Dielectrics and Electrical Insulation 8(4), 629–636 (2001)
- [74] Mallat, S.: Wavelet Tour of Signal Processing. Academic Press, London (2008)
- [75] Jong-Myoung, K., Joo-Hyun, H.O., Myeong-Chan, C., Eun-Jong, C., Tae-Soo, L.: Wireless biomedical signal monitoring device on wheelchair using noncontact electro-mechanical film sensor. In: Proceedings IEEE EMBS 2007, pp. 574–577 (2007)
- [76] Junilla, S., Akhbardeh, A., Värrí, A.: An electromechanical film sensor based wireless ballistocardiographic chair: Implementation and performance. Journal of Signal Processing Systems 57(3), 305–320 (2009)
- [77] Droitcour, A.D., Lubecke, V.M., Lin, J., Boric-Lubecke, O.: A microwave radio for Doppler radar sensing of vital signs. In: Proceedings of IEEE MTT-S Int. Microw. Symp. Dig., pp. 175–178 (2001)
- [78] Xiao, Y., Lin, J., Boric-Lubecke, O., Lubecke, V.: Frequency-Tuning technique for remote detection of heart beat and respiration using low-power Double-Sideband Transmission in the Ka-Band. IEEE Trans on microwave theory and techniques 54(5), 2023–2031 (2006)
- [79] Musch, T.: A high precision 24-GHz FMCW Radar based on a fractional-N Ramp-PLL. IEEE Trans on Instrum. and Meas. 52, 2 (2003)

- [80] Wenger, J.: Automotive radar - status and perspectives. In: Proceedings of IEEE Compound Semiconductor Integrated Circuit Symposium, CSIC 2005, pp. 21–24 (2005)
- [81] Kułuzynski, K., Kret, T., Siénko, J., Czajkowski, K., Pałko, T.: Automatic detection of ultrasonic Doppler signal episodes resulting from fetal breathing movements. *Medical Engineering & Physics* 30, 426–433 (2008)
- [82] Karlsson, B., Berson, M., Helgason, T., Geirsson, R.T., Pourcelet, L.: Effects of fetal and maternal breathing on the ultrasonic Doppler signal due to fetal heart movement. *European Journal of Ultrasound* 11, 47–52 (2000)
- [83] Mostafanezhad, I., Boric-Lubecke, O., Lubecke, V., Mandic, D.P.: Application of empirical mode decomposition in removing fidgeting interference in Doppler Radar life signs monitoring devices. In: Proc. 31st Annual International Conference of the IEEE EMBS, September 2-6, pp. 340–343 (2009)
- [84] Matsui, T., Hagisawa, K., Ishizuka, T., Takase, B., Ishihara, M., Kikuchi, M.: A novel method to prevent secondary exposure of medical and rescue personnel to toxic materials under biochemical hazard conditions using microwave Radar and Infrared Thermography. *IEEE Transactions on Biomedical Engineering* 51(12), 2184–2188 (2004)
- [85] Matsui, T., Arai, I., Gotoh, S., Hattori, H., Takase, B., Kikuchi, M., Ishihara, M.: A novel apparatus for non-contact measurement of heart rate variability: a system to prevent secondary exposure of medical personnel to toxic materials under biochemical hazard conditions, in monitoring sepsis or in predicting multiple organ dysfunction syndrome. *Biomedicine & Pharmacotherapy* 59, S188–S191 (2005)
- [86] Suzuki, S., Matsui, T., Imuta, H., Uenoyama, M., Yura, H., Ishihara, M., Kawakami, M.: A novel autonomic activation measurement method for stress monitoring: non-contact measurement of heart rate variability using a compact microwave radar. *Medical& Biological Engineering& Computing* 46, 709–714 (2008)
- [87] Fletcher, R., Han, J.: Low-cost differential front-end for Doppler Radar vital signs monitoring. In: Proceedings IEEE International Microwave Symposion, pp. 1325–1328 (2009)
- [88] Postolache, O., Girao, P., Madeira, R., Postolache, G.: Microwave FMCW Doppler radar implementation for in-house pervasive health care system. In: Proc. IEEE International Workshop on Medical Measurements and Applications (2010)

The Method of Increasing the Accuracy of Mean Opinion Score Estimation in Subjective Quality Evaluation

A. Ostaszewska and S. Żebrowska-Łucyk

Warsaw University of Technology, Faculty of Mechatronics,
Sw. Andrzeja Boboli 8 Str., Warsaw, 02-525, Poland

Abstract. The paper presents a method of reliability estimation of scores obtained in subjective quality evaluation, which was inspired by procedures used in between-laboratory tests for determination of repeatability and reproducibility of measurement methods. The proposed use of Madel's k and h statistics enables for significant decrease of MOS standard deviation, which is exemplified by SSCQE of compressed video results.

1 Introduction

In case of wearable devices each issue starts and ends on a human being and apart from saving life it is also very important to improve its comfort and quality. No matter the definition of comfort or quality is, the only source of knowledge on human sensation and experience is subjective evaluation.

Subjective evaluation is conducted with a group of users of the technology that is being under investigation. Evaluation can be performed with the use of paper questionnaires or with the newer technologies that enable for continuous evaluation for example and need some special equipment. The method of subjective evaluation depends on the character of examined device or technology. Although various methods provide different type of scores, the common problem is the fact, that each of the subjects has his individual requirements, expectations and the level of satisfaction. Hence, the main problem associated with subjective assessments (apart from the fact that they are time- and cost-consuming) is a large dispersion of individual scores, which make estimates of population parameters obtained from experiments - generally speaking – of a little precision. In the language of statistics it means that the confidence intervals of calculated parameters are wide, and in the language of metrology it means a big uncertainty of measurements.

The accurate estimation of the expected value is of great practical importance. The most common estimator of the population mean is Mean Opinion Score (MOS)- mathematically averaged opinionated scores.

MOS is for example used in the area of subjective quality evaluation of compressed video. This area of evaluation came into existence and evolved parallel to

digital compression. As digital video has a wide audience, a lot had been done to improve the technology. There are recommendations on performing the quality evaluation with the detailed description of the various methods of collecting data. However, there is a problem with wide uncertainty intervals still, despite the fact that there are some ideas proposed of how to deal with that fact.

The paper presents the new method of data filtration, which enables for decreasing confidence intervals for the mean. The method is used for data that regard subjective continuous quality evaluation of compressed video, but the same attitude can be used in any area of measurement with the human audience.

Subjective quality assessment consists in evaluating the quality of the test sequence by the appropriately numerous group of observers and coming to a conclusion on the basis of the set of individual scores.

2 Subjects Selection

In case of subjective quality evaluation the key role is played by the observers. Their ability to focus, perceptiveness, the skill to translate their impressions to a measurement scale and reproducibility (in the meaning of the degree of compliance of scores in the repeated evaluation of the same sequence) influence not only measurement accuracy but also the usefulness of the experiment. Obviously not everyone has the right set of features to be predestined to accurate quality evaluation. Besides even a subject with the best perceptual features may in some adverse circumstances perform poorly due to the attention deficit.

That's why the procedure of subjects' selection should include two complementary phases. The first is the preliminary test (pretest), which is the psychometric test for skills and abilities to perform the task of constant observation and evaluation of a test material. The subject would be admitted to the further tests on the basis of the pretest result. The second phase of the selection process should base on critical analysis of individual scores given during the final test session. The scores which don't fulfill the criteria (for) shouldn't be taken into consideration whilst MOS computing.

In ITU Recommendations [3, 4, 5], which set the way of data proceeding for R&D centers all over the world, there admittedly is a similar attitude contained, but result of using it is not satisfactory. The pretest segment is limited to screening for normal visual acuity or corrected-to-normal acuity and for normal color vision. According to ITU Recommendations, subjects should not be directly involved either in picture or audio quality evaluation as part of their work and should not be experienced assessors. These undoubtedly are necessary conditions but not sufficient, as it doesn't take into consideration the ability to express the impression with the use of measurement scale nor the ability to maintain attention for a time of a test session. ITU Recommendations allow to discard the scores from the final test session, although the proposed methods don't have sufficient mathematical substantiation. Furthermore the experiments conducted in IMIIB PW show the proposed by ITU methods of discarding are not effective.

The necessity of improving methods and criteria of selection of subjects is obvious for computer scientists who work in the area of multimedia data compression

and transmission [6]. This issue is a subject of interest among scientists, who use statistical tools from the area of psychology [7].

The paper presents the metrological attitude to the issue, inspired with methods used in inter-laboratory comparisons and proficiency testing programs. The main feature of this method is concentrating on the quantitative results of individual scores instead of analyzing elementary causes of occurrence of unreliable scores.

The main idea is that the set of features tested in pretest should depend on the evaluation method (continuous, punctual, with or without a reference), so pretest conditions should be as close to the conditions of a chosen method as possible. The proposed method can be used both during the pretest and the decisive evaluation.

3 Scores Accuracy Examination

3.1 Between-Laboratory Tests

Quality evaluation of compressed video is the analogical issue to metrology tests, where the reference value does not exist and it is computed on the basis of statistical analysis of results obtained in laboratories which take part in a balanced uniform-level experiment [11, 12, 13, 14]. On the basis of experiment, not only the final result of the test is computed, but also the measurement accuracy is estimated. The concept of accuracy comprises trueness (the closeness of agreement between a test result and the accepted reference value) and precision (the closeness of agreement between independent test results obtained under stipulated conditions).

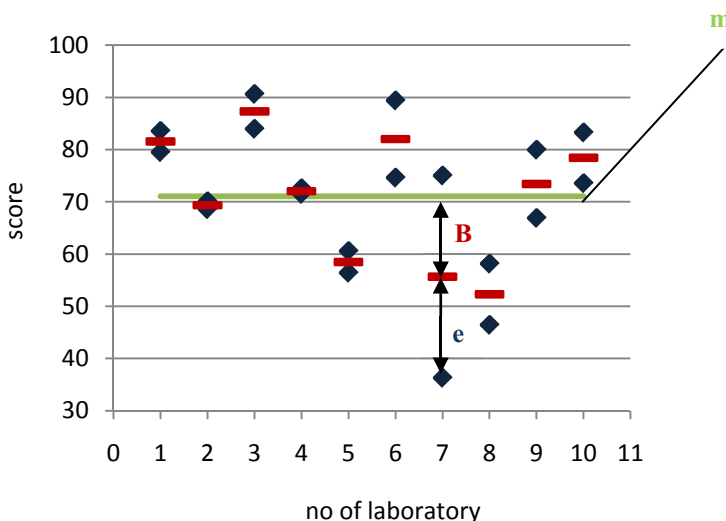


Fig. 1. Statistical model of the between-laboratory test

Analysis and interpretation of the test results is based on a statistical model as follows (fig. 1):

$$y = m + B + e, \quad (1)$$

where:

y – the test result, m – the general mean (expectation), B – the laboratory component of bias under repeatability conditions, e – the random error occurring in every measurement under repeatability conditions.

The general mean, m is the level of the test. In case of examining the difference between test results obtained by the same measurement method, the bias of the measurement method will have no influence and can be ignored.

The term B is considered as the sum of both random and systematic components. It is assumed to remain constant during any series of tests performed under repeatability conditions. The variance of B is called the between-laboratory variance and is expressed as:

$$\text{var}(B) = \sigma_L^2 \quad (2)$$

which includes the between-operator and between-equipment variabilities.

The term e represents a random error occurring in every test result and is assumed to be of an approximately normal distribution. Within a single laboratory, its variance under repeatability conditions is called the within-laboratory variance and is expressed as:

$$\text{var}(e) = \sigma_w^2 \quad (3)$$

and the arithmetic mean of the within-laboratory variances is called the repeatability variance and is designated by:

$$\sigma_r^2 = \overline{\text{var}(e)} = \overline{\sigma_w^2} \quad (4)$$

The reproducibility variance is expressed as:

$$\sigma_R^2 = \sigma_L^2 + \sigma_r^2 \quad (5)$$

In case of this type of experiment it is very important to find the proper method for detection inconsistent results and to develop criteria of rejection of unreliable data.. international standards [11] recommend two groups of consistency tests: graphical and numerical (tab. 1)

Table 1. Techniques of scrutiny for consistency according to ISO 5725

	Scrutiny for within-laboratory consistency	Scrutiny for between-laboratory consistency
graphical techniques	Mandel's k statistic	Mandel's h statistic
numerical techniques	Cochran's test	Grubbs' test

On the basis of the test chosen, inconsistent results are rejected and the general mean m and its confidence intervals are calculated. The results from the individual observers who participate in a quality evaluation of compressed video can be submitted the analogous procedure.

3.2 A Subject as a Laboratory

Looking at a procedure of compressed video quality evaluation from metrological point of view, it could be assumed that each of subjects (qualified to take part in a final test) could represent a single laboratory, which produces test results under repeatability conditions. The expected result is within-laboratory repeatability, which means producing consistent results under repeatability conditions. In case of subjective experiment it means coherent scores for the same test material. If a subject produces some inconsistent scores, they should be rejected and not taken into account during the further analysis.

From the scores that are inter-consistent it is necessary to discard those, which were given by the observers who do not perceive the compression errors or respond to other stimuli such as the scene content for example.

Similarly as in between-laboratory consistency tests, results produced under reproducibility conditions are expected to be in accordance with the opinion of the rest of the audience.

4 Proposed Method Verification

The filtration method proposed in the paper was used for processing data from Single Stimulus Continuous Quality Evaluation (SSCQE) experiment [4, 5].

As SSCQE is the single stimulus method, only the compressed video is displayed and there is no reference material given. Each of the observers has his own slider device with the scale attached and gives the scores which reflects the quality perceived constantly.

The scale ranges from 0 to 100, where a 100 means the perfect quality. No semantic scale was used, because there are some evidence that the use of it can change the scale to non-linear. The kind and the strength of this phenomena depends on the language used [8, 9, 10].

According to ITU-T References [5] the test material should be built of variously coded scenes, each of them at least 5 minutes long. Though the entire test session shouldn't be longer than 30 minutes.

In order to examine as wide range of coding parameters as possible, the material coded with the same parameters was one minute long and consisted of four 15-seconds scenes of one kind of content: 'bbc3' (bbc3), 'mobile' (mobi), 'cactus' (cact) and 'susie' (susi). Ten levels of bitrate were used in the experiment in a range from 2 Mbps to 5 Mbps. All test material was coded with MPEG-2, 13-picture Group of Pictures (GOP), with two B-frames in a structure. Individual

levels of coding were arranged randomly in the test material. Although the whole was ten minutes long, the experiment lasted 20 minutes, as the test material was displayed twice to the observers. The audience was not aware of this repetition.

45 students aged 20 – 25 participated in the experiment.

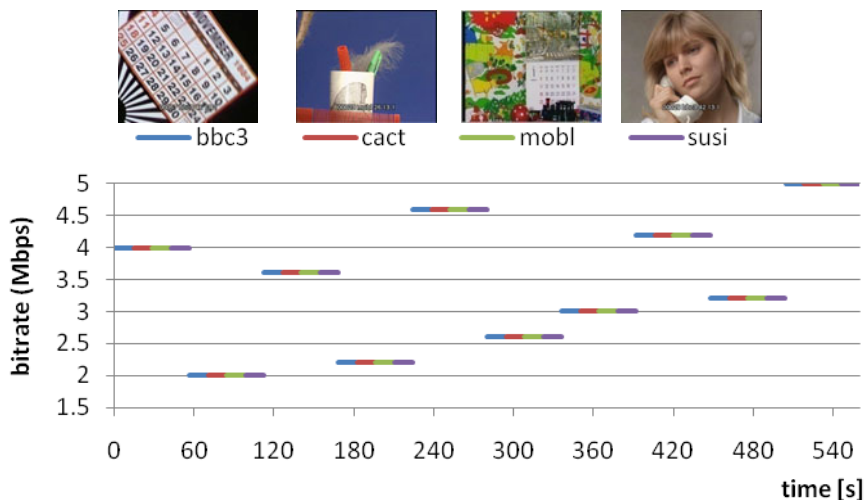


Fig. 2. Diagram of the test material: a) frames from four scenes used in the test, b) the test material distribution for a single session

5 Processing and Filtration Method

The raw measurement data were individual signals from each observer, sampled twice a second during the whole 20-minutes test.

For the purpose of examining the inter- and intra-consistency of observers' data, it was necessary to separate 15-seconds sectors of signals which related to each of the four scenes, as the scene content influences the character of scores strongly ($a = \text{bbc3, cact, mobl, susi}$).

To minimize the influence of individual dynamic of reaction, the filtration was carried out on the mean of scores given in time by the i -th observer ($i = 1, \dots, 45$) for the j -th level of coding ($j = 1, \dots, 10$) and for the k -th repetition ($k = 1, \dots, 2$), where $t' = 10$ is the number of samples from the beginning of the scene that are rejected to eliminate the „recency effect” [3] (fig. 3)

$$\bar{y}_{ijk.a} = \frac{1}{T - t'} \sum_{t=t'}^T y_{ijkta} \quad (6)$$

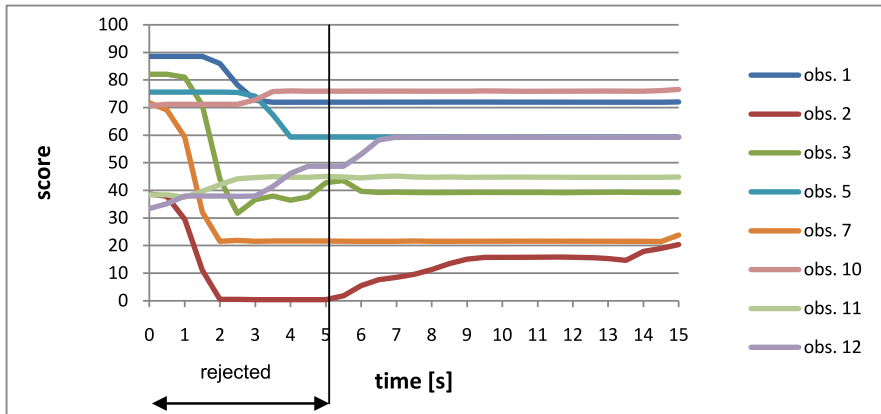


Fig. 3. Rejection of the first samples of measurement signal

The first step of filtration was qualifying the observer's scores to the further analysis – checking if he responds to the stimuli at all and if his reaction is not incoherent with the reaction of the rest of the audience. For this purpose there were computed consecutively:

- a. mean of scores given by the i -th observer in n repetitions ($n = 2$) for each j -th level of coding ($j = 10$):

$$\bar{y}_{ij..a} = \frac{1}{n} \sum_{k=1}^n \bar{y}_{ijk.a}, \quad (7)$$

- b. MOS (Mean Opinion Score) – mean of scores from the audience for each of j -th level of coding:

$$\bar{y}_{.j..a} = \frac{1}{p} \sum_{i=1}^p \bar{y}_{ij..a}, \quad (8)$$

- c. Spearman rank correlation R_{ij} between scores from i -th observer and MOS for the j -th level of coding, for each of a -scenes ($a = 4$) separately.

Signals from the observer for whom $R_{ij} < 0,5$ were rejected. In this experiment it was 17% signals discarded. Amongst them there were scores from observers, who didn't respond at all (fig. 4, b-series) or who generated random scores (fig. 4, a-series).

As the mean score and the range of scores used vary between individual observers, it is proper to treat the subjects as measurement tools with different sensitivity (fig. 5). To make comparison of measurement signals, it was necessary to standardize them first. The operation starts with normalization, which makes all individual means of the same value and the same range of scale used). Then the

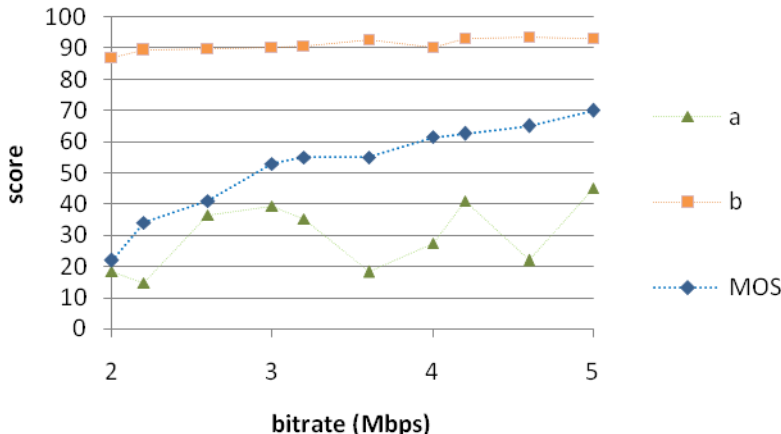


Fig. 4. Examples of individual scores assigned to be unreliable with the signal form the audience in the bacground; MOS – mean opinion score form all the subjects display expected increase of quality corelated with the increase of bitrate, a – individual scores assumed to be random (with no consistency with the trend of MOS, b – the lack of reaction to the changes of quality

data are multiplied by standard deviation of scores given by the audience (pooled standard deviation) and the mean of all scores is added to come back to the original scale:

$$\bar{y}_{ijk_norm} = \frac{\bar{y}_{ijk.a} - \bar{y}_{i...a}}{\sqrt{\frac{\sum_{j=1}^q (\bar{y}_{ijk.a} - \bar{y}_{i...a})^2}{q}}} \sqrt{\frac{\sum_{i=1}^{p_R} \sum_{j=1}^q (\bar{y}_{ij..a} - \bar{y}_{i...a})^2}{p_R q - 1} + \bar{y}} \quad (9)$$

where:

$i = 1 \dots p_R$, where p_R – number of observers after the first step of filtration (Spearman rank correlation)

$\bar{y}_{i...a}$ - mean of scores from the i -th observer given for all levels of coding of the scene a:

$$\bar{y}_{i...a} = \frac{1}{q} \sum_{j=1}^q \bar{y}_{ij..a} \quad (10)$$

$\bar{y}_{....a}$ - mean from all means from all observers:

$$\bar{y}_{...a} = \frac{1}{p_R} \sum_{i=1}^{p_R} \bar{y}_{i...a} \quad (11)$$

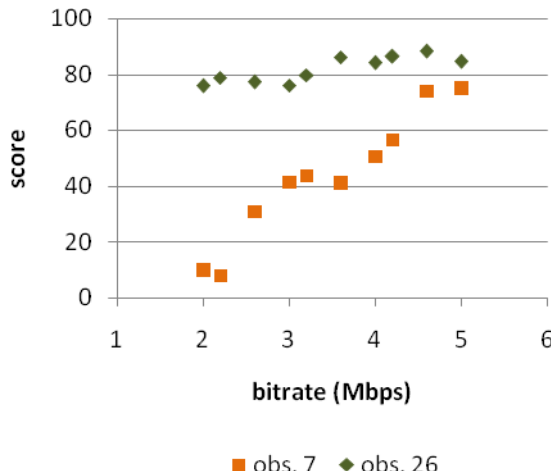


Fig. 5. Mean of scores given for the certain bitrate by two individual observers with different sensitivity

Figure 6 shows the effect of standardization of two signals.

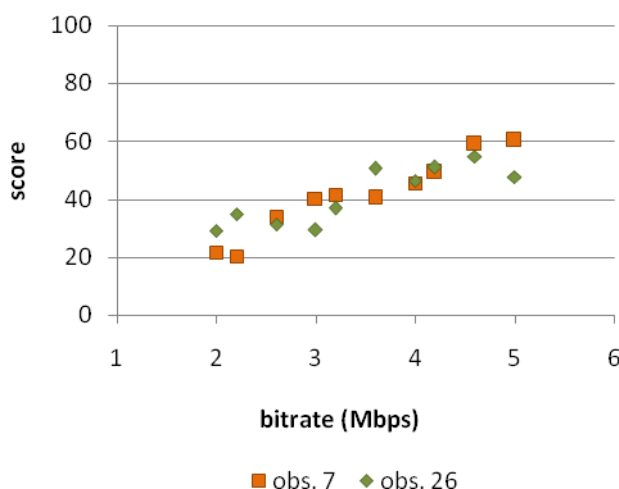


Fig. 6. Mean of scores given for the certain bitrate by two individual observers with different sensitivity

In the next step each level of coding was processed separately. The criteria for keeping or rejecting the data was based on the difference of scores:

- given by the same observer for the repeated measurement – checking inter-consistency,
- given by the observer and MOS – checking intra-consistency.

In order to check the inter-consistency the Mandel's k statistic was used, where k for the i-th observer for the j-th level of coding is computed according to the following formula:

$$k_{ija} = \frac{s_{ija}}{s_{rja}} \quad (12)$$

where:

s_{ija} - the standard deviation for the i-th observer and j-th level:

$$s_{ija} = \sqrt{\frac{\sum_{k=1}^n (\bar{y}_{ijk.a} - \bar{y}_{ij..a})^2}{n-1}} \quad (13)$$

where:

s_{rja} - the repeatability standard deviation:

$$s_{rja} = \sqrt{\frac{\sum_{i=1}^p s_{ija}^2}{p}} \quad (14)$$

and the critical value of k_c is computed

$$k_c = \sqrt{\frac{pF\{\alpha, f_1, f_2\}}{F\{\alpha, f_1, f_2\} + (p-1)}} \quad (15)$$

$$f_1 = n-1$$

$$f_2 = (n-1)(p-1)$$

α – significance level $\alpha = 0,05$

$F\{\alpha, f_1, f_2\}$ – quantile from the F-distribution with f_1 and f_2 degrees of freedom (numerator and denominator).

The results of Mandel's k statistic usage for all 10 levels of coding of scene mobl are displayed in the figure 7. Horizontal lines show the critical values – boundaries between acceptable results and those which qualify for rejection because of the lack of intra-consistency.

The intra-inconsistent scores were rejected with the use of Mandel's h statistic, where h value was computed as follows:

$$h_{ija} = \frac{\bar{y}_{ij..a} - \bar{y}_{.j..a}}{s_{mja}} \quad (16)$$

where:

$$s_{mja} = \sqrt{\frac{\sum_{i=1}^p (\bar{y}_{ij..a} - \bar{y}_{.j..a})^2}{p}} \quad (17)$$

and hc given by formula:

$$h_c = \frac{(p-1)t\{\alpha, f\}}{\sqrt{p(t^2\{\alpha, f\} + p-2)}} \quad (18)$$

$$f = p-2$$

α – significance level $\alpha = 0,05$

$t\{\alpha, f\}$ – quantile of t-Student distribution with f degrees of freedom

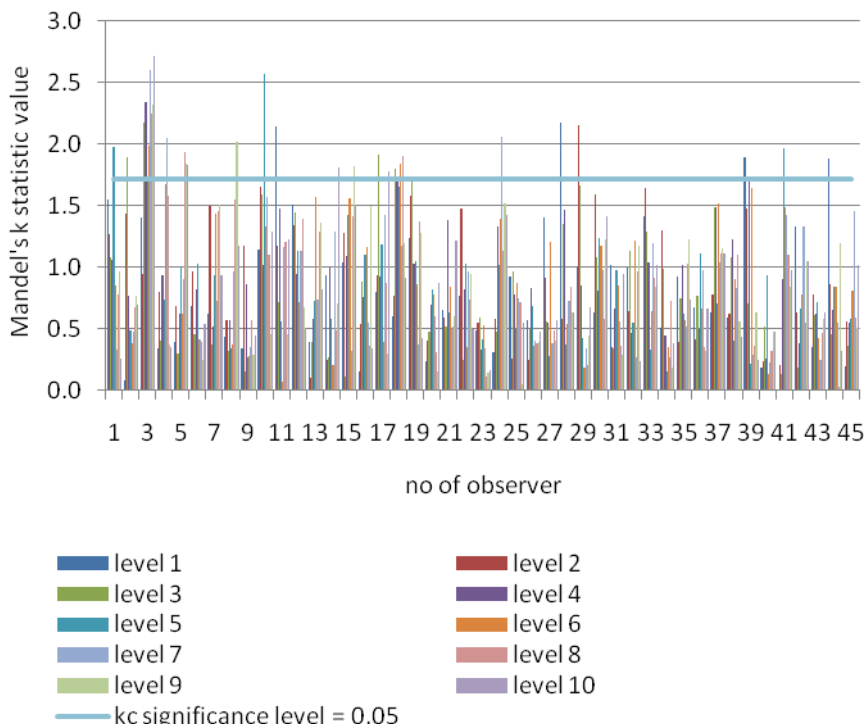


Fig. 7. Graphic illustration of the Mandel's k statistic results

The results of Mandel's statistic usage for the 'mobl' scene are presented in the fig. 8. The value of the test can be either positive or negative, so the critical values of Mandel's h statistic are shown as two horizontal lines (fig. 8).

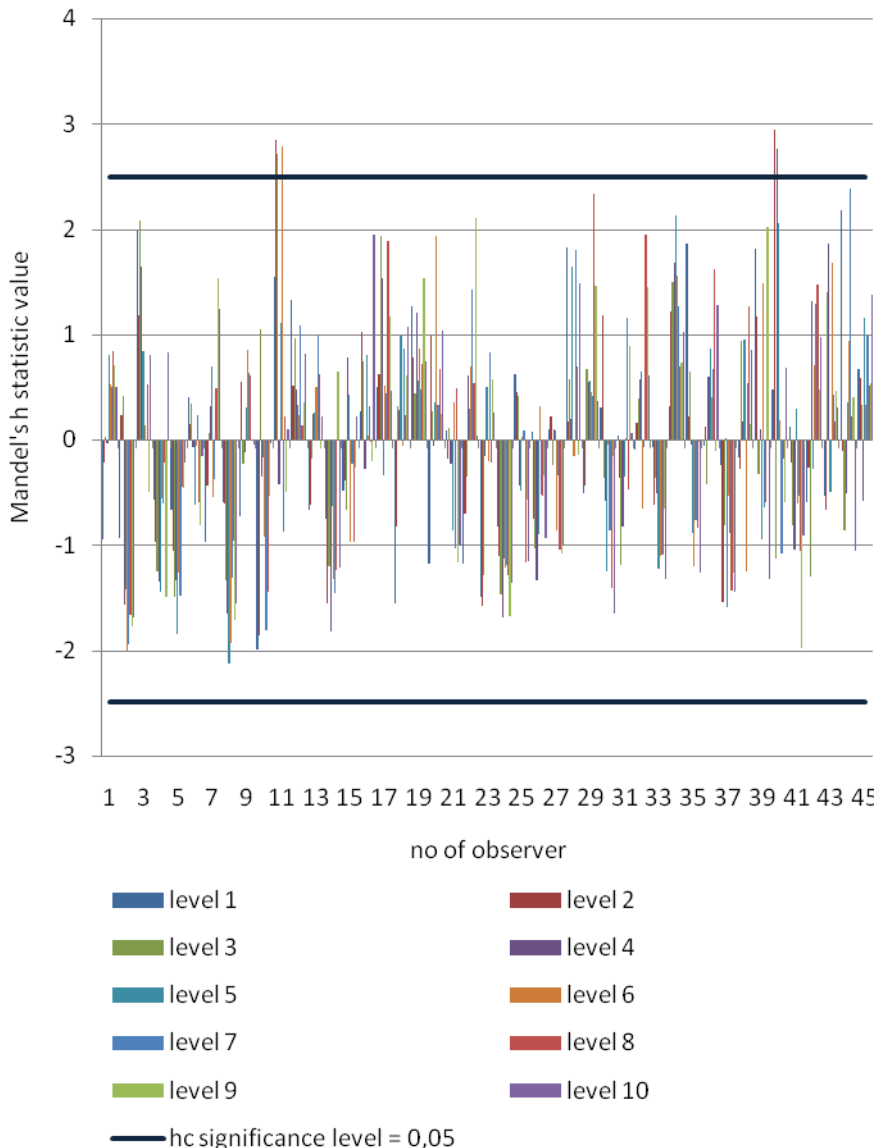


Fig. 8. Graphic illustration of the Mandel's h statistic results

The result of the proposed method of data filtration is decreasing the standard deviation of mean of scores given for each level of coding from 14 – 18 % (fig. 10) of the measurement scale to 7 – 9 % (fig. 11).

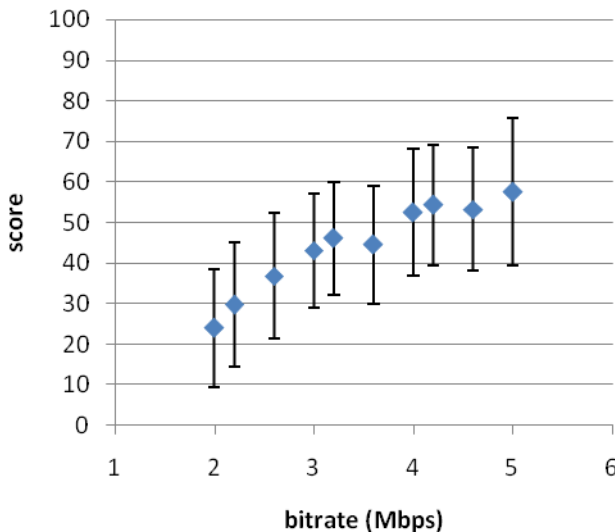


Fig. 9. Mean opinion scores (MOS) and standard deviation of MOS, SSCQE results (45 subjects, ‘mobl’ scene) computed on the basis of raw data

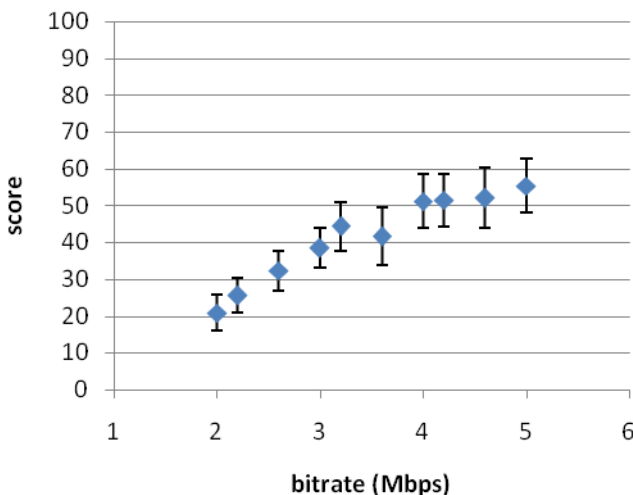


Fig. 10. Mean opinion scores (MOS) and standard deviation of MOS, SSCQE results (45 subjects, ‘mobl’ scene) computed on the basis of filtered data

6 Conclusions

Both the thorough analysis of the results obtained from subjective tests and keeping the proper conditions under which the experiment is carried out contribute to expanding the state of the art in the area of compression errors perception.

The proposed method of inconsistent scores rejection enables for more precise evaluation of expected population mean score without the necessity of increasing the number of observers. The method is based on the objective mathematical criteria, which should always be taken a priori (for example the significance level of tests used, the minimal number of observers) the way to limit the risk of making errors of the first and of the second kind.

In case of continuous methods of assessment, like SSCQE for example, presented method of data analysis enables for rejection not only the whole signals from the unreliable observer, but also just the part of it, where the bias is substantial. Thanks to that the data collected in the experiment is effectively used.

The discussed approach is recommended to use for any subjective evaluation, wherever the standard deviation is too large to draw conclusions on the assumed significance level.

References

- [1] Lauterjung, J.: First results of digital video quality measurements in DVB networks, Rohde & Schwarz (January 2006)
- [2] Morris, T., Angus, K., Butt, R., Chilton, A., Dettman, P.: CQA – Subjective Video Codec Quality Analyser. BMVC 1999 Image Matching and Retrieval (1999)
- [3] ITU-T P 910 Subjective video quality assessment methods for multimedia applications (2008)
- [4] ITU-T P 911, Subjective audiovisual quality assessment methods for multimedia applications (1998)
- [5] ITU-R BT 500-12 Methodology for the subjective assessment of the Quality of Television Picture (2009)
- [6] Grega, M., Janowski, L., Leszczuk, M., Romaniak, P., Papir, Z.: Quality of experience evaluation for multimedia services. Przegląd Telekomunikacyjny i Wiadomości Telekomunikacyjne (April 2008)
- [7] Uebersax, J.: Statistical methods for rater agreement, <http://ourworld.compuserve.com/homepages/jstuebersax/agree.htm>
- [8] Jones, B.L., McManus, P.R.: Graphicscaling of qualitative terms. SMPTE Journal (November 1986)
- [9] Narita, N.: Graphic scaling and validity of Japanese descriptive terms used in subjective evaluation tests. SMPTE Journal (July 1993)
- [10] Virtanen, M.T., Gleiss, N., Goldstein, M.: On the use of evaluative category scales in telecommunications. In: Proc. Human Factors in Telecommunications (1995)
- [11] ISO 5725:1994, Accuracy (trueness and precision) of measurement methods and results

- [12] ISO/IEC Guide 43-1:1997 Proficiency testing by interlaboratory comparisons – Part 1: Development and operation of proficiency testing schemes
- [13] ISO/IEC Guide 43-2:1997 Proficiency testing by interlaboratory comparison – Part 2: Selection and use of proficiency testing schemes by laboratory accreditation bodies
- [14] ISO/IEC 17025:2005 General requirements for the competence of testing and calibration laboratories

Wearable Assistive Devices for the Blind

Ramiro Velázquez

Universidad Panamericana, Aguascalientes, Mexico

Abstract. Assistive devices are a key aspect in wearable systems for biomedical applications, as they represent potential aids for people with physical and sensory disabilities that might lead to improvements in the quality of life. This chapter focuses on wearable assistive devices for the blind. It intends to review the most significant work done in this area, to present the latest approaches for assisting this population and to understand universal design concepts for the development of wearable assistive devices and systems for the blind.

Keywords: assistive technology, reading/mobility aids, wearable devices and systems.

1 Introduction

1.1 Target Population

Globally, an estimated 40 to 45 million people are totally blind, 135 million have low vision and 314 million have some kind of visual impairment [1]. The incidence and demographics of blindness vary greatly in different parts of the world. In most industrialized countries, approximately 0.4% of the population is blind while in developing countries it rises to 1%. It is estimated by the World Health Organization (WHO) that 87% of the world's blind live in developing countries.

Over the last decades, visual impairment and blindness caused by infectious diseases have been greatly reduced (an indication of the success of international public health action), but there is a visible increase in the number of people who are blind or visually impaired from conditions related to longer life expectancies. The great majority of visually impaired people are aged 65 years or older. It is estimated that there is a per-decade increase of up to 2 million persons over 65 years with visual impairments. This group is growing faster than the overall population.

In younger groups, blindness and visual impairment is mainly due to birth defects and uncorrected refractive errors. In the first case, most of the causes are in the brain rather than in the eye while in the second one, they are conditions that could have been prevented if diagnosed and corrected with glasses or refractive surgery on time.

It is estimated that by the year 2020, all blind-related numbers will double.

1.2 Dimension of the Problem

Of all sensations perceived through our senses, those received through sight have by far the greatest influence on perception. Sight combined with the other senses, mainly hearing, allow us to have a world global perception and to perform actions upon it. For the blind, the lack of sight is a major barrier in daily living: information access, mobility, way finding, interaction with the environment and with other people, among others, are challenging issues.

In fact, school and working-age blind have very high analphabet and unemployment rates. For example, in the US, the blind unemployment rate is around 75% while only 10% of the blind children receive instruction in Braille [2]. Despite efforts, a true is that most schools and employers cannot accommodate blind people. In consequence, the person who is blind and his/her family face important socioeconomic constraints.

The issue of the blind becomes a very serious problem in terms of health and social security. Costly-in home expenses, nursing home care and welfare expenses on unemployment and health services have to be absorbed by the state.

A state action to enable the blind/visually impaired to live independent and productive lives has been to teach them new ways to accomplish routine daily tasks. A great variety of specialists is involved: special education teachers, Braille teachers, psychologists, orientation and mobility specialists, low-vision specialists and vision rehabilitation therapists to name a few.

Evidently, this involves a very high cost that has to be absorbed by the state. Moreover, the availability of funding and qualified personnel is insufficient to cover the actual population's demand. Other means are urgently needed to assist this population.

1.3 Assistive Technology

Advances of technology and better knowledge in human psycho-physiological 3D world perception permit the design and development of new powerful and fast interfaces assisting humans with disabilities. For the blind, research on supportive systems has traditionally focused on two main areas: information transmission and mobility assistance. More recently, computer access has been added to the list [3].

Problems related to information transmission concern reading, character recognition and rendering graphic information about 2D and 3D scenes. The most successful reading tool is the Braille dot code. Introduced by Louis Braille in the 19th century, it has now become a standard worldwide. Inventions addressing the problems of character recognition and pictorial representation mostly consist of tactile displays. They permit character and graphic recognition by feeling a tactile version of them.

Problems related to mobility assistance are more challenging. They involve spatial information of the immediate environment, orientation and obstacle avoidance. Many electronic travel aids (ETAs) for safe and independent mobility of the blind have been proposed over the last decades. They all share the same operation principle: they all scan the environment (using different technologies) and display the information gathered to other sense (mainly hearing and touch).

With the internet revolution of the last years, problems related to computer access for the blind arose. Popular solutions are voice synthesizers, screen magnifiers and Braille output terminals. Voice synthesizers practically read the computer screen; screen magnifiers enable on-screen magnification for those with low-vision and Braille output terminals are plugged to the computer so that information on the screen is displayed in Braille.

1.4 Wearable and Portable Devices

This chapter reviews wearable assistive devices for the blind and less portable assistive devices. There is a slight difference between both.

Wearable devices are distinctive from portable devices by allowing hands-free interaction, or at least minimizing the use of hands when using the device. This is achieved by devices that are actually worn on the body such as head-mounted devices, wristbands, vests, belts, shoes, etc.

Portable devices are usually compact, lightweight, they can be easily carried (but not worn) by the user and require constant hand interaction. For example: tactile displays, electronic canes, mobile phones, laptop computers, etc.

The area of wearable devices is currently a “hot” research topic in assisting people with disabilities such as the blind. As this area is still very much young and experimental, there are not many mature commercial products with a wide user base.

2 Wearable Technologies for the Blind

A number of wearable assistive devices have been developed as task-specific solutions for activities such as reading and travel. Given the fact that sight is missing, they try to open new communication channels through hearing and touch. Devices are as diverse as the technology used and the location on the body. Fig. 1 overviews the body areas involved in wearable assistive devices: fingers, hands, wrist, abdomen, chest, feet, tongue, ears, etc. have been studied to transmit visual information to the blind. This chapter intends to review several prototypes so that their potential can be appreciated.

2.1 Considerations on Hearing and Touch

After sight, hearing and touch are definitively the second and third major human senses, respectively. For the blind, they evidently become the first and second ones, respectively.

Blind people rely on hearing environmental cues for key tasks such as: awareness, orientation, mobility and safety. A representative example is when trying to cross a street intersection all alone: they stand-still listening to the environment and will not cross until the traffic light sequence is fully understood.

The ear is the sense organ that detects sound vibrations. It is responsible for transducing these vibrations into nerve impulses that are perceived by the brain.

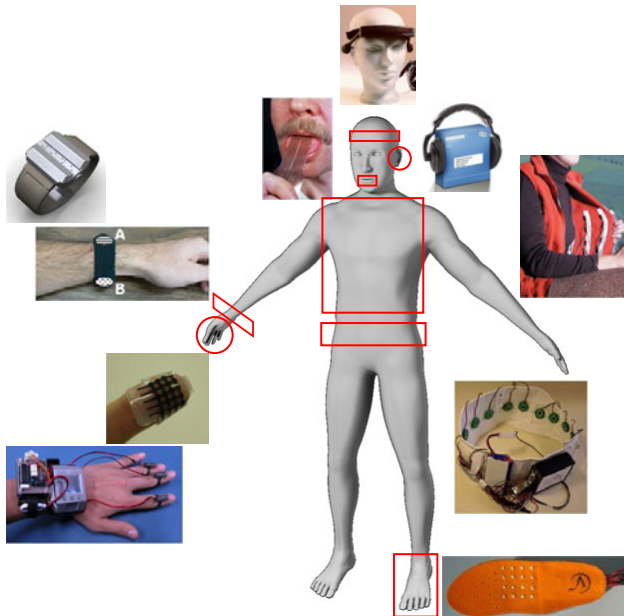


Fig. 1. Overview of wearable assistive devices for the blind.

After brain processing, it is possible for humans to detect several characteristics of sound such as loudness, pitch or frequency, timbre, direction and distance to the source.

Roughly, the audible frequency range of the human ear is 20 Hz to 20 kHz with a remarkable discrimination of 0.5 to 1 Hz. Hearing a sound mainly depends on 2 parameters: sound intensity and frequency.

Fig. 2 shows the measured threshold of hearing curve that describes the sound intensity required to be heard according to frequency. The standard threshold of hearing at 1 kHz is nominally taken to be 0 dB, but it is actually about 4 dB. Note that there is a marked difference between low and high frequencies: while about 60 dB is required to be heard at 30 Hz, about 18 dB is required at 10 kHz. The high sensitivity region at 2 to 5 kHz is very important for the understanding of speech.

Human tolerance to sound intensity goes from the threshold of hearing at 4 dB to the threshold of pain at 120 dB, which can be produced by a jet engine.

It has been demonstrated that 8 hours of 90 dB sounds can cause damage to the ears, 1 minute of 110 dB causes hearing loss and any exposure to 140 dB sounds causes immediate and irreversible damage [4].

Additional related problems are the degradation and overload of the hearing sense. Recent studies [5] have shown that a 20-30 minute listening to music/speech/sound activity causes degradation to human sensors information registration, reduces human capacity to perform usual tasks and affects the posture and equilibrium.

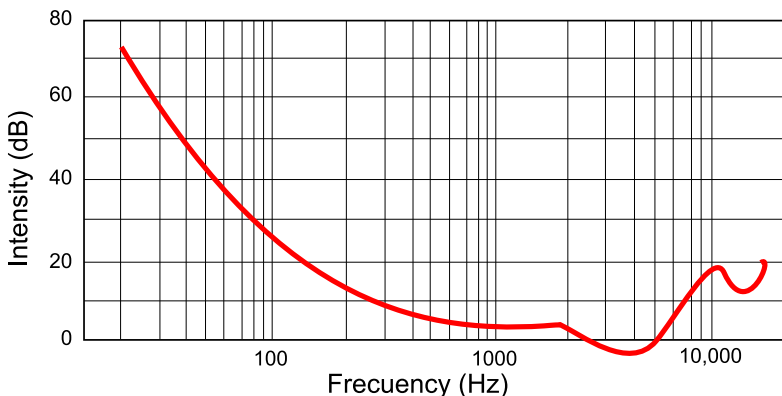


Fig. 2. Threshold of hearing: sound intensity minimal thresholds as function of frequency, after [4].

All these facts must be taken into account when designing assistive devices that exploit hearing as the substitution sense.

In healthy-sighted, touch is generally used as an additional independent sensory modality to convey information or as a redundant modality to increase information coming from vision and hearing.

For the blind, touch becomes the primary input for the receipt of non-audible physical information. Blind people can rapidly and accurately identify three-dimensional objects by touch. They can also locate and orient themselves in known environments by touching objects. Braille readers access information through touch.

The skin is the sense organ that contains the essential biological sensors of touch. It encompasses 3 main groups of sensors organized by biological function: the thermoreceptors, responsible for thermal sensing, the nociceptors, responsible for pain sensing and the mechanoreceptors, sensitive to mechanical stimulus and skin deformation.

Our interest focuses on the mechanoreceptors as they are responsible for sensing and transmission of physical deformations by external forces to the nervous system. Four kinds of mechanoreceptors can be found on the human glabrous skin: Pacini corpuscles, Ruffini endings, Merkel cells and Meissner corpuscles.

According to [6], Meissner corpuscles respond to touch, Pacini corpuscles respond to vibration, Ruffini endings respond to lateral extension of the skin and articular movement and Merkel cells perceive pressure.

Our interest mainly focuses on Meissner and Pacini skin mechanoreceptors since they are involved in hand feeling during object exploration.

Similar to the relationship found for hearing, feeling a deformation on the skin depends on the relation between the amount of skin indentation and frequency. Fig. 3 shows this relation for Meissner and Pacini mechanoreceptors. Note that while Pacini corpuscles are sensitive to low amplitude-high frequency stimuli, Meissner ones are sensitive to high amplitude-low frequency stimuli.

The ability to discriminate stimuli on the skin varies throughout the body. The two-point discrimination threshold (TPDT) is a measure that represents how far apart two pressure points must be in order to be perceived as two distinct points on the skin [8]. This measurement usually aids designers in choosing the density of a tactile display depending on the part of the body the tactile display will be

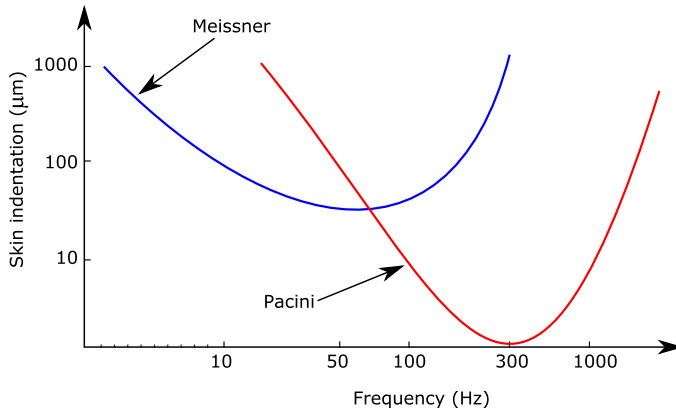


Fig. 3. Skin indentation minimal detection thresholds as function of frequency, after [7].

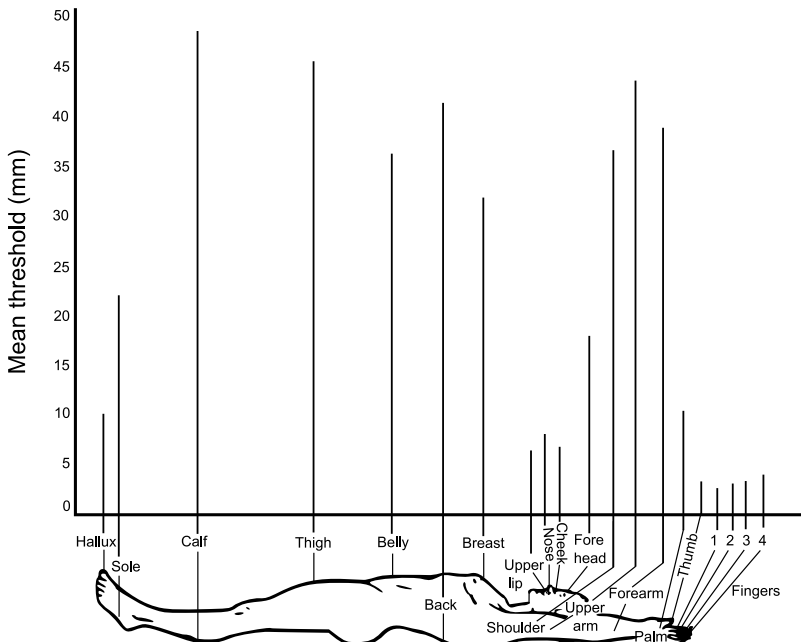


Fig. 4. TPDT for different areas of the body, after [9].

mounted. Fig. 4 shows the TPDT for different areas of the body. The TPDT is 2.54 mm for the fingertips, 18 mm for the forehead, 40 mm for the forearm, 42 mm for the back, 49 mm for the calf, etc.

Figs. 3 and 4 are the basis for designing wearable touch stimulation devices such as tactile displays. For example, for correctly stimulating the fingertips, a tactile display should integrate an actuator array of 2.54 mm interspacing (Fig. 4) and produce an effective skin indentation of 1 mm at 1 Hz (Meissner curve, Fig. 3) or have an array of contact pins at 2.54 mm interspacing and produce 10 μm of skin indentation at 100 Hz (Pacini curve, Fig. 3).

2.2 Assistive Devices Worn on Fingers and Hands

Most of the assistive devices for the blind that exploit touch as the substitution sense are tactile displays for the fingertips and palms. Typical tactile displays involve arrays of vibrators or upward/downward moveable pins as skin indentation mechanisms.

Many tactile devices have been developed using a wide range of technologies. Approaches range from traditional actuation technologies such as servomotors, electromagnetic coils, piezoelectric ceramics and pneumatics [10-13] to the new ones: shape memory alloys (SMAs), electroactive polymers (EAPs), electrorheological (ER) fluids and airbone ultrasound [14-17].

However, most of the tactile displays found in the literature are at best good examples of portable devices. Wearable devices for the fingers and palms were not found in the literature until recently. Two examples are the band-aid-size tactile display from Sungkyunkwan University (Korea) and the Finger-Braille interface from Tokyo University (Japan).



Fig. 5. Wearable tactile display for the fingertip.

The bandage-sized tactile display is an innovative touch stimulation device based on EAP soft actuator technology (Fig. 5). It is soft and flexible and can be wrapped around the finger like a band-aid. This new wearable display could be used as a Braille display or as a multi-purpose tactile display to convey visual information to the blind.

The first prototype developed is a thin polymer sheet of 210 μm thick with 20 EAP soft actuators distributed in an active area of $14 \times 11\text{mm}^2$ which covers most

of the fingertip's touch-sensitive area. Tactile feel is produced by actuating the 20 contact points independently. Both vibration and upward/downward patterns can be generated using an external user computer interface [18].

The Japanese Finger-Braille interface is a wearable assistive device to communicate information to the deaf-blind. In this system, the fingers are regarded as Braille dots: 6 fingers, 3 at each hand, are enough to code any 6-dot Braille character. Some examples of translation are shown in fig. 6.

Using this codification, 6 small lightweight vibrating DC motors were attached to the fingers (Fig.7). They provide a 120 Hz vibration to stimulate the back of the finger. Each 3 motor-hand is controlled by a Citizen-IBM wristwatch computer and an electronic module that includes the batteries and control circuitry. The wristwatch computer is capable of communicating with external devices via Bluetooth technology. The total weight of the equipment, including battery, is approximately 170 g per hand.

The creators of the Finger-Braille interface report in [19] high recognition rates from experiments conducted with deaf-blind subjects which shows the prototype's potential for providing Braille information.

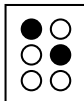
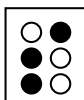
Character	Braille code	Finger-Braille
e		
s		

Fig. 6. Finger-Braille code.



Fig. 7. Finger-Braille interface with wristwatch computers.

2.3 Assistive Devices Worn on the Wrist and Forearm

Researchers at the University of British Columbia (Canada) have developed two prototypes of vibrotactile displays that can be worn on the forearm and wrist (Fig. 8(a)).

Both displays consist of 2 vibrating DC motors spaced 60 mm apart that generate vibrations at 140 Hz [20].

These tactile devices convey information using intermittent alert-like signals and were used to alert clinicians of adverse changes in a patient's heart rate without distracting their attention with auditory alarms. Experiments conducted with these prototypes showed that there was no difference between the wrist and forearm: comfort and accuracy of information were perceived to be the same.

Similarly to this application, these devices could be used to convey simple patterns such as alert-like information to the blind for example when approaching an obstacle.

A popular wearable assistive device for the wrist is of course the Braille watch (Fig. 8(b)). On the basis that a watch is a primary necessity for living a normal life, several companies are nowadays commercializing Braille watches.

These watches, which have the exact same mechanism as the regular ones, display time information as raised patterns on the dial or as Braille numbers which blind people will sense.



Fig. 8. (a) Tactile display prototypes for the forearm and wrist and (b) Braille watch.

2.4 Assistive Devices Worn on the Tongue

In normal vision, the eyes send signals to the middle of the brain. From there, these signals are sent directly to the visual cortex. Not so for the blind.

In 1998, the University of Wisconsin (USA) introduced the TDU (Tongue Display Unit). The TDU proposed to retrain the way the brain processes visual information by first stimulating the tongue with an electrode array. The nerves in the tongue send signals through a different pathway to the brain stem in the area that deals with touch. Eventually, the blind person learns to interpret touch as sight in the virtual cortex.

The TDU first prototype translated optical images picked up by a camera into electro-tactile stimuli which were delivered to the dorsum of the tongue via a 12 x 12 flexible electrode array placed in the mouth (Fig. 9(a)). Experiments report that after sufficient training (15 h), the user loses awareness of on-the-tongue sensations and perceives the stimulation as shapes and features in space [21].

Inspired by the TDU, researchers at the University of Montreal (Canada) proposed a tongue display to help blind people navigate around obstacles (Fig. 9(b)) [22]. This device, under the name of Brainport Vision Technology, is expected to be commercially available in the near future.

Another TDU-based display is the one developed by researchers at Joseph Fourier University (France). Their prototype consists of a matrix of 36 electrodes that transmit electrical impulses to the tongue (Fig. 9(c)). This device is currently being used to detect and correct stability and posture [23].

The ultimate goal of the TDUs is to develop a compact, cosmetically acceptable, wireless system that can be worn like a dental orthodontic retainer.

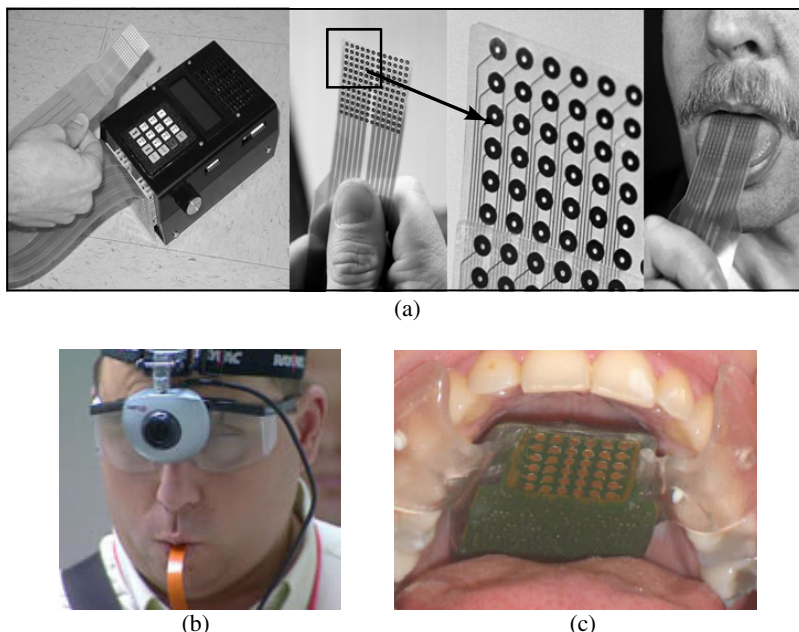


Fig. 9. TDU systems. Prototypes of: (a) the University of Wisconsin, (b) the University of Montreal and (c) Joseph Fourier University.

2.5 Head-Mounted Assistive Devices

Head-mounted devices (HMDs) such as headsets and headbands are the most popular kind of wearable assistive devices.

The head is the rostral part of the human body that comprises the brain, eyes, ears, nose and mouth (all of which are responsible for sensory functions). In

particular, the ears, the only sensory organ responsible for hearing throughout the body and the main substitution pathway for the blind, are located on the head. Moreover, humans use head motion to gather information from the environment. It is easy to deduce that devices worn on the head acquire that freedom of motion for environment scanning.

A number of HMDs have been developed for reading and travel assistance of the blind. For reading, the most representative example is the audio book. Entire text books are recorded in the form of speech and reproduced by wearable headset systems (earphones and player).

Since 1950, audio books have benefited the blind population by offering a simple, low-cost, non-Braille reading option. Thousands of titles are available, and with today's technology they can be downloaded for example, from the National Library Service for the Blind and Physically Handicapped (NLS) [24]. Even though the undisputable advantages of audio books, two issues have to be considered:

- **Availability.** Even though there are thousands of titles, not all books are systematically converted to audio books and there is a significant delay with new books. Months, years (or never) could take to have a new book available in audio form.
- **Audio books should not be considered as the reading solution for blind people.** It is true that they fit perfectly for the elderly and non-Braille readers. However as healthy-sighted do prefer to read a book instead of hearing it, why do we assume that a blind person prefers to listen to a book instead of reading it? For the blind, reading a book heightens the self-esteem and independence. Moreover, it trains their orthography which is in most cases quite bad.

For travel assistance, several HMDs have been proposed. In the early years, the most sophisticated device that first became commercially available was the Binaural Sonic Aid (SonicGuide) [25]. The SonicGuide consisted of an ultrasonic wide-beam equipment mounted on spectacle lenses (Fig. 10(a)). Signals reflected back from the 3D world were presented to the user as audio indicating the presence of an obstacle and its approximate distance to the user.

Over the years, the SonicGuide has undergone continuous improvements and its latest version is the system called KASPA [26]. KASPA is worn as a headband

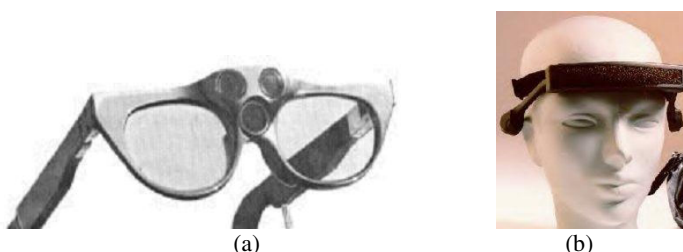


Fig. 10. (a) The SonicGuide (1974) and (b) its latest version, the KASPA system (2002).

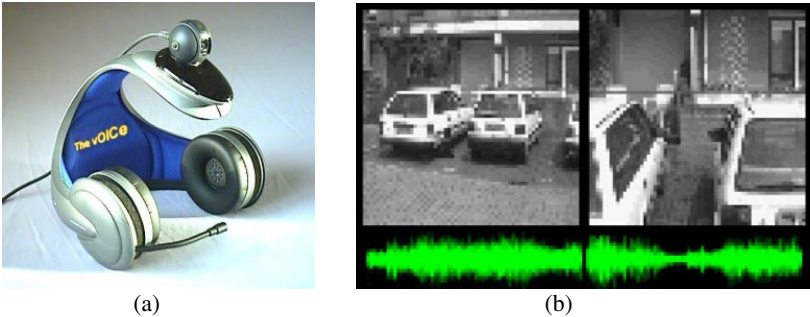


Fig. 11. (a) The vOICe system and (b) an example of its image-to-sound rendering.

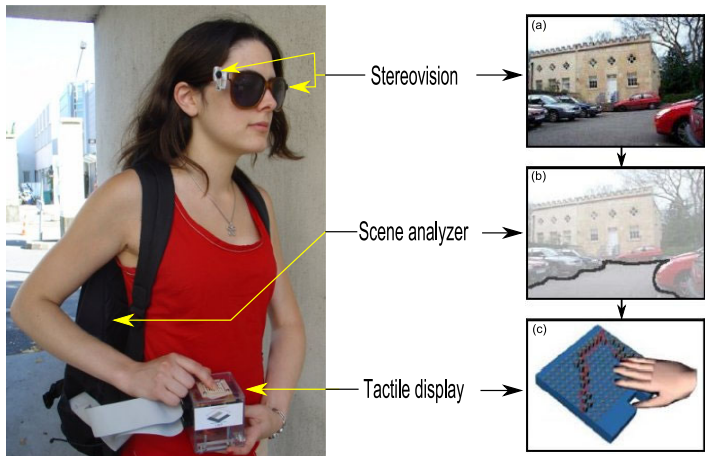


Fig. 12. The IG wearable system and an example of its image-to-tactile rendering.

(Fig. 10(b)) and creates an auditory representation of the objects ahead of the user. With sufficient training, allows users to distinguish different objects and even different surfaces in the environment.

Many portable ETAs like the SonicGuide and the Kaspa system have been developed in the form of hand held devices [27-28]. All these devices are similar to radar systems: a laser or ultrasonic beam is emitted in a certain direction in space and the beam is reflected back from objects that it confronts on its way. A sensor detects the reflected beam, measures the distance to the object and indicates that information to the user through audio or tactile signals.

A new generation of ETAs aims to provide a sensory substitution/supplementation more than merely obstacle detection. The information is acquired using video cameras and its processing is more at cognitive level (brain plasticity, perception, intentionality, etc.). Two representative examples are here presented.

The vOICe system (Fig. 11(a)), patented by Philips Co., converts visual depth information into an auditory representation [29]. This is the first device that

successfully uses a camera as an input source. An image is translated to sounds where frequency and loudness represents different scene information parameters such as position, elevation and brightness (Fig. 11(b)). Simple things like finding an object may be mastered in minutes but fully mastering the vOICe's visual-to-auditory language may well take years.

The vOICe is nowadays a mature commercial product [30] and a large number of testimonials show that it is actually improving the quality of life of blind users.

The Intelligent Glasses (IG) is a combined HMD and tactile display system developed at Paris 6 University (France). The IG is a new generation ETA that provides tactile maps of visual spaces and allows users to deduce possible paths for navigating these spaces in order to perform independent, safe and efficient mobility tasks.

The IG system is basically composed of 3 main modules: vision module, scene analyzer and tactile display. Fig. 12 shows the IG first wearable prototype and its operation principle: (a) a pair of stereo-cameras mounted on the glasses frame acquire the environment's representation. (b) Vision algorithms are then applied in order to identify the obstacles in the scene and their user-related position. (c) Finally, this information is displayed on a tactile display for fast exploration by the user. The resulting tactile map is a simple edge-like representation of the obstacles' locations in the scene. All obstacles are considered and displayed in tactile domain as binary data: presence or absence of an obstacle.

Results in [31] show that healthy-sighted blindfolded subjects are able to understand, interact and navigate spaces using tactile maps. Upon training, subjects become more efficient and used to the IG system and tactile maps.

2.6 Vests and Belts

Researchers at Carnegie Mellon University (USA) presented in [32] the Kahru Tactile Outdoor Navigator (Fig. 13(a)). The Kahru system is a wearable tactile harness-vest display that provides simple directional navigation instructions. A set of 6 vibrating motors generates tactile messages such as forward, back, left, right, speed up and slow down to guide the user through an environment. Communication with the vest is ensured by a belt-worn infrared receiver.

TNO Human Factors, an applied scientific research institute in the Netherlands, has developed a tactile display that consists of 128 vibrating elements attached to a vest (Fig. 13(b)). Vibrations at 160 Hz present 3D spatial information to the user. This vest is currently being used to convey flight information to pilots in an intuitive way [33]. Similarly, it could be used for the blind.

Researchers at MIT (USA) have developed a tactile display embedded in a vest that fastens around the lower torso (Fig. 13(c)). This tactile display consists of a 4 x 4 array of vibrating motors which are independently controlled by an electronic unit. The electronic unit receives commands wirelessly from a remote computer.

This tactile vest display can be used as a navigation aid outdoors, as experiments in [34] have proved that 8 different vibrotactile patterns can be interpreted as directional (for example: stop, look left, run, proceed faster or

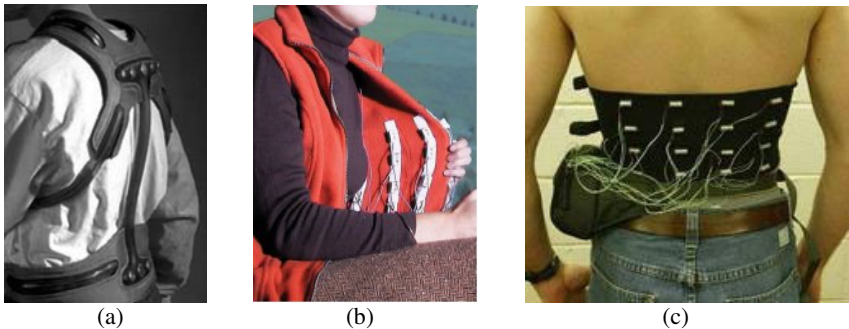


Fig. 13. Tactile vest displays. Prototypes of: (a) Carnegie Mellon University, (b) TNO Human Factors and (c) MIT.

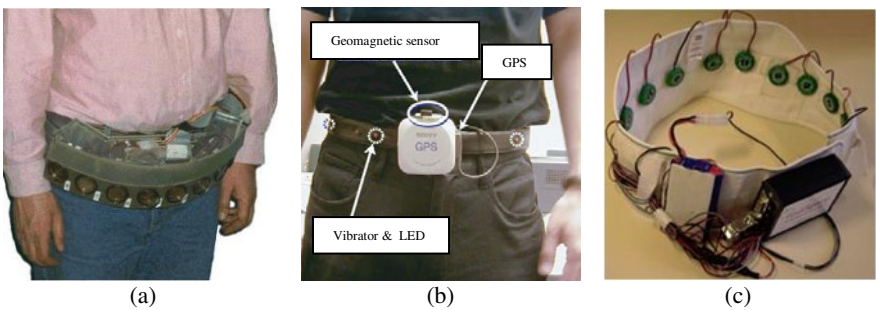


Fig. 14. Belt-worn assistive devices. Prototypes of: (a) the University of Michigan, (b) Keio University and (c) the University of Osnabrück.

proceed slower) or instructional cues (for example: raise arm horizontally, raise arm vertically) with almost perfect accuracy.

The NavBelt [35], a wearable ETA proposed by the University of Michigan (USA), provides acoustical feedback from an array of ultrasonic sensors mounted on a belt around the abdomen (Fig. 14(a)). These sensors provide information on very local obstacles placed in a 120° wide sector ahead of the user.

Researchers at Keio University (Japan) proposed in [36] the ActiveBelt, a belt-type tactile display for directional navigation. The ActiveBelt consists of a GPS, a geomagnetic sensor and 8 vibrators distributed at regular intervals around the torso (Fig. 14(b)).

Vibrations within the range of 33 to 77 Hz are supplied by the ActiveBelt to indicate directions to the user. A set of experiments confirmed that subjects are able to identify the 8 directions while walking.

Another belt-type assistive device is the one developed at the University of Osnabrück (Germany). The prototype consists of an electronic compass and 13 vibrators located around the abdomen (Fig. 14(c)). This belt enables its user to continuously feel his orientation in space via vibrotactile stimulation. Navigation accuracy and long-term usage of the belt are currently being evaluated [37].

2.7 Assistive Devices Worn on the Feet

The human foot is a highly functional structure yet its full capabilities have not been thoroughly explored.

What we know about the human foot is that it combines mechanical complexity and structural strength. The ankle serves as foundation, shock absorber and propulsion engine. The foot can sustain enormous pressure and provides flexibility and resiliency. Sensory input from the foot, particularly from the foot sole, has long been recognized as an important source of sensory information in controlling movement and standing balance [38]. As the load on the foot is transferred from heel to toe, pressure signals are automatically fed back to the brain to provide important information about the body's position with respect to the supporting surface.

Our work at Panamericana University (Mexico) has focused on evaluating the performance of the foot sole receptors for information transmission.

For this purpose, we have developed a shoe-integrated vibrotactile display to study how people understand information through their feet and to evaluate whether or not this comprehension level is sufficient to be exploited for assistance of the blind.

Based on the physiology of the plantar surface of the foot, a first prototype consisting of a 16-point array of actuators has been designed and implemented (Fig. 15). All 16 vibrators have been successfully integrated in a regular foam shoe-insole with 10 mm interspacing. They provide vibrating frequencies between 10-55 Hz. Each vibrator is independently controlled with a specific vibrating frequency command.

One of the advantages of this mechatronic shoe-insole is that it can be further inserted into a shoe making it an inconspicuous and visually unnoticeable assistive device. Unlike other portable/wearable assistive devices, an on-shoe device does not heighten the handicapped image that affects the user's self-esteem.



Fig. 15. Shoe-integrated tactile display: back and forth. Prototype of Panamericana University.

Experiments involving direction, shape, pattern recognition and navigation in space have been conducted with healthy blindfolded-sighted and blind people to gain insights into the capabilities of tactile-foot perception [39].

Results show that both healthy-sighted and blind subjects understand easily vibrations encoding simple information such as directional instructions (for example: go forward, backward, turn left, turn right and stop) and familiar patterns (for example: SMS, phone call, caution) but do not understand vibrations encoding more complex information such as shapes. Although it seems that the feet are not appropriate for precise information recognition, collected data show that it is feasible to exploit podotactile information for navigation in space.

Current work evaluates (1) whether long-term vibrating stimuli on the foot affects balance and walking and (2) user performance depending on cognitive load. The final goal is to integrate the concept of podotactile stimulation in ETAs for the blind.

3 Synthesis and Conclusions

The miniaturization of actuators and electronics has allowed the creation of new devices and systems that can be embedded into clothing. These wearable systems facilitate the user's ability to perform normal daily tasks without feeling encumbered by burdensome devices.

In particular, this chapter has focused on wearable assistive devices for the blind. A brief non-exhaustive survey of wearable assistive devices for this population has been presented to illustrate the most representative work done in this area. Devices worn on the finger, hands, wrist, forearm, tongue, head, chest, abdomen and feet have been proposed over the last decades to provide wearable solutions to the problems of reading and mobility.

For the blind, hearing and touch become the first and second major senses, respectively. They will never replace vision but they still gather much information from the environment for daily tasks. That is the reason why assistive devices provide acoustical and tactile feedback to compensate for visual information. In contrast, smell and taste are largely ignored as being essential to the interaction with the environment.

Several universal design concepts for acoustical/tactile based assistive devices have been presented. They provide guidelines to stimulate both hearing and touch in order to obtain the best performance from these senses. Yet, some considerations must be taken into account:

- **Sensory overload.** The brain simultaneously processes stimuli from several or all of the sensory modalities to interpret the surrounding environment. Because humans have a limited capacity to receive, hold in working memory and cognitively process information taken from the environment, the use of only one sensory modality to convey information can quickly overload that modality. After a while, users may be limited in the perception of acoustical or tactile signals coming from assistive devices.

- **Long learning/training time.** Learning and mastering the visual-to-sound or visual-to-tactile new language is quite a challenge and requires long training time, patience and great effort from the user.
- **Acoustical feedback** is useful only for reading applications. For mobility applications, it might interfere with the blind person's ability to pick up environmental cues. Moreover, continuous acoustic feedback (20-30 min) might affect posture and equilibrium.
- **Tactile feedback** is a viable choice for mobility applications. However, the information presented must be in accordance with the location of the tactile display on the body. Precise information can only be recognized with the fingers and tongue while simple information can be displayed on the rest of the body. It seems that simple directional information is the best choice for mobility of the blind. It does not require constant activity and cognitive effort that reduces walking speed and quickly fatigues the user.

Despite efforts and the great variety of wearable assistive devices available, user acceptance is quite low. Audio books and Braille displays (for those who can read Braille) and the white cane and guide dog will continue to be the most popular reading/travel assistive devices for the blind.

Acceptance of any other portable or wearable assistive device is always a challenge in blind population. Motivation, cooperation, optimism, willingness/ability to learn or adapt new skills is not a combination that can be taken for granted.

References

1. World Health Organization, Visual impairment and blindness - Fact Sheet N°282 (2009), <http://www.who.int/mediacentre/factsheets/fs282/en/>
2. Blind World Magazine, Breaking the chains of paternalism (2006), <http://home.earthlink.net/~blindworld/NEWS/6-06-14-02.htm>
3. Brabyn, J., Seelman, K., Panchang, S.: Aids for people who are blind or visually impaired. In: Cooper, R., Ohnabe, H., Hobson, D. (eds.) An Introduction to Rehabilitation Engineering, pp. 287–313. Taylor & Francis, Abington (2007)
4. Moore, B.: An introduction to the psychology of hearing, 5th edn. Elsevier Academic Press, Amsterdam (2003)
5. Hakkinen, J., Vuori, T., Paakka, M.: Postural stability and sickness symptoms after HMD use. In: Proc. of IEEE International Conference on Systems, Man and Cybernetics, Hammamet, Tunisia, pp. 147–152 (2002)
6. Kandel, E., Jessell, T.: Touch. In: Kandel, E., Schwartz, J., Jessell, T. (eds.) Principles of neural science, 3rd edn., pp. 349–414. Oxford University Press, Oxford (1991)
7. Sekuler, R., Blake, R.: Perception. McGraw-Hill Education, New York (2002)
8. Geiger, S.: Handbook of physiology section 1: the nervous system. American Physiological Society (1984)
9. Weinstein, S.: Intensive and extensive aspects of tactile sensitivity as a function of body part, sex, and laterality. In: Kenshalo, D. (ed.) The skin senses, Charles C. Thomas, pp. 195–222 (1968)

10. Wagner, C., Lederman, S., Howe, R.: Design and performance of a tactile shape display using RC servomotors. In: Proc. of 10th Symposium on Haptic Interfaces for Virtual Environment and Teleoperator Systems, Orlando, FL, USA, pp. 354–355 (2002)
11. Fischer, H., Neisius, B., Trapp, R.: Tactile feedback for endoscopic surgery. In: Satava, R., Morgan, K., Sieburg, H., Mattheus, R., Christensen, J. (eds.) Interactive Technology and the New Paradigm for Healthcare, pp. 114–117. IOS Press, Amsterdam (1995)
12. Summers, I., Chanter, C.: A broadband tactile array on the fingertip. *Journal of the Acoustical Society of America* 112, 2118–2126 (2002)
13. Vidal, F., Madueño, M., Navas, R.: Thermo-pneumatic actuator for tactile displays and smart actuation circuitry. In: Proc. of SPIE International Symposium on Microtechnologies for the New Millennium, Sevilla, Spain, pp. 484–492 (2005)
14. Velazquez, R., Pissaloux, E., Hafez, M., Szewczyk, J.: Tactile rendering with shape memory alloy pin-matrix. *IEEE Transactions on Instrumentation and Measurement* 57(5), 1051–1057 (2008)
15. Konyo, M., Tadokoro, S., Takamori, T.: Artificial tactile feel display using soft gel actuators. In: Proc. of IEEE International Conference on Robotics and Automation, San Francisco, CA, USA, pp. 3416–3421 (2000)
16. Taylor, P., Pollet, D., Hosseini, A., Varley, C.: Advances in an electrorheological fluid based tactile array. *Displays* 18, 135–141 (1998)
17. Hoshi, T., Iwamoto, T., Shinoda, H.: Non-contact tactile sensation synthesized by ultrasound transducers. In: Proc. of 3rd Joint Eurohaptics Conference and Symposium on Haptic Interfaces for Virtual Environment and Teleoperator Systems, Salt Lake City, UT, USA, pp. 256–260 (2009)
18. Koo, I., Kwangmok, J., Koo, J., Nam, J., Lee, Y., Choi, H.: Development of soft-actuator-based wearable tactile display. *IEEE Transactions on Robotics* 24(3), 549–558 (2008)
19. Amemiya, T., Yamashita, J., Hirota, K., Hirose, M.: Virtual leading blocks for the deaf-blind: a real-time way-finder by verbal-nonverbal hybrid interface and high-density RFID tag space. In: Proc. of IEEE Virtual Reality, Chicago, IL, USA, pp. 165–172 (2004)
20. Ng, G., Barralon, P., Dumont, G., Schwarz, S., Ansermino, J.: Optimizing the tactile display of physiological information: vibro-tactile vs. electro-tactile stimulation, and forearm or wrist location. In: Proc. of Annual International Conference of the IEEE Engineering in Medicine and Biology Society, Lyon, France, pp. 4202–4205 (2007)
21. Bach-Rita, P., Kaczmarek, K., Tyler, M., Garcia-Lara, J.: From perception with a 49-point electrotactile stimulus array on the tongue: a technical note. *Journal of Rehabilitation Research and Development* 35(4), 427–430 (1998)
22. Ptito, M., Moesgaard, S., Gjedde, A., Kupers, R.: Cross-modal plasticity revealed by electrotactile stimulation of the tongue in the congenitally blind. *Brain* 128, 606–614 (2005)
23. Vuillerme, N., Pinsault, N., Chenu, O., Fleury, A., Payan, Y., Demongeot, J.: A wireless embedded tongue tactile biofeedback system for balance control. In: Pervasive and Mobile Computing, vol. 5, pp. 268–275 (2009)
24. National Library Service for the Blind and Physically Handicapped. Updated information, <http://www.loc.gov/nls/>
25. Kay, L.: A sonar aid to enhance spatial perception of the blind: engineering design and evaluation. *Radio and Electronic Engineer* 44(11), 605–627 (1974)

26. SonicVision. Updated information, <http://www.sonicvision.co.nz>
27. GDP Research Australia Updated information, <http://www.gdp-research.com.au>
28. Bay Advanced Technologies Ltd. Updated information, <http://www.batforblind.co.nz>
29. Meijer, P.: An experimental system for auditory image representations. *IEEE Transactions on Biomedical Engineering* 39(2), 112–121 (1992)
30. Seeing with Sound - The vOICe. Updated information, <http://www.seeingwithsound.com>
31. Velazquez, R., Fontaine, E., Pissaloux, E.: Coding the environment in tactile maps for real-time guidance of the visually impaired. In: Proc. of IEEE International Symposium on Micro-NanoMechatronics and Human Science, Nagoya, Japan (2006)
32. Gemperle, F., Ota, N., Siewiorek, D.: Design of a wearable tactile display. In: Proc. of 5th International Symposium on Wearable Computers, Zurich, Switzerland, pp. 5–12 (2001)
33. van Veen, H., van Erp, J.: Providing directional information with tactile torso displays. In: Proc. of EuroHaptics 2003, Dublin, Ireland, pp. 471–474 (2003)
34. Jones, L., Lockyer, B., Piateski, E.: Tactile display and vibrotactile pattern recognition on the torso. *Advanced Robotics* 20, 1359–1374 (2006)
35. Borenstein, J.: The NavBelt - A computerized multi-sensor travel aid for active guidance of the blind. In: Proc. of CSUN's 5th Annual Conference on Technology and Persons with Visual Disabilities, Los Angeles, CA, USA, pp. 107–116 (1990)
36. Tsukada, K., Yasumrua, M.: ActiveBelt: belt-type wearable tactile display for directional navigation. In: Davies, N., Mynatt, E.D., Siio, I. (eds.) *UbiComp 2004*. LNCS, vol. 3205, pp. 384–399. Springer, Heidelberg (2004)
37. Nagel, S., Carl, C., Kringe, T., Märtin, R., König, P.: Beyond sensory substitution-learning the sixth sense. *Journal of Neural Engineering* 2, R13–R26 (2005)
38. Allum, J., Bloem, B., Carpenter, M., Hulliger, M., Hadders, M.: Proprioceptive control of posture: a review of new concepts. *Gait and Posture* 8, 214–242 (1998)
39. Velazquez, R., Bazan, O., Magaña, M.: A shoe-integrated tactile display for directional navigation. In: Proc. of IEEE/RSJ International Conference on Intelligent Robots and Systems, St. Louis, MO, USA, pp. 1235–1240 (2009)

Intrabody Communication in Biotelemetry

Željka Lučev, Igor Krois, and Mario Cifrek

University of Zagreb, Faculty of Electrical Engineering and Computing

Abstract. Biotelemetry is remote monitoring, measuring and recording of a living organism's function, activity or condition. Network of sensor nodes placed on or implanted inside the body of a subject is called Body Area Network (BAN). In this work we will describe the principles of a wireless body area network which uses the human body as a transmission medium, namely intrabody communication (IBC). We will describe the limitations set on the IBC systems, describe dielectric properties of the human body as a transmission medium, specify different ways of transmitting signals through the human body and compare characteristics of the IBC systems found in the literature.

Keywords: biotelemetry, intrabody communication (IBC), capacitive coupling, galvanic coupling.

1 Introduction

Biotelemetry is the use of telemetry methods for sending signals from a living organism over some distance to the receiver [23]. It is used to remotely observe, measure and document a human or animal functions, activities, or locations. It consists of several subfields, like medical and human research biotelemetry, implantable biotelemetry and animal biotelemetry. Medical biotelemetry is used to remotely track physiological functions of patients, like body temperature, heart rate, blood pressure, ECG, EEG signals, etc., and even to operate devices such as drug delivery systems and prosthetics. Implantable biotelemetry focuses on the transmitter devices implanted in the human or animal being studied, like cochlear implants or implantable pacemakers. Animal biotelemetry is widely used to conduct research on animal behaviour in their natural environment or on animal migration patterns. In this work we will focus our attention on biotelemetry systems used for monitoring human functions only, i.e. medical and implantable biotelemetry systems.

The main constituents of a biotelemetry system are sensors of physiology functions located on the transmitters, transmission path and receivers. Transmitters with sensors are placed on the surface of or implanted inside the human body. In contrast to the medical biotelemetry, the implantable implies the absence of wires as a transmission medium between a transmitter and a receiver. Still, the wires are impractical for monitoring, since they disturb the patient and the medical personnel. Using different wireless technologies provides better freedom of movements and the mobility of the patient, which is of particular importance in a long-term

monitoring, every-day activities of non-ambulatory patients and during the surgeries. Wearable sensor network placed on the human body is called Body Area Network (BAN) and it must comply with the following demands:

- it must not interfere with the human body functions, therefore sensor nodes placed on the body must be in accordance with the existing regulations and guidelines [22, 28];
- it must provide real-time communication;
- low-power requirements;
- no electromagnetic interference between the sensor nodes;
- the presence of the system must not disturb normal movements of the patient, i.e. the sensor network must be lightweight and small-sized.

Two main concerns in a low-power lightweight wireless system design are the distance over which the signal can be received, and the transmitter design, both of which are related to the power source used by the transmitter. Considering that surface mount technology is used in design, the batteries are usually the largest part of the transmitter package. There is a trade off between freedom of the subject's movement and power of transmitter determined by the battery size and capacity: the more powerful transmitters with larger batteries can transmit signals over greater distances, but are more difficult to place on or implant in the human body without severely affecting the subject's behaviour and energetics.

2 Regulations

Safety restrictions on the effects of exposure to time-varying electric, magnetic, and electromagnetic fields (EMF) are based on established health effects, as described in international guidelines by the International Commission on Non-Ionizing Radiation Protection (ICNIRP) [22] together with different national considerations [28]. The exposure to EMF results in internal body currents and energy absorption in tissues. Protection against adverse health effects requires that proposed basic restrictions are not exceeded.

Guidelines and legal regulations that set basic limitations on exposure to the electromagnetic fields define two types of population [22, 28]. The occupationally exposed population consists of adults who are generally exposed under known conditions and are trained to be aware of potential risk and to take appropriate precautions. The other group is the general public, which comprises of individuals of all ages and of varying health status, and may include particularly susceptible groups or individuals, like children, women and chronically ill people. Therefore, more stringent exposure restrictions are advised for the general public than for the occupationally exposed population, what we take into account in this discussion.

Depending on the frequency of the field, the physical quantities used to specify the basic restrictions on exposure to EMF are as follows, [22, 28], Fig. 1:

- current density (J) in the frequency range 1 Hz – 10 MHz;
- specific energy absorption rate (SAR) in the frequency range 100 kHz – 10 GHz;
- power density (S), in the frequency range 10–300 GHz.

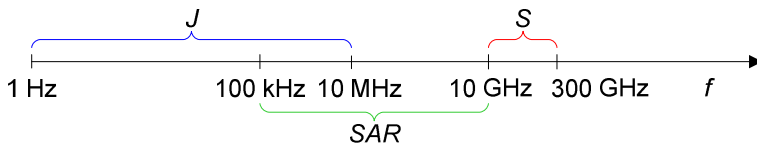


Fig. 1. Restrictions on exposure to electromagnetic fields

Restrictions on current density are provided to prevent effects on nervous system functions. The most stringent restrictions are set in the frequency range between 4 Hz and 1 kHz, where the maximum current density is 2 mA/m^2 , due to a low threshold for nerve stimulation in this frequency range. Below 4 Hz and above 1 kHz the basic restrictions on induced current density increase. Basic restrictions on the induced current density rms values are given in Table 1., where f is the frequency in hertz.

Table 1. Maximum current density for head and trunk (rms) [22]

Frequency range, f	J_{max} [mA/m^2]
< 1 Hz	8
1–4 Hz	$8/f$
4 Hz – 1 kHz	2
1 kHz – 10 MHz	$f/500$

Between 100 kHz and 10 GHz basic restrictions on specific energy absorption rate are provided to prevent whole-body heat stress and excessive localized tissue heating. Maximum recommended SAR values for the general public population are as follows: a whole-body average SAR 0.08 W/kg, localized SAR in head and trunk 2 W/kg, and localized SAR in limbs 4 W/kg. Restrictions on power density are provided to prevent excessive heating in tissue at or near the body surface. Maximum recommended power density value for the general public is set to 10 W/m^2 .

A quantity that considers human perception and other indirect effects is contact current. I_c is a current that flows when the human body comes into contact with an object at a different electric potential, that is when either the body or the object is charged by an electromagnetic field, [22]. Reference levels for contact current are given in order to avoid shock and burn hazards, for the frequencies up to 110 MHz. The point contact reference levels are shown in Table 2. (f is the frequency in kHz).

Table 2. Reference levels for time varying contact currents from conductive objects [22]

Frequency range, f	$I_{d,max}$ [mA]
< 2.5 kHz	0.5
2.5–100 kHz	$0.2f$
100 kHz – 110 MHz	20

Reference level for current induced in any limb at frequencies between 10 MHz and 110 MHz is below the basic restrictions on localized SAR. This value is set to 45 mA for general public.

3 Wireless Biotelemetry Systems

In this chapter, we analyse a typical wireless electromyography system as an example of a wireless sensor network. A wireless electromyography system consisting of four EMG sensor nodes placed on the body and a single medical data acquisition system placed a few meters away is depicted in Fig. 2. Sensor nodes and a central unit communicate using a standard wireless link, like WLAN, Bluetooth, RFID or ZigBee. Although often used in biotelemetry, these standards are optimized for other applications: WLAN for data transfer, Bluetooth for voice transmission, RFID for identification and tracking, and ZigBee for industrial applications. Data rate of WLAN and Bluetooth communication modules is fast enough for biomedical applications, but they emit high levels of EMF radiation, which can lead to tissue overheating and irritation. High transmitted power also requires frequent replacement of batteries, which is undesirable in the case of implanted sensors. ZigBee and RFID modules have lower consumption, but their achievable data rates are insufficient for biomedical applications. Common to all of these standards is that they are designed for communication at a distance of several tens of meters, so they inherently generate excessive power.

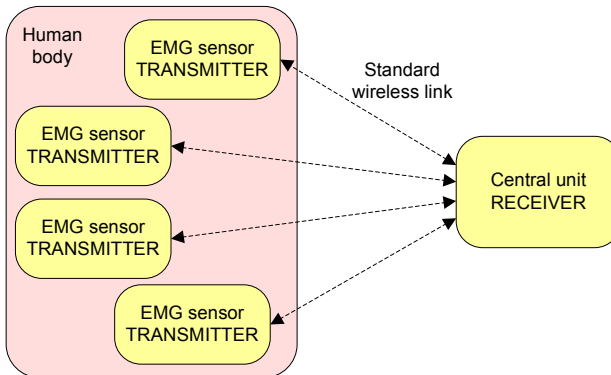


Fig. 2. Typical wireless electromyography system

Considering this, a new method of wireless data transmission called intrabody communication (IBC) is developed. IBC uses the human body as a signal transmission medium. It is a short range (up to 2 m) communication with very low consumption (< 1 mW), and a data rate fast enough for biotelemetry applications. All transmitter nodes do not communicate directly with the distant central unit as in Fig. 2, but with a single receiver placed on the human body, in their close vicinity as in Fig. 3, hence further reducing the power consumption. Only the receiver unit

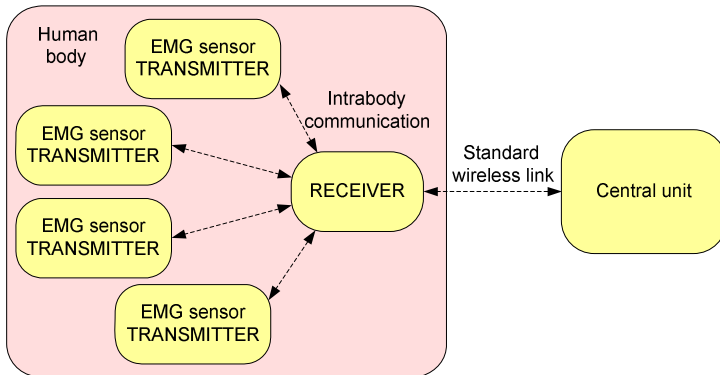


Fig. 3. IBC wireless electromyography system

communicates with the distant central unit, using a standard wireless protocol. Intrabody communication uses lower frequencies and lower power for short-distance communication through fairly conductive medium of the human body, so the consumption of such a system is lower than of Bluetooth or WLAN systems.

Main components of an intrabody communication system are shown in Fig. 4. IBC system consists of a number of transmitters and a receiver which communicates with the remote central medical unit (due to the low power requirements). Some transmitters can be modified to serve as a signal router. A typical transmitter incorporates sensors of physiological functions for obtaining biomedical signals, signal encoder, a modulator and a coupler. The receiver consists of a detector, demodulator, signal decoder and a signal processing unit.

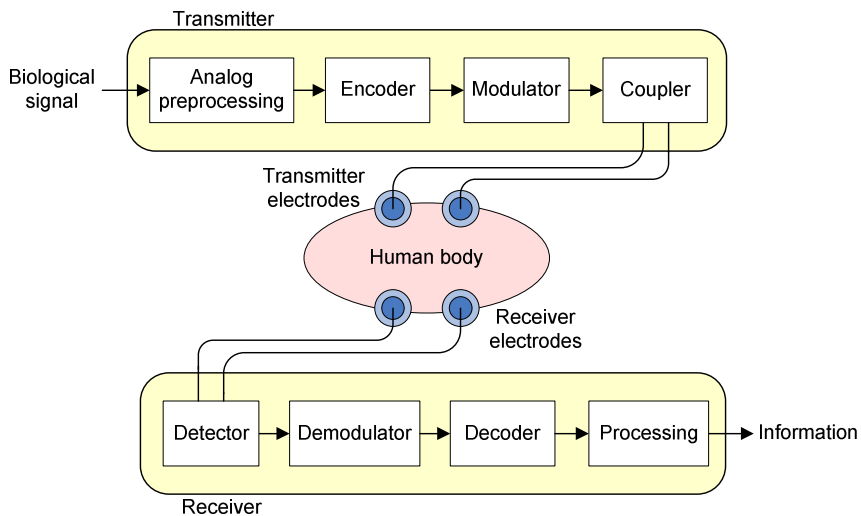


Fig. 4. Intrabody communication system

The choice of the modulation, a coupling method, the position of the transmitters with respect to the receiver, and arrangement of the electrodes depend on the coupling method and the application.

4 Dielectric Properties of Human Tissues

The dielectric properties of the human body, electrical conductivity and relative permittivity, determine the flow of electric current and the magnitude of polarization effects, respectively. The dielectric properties of biological tissues for frequency range from 10 Hz to 10 GHz were described and summarized in [9–11] by Gabriel et al. It is shown that the dielectric properties of tissues depend on the type of tissue, frequency, temperature, and the amount of water in a particular tissue, [11]. Frequency dependence of conductivity σ and relative permeability ϵ_r of human tissues that contribute to the transfer of signals the most (wet and dry skin, muscle in the longitudinal direction, fat and hard bone) at a temperature of 37 °C are shown in Figs. 5 and 6, respectively. It is assumed that the signals travel through a particular tissue homogeneously, because the penetration depth at the observed frequencies is larger than the dimensions of the body [20].

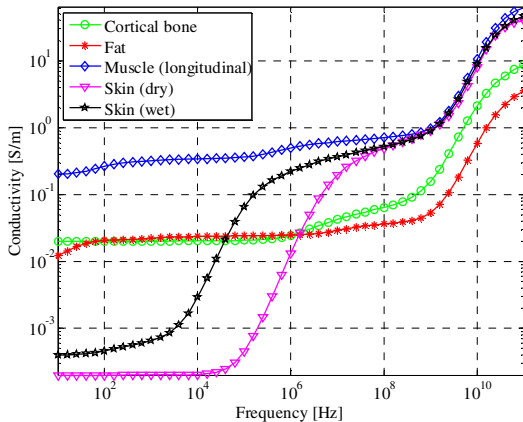


Fig. 5. Frequency dependence of conductivities for different human body tissues. Adapted from [20]

The signals propagate best through the muscles due to their high conductivity in the whole frequency range, Fig 5. The conductivity and permittivity of the wet and dry skin differ for the frequencies up to 1 MHz. For higher frequencies their values are almost equal to those of the muscles. Above 100 MHz the conductivity of all considered tissues increases rapidly.

The selection of the appropriate carrier frequency for intrabody communication is a trade-off between several requirements: constraints imposed by the safety regulations in order to prevent interference with normal biological signals,

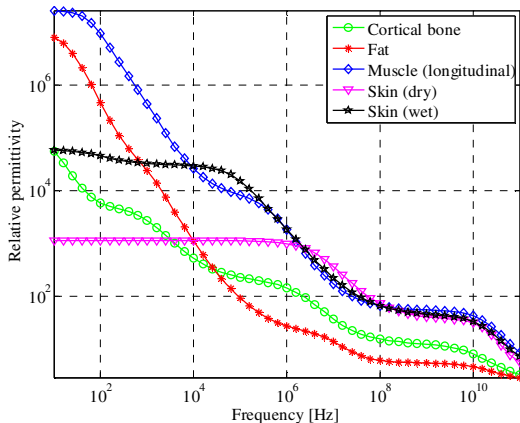


Fig. 6. Frequency dependence of relative permittivities for different human body tissues. Adapted from [20]

ultra-low power requirements, and high tissue conductance at the signal carrier frequency (achieved at higher frequencies).

5 Human Body as a Signal Transmission Medium

Transmission characteristic of an IBC system depend on the properties of tissue and a signal path, which is defined by the position of the transmitter relative to the receiver, signal transmission method, signal amplitude, and carrier frequency and type of modulation used. Electric fields external to the body induce a surface charge on the body, which results in induced currents in the body. The distribution of these currents depends on exposure conditions, on the size and shape of the body, and on the body's position in the field. There are different ways to send and receive signals through the human body, which can be reduced to two main methods:

- capacitive signal coupling;
- galvanic signal coupling.

In capacitive signal coupling the signal is controlled by an electric potential between the transmitter electrodes. In galvanic signal coupling the signal is controlled by a current flow through the body.

5.1 Capacitive Signal Coupling

The use of the human body as a signal transmission medium was proposed at MIT in 1995 [43], and first used in a system known as the Personal Area Network (PAN) [43, 44]. PAN system consists of a transmitter and a receiver, each of which is battery powered and incorporates a pair of electrodes: a signal electrode attached to the human body, and a ground electrode oriented towards the environment. Zimmerman et al. noticed that in the presence of a weak electric

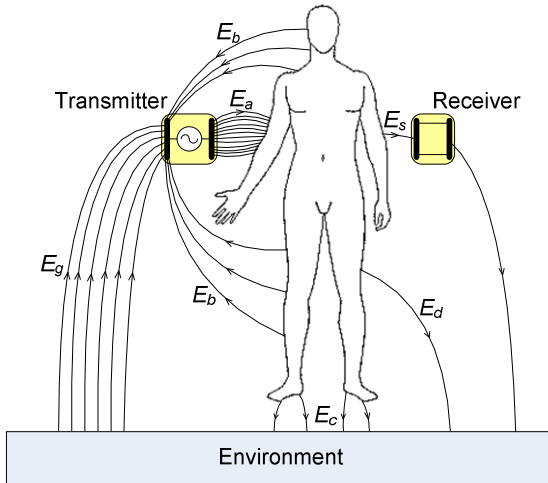


Fig. 7. Electric fields induced by capacitive intrabody communication

field the human body acts as a signal guide and couples the signal electrostatically (capacitively), while the return path is provided by the environment (air and various other objects in the vicinity of the body). Signal transmission is achieved by modulating the voltage between signal electrodes, which is detected and decoded by the receiver. The induced current conducted through the body is in order of magnitude of picoamperes, and is not harmful to the organism.

In the capacitive intrabody communication, as shown in Fig. 7, the induced electric fields are established between all parts of the system that are at different potentials. The transmitter imposes an oscillating potential on the body, relative to the earth ground, causing electric fields E_a between transmitter signal electrode and the body, E_b between the body and the transmitter ground electrode, fields E_c and E_d between the body and the environment, and a field E_s between the body and the receiver signal electrode:

$$E_a = E_b + E_c + E_d + E_s \quad (1)$$

The return path to the transmitter is closed by the field E_g between the environment and the transmitter ground electrode. Due to the existence of electric fields E_b , E_c and E_d a large part of the transmitted signal closes back to the transmitter ground electrode and the received field E_s is extremely small, but sufficient to obtain the desired information. Since the field E_s additionally decreases with the cube of the distance [44], capacitive intrabody communication can be achieved only at a close distance.

In the capacitive coupling approach the received signal level is affected by the orientation of the transmitter with respect to the receiver, the number of ground electrodes connected to the body, the size of the receiver ground plane, and the surrounding environment ([4], [18], [25]). There is still no agreement on which electrode arrangement is the best, since it highly depends on the application the

system is designed for and the signal carrier frequency used. The most common arrangements that yield the largest received signal level are depicted in Fig. 8. In the left one both transmitter electrodes are connected to the body along the line of the signal propagation, and in the right one only the transmitter signal electrode is connected to the body. In both cases the ground electrode of the receiver remains disconnected from the body. The fact that all four electrodes do not necessarily need to be in direct contact with the body allows a successful communication even through the clothes of the subject. Also, increasing the size of the receiver ground plane can strengthen the received signal level, [26].



Fig. 8. Positions of the electrodes: longitudinal direction (left), two-electrode arrangement (right). TX is a transmitter, RX is a receiver; S denotes a signal electrode and G denotes a ground electrode, [25]

The signal transmission path highly depends on the configuration of the environment, what must be taken into account when using capacitive IBC approach. Selection of the appropriate carrier frequency is also very important factor in design of the IBC system, because an increase of the signal frequency increases the amount of field emitted through the air by radiation, and reduces the field between the receiver and body that we measure.

5.2 Galvanic Signal Coupling

In the galvanic intrabody communication both transmitter and receiver electrodes are connected to the human body and an alternating current signal is used as a signal carrier, as in Fig. 9. The main (primary) current flow is applied differentially between the transmitter electrodes, while a small part of a current propagates through the body and causes an alternating potential difference between the

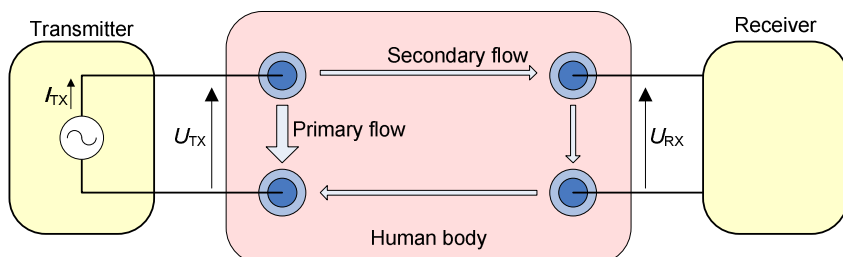


Fig. 9. Galvanic intrabody communication

receiver electrodes. In galvanic coupling approach the transmission path is closed entirely through the subject's body, so the characteristics of a received signal do not depend on the characteristics of the environment, as in a capacitive coupling approach. The main parts of the galvanic IBC system are the same as in a capacitive IBC system, with the exception of the coupler which is adapted to current controlled signal transmission.

6 IBC Technology Overview

Several groups from all parts of the world are involved in the development of IBC devices. Various developed IBC systems can be found in the literature, some of which are more oriented to medical applications, while the others are oriented to various non-medical purposes. Because IBC is a brand new technology, IBC devices are not yet available on the market, but many of the concepts of their application have been thoroughly worked out. The developed systems differ by the coupling method, the coupling amplitude, the chosen frequency range, the signal modulation method, and the achieved data rates.

The concept of Personal Area Networks (PANs) was presented in 1995 to demonstrate how electronic devices on and near the human body can exchange digital information through near-field electrostatic coupling [43]. The first successful PAN prototype used a capacitive signal coupling, a signal with an amplitude of 30 V, 330 kHz carrier frequency, and on-off keying (OOK) modulation. Data rate of 2400 bps and a power consumption of 1.5 mW [44] were achieved. For defining the shape and size of the IBC devices Zimmerman suggested items that are often used in everyday life: watches, credit cards, eyeglasses, identification badges, belts or shoe pads. Depending on the shape and position of an IBC device on the body he suggested a possible application of a new technology: devices such as head-sets, hearing aids, microphones and various indicators may be worn on the head, and identification devices, such as electronic tags, can be placed in a pocket. Indicators, microphones, cameras and speakers can be easily incorporated in a watch, and the heavier devices (PDA, mobile phones, keyboards ...) can be placed around the waist. Also, different physiological sensors can be incorporated in IBC devices and they can monitor the physiological functions of the organism, such as the heart rate, blood pressure, breathing, etc. In the end, Zimmerman suggests the possibility of using devices that are inserted into the shoe, such as pads, which gain the energy from the environment, and are used for communication with IBC devices in their vicinity or as transceivers which detect the position and the identity of the people who wear it.

After Zimmerman, at MIT Gray explores the physical limits of intrabody communication [12]. Analysis of the transmission channel showed that the amplifier noise and crosstalk with other IBC devices on the body have the most influence on the received signal. He tested the on-off keying (OOK) and phase shift keying (PSK) modulation at data rates of up to several thousand bits per second. The final version of the hardware [33] was based on frequency shift keying (FSK) modulation and it achieved a data rate of 9600 bps. Analog demodulation at the receiver side was performed using a PLL (phase-locked loop) unit.

Wireless system with very small consumption designed for monitoring the ECG signal was developed by Handa et al. at Waseda University (Japan) [19]. The system consisted of ECG detector placed on the chest of the patient and a receiver placed around the wrist. Alternating current signal with an amplitude of $20 \mu\text{A}$ was galvanically transmitted between the ECG detector and a receiver. Pulse-width modulation (PWM) with a carrier frequency of 70 kHz was used. Total power consumption of the system was very small, around $8 \mu\text{W}$.

M. Fukumoto et al. from NTT Human Interface Laboratories developed a wireless wearable system for the finger-tip typing detection called FingeRing [8]. A test subject on each finger has a ring with a transmitter which registers finger movements when playing or typing. The receiver is located on the wrist, integrated into a wristwatch. Communication system, based on a variant of capacitive IBC, uses an analog frequency modulation with carrier frequencies between 50 kHz and 90 kHz and a consumption of 1.75 mW .

The goal of Derek P. Lindsey et al. [24] was the reduction of volume of implantable devices for *in vivo* biometric measurements. They developed a method that uses ionic properties of the human body for the signal transmission, and tested it by measuring tension in anterior cruciate ligament (ACL) grafts of the cadaver. Transmitter platinum electrodes were implanted into the lateral femoral epicondyle, and the signal was detected by surface electromyography electrodes. They studied the effect of transmission frequency, the current injected, the distance between the electrodes, the distance of the electrodes from the joint line and the position of surface electrodes on the signal attenuation. For this application the best results were obtained using a current with amplitude of 3 mA and a frequency modulated (FM) signal with carrier frequency of 37 kHz .

K. Partridge et al. from the University of Washington have, based on the Zimmerman PAN prototype, developed and described a system [31] with which they had achieved a data rate of up to 38.4 kbps . They used carrier frequencies of 180 kHz and 140 kHz with FSK modulation and a signal with an amplitude of 22 V . They compared the data error rates and the received signal strengths for different distances between the body and the electrodes, positions of electrodes on the body, size and shape of the receiver signal electrode, and some other factors. They concluded that the size and the shape of the receiver electrodes have only a small effect on signal transmission, in contrast to the distance between the electrodes and the body, which significantly affects the transfer. They also found that the path of the return signal, which closes through the environment, has the greatest influence on the signal transmission, because the useful capacitance of air couplers through the environment is extremely small: it has the order of magnitude in femtofarads [43].

At the university in Chiba (Japan) K. Fujii and K. Ito investigated transmission characteristics of the human body in the IBC system. In [2] they described the FDTD (finite-difference time-domain) simulation of electric field distribution around the numerical model of the human arm approximated by parallelepiped with following characteristics: dimensions $5 \text{ cm} \times 5 \text{ cm} \times 45 \text{ cm}$, relative permittivity $\epsilon_r = 81$ and conductivity $\sigma = 0.62 \text{ S/m}$ (dielectric parameters of the muscle). IBC transmitter that generates a signal amplitude of 3 V and a frequency of

10 MHz was used as a source of an electric field. They showed that the field was formed around the arm, and that the received signal attenuation was lower when both the signal and the ground electrode of the transmitter were in contact with the body, than when the ground electrode was disconnected from the body. In [3] they added the receiver and monitored the influence of the position of the receiver and transmitter electrodes on the signal transmission through the biological tissue-equivalent solid phantom arm (the same dimensions as the numerical model of the arm) and in FDTD simulation. The configuration in which both transmitter electrodes were attached to the body, while the receiver signal electrode was connected, and the receiver ground electrode disconnected from the body proved to be the best. In [4] they showed that the transmitter electrodes should be placed along the line of the signal propagation from transmitter to the receiver, and that the size of the transmitter and its electrodes significantly affects the strength of the received signal. On the other hand, the change in carrier frequency in interval between 10 MHz and 100 MHz had little effect on signal transmission through the human body. Fujii et al. combined all the previous results in [5], where they compared the results obtained in simulations with the results measured using the biological tissue-equivalent solid phantom arm. They found that the signal was spread as a surface electromagnetic wave along the surface of the skin. Simulation results were confirmed on realistic models of Japanese adults (male and female) [6, 7] and in [7] they presented the spatial distribution of electric field around the numerical model of the arm on which the IBC system was placed.

K. Hachisuka et al. used capacitive method of signal transmission, which they called the electromagnetic wave, for intrabody communication. They showed that in the frequency range from 0.5 MHz to 50 MHz, frequencies around 10 MHz are optimal for the carrier frequency of IBC system with minimal power consumption [15, 16]. The carrier frequency they have chosen for their system was 10.7 MHz, due to the large number of (cheap) components on the market that support it. Measurements were conducted on the phantom hand (described in [15] and [17]) and *in vivo*. The developed transmitters and receivers were the size of 30 mm x 30 mm, weighted around 5 g, and used a 3 V battery as the power supply. The signal amplitude of 3 V and frequency of 10.7 MHz was successfully detected and demodulated at the receiver, for both the frequency (FM) [16] and the digital FSK modulation [15]. Data rate achieved using the FSK modulation was 9.6 kbps. They investigated the optimal position of the transmitter and receiver electrodes for different distances, frequencies and body positions. The two-electrode arrangement, in which only the signal electrode is attached to the body, was found to be 20 dB better in the kilohertz band than the four-electrode arrangement in which all four electrodes are in contact with the body [18]. They suggested that the IBC devices could be used in healthcare, in electronic money transactions, for exchange of a business data and for music files sharing.

Japanese phone company NTT (Nippon Telegraph and Telephone Corporation) and its subsidiary NTT DoCoMo Inc. are among the first to use intrabody communication technology to successfully realize communication between electronic devices in everyday life. Their implementation of intrabody communication is called RedTacton [29], and it achieves the data rate of up to 10 Mbps using the

capacitive signal transmission method. High data rate is achieved using the electrooptic crystals in the receiver, where change in the electric field with frequency of 10 MHz (which carries the information about the signal), causes measurable change of polarization of the laser beam passing through the crystal [39]. Some of the applications of RedTacton technologies that the NTT proposes are the exchange of data between different devices, identification of users of different services, the use in security systems, etc.

At Waseda University (Tokyo, Japan) a broadband IBC system was developed [34]. The largest attenuation of the received signal was achieved when the signal electrodes of the transmitter and receiver only, having 2 cm in diameter, were connected to the body of the test subjects. Researchers have investigated the properties of the human body as a signal transmission medium up to the frequency of 2.5 GHz. Regarding the signal attenuation and time delay, they discovered that BPSK or MSK modulation [35, 36] at the frequencies between 200 MHz and 600 MHz [35] showed the best transmission characteristics for fast broadband intrabody communication. Some of the developed IBC devices [37] were specialized for helping people with special needs, such as a system to help blind and visually impaired people for the orientation in space [37] or a system for mute people to communicate using a wireless keyboard [37]. This system is able to identify which finger the person is using to touch the device and, depending on the selected settings, to reproduce the voice or words on the built-in speakers. They also proposed the use of IBC devices for advertising in trains [37], as well as a personalized system for monitoring the health of the patients [1].

As a part of the European IMEC international corporation with headquarters in Belgium within the Human++ project [21], a sensor network for monitoring vital functions of the human body was developed. Miniature, autonomous and intelligent sensor nodes [13] with extremely low consumption ($21 \mu\text{A} @ 3 \text{ V}$) that record the biological signals of the patients (EEG, ECG, EMG - [14]) and send them to different medical central units, where the data is further processed, have been developed as a part of the research. A very small amount of electrical energy is needed for powering the sensors, and it is obtained by thermal harvesting [32]. The ultra-wide frequency modulation (UWB) between 3 GHz and 5 GHz, with a width of signal spectrum from 500 MHz to 2 GHz is used for communication.

Marc Wegmüller from the ETH Zurich used galvanic intrabody communication [32, 33]. Developed transmitters were connected to the body over two electrodes which generate a current signal with maximal amplitude of 1 mA. Wegmüller investigated the characteristics of the intrabody signal transmission for the signals with frequencies from 10 kHz to 1 MHz. The data rate of 64 kbps was achieved for a carrier frequency of 256 kHz and the QPSK modulation, with a total power consumption of 20 mW. The theoretical results were confirmed by measuring the ECG signal on 20 subjects. It was discovered that the signal transmission depends on the proportion of individual tissues to total body weight and the condition of certain tissues, and that the received signal attenuation was smaller for the greater skin moisture and higher proportion of water in a tissue. The ideal patient for the transmission of signal of frequency from 100 kHz to 500 kHz should have the

muscle mass over 45% and the intercellular body water value greater than 60%. Also, a small skin fold thickness positively influences the communication.

At the University of Zagreb, Lučev et al. have used a capacitive IBC approach in a design of an electromyography system. The transmitters generate signals with an amplitude of $1.15 \text{ V}_{\text{pp}}$, and approximately 1 MHz carrier frequency [25]. Typical achieved data rate was 8 kbps, and the maximal tested data rate was 64 kbps. The researchers investigated relation between the received signal strength and mutual position of the receiver and transmitter in developed IBC system. *In vivo* measurements showed that the signal propagates through the human body, and not through the surrounding air [25]. The researchers concluded that received signal strength was higher for longitudinal direction of the transmitter electrodes (Fig. 8., left) for the transmitter located on the same arm as the receiver. For the transmitter located on the opposite arm, the signal was stronger in the two-electrode arrangement (Fig. 8., right) [25, 26]. They also found that increasing the surface reference electrode receiver up to 600 cm^2 has an impact on improving the transmission of signals [26]. In addition to this, *in vivo* measurements of surface electromyography signals showed that developed IBC system can be used to monitor muscle fatigue, what is of special importance in kinesiology and rehabilitation [27].

Besides the above applications it is interesting to mention the use of IBC capsules as miniature endoscopic devices [42]. After the patient swallows the capsule it collects data of the state of the desired part of the body from the inside (digestive system) and then sends it through the human tissue to the receiver on the surface of the body.

A comparison between the most important capacitive and galvanic IBC system found in the literature is given in Table 3. The authors of each system, the amplitude and frequency of signals used, the method of modulation used and the maximum achieved data rate are all provided.

Table 3. Comparison of intrabody communication systems. Adopted from [41]

Authors	Year	Coupling method	Coupling amplitude	Carrier frequency	Modulation	Data rate [bps]
Zimmerman	1995	capacitive	30 V	330 kHz	OOK	2.4 k
Fukumoto	1997	capacitive	21 V	90 kHz	FM	0.1 k
Reynolds	1997	capacitive	10 V	70 kHz	FSK	9.6 k
Partridge	2001	capacitive	22 V	160 kHz	FSK	38.4 k
Fujii/Ito	2002	capacitive	3 V	10 MHz	OOK	/
Hachisuka	2003	capacitive	1 V	10.7 MHz	FSK	9.6 k
NTT/DoCoMo	2003	capacitive	25 V	10 MHz	OOK	10 M
Ruiz/Shimamoto	2005	capacitive	/	200–600 MHz	MSK	/
IMEC	2005	capacitive	/	2.4 GHz	UWB	/
Lučev	2009	capacitive	1.15 V	1 MHz	FM	64 kbps
Handa	1997	galvanic	$20 \mu\text{A}$	70 kHz	PWM	0.9 k
Lindsey	1998	galvanic	3 mA	37 kHz	FM	/
Oberle	2002	galvanic	4 mA	60 kHz	CPFSK	4.8 k
Wegmüller	2007	galvanic	1 mA	256 kHz	BPSK	64 k

7 Conclusion

In this work we described the principles of intrabody communication (IBC), with an emphasis on the IBC systems used in biotelemetry. IBC systems utilize conductive properties of the human body for the transmission of the electrical signals. They work at lower frequencies and lower range than standard wireless systems and, accordingly, they have lower power consumption. Due to the reduced power consumption, heating and tissue irritation of the patients are lower, and the battery lifetime is longer. We presented the restrictions set on the IBC systems due to the patient safety requirements, taking into account the stringent exposure restrictions advised for the general public, which may include particularly susceptible groups or individuals, like children, women and chronically ill people.

Two main methods of intrabody communication are capacitive and galvanic signal coupling. In a capacitive signal coupling the signal is controlled by an electric potential between the transmitter electrodes, and in a galvanic signal coupling the signal is controlled by a current flow through the body. The literature we reviewed on the subject is abundant with different choices of modulation techniques, coupling methods, and transmitter-receiver arrangements, which all depend on the coupling method and the application. Possible applications of IBC technology are very broad: from biotelemetry and medicine on one side to the communication between various electronic devices and security systems on the other side.

There is still a need for a detail investigation of the properties of the human body as a transmission medium for IBC signals, in order to define criteria for the selection of a coupling method and the optimization of the position of the electrodes. The choice of the modulation, carrier frequency and coupling amplitude must be carefully performed, with respect to the criteria of consumption, probability of the error, and data rate.

References

1. Alshehab, A., Kobayashi, N., Kikuchi, R., Ruiz, J.A., Shimamoto, S., Ishibashi, H.: A study on intra-body communication for personal healthcare monitoring system. In: 10th International Conference on e-health Networking, Applications and Services (HealthCom 2008), Singapore, pp. 219–220 (2008)
2. Fujii, K., Ito, K., Tajima, S.: Signal propagation of wearable computer using human body as transmission channel. In: Proceedings of the International Symposium on Antennas and Propagation, ISAP 2002, pp. 512–515 (2002)
3. Fujii, K., Ito, K., Tajima, S.: A study on the receiving signal level in relation with the location of electrodes for wearable devices using human body as a transmission channel. In: IEEE Antennas and Propagation Society International Symposium, vol. 3, pp. 1071–1074 (2003)
4. Fujii, K., Ito, K.: Evaluation of the received signal level in relation to the size and carrier frequencies of the wearable device using human body as a transmission channel. In: IEEE Antennas and Propagation Society International Symposium, vol. 1, pp. 105–108 (2004)

5. Fujii, K., et al.: Study on the transmission mechanism for wearable devices using the human body as a transmission channel. *IEICE Trans. Commun.* E88-B(6), 2401–2410 (2005)
6. Fujii, K., Takahashi, M., Ito, K.: Study on the electromagnetic field distributions of realistic Japanese adult male and female models with a wearable device using the human body as a transmission channel. In: *IEEE Antennas and Propagation Society International Symposium*, Albuquerque, NM, USA, vol. 1, pp. 2121–2124 (2006)
7. Fujii, K., Takahashi, M., Ito, K.: Electric field distributions of wearable devices using the human body as a transmission channel. *IEEE Transactions on Antennas and Propagation* 5(7), 2080–2087 (2007)
8. Fukumoto, M., Tonomura, Y.: Body coupled FingeRing: Wireless wearable keyboard. In: *CHI 1997 Conference on Human Factors in Computing Systems*, pp. 147–154 (1997)
9. Gabriel, C., Gabriel, S., Corthout, S.: The dielectric properties of biological tissues: I. Literature survey. *Physics in Medicine and Biology* 41, 2231–2249 (1996)
10. Gabriel, S., Lau, R.W., Gabriel, C.: The dielectric properties of biological tissues: II. Measurements in the frequency range 10 Hz to 20 GHz. *Physics in Medicine and Biology* 41, 2251–2269 (1996)
11. Gabriel, S., Lau, R.W., Gabriel, C.: The dielectric properties of biological tissues: III. Parametric models for the dielectric spectrum of tissues. *Physics in Medicine and Biology* 41, 2271–2293 (1996)
12. Gray, M.: Physical limits of intrabody signalling. Bachelor thesis, MIT Media Laboratory, Cambridge, MA, USA (1997)
13. Gyselinckx, B., Van Hoof, C., Ryckaert, J., Yazicioglu, R.F., Fiorini, P., Leonov, V.: Human++: autonomous wireless sensors for body area networks. In: *Proceedings of the IEEE Custom Integrated Circuits Conference*, pp. 13–19 (2005)
14. Gyselinckx, B., et al.: Human++: Emerging Technology for Body Area Networks. In: *IFIP International Conference on Very Large Scale Integration*, Nice, France, pp. 175–180 (2006)
15. Hachisuka, K., et al.: Development and performance analysis of an intra-body communication device. In: *12th International Conference on Transducers, Solid-State Sensors, Actuators and Microsystems*, Boston, USA, vol. 2, pp. 1722–1725 (2003)
16. Hachisuka, K., et al.: Development of wearable intra-body communication devices. *Sensors and actuators A: Physical* 105, 109–115 (2003)
17. Hachisuka, K., Takeda, T., Terauchi, Y., Sasaki, K., Hosaka, H., Itao, K.: Intra-body data transmission for the personal area network. *Microsystem Technologies* 11(8-10), 1020–1027 (2005)
18. Hachisuka, K., et al.: Simplified circuit modelling and fabrication of intra-body communication devices. *Sensors and actuators A: Physical* 130-131, 322–330 (2006)
19. Handa, T., Shoji, S., Ike, S., Takeda, S., Sekiguchi, T.: A very low-power consumption wireless ECG monitoring system using body as a signal transmission medium. In: *Proc. of the 1997 International Conference on Solid-State Sensors and Actuators*, Chicago, USA, pp. 1003–1006 (1997)
20. IFAC, Dielectric properties of body tissues calculator (2000),
<http://niremf.ifac.cnr.it/tissprop/> (December 2009)
21. IMEC Human++ projekt. Available online (December 2009),
http://www2.imec.be/imec_com/imec_com_homepage.php
22. INCIRP, Guidelines for Limiting Exposure to Time-Varying Electric, Magnetic, and Electromagnetic Fields (up to 300 GHz). *Health Physics* 74(4), 494–522 (1998)

23. International Society on Biotelemetry ISOB (December 2009),
<http://www.biotelemetry.org/>
24. Lindsey, D.P., McKee, E.L., Hull, M.L., Howell, S.M.: A new technique for transmission of signals from implantable transducers. *IEEE transactions on biomedical engineering* 45, 614–619 (1998)
25. Lučev, Ž., Krois, I., Cifrek, M.: A multichannel wireless EMG measurement system based on intrabody communication. In: XIX IMEKO World Congress. Fundamental and Applied Metrology, Lisbon, Portugal, pp. 1711–1715 (2009)
26. Lučev, Ž., Krois, I., Cifrek, M., Džapo, H., Tonković, S.: Effects of Transmitter Position and Receiver Ground Plane on Signal Transmission in Intrabody Wireless EMG Measurement System. In: Proceedings of XI World Congress on Medical Physics and Biomedical Engineering, Munich, Germany, pp. 887–890 (2009)
27. Lučev, Ž., Krois, I., Cifrek, M.: Application of wireless intrabody communication system to muscle fatigue monitoring. In: International Instrumentation and Measurement Conference, Austin, TX, USA (2010) (accepted for publication)
28. Ministry of Health, Regulations for protection against electromagnetic fields (Pravilnik o zaštiti od elektromagnetskih polja), no. 3306, in croatian (2003)
29. NTT RedTacton (2009), <http://www.redtacton.com/en/index.html>
30. Oberle, M.: Low power system-on-chip for biomedical application. PhD thesis Diss. ETH No. 14509, ETH Zürich, Suisse (referenced after [41]) (2002)
31. Partridge, K., et al.: Empirical measurements of intrabody communication performance under varied physical configurations. In: UIST 2001: Proceedings of the 14th annual ACM symposium on User interface software and technology, Orlando, Florida, USA, pp. 183–190 (2001)
32. Penders, J., et al.: Human++: From technology to emerging health monitoring concepts. In: ISSS-MDBS 2008, Hong Kong, pp. 94–98 (2008)
33. Post, E.R., Reynolds, M., Gray, M., Paradiso, J., Gershenfeld, N.: Intrabody buses for data and power. In: First International Symposium on Wearable Computers, pp. 52–55 (1997)
34. Ruiz, J.A., Shimamoto, S.: A study on the transmission characteristics of the human body towards broadband intra-body communications. In: Proceedings of the 9th International Symposium on Consumer Electronics (ISCE 2005), pp. 99–104 (2005)
35. Ruiz, J.A., Xu, J., Shimamoto, S.: Propagation characteristics of intra-body communications for body area networks. In: IEEE Consumer Communications and Networking Conference (CCNC), vol. 1, pp. 509–513 (2006)
36. Ruiz, J.A., Shimamoto, S.: Experimental Evaluation of Body Channel Response and Digital Modulation Schemes for Intra-body Communications. In: IEEE International Conference on Communications, Istanbul, Turkey, vol. 1, pp. 349–354 (2006)
37. Ruiz, J.A., Shimamoto, S.: Novel communication services based on human body and environment interaction: applications inside trains and applications for handicapped people. In: IEEE Wireless Communications and Networking Conference (WCNC 2006), Las Vegas, NV, USA, vol. 4, pp. 2240–2245 (2006)
38. Shimamoto, S., Alsehab, A.M., Kobayashi, N., Dovchinbazar, D., Ruiz, J.A.: Future applications of body area communications. In: 6th International Conference on Information, Communications & Signal Processing, Singapore, pp. 1–5 (2007)
39. Shinagawa, M., Fukumoto, M., Ochiai, K., Kyuragi, H.: A near-field-sensing transceiver for intrabody communication based on the electrooptic effect. *IEEE Transaction on Instrumentation and Measurement* 53, 1533–1538 (2004)

40. Wegmüller, M.S., Oberle, M., Kuster, N., Fichtner, W.: From dielectrical properties of human tissue to intra-body communications. In: Proc. of IFMBE, World Congress on Medical Physics and Biomedical Engineering 2006, Seoul, Korea, vol. 14(2), pp. 613–617 (2006)
41. Wegmüller, M.S.: Intra-Body Communication for Biomedical Sensor Networks. PhD thesis, Diss. ETH No. 17323, ETH Zürich, Suisse (2007)
42. World Intellectual Property Organization, Capsule type endoscope, patent WO 2008/065839 A1 (2008)
43. Zimmerman, T.G.: Personal Area Networks (PAN): Near-field intrabody communication. MIT Media Laboratory, Cambridge (1995)
44. Zimmerman, T.G.: Personal Area Networks: Near-field intrabody communication. IBM Systems Journal, IBM Corp 35, 609–617 (1996)

SPINE-HRV: A BSN-Based Toolkit for Heart Rate Variability Analysis in the Time-Domain

Alessandro Andreoli^{1,2}, Raffaele Gravina^{2,3}, Roberta Giannantonio⁴,
Paola Pierleoni¹, and Giancarlo Fortino^{3,*}

¹ Università Politecnica delle Marche, Ancona, Italy

² WSN Lab Berkeley, California, USA

³ Università della Calabria, Rende (CS), Italy

g.fortino@unical.it

⁴ Telecom Italia, Torino, Italy

Abstract. The Heart Rate Variability (HRV) is based on the analysis of the R-peak to R-peak intervals (RR-intervals) of the ECG signal in the time and/or frequency domains. Doctors and psychologists are increasingly recognizing the importance of HRV; in fact, a number of studies have demonstrated that patients with anxiety, phobias and post-traumatic stress disorder consistently show lower HRV, even when not exposed to a trauma related prompt. Importantly, this relationship existed independently of age, gender, trait anxiety, cardio-respiratory fitness, heart rate, blood pressure and respiration rate. In this paper, we present a toolkit based on body sensor networks (BSN) for the time-domain HRV analysis, namely SPINE-HRV (Signal Processing In Node Environment-HRV). The SPINE-HRV is composed of a wearable heart activity monitoring system to continuously acquire the RR-intervals, and a processing application developed using the SPINE framework. The developed system consists of a wireless chest band, a wireless wearable sensor node and a base station. The RR-intervals are processed using the SPINE framework at the base station side through a time-domain analysis of HRV. The analysis provides seven common parameters known in medical literature to help cardiologists in the diagnosis related to several heart diseases. In particular, SPINE-HRV is applied for stress detection of people during activities in their everyday life. Experimentations carried out by monitoring subjects in specific activities have shown the effectiveness of SPINE-HRV in detecting stress.

Keywords: Body Sensor Networks, Domain specific frameworks, SPINE, Health care, HRV, stress detection.

1 Introduction

During the last few years the death rate has been increased constantly due to heart diseases coming from the change of dietary life style. Therefore, if the heart could

* Corresponding author.

be monitored constantly in daily life, the unexpected heart diseases would be more easily predicted not only for patients with heart pathologies but also for healthy people who exercise daily. Among many factors affecting the cardiovascular human system, in this work, we focus on stress that is currently considered of notable importance. Many studies show connections between long-term exposure to stress and risk factors for poorer immune functions and cardiovascular diseases [8][5]. In particular, in [8], authors showed that chronic forms of stress were accompanied by reduced cytotoxicity of natural killer cell, suppressed proliferative responses of lymphocyte, and blunted humoral responses to immunization. Moreover, [5] found out that long-term exposure to adverse psychosocial circumstances linked cardiovascular risk factors such as high blood pressure and high blood cholesterol. Although the exact mechanisms of how stress exerts these effects are not well known, a stress monitoring technique which would measure stress levels may significantly support the development of methods for the mitigation of long-term stress and promote healthy life style. Despite the complexity of measuring the stress level directly, it is quite possible to annotate stressful events and relate them to physiological signal changes that can be easily measured. Thus, it is important to measure physiological signals accurately anytime and anywhere. As the progress in electronics is made, healthcare devices have become miniaturized, more sophisticated, and more personalized [21]. A real-time personal stress monitor would benefit individuals by providing continuous feedback about their stress levels. In essence, the use of a wearable sensor for monitoring stress levels enables an individual to monitor oneself anytime and anywhere.

Heart Rate Variability (HRV) could be one of the most promising markers for this purpose. HRV represents the variations in the beat-to-beat alteration in the heart rate. HRV analysis is prevalently used to assess the effect of autonomic regulation on the heart rate. It provides a dynamic nature of the interplay between the sympathetic and parasympathetic branches. The activation of Sympathetic Nervous System (SNS) causes the increase of sympathetic branch activity that accelerates the heart rate, constricts blood vessels, and raises blood pressure. The parasympathetic branch induces the relaxation response that slows down the heart rate and decreases the force of the heart contractions. There is a balance between these systems under normal situations, placing the body in a state of homeostasis. However, under a state of mental stress, this balance will be altered [6]. Hence, HRV can be used to detect the change in system balance as measures of mental activity and mental stress [2]. Moreover, HRV has been used in clinical research to assess the prognosis of different pathologies in several cardiological and non-cardiological diseases such as myocardial dysfunction, diabetes and arrhythmias [10]. In normal subjects, both sympathetic and parasympathetic tone fluctuates throughout the day [4]. HRV indices such as the ratio of the low-frequency (LF) to high frequency (HF) power or the fractional LF power have been used to describe sympathovagal balance. In the absence of any sympathetic or parasympathetic input to the sinus node, the sinus node fires at its intrinsic rate. When vagal effects predominate, the heart rate is less than the intrinsic heart rate; when sympathetic

effects predominate, the heart rate is greater than the intrinsic heart rate [12]. It was found that the HRV decreases with age and for an individual, the HRV is maximum during sleep. It is also dependent on the heart rate, i.e. the HRV is more at lower heart rates [13].

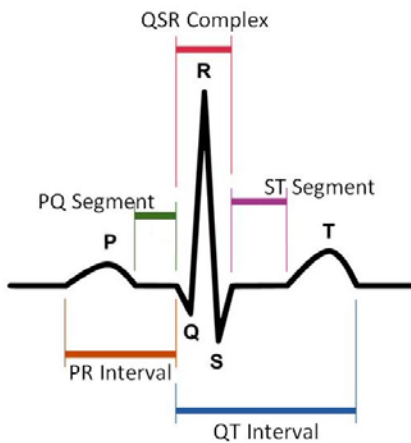
The interest on the HRV analysis is growing fast in the research community as HRV has been demonstrated to be a valid marker for several physiological conditions. Recently, a few research projects are aiming to combine the well-known benefits of Wireless Body Sensor Network (WBSN) technologies to monitor the HRV continuously and non invasively. In particular, research has been focused on ear-worn wireless pulse oximeter sensors, used to detect the heart beats from the oxygen saturation of the blood. However, such in-ear devices are influenced by motion noise, particularly due to jaws movements. Moreover a few commercial emotional stress monitor products are also available today. However, since they are based on hand- held devices or ear-clip connected via USB to a PC, they are designed for temporary monitoring and not intended for continuous use.

In this paper we propose a toolkit for the time-domain HRV analysis, namely SPINE-HRV. The proposed system detects in real-time the heart beats to extract the characteristic RR intervals (or RR_i). Time-domain features are in turn extracted from the RR_i to indentify the stress level of the monitored subject. The system is composed of a wireless chest band, a wireless wearable device acting as a mobile gateway to a central coordinator, and a user friendly application running on a laptop or PC. The main strength of the proposed system relies in its comfortable wearability, robustness to noise due to body movements and its ability to identify emotional stress in real-time, with no need to rely on offline analysis. The remainder of the paper is organized as follows. Section 2 provides an overview on HRV and some related work. Section 3 describes the SPINE framework, atop which the proposed solution has been implemented. Section 4 describes the proposed SPINE-HRV tool system. Section 5 reports experimental results obtained under real life situations. Finally, the main contributions of the paper are discussed in Section 6.

2 Background and Related Work

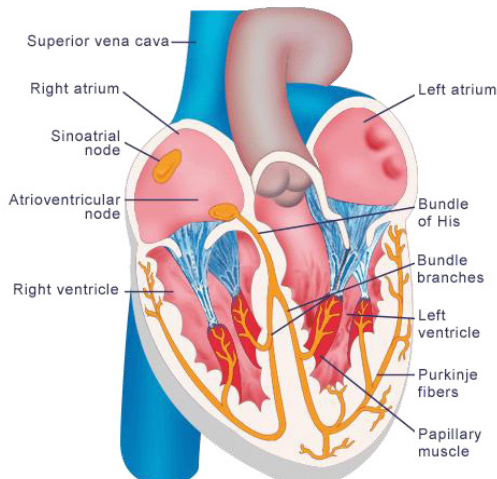
Heart rate variability (HRV) describes the variations between consecutive heartbeats. The rhythm of the heart is controlled by the sinoatrial (SA) node, which is modulated by both the sympathetic and parasympathetic branches of the autonomic nervous system. Sympathetic activity tends to increase heart rate and its response is slow (few seconds). Parasympathetic activity, on the other hand, tends to decrease heart rate and mediates more quickly (0.2-0.6 seconds). The term HRV refers, in general, to changes in heart beat interval that is a reciprocal of the heart rate.

The starting point for HRV analysis is the electrocardiogram (ECG) recording from which the HRV time series can be extracted. The ECG signal consists of a quasi-periodic sequence of P, QRS and T-wave (see Fig. 1). In the formulation of

**Fig. 1.** QRS complex

the HRV time series, a fundamental issue is the determination of the heart beat period. The aim in HRV analysis is to examine the sinus rhythm modulated by the autonomic nervous system. Therefore, in principle, we should detect the occurrences of the SA-node action potentials. This is, however, impossible in practice and, thus, the fiducial points for the heart beat are usually determined from the ECG recording. The nearest observable activity in the ECG compared to SA-node firing is the P-wave resulting from atrial depolarization (see Fig. 2).

The heart beat period is commonly evaluated as the time difference between the easily detectable QRS complexes being the part with the highest amplitude with in the ECG signal (see Fig. 1).

**Fig. 2.** Electrophysiology of the heart

After the QRS complex occurrences have been estimated, the HRV time series can be derived. The inter-beat, or RR_i , are obtained as the time difference between successive R-wave occurrences. That is, the i^{th} RR interval (see Fig. 3) is obtained as the difference between the R-wave occurrences at time i and $i-1$: $RR_i = t_i - t_{i-1}$.

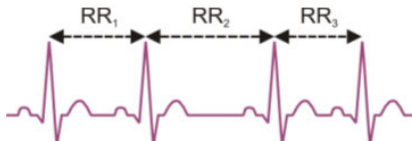


Fig. 3. RR interval tachogram

Variations in heart rate may be evaluated by a number of methods. Perhaps the simplest one to perform is based on the time-domain measures. In particular, the most evident measure is the mean value of RR_i (\bar{RR}) or, correspondingly, the mean (\overline{RR}). In addition, several variables that measure the variability within the RR series exist: the standard deviation of RR_i (SDNN). The most commonly used measures derived from interval differences also include the root mean square of successive differences (RMSSD). Another measure calculated from successive RR_i differences is the NN50 which is the number of successive intervals differing by more than 50 ms and pNN50 that is the proportion derived by dividing NN50 by the total number of RR_i . Table 1 shows in detail the various time domain HRV parameters [10].

Table 1. Time domain HRV parameters

Parameter	Units	Description
NN50 count		Number of adjacent RR intervals differing by more than 50 ms in entire ECG recording
pNN50	%	NN50 count divided by the total number of all RR intervals
SDNN	ms	Difference between shortest and longest RR interval
SDNN index	ms	Mean of the standard deviations of all RR intervals for all 5 min segments in the entire recordings
SDNN	ms	Standard deviation of averages of RR intervals for all 5 min segments in the entire recordings
RMSSD	ms	Root mean square of the difference of successive RR intervals
SDSD	ms	Standard deviation of differences between adjacent RR intervals
HRV index	ms	Total number of all RR intervals divided by amplitude of all RR interval

In contrast to the time domain measures of HRV mentioned above, recent developments in microprocessor technology has enabled the calculation of frequency measures on the same ECG data. Frequency measures involve the spectral analysis of HRV. The RR interval time series is an irregularly time-sampled signal. This is not an issue in time domain, but in the frequency-domain it has to be taken into

Table 2. Frequency-domain HRV parameters

Parameters (units)	Definition	Interpretation
Total power (ms²)	Total area under the power density function (0.003 - 0.04 Hz)	Total variability (HRV), equal to (SDNN)
HFP or HF (ms²)	Area under the power density function in the frequency (0.15-0.4 Hz)	Parasympathetic modulation of HR (respiratory sinus arrhythmia)
LFP og LF (ms²)	Area under the power density function in the frequency (0.04-0.15 Hz)	Sympathetic modulation of HR with contribution from parasympathetic activity
VLF (ms²)	Area under the power density function in the frequency range (0.003-0.04 Hz)	Modulation of HR by slow blood pressure regulating systems
HF n.u. (normalized units)	HF/(TP-VLF)	Same as HF
LF n.u. (normalized units)	LF/(TP-VLF)	Same as LF
LF/HF	LF/HF	"Autonomic balance", i.e. the balance between sympathetic and parasympathetic activity.

account. If the spectrum estimate is calculated from this irregularly time-sampled signal, additional harmonic components appear in the spectrum. Therefore, the RR_i signal is usually interpolated before the spectral analysis to recover an evenly sampled signal from the irregularly sampled event series. In the frequency-domain analysis power spectral density (PSD) of the RR series is calculated. The HRV spectrum contains the high frequency (0.18 to 0.4 Hz) component, which is due to respiration and the low frequency (0.04 to 0.15 Hz) component that appears due to both the vagus and cardiac sympathetic nerves [7]. Ratio of the low-to-high frequency spectra is used as an index of parasympathetic-sympathetic balance. Frequency domain HRV parameters are detailed in Table 2.

HRV has been extensively studied during the last decades, and numerous research articles have been already published [7][10]. Many industry research projects also focus on HRV. Many of these works aim to find a connection between different features extracted from RR_i data and related heart diseases. An interesting research [4] proves the existence of a relation between time-domain HRV parameters and stressful driving situation on the road. This work demonstrates that driving is a powerful stressor. In fact, as the subjects started driving, the HRV parameters changed rapidly; in particular, the SSDN, RMSSD and NN50 decreased, while the HR increased. In [9] a statistical oriented framework, called Kubios HRV developed by University of Kuopio is proposed. This is an advanced tool for studying the variability of heart beat intervals. The software is mainly designed for the analysis of normal human HRV, but should also be usable for animal research. Kubios HRV supports all data of two commonly used heart rate monitors: SUUNTO SDF/STE and POLAR HRM files [22]. Kubios HRV includes all the commonly used time- and frequency-domain parameters of HRV. The frequency-domain parameters are calculated for both nonparametric (Fourier transform based) and parametric (autoregressive modelling based) spectrum estimates. In addition, several non-linear HRV parameters are calculated such as Poincare' plot, recurrence plot analysis, detrended fluctuation analysis, approximate and sample entropies, and correlation dimension. There are a few commercial products for stress monitoring. StressEraser [1] is a tangible biofeedback device that was specifically designed to help finding the unique breathing pattern that maximizes Respiratory Sinus Arrhythmia (RSA). Stress Monitor [23] is commercialized by Health

Reviser and is designed for monitoring the stress level while working. In particular, it is composed by a USB ear-clip to be connected to a PC, and a GUI application for real-time evaluations as well as historical reports. Because it is necessary to connect the ear-clip to a PC, Stress Monitor is not intended for continuous daily monitoring. The emWave Personal Stress Reliever [24] is a handheld portable device with audio and LEDs feedbacks to monitor the stress level. However, none of these solutions are designed for continuous monitoring, as they must be handled in hand to work.

To date a number of BSN-based research projects have been dedicated on heart monitoring, most of the time by analyzing the ECG signal. However HRV analysis is still today mainly performed offline on data collected previously. A few works focused the attention on using a BSN-based approach to perform online HRV analysis. For instance, in [18], an in-ear micro-optic sensor to gather pulseoxymetric measurements is described. The pulse oximeter is used as an alternative to the ECG to deduce the HRV analysis from the photoplethysmograph (PPG) signal. The authors suggest the use of an in-ear sensor to reduce the strong motion artifacts that are common in finger-tip sensors. In fact, with respect to the arms, the relative position of the auditory canal is almost constant. Moreover, the body temperature, which influences the pulse oximeter sensor, has smaller oscillations in the ear than on the fingers. On the other hand, jaw motions can corrupt the signal. In particular, the precise observation of the heart beat by pulse oxymetric measurements inside the ear fails in the presence of a moving jaw. Several methods have been proposed for analyzing the variability of the heart rate [10]. Most of them describe the fluctuations in the heart beat intervals by well established time or frequency domain measurements, such as mean, standard deviation, the ratio of low-to-high frequency spectral bands, or the PSD of the signal. Usually the PSD of a signal is estimated by performing the Fast Fourier Algorithm (FFT). This technique can be easily applied to evenly sampled time series. In contrast to this, for unevenly sampled time series, which are common in long term monitoring of physiological parameters in normal daily life due to missing data during the observation, the estimation of the correlation or the spectral properties is a difficult task. To tackle this issue, the authors estimate the PSD using Lomb-periodograms [19]. In particular, up to 25% of missing data in the tachogram will affect the original pulse signal, but will not influence the HRV analysis.

In [20], the authors propose another in-ear PPG sensor based solution to analyze the HRV. With respect to the work mentioned above, in this study, a built-in accelerometer sensor has been used to detect the level of the head motion and compensate the motion artifact in the PPG signal. In particular, when the motion level was larger than a pre-defined threshold, which had been pre-determined by tests on individual subjects, the HR obtained during this period was eliminated and replaced by the HR measured just prior to the motion period.

With respect to the current literature, we propose a different approach which involves a wireless chest belt commercially available by POLAR. Using a wireless chest belt makes the system more comfortable than wired electrodes. Furthermore, because the chest belt is a commercial product for sport and fitness activities, it

has been designed to be much robust against body movements. Finally, we propose a BSN-based solution that explicitly uses HRV to detect stress of the monitored subject.

3 The SPINE Framework

Programming BSN applications is a complex task mainly due to the hard resource constraints of wearable devices and to the lack of proper and easy to use software abstractions. Typically, BSN applications have in common several requirements. For example, most BSN systems need signal processing intensive tasks such as signal filtering, feature extraction and decision support tools. Security and data encryption must often be taken into account as most of the communication involves sensible medical data of the users, such as their heart condition, glucose level, physical activity being performed, or simply their location. Device discovery and advertising are considered very useful if not necessary, due to the variety of physical sensors and functionalities supported by the wearable devices. Scalability and flexibility are also important to allow higher performance (e.g. more accurate event classification having availability of more data sources) and easier updates in the system requirements. Optimising power consumption of both the wearable devices and the coordinator unit is also critical, as in many cases, especially for BSNs with medical purposes, the system must be used for continuous monitoring twenty four hours a day, seven days a week. It is well known that wireless communication has a critical influence in power consumption; as a consequence, programming a BSN must also address the issue of achieving low radio duty cycling most of the time. Many BSN applications need handling of multiple sensor signals at the same time, which is sometime referred as sensor data fusion and context awareness (e.g. accelerometer, electrocardiogram and location data to identify physical activities).

To address these requirements in a systematic way, software frameworks have been proposed, specifically for BSNs (CodeBlue [17]), or adapted to BSNs scenarios (Titan [15]). CodeBlue is a framework running on TinyOS specifically designed for integrating wireless medical sensor nodes and other devices. CodeBlue allows these devices to discover each other, report events, and establish communications. CodeBlue relies on a publish/subscribe-based data routing framework in which sensors publish relevant data to a specific channel and end-user devices subscribe to channels of interest. It includes a naming scheme, a multi-hop communication protocol, authentication and encryption capabilities, location tracking and in-network filtering and aggregation. CodeBlue provides end-user devices with a query interface for retrieving data from previously discovered sensor nodes. Although CodeBlue provides a sensor driver abstraction architecture which allows an easy integration of new sensors within the system, selection of sensor types or physical node identifiers as data sources, tuning of the data rate and definition of threshold-based filters to avoid unnecessary data being transmitted, it does not allow inserting complex signal processing functionalities into the sensor nodes. It supports just simple threshold-based triggers on the sensor readings that do not

give enough flexibility for the variety of requirements of the BSN applications. A higher-level approach is adopted by Titan [15]. Titan, which is implemented in TinyOS, is a general-purpose middleware that supports implementation and execution of context recognition algorithms in dynamic WSN environments. Titan represents data processing by a data flow from sensors to recognition results. The data is processed by tasks, which implement elementary computations. Tasks and their data flow interconnections define a task network, which runs on the sensor network as a whole. Tasks are mapped onto each sensor node according to the sensors and the processing resources it provides. Titan dynamically reprograms the WSN to exchange context recognition algorithms, handle defective nodes, variations in available processing power, or broken communication links. The architecture of Titan is composed of several software components, which enhance modularity. Although Titan raises the programming abstraction level by offering a middleware for effectively developing signal processing applications in WSNs, it is based on too generic mechanisms for providing efficient solutions in the specific BSN application domain. In fact, the programming of a feature extraction operation on the sensor node, which is often carried out in a BSN application, requires the creation of at least five tasks (sampling, buffering, loading, feature calculation, transmission). Moreover, some overhead can be introduced due to the connections of the output and input ports among tasks through which data are exchanged.

As discussed, existing frameworks do not cover properly all the requirements of a typical BSN application. However, a solution resides in a quite novel software engineering approach called “domain-specific framework”. Domain-specific frameworks are in the middle between application-specific code and general-purpose middleware approaches. They specifically address and standardize the core challenges of WSN design within a particular application domain. While maintaining high efficiency, such frameworks allow for a more effective development of customized applications with little or no additional hardware configuration and with the provision of high-level programming abstractions tailored for the reference application domain.

To support the design of optimized BSN applications while minimizing the design time and efforts, a domain-specific framework, called SPINE (Signal Processing In-Node Environment) [14], has been developed. SPINE is designed to support flexible and distributed signal-processing for BSN systems. The main goal of SPINE is to provide BSN developers with support for rapid prototyping of signal-processing applications. It provides higher-level abstractions and support to quickly explore implementation tradeoffs through fast prototyping. SPINE focuses on making a variety of functionality easily and conveniently accessible, yet configurable by designers. SPINE is based on the following principles:

- *Open Source.* The SPINE project [16] is Open Source to establish a community of users and developers. The SPINE code is available under the LGPL license.
- *Interoperability through APIs.* SPINE provides local and remote applications with lightweight Java APIs that they can use to manage the sensor nodes or

issue service requests. The APIs are easily portable to devices of various capabilities, such as PCs or smartphones.

- *High-level abstractions.* SPINE provides libraries of protocols, utilities and data processing functions and support to easily specify new services and features. The layer defined by the SPINE service libraries allows application designers to program at higher levels of abstraction than TinyOS.
- *Distributed implementations of data processing and interpretation algorithms.* SPINE helps designers to evaluate the efficiency of distributed implementations of data classification algorithms with respect to the use of energy and channel bandwidth.

Table 3 introduces the most common tasks handled on the wearable sensor nodes and required in most of the BSN systems. It is worth noting that they are all available in SPINE.

Table 3. Common tasks supported by BSN applications at node-side

Service	Description
Sampling	The sensor sampling process represents the first step for developing a BSN application. Selecting the appropriate sampling time to satisfy the application requirements is important because the amount of data generated and processed and “under certain degree” the energy consumed depend on it.
Feature extraction	Classification algorithms very rarely use raw data. Instead, attributes (or features) are typically extracted on data windows and used to detect events and classify activities. Extracting features directly on the wireless nodes also allows the reduction of the radio usage, as aggregated results are sent instead of several raw data values.
Queries	Support for selective queries on the available sensors of a node is important because application requirements can change over time and not all the sensors are necessarily involved for algorithms execution at any time.
Node synchronization	In a WBSN, nodes should be kept synchronized when sampling the sensors and processing data, because data gathered from multiple wearable nodes must refer to the same time interval to be aggregated to recognize correctly physical activities or other events of interest.
Duty cycling	Duty cycling is a mechanism for handling the radio status (idle, on, off) to reduce power consumption of a sensor node and therefore its battery lifetime. In particular, radio duty cycling must be tuned very carefully, reducing as much as possible the active time (transmitting, receiving, and listening).

In SPINE, sensors and common processing blocks, such as math aggregators and threshold-based alarms, can be configured independently and connected together arbitrarily at run-time based on external controls. Such an approach allows heterogeneous applications to be built atop the same basic software components, enhancing code reusability and, more importantly, removes the need for redeploying the node-side code based on a particular application. Obviously, to support different applications, the wearable sensing node(s) must be equipped with all the required sensors.

The BSN architecture supported by SPINE includes multiple sensor nodes and one coordinator node. Currently, the network architecture of SPINE is organized as a star topology, which is very common for BSN applications, where sensor

nodes communicate only with the coordinator. The coordinator manages the network, collects and analyzes the data received from the sensor nodes, and acts as a gateway to connect the BSN with wide area networks for remote data access. Sensor nodes measure local physical parameters and send raw or processed data to the coordinator.

The SPINE framework consists of two main components, implemented, respectively, on the coordinator (e.g. a PC or a smartphone) and on the BSN nodes. A high level view of the software layering of SPINE is shown in Fig. 4.

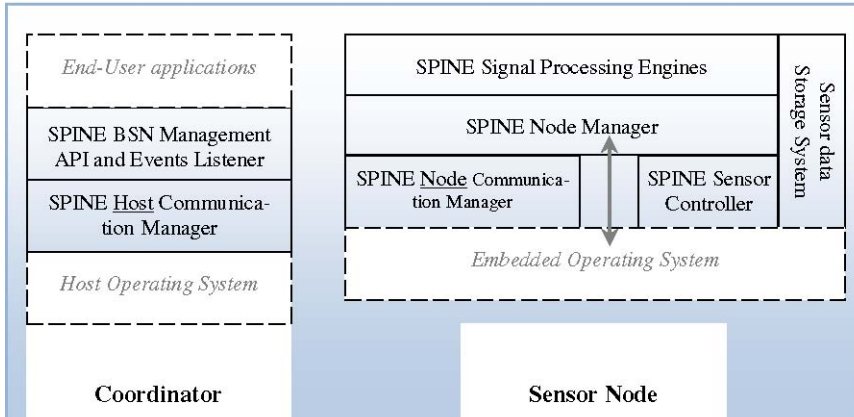


Fig. 4. SPINE Software Layers

On the coordinator side, SPINE provides application developers with a very intuitive interface to the BSN that is placed between end-user applications and the hardware and software host platform. On the node side, the SPINE framework is responsible for providing developers with abstractions of hardware resources such as sensors and the radio, a default set of ready-to-use common signal processing functions and, most important, a flexible and modular architecture to customize and extend the framework itself to support new physical platforms and sensors and introduce new signal processing services.

4 Spine HRV Toolkit

The SPINE-HRV tool is a full-fledged heart monitoring system. The hardware is specially designed to be non-restricted, non-aware and non-invasive, therefore suitable in daily life use. In fact, the required hardware modules communicate with each other through wireless connections. The software layer development has been simplified by the use of the SPINE framework [3]. Thus, most of the programming efforts have been dedicated to the implementation of the HRV analysis algorithms.

4.1 Hardware

The hardware architecture of our system is composed of a wireless chest band, a wireless wearable node and a coordinator station. The wireless chest band detects heart beats and transmits a pulse message over the air each time a heart beat has been detected. It does not require manual power on or any software configuration. The wearable node is a TelosB mote equipped with the CardioShield (see Fig. 5), a custom board that has a dedicated receiver for the heart beat messages sent by the chest band.

There are two type of chest band that the receiver can use, the former is a non coded chest band, the latter utilizes a coded modulation that allows to be more robust again the noise. Furthermore, the use of the modulated one chest band allows exploiting multiple copies of the same wireless network in the same environment. This is a realistic situation in a typical hospital environment, where patients perform the same exams in the same environment at the same time.



Fig. 5. TelosB CardioShield

Such receiver in turn triggers a hardware interrupt to the GPIO 27 of the MSP430 microcontroller of the TelosB mote. When two "heart beats" interrupt signals are intercepted by the microcontroller, the time intervals (with milliseconds resolution) between the pulses are calculated and the instantaneous heart rate is determined. The receiver on the node and the chest band must stay within the range up to 80 cm, so that the node can be easily worn on the waist. The board also has a built-in three-axis accelerometer. An interesting consideration can also be done with respect to the power consumption of the entire CardioShield board. The heart beat receiver has a typical power consumption of $60\mu\text{A}$ only. The overall consumption rise to 7mA , considering the accelerometer, the heart beat receiver, the radio CC2420 and the microcontroller power. Thus it permits up to 28 hours of battery life, with a typical battery of 600mAh . This feature is useful for long-term recordings where sequences of RR_i are taken during the entire 24-hours period. The wearable node runs the TinyOS operating system and is powered by the SPINE framework. The coordinator station is a PC or a smartphone running a Java application built atop SPINE, which allows application level bidirectional communication to setup the wearable node and retrieve heart beats as well as accelerometer data.

4.2 Software

The wearable mote runs the SPINE framework, which has been extended with a custom defined processing function to support the CardioShield board. In particular, the function takes care of enabling/disabling interrupts from the heart beat dedicated receiver based on coordinator requests. When the function is instructed by the SPINE coordinator to start computing, interrupts corresponding to heart beats are timestamped using a counter with millisecond resolution provided by TinyOS. Then, the interval between subsequent heart beats, commonly known as RR_i , is calculated and transmitted over-the-air as a SPINE data message. The node can also be setup at runtime to transmit activity counts from the accelerometer along with the measured RR_i . Activity counts is a SPINE feature that can be used to calculate the calories consumed. This feature is particularly accurate when wearing the node on the waist. It is useful to combine the two data types, for instance, to verify if an increased heart rate is due to the physical activity being performed. The developed Java application (see its GUI in Fig. 6) uses RR_i data, gathered from the wearable node through SPINE, to compute the average heart beat rate expressed in beat per minute (BPM), the maximum and minimum heart rate, and to analyze the stress level of the monitored subject. A time series plot diagram shows in real time the instantaneous heart rate, and it is very useful to quickly visualize arrhythmias such as Premature Ventricular Contractions (PVCs), happening when the heart skip a contraction, or accessory pathway tachycardias, causing the heart to beat unusually fast. Furthermore, the calories consumed per minute are computed from the activity counts feature, and expressed in Kcal/min. The calories consumed are also reported in a time series plot diagram.

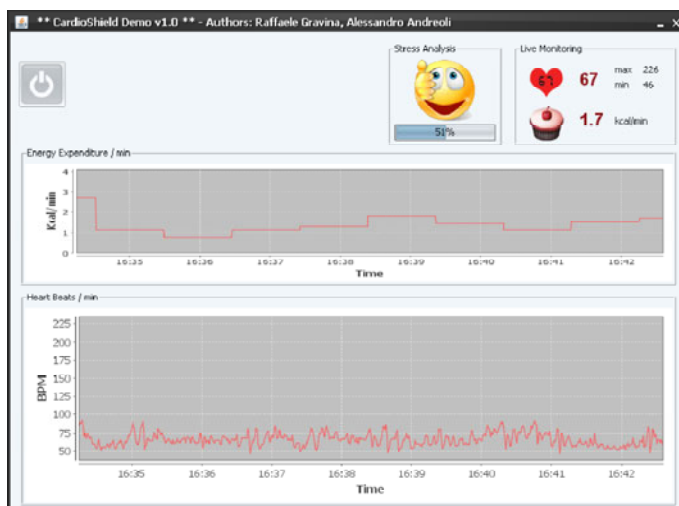


Fig. 6. SPINE-HRV toolkit

Furthermore, the SPINE-HRV toolkit provides a useful interface to record raw RR_i into a POLAR compliant file [22], where each line of the file represent a RR_i time with millisecond resolution. The feature permits also to use SPINE-HRV toolkit as bridge to other software (for example Kubios [9]) to perform other kinds of HRV analysis.

4.3 Stress Analysis Engine

The heart rate is computed from the RR_i values, sent by the wearable node and expressed in milliseconds. It worth noting that we assume a reliable communication between the wireless chest band and the wearable node. Evident lost heart beat packets are transparently filtered out by the embedded code running on the node. Also, we decided not to interpolate dropped RR_i messages sent by the wearable node to avoid further bias while executing the analysis. This approach is simplified by the event-based programming model provided by SPINE. Specifically, we use a 20-point moving average filter over the inter-beat intervals. Maximum and minimum heart rate, however, are computed instantaneously by dividing the current RR_i received from the wireless node by one minute. The stress level of the subject is refreshed every ten minutes, as previous works have shown that this is the minimum collection time to get significant results [11]. In our work we utilize only time-domain analysis that is fair enough to evaluate the stress condition as demonstrated in [11]. In particular, we compute the following features: \overline{RR}_j (computed by averaging on 15 heartbeats) proportional to \overline{HR} , pNN50, SDNN and RMSSD as follows:

$$\overline{RR}_j = \frac{1}{15} \sum_{j=1}^{15} RR_j \quad (1)$$

$$SDNN = \sqrt{\frac{1}{N-1} \sum_{j=1}^N (RR_j - \overline{RR})^2} \quad (2)$$

$$RMSSD = \sqrt{\frac{1}{N-1} \sum_{j=1}^{N-1} (RR_{j+1} - RR_j)^2} \quad (3)$$

$$pNN50 = \frac{NN50}{N-1} \times 100 \quad (4)$$

where RR_j denotes the value of j^{th} RR interval and N is the total number of successive intervals. SDNN is the primary measure used to quantify HRV change, since SDNN reflects all the cyclic components responsible for variability in the period of recording. Usually under negative emotions, the activation of autonomic

nervous system (ANS) is decreased compared to positive emotions; hence, higher SDNN might serve as an indicator for ANS activation.

In this work, we focus on determining whether the monitored subject is under emotional stress or not. Thus, it is a decision problem that we solve with a threshold-based approach.

In Table 4 the threshold values we have adopted, which have been extracted from the results found in [11] are reported. The final decision is made on a simple majority vote: if three out of the four features exceed the threshold, we classify the emotional state as stressed.

Table 4. Stress threshold for HRV parameters

Feature	Threshold	Unit
HR	>85	1/min
pNN50	<7	%
SDNN	<55	ms
RMSD	<45	ms

5 An Experimentation for Stress Detection

To evaluate the proposed BSN-based emotional stress indicator system, we collected data from several subjects under different stimulus sessions. All participants had normal auditory function; none had neurological disorders. They were asked to be free of coffee and alcoholic drinks at least three hours before each experiment. All of them were given written informed consent to complete the questionnaires and the psycho-physiological protocols. We organized the experiments in five different sessions:

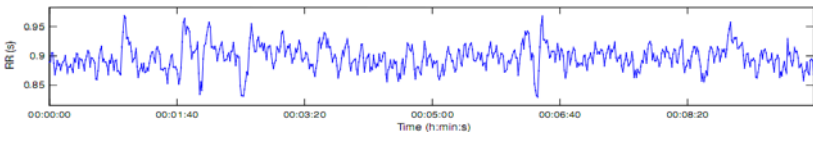
1. sleeping
2. watching TV
3. walking
4. working at the PC
5. driving a car

For the sake of explanation, we will show the obtained results of the subject where the different reactions were more evident. Furthermore, we will focus on a ten minutes window that is the minimum time required to perform accurately the stress analysis. We used our system to record the time-domain based stress analysis results, and to store the RR_i signal itself into a file to compare the obtained results with a frequency-domain HRV analysis using the Kubios software (see Fig. 7 – 11).

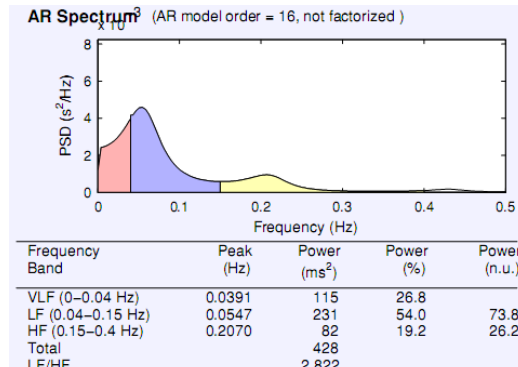
Table 5 summarizes, for the reported subject, how our system classified the selected sessions.

Table 5. Stress evaluation of different sessions.

Session	Emotional State
Sleep	Non Stressed
Watch TV	Non Stressed
Walk	Non Stressed
Office Work	Stressed
Drive	Stressed



(a)



(b)

Fig. 7. Sleeping: (a) RR_i signal / time-domain; (b) PSD / frequency-domain analysis

As discussed in Section 1 and 2, the parasympathetic nervous system is predominant in the HF band, while the sympathetic nervous system is predominant in the VLF and LF bands. Furthermore we briefly remind that the sympathetic system, which is responsible of increasing the heart rate, is much more quickly influenced by “emotions” variations. Given that, we note that in the driving and working sessions, which have been classified by our system as “stressed”, the PSD is more concentrated in the VLF and LF bands compared to the walking, TV watching, and sleeping sessions, which have been classified as “non stressed”. We can then conclude that reasonably good results in identifying emotional stress can be achieved without recurring to frequency domain analysis of the HRV, and just by analysing features extracted in the time-domain. This has facilitated the realization of a real-time BSN-based stress monitor such as SPINE-HRV.

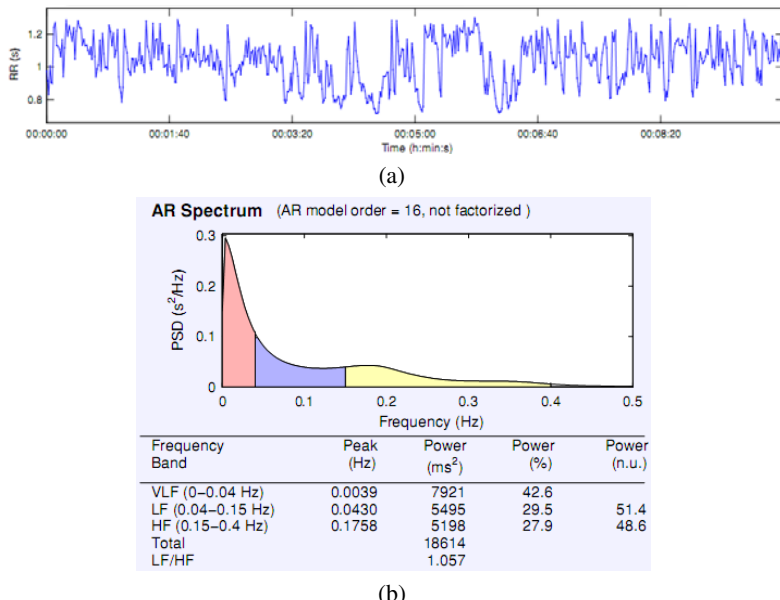


Fig. 8. *Watching TV:* (a) RR_i signal / time-domain; (b) PSD / frequency domain analysis

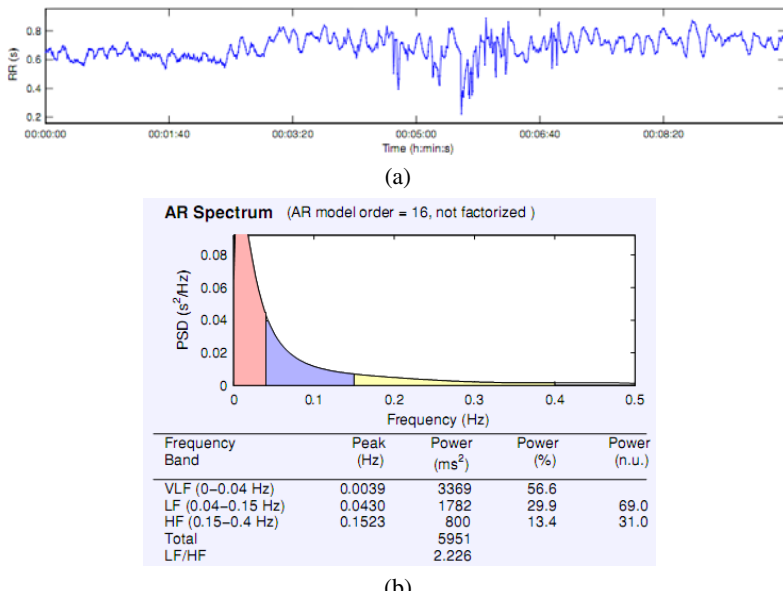


Fig. 9. *Walking:* (a) RR_i signal / time-domain; (b) PSD / frequency domain analysis

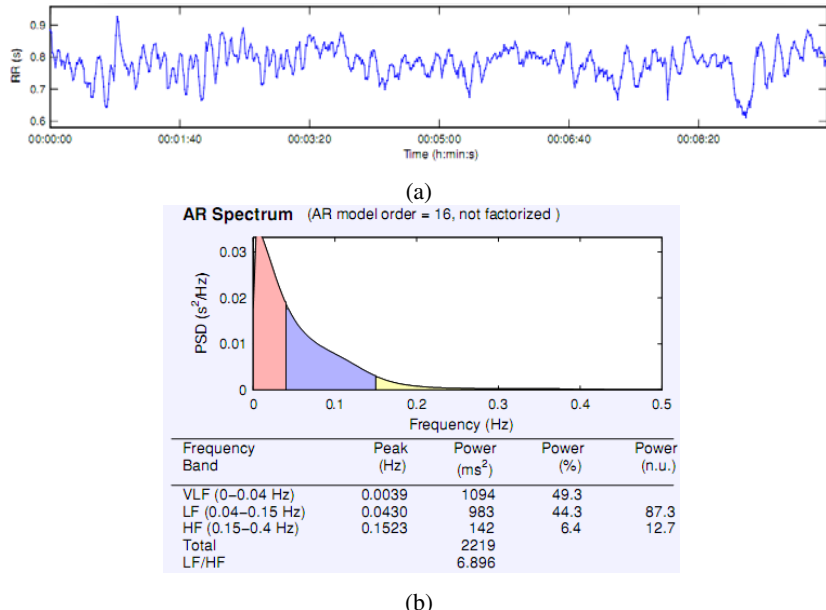


Fig. 10. Working at PC: (a) RR_i signal / time-domain; (b) PSD / frequency domain analysis

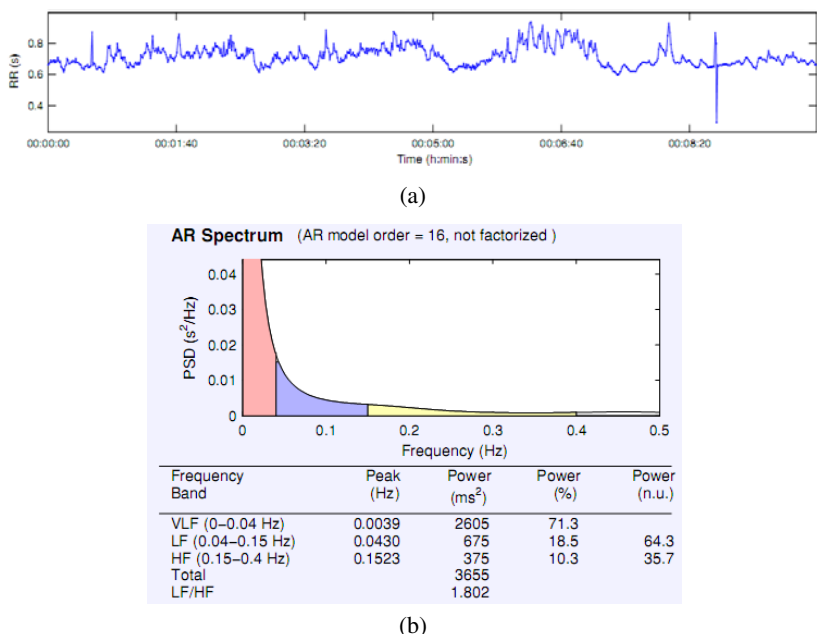


Fig. 11. Driving: (a) RR_i signal / time-domain; (b) PSD / frequency domain analysis

6 Conclusion

HRV is being catalyzing attention as an important medical indicator; in fact, a number of studies have demonstrated that patients with anxiety, phobias and post-traumatic stress disorder consistently show lower HRV, even when not exposed to a trauma related prompt. In this paper we have presented SPINE-HRV, a toolkit for the time-domain analysis of HRV. In particular, SPINE-HRV consists of a wireless chest band, a wireless wearable device acting as a mobile gateway to a central coordinator, and a user friendly application running on a laptop, PC or smartphone. The software is completely based on the SPINE framework which allows for efficient sensing, flexible in-node processing, and rapid prototyping. Currently few research prototypes based on BSNs exist that allow for HRV analysis. However SPINE-HRV represents the first prototype using a wireless chest belt so making the system more comfortable than systems using wired electrodes or handheld devices. Furthermore, because the chest belt is a commercial product for sport and fitness activities, it has been designed to be robust against body movements. SPINE-HRV is currently applied to stress detection that is computed through an effective threshold-based algorithm. The experimentation of such an application has been carried out on different subjects performing different activities of the everyday life: walking, working at the PC, watching TV, sleeping, and driving. The obtained result are interesting as they show that SPINE-HRV is able to detect stress by performing only a time-domain analysis of HRV with respect to more complex computational methods based on the frequency-domain analysis. Thus, SPINE-HRV can be actually used to detect stress of human beings in real-time.

Currently, we are focusing our research efforts in improving the stress analysis algorithm by introducing frequency domain features as well as comparing the obtained results to the clinical blood test for the stress hormone, which has been identified by the medical community as the quantitative measurement of the emotional stress level. Furthermore our stress analysis algorithm can also be improved using ElectroEncephaloGram (EEG) alpha biofeedback.

Acknowledgments

This work has been partially supported by CONET, the Cooperating Objects Network of Excellence, funded by the European Commission under FP7 with contract number FP7-2007-2-224053.

References

1. Stress Eraser, <http://stresseraser.com/>
2. Bernardi, L., Wdowczyk-Szulc, J., Valenti, C., Castoldi, S., Passino, C., Spadacini, G., Sleight, P.: Effects of controlled breathing, mental activity and mental stress with or without verbalization on heart rate variability. *J Am. Coll. Cardiol.* 35(6), 1462–1469 (2000)

3. Gravina, R., Guerrieri, A., Fortino, G., Bellifemine, F., Giannantonio, R., Sgroi, M.: Development of body sensor network applications using spine. In: IEEE International Conference on Systems, Man and Cybernetics, 2008. SMC 2008, pp. 2810–2815 (October 2008)
4. Lee, H.B., Kim, J.S., Kim, Y.S., Baek, H.J., Ryu, M.S., Park, K.S.: The relationship between hrv parameters and stressful driving situation in the real road. 198–200
5. McEwen, B.S.: Protective and Damaging Effects of Stress Mediators. *N. Engl. J. Med.* 338(3), 171–179 (1998)
6. Rani, P., Sims, J., Brackin, R., Sarkar, N.: Online stress detection using psychophysiological signals for implicit human-robot cooperation. *Robotica* 20(6), 673–685 (2002)
7. Salahuddin, L., Kim, D.: Detection of acute stress by heart rate variability using a prototype mobile ecg sensor, vol. 2, pp. 453–459
8. Segerstrom, S.C., Miller, G.E.: Psychological stress and the human immune system: A meta-analytic study of 30 years of inquiry
9. Tarvainen, M.P., Niskanen, J.-P., Lippinen, J.A., Ranta-Aho, P.O., Karjalainen, P.A.: Kubios hrv - a software for advanced heart rate variability analysis
10. Task Force European Society of Cardiology the North American Society of Pacing. Heart Rate Variability: Standards of Measurement, Physiological Interpretation, and Clinical Use. vol. 93, pp. 1043–1065
11. Yang, H.-K., Lee, J.-W., Lee, K.-H., Lee, Y.-J., Kim, K.-S., Choi, H.-J., Kim, D.-J.: Application for the wearable heart activity monitoring system: Analysis of the autonomic function of hrv
12. Goldberger, J.J.: Sympathovagal balance: how should we measure it? *Am. J. Physiol (Heart Circ. Physiol.)* 4 276, H1273–H1280 (1999)
13. Al-Hazimi, A., Al-Ama, N., Syamic, A., Qosti, R., Abdel-Galil, K.: Time domain analysis of heart rate variability in diabetic patients with and without autonomic neuropathy. *Annals of Saudi Medicine* 22(5-6), 400–402 (2002)
14. Gravina, R., Guerrieri, A., Fortino, G., Bellifemine, F., Giannantonio, R., Sgroi, M.: Development of body sensor network applications using spine. In: IEEE International Conference on Systems, Man and Cybernetics, SMC 2008., October 2008, pp. 2810–2815 (2008)
15. Lombbriser, C., Roggen, D., Stäger, M., Tröster, G.: Titan: A tiny task network for dynamically reconfigurable heterogeneous sensor networks. In: 15. Fachtagung Kommunikation in Verteilten Systemen (KiVS), Informatik aktuell, pp. 127–138. Springer, Heidelberg (2007)
16. SPINE open source project, <http://spine.tilab.com/>
17. Shnayder, V., Chen, B.-r., Lorincz, K., Jones, T.R.F.F., Welsh, M.: Sensor networks for medical care. In: Technical Report TR-08-05, Division of Engineering and Applied Sciences. Harvard University (2005)
18. Wartzek, T., Vogel, S., Hennig, T., Brodersen, O., Hulsbusch, M., Herzog, M., Leonhardt, S.: Analysis of Heart Rate Variability with an In-Ear Micro-Optic Sensor in View of Motion Artifacts. In: Sixth International Workshop on Wearable and Implantable Body Sensor Networks, pp. 168–172 (2009)
19. Lomb, N.R.: Least-squares frequency analysis of unequally spaced data. *Astrophys Space Sci.* 39, 447–462
20. Wang, C.Z., Zheng, Y.P.: Home-telecare of the elderly living alone using an new designed ear-wearable sensor. In: Proc. 5th Int. Workshop on Wearable and Implantable Body Sensor Networks, Hong Kong, China (2008)

21. Wang, B., Wang, L., Lin, S.J., Wu, D., Huang, B.Y., Zhang, Y.T., Yin, Q., Chen, W.: A Body Sensor Networks Development Platform for Pervasive Healthcare. In: 3rd International Conference on Bioinformatics and Biomedical Engineering, ICBBE 2009, June 11-13, pp. 1-4 (2009)
22. Polar HRM2 File Format Description, Polar (2009)
23. Health Reviser Stress Monitor,
<http://www.healthreviser.com/content/stress-monitor>
24. emWave Personal Stress Reliever,
http://www.myemwave.org/about_emwave_stress.html

Measuring Finger Movement in Arthritic Patients Using Wearable Glove Technology

J. Condell¹, K. Curran¹, T. Quigley², P. Gardiner³, M. McNeill¹,
J. Winder⁴, E. Xie¹, and Zhang Qi¹

¹ Faculty of Computing and Engineering, Magee College, University of Ulster,
Londonderry, N. Ireland

² Faculty of Arts, Magee College, University of Ulster, Londonderry, N. Ireland

³ Western Health and Social Care Trust, Altnagelvin Hospital, Londonderry, N. Ireland

⁴ School of Health Sciences, University of Ulster, Jordanstown, N. Ireland

Abstract. This paper outlines the initial ideas and results surrounding the development of an accurate hand movement measurement tool. This tool will assist medical clinicians, specifically rheumatologists and orthopaedic hand surgeons, with measuring the loss of movement in the human hand. This has many direct applications within medical practice including diagnosis, prognosis and recovery assessment of patients with conditions specific to the hand e.g. to measure how far a patient can close their fingers (with a flare up in arthritis patients may not be able to make a fist).

Current measurement techniques available to clinicians are either invasive (x-rays) or rely heavily on manual evaluation such as vision and touch which are dependent on training and experience and results often vary between observers. Measuring tape is commonly used to measure distances e.g. between palm and fingertip which also leads to issues with accuracy, as well as patient self questionnaires which allow for interpretation.

Keywords: medical informatics, healthcare technology, rheumatology, assisted technology.

1 Introduction

In society today, arthritis remains a disabling and agonizing disease. The term arthritis is used to describe more than 100 rheumatic diseases and 67 million (25%) adults aged 18 years and older will have doctor-diagnosed arthritis by the year 2030, and an estimated 25 million adults (37%) of those with arthritis will report arthritis-attributable activity limitations. In addition to these estimates, the personal treatment required for each individual becomes limited with every new patient as there is an increasing gap between the ideal and realistic number of doctors demanded. As a result, traditional measurements of arthritis requires exhaustive personal examination and labour so that medical staff may offer hasty, ambitious, and at many times, unconstructive conclusions that may hinder the enactment and analysis of arthritis rehabilitation. If patients are to receive the care

they need and doctors the time, scientists require more accurate and less laborious methods of analysis in regards to arthritis consultation. Therefore, an improved measurement in the region of arthritis rehabilitation is to be welcomed. Wearable Data Glove solutions are increasingly proving to offer reliable, accurate assessments with high cost effectiveness.

This research project aligns people with skill sets from the Creative Arts, Computing & Engineering, Programming and Rheumatology all of which have a vision and appreciation of how available and evolving technologies can be integrated to have a positive, direct impact on real clinical practice. The prototype is developed with insight from an active clinician in the field of Rheumatology. This facilitates direct measurement of the benefits and impact the project could have in daily clinical practice.

Knowledge of the nature and extent of the movement of hand joints greatly enhances the understanding of how sections of the body work. Measurement of joint range is a concern of many health care professionals and is used to establish a baseline and to record progress [4, 8]. Current measurement techniques available to clinicians are either invasive (x-rays) or rely heavily on manual evaluation such as vision and touch which are dependent on training and experience and results often vary between observers. Measuring tape is commonly used to measure distances e.g. between palm and fingertip which also leads to issues with accuracy, as well as patient self questionnaires which allow for interpretation. Hand measurement has many direct applications within medical practice including diagnosis, prognosis and recovery assessment of patients with conditions specific to the hand e.g. to measure how far a patient can close their fingers (with a flare up in arthritis patients may not be able to make a fist).

The aim of this project is to develop a solution of measuring hand joint movement that is accurate, easy to use and delivers useful data to the clinician through a user interface. Custom developed 3D CG graphics of the human hand will be integrated to enhance the user experience and add educational value. In order to achieve this accurate motion capture data of hand coordinates will be used with the 5DT Data Glove 14. This hardware is compatible with 3Ds Max, Motion Builder and 3D development software which will aid in the creation of an interface to present the measurement data in a user friendly format, enabling clinicians to efficiently make informed decisions on loss of movement.

2 Related Work

A number of devices and techniques have been investigated over the years to determine the range of movement of joints of the hand. However no fast and user friendly device has yet been identified to measure the movements of all of the small joints of the hand [5, 6]. One study examined the accuracy and precision of the 3Space Isotrak system for the measurement of known angles on a model and of metacarpophalangeal (MCP) joint range in the hand [8]. The 3Space Isotrak is an electromagnetic device that measures the position and orientation of a sensor in space. Results in studies [2] have validated the system as being accurate however

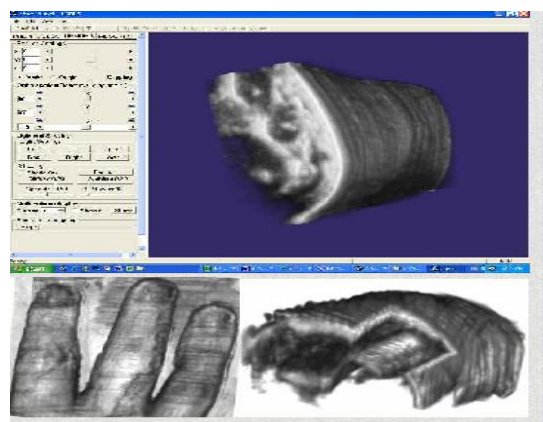


Fig. 1. 3D Ultrasound Imaging for Musculoskeletal Tissues¹

the unwieldy setup required to record such measurements render such a system impractical in practice.

3D ultrasound is an imaging sensor system (see Figure 1) typically used in clinical diagnosis and treatment monitoring. Through the use of projected and retrieved sound waves, scientists and physicians may observe 3D images of the musculoskeletal system, detecting such problems as tendonitis, bursitis, muscle injury, and arthritis.

Recently, portable freehand 3D ultrasound imaging systems have been created to allow various fields of research ease of access to its advantages. Specifically, such devices have proved useful in the scanning and treatment of rheumatoid arthritis patients. Before ultrasound, doctors could scan patients using an MRI and consequently prescribe their medications. However, the progress of treatment would initially rely on the patient's interpretation of their own pain. Furthermore, the indication of less pain is not always an indication of lessening inflammation. 3D ultrasounds allow physicians to assess the level of inflammation directly, rather than acting solely upon interpretation. Nevertheless, ultrasound is not without disadvantages, particularly in its lack of affordability and availability. Chief limitations arise in that the ultrasound devices must be placed in specific locations and at proper angles for the device to work. While ultrasound detects muscular systems quite efficiently, ultrasound cannot image bone, a serious problem if bone damage exists in the patient. If ultrasound must penetrate thick tissue, images may also prove unreliable, another problem if the patient is muscular or obese. In conclusion, ultrasound has proven its most effective use in fatal recognition, yet overall has limited testing in regards to other areas of the medical field. Certainly Ultrasound deserves more experimentation, yet it must also become more easily available for additional tests to become a reality.

¹ <http://www.tups.org/>

The Humanglove is a sensitized, elastic fabric glove designed and commercialized by Humanware². The Humanglove is equipped with 20 Hall effect sensors that are distributed as shown in Figure 1.



Fig. 2. Humanglove

Each sensor measures data related to a DOF of the hand. The nominal sensor characteristics are resolution, 0.4° over a range up to 90°; linearity, about 1 percent full-scale output, and accuracy about 1°. However, no information about the sensors is available concerning their performance when they are mounted on the elastic fabric glove. The glove control unit is connected to the host computer through a standard RS-232 at 38400 baud; the host computer can be any kind of workstation, PC, or Macintosh. Data acquisition is performed through a proprietary software package called Graphical Virtual Hand (GVH). This program calibrates the glove and displays an animated hand that mirrors movements of the user's hand. Data acquisition and storage in ASCII format can be performed both with and without the GVH interface (with a non-graphical version of the data acquisition software).

The TUB-sensor glove developed at the Technische Universität Berlin (TUB) enables continuous measurement of grip power, which can be depicted in load-time diagrams. The strength distribution pattern of the grip is recorded through ten sensors applied to the palm surface of the hand and evaluated on a computer. Studies have been conducted using this glove to determine whether it is possible to assign an individual strength distribution pattern to the different grip sizes of the dynamometer³ they have also studied whether it is possible to recognise sub maximal effort, corresponding to a pretended loss of strength on the basis of characteristics in the strength distribution pattern.

The AcceleGlove is a portable, glove based input interface, designed as an assistive device that translates hand and gesture based languages (such as American Sign Language) into written and spoken language. The AcceleGlove consists of a group of sensors and accelerometers that are strapped to the hand, arm, and shoulder and a set of algorithms that decipher and categorize the movements of the hand and arm. The AcceleGlove has the capability to translate both finger spelling

² Humanware S.R.L.. Humanglove developers manual; Pisa, Italy; 1998.

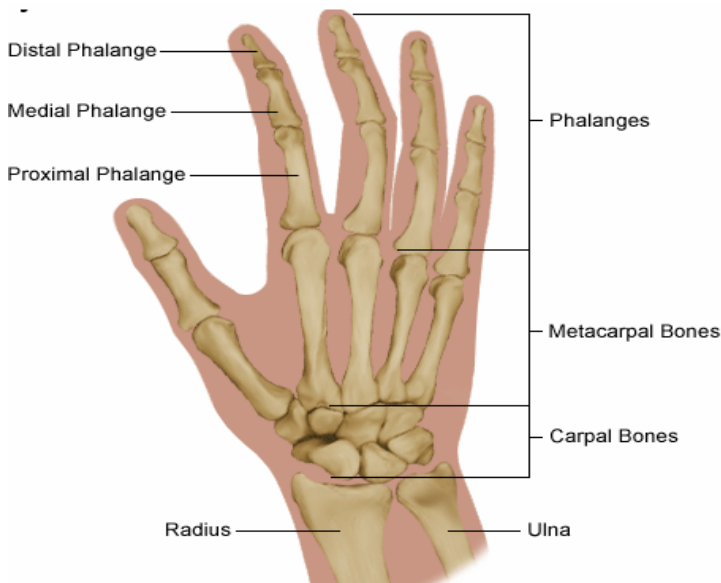


Fig. 3. Structure of a hand³

and more complicated, gesture-based signs. Additionally, the AcceleGlove unit is more portable than comparable technologies and can be built at a fairly low price per unit. Eval⁴, Clinical Hand Master⁵, and Dexter⁶ have also proven to be well-developed, computer-based hand diagnosis and rehabilitation systems with the capability of data collection.

Virtual Reality (VR) has been promising as an effort to provide substitute environmental experiences for repetitive practice in a task-oriented context within a clinical setting [1,3,7]. VR allows individuals to practice movements in several different environments and indeed perform rapid transition between tasks. Clinicians then possess the capability of creating challenging tasks through which intensive, repetitive practice of new motor skills can be delivered and monitored [7]. These aspects of research however focus more on the tasks and rehabilitation as opposed to our quest to provide accurate measurements for diagnosis and assessment.

One of the main shortcomings of the traditional manual measurement for arthritis patients recovering after proper treatment or undergoing diagnosis is the lack of accurate, repeatable, and reliable tools. Presently, such methods involve questionnaires (Arthritis Impact Measurement Scales 2 Short Form (AIMS2-SF), The Functional Index of Hand OA (FIHOA), the Health Assessment Questionnaire (HAQ), etc.), X-ray, rulers, protractors, strings, or even water. Arthritis physicians

³ <http://arthritis-symptom.com/images/Hand-Fracture.gif>

⁴ <http://www.greenleafmed.com/Products/pointofcase.htm>

⁵ <http://www.cs.utah.edu/classes/cs6360/Nahvi/haptic.html>

⁶ <http://www.cedaron.com/>

use diagnostic reports to give patients individual treatment, yet potentially inaccurate diagnoses will undoubtedly lead to unbeneficial and even dangerous conclusions. Therefore, it is necessary to find new advanced techniques to produce more accurate and repeatable results.

As a sensitive electronic device, the data glove was created with the purpose of measuring hand dexterity using precise algorithms. There is a growing body of research to attest to the reliability of data gloves for goniometric measurements. Repeatability results showed an overall error of 3.4°, compared to 5.5° and 5.7° reported with other ... manual measurements (5-8°) [12] and elsewhere results show an overall error of 5.6 degrees, as compared to an error of between 5 and 8 degrees with manual measurement [13]. In another study, the Humanglove was seen as adequate for several applications in the field of rehabilitation engineering and comparable to repeatability of manual goniometric measurements in normal subjects [11].

When we take a close look at the human hand, we will find there are several constraints within which one can use range measuring for the stiffness measurement.

The interfinger constraint is between the joints of the same finger (see Figure 1). Using this type of constraint, pinkie, index, middle, ring, distal interphalange (DIP) joints' movements can be approximated by the following equation:

$$\theta_{DIP} = \frac{2}{3} \theta_{PIP}$$

Equation 1 Interfinger constraints

The angle range constraint refers to the limits of the range of finger motions as a result of hand structure, normally within the following ranges:

$$\begin{aligned} 0^\circ &\leq \theta_{PIP_FLEXION} \leq (90^\circ \sim 100^\circ) \\ 0^\circ &\leq \theta_{Thumb_DIP_FLXION} \leq 90^\circ \\ 0^\circ &\leq \theta_{MCP_FLEXION} \leq 90^\circ \end{aligned}$$

Equation 2 Angle range constraints

The bending direction constraint is available for DIP, PIP, and Thumb PIP joints. [14] mapped finger angles to the torque and found a non-linear relationship. Other work supported their findings [12]. Simone et al evaluated the usefulness of a wireless custom monitor in measuring real-time finger posture over an extended period of time as the wearer went about daily life activities. Signal conditioning electronics, memory storage, and the wireless transmission system were located in a small box that could be strapped to the arm and the core of the system was a Tmote Sky device [9]. One individual wore the device for 25 continuous hours in the research facility and at home. The study found that real time joint motion can be used to evaluate compliance with therapy regimens and true function effects of an intervention, and to assess overall functional levels and objective hand use outside the clinic. This supports our research aims.

3 Tests

The overall aim is to develop a software tool using a commercial data glove to assist medical clinicians with the accurate measurement of the common condition of loss of movement in the human hand in patients with arthritis. We had therefore to determine the feasibility of the Data Glove by implementing a series of tests. Our initial aims were to prove the feasibility of the Data Glove, determine accuracy of the Data Glove and to discover what precisely the Data Glove can measure. Therefore we devised a series of tests to achieve this. Testing would be carried out through a series of studies which are designed to inform the aims of final stages of the project.

Study A – Repeatability testing of Data Glove on rigid hand model

The purpose of this study is to determine how repeatable tests from the Data Glove are. To avoid issues of hand movement we will use a static rigid hand. This study will be carried out by the team over the period of one half day. No volunteers required. Equipment required would be our Data Glove, rigid hand model and a camera and tripod.

Process

- Obtain a rigid hand model
- Secure hand model to surface (e.g. vice grip)
- Place glove onto hand aligning the top of each bend sensor to the PIP joint, and the bottom of each sensor to the MCP joint
- Once in position record output values from Data Glove
- Repeat process 10 times

Outcomes

Statistical analysis

1. Variation in sensor data from each channel of the Data Glove

The results table for this study takes the following format as shown in

Table 1. Study A results capture format

Channel / Sensor	Description	Mean measure	Standard Deviation of measurement	% Variance
1	Pinky finger	1022	1	0.45
2...	Ring finger	855	2	0.08

The outputs from this study would be used to inform clinical researchers of the repeatability achievable using the Data Glove as a measurement tool for a static hand. The study would also enable us to determine a quantifiable measurement of error in repeatable measurements taken by the Data Glove.

Study B – Repeatability testing of application of Data Glove onto rigid hand model

The purpose of this study is to determine the likely range of error by a trained technician in placing the Data Glove onto a patient's hand. To avoid issues of hand movement we will use a static rigid hand. This study will be conducted simultaneously with Study A.

Process

- Set up camera in fixed alignment with the glove
- Record camera lens used, aperture & shutter speed and camera distance from Data Glove
- Photograph the glove placement 10 times

Outcomes

Statistical analysis

1. Variation in positioning of sensors

We would anticipate our results table will take the following format for each sensor.

Table 2. Study B capture results format

Photo	Channel / Sensor	Description	Position (X,Y) mm	Standard Deviation of measurement	% Variance
1	1	Pinky finger	48, 129	1	0.45
2	1	Pinky finger	49, 127	2	0.02
3	1	Pinky finger	49, 128	3	0.2
4...	1	Pinky finger	47, 126	4	0.38

The outputs from this study will inform the team of the repeatability achievable by a trained technician placing the glove onto a static hand. The study will enable us to determine a quantifiable measurement of repeatability for sensor placement.

Studies A and B both involve the following procedures:

1. Secure hand model to surface (Vice)
2. Place Data Glove onto hand model aligning top of each sensor to the PIP joint and bottom of each sensor to the MCP joint
3. Set up camera on tripod in alignment with hand model and Data Glove
4. Record lens type, aperture, shutter speed and camera distance from Data Glove
5. Record output values from Data Glove
6. Mark each photograph with clapper board
7. Repeat process 10 times

Study C – Accuracy testing of Data Glove on animated hand model

The purpose of this study is to determine how accurate the Data Glove is in comparison to an animated mechanical hand setup. Ideally the mechanical hand should itself be accurate and reliable. Testing will focus on one movement, flexion at one joint of one finger. We believe it is best to use a robotic hand / finger here or a replica hand / finger with joints possessing the ability to snap or click into 3, or more, positions e.g. Bend PIP joint by 30 deg, 60 deg and 90 deg. We can then compare against the value outputs from the Data Glove. This study is carried out by the team over the period of one half day. No volunteers required. Equipment required will be our Data Glove, animatable hand / finger model.

Process

- Obtain an animatable hand / finger model
- Secure hand model to surface (e.g. vice grip)
- Place glove onto hand / finger aligning the top of each bend sensor to the PIP joint, and the bottom of each sensor to the MCP joint
- Once in position record output values from Data Glove
- Repeat process 10 times

Outcomes

Statistical analysis

1. Variation in measurement data taken from animatable hand / finger model and Data Glove.

The results table takes the following format

Table 3. Study B results capture format

Robotic Hand	Channel / Sensor	Description	Mean measure	Standard Deviation of measurement	% Variance
0° Flexion	1	Pinky finger MCP	0095	1	0.45
30° Flexion	1	Pinky finger MCP	0725	2	0.08
60° Flexion	1	Pinky finger MCP	1562	3	0.25
90° Flexion	1	Pinky finger MCP	3622	4	0.21

The outputs from this study will inform clinical researchers of the accuracy in measuring joint angular data using the Data Glove. As a follow up study perhaps we may consider repeating this test on a human hand where the PIP and DIP joints are secured and unable to bend so we are only getting data for the MCP joint as in this study. Study C involves the following procedures:

1. Secure hand model to surface (Vice)
2. Place glove onto hand aligning the top of each bend sensor to the PIP joint, and the bottom of each sensor to the MCP joint
3. Once in position record output values from Data Glove
4. Repeat process 10 times

4 Measurement Glove Prototype

The project involves the development of a tool to assist medical clinicians with the accurate measurement of the common condition of loss of movement in the human hand in patients with arthritis. The main aim is to develop a solution that is accurate, easy to use and delivers useful data such as historical patient hand movement data to the clinician through a user interface. The main targets and stages of the project include:

- *Interface Development* – The development of a user friendly front end UI with specific requirements from Rheumatologist e.g. patient friendly.
- *Database development* - The database allows the clinician to store and access patient data. For instance, the clinician can view patients past tests while wearing the glove and view on screen the actual movements in the form of an animation of the moving hand taken from the previously recorded movements on the day of the actual test. This is unique in this field. Consideration would be taken of ethical issues and so various options would be investigated e.g. storing hand images only classified by patient number (no reference made to patient name or identity).
- *3D environment (XNA) set up and customization* - This allows the clinician to see in real-time the movements of the patients hand on screen which mirrors the patients' movements inside the glove.
- *Data refinement* - This involves work on attaining high accuracy levels to improve results in addition to the creation of graphs for the presentation of patient measurements in various ways for use during consultation. This may lead to insights previously hidden through use of basic manual measurements.

The data glove we used was the 5DT Data Glove 5. It is easy to use and comfortable giving high quality, high rate, low cross-correlation data ideal for realistic real-time animation and motion capture. It has sensors attached to each finger to measure finger flexure and also a tilt sensor attached to the exterior of the hand.

Custom developed 3D CG graphics of the human hand are integrated to enhance the user experience and add educational value. In order to achieve this accurate motion capture, data of hand coordinates are used with the 5DT Data Glove 5 to set up an initial system.

This hardware is compatible with 3Ds Max, Motion Builder and 3D development software. An interface is being developed to present the measurement data in a user friendly format, enabling clinicians to efficiently make informed

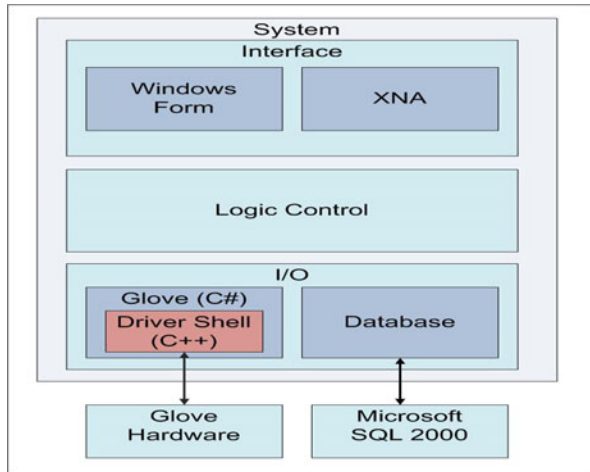


Fig. 4. Structure of the program

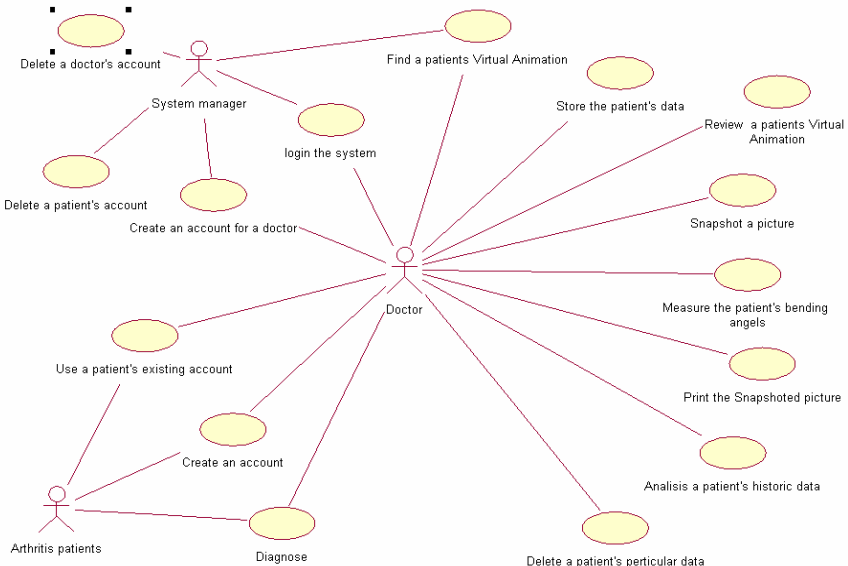


Fig. 5. System Architecture Use Cases

decisions on loss of movement. The program structure is shown in Figure 1. This shows how the Data Glove hardware integrates with Microsoft SQL using C++ and a database to process the information and display results on the interface accordingly.

The data glove works in measuring arthritis stiffness as the resistance of the sensor changes as each finger moves. For example, when a user bends their

fingers, less light will emit from the LED (Light-emitting diode) in the optical data glove, causing the resistance change and thus resulting in a numerical value in the sensors feedback.

Figure 2 provides an overview of the system architecture. We have designed the system so that the doctor takes a key role as the main operator. They can use it to create an account for an arthritis patient and record the current illness situation information in the database. Each patient wears the data glove and does the motion that the doctor asks them to do. This motion is then captured. The 5DT Data Glove 5 measures finger flexure (1 sensor per finger) and the orientation (pitch and roll) of the user's hand. It can emulate a mouse as well as a baseless joystick. The interface we have created is shown in Figure 3. This demonstrates how each finger on the right and data glove is sending data to the system which is then displaying the information for the clinician to analyse. Each finger is labeled as one of the first five sensors (sensor 1 to sensor 5) and sensor 6 and sensor 7 relate to the 2-axis tilt sensor. It can also be seen that the value displayed for each sensor relates to the degree of movement of each finger being recorded by the system.

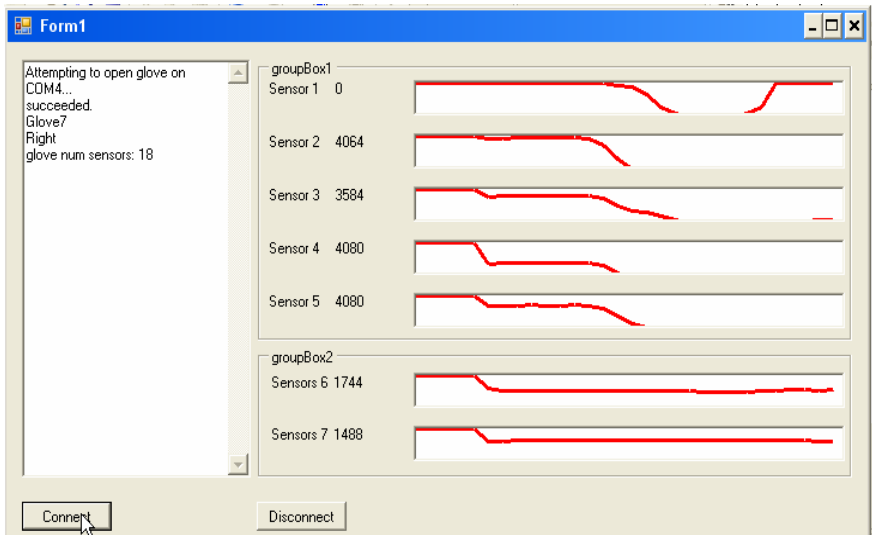


Fig. 6. Interface processing information from each sensor (finger) on data glove

Figure 4 shows a close up of the hand model that we created in 3Ds Max which allows us to monitor the patient performing movement exercises (or tests). This also is the model that we see repeating the tests when we choose to reply examinations at a later date. This aspect is interesting as the physician can now see in real time the previous test(s) and compare them to the current set of tests and this may possibly lead to more a more accurate diagnosis but this of course is yet to be examined and we can only speculate at this moment as to any future benefits of having real time animation playback of examinations.

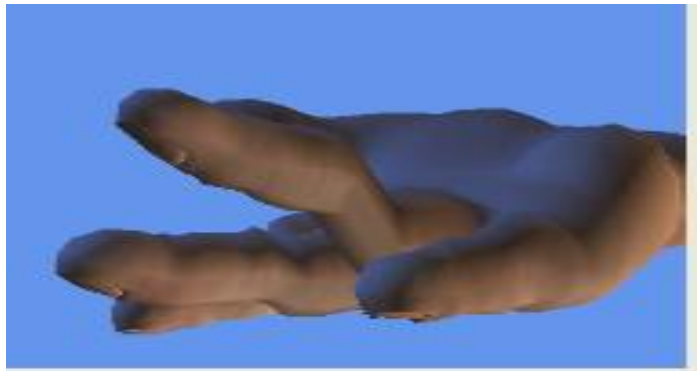


Fig. 7. Close up of hand model

Figure 5 also shows the hand model animated alongside the sensor data being processed from the data glove. It is important that the system is able to recognize a broad range of finger gestures and record movement associated with them.

The range of gestures recognized by the system currently is shown in Figure 6. One key concept of the project is that the system can replay the movement of the hand in an animated sequence so that the clinician can get an idea of the speed of the movement and also quantify the joint stiffness. This would also be useful for physiotherapists who may prefer to see a visual display of the hand movement. Ideally the tests would be done at the patient's home (or in their own time) before their routine appointment with the clinician. This would save clinician's time and allow for a very efficient clinical service.



Fig. 8. Animated hand alongside sensor data from glove

The system should relay back to the clinician some main measurements:

- The *degree of deformity* of the hand and an objective measurement of the stiffness of the moving joints. It is well known that patients usually move their hands slowly if their hands are stiff. This measurement tool should quantify this stiffness.

- The *amount of joint swelling*. Usually clinicians simply assess this visually and through pressing the hand. A volumetric measurement is required which could be integrated into the final system.
- *Maximum and minimum range of movement* of hand e.g. the extension and inflexion as in how far the fingers and hand can be moved. Individual data would be stored per finger showing the range of movement for each individual joint in the hand.
- *Rate of movement of hand* – the speed of movements aid the clinician in the diagnosis of condition.

For these measurements the system records the average, minimum and maximum values over a period of time or number of tests. This allows the clinician to have a historical view of the hand movement and make a prognosis based on key indicators.

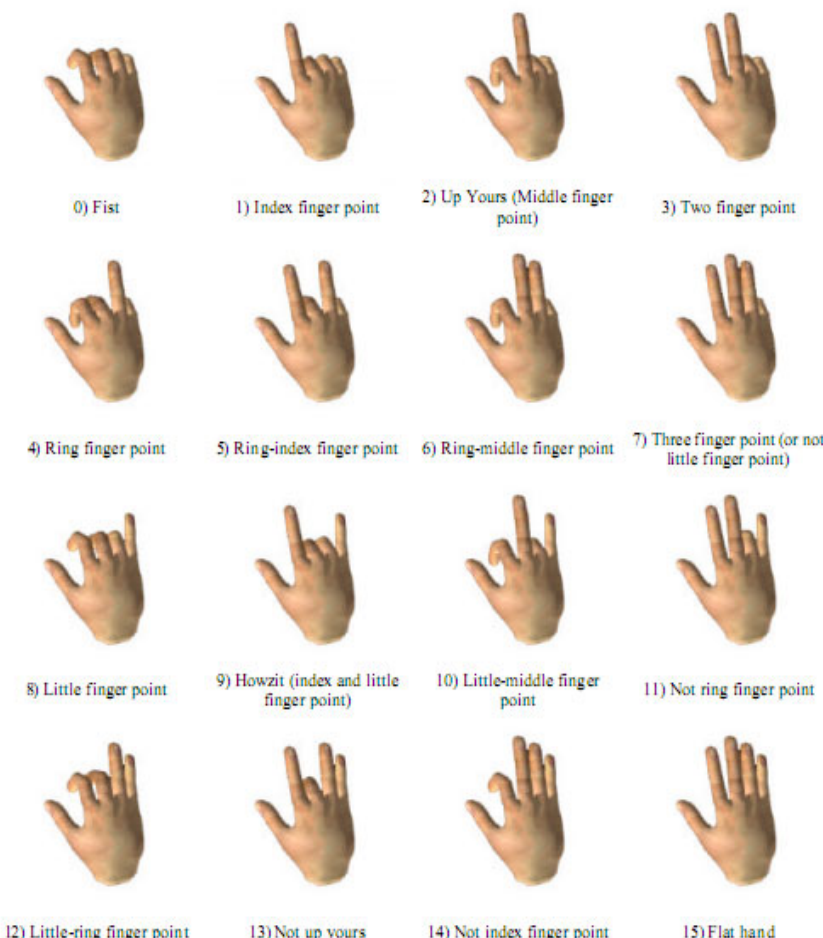


Fig. 9. Gestures recognised by system

5 Conclusion

This project aligns researchers & practitioners with skill sets from a diverse range of research areas, all of which appreciate how available and evolving technologies can be integrated to have a positive, direct impact on real clinical practice. This idea has obvious commercial potential and should provide an ideal environment for interdisciplinary community arts projects which more and more are embracing digital technologies as indeed is the field of educational medicine. Further work will therefore involve the exploration of further applications within clinical and educational practice. Future work will integrate mean and standard deviation error measures [10] with the recorded data and accurate ‘normal’ data to produce data charts and graphs which will allow the clinician to automatically and efficiently analyse the patient’s range of movement.

One research concept which is of particular interest for future work is the development of a data belt. This belt would be positioned around the spine to measure distance and change or movement of the spine. Currently these measurements are taken using a basic tape measure. A more automated system would be of considerable benefit to clinicians. Patients would wear the belt at set times of the day and before each clinical appointment. Data would be logged and graphed, making the clinicians analysis more efficient and accurate as a result.

References

- [1] Boian, R., Sharma, A., Han, C., Merians, A., Burdea, G., Adamovich, S., Recce, M., Tremaine, M., Poizner, H.: Virtual reality-based post-stroke hand rehabilitation. *Stud. Health Technol. Inform.* 85, 64–70 (2002)
- [2] Culham, E., Peat, M.: Spinal and shoulder complex posture. I: Measurement using the 3Space IsotraK. *Clinical Rehabilitation* 7, 309–318 (1993)
- [3] Finley, M., Fasoli, S., Dipietro, L., Ohlhoff, J., Maclellan, L., Meister, C., Whitall, J., Macko, R., Bever, C., Krebs, J.H., Hogan, N.: Short-duration robotic therapy in stroke patients with severe upper-limb motor impairment. *J. Rehabil Res. Dev.* 42(5), 683–692 (2005)
- [4] Greene, B., Wolf, S.: Upper extremity joint movement: Comparison of two measurement devices. *Archives of Physical Medicine and Rehabilitation* 70, 288–290 (1989)
- [5] Hamilton, G.F., Lachenbruch, P.A.: Reliability of goniometers in assessing finger joint angle. *Physical Therapy* 49, 465–469 (1969)
- [6] Hasselkus, B.R., Kshepakan, K.K., Houge, J.C., Plautz, K.A.: Rheumatoid arthritis: A two-axis goniometer to measure metacarpophalangeal laxity (1981)
- [7] Jial, Y., Toro, M., Luo, X., Lau, S., Kenyon, R., Kamperl, D.: Integration of Virtual Reality and an Assistive Device for Hand Rehabilitation Following Stroke. *Intern. Confer.Complex Medical Eng.* (2007)
- [8] Kulkarni-Lambore, S., Peat, M.: Reliability and validity of 3Space IsotraK in the measurement of metacarpophalangeal joint range. *Physiotherapy Theory and Practice* 16(4), 219–227 (2000)

- [9] Simone, L., Nappinnai, S., Luo, X., Jia, Y., Kamper, D.: Measuring Finger Flexion and Activity Trends over a 25 Hour Period using a Low Cost Wireless Device. In: Proceedings of the 28th International Conference of the IEEE Engineering in Medicine and Biology Society (EMBC 2006), New York, NY (2006)
- [10] Alvi, A.K., Muxxaffar, A., Usman, M., Mumtaz, S., Azhar, Y.B.: Pakistan Sign Language Recognition, Sir Syed University of Technology and Engineering, Boltay Health – Final Report (2005)
- [11] Dipietro, L., Sabatini, A., Dario, P.: Evaluation of an instrumented glove for hand-movement acquisition. *Journal of Rehabilitation Research & Development* 40(2), 179–190 (2003)
- [12] Simone, L.: A Low Cost Method to Measure Finger Flexion in Individuals with Reduced Hand and Finger Range of Motion. *Journal of NeuroEngineering and Rehabilitation* 13(3) (2005)
- [13] Wise, S., Gardner, W., Sabelman, E., Valainis, E., Wong, Y., Glass, K., Drace, J., Rosen, J.: Evaluation of a fiber optic glove for semi-automated goniometric measurements. *Journal of Rehabilitation Research and Development* 27(4), 411–424 (Fall 1999)
- [14] Luster, S., Patterson, P., Cioffi, W., Mason, A., McManus, W., Pruitt, B.: An Evaluation Device for Quantifying Joint Stiffness in the Burned Hand. *Journal of Burn Care and Research* 11(4) (July/August 1990)

Author Index

- Amato, F. 137
Andò, Bruno 97
Andreoli, Alessandro 369
Antonio, Greco 31
Araújo, Pedro 115

Baglio, Salvatore 97
Barroca, Norberto 115
Benito-Lopez, Fernando 177
Bhushan, Abhinav 55
Borges, Luís M. 115
Boukallel, Mehdi 155
Bourke, Alan 1
Byrne, Robert 177

Calabrese, B. 137
Cannataro, M. 137
Cifrek, Mario 351
Cocorullo, G. 137
Condell, J. 391
Coyle, Shirley 177
Curran, K. 391

Davis, Cristina E. 55
De Capua, Claudio 195, 207
Desmaële, Denis 155
Diamond, Dermot 177

Ferrari, Marco 97
Ferrari, Vittorio 97
Ferro, João M. 115
Fortino, Giancarlo 369
Francesco, Conversano 31

Gambardella, A. 137
Gammaitoni, Luca 97
Gardiner, P. 391
Giannantonio, Roberta 369
Girão, Pedro Silva 277
Gravina, Raffaele 369
Guzzi, P.H. 137

Hegeduš, Hrvoje 259

Inoue, Yoshio 219

Jabłoński, Ireneusz 75
Jurčević, Marko 259

Kenyon, Nicholas J. 55
Krois, Igor 351

Lanuzza, M. 137
Lay-Ekuakille, Aimé 259
Lebres, António S. 115
Li, Chunguang 219
Liu, Tao 219
Lučev, Željka 351
Lymberis, Andreas 237

Malarić, Roman 259
Martinez-de-Oliveira, J. 115
McNeill, M. 391
Morello, Rosario 195, 207
Mostarac, Petar 259
Mroczka, Janusz 75

Nelson, John 1

- O'Brien, Hugh 1
Ostaszewska, A. 315
- Palumbo, A. 137
Pierleoni, Paola 369
Pinheiro, Eduardo 277
Postolache, Gabriela 277
Postolache, Octavian 277
- Qi, Zhang 391
Quigley, T. 391
- Régnier, Stéphane 155
Rente, Andreia 115
- Salvado, Rita 115
Schivo, Michael 55
Sergio, Casciaro 31
- Shibata, Kyoko 219
Sturniolo, M. 137
- Trigona, Carlo 97
- van de Ven, Pepijn 1
Velázquez, Ramiro 331
Velez, Fernando J. 115
Veltri, P. 137
Vizza, P. 137
- Winder, J. 391
- Xie, E. 391
- Żebrowska-Lucyk, S. 315
Zhao, Weixiang 55